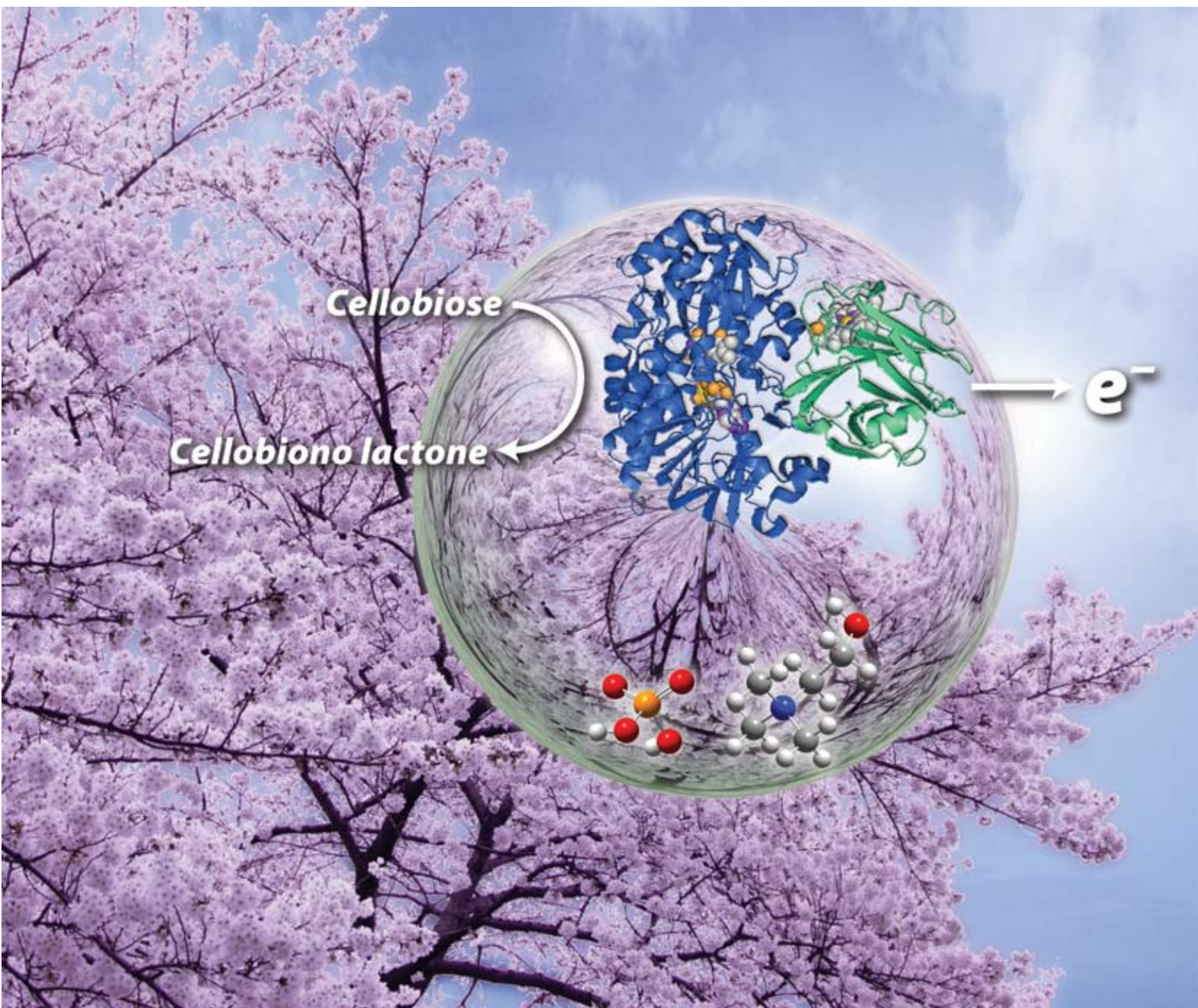


Green Chemistry

Cutting-edge research for a greener sustainable future

www.rsc.org/greenchem

Volume 11 | Number 3 | March 2009 | Pages 297–436



ISSN 1463-9262

RSC Publishing

Ohno *et al.*
Biocatalytic oxidation of cellobiose

Guo *et al.*
Simultaneous esterification and transesterification of soybean oil

Tan *et al.*
Extraction of lignin from lignocellulose

Jessop *et al.*
Switching the hydrophilicity of a solute



1463-9262(2009)11:3;1-B

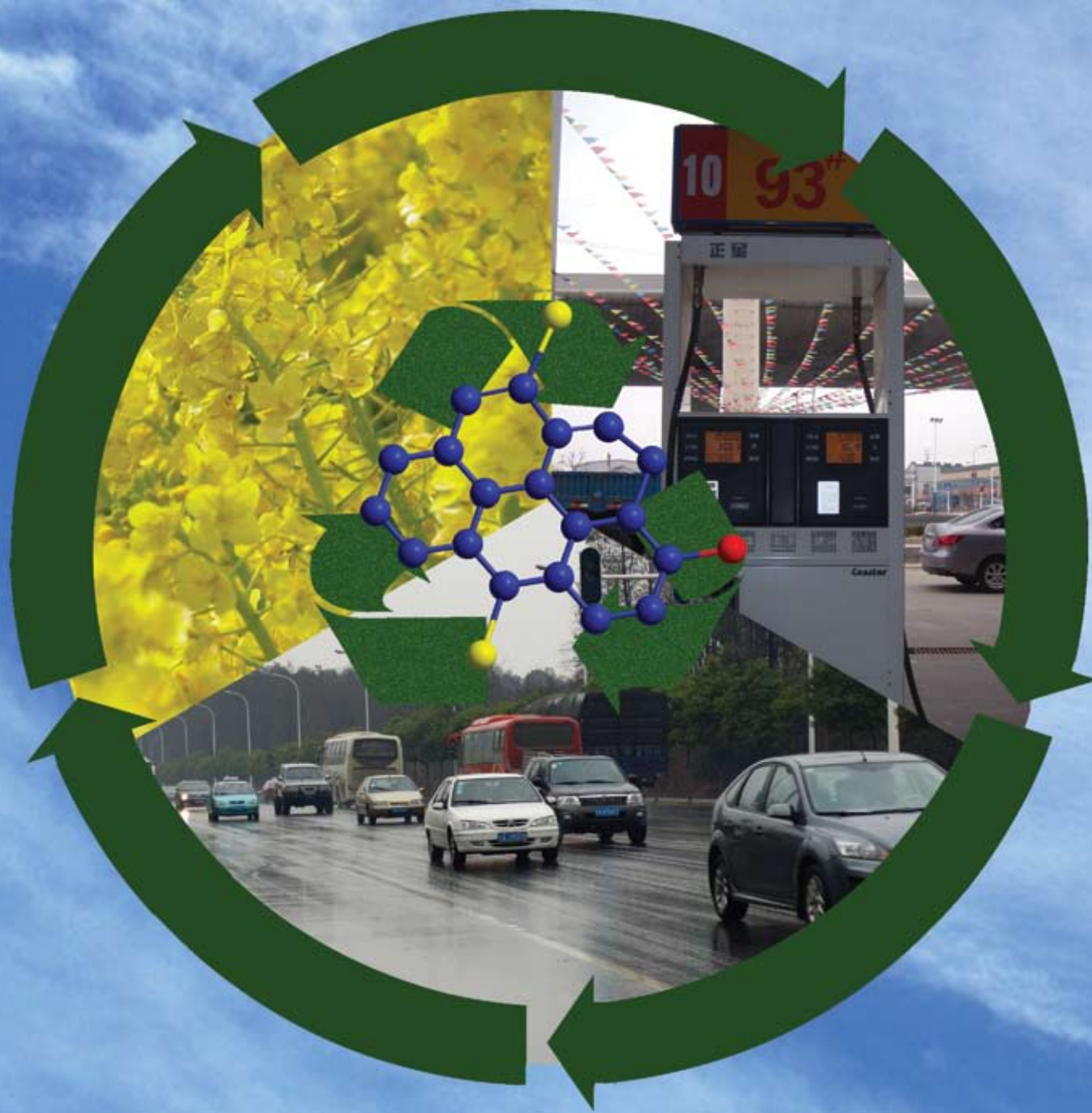
Green Chemistry

Cutting-edge research for a greener sustainable future

www.rsc.org/greenchem

Volume 11 | Number 3 | March 2009 | Pages 297–436

Downloaded on 21 November 2010
Published on 09 March 2009 on <http://pubs.rsc.org> | doi:10.1039/B903786C



ISSN 1463-9262

Zheng *et al.*
Biont shell catalyst for biodiesel
production

Oelgemöller *et al.*
Green photochemistry

Li *et al.*
Basic metal carbonate supported
gold nanoparticles

Nagarajan *et al.*
A stable biomimetic redox catalyst

RSC Publishing

Green Chemistry

Cutting-edge research for a greener sustainable future

www.rsc.org/greenchem

RSC Publishing is a not-for-profit publisher and a division of the Royal Society of Chemistry. Any surplus made is used to support charitable activities aimed at advancing the chemical sciences. Full details are available from www.rsc.org

IN THIS ISSUE

ISSN 1463-9262 CODEN GRCHFJ 11(3) 297–436 (2009)



Cover

See Ohno *et al.*, pp. 351–354. Enzymatic oxidation of cellobiose in hydrated IL opens a new technology for biomass energy conversion. A ribbon image of cellobiose dehydrogenase was reproduced from the protein data bank ID 1kdg and 1d7c. Image reproduced with permission from Hiroyuki Ohno from *Green Chem.*, 2009, **3**, 351.



Inside cover

See Zheng *et al.*, pp. 355–364. A tri-step synthetic strategy was devised to obtain a high-performance and ecologically friendly heterogeneous biodiesel catalyst derived from biont shell. Image reproduced with permission from Xinsheng Zheng from *Green Chem.*, 2009, **3**, 355.

CHEMICAL TECHNOLOGY

T17

Drawing together research highlights and news from all RSC publications, *Chemical Technology* provides a 'snapshot' of the latest applications and technological aspects of research across the chemical sciences, showcasing newsworthy articles and significant scientific advances.

Chemical Technology

March 2009/Volume 6/Issue 3

www.rsc.org/chemicaltechnology

COMMUNICATIONS

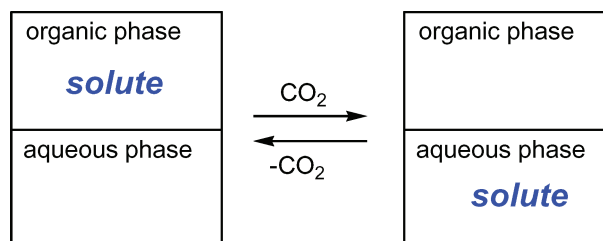
307



Switching the hydrophilicity of a solute

Lam Phan and Philip G. Jessop*

An amidine appendage gives a solute switchable hydrophilicity. The introduction of CO₂ gas reversibly changes the solute's oil/water partition coefficient by >2 orders of magnitude.



EDITORIAL STAFF

Editor

Sarah Ruthven

Assistant editors

Sarah Dixon, Katie Dryden-Holt

Publishing assistant

Jessica-Jane Doherty

Team leader, Informatics

Stephen Wilkes

Technical editor

Edward Morgan

Production administration coordinator

Sonya Spring

Administration assistants

Aliya Anwar, Jane Orchard, Julie Thompson

Publisher

Emma Wilson

Green Chemistry (print: ISSN 1463-9262; electronic: ISSN 1463-9270) is published 12 times a year by the Royal Society of Chemistry, Thomas Graham House, Science Park, Milton Road, Cambridge, UK CB4 0WF.

All orders, with cheques made payable to the Royal Society of Chemistry, should be sent to RSC Distribution Services, c/o Portland Customer Services, Commerce Way, Colchester, Essex, UK CO2 8HP. Tel +44 (0) 1206 226050; E-mail sales@rscdistribution.org

2009 Annual (print + electronic) subscription price: £1027; US\$2013. 2009 Annual (electronic) subscription price: £924; US\$1811. Customers in Canada will be subject to a surcharge to cover GST. Customers in the EU subscribing to the electronic version only will be charged VAT.

If you take an institutional subscription to any RSC journal you are entitled to free, site-wide web access to that journal. You can arrange access via Internet Protocol (IP) address at www.rsc.org/ip. Customers should make payments by cheque in sterling payable on a UK clearing bank or in US dollars payable on a US clearing bank. Periodicals postage paid at Rahway, NJ, USA and at additional mailing offices. Airfreight and mailing in the USA by Mercury Airfreight International Ltd., 365 Blair Road, Avenel, NJ 07001, USA.

US Postmaster: send address changes to Green Chemistry, c/o Mercury Airfreight International Ltd., 365 Blair Road, Avenel, NJ 07001. All despatches outside the UK by Consolidated Airfreight.

PRINTED IN THE UK

Advertisement sales: Tel +44 (0) 1223 432246; Fax +44 (0) 1223 426017; E-mail advertising@rsc.org

For marketing opportunities relating to this journal, contact marketing@rsc.org

Green Chemistry

Cutting-edge research for a greener sustainable future

www.rsc.org/greenchem

Green Chemistry focuses on cutting-edge research that attempts to reduce the environmental impact of the chemical enterprise by developing a technology base that is inherently non-toxic to living things and the environment.

EDITORIAL BOARD

Chair

Professor Martyn Poliakoff
Nottingham, UK

Scientific Editor

Professor Walter Leitner
RWTH-Aachen, Germany

Associate Editors

Professor C. J. Li
McGill University, Canada

Members

Professor Paul Anastas
Yale University, USA

Professor Joan Brennecke
University of Notre Dame, USA

Professor Mike Green
Sasol, South Africa

Professor Buxing Han
Chinese Academy of Sciences,
China

Professor Shu Kobayashi,
University of Tokyo, Japan

Dr Alexei Lapkin
Bath University, UK

Professor Steven Ley
Cambridge, UK

Dr Janet Scott
Unilever, UK

Professor Tom Welton
Imperial College, UK

ADVISORY BOARD

James Clark, York, UK
Avelino Corma, Universidad
Politécnica de Valencia, Spain
Mark Harmer, DuPont Central
R&D, USA

Herbert Hugl, Lanxess Fine
Chemicals, Germany
Roshan Jachuck,
Clarkson University, USA

Makato Misono, nite,
Japan

Colin Raston,
University of Western Australia,
Australia

Robin D. Rogers, Centre for Green
Manufacturing, USA

Kenneth Seddon, Queen's
University, Belfast, UK

Roger Sheldon, Delft University of
Technology, The Netherlands

Gary Sheldrake, Queen's
University, Belfast, UK

Pietro Tundo, Università ca
Foscari di Venezia, Italy

INFORMATION FOR AUTHORS

Full details of how to submit material for publication in Green Chemistry are given in the Instructions for Authors (available from <http://www.rsc.org/authors>). Submissions should be sent via ReSource: <http://www.rsc.org/resource>.

Authors may reproduce/republish portions of their published contribution without seeking permission from the RSC, provided that any such republication is accompanied by an acknowledgement in the form: (Original citation) – Reproduced by permission of the Royal Society of Chemistry.

© The Royal Society of Chemistry 2009. Apart from fair dealing for the purposes of research or private study for non-commercial purposes, or criticism or review, as permitted under the Copyright, Designs and Patents Act 1988 and the Copyright and Related Rights Regulations 2003, this publication may only be reproduced, stored or transmitted, in any form or by any means, with the prior permission in writing of the Publishers or in the case of reprographic reproduction in accordance with the terms of licences issued by the Copyright Licensing Agency in the UK. US copyright law is applicable to users in the USA.

The Royal Society of Chemistry takes reasonable care in the preparation of this publication but does not accept liability for the consequences of any errors or omissions.

Ⓢ The paper used in this publication meets the requirements of ANSI/NISO Z39.48-1992 (Permanence of Paper).

Royal Society of Chemistry: Registered Charity No. 207890

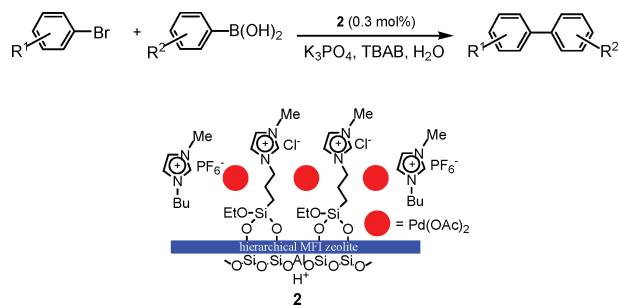
COMMUNICATIONS

309

Palladium acetate immobilized in a hierarchical MFI zeolite-supported ionic liquid: a highly active and recyclable catalyst for Suzuki reaction in water

Myung-Jong Jin,* Abu Taher, Hee-Jae Kang, Minkee Choi and Ryong Ryoo*

Palladium acetate was immobilized in ionic liquid layers on the mesopore wall of hierarchical MFI zeolite, and tested as a catalyst for Suzuki coupling reaction in water.

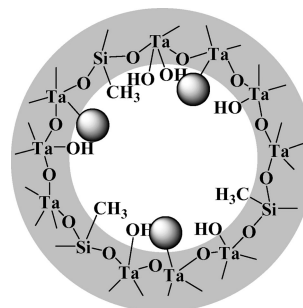


314

Simultaneous esterification and transesterification of soybean oil with methanol catalyzed by mesoporous Ta₂O₅/SiO₂-[H₃PW₁₂O₄₀/R] (R = Me or Ph) hybrid catalysts

Leilei Xu, Yonghui Wang, Xia Yang, Jianglei Hu, Wei Li and Yihang Guo*

Mesoporous Ta₂O₅/SiO₂-[H₃PW₁₂O₄₀/R] hybrid catalysts for the simultaneous esterification and transesterification of soybean oil with methanol.

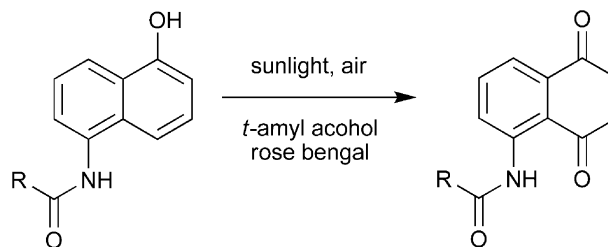


318

Green photochemistry: solarchemical synthesis of 5-amido-1,4-naphthoquinones

Elodie Haggiage, Emma E. Coyle, Kieran Joyce and Michael Oelgemöller*

Dye sensitized photooxygenations of 5-amido-1-naphthols gave the corresponding 5-amido-1,4-naphthoquinones in moderate to excellent yields. The solar process gave higher yields in almost all cases studied and allowed for significant energy savings.

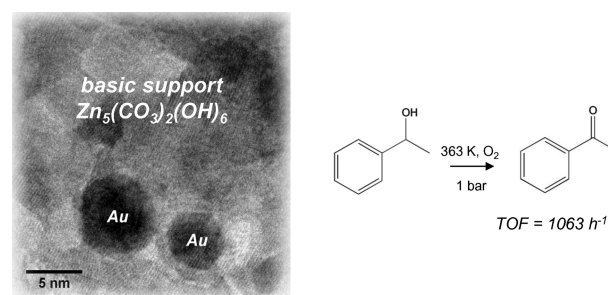


322

Basic metal carbonate supported gold nanoparticles: enhanced performance in aerobic alcohol oxidation

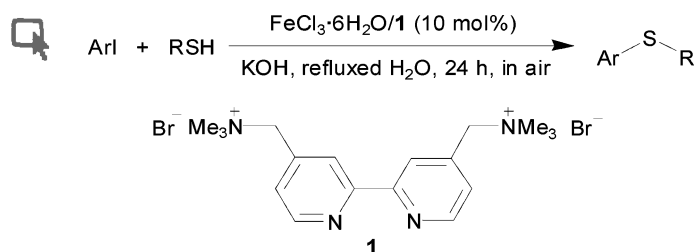
Jie Yang, Yejun Guan, Tiny Verhoeven, Rutger van Santen, Can Li* and Emiel J. M. Hensen*

Gold nanoparticles supported by basic metal carbonates such as hydrozincite and bismuth carbonate are excellent catalysts for liquid-phase aerobic alcohol oxidation in the absence of a soluble base.



COMMUNICATIONS

326

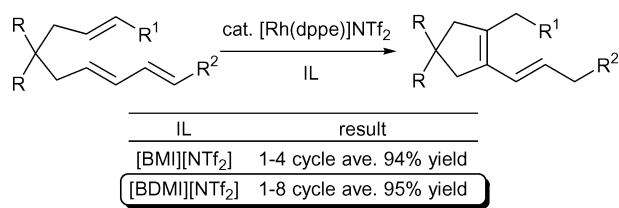


A reusable FeCl₃·6H₂O/cationic 2,2'-bipyridyl catalytic system for the coupling of aryl iodides with thiols in water under aerobic conditions

Wei-Yi Wu, Jui-Chan Wang and Fu-Yu Tsai*

A cationic 2,2'-bipyridyl/FeCl₃·6H₂O system catalyzed coupling of aryl iodides with thiols to give thioethers in water under aerobic conditions. The residual aqueous solution after extraction could be reused for several cycles without a significant decrease in activity.

330



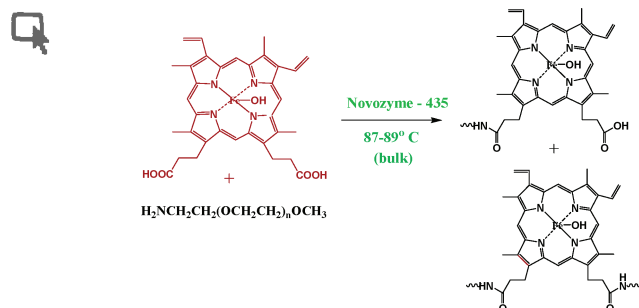
Study on Rh(I)-catalyzed cycloisomerization of dienes with alkenes in ionic liquids: effect of the structure of ILs on catalyst recyclability

Yoshihiro Oonishi, Akira Saito and Yoshihiro Sato*

A Rh(I)-catalyzed cycloisomerization of dienes with alkenes using ILs as reaction media was investigated. It was found that the structure of ILs strongly affected the recyclability of the catalyst in this cycloisomerization, and a [BDMI]⁺-based IL was more effective than a [BMI]⁺-based one.

PAPERS

334

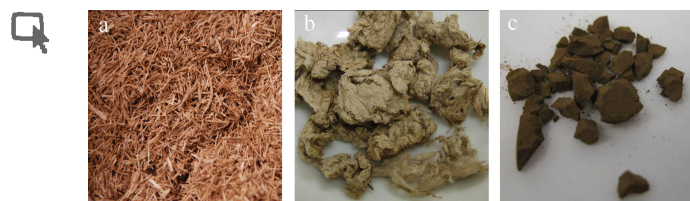


A stable biomimetic redox catalyst obtained by the enzyme catalyzed amidation of iron porphyrin

Subhalakshmi Nagarajan, Ramaswamy Nagarajan, Ferdinando Bruno, Lynne A. Samuelson and Jayant Kumar

The synthesis of hematin tethered with methoxypolyethylene glycol amine chains as a stable and water-soluble biomimetic catalyst is reported. This one step synthesis was performed under solventless conditions and was catalyzed by a lipase, Novozyme-435.

339



Extraction of lignin from lignocellulose at atmospheric pressure using alkylbenzenesulfonate ionic liquid

Suzie S. Y. Tan,* Douglas R. MacFarlane, Jonathan Upfal, Leslie A. Edey, William O. S. Doherty, Antonio F. Patti, Jennifer M. Pringle and Janet L. Scott

An ionic liquid mixture containing the 1-ethyl-3-methylimidazolium cation and a mixture of alkylbenzenesulfonates with xylenesulfonate as the main anion was used to extract lignin from sugarcane plant waste at atmospheric pressure and elevated temperatures (170–190 °C).

346

Purification of hexane with effective extraction using ionic liquid as solvent

Ana B. Pereiro and Ana Rodriguez*

An experiment with a laboratory-scale packed column, under steady-state conditions, was carried out with the purpose of removing hexane from its azeotropic mixture using the proposed ionic liquid 1-butyl-3-methylimidazolium methyl sulfate as the azeotrope-breaker.

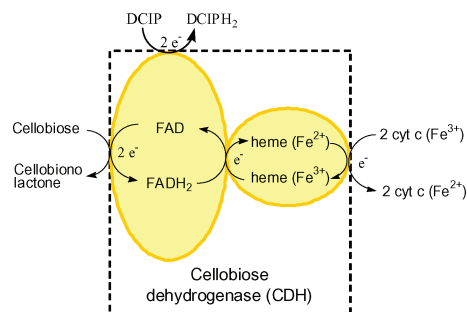


351

Biocatalytic oxidation of cellobiose in an hydrated ionic liquid

Kyoko Fujita, Nobuhumi Nakamura, Kiyohiko Igarashi, Masahiro Samejima and Hiroyuki Ohno*

Cellobiose dehydrogenase was successfully dissolved in hydrated choline dhp and realized both inter- and intra-electron transfer.

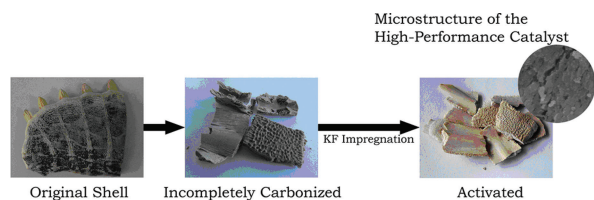


355

Biont shell catalyst for biodiesel production

Jie Xie, Xinsheng Zheng,* Ai Qin Dong, Zhidong Xiao and Jinhua Zhang

A new, ecologically friendly tri-step synthetic strategy was devised to obtain a novel high-performance heterogeneous biodiesel catalyst derived from biont shell. The method is facile, inexpensive, environmentally benign, and amenable to scale-up and processing.

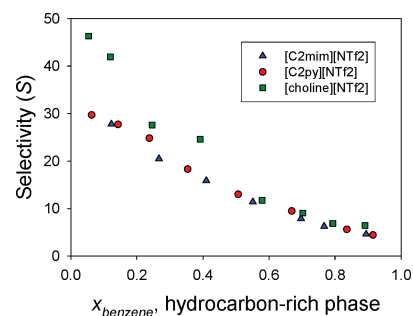


365

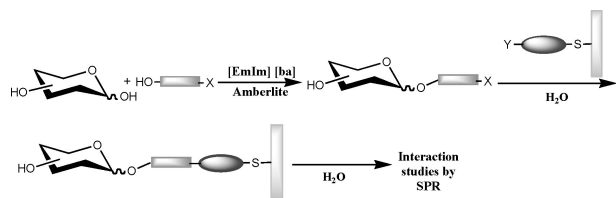
Bis{(trifluoromethyl)sulfonyl}amide ionic liquids as solvents for the extraction of aromatic hydrocarbons from their mixtures with alkanes: effect of the nature of the cation

Alberto Arce, Martyn J. Earle,* Héctor Rodríguez, Kenneth R. Seddon and Ana Soto

The effect of the cation nature in bis{(trifluoromethyl)sulfonyl}amide ionic liquids has been evaluated in terms of their ability to act as solvents for the separation of mixtures of benzene and hexane.



373



Green glycosylation using ionic liquid to prepare alkyl glycosides for studying carbohydrate–protein interactions by SPR

F. Javier Muñoz, Sabine André, Hans-Joachim Gabius, José V. Sinisterra, María J. Hernáiz* and Robert J. Linhardt*

A simple green glycosidation approach using an ionic liquid to prepare alkyl glycosides for studying carbohydrate–protein interactions by surface plasmon resonance (SPR).

380

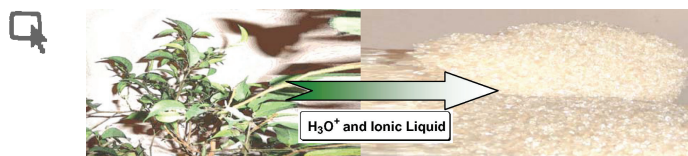


Use of life cycle assessment to characterize the environmental impacts of polyol production options

Richard K. Helling* and David A. Russell

This work and its results represent an exciting and unique combination of environmental analysis, novel technologies, and alternative feedstocks, leading to the development and commercialization of new materials and products.

390

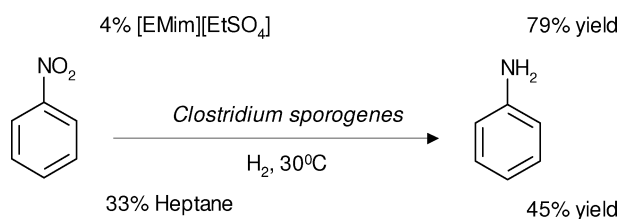


Kinetic model for the hydrolysis of lignocellulosic biomass in the ionic liquid, 1-ethyl-3-methyl-imidazolium chloride

Laurent Vanoye, Markus Faselow, John D. Holbrey, Martin P. Atkins and Kenneth R. Seddon

The acid catalysed conversion of cellobiose to glucose was achieved efficiently in ionic liquids; which was an efficient model for lignocellulosic biomass digestion.

397



Effects of water-miscible ionic liquids on cell growth and nitro reduction using *Clostridium sporogenes*

Olutosin Dipeolu, Edward Green and Gillian Stephens*

[EMim][EtSO₄] suppresses unproductive substrate consumption during biocatalytic nitro reduction.

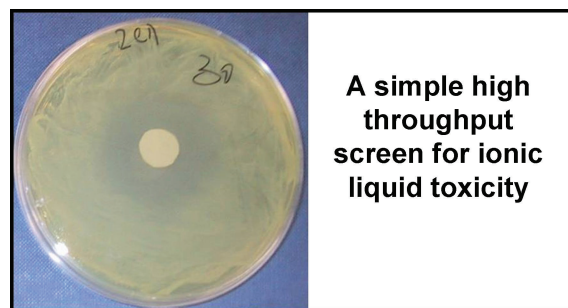
PAPERS

402

A high throughput screen to test the biocompatibility of water-miscible ionic liquids

Martin Rebros, H. Q. Nimal Gunaratne, Jamie Ferguson, Kenneth R. Seddon and Gillian Stephens*

A high throughput screen was used to test the biocompatibility of water-miscible ionic liquids.

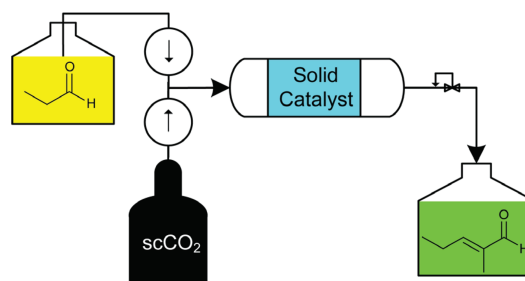


409

The continuous self aldol condensation of propionaldehyde in supercritical carbon dioxide: a highly selective catalytic route to 2-methylpentenal

James G. Stevens, Richard A. Bourne and Martyn Poliakoff*

The aldol reactions of propionaldehyde and butyraldehyde have been explored in supercritical carbon dioxide over a variety of heterogeneous acidic and basic catalysts; they exhibit increased selectivity compared to using neat reactants.

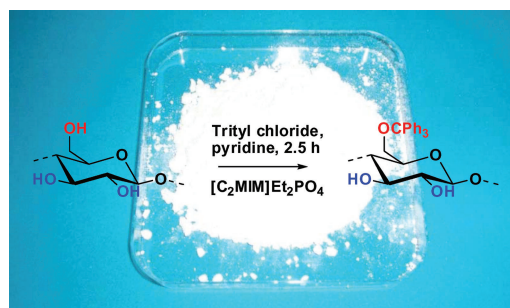


417

Extended dissolution studies of cellulose in imidazolium based ionic liquids

Jürgen Vitz, Tina Erdmenger, Claudia Haensch and Ulrich S. Schubert*

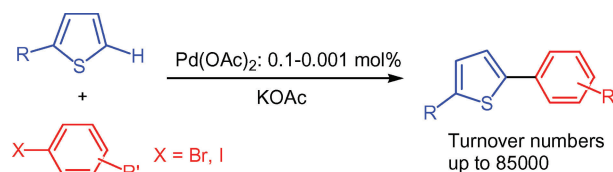
In the present work, different ionic liquids were screened for the dissolution of cellulose.



425

Ligand-less palladium-catalyzed direct 5-arylation of thiophenes at low catalyst loadings

Julien Roger, Franc Požgan and Henri Doucet*


Pd(OAc)₂ provides a very efficient catalyst for the direct 5-arylation of thiophene derivatives. With this catalyst, a low palladium concentration (0.1–0.001 mol%) should be employed in order to obtain high yields of coupling products.

AUTHOR INDEX

- André, Sabine, 373
 Arce, Alberto, 365
 Atkins, Martin P., 390
 Bourne, Richard A., 409
 Bruno, Ferdinando, 334
 Choi, Minkee, 309
 Coyle, Emma E., 318
 Dipeolu, Olutosin, 397
 Doherty, William O. S., 339
 Dong, Aiqin, 355
 Doucet, Henri, 425
 Earle, Martyn J., 365
 Edey, Leslie A., 339
 Erdmenger, Tina, 417
 Fanselow, Markus, 390
 Ferguson, Jamie, 402
 Fujita, Kyoko, 351
 Gabius, Hans-Joachim, 373
 Green, Edward, 397
 Guan, Yejun, 322
 Gunaratne, H. Q. Nimal, 402
 Guo, Yihang, 314
- Haensch, Claudia, 417
 Haggiage, Elodie, 318
 Helling, Richard K., 380
 Hensen, Emiel J. M., 322
 Hernáiz, María J., 373
 Holbrey, John D., 390
 Hu, Jianglei, 314
 Igarashi, Kiyohiko, 351
 Javier Muñoz, F., 373
 Jessop, Philip G., 307
 Jin, Myung-Jong, 309
 Joyce, Kieran, 318
 Kang, Hee-Jae, 309
 Kumar, Jayant, 334
 Li, Can, 322
 Li, Wei, 314
 Linhardt, Robert J., 373
 MacFarlane, Douglas R., 339
 Nagarajan, Ramaswamy, 334
 Nagarajan, Subhalakshmi, 334
 Nakamura, Nobuhumi, 351
 Oelgemöller, Michael, 318
- Ohno, Hiroyuki, 351
 Oonishi, Yoshihiro, 330
 Patti, Antonio F., 339
 Pereiro, Ana B., 346
 Phan, Lam, 307
 Poliakov, Martyn, 409
 Požgan, Franc, 425
 Pringle, Jennifer M., 339
 Rebros, Martin, 402
 Rodriguez, Ana, 346
 Rodríguez, Héctor, 365
 Roger, Julien, 425
 Russell, David A., 380
 Ryoo, Ryong, 309
 Saito, Akira, 330
 Samejima, Masahiro, 351
 Samuelson, Lynne A., 334
 Sato, Yoshihiro, 330
 Schubert, Ulrich S., 417
 Scott, Janet L., 339
 Seddon, Kenneth R., 365, 390, 402
 Sinisterra, José V., 373
- Soto, Ana, 365
 Stephens, Gillian, 397, 402
 Stevens, James G., 409
 Taher, Abu, 309
 Tan, Suzie S. Y., 339
 Tsai, Fu-Yu, 326
 Upfal, Jonathan, 339
 Vanoye, Laurent, 390
 van Santen, Rutger, 322
 Verhoeven, Tiny, 322
 Vitz, Jürgen, 417
 Wang, Jui-Chan, 326
 Wang, Yonghui, 314
 Wu, Wei-Yi, 326
 Xiao, Zhidong, 355
 Xie, Jie, 355
 Xu, Leilei, 314
 Yang, Jie, 322
 Yang, Xia, 314
 Zhang, Jinhua, 355
 Zheng, Xincheng, 355

FREE E-MAIL ALERTS AND RSS FEEDS


Contents lists in advance of publication are available on the web *via* www.rsc.org/greenchem – or take advantage of our free e-mail alerting service (www.rsc.org/ej_alert) to receive notification each time a new list becomes available.

 Try our RSS feeds for up-to-the-minute news of the latest research. By setting up RSS feeds, preferably using feed reader software, you can be alerted to the latest Advance Articles published on the RSC web site. Visit www.rsc.org/publishing/technology/rss.asp for details.

ADVANCE ARTICLES AND ELECTRONIC JOURNAL

Free site-wide access to Advance Articles and the electronic form of this journal is provided with a full-rate institutional subscription. See www.rsc.org/ejs for more information.

* Indicates the author for correspondence: see article for details.

 Electronic supplementary information (ESI) is available *via* the online article (see <http://www.rsc.org/esi> for general information about ESI).

RSC online shop

Simple, secure, *fast!*

24/7 access: The RSC online shop gives you continuous access to class leading products and services, expertly tailored to cater for your training and educational needs.

Browse and buy: Visit our shop to browse over 750 book titles, subscribe or purchase an individual article in one of our journals, join or renew your RSC membership, or register to attend a conference or training event.

Gift ideas: If you're looking for gift ideas, look no further. In our online shop you'll find everything from popular science books like *The Age of the Molecule* and the inspirational *Elegant Solutions* from award winning writer, Philip Ball, to our stunning Visual Elements wall chart and jigsaw.

With secure online payment you can shop online with confidence.

The RSC has so much to offer...*why not go online today?*

19120654b

RSC Publishing

www.rsc.org/shop

Registered Charity Number 207890



Chemical Technology

Holographic discs store more information than DVDs

Polymers branch into data storage

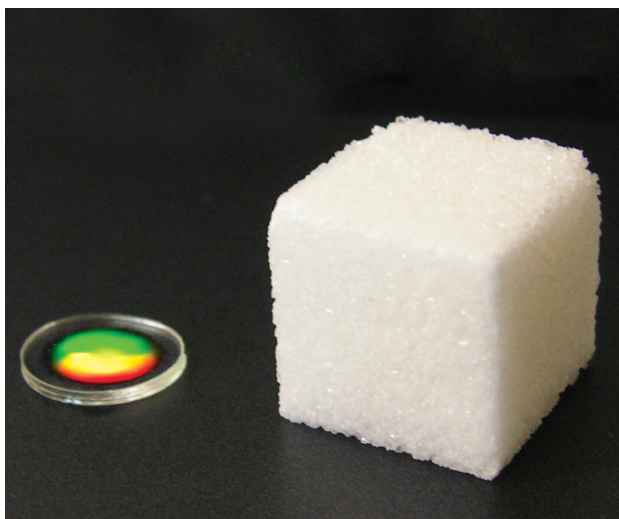
Scientists have harnessed the power of holography to store large amounts of data in a postage stamp-sized disc.

Craig Hawker, at the University of California, Santa Barbara, US, and colleagues designed photopolymers that can store up to 50 times more data than a DVD.

Unlike a DVD, which only uses a disc's surface, holographic data storage uses the whole volume of the disc. As a result, holography promises terabytes (1000 gigabytes) of storage capacity in a recording disc the size of a postage stamp, says Hawker. A typical DVD holds only 4.7 gigabytes.

Recently, researchers have investigated light-sensitive polymers – which are used to make the holograms seen in driving licences – for data storage. But these photopolymers shrink as the molecules polymerise during the recording process, making it difficult to accurately retrieve the recorded data.

Hawker overcame this problem by making a series of



highly branched monomers. He showed that when the molecules polymerised, the volume change was much smaller than for previous photopolymers and so the shrinkage was negligible.

'Of particular note is finding that a holographic medium prepared using one of our monomers exhibits 50 times more storage

Although the disc is smaller than a sugar cube, it can hold 50 times more information than a typical DVD

Reference
A Khan *et al.*, *Chem. Commun.*, 2009, 425 (DOI: 10.1039/b816298k)

capacity than a conventional DVD,' says Hawker. 'To reach the terabyte goal, you need to have very high efficiency and fidelity during the recording process.'

The polymer's refractive index, which is a measure of how much it reduces the speed of light passing through it, is key to increased storage capacity, explains Hawker. He is working on a system that combines a low refractive index scaffold with ultra-high refractive index monomers, which he expects to show improved results.

'This work illustrates the power of modern polymer synthesis to custom-design organic materials with advantageous properties,' says Stefan Hecht, an expert in organic functional materials at Humboldt University, Berlin, Germany. 'By fine tuning the macromolecular architecture, Hawker and co-workers have created new high performance data storage materials, overcoming limitations of conventional polymer chemistry.'
Sarah Corcoran

In this issue

HIV diagnosis improved

Microfluidic module enables sensitive and selective cell counting

Solar power kills bacteria in water

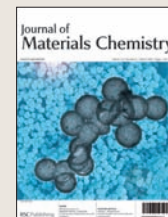
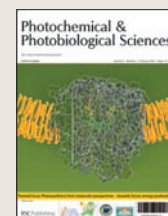
A ray of sunshine in the fight against disease

Interview: From macro to nano

Detlef Günther discusses nanoanalytics, football and the largest crystals in the world

Instant insight: Size matters

Andrew Houlton and colleagues explain how DNA can direct electronic materials to grow on the nanoscale



The latest applications and technological aspects of research across the chemical sciences

Application highlights

Catalyst-bound fluorescent dye monitors ion binding

Lighting up the active site

Belgian scientists have developed a system that could provide information about catalytic cycles at the single molecule level.

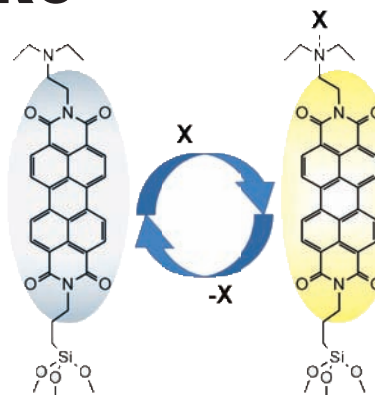
Single molecule fluorescence spectroscopy is an important tool for monitoring discrete events in catalytic reactions that would not normally be detected in bulk measurements. Usually this involves attaching a marker to a reactant that fluoresces upon conversion to the product. However, this route offers an indirect approach to obtaining information about the catalytic cycle. Now a team, led by Johan Hofkens and Dirk De Vos at the Catholic University of Leuven, has attached the fluorescent reporter group to the catalyst itself to provide a more direct method for monitoring the cycle.

The team linked a tertiary amine,

the system's catalytic active site, to a perylene-based dye, which acts as the reporter group. They then anchored the dye to a microscope cover slide so they could test the catalyst under different conditions.

Electron transfer from the free amine to the reporter quenched the reporter's fluorescence. But when the amine bound to a molecule or ion, such as a proton in a base-catalysed reaction, electron transfer was hindered and the reporter fluoresced. 'This opens perspectives on monitoring complexation by the amine group in a more direct way than present state of the art techniques,' says Hofkens.

'In recent years, beautiful tools have been developed to study



The reporter fluoresces when a proton or metal ion (X) binds to the amine

Reference
R Ameloot *et al.*, *Photochem. Photobiol. Sci.* 2009, DOI: 10.1039/b821657f

catalytic reactions at the single molecule level,' says Philip Tinnefeld, who investigates fluorescence imaging techniques at the Ludwig Maximilian University of Munich, Germany. 'Reporters such as this are certainly important for the development of this field.'

Although the system worked well, Hofkens says that unexpected dark states, where the individual molecules' fluorescence was not detected irrespective of their binding state, could also be seen. The group aim to modify the system, for example by changing the link between the reporter and the cover slide, to eliminate this problem so that the system can be applied to the field of catalysis. *Bailey Fallon*

Chemistry and Medicines

An Introductory Text

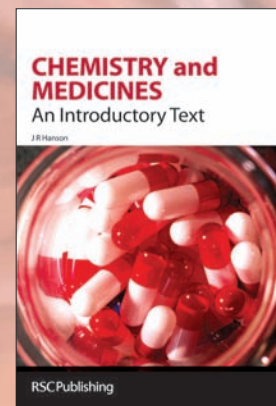
By J R Hanson

This text book covers all areas of medicinal chemistry including:

- bio-organic chemistry
- organic synthetic methods
- physical organic chemistry
- organic reaction mechanisms

It also describes the underlying chemistry for synthesis of key drugs used to combat diseases of central nervous system, infectious diseases and cancers. Ideal for advanced undergraduates and post graduates.

BB Hardback | 166 pages | ISBN 9780854046454 | 2006 | £27.50



RSC Publishing

www.rsc.org/books

Registered Charity Number 207890

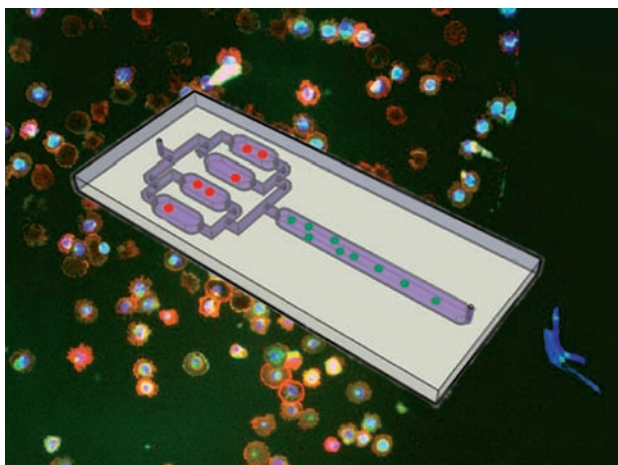
Microfluidic module enables more sensitive and selective cell counting

HIV diagnosis improved

A cheaper and easier way to monitor HIV in patients could revolutionise global health care, according to scientists in the US.

The World Health Organization estimates that more than 33 million people worldwide have HIV. HIV destroys white blood cells called CD4+ T lymphocytes that are crucial for fighting disease. It also reduces the body's ability to replace these cells. Scientists use a technique called flow cytometry to monitor changes in patients' CD4+ levels – when they drop below 200 cells per microlitre, the patient is diagnosed with AIDS and prescribed anti-retroviral drugs. But flow cytometry requires expensive equipment and highly trained scientists to use it.

Mehmet Toner and colleagues at Massachusetts General Hospital, Boston, have modified a microfluidic device they



were working on previously to overcome its major pitfall – sample contamination with another type of white blood cell called monocytes. They developed an upstream monocyte depletion module, which separates monocytes from blood samples before the lymphocytes

The device removes the monocytes from blood then counts the lymphocytes

Reference
X Cheng *et al*, *Lab Chip*, 2009, DOI:10.1039/b818813k

are counted. Using the module, Toner measured the lymphocyte count with higher selectivity and sensitivity than before. Toner says the device has 'the potential to be one of the holy grails of global health'.

'The device assertively contributes to point of care testing from whole blood and may additionally facilitate other on-chip integrated whole blood-based assays,' says Philip Day, an expert in tool miniaturisation for quantitative molecular biology from the University of Manchester, UK.

Toner says his device is simpler and cheaper than flow cytometry, meaning it could be used in the resource-scarce settings of developing countries. The method, combined with the recent fall in HIV drug prices, should lead to significant progress in the fight against HIV, he adds.

Jennifer Newton

A ray of sunshine in the fight against disease

Solar power kills bacteria in water

Scientists have improved solar water decontamination techniques in an attempt to reduce the spread of water borne diseases in developing countries.

Solar water disinfection is a simple way to kill bacteria in water. It is used by households in developing countries where safe drinking water is scarce. People fill plastic bottles with water and leave them in sunlight, where the UV radiation and increased water temperature kill the bacteria within six hours. But the method requires strong sunlight and can only treat limited volumes of water.

Kevin McGuigan, from The Royal College of Surgeons in Ireland, Dublin, and colleagues investigated solar disinfection of *Escherichia coli*-contaminated water in large volume flow reactors. A pump circulated the water between a holding tank and a glass tube surrounded by solar collectors that focus the sun's energy

onto the tube. They found that *E. coli* inactivation depends on the total dose of sunlight rather than the light's intensity. They also showed that the reactors can be ineffective because the bacteria receive an intermittent dose of radiation as they flow between the dark holding tank and the see-through tube. If the bacteria are not completely inactivated by the sunlight, the dark periods give them time to recover from the radiation damage, making them more resistant when reilluminated.

'For me, the major significance of the research is that these methods can be effective, but recalculating flow through solar disinfection reactors must be carefully designed in order to avoid the possibility of resistant sub-populations of pathogens remaining viable due to incomplete sunlight exposure,' says McGuigan.

'This work is an important



Sunlight can disinfect water in plastic bottles but the treatable volumes are limited

Reference
E Ubomba-Jaswa *et al*, *Photochem. Photobiol. Sci.*, 2009, DOI 10.1039/b816593A

contribution that points out potential advantages and limitations of solar disinfection, depending on the type of solar photoreactor and operation mode,' comments Cesar Pulgarin, an expert in biological decontamination processes at the Swiss Federal Institute of Technology in Lausanne, Switzerland. 'It is also the first attempt that assesses the minimal UV dose required for complete bacterial inactivation by solar disinfection.'

The World Health Organization estimates that more than one billion people lack access to safe drinking water, resulting in millions of deaths each year from water-related diseases such as diarrhoea. McGuigan says he plans to introduce the flow reactor technology into developing countries, where he hopes it could provide emergency relief to communities affected by famine, flood and war.

Phillippa Ross

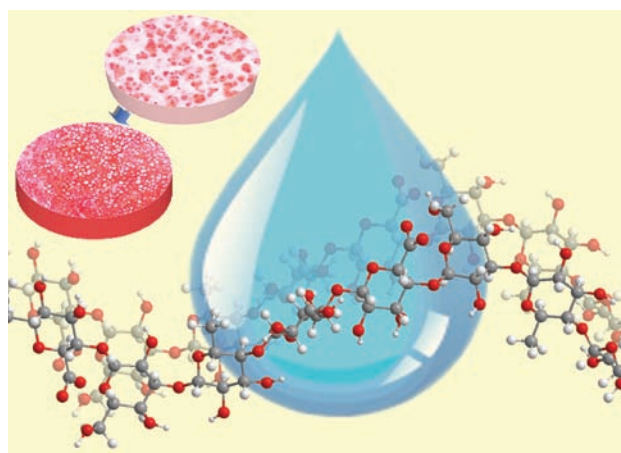
Cell-laden gel encourages growth of new cartilage

Food additive promotes tissue regeneration

Scientists in Singapore have developed an injectable hydrogel that can be used to regenerate cartilage in injured patients.

Dong-an Wang and colleagues at Nanyang Technological University modified gellan gum, a widely used polysaccharide food additive, to transform it into a cell-carrying hydrogel. Cell-containing hydrogel solutions can be injected into target sites in the body, where they are cooled to form cell-laden gels that encourage tissue regeneration. But gellan forms a hydrogel at temperatures higher than body temperature and so until now has been unsuitable for tissue engineering because it can't be injected as a solution.

Wang chemically cut gellan molecules to reduce their size. He found that the shorter molecules formed a hydrogel when below body temperature. Wang loaded the gel



with cells and monitored its ability to promote tissue regeneration in vitro. The gellan-based gels were faster at promoting cartilage growth than agarose gels, which are widely used in tissue regeneration.

So far, Wang has only tested the

Chemically cutting the gellan molecules lowers their gelation temperature

Reference

Y Gong *et al*, *J. Mater. Chem.*, 2009, DOI: 10.1039/b818090c

gels in vitro but he predicts that the technology will transfer to patients. 'We believe our scaffolding system promises to bridge the gap between bench and bedside,' he says. 'One could envisage a cell-carrying gellan solution being injected into any randomly shaped veins, forming gels in situ that encapsulate therapeutic cells working on tissue regeneration.' Wang says he also plans to investigate the degradation properties of modified gellan.

'Many approaches to regenerate cartilage tissue in the clinic have failed in the past,' says Matthias Lutolf, who investigates the interface between biomolecular engineering and adult stem cell biology at the Swiss Federal Institute of Technology, Lausanne. 'It will be interesting to see how this technology performs in a more relevant in vivo scenario, for example in a rabbit model.'

Vikki Chapman

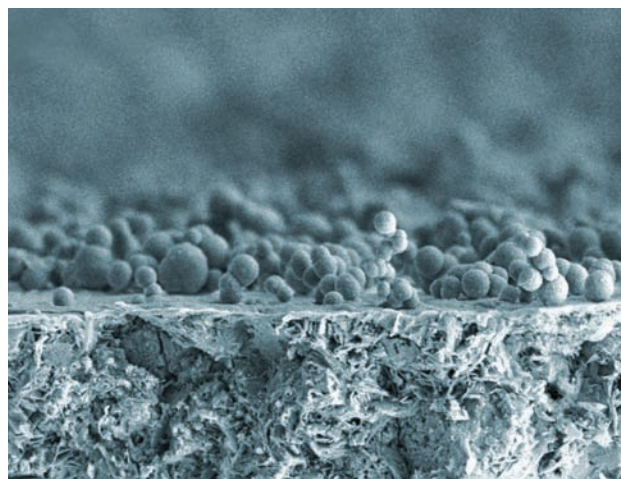
Bioactive cement enhances the growth of bone-building cells

Silicate performs strongly at bone repair

Biomaterials scientists in Taiwan have developed a quick-setting cement that could help broken bones to regenerate.

Calcium phosphates were developed over 20 years ago as alternatives to polymer-based cements for mending damaged bones. Their chemical similarity to bone means that they are good repair materials. They are also less toxic and more fracture-resistant than polymer cements. However, the absence of silicon – thought to be an important trace element in the early stages of bone formation – means that calcium phosphate cements are not perfect when it comes to integrating with living tissue.

By using silicate rather than phosphate, a team led by Shinn-Jyh Ding at Chung-Shan Medical University, Taichung, has developed a quick-setting cement with promising biological properties. Earlier calcium silicate formulations had setting times of over an hour,



which is too long for clinical applications, says Ding. The new cement sets in just five minutes. It should be a good candidate for bone replacements, he adds, because a biocompatible layer of bone-like apatite nodules forms on the surface when immersed in a physiological

A layer of bone-like nodules forms on the cement's surface

Reference

S-J Ding *et al*, *J. Mater. Chem.*, 2009, 19, 1183 (DOI: 10.1039/b819033j)

solution. Ding says that tests in vitro suggest that the cement should encourage the growth of osteoblasts – the cells that are responsible for generating bone tissue – opening up the possibility of its use as an implant material.

Future research by the group, says Ding, will focus on improving the injectability and durability of their cement, which he suggests might be achieved by adding natural materials such as gelatin and chitosan.

Jake Barralet, a specialist in bioceramics at McGill University, Montreal, Canada, says that materials that stimulate tissue repair are the 'next big thing' in regenerative medicine. 'It is not yet clear precisely what material parameters cause cell differentiation and tissue regeneration in bone, but this work broadens our knowledge in this growing field and I look forward to reading further studies by this group,' he says.

David Barden

Interview

From macro to nano

Detlef Günther talks to May Copsey about nanoanalytics, football and measuring the largest crystals in the world



Detlef Günther

Detlef Günther is professor for trace element and micro analysis at the Swiss Federal Institute of Technology Zurich and chair of the *Journal of Analytical Atomic Spectrometry* Editorial Board. His research focuses on fundamental and applied aspects of plasma-based mass spectrometry techniques, ion generation and ion extraction procedures and laser ablation-inductively coupled plasma-mass spectrometry for elemental and isotope analysis.

What inspired you to become a chemist?

I grew up in a little village with a very small school. Our chemistry teacher was also the coach of our football team – so being good at chemistry helped me to get picked for the team. Later on, in high school, I had an excellent teacher who showed us experiments not normally allowed at school. We really had the smell and the taste of chemistry very early on in the classroom.

Did you always want to work in analytical chemistry?

To begin with I was much more interested in organic chemistry. Chemistry was a popular subject because my university (Martin Luther University Halle-Wittenberg) was very close to some of the major chemical companies in East Germany. We had two branches, synthetic chemistry and technical chemistry. However, all the places had been filled for synthetic chemistry and I couldn't switch. I went on to pass the major exams in analytical chemistry and it was then I realised that if I couldn't synthesise something new, I might be able to analyse something. So that was the start.

What led you to choose a PhD in analytical chemistry?

Where I did my PhD was very special because we had one of the first inductively coupled plasma-optical emission systems (ICP-OES) in East Germany. That was fantastic because most of our colleagues at other universities had no access to this technology. My PhD supervisor, Professor Moenke, was well-known in the field of laser ablation (LA) and she worked very hard to obtain such an instrument for LA-ICP-OES.

With the experience of working in other areas of science, do you think chemists have much to learn from other disciplines?

The field of atomic spectrometry involves quite a lot of fundamental work but the highest recognition it receives is always related to application. Transferring fundamental understanding from the analytical side to clever applications can bring a breakthrough and further recognition. The future of our field is somewhere at this interface.

Can you tell us about your current research and collaborations?

The most interesting ongoing research involves the fundamental development of ICP-mass spectrometry. The project aims to increase the sensitivity of this technique by producing a larger number of ions that can be measured. We hope that this can be done by using a new interface configuration. This research might take us closer to nanoanalytics, which is necessary, particularly for solid analysis using laser ablation.

In my field, we have the opportunity to touch many different areas of science. For example, we are just about to go to Mexico with a colleague from Bologna to look at the Naica crystals. These are the largest gypsum crystals ever found and there is still a lot of work to do in figuring out how and why they are formed.

We also have some collaboration with industry. The quality control of raw products is becoming more important, as everything that had been at the microgram per gram level a couple of years ago is now reduced to the nanogram per gram level and is harder to detect. So we have the challenge of providing the method to do this.

What's the secret of having a successful research group?

Getting the right people together and always looking for the people who have more knowledge in areas that we are not familiar with. In 2008, my group celebrated our 10th anniversary and it was really nice to reflect on what we had done over the last 10 years. Publications will not make us famous in the future; I simply think our contribution is to generate well-trained PhD students so that they will pass on our intentions and our enthusiasm for research.

What message do you have for someone starting out on a research career?

My advice is to search for projects that you are really interested in because fascination and dedication produces the extra energy necessary to carry out a project. That is the best advice because if you are fascinated then you can do almost everything.

What do you like doing when you are not in the lab?

If I'm not talking about lasers, then I talk about football. I am a devoted supporter of Bayern Munich and of course, the German national team. Since living in Switzerland I have adapted to almost everything, but when it comes to football, I'm German.

ISOLUTE® SLE+

Supported Liquid Extraction plates are now available in 200 mg and new 400 mg size.



**Effective
Sample
Preparation
without ACN**

Replace traditional liquid-liquid extraction techniques with faster more efficient SLE+ Plates

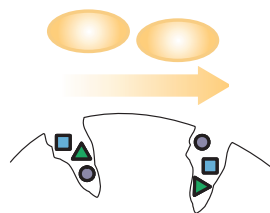
- Easily transfer a current LLE method to SLE
- Improved productivity
- Improved drug recovery
- Reduced ion suppression

EVOLUTE®

An affordable next generation polymer-based SPE sorbent for cleaner samples.

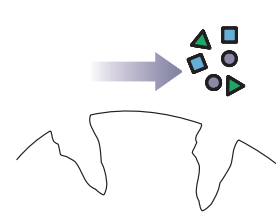
- **EVOLUTE ABN** extracts Acids, Bases and Neutrals
- **EVOLUTE CX** extracts Basic compounds and completely removes phospholipids from biological matrices

Sample Application



Drugs are retained while proteins pass straight to waste

Analyte Elution



Drugs are eluted

Go to www.biotage.com for more information, application notes, and to request a **FREE** sample.

Instant insight

Size matters

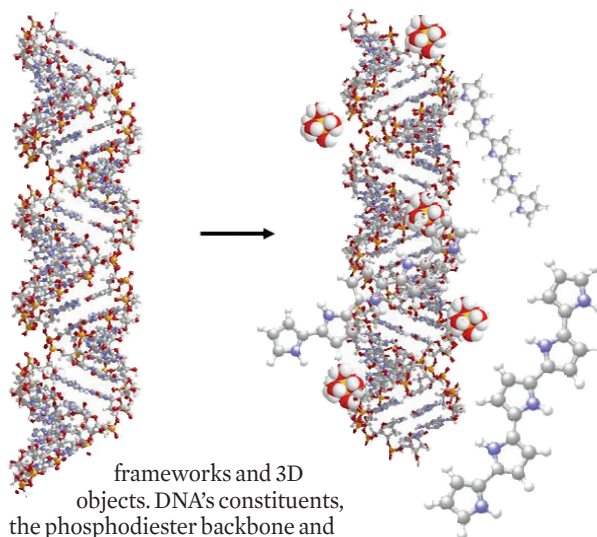
Andrew Houlton, Benjamin Horrocks, Andrew Pike and Miguel Galindo of the Chemical Nanoscience Laboratories at Newcastle University, UK, explain how DNA can direct electronic materials to grow on the nanoscale

Industrial, research and consumer sectors are relying more and more on semiconductor materials. In both existing and newly emerging markets, these materials are required on an ever smaller scale – the nanoscale. The International Technology Roadmap for Semiconductors predicts that silicon-based electronics smaller than 30 nanometres will be in use by the end of the decade. A wide range of other semiconductors, providing us with everything from protection from the sun (titanium dioxide) to new insights into cellular processes (cadmium selenide in bio-markers), also rely on nanoscale materials.

Semiconductors become particularly interesting at such small sizes because their electronic structure changes dramatically. On the nanoscale, semiconductors become more molecule-like and their energy levels change from continuous to discrete. This phenomenon, known as quantum confinement, gives rise to unusual optical and electronic properties, such as luminescence at visible wavelengths in silicon. However, preparing nanoscale materials and assembling them into functional systems is challenging, both technically and economically.

Materials scientists are exploring a new approach to overcome this challenge that draws inspiration from biology, where complex hierarchical systems are assembled from simpler building blocks. One of the most promising strategies for synthesising and organising nanomaterials makes use of nature's own storage medium for the genetic code, DNA.

For a biomolecule, DNA is remarkably robust. It can be readily prepared at precise lengths using biological or chemical synthesis. The four letter genetic code, ATGC, allows scientists to build well-defined structures, including extended 2D



frameworks and 3D objects. DNA's constituents, the phosphodiester backbone and nucleobases, ensure that a wide range of precursors, such as metal ions and monomer units, can interact with the biopolymer. This, along with DNA's long thin shape, means that single DNA molecules can act as excellent templates for growing technologically useful materials at the smallest of sizes.

Scientists have made inorganic compounds, such as cadmium sulfide, lead sulfide and copper sulfide, as nanoscale solids using DNA strands as templates. This is done in a two-step process, where DNA is first doped with metal ions and then incubated with sulfide anions. The size and shape of the resulting material can be controlled by adapting the reaction conditions. For example, it is possible to prepare continuous strands of cadmium sulfide – so-called nanowires – as well as chains of nanoparticles. The nanoparticles show clear evidence of quantum confinement and their assembly into chains represents the first step towards quantum logic arrays, an exciting new architecture for low-power electronics. The continuous nanowires, formed in solution-phase reactions, are electrically conducting and have been used as ultra-small components in

DNA acts as a template for growing and organising nanomaterials

simple electrical circuits.

Researchers have also demonstrated DNA-templating of conducting polymers. These materials are important because, being molecular-based, their properties can be easily tuned. They can also be readily functionalised using synthetic chemistry, which enables scientists to attach probe molecules and develop nanowire-based sensors. This is an exciting area for future application that takes advantage of the sensitivity of nanowires' electrical conductivity to external changes.

DNA-templating also provides traditional conducting polymer materials, such as polypyrrole, in a more processable form. Ordinarily, this material is prepared as highly insoluble films, but when synthesised as nanowires, the resulting material can be manipulated by aligning or stretching. This type of DNA-polymer hybrid also self-organises into ordered rope-like strands and extended networks, features which may be useful in device fabrication and plastic electronics.

In other recent developments, as an alternative to using DNA as a template, researchers have used synthetic chemistry to modify the basic structure of DNA by incorporating new functional groups. This approach raises the fascinating scenario of biological processing of electronic materials and the possibility of 'growing' nanoscale structures and circuits using the intrinsic properties of biomolecules themselves.

In more ways than one, it looks like DNA will be central to nanoscience's evolution to nanotechnology and will bring about the low-cost, functional, nanoscale systems of the future.

Reference
A Houlton *et al.*, *Chem. Commun.*, 2009, DOI:10.1039/b818456a

Read more in 'DNA-based routes to semiconducting nanomaterials' in issue 12 of *ChemComm*

Essential elements

2009 spring conferences

With the 2009 spring conference season about to begin, RSC Publishing staff will be spread around the globe at a number of major conferences over the forthcoming weeks.

Meet RSC staff at Pittcon in Chicago, US, from 8–12 March. This comprehensive annual meeting on laboratory science this year celebrates 60 years of service to the scientific community. Visit the RSC at booth #3410 and meet Niamh O'Connor, the editor of *Analyst* and JAAS, the market leader in spectrometric techniques. Pick up free copies of RSC journals and enter our competition to win an iPod touch when you sign up to journal e-alerts. Keep up-to-date with forthcoming RSC Pittcon announcements at www.rsc.org/publishing

The RSC will also be at the American Physical Society (APS) meeting in Pittsburgh, PA,

DEPARTURES			
TIME	DESTINATION	FLIGHT	GATE
09 20	CHICAGO	AA343	A12
09 30	PITTSBURG	UA882	A34
11 40	SALT LAKE CITY	RF453	B45

US, from 16–20 March, where around 7000 scientists gather to share research on a wide range of physics and physics-related topics. Visit us at booth #117.

Salt Lake City, US, hosts the 237th ACS National Meeting & Exposition, from 22–26 March. Enjoy the rich programme of scientific papers on a variety of multidisciplinary topics, including thematic programming around nanoscience. Meet Geoff Ozin (a speaker in the Naturally Nano session on Tuesday 24 March) who will be at RSC booth #1525 signing copies of his best

selling book, *Nanochemistry*. The 2nd edition highlights the latest breakthroughs using more than eighty new case histories, problem sets and teaching principles.

If you're travelling to these or other conferences, look out for RSC Publishing staff – they will be happy to meet you. Visit our stand and pick up sample copies of journals, look out for special offers on the RSC book collection and keep up-to-date with the latest developments and exciting new announcements from RSC Publishing.

Faraday Discussions grow in popularity

Faraday Discussions, the long-established series of meetings providing unique international views on newly acquired physical chemistry, chemical physics and biophysical chemistry results, has increased its frequency this year from three to four meetings. These meetings take a special format, in which papers are distributed to all participants in advance of the conference and almost all of the meeting is devoted to discussion of the papers.

Previous *Faraday Discussions* volumes are available to buy online at www.rsc.org/books.

Faraday Discussions' latest impact factor is 5.0, emphasising its highly cited and well respected accounts by world-class experts in physical chemistry. Philip Earis, editor for *Faraday Discussions* comments: 'The unique format of *Faraday Discussions*, and the world-class speakers that discussions attract, lead to outstanding and stimulating

debate in topical areas of physical chemistry.'

2009 sees the discussion of Cold and ultracold molecules; Soft nanotechnology; Multi-scale modelling of polymers, colloids, mesophases and membranes; and Frontiers in physical organic chemistry. Registration is now open for the first meeting in April which will be held at Durham University, UK. Visit www.rsc.org/faraday for further information on past and future *Faraday Discussions*.

Chemical Technology (ISSN: 1744-1560) is published monthly by the Royal Society of Chemistry, Thomas Graham House, Science Park, Milton Road, Cambridge UK CB4 0WF. It is distributed free with *Chemical Communications*, *Journal of Materials Chemistry*, *The Analyst*, *Lab on a Chip*, *Journal of Atomic Absorption Spectrometry*, *Green Chemistry*, *CrystEngComm*, *Physical Chemistry Chemical Physics*, *Energy & Environmental Science* and *Analytical Abstracts*. *Chemical Technology* can also be purchased separately. 2009 annual subscription rate: £199; US \$396. All orders accompanied by payment should be sent to Sales and Customer Services, RSC (address above). Tel +44 (0) 1223 432360, Fax +44 (0) 1223 426017 Email: sales@rsc.org

Editor: Joanne Thomson

Deputy editor: Sarah Dixon

Associate editors: Celia Gitterman, Elinor Richards

Interviews editor: Ruth Doherty

Web editors: Nicola Convine, Michael Townsend, Debora Giovaneli

Essential elements: Christine Hartshorne, Rebecca Jeeves

Publishing assistant: Jackie Cockrill

Publisher: Graham McCann

Apart from fair dealing for the purposes of research or private study for non-commercial purposes, or criticism or review, as permitted under the Copyright, Designs and Patents Act 1988 and the copyright and Related Rights Regulations 2003, this publication may only be reproduced, stored or transmitted, in any form or by any means, with the prior permission of the Publisher or in the case of reprographic reproduction in accordance with the terms of licences issued by the Copyright Licensing Agency in the UK. US copyright law is applicable to users in the USA.

And finally...

As part of this year's food theme, the RSC's book programme will showcase titles focused on, or related, to the food sciences. The RSC already has an extensive food science list catering for scientists at all levels from schools and universities through to industry. *The Science of Chocolate*, *Chemistry and Biology of Winemaking* and *Food: The Chemistry of its Components* (5th edition) are already established as best selling titles, used by the scientific community and professionals globally.

2nd Edition

The Science of Chocolate

Stephen T Beckett



2009 begins with the publication of the *Microbiology Handbook (Diary)*, shortly followed by other exciting new food titles including *Nanotechnologies in Food* (from the RSC's landmark *Nanoscience and Nanotechnology* series) and *Handbook of Culture Media for Food and Water Microbiology*. These titles will be complemented further by other exciting projects to be published throughout the year.

For more information please visit www.rsc.org/books

The Royal Society of Chemistry takes reasonable care in the preparation of this publication but does not accept liability for the consequences of any errors or omissions. The RSC is not responsible for individual opinions expressed in *Chemical Technology*. Content does not necessarily express the views or recommendations of the RSC.

Royal Society of Chemistry: Registered Charity No. 207890.

RSC Publishing

Switching the hydrophilicity of a solute†

Lam Phan and Philip G. Jessop*

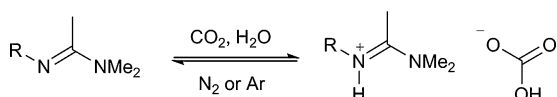
Received 28th November 2008, Accepted 5th January 2009

First published as an Advance Article on the web 15th January 2009

DOI: 10.1039/b821239b

An amidine appendage gives a solute switchable hydrophilicity. Upon the introduction of CO₂ gas, a hydrophobic solute can turn into a hydrophilic solute, with the corresponding partition coefficient changed by over 2 orders of magnitude.

Building switchability into basic chemicals facilitates cleaner reactions and less energy-intensive separations. In collaboration with others, we have already shown that incorporation of an amidine functional group into a solvent^{1,2} or a surfactant³ allows the chemical to have switchable properties in the presence or absence of CO₂ (Scheme 1). For example, a long chain amidine can be switched between a surfactant form and a demulsifier form just by the introduction or removal of CO₂ gas at 1 atm. The same kind of switchability could be very desirable in some solutes, giving one control over the solubility properties of the solute, including controlling absolute solubility and relative solubility (partitioning). A solute in a biphasic water/organic solvent mixture could be made to switch between partitioning preferentially into the organic phase (Fig. 1, left side) to partitioning preferentially into the aqueous phase (Fig. 1, right side).



Scheme 1 An amidine-based switchable surfactant (R = C₈H₁₇, C₁₂H₂₅, C₁₆H₃₃), where the left form is a demulsifier and the right form is a surfactant.

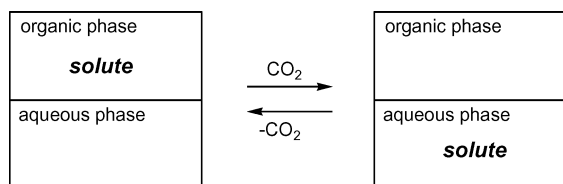


Fig. 1 Switching a solute's partitioning behaviour.

Solutes having controllable partitioning between organic and aqueous phases would be highly desirable as a method for facilitating post-reaction separations, which is an important goal of green chemistry, especially when the separating agents are as

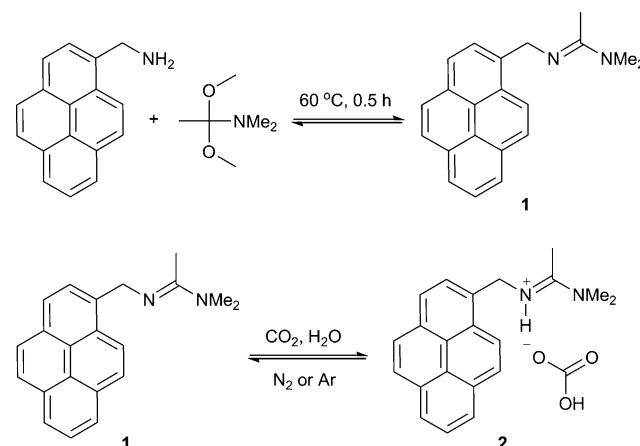
Department of Chemistry, Queen's University, 90 Bader Lane, Kingston, Ontario, Canada K7L 3N6. E-mail: jessop@chem.queensu.ca;

Fax: 1 (613) 533-6669; Tel: 1 (613) 533-3212

† Electronic supplementary information (ESI) available: UV/visible spectra of **1** and **2** in water, toluene and a biphasic mixture thereof. Fluorescence excitation and emission spectra of **1** and **2** in water, 1-octanol and a biphasic mixture thereof. See DOI: 10.1039/b821239b

benign as CO₂ and water. For example, attachment of an amidine group as a molecular tag on a reagent could make it particularly easy to remove excess reagent (or tag-containing byproducts) from the product mixture; a simple wash with carbonated water would suffice. Similarly, amidine-tagged chelating agents could be used to trap heavy metal impurities from oils and then could be removed from the oil by washing with carbonated water. Separation of homogeneous catalysts from products could also be performed in this manner. Andreetta *et al.*⁴ demonstrated such a phase-switching solute in their work with catalyst recovery, where they chose Co and Rh complexes with ligands such as P(CH₂CH₂CH₂NEt₂)₃ or P(CH₂CH₂CH₂NMe₂)₃ that can help “move” the catalyst from an organic media by CO₂ treatment, and recover the catalyst by displacement of the CO₂ afterwards. Cole-Hamilton and colleagues have used an amidine group attached to PPh₃ for a similarly switchable catalyst.⁵ We quantitatively demonstrate, in this paper, that an amidine appendage causes a solute to change its partition coefficient dramatically.

We have now found that the 1-octanol:water and toluene:water partition coefficients of a solute containing an amidine appendage could be controlled by the introduction and removal of 1 atm of CO₂. Herein, we describe such a solute, compound **1**, synthesized from 1-pyrenemethylamine by Scoggin's⁶ method for amidine synthesis (Scheme 2). 1-Pyrenemethylamine (0.57 mmol) was added to a flask containing acetonitrile (5 mL) and *N,N*-dimethylacetamide dimethylacetal (2.3 mmol). The solution was stirred at 65 °C for 30 min. After the solution was cooled, methanol byproduct was removed by rotoevaporation. The remaining liquid was cooled and a pale yellow precipitate was collected and washed with cold acetonitrile.‡



Scheme 2 Synthesis of *N,N*-dimethyl-*N'*-(pyren-1-ylmethyl)acetimidamide (**1**) and its reaction with CO₂ and water to create *N,N*-dimethyl-*N'*-(pyren-1-ylmethyl)acetimidinium bicarbonate salt **2**.

An aqueous solution of the bicarbonate salt was prepared (*in situ*) by dissolving 1.1 mg of **1** in 5.0 ml of distilled water and slowly bubbling CO₂ into the mixture for 1 h (hereafter referred to as stock solution A); this gave an *in situ* formation of *N,N*-dimethyl-*N'*-(pyren-1-ylmethyl)acetamidinium bicarbonate salt **2** (Scheme 2).§

The phase-switching behaviour of **1** and **2** (hereafter collectively referred to as the dye) was tested qualitatively by dissolving 1.0 mg of **1** in 5.0 ml toluene (hereafter referred to as stock solution B). Two vials containing 4 ml each of toluene and water were prepared; to one of these, 0.05 ml from stock solution A was added and the mix flushed with CO₂. To the other, the same amount of solution B was added. When the vials were illuminated with a short-wave, 320–400 nm, UV lamp (Fig. 2), visible fluorescence showed that the dye preferentially partitions into the toluene phase when in the **1** form, and partitions into the water phase when in the **2** form. The switching of phase partitioning can be achieved by either bubbling CO₂ or purging with N₂ and heating for 1 hour.

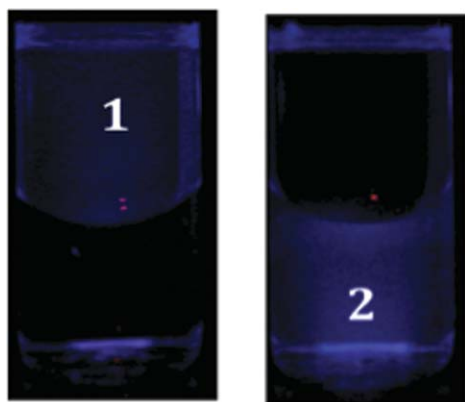


Fig. 2 Phase switching behaviour of the dye in a toluene:water mixture (4 ml each), illuminated with a short-wave, 320–400 nm, UV lamp. Left: compound **1**. Right: compound **2**.

Similar qualitative tests were performed with 1.2 mg of **1** dissolved in 5.0 ml of 1-octanol (stock solution C). This time, an aliquot was added to a 1:1 mixture of 1-octanol and water. Again, the same partitioning behaviour was exhibited by the dye, with the **1** form partitioning into the organic phase, and **2** form partitioning into the aqueous phase (Fig. 3).

The toluene/water partition coefficient $K_{\text{tol/w}}$ was measured for the pyrene amidine in the presence and absence of CO₂, to quantify the change in partitioning behaviour. The concentrations of pyrene dye were determined in each phase by UV/visible spectrometry (see ESI†). The log $K_{\text{tol/w}}$ values were obtained by taking the average of triplicate trials. In a toluene:water mixture, the partition coefficient $K_{\text{tol/w}}$ clearly changes over two orders of magnitude (Table 1). Note that the log $K_{\text{tol/w}}$ changes from a positive value (meaning preferential partitioning into the toluene) to a negative value (partitioning into the water), demonstrating that the desired shuttling of the solute from one phase to another is quite possible.

The 1-octanol/water partition coefficient P ($\equiv K_{\text{oct/w}}$) was also measured. In this case, spectrofluorometry was employed because UV/visible spectrometry was insufficiently sensitive to detect the low concentrations in the aqueous phase. Excitation

Table 1 Partition coefficients of the pyrene amidine dye in equal volume mixtures of 1-octanol:water and toluene:water

	In the absence of CO ₂	In the presence of CO ₂
log $K_{\text{tol/w}}$	1.2 ± 0.3	-1.1 ± 0.2
log P (excitation)	2.9 ± 0.2	0.3 ± 0.2
log P (emission)	3.1 ± 0.4	0.3 ± 0.2

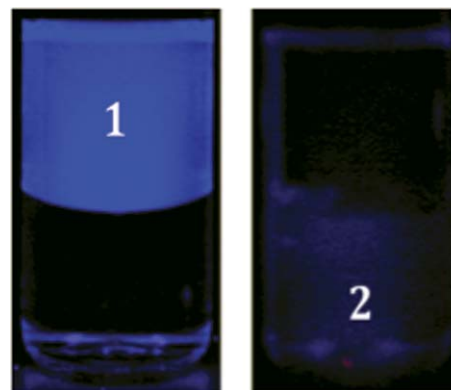


Fig. 3 Phase switching behaviour of the dye in a 1-octanol:water mixture (4 ml each), illuminated with a short-wave, 320–400 nm, UV lamp. Left: compound **1**. Right: compound **2**.

and emission data resulted in essentially the same partition coefficients. The P value is significantly larger than the $K_{\text{tol/w}}$ value because 1-octanol is a better solvent for the pyrene amidine. P drops almost 3 orders of magnitude when CO₂ is bubbled through the mixture, but because log P never drops below 0, a substantial fraction of the dye molecules remain in the octanol phase.

In conclusion, we have successfully synthesized a solute having switchable partitioning behaviour, partitioning far more strongly into organic solvents when under air and much less strongly when in the presence of CO₂. No elevated pressures are required for this effect.

Notes and references

† ¹H NMR (acetone-d₆): δ 7.9–8.4 (m, 9H, aromatic), 5.16 (s, 2H, CH₂N=C), 2.99 (s, 6H, N(CH₃)₂), 2.12 (s, 3H, N=C-CH₃). ¹³C{¹H} NMR (acetone-d₆): δ 159.0 (N=C), 51.3 (CH₂N=C), 37.3 (N(CH₃)₂), 12.0 (N=C-CH₃). IR (KBr): 1619 (s) cm⁻¹. MS (EI+): obs. 300.1617, calc. for C₂₁H₂₀N₂, 300.1626. The observed ¹³C NMR data very closely match those reported for PhCH₂N=C(Me)NMe₂, as reported by J. Jaroszevska-Manaj *et al.*⁷

§ ¹H NMR (acetone-d₆): δ 7.9–8.4 (m, 9H, aromatic), 5.32 (s, 2H, CH₂N=C), 3.18 (s, 6H, N(CH₃)₂), 2.21 (s, 3H, N=C-CH₃). ¹³C{¹H} NMR (acetone-d₆): δ 162.7 (N=C), 51.7 (CH₂N=C), 38.7 (N(CH₃)₂), 12.9 (N=C-CH₃). IR (KBr): 841 (s), 1334 (s), 1614 (s) cm⁻¹.

- P. G. Jessop, D. J. Heldebrant, L. Xiaowang, C. A. Eckert and C. L. Liotta, *Nature*, 2005, **436**, 1102.
- L. Phan, X. Li, D. J. Heldebrant, R. Wang, D. Chiu, E. John, H. Huttenhower, P. Pollet, C. A. Eckert, C. L. Liotta and P. G. Jessop, *Ind. Eng. Chem. Res.*, 2008, **47**, 539–545.
- Y. Liu, P. G. Jessop, M. Cunningham, C. A. Eckert and C. L. Liotta, *Science*, 2006, **313**, 958–960.
- A. Andreatta, G. Barberis and G. Gregorio, *Chim. Ind.*, 1978, **60**, 887–891.
- D. J. Cole-Hamilton, *Private Communication*, 2008.
- M. W. Scoggins, *J. Chromatogr. Sci.*, 1975, **13**, 146–148.
- J. Jaroszevska-Manaj, J. Oszczapowicz and W. Makulski, *J. Chem. Soc., Perkin Trans. 2*, 2001, 1186–1191.

Palladium acetate immobilized in a hierarchical MFI zeolite-supported ionic liquid: a highly active and recyclable catalyst for Suzuki reaction in water

Myung-Jong Jin,^{*a} Abu Taher,^a Hee-Jae Kang,^a Minkee Choi^b and Ryong Ryoo^{*b}

Received 10th October 2008, Accepted 6th January 2009

First published as an Advance Article on the web 15th January 2009

DOI: 10.1039/b817855k

Palladium acetate was immobilized in thin ionic liquid layers on the mesopore wall of hierarchical MFI zeolite, and tested as a catalyst for Suzuki coupling reaction in water. The catalyst exhibited very high activity in the coupling of various aryl bromides with arylboronic acids. Moreover, the catalyst could be recycled without a significant loss of catalytic activity.

Introduction

Suzuki coupling of aryl halides with arylboronic acids has served as a powerful reaction for the construction of biaryl units in organic synthesis.¹ Various kinds of homogeneous palladium catalysts are used for the Suzuki reaction.² One practical limit to performing homogeneously catalyzed reactions is the difficulty of separating the product from the catalyst or removing the product continuously. This limit is of environmental and economic concern in large scale-synthesis. Homogeneous catalysts are often immobilized in a porous inorganic or organic support in order to overcome these problems facing green chemistry.^{3,4} Recently, ionic liquids have received much attention as promising green media to reuse homogeneous catalysts.⁵ However, the reactions which involve ionic liquids as solvents suffer from severe problems related with expensive cost and high viscosity of the ionic liquids. It would be desirable to minimize the amount of ionic liquid in a potential process. In this regard, a new concept of a supported ionic liquid phase has been adopted for immobilization of catalysts.⁶ This strategy is to physically coat an ionic liquid containing homogeneous catalyst as a thin film on the surface of a solid support, which leads to a significant decrease in the amount of ionic liquid as well as a large increase in the contact area between the two phases. Recently, Hagiwara *et al.* have demonstrated that the ionic liquid layer can be stabilized when amino groups are grafted on the surface of silica support.^{6d} Research for efficient, convenient and recyclable catalytic systems based on supported ionic liquids is still a major challenge. Our interest in this area has prompted us to explore immobilization of palladium acetate with ionic liquid in the mesoporous channels of a hierarchically porous MFI zeolite. In addition to the use of the acidic hierarchical zeolite, our

approach is to effectively immobilize the ionic liquid layer by covalently grafting ionic liquid molecules on the surface of the mesopore walls.

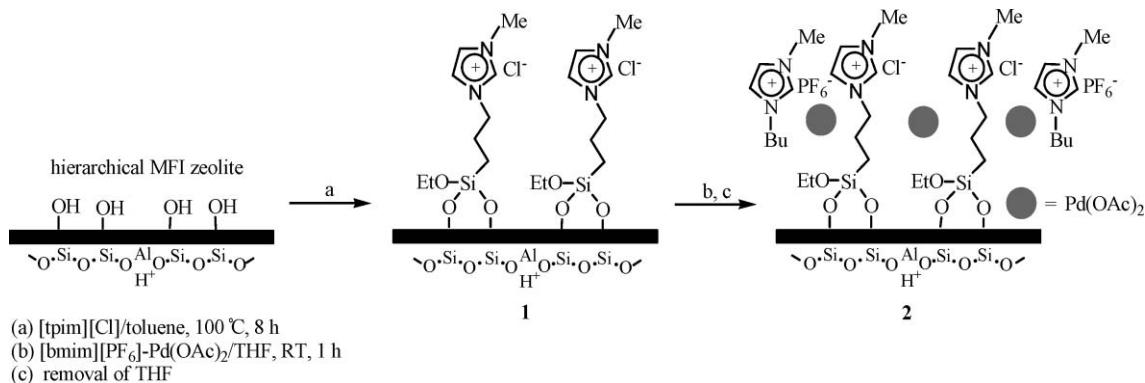
Previously, Ryoo and co-workers have developed a synthesis route to the highly mesoporous, hierarchically porous zeolites, which can serve as a potentially new support for the immobilization of homogeneous catalysts.⁷ In the case of hierarchical MFI zeolite, the mesopore diameters are uniform and tailored, typically in the range of 3–10 nm. The mesopore walls are made of crystalline microporous zeolite frameworks. The zeolite frameworks are terminated at the surface of mesopore walls with a high concentration of silanol groups. Through condensation of the silanol groups with organosilanes, the mesopore walls can be easily functionalized with organic groups. In particular, the functionalized MFI zeolite with a crystalline zeolite framework exhibited higher hydrothermal stability than other mesoporous materials without crystalline framework such as SBA-15 and MCM-41.⁸

As shown in Scheme 1, the immobilization of palladium acetate in the present work was performed in two steps. A hierarchical MFI zeolite with a narrow distribution of mesopore diameters around 3.3 nm was hydrothermally synthesized using dodecyltrimethyl[3-(trimethoxysilyl)propyl]ammonium chloride as a mesopore-directing agent.⁹ The hierarchical zeolite had the specific BET surface area of 502 m²/g and pore volume of 0.46 cm³/g. Mesopore walls of the MFI zeolite **1** were functionalized by the treatment with 1-(3-triethoxysilylpropyl)-3-methylimidazolium chloride ([tpim][Cl])¹⁰ in refluxing toluene. Loading of the imidazolium ionic liquid could be increased up to 1.3 mmol/g. The functionalization capacity was higher than those for amorphous silica gel¹¹ (0.87 mmol/g) and SBA-15 mesoporous silica¹² (1.0 mmol/g) under the same treatment conditions. The MFI zeolite has an approximately two times smaller surface area of the mesopore walls than SBA-15. Thus, the surface functionalization density should be at least two times higher at the mesopore walls of the hierarchical zeolite than SBA-15. The high density of surface functionalization in the case of hierarchical zeolite seemed to be due to densely populated silanol groups that were available on the mesopore walls.⁸ Such a mesoporous material may be a preferable choice in the development of supported ionic liquid catalysts because the covalently grafted ionic liquid moieties in a high density are supposed to immobilize free ionic liquid with catalytic species effectively.

In the second step for immobilization, the modified zeolite **1** (1.1 mmol/g) was immersed in a THF solution containing ionic liquid 1-butyl-3-methylimidazolium hexafluorophos-

^aSchool of Chemical Science and Engineering, Inha University, Incheon, 402-751, Korea. E-mail: mjjin@inha.ac.kr; Fax: +82-32-872-0959; Tel: +82-32-860-7469

^bNational Honor Scientist Program in Korea, Center for Functional Nanomaterials and Department of Chemistry, Korea Advanced Institute of Science and Technology, Daejeon, 305-701, Korea. E-mail: rryoo@kaist.ac.kr; Fax: +82-42-869-8130; Tel: +82-42-869-8131



Scheme 1 Preparation of MFI-supported Pd(OAc)₂-ionic liquid.

phate ([bmim][PF₆])¹³ and Pd(OAc)₂. Their weight ratio was 0.07 Pd(OAc)₂/0.14 ionic liquid/1.0 modified MFI zeolite **1**. The THF solvent was removed by evaporation, and the zeolite sample was washed with diethyl ether. The ether washing was to remove weakly adsorbed Pd(OAc)₂ without loss of the insoluble [bmim][PF₆]. Inductively coupled plasma (ICP) emission analysis showed a Pd content of 0.24 mmol/g in the resultant sample, in good agreement with the initial loading. This is similar to the strategy of Hagiwara *et al.* who grafted amino groups on silica gel.^{6d} In contrast, we grafted ionic liquid moieties on the mesopore walls of the zeolite. We believe that the added Pd(OAc)₂-[bmim][PF₆] matrix can be strongly incorporated into the covalently grafted ionic liquid layer through the interaction between the free ionic liquid and the grafted ionic liquid moiety. Transmission electron microscopic (TEM) and scanning electron microscopic (SEM) images showed that the resultant sample **2** is very similar to that of the parent MFI (Fig. 1).

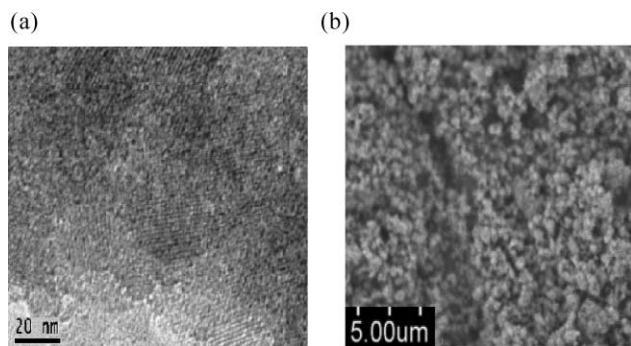


Fig. 1 (a) TEM image and (b) SEM image of MFI-IL-Pd(OAc)₂ **2**.

The heterogeneous Suzuki coupling has been mainly studied with reactive but expensive aryl iodides. The use of aryl bromides instead of aryl iodides would be more desirable for the large-scale applications. Suzuki coupling is generally performed in an organic solvent or water-organic mixture. The use of water as a safe and environmentally sustainable reaction medium has attracted much attention due to increasing environmental concerns in recent years. We tested the coupling of 4-bromoanisole with phenylboronic acid in water as a model reaction (Table 1). The reaction was initially performed using 0.3 mol% of catalyst **2** and K₃PO₄ as base in neat water.

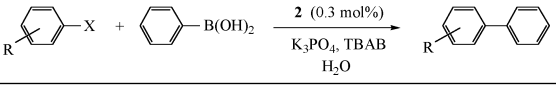
Table 1 Suzuki coupling of 4-bromoanisole with phenylboronic acid in water^a

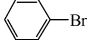
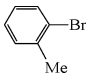
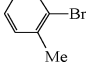
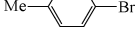
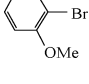
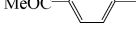
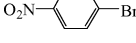
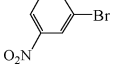
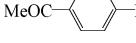
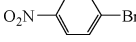
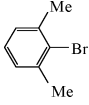
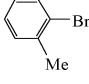
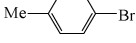
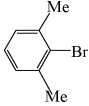
Entry	2 (mol%)	TBAB	<i>T</i> (°C)	Time (h)	yield ^b (%)
1	0.3	0	95	5.0	90 (92)
2	0.3	0.2	65	0.7	90 (93)
3	0.3	0.4	65	0.5	96 (99)
4	0.3	0.6	65	0.5	97 (99)
5 ^c	0.3	0.4	65	0.5	91 (96)
6 ^d	0.3	0.4	65	0.5	91 (95)
7	0.1	0.4	65	0.5	94 (98)
8	0.05	0.4	65	0.5	92 (96)
9	0.3	0.4	40	1.5	90 (95)
10	0.1	0.4	40	2.5	87 (92)

^a Molar ratio: bromobenzene (1.0 equiv.), phenylboronic acid (1.1 equiv.), **2** (0.3–0.05 mol%, Pd loading ratio: 0.24 mmol/g), and K₃PO₄ (2.0 equiv.). ^b Isolated yields (GC yield in parenthesis). ^c Na₂CO₃ was used instead of K₃PO₄. ^d Cs₂CO₃ was used instead of K₃PO₄.

High conversion was obtained at 95 °C in 5 h (entry 1). A phase transfer agent, tetrabutylammonium bromide (TBAB), was added to enhance the reactivity of the reaction. The TBAB effect on catalytic activity was surveyed with different amounts of TBAB (entries 2–4). The biphasic coupling reaction was found to be very efficient in the presence of 0.4 equiv. of TBAB. 4-Bromoanisole could be cleanly coupled with phenylboronic acid in 99% yield within a very short reaction time. Use of Na₂CO₃ or Cs₂CO₃, instead of K₃PO₄ resulted in slightly less effective coupling (entries 5 and 6). It is remarkable that high reactivity could be observed at a very low catalyst loading of 0.1–0.05 mol% (entries 7 and 8). The turnover frequency (TOF) was as high as 3840 h⁻¹ for the coupling. It is also noteworthy that catalyst **2** shows outstanding performance even at a low temperature of 40 °C (entries 9 and 10).

In order to investigate the scope on aryl bromides in the coupling with phenylboronic acid, different aryl bromides were employed in the reaction (Table 2). High catalytic activity for both bromobenzene and deactivated aryl bromides such as 2-bromotoluene, 4-bromotoluene, and 2-bromoanisole was observed, affording the corresponding biphenyl compounds in excellent yields (entries 1–5). Activated 4-bromoacetophenone, 1-bromo-4-nitrobenzene and 1-bromo-3-nitrobenzene were

Table 2 Suzuki coupling of aryl bromide with phenylboronic acid in water^a


Entry	Aryl bromide	Time (h)	T (°C)	Yield ^b (%)
1		0.5	65	95 (97)
2		0.7	65	88 (92)
3		2	50	87 (92)
4		0.7	65	85 (90)
5		0.5	65	93 (94)
6		0.3	65	95 (100)
7		0.4	65	98 (100)
8		0.4	65	97 (100)
9		2.0	RT	94 (98)
10		3.0	RT	97 (97)
11		1.2	95	85 (91)
12 ^c		0.5	65	71 (75)
13 ^c		0.7	65	72 (79)
14 ^c		1.2	95	51 (53)

^a Unless otherwise noted, reaction was run employing aryl bromide (1.0 equiv.), phenylboronic acid (1.1 equiv.), **2** (0.3 mol%), TBAB (0.4 equiv.) and K₃PO₄ (2.0 equiv.). ^b Isolated yields (GC yield in parenthesis). ^c Reaction was carried out in the presence of Pd(OAc)₂ instead of **2**.

rapidly coupled at 65 °C or even room temperature in quantitative yields (entries 6–10). Activated aryl bromides possessing electron-withdrawing groups showed higher reactivity than those possessing electron-donating groups. A slightly shorter reaction time was required to reach almost quantitative conversion. It should be noted that sterically hindered 2-bromo-

1,3-dimethylbenzene could be coupled in high yield (entry 11). For comparison, unsupported Pd(OAc)₂ was tested as catalyst under the same reaction conditions (entries 12–14). Comparison of entries 2 vs. 12, 4 vs. 13, and 11 vs. 14 indicated that the supported catalyst **2** was superior to unsupported Pd(OAc)₂. A more significant difference was observed in the coupling of less reactive 2-bromo-1,3-dimethylbenzene with steric hindrance. The results indicate that the use of a supported ionic liquid system is beneficial in enhancing the reactivity. The high efficiency of catalyst **2** is probably attributed to the fact that Pd(OAc)₂ is well-spread in the ionic liquid phase, and therefore more readily accessible for the reactants. Moreover, the anchored ionic liquid induces the formation of a hydrophobic environment on the surface of the MFI zeolite.

The catalytic system was further extended to the coupling reaction of aryl bromides with different arylboronic acids (Table 3). The results show that the catalytic system is very efficient for Suzuki coupling reaction of aryl bromides with different arylboronic acids. Deactivated aryl bromides could react with electron-rich 4-methylphenylboronic acid, and 4-methoxyphenylboronic acid afforded the corresponding products with high yields (entries 1–8). Besides, these conditions allow for the coupling of the deactivated aryl bromides with electron-deficient 4-chlorophenylboronic acid, 2-chlorophenylboronic acid, and 3-nitrophenylboronic acid (entries 9–17). Nearly complete conversions were also achieved for the reactions within short reaction times. The sterically hindered 2-bromo-1,3-dimethylbenzene could undergo coupling reactions with different arylboronic acids catalyzed by only 0.3 mol% of **2** to yield similar results, although a higher temperature and longer time were required (entries 18 and 19). The catalytic system was applicable to a wide range of arylboronic acids in all cases.

We turned our attention to the reusability of our catalyst. The recycling of the catalyst is an important issue in the heterogeneous reaction. As we described above, the major advantages of immobilized catalyst is its easy recovery by filtration or centrifugation. The recycling of **2** was investigated by the coupling of 4-bromoanisole and 1-bromo-4-nitrobenzene with phenylboronic acid in water. As shown in Table 4, the catalyst could be recovered and reused five times without significant loss of activity. Furthermore, ICP analysis of the solution indicated that less Pd metal (1.5 ppm) leached into the reaction solution during the first run. The isolated solution did not exhibit any further reactivity. This excellent reusability and high stability of the catalyst would be explained by strong binding of Pd(OAc)₂ to MFI-supported ionic liquid and site isolation, that is, the absence of interactions between catalytic sites, which causes aggregation of the Pd complex and formation of less active Pd catalyst. In addition to the high activity, the successful recycling of this catalytic system allows for a more economic and environmentally friendly process.

Experimental

Synthesis of hierarchical MFI zeolite

Hierarchical MFI zeolite was hydrothermally synthesized with dodecyltrimethyl[3-(trimethoxysilyl)propyl]ammonium chloride

Table 3 Suzuki coupling of aryl bromide with arylboronic acid in water^a

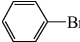
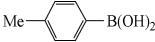
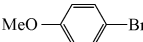
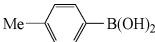
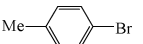
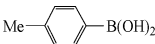
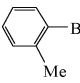
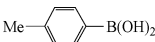
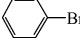
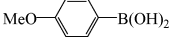
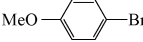
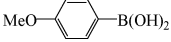
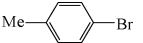
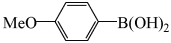
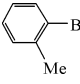
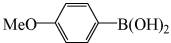
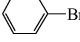
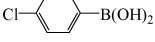
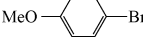
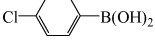
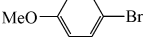
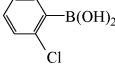

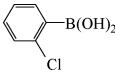
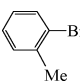
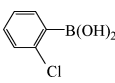
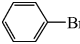
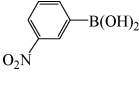
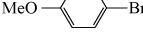
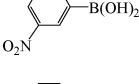
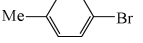
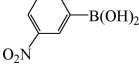
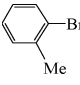
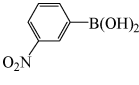
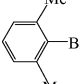
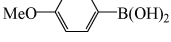
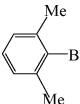
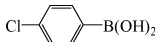
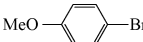
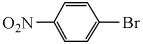
Entry	Aryl bromide	Arylboronic acid	Time (h)	Yield ^b (%)
1			0.5	94 (95)
2			0.5	92 (95)
3			1.0	95 (97)
4			0.5	91 (96)
5			0.5	94 (95)
6			0.5	91 (96)
7			1.0	91 (97)
8			0.5	93 (97)
9			0.5	95 (96)
10			0.5	93 (92)
11			0.5	90 (93)
12			2.0	85 (90)
13			1.0	87 (91)
14			0.5	96 (98)
15			0.5	96 (99)
16			0.5	92 (96)
17			0.5	92 (97)
18 ^c			2.5	84 (90)

Table 3 (Contd.)

Entry	Aryl bromide	Arylboronic acid	Time (h)	Yield ^b (%)
19 ^c			2.5	85 (91)

^a Unless otherwise noted, reaction was run employing aryl bromide (1.0 equiv.), arylboronic acid (1.1 equiv.), **2** (0.3 mol%), TBAB (0.4 equiv.) and K₃PO₄ (2.0 equiv.) at 65 °C. ^b Isolated yields (GC yield in parenthesis). ^c Reaction temp. was 90 °C.

Table 4 Recycling of catalyst **2** in Suzuki coupling of aryl bromide with phenylboronic acid^a

Aryl halide	Cycle	Yield ^b (%)	Cycle	Yield ^b (%)
	1	99	4	96
	2	97	5	96
	3	98		
	1	100	4	99
	2	100	5	99
	3	100		

^a Reaction was carried out using aryl bromide (1.0 equiv.), phenylboronic acid (1.1 equiv.), **2** (0.3 mol%), TBAB (0.4 equiv.) and K₃PO₄ (2.0 equiv.) at 65 °C for 0.5 h. ^b GC yield.

as a mesopore-directing agent.⁹ The product was dried in an oven at 373 K and subsequently calcined in air at 823 K. The sample was ion-exchanged into the NH₄⁺ form by repeating the ion-exchange treatment three times with a 1 M aqueous solution of NH₄NO₃ at 353 K for 4 h. The zeolite was calcined at 823 K for 6 h to convert it to the H⁺ form.

Modification of the surface of MFI zeolite with ionic liquid

To a solution of 1-(3-triethoxysilylpropyl)-3-methylimidazolium chloride (1.0 g, 3.1 mmol) in toluene was added MFI zeolite (2.0 g). The mixture was stirred at 100 °C for 10 h. After cooling, the reaction mixture was filtered and washed with CH₂Cl₂ several times, and dried at 60 °C under vacuum to yield MFI zeolite-supported ionic liquid **1** (2.57 g). Elemental analysis and weight gain showed that 1.2 mmol of 1-(3-triethoxysilylpropyl)-3-methylimidazolium chloride was anchored on 1.0 g of **1**.

Immobilization of Pd(OAc)₂-ionic liquid onto modified MFI zeolite

To a stirred solution of Pd(OAc)₂ (66 mg, 0.29 mmol) and 1-butyl-3-methylimidazolium hexafluorophosphate (165 mg, 0.58 mmol) in THF (10 mL), modified MFI zeolite **1** (1.0 g, 1.20 mmol/g) was added. The mixture was stirred for 40 min at room temperature, and then THF was slowly removed under reduced pressure. The resulting powder was washed with diethyl ether and dried under vacuum at 60 °C to give MFI zeolite-supported Pd(OAc)₂-ionic liquid **2** (1.21 g). The Pd content of

0.22 mmol/g was measured by inductively coupled plasma (ICP) analysis.

General procedure for heterogeneous Suzuki reaction

Aryl halide (1.0 mmol), phenylboronic acid (134 mg, 1.1 mmol), K_3PO_4 (424 mg, 2.0 mmol), TBAB (129 mg, 0.4 mmol), dodecane (40 mg, internal standard) and catalyst **2** (13.5 mg, 0.22 mmol/g, 0.3 mol%) were mixed in H_2O (3.0 mL). The mixture was stirred at 65 °C in an air atmosphere. The crude was analysed by GC/GC-MS. The reaction mixture was filtered and washed with H_2O and Et_2O . The organic phase was separated and dried over $MgSO_4$, and the solvent was evaporated under reduced pressure. The product was purified by column chromatography on silica gel.

The reuse of MFI zeolite-supported catalyst **2**

In the recycling experiment, the reaction was performed by using a mixture of aryl halide (1.0 mmol), phenylboronic acid (134 mg, 1.1 mmol), K_3PO_4 (424 mg, 2.0 mmol), TBAB (129 mg, 0.4 mmol) and catalyst **2** (13.5 mg, 0.3 mol%) in H_2O (3.0 mL) at 65 °C for 0.5 h. After completion of the reaction, the catalyst in the reaction mixture was separated from the solution by a centrifuge. The solution was worked up as described above. The separated catalyst was successively reused for the next reaction without any pretreatment.

Conclusions

In conclusion, hierarchical MFI zeolite was used as a support for immobilization of $Pd(OAc)_2$ -ionic liquid matrix. In this work, ionic liquid fragments were anchored on the mesopore walls of the zeolite. An ionic liquid phase with $Pd(OAc)_2$ was then immobilized into the covalently grafted ionic liquid framework. The resulting catalyst exhibited excellent catalytic activity and high stability for Suzuki coupling reactions in water. This catalyst was recycled four times without a significant loss in the catalytic activity. Hierarchical MFI zeolite was proven to be a promising support for the supported ionic liquid catalysis.

Acknowledgements

This work was supported by the National Honor Scientist Program of the Ministry of Education, Science and Technology in Korea.

References

1 For reviews, see: (a) N. Miyaura and A. Suzuki, *Chem. Rev.*, 1995, **95**, 2457–2483; (b) S. R. Chemler, D. Trauner and S. J. Danishefsky,

Angew. Chem., Int. Ed., 2001, **40**, 4544–4568; (c) S. Kotha, K. Lahiri and D. Kashinath, *Tetrahedron*, 2002, **58**, 9633–9695; (d) K. C. Nicolaou, P. G. Bulger and D. Sarlah, *Angew. Chem., Int. Ed.*, 2005, **44**, 4442–4489; (e) M. G. Banwell, T. E. Goodwin, S. Ng, J. A. Smith and D. J. Wong, *Eur. J. Org. Chem.*, 2006, 3043–3060; (f) N. T. S. Phan, M. V. D. Sluys and C. W. Jones, *Adv. Synth. Catal.*, 2006, **348**, 609–679; (g) S. Kotha and K. Lahiri, *Eur. J. Org. Chem.*, 2007, 1221–1236.

- 2 (a) J. P. Wolfe, R. A. Singer, B. H. Yang and S. L. Buchwald, *J. Am. Chem. Soc.*, 1999, **121**, 9550–9561; (b) A. D. Littke, C. Dai and G. C. Fu, *J. Am. Chem. Soc.*, 2000, **122**, 4020–4028; (c) M. R. Netherton, C. Dai, K. Neuschütz and G. C. Fu, *J. Am. Chem. Soc.*, 2001, **123**, 10099–10100; (d) J. Yin, M. P. Rainka, X.-X. Zhang and S. L. Buchwald, *J. Am. Chem. Soc.*, 2002, **24**, 1162–1163; (e) R. B. Bedford, C. S. J. Cazin and S. L. Hazelwood, *Angew. Chem., Int. Ed.*, 2002, **41**, 4120–4122; (f) F. Churrua, R. SanMartin, B. Inés, I. Tellitu and E. Domínguez, *Adv. Synth. Catal.*, 2006, **348**, 1836–1840.
- 3 For reviews, see: (a) N. E. Leadbeater and M. Marco, *Chem. Rev.*, 2002, **102**, 3217–3274; (b) L. Yin and J. Liebscher, *Chem. Rev.*, 2007, **107**, 133–173.
- 4 (a) L. Djakovitch and K. Koehler, *J. Am. Chem. Soc.*, 2001, **123**, 5990–5999; (b) Y. M. A. Yoichi, K. Takeda, H. Takahashi and S. Ikegami, *Org. Lett.*, 2002, **20**, 3371–3374; (c) S. Paul and J. H. Clark, *Green Chem.*, 2003, **5**, 635–638; (d) A. Corma, H. Garcia, A. Leiva and A. Primo, *Appl. Catal. A: Gen.*, 2003, **247**, 41–49; (e) A. Corma, H. Garcia, A. Leiva and A. Primo, *Appl. Catal. A: Gen.*, 2004, **257**, 77–83; (f) J. J. E. Hardy, S. Hubert, D. J. Macquarrie and A. J. Wilson, *Green Chem.*, 2004, **6**, 53–56.
- 5 (a) P. Wasserscheid and W. Keim, *Angew. Chem., Int. Ed.*, 2000, **39**, 3772–3789; (b) J. Dupont, R. F. de Souza and P. A. Z. Suarez, *Chem. Rev.*, 2002, **102**, 3667–3691; (c) N. Jain, A. Kumar, S. Chauhan and S. M. S. Chauhan, *Tetrahedron*, 2005, **61**, 1015–1060; (d) T. Akiyama, A. Suzuki and K. Fuchibe, *Synlett*, 2005, 1024–1026; (e) B. C. Ranu, S. Banerjee and R. Jana, *Tetrahedron*, 2007, **63**, 776–782.
- 6 (a) C. P. Mehnert, R. A. Cook, N. C. Dispenziere and M. Afeworki, *J. Am. Chem. Soc.*, 2002, **124**, 12932–129336; (b) S. Breitenlechner, M. Fleck, T. E. Müller and A. Suppan, *J. Mol. Catal. A*, 2004, **214**, 175–179; (c) C. P. Mehnert, *Chem. Eur. J.*, 2005, **11**, 50–56; (d) H. Hagiwara, K. H. Ko, T. Hoshi and T. Suzuki, *Chem. Commun.*, 2007, 2238–2840.
- 7 M. Choi, H. S. Cho, R. Srivastava, C. Venkatesan, D.-H. Choi and R. Ryoo, *Nat. Mater.*, 2006, **5**, 718–723.
- 8 D.-H. Lee, M. Choi, B.-W. Yu and R. Ryoo, *Chem. Commun.*, 2009, 74–76.
- 9 V. N. Shetti, J. Kim, R. Srivastava, M. Choi and R. Ryoo, *J. Catal.*, 2008, **254**, 296–303.
- 10 (a) B. Gadenne, P. Hesemann and J. J. E. Moreau, *Chem. Commun.*, 2004, 1768–1769; (b) S. Brenna, T. Posset, J. Furrer and J. Blumel, *Chem. Eur. J.*, 2006, **12**, 2880–2888.
- 11 (a) D. Zhao, Q. Huo, J. Feng, B. F. Chemlka and G. D. Stucky, *J. Am. Chem. Soc.*, 1998, **120**, 6024–603611; (b) A. P. Wight and M. E. Davis, *Chem. Rev.*, 2002, **102**, 3586–3613; (c) G. Du, S. Lim, M. Pinault, C. Wang, F. Fang, L. Pfefferle and G. L. Haller, *J. Catal.*, 2008, **253**, 74–90.
- 12 (a) M. K. Richmond, S. L. Scott and H. Alper, *J. Am. Chem. Soc.*, 2001, **123**, 10521–1052512; (b) C. Baleizao, A. Corma, H. Garcia and A. Leyva, *Chem. Commun.*, 2003, 606–607; (c) P.-H. Li and L. Wang, *Adv. Synth. Catal.*, 2006, **348**, 681–685.
- 13 J. G. Huddleston, A. E. Visser, W. M. Reichert, H. D. Willauer, G. A. Broker and R. D. Rogers, *Green Chem.*, 2001, **53**, 156–164.

Simultaneous esterification and transesterification of soybean oil with methanol catalyzed by mesoporous Ta₂O₅/SiO₂-[H₃PW₁₂O₄₀/R] (R = Me or Ph) hybrid catalysts†

Leilei Xu, Yonghui Wang, Xia Yang, Jianglei Hu, Wei Li and Yihang Guo*

Received 2nd September 2008, Accepted 8th January 2009

First published as an Advance Article on the web 16th January 2009

DOI: 10.1039/b815279a

The mesoporous Ta₂O₅ material functionalized with both alkyl groups and a Keggin-type heteropoly acid, Ta₂O₅/SiO₂-[H₃PW₁₂O₄₀/R] (R = Me or Ph), was prepared in a single step by the combination of sol-gel co-condensation, templated self-assembly, and hydrothermal treatment in the presence of a triblock copolymer surfactant. Compared with alkyl-free H₃PW₁₂O₄₀/Ta₂O₅ catalyst, the as-prepared hybrid catalyst exhibited much higher catalytic activity and stability to simultaneous esterification and transesterification of soybean oil (in the presence of 20 wt% myristic acid) with methanol under mild conditions.

Transesterification of vegetable oils with short chain alcohols to form fatty acid methyl esters (FAMES) has been a focus of much recent research because of the need to replace fossil fuel energy sources with renewable biofuels.¹ Generally, use of low quality feedstocks, such as waste cooking oils, will help to improve the economical feasibility of biodiesel, but the presence of undesirable components, such as free fatty acids (FFAs) and water, makes the process complicated. High FFA content leads to the conventional base-catalyzed transesterification route being inappropriate due to soap formation. For feedstocks with high FFA contents, acid catalysis is preferable to base catalysis because it allows the simultaneous esterification of FFAs and transesterification of triglycerides under appropriate reaction conditions, without the formation of soap.² However, inherent drawbacks to the use of liquid acids as catalysts, such as slow reaction rate, requirement of high temperature, high molar ratio of oil and alcohol, separation of the catalyst, and serious environmental and corrosion related problems, render liquid acids impractical for biodiesel production.

Solid acid catalysts, which are recyclable and readily separable from the reaction product, offer the opportunity to reduce the impact on the environment and increase industrial interest for biodiesel production.^{3,4} As a super strong Brønsted acid, heteropoly acid (HPA) has potential economic and green benefits for biodiesel production.⁵ Nevertheless, HPA in the bulk form is of poor efficiency due to its small surface area (lower than 5 m² g⁻¹); additionally, separation and recovery of HPA is difficult owing to its high solubility in many solvents.

To overcome the above disadvantages, we have immobilized a Keggin-type HPA onto a Ta₂O₅ support *via* a direct sol-gel co-condensation method. The selection of Ta₂O₅ as the support was based on its acidic properties, and its acid strength can be further improved by incorporation with H₃PW₁₂O₄₀ due to the formation of new (≡Ta-OH₂)_n⁺(H₃PW₁₂O₄₀)ⁿ⁻ active sites in the H₃PW₁₂O₄₀/Ta₂O₅ composite. On the other hand, the composite possesses a well-distributed three-dimensionally interconnected porous structure with a large surface area. Both advantages ensure that the composite exhibits high catalytic activity, selectivity, and stability towards the simultaneous esterification of lauric acid or myristic acid and transesterification of tripalmitin under mild conditions.⁶ However, the formation of significant quantities of water from esterification of FFAs inhibits the reactants from approaching active sites and thereby decreases the catalytic activity. This effect is exacerbated by the hydrophilicity of the reaction environment within the pores. In addition, the relative affinity of the catalyst for the highly hydrophilic methanol or glycerol and the rather hydrophobic oil or FFAs also influences the catalytic activity.⁷ Therefore, the catalytic performance of H₃PW₁₂O₄₀/Ta₂O₅ composite for both esterification and transesterification reactions is expected to be further improved by tuning its hydrophobic/hydrophilic balance. It has been reported the catalytic activity of the esterification reaction was improved by modification of sulfonic acid-functionalized mesoporous silica with alkyl groups.⁸ However, the utilization of this kind of multifunctionalized material for the production of biodiesel in a single step, namely catalyzing esterification and transesterification reactions simultaneously, has not been investigated so far. Herein, multifunctionalized mesoporous organic-inorganic hybrid tantalum pentoxide materials containing both alkyl groups and the Keggin unit, Ta₂O₅/SiO₂-[H₃PW₁₂O₄₀/R] (R = Me and Ph), were prepared in a single step by the combination of sol-gel co-condensation, templated self-assembly, and hydrothermal treatment in the presence of a triblock copolymer surfactant. The catalytic performance of as-prepared Ta₂O₅/SiO₂-[H₃PW₁₂O₄₀/R] was evaluated by direct use of soybean oil for biodiesel production in the presence of 20 wt% myristic acid under mild conditions (atmosphere refluxing).

Experimental

P123 (0.043 mmol) was dissolved in ethanol (171.7 mmol), and then TaCl₅ (1.7 mmol) was added. After vigorous stirring, aqueous H₃PW₁₂O₄₀ (11.3 mol L⁻¹, 2 mL) was introduced, and

School of Chemistry, Northeast Normal University, Changchun, P. R. China 130024. E-mail: guoyh@nenu.edu.cn; Fax: +86-431-85098705; Tel: +86-431-85098705

† Electronic supplementary information (ESI) available: Raman spectra and adsorption-desorption isotherms. See DOI: 10.1039/b815279a

then methyltrimethoxysilane (MeTMS) or phenyltrimethoxysilane (PhTMS) (0.57 mmol) was added. The resulting sol was aged at 40 °C for 24 h and then subjected to hydrothermal treatment at 80 °C for 48 h at a heating rate of 2 °C min⁻¹. The formed white hydrogel was dehydrated slowly at 60 °C in a vacuum for 24 h until a complete gel particulate was produced. P123 was removed by boiling ethanol extraction for 6 h. The products are represented by Ta₂O₅/SiO₂-[H₃PW₁₂O₄₀/R], where R = Me or Ph. Loading of H₃PW₁₂O₄₀ in the composite is 10.0%, determined by a ICP-AES. SiO₂-[H₃PW₁₂O₄₀/Me] with 9.6% H₃PW₁₂O₄₀ loading was prepared by a similar method, and tetraethoxysilane was used as the silicon source.

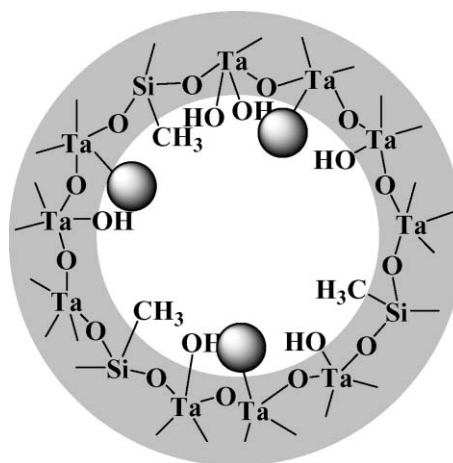
For comparison, a post-synthesis grafting method was also applied to prepare the composite. Ta₂O₅ was synthesized firstly according to the procedure described in the literature.⁹ The dried Ta₂O₅ (0.68 mmol) was suspended in a mixture of MeTMS or PhTMS (22.5 mmol L⁻¹) and H₃PW₁₂O₄₀ (5.5 mmol L⁻¹) in ethanol (20 mL) and refluxed for 24 h. The product was dried at 45 °C for 24 h and 120 °C for 2 h in vacuum, respectively. The products are represented by [H₃PW₁₂O₄₀/R]-Ta₂O₅/SiO₂. Loading of H₃PW₁₂O₄₀ in [H₃PW₁₂O₄₀/R]-Ta₂O₅/SiO₂ composite is 7.5%, determined by ICP-AES.

Simultaneous esterification and transesterification of soybean oil in the presence of myristic acid was carried out using as-prepared catalysts under atmosphere refluxing (65 °C) for 24 h. For a typical run, the reaction mixture consisted of 0.66 mmol soybean oil with 20 wt% myristic acid, 59.5 mmol methanol, and 2 wt% catalyst (referred to the amount of whole reaction mixture). Through GC-MS analysis, methyl palmitin (C16), methyl oleate (C18:1), methyl linoleate (C18:2), and methyl myristate (C14) are the main products in the above reaction system.

The performance of the catalysts was evaluated quantitatively by the yield of each FAME (% Y), and $Y = (M_D/M_T) \times 100$, where M_D and M_T are the number of moles of each FAME produced and expected, respectively. The concentrations of FAME were determined periodically on an Agilent 6890 GC fitted with a HP-INNOWax capillary column and flame ionization detector. Ethyl laurate was applied as an internal standard.

Results and discussion

Raman scattering studies (Fig. S1 of ESI[†]) confirmed both alkyl (Me or Ph) groups and the Keggin unit were incorporated into the products during the formation of the hybrid network by using a co-condensation method. In this “one-pot” method, the organosilanes were co-hydrolyzed and condensed with TaCl₅ in the presence of H₃PW₁₂O₄₀ to create Ta₂O₅/SiO₂-[H₃PW₁₂O₄₀/R] hybrid materials. The peaks found at 930.5, 992.5, and 1010.7 cm⁻¹ originate from the Keggin unit,¹⁰ while the peaks appearing at 3000.0, 1367.5, and 1594.3 cm⁻¹ are due to aromatic C–H bonds and C–C rings, respectively (Fig. S1b of ESI[†]).¹¹ In addition, the strong scattering peaks at 2910.0 and 2978.4 cm⁻¹ correspond to stretch vibrations of aliphatic C–H bonds (Fig. S1c of ESI[†]).¹¹ Based on the above information and the preparation method applied, a proposed schematic representation of the product is shown in Scheme 1. In this hybrid network, alkyl groups and the Keggin unit are



Scheme 1 Schematic representation of the multifunctionalized Ta₂O₅/SiO₂-[H₃PW₁₂O₄₀/Me]. ● refers to the H₃PW₁₂O₄₀ unit.

connected with the Ta₂O₅ matrix through Ta–O–Si–C and Ta–O–W covalent bonds, respectively.

Alkylated H₃PW₁₂O₄₀/Ta₂O₅ catalysts prepared with different methods exhibit different morphologies, which were revealed by TEM observations (Fig. 1). The co-condensed samples (Ta₂O₅/SiO₂-[H₃PW₁₂O₄₀/R]) exhibit a wormhole structure (Fig. 1a and 1b), while the grafted one ([H₃PW₁₂O₄₀/Me]-Ta₂O₅/SiO₂) possesses an ordered hexagonal array of mesopores (Fig. 1c).

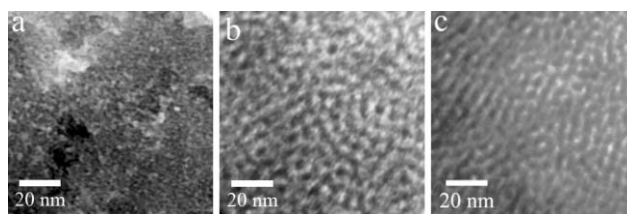


Fig. 1 TEM images of co-condensed and grafted hybrid catalysts. (a) Ta₂O₅/SiO₂-[H₃PW₁₂O₄₀/Me]; (b) Ta₂O₅/SiO₂-[H₃PW₁₂O₄₀/Ph]; (c) [H₃PW₁₂O₄₀/Me]-Ta₂O₅/SiO₂.

The N₂ adsorption–desorption isotherms of Ta₂O₅/SiO₂-[H₃PW₁₂O₄₀/R] are Type IV with an H2-type hysteresis loop, which is indicative of the well-distributed mesostructure of the materials tailored by nonionic templates (Fig. 2). A

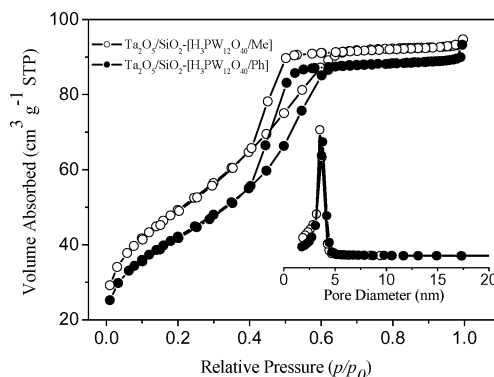


Fig. 2 Nitrogen adsorption–desorption isotherms and pore size distribution profiles (inset) of co-condensed Ta₂O₅/SiO₂-[H₃PW₁₂O₄₀/R] hybrid catalysts.

triangular hysteresis loop implies three-dimensionally interconnected mesoporosity of $\text{Ta}_2\text{O}_5/\text{SiO}_2\text{-}[\text{H}_3\text{PW}_{12}\text{O}_{40}/\text{R}]$ materials, which is in good agreement with the TEM results. $\text{Ta}_2\text{O}_5/\text{SiO}_2\text{-}[\text{H}_3\text{PW}_{12}\text{O}_{40}/\text{R}]$ possess larger surface areas than the alkyl-free sample ($\text{H}_3\text{PW}_{12}\text{O}_{40}/\text{Ta}_2\text{O}_5$, $114.7 \text{ m}^2 \text{ g}^{-1}$); moreover, methylated $\text{Ta}_2\text{O}_5/\text{SiO}_2\text{-}[\text{H}_3\text{PW}_{12}\text{O}_{40}/\text{Me}]$ has a larger surface area ($178.2 \text{ m}^2 \text{ g}^{-1}$) compared with phenylated $\text{Ta}_2\text{O}_5/\text{SiO}_2\text{-}[\text{H}_3\text{PW}_{12}\text{O}_{40}/\text{Ph}]$ ($152.1 \text{ m}^2 \text{ g}^{-1}$). The pore size distribution curves are centered at a pore diameter of 3.0–3.5 nm for $\text{Ta}_2\text{O}_5/\text{SiO}_2\text{-}[\text{H}_3\text{PW}_{12}\text{O}_{40}/\text{R}]$ catalysts, and the narrow pore size distributions imply the pores within the composites are uniform. Introduction of both the Keggin unit and alkyl groups by the grafting technique has little effect on the surface area of the products ($110.6 \text{ m}^2 \text{ g}^{-1}$ for $[\text{H}_3\text{PW}_{12}\text{O}_{40}/\text{Me}]\text{-Ta}_2\text{O}_5/\text{SiO}_2$ and $94.3 \text{ m}^2 \text{ g}^{-1}$ for $[\text{H}_3\text{PW}_{12}\text{O}_{40}/\text{Ph}]\text{-Ta}_2\text{O}_5/\text{SiO}_2$) compared with the alkyl-free sample, but both the size of the hysteresis loop (Fig. S2 of ESI†) and pore volume decrease, suggesting a possible accumulation of the grafted components around the pore openings.

The co-condensed hybrid materials ($\text{Ta}_2\text{O}_5/\text{SiO}_2\text{-}[\text{H}_3\text{PW}_{12}\text{O}_{40}/\text{R}]$) were successfully tested by the simultaneous transesterification of triglycerides and esterification of myristic acid (20 wt%) in soybean oil with methanol under identical reaction conditions, namely a reaction temperature of 65°C , reaction time of 24 h, 1:90 molar ratio of oil and methanol, and 2 wt% catalyst (Fig. 3a and b). For comparison, the silica-based hybrid catalyst ($\text{SiO}_2\text{-}[\text{H}_3\text{PW}_{12}\text{O}_{40}/\text{Me}]$, Fig. 3c), the grafted hybrid catalysts ($[\text{H}_3\text{PW}_{12}\text{O}_{40}/\text{R}]\text{-Ta}_2\text{O}_5/\text{SiO}_2$), and alkyl-free catalyst ($\text{H}_3\text{PW}_{12}\text{O}_{40}/\text{Ta}_2\text{O}_5$) were also examined under the same conditions.

Both $\text{Ta}_2\text{O}_5/\text{SiO}_2\text{-}[\text{H}_3\text{PW}_{12}\text{O}_{40}/\text{Me}(\text{Ph})]$ and $\text{H}_3\text{PW}_{12}\text{O}_{40}/\text{Ta}_2\text{O}_5$ showed significantly high esterification reactivity, and the yields of methyl myristate reached higher than 99% under the above conditions. However, the yield was only 53.6% by using $\text{SiO}_2\text{-}[\text{H}_3\text{PW}_{12}\text{O}_{40}/\text{Me}]$ under the same conditions.

As for the transesterification reaction, $\text{Ta}_2\text{O}_5/\text{SiO}_2\text{-}[\text{H}_3\text{PW}_{12}\text{O}_{40}/\text{R}]$ exhibited the highest catalytic activity among all tested catalysts. After the reaction was performed for 24 h, the yields of methyl linoleate, methyl palmitin, and methyl oleate reached 81.2%, 65.9%, and 53.9%, respectively, catalyzed by $\text{Ta}_2\text{O}_5/\text{SiO}_2\text{-}[\text{H}_3\text{PW}_{12}\text{O}_{40}/\text{Me}]$; by using $\text{H}_3\text{PW}_{12}\text{O}_{40}/\text{Ta}_2\text{O}_5$, the corresponding yields were 30.4%, 24.9%, and 20.5%, respectively. In the cases of the two hybrid catalysts with different supports, $\text{SiO}_2\text{-}[\text{H}_3\text{PW}_{12}\text{O}_{40}/\text{Me}]$ and $\text{Ta}_2\text{O}_5/\text{SiO}_2\text{-}$

$[\text{H}_3\text{PW}_{12}\text{O}_{40}/\text{Me}]$, the former was obviously less active than the latter under the same conditions, and the yields of methyl linoleate, methyl palmitin, and methyl oleate were 9.3%, 10.5%, and 16.0%, respectively. Finally, the grafted catalysts showed a much lower transesterification activity, and the corresponding yields were only 3.3%, 2.9%, and 2.0% for $[\text{H}_3\text{PW}_{12}\text{O}_{40}/\text{Me}]\text{-Ta}_2\text{O}_5/\text{SiO}_2$ and 1.5%, 1.2%, and 0.9% for $[\text{H}_3\text{PW}_{12}\text{O}_{40}/\text{Ph}]\text{-Ta}_2\text{O}_5/\text{SiO}_2$.

The high catalytic activity of the co-condensed $\text{Ta}_2\text{O}_5/\text{SiO}_2\text{-}[\text{H}_3\text{PW}_{12}\text{O}_{40}/\text{R}]$ materials is mainly determined by its strong Brønsted acid sites, $(\equiv\text{Ta-OH}_2)_n^+(\text{H}_2\text{PW}_{12}\text{O}_{40})_n^-$, which were formed at the surface of the hybrid catalyst *via* Ta–O–W bonds.⁶ Additionally, homogeneously dispersed inert hydrophobic organic groups (Me or Ph) in the materials do appear to improve the catalytic activity. For the esterification reaction, it created a hydrophobic environment within pores, which served to exclude the yielded water from the active sites, leading to the catalyst sustaining a higher reaction rate. As for the transesterification reaction, it tuned the hydrophobic/hydrophilic balance of the catalyst, which is beneficial to the reaction with the highly hydrophobic triglyceride reactant and rather hydrophilic glycerol product. Therefore, the relative affinity of the catalyst to triglyceride and glycerol was changed, leading to relatively weak adsorption of glycerol molecules and strong adsorption of triglyceride molecules on the multifunctionalized hybrid catalyst surface. As a consequence, higher activity and much lower catalyst deactivation (see Fig. 4) were obtained compared to alkyl-free $\text{H}_3\text{PW}_{12}\text{O}_{40}/\text{Ta}_2\text{O}_5$. By using the grafted method, it was difficult to form the $(\equiv\text{Ta-OH}_2)_n^+(\text{H}_2\text{PW}_{12}\text{O}_{40})_n^-$ species in $[\text{H}_3\text{PW}_{12}\text{O}_{40}/\text{R}]\text{-Ta}_2\text{O}_5/\text{SiO}_2$ materials. In addition, uneven distribution of the Keggin unit and alkyl groups in the grafted catalyst significantly decreased the accessibility to the active centre and diffusion rate of the reactants. Moreover, weak physical interactions between the Keggin unit and surface Ta–OH group resulted in leaching part of $\text{H}_3\text{PW}_{12}\text{O}_{40}$ species into the system during the catalytic process (determined by ICP-AES). All of the above factors lead to very poor catalytic activity of the grafted catalyst for the transesterification reaction.

$\text{Ta}_2\text{O}_5/\text{SiO}_2\text{-}[\text{H}_3\text{PW}_{12}\text{O}_{40}/\text{Me}]$ was selected to investigate the recyclability of as-prepared hybrid catalysts. The catalyst separated from the reaction mixture by centrifugation was washed with dichloromethane for three times and dried at 60°C overnight for subsequent catalytic cycles. As shown in

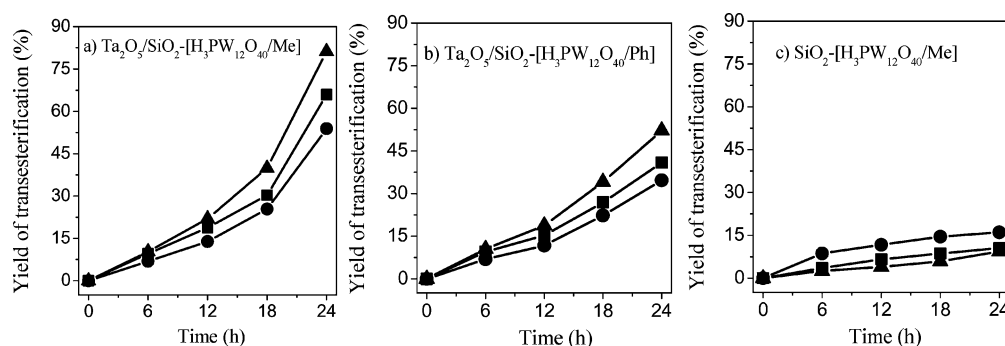


Fig. 3 Yield of transesterification vs. reaction time for $\text{Ta}_2\text{O}_5/\text{SiO}_2\text{-}[\text{H}_3\text{PW}_{12}\text{O}_{40}/\text{R}]$ hybrid catalysts compared with $\text{SiO}_2\text{-}[\text{H}_3\text{PW}_{12}\text{O}_{40}/\text{Me}]$ catalyst at 65°C , molar ratio of SB:MeOH = 1:90, 20 wt% of myristic acid, and 2 wt% catalyst: methyl palmitin (■), methyl oleate (●), and methyl linoleate (▲).

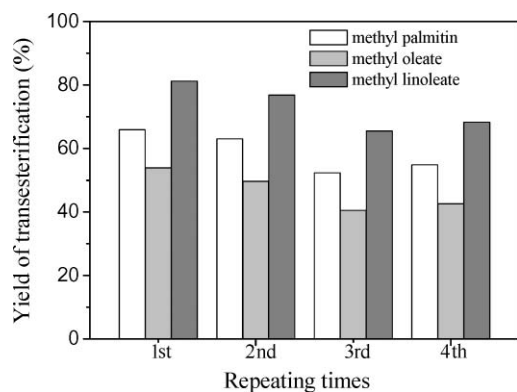


Fig. 4 Recyclability of the $\text{Ta}_2\text{O}_5/\text{SiO}_2\text{-}[\text{H}_3\text{PW}_{12}\text{O}_{40}/\text{Me}]$ for the transesterification of soybean oil with methanol in the presence of 20 wt% of myristic acid. Molar ratio of SB:MeOH = 1:90, 2 wt% catalyst, 24 h, and 65 °C.

Fig. 4. $\text{Ta}_2\text{O}_5/\text{SiO}_2\text{-}[\text{H}_3\text{PW}_{12}\text{O}_{40}/\text{Me}]$ showed excellent stability and maintained a similar level of activity after four reaction cycles; meanwhile, P or W was hardly detected by ICP-AES in the catalyst-free reaction solutions. The results confirm that as-prepared $\text{Ta}_2\text{O}_5/\text{SiO}_2\text{-}[\text{H}_3\text{PW}_{12}\text{O}_{40}/\text{R}]$ hybrid materials can function as recyclable and robust solid acid catalysts for simultaneously catalyzing esterification as well as the transesterification reaction.

In summary, a more active and stable mesoporous $\text{H}_3\text{PW}_{12}\text{O}_{40}/\text{Ta}_2\text{O}_5$ catalyst for simultaneously catalyzing transesterification of triglycerides and esterification of FFAs present in soybean oil to FAMES can be obtained by further

functionalizing with alkyl groups. The current work suggests that the catalytic performance of the supported HPA for the above two reactions can be improved by tuning its hydrophobic/hydrophilic balance.

Acknowledgements

This work is supported by the Key Project of Chinese Ministry of Education (No. 308008), the program of Changjiang Scholars and Innovative Research Team in University, and Analysis and Testing Foundation of Northeast Normal University.

Notes and references

- 1 S. Al-Zuhair, *Biofuels, Bioprod. Bioref.*, 2007, **1**, 57.
- 2 E. Lotero, Y. Liu, D. E. Lopez, K. Suwannakarn, D. A. Bruce and James G. Goodwin, Jr., *Ind. Eng. Chem. Res.*, 2005, **44**, 5353.
- 3 T. Lacombe, G. Hillion, B. Delfort, R. Revel, S. Leporc and F. Paille, *FR Pat.* 2855518-A1, 2005.
- 4 G. Hillion, B. Delfort and I. Durand, *FR Pat.* 2866653-A1, 2005.
- 5 P. Morin, B. Hamad, G. Sapaly, M. G. Carneiro Rocha, P. G. Pries de Oliveira, W. A. Gonzalez, E. Andrade Sales and N. Essayem, *Appl. Catal. A: Gen.*, 2007, **330**, 69.
- 6 L. Xu, Y. Wang, X. Yang, X. Yu, Y. Guo and J. H. Clark, *Green Chem.*, 2008, **10**, 746.
- 7 I. Díaz, C. Márquez-Alvarez, F. Mohino, J. Pérez-Pariente and E. Sastre, *J. Catal.*, 2000, **193**, 283.
- 8 I. K. Mbaraka and B. H. Shanks, *J. Catal.*, 2005, **229**, 365.
- 9 B. Lee, D. Lu, J. N. Kondo and K. Domen, *J. Am. Chem. Soc.*, 2002, **124**, 11256.
- 10 Y. Guo, K. Li and J. H. Clark, *Green Chem.*, 2007, **9**, 1.
- 11 D. Lin-Vien, N. B. Colthup, W. B. Fateley and J. G. Graselli, *The Handbook of Infrared and Raman Characteristic Frequencies of Organic Molecules*, Academic Press, Boston, 1991.

Green photochemistry: solarchemical synthesis of 5-amido-1,4-naphthoquinones†

Elodie Haggiage,^a Emma E. Coyle,^a Kieran Joyce^a and Michael Oelgemöller^{*a,b}

Received 24th September 2008, Accepted 6th January 2009

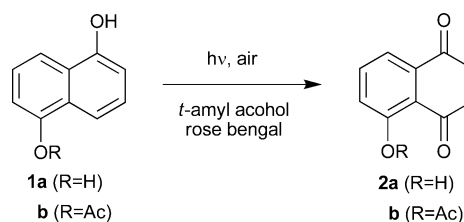
First published as an Advance Article on the web 20th January 2009

DOI: 10.1039/b816676e

Dye sensitized photooxygenations of 5-amido-1-naphthols were investigated with artificial light and sunlight, and the corresponding 5-amido-1,4-naphthoquinones were isolated in moderate to excellent yields. Under sunny conditions the yields were higher for almost all cases studied. The energy demand of the equipment used was determined, revealing significant energy savings for solar exposures.

Recent concerns regarding global warming and climate change have led to the establishment of *green chemistry* and its principles in academia and industry.¹ Among the many different *green chemical* approaches, photochemistry can play a central role since light is regarded as a *clean reagent*.² So far, however, the high energy demand of most common artificial light-sources has prevented widespread usage of photochemical methods in industry. To overcome this disadvantage, sunlight (direct or concentrated) has recently been applied as sustainable light-source.³ This concept leads back to the origin of organic photochemistry in the late 19th century.⁴ In recent years, we have demonstrated the feasibility of solarchemical syntheses for a number of commodity chemicals.⁵ During our ongoing study on photoacylation reactions,⁶ we became especially interested in the synthesis of 1,4-naphthoquinones through solar photooxygenations.⁷ 1,4-Naphthoquinones are important natural products, serve as valuable building blocks in synthesis and are key-moieties in biologically active compounds.⁸ They are most commonly synthesized from the corresponding 1-naphthols by oxidation,⁹ but these thermal pathways suffer from severe disadvantages concerning selectivity, sustainability or scale-up.^{9a} Dye sensitized photooxygenations represent a useful alternative, and various examples have been reported in the literature.^{7,10}

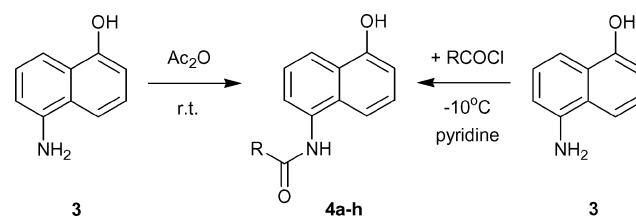
The photooxygenation of 1,5-dihydroxynaphthalene **1** to Juglone (**2**, 5-hydroxy-1,4-naphthoquinone) was selected as a model system to establish the most sustainable reaction conditions (Scheme 1). We were in particular interested in developing an entirely 'green' procedure and, for example, applied the solvent selection criteria developed by Pfizer¹¹ for the photochemical key-step and the subsequent purification.



Scheme 1 Photooxygenation to Juglone **2a** and 5-acetoxy-1,4-naphthoquinone **2b**.

The original irradiation procedures required the usage of the hazardous solvents dichloromethane, acetonitrile or methanol.¹⁰ After extensive optimization we found *tert*-amyl alcohol to be a suitable 'green' substitute instead. Following a standardized procedure, a solution of 1,5-dihydroxynaphthalene **1a** was irradiated in a Schlenk-flask with a 500 W halogen lamp in the presence of rose bengal as a sensitizer while the solution was purged with air. After 2.5 h, Juglone was isolated *via* column chromatography in a yield of 62%. In an attempt to synthesize functionalized derivatives of Juglone, the mono-acetate **1b** was irradiated under the same conditions for 4 to 5.5 h. The outcome of this reaction was somewhat sensitive to workup conditions.‡ When the solvent was evaporated at elevated temperature, Juglone **2a** was isolated in 30% yield as the only product. When the water bath temperature was kept below 40 °C during evaporation, Juglone was only detected in trace amounts by TLC and the 5-acetoxy-1,4-naphthoquinone **2b** was isolated in a yield of 35% instead.

We thus became interested in using 5-amido-1-naphthols as starting materials. Subsequent photooxygenation would yield the corresponding 5-amido-1,4-naphthoquinones, and these compounds are known to show antibiotic properties.¹² The desired starting compounds **4a–h** were readily available through standard acylation from 5-amino-1-naphthol **3** in yields of 15–61% (Scheme 2).¹³



Scheme 2 Synthesis of 5-amido-1-naphthols **4a–h**.

When the amido-derivatives **4a–h** were irradiated for 4 h following the general photooxygenation procedure, the

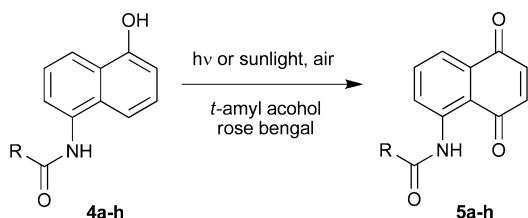
^aDublin City University, School of Chemical Sciences and NCSR, Glasnevin, Dublin, 14, Ireland

^bSchool of Pharmacy and Molecular Sciences, James Cook University, Townsville, Queensland, 4811, Australia.

E-mail: michael.oelgemoller@jcu.edu.au; Fax: +61-7-4781-6078; Tel: +61-7-4781-4535

† Dedicated to Prof. Robert S. H. Liu (University of Hawaii) on the occasion of his 70th birthday.

corresponding naphthoquinones **5a–h** were obtained in yields of 12–72% (Scheme 3). When irradiation was extended to 24 h, conversions and consequently yields increased and the desired products were isolated in amounts of 40–96% (Table 1). In July and August 2008, we repeated the photooxygenation reactions under ‘outdoor’ conditions at Dublin City University (latitude 53°23' N, 6°15' W, 50 m above sea level). Solutions of **4a–h** and rose bengal were exposed to direct sunlight for 6 h while the solution was purged with a gentle stream of air. During the course of each illumination the reaction mixture significantly darkened due to the formation of the strongly colored product. All solar experiments went smoothly and gave moderate to excellent yields of **5a–h** without any noticeable side-products or photodecomposition (Table 1). Under sunny or partly sunny conditions, the yields were comparable or higher than those after irradiation with artificial light for 24 h. Even under poor illumination conditions with mainly diffuse radiation the desired products were isolated in moderate to good yields, hence unambiguously proving the feasibility of solar synthesis. Likewise, solar exposure of the diol **1a** under sunny conditions for 4 h furnished Juglone **2a** in 70% yield and excellent quality.



Scheme 3 Photooxygenation of 5-amido-1-naphthols **4a–h**.

In order to compare the energy efficiency of solar exposure vs. irradiations with artificial light we measured the energy consumption per hour of operation of all electrical devices applied (Table 2) using a commercially available domestic electricity meter (Nikkai power, N67FU).¹⁴ The 500 W halogen lamp consumed the by far largest amount of electrical power with 0.432 kWh (or 1555.2 kJ). Due to the significant generation of heat by the lamp, the ‘indoor’ procedure required additional cooling by an electrical fan thus adding 0.018 kW (or 64.8 kJ) for its operation. In contrast, the ‘outdoor’ procedure solely required the use of an air pump (common for both processes), which consumed just 0.002 kWh (or 7.2 kJ) of energy. Purging additionally avoided the need of a magnetic stirrer. Notably, the mild climate of Dublin (Ireland) in combination with the relatively high boiling point of *tert*-amyl alcohol (102 °C) does not necessarily require the need for cooling water, thus reducing the overall energy demand further.¹⁵ Alternatively, the concept of using natural or artificial water reservoirs as heat sinks has been recently demonstrated by Liu and coworkers.¹⁶ In comparison with the energy demand of a conventional hot plate/magnetic stirrer it is interesting to note that the selected artificial light-source required far more electrical energy per hour of operation.

Conclusions

In conclusion, the photooxygenation of a series of 5-amido-1-naphthols results in the formation of 5-amido-1,4-naphthoquinones in moderate to excellent yields. Solar illuminations under ideal conditions gave significantly higher yields for almost all cases examined. The energy demand of the equipment has been compared for solar exposure vs. irradiation for the first time. Significant energy savings could be achieved by completely avoiding artificial light. Hence, this transformation

Table 1 Isolated yields of photooxygenations to **4a–h**

5	R	Artificial light		Sunlight	
		4 h	24 h	6 h	Weather
a	Me	12%	80%	90%	sunny
b	Et	34%	89%	53%	cloudy ^a
c	<i>cyclo</i> -Pr	36%	54%	53%	partly sunny
d	<i>t</i> -Bu	72%	94%	54%	sunny spells
e	Ph	17%	58%	80%	partly sunny
f	<i>p</i> -ClC ₆ H ₄	68%	72%	54%	cloudy ^a
g	<i>p</i> -MeC ₆ H ₄	24%	40%	63%	partly sunny
h	<i>p</i> -NCC ₆ H ₄	35%	96%	23%	cloudy ^a

^a Mainly diffuse radiation.

Table 2 Energy consumption of equipment used^a

	Model	E/kWh	E/kJ
Halogen lamp	IQ group HB-DFL-500, Armley lamp	0.432	1555.2
Air pump	Hagen Elite 800	0.002	7.2
Electric fan	GET, 9" desk fan, G9DFAN	0.018	64.8
Oil bath (heating to 100 °C) ^b	IKA, yellowline MST basic	0.084	302.4
Oil bath (maintained at 100 °C) ^c	IKA, yellowline MST basic	0.054	194.4

^a Energy consumption as measured by a Wattmeter for 1 h of operation. ^b Setting to 100 °C on the TC 1 probe (electronic contact thermometer) and 150 °C on the dial; 50 min heat up time, 10 min maintaining the temperature; 14 cm Ø crystallization dish; 600 ml silicon oil (Fluka). ^c Same settings and conditions as [b].

can be regarded as another example of 'green photochemistry'¹⁷ and a further contribution to Giacomo Ciamician's vision of 'the photochemistry of the future' (presented at the International Congress of Applied Chemistry in New York in 1912).^{18,19}

Experimental

Compound **4a** was synthesized as described by Jindal and co-workers.^{13a} All other 5-amido-1-naphthols **4b–h** were prepared following a modified procedure reported by Neidlein and Moller.^{13b} **General procedure:** 7.0 g (44 mmol) of 5-amino-1-naphthol **3** were dissolved in 75 ml of pyridine. 60 mmol of the corresponding acid chloride were added dropwise to the solution at -10°C . After stirring for 3 h, the reaction mixture was poured onto ice-water. The precipitate was filtered off and washed twice with cold water. The crude product was recrystallized from ethanol–water or ethyl acetate–cyclohexane. Exemplary details for **5-pivaloylamino-1-naphthol (5d)**. Purple solid; m.p.: 258°C ; ^1H NMR (400 MHz, DMSO- d_6): $\delta = 1.31$ (s, 9H), 6.86 (dd, $^3J = 6.4$, $^4J = 2.4$ Hz, 1H), 7.30 (dd, $^3J = 6.4$ Hz, 1H), 7.34–7.43 (m, 3H), 8.02 (d, $^3J = 8.0$ Hz, 1H), 9.37 (br. s, 1H), 10.17 ppm (br. s, 1H). ^{13}C NMR (100 MHz, DMSO- d_6): $\delta = 27.5$, 38.9, 108.0, 113.7, 120.2, 124.0, 124.5, 126.3, 125.4, 131.1, 133.8, 153.4, 177.1 ppm; IR (KBr): $\nu = 3284$, 2970, 1655, 1599, 1577, 1493, 1408, 1274, 1209, 1141, 960, 779, 736, 555 cm^{-1} .

General Procedure for photooxygenation

1 mmol of 5-amido-1-naphthol **4** and 50 mg of rose bengal were dissolved in 100 ml of *tert*-amyl alcohol. The clear solution was irradiated (500 W halogen lamp) or exposed to direct sunlight in a Pyrex Schlenk-flask equipped with a cold finger and a reflux condenser for 4, 6 or 24 h at ambient temperature while purging with a gentle stream of air. Evaporated solvent should be refilled whenever necessary. The progress of the reaction was monitored by TLC analysis (SiO_2 , cyclohexane:ethyl acetate 3:1). The solvent was removed under vacuum, and the residue was purified by column chromatography (SiO_2 , cyclohexane:ethyl acetate 3:1). Experimental details and results are given in Table 1. Exemplary details for **5-pivaloylamino-1,4-naphthoquinone (5d)**. Yellow solid; m.p.: 186°C ; ^1H NMR (400 MHz, acetone- d_6): $\delta = 1.36$ (s, 9H), 7.04 (d, $^2J = 14.4$ Hz, 1H), 7.06 (d, $^2J = 14.4$ Hz, 1H), 7.78 (dd, $^3J = 7.6$, $^4J = 1.2$ Hz, 1H), 8.85 (dd, $^3J = 7.6$, 8.4 Hz, 1H), 9.14 (dd, $^3J = 8.4$, $^4J = 1.2$ Hz, 1H), 12.13 ppm (br. s, 1H). ^{13}C NMR (100 MHz, CDCl_3): $\delta = 27.7$, 40.8, 116.4, 121.9, 126.3, 132.3, 135.9, 138.1, 140.1, 141.9, 179.1, 184.7, 189.3 ppm; IR (KBr): $\nu = 3249$, 2965, 1687, 1646, 1604, 1577, 1491, 1408, 1304, 1254, 1152, 1100, 944, 836, 740, 550, 448 cm^{-1} .

Acknowledgements

This research project was financially supported by Dublin City University (Research Alliance Funds 2005 and 2008), the Irish Research Council for Science, Engineering and Technology (IRCSET) and the Environmental Protection Agency (EPA, 2007-PhD-ET-7). Elodie Haggiage thanks ERASMUS for a Visiting Fellowship. The authors thank Dr Peter J. Dunn (Pfizer) for the generous donation of *tert*-amyl alcohol.

References

‡ This phenomenon is currently being further investigated. The synthesis of Juglone starting from **1b** has previously been reported.^{7b,10g}

- (a) P. Tundo, P. Anastas, D. St. C. Black, J. Breen, T. Collins, S. Memoli, J. Miyamoto, M. Polyakoff and W. Tumas, *Pure Appl. Chem.*, 2000, **72**, 1207–1228; (b) P. T. Anastas, and J. C. Wagner, *Green Chemistry: Theory and Practice*, Oxford University Press, Oxford, 1998.
- (a) A. Albin, and M. Fagnoni, in *Green Chemical Reactions (NATO Science for Peace and Security Series, Series C: Environmental Security)*, ed. P. Tundo and V. Esposito, Springer, Dordrecht, 2008, pp. 173–189; (b) C. L. Ciana and C. G. Bochet, *Chimia*, 2007, **61**, 650–654; (c) J. Mattay, *Chem. unseiner Zeit*, 2002, **36**, 98–106.
- (a) B. Pohlmann, H.-D. Scharf, U. Jarolimek and P. Mauermann, *Solar Energy*, 1997, **61**, 159–168; (b) P. Esser, B. Pohlmann and H.-D. Scharf, *Angew. Chem., Int. Ed.*, 1994, **33**, 2009–2023.
- (a) H. D. Roth, *Pure Appl. Chem.*, 2001, **73**, 395–403; (b) H. D. Roth, *Angew. Chem., Int. Ed.*, 1989, **28**, 1193–1207.
- (a) M. Oelgemöller, C. Jung and J. Mattay, *Pure Appl. Chem.*, 2007, **79**, 1939–1947; (b) M. Oelgemöller, C. Jung, J. Ortner, M. Mattay, C. Schiel and E. Zimmermann, *The Spectrum*, 2005, **18**, 28–33; (c) M. Oelgemöller, C. Jung, J. Ortner, J. Mattay, C. Schiel, and E. Zimmermann, in *Proc. 2004 International Solar Energy Conference—Portland, USA*, ASME, Boulder, 2004, pp. 1–9, ISBN 0-89553-176-3 (CD-ROM), ISEC 2004-65021.
- (a) F. Friedrichs, B. Murphy, D. Nayrat, T. Ahner, M. Funke, M. Ryan, J. Lex, J. Mattay and M. Oelgemöller, *Synlett*, 2008, 3137–3140; (b) P. A. Waske, J. Mattay and M. Oelgemöller, *Tetrahedron Lett.*, 2006, **47**, 1329–1332; (c) M. Oelgemöller, C. Schiel, R. Fröhlich and J. Mattay, *Eur. J. Org. Chem.*, 2002, 2465–2474; (d) C. Schiel, M. Oelgemöller and J. Mattay, *Synthesis*, 2001, 1275–1279; (e) C. Schiel, M. Oelgemöller, J. Ortner and J. Mattay, *Green Chem.*, 2001, **3**, 224–228; (f) C. Schiel, M. Oelgemöller and J. Mattay, *J. Inf. Rec.*, 1998, **24**, 257–260.
- (a) M. Oelgemöller, N. Healy, L. de Oliveria, C. Jung and M. Mattay, *Green Chem.*, 2006, **8**, 831–834; (b) O. Suchard, R. Kane, B. J. Roe, E. Zimmermann, C. Jung, P. A. Waske, J. Mattay and M. Oelgemöller, *Tetrahedron*, 2006, **62**, 1467–1473; (c) M. Oelgemöller, C. Jung, J. Ortner, M. Mattay and E. Zimmermann, *Green Chem.*, 2005, **7**, 35–38.
- (a) R. H. Thomson, *Naturally Occurring Quinones IV*, Blackie, London, 1997; (b) R. H. Thomson, *Naturally Occurring Quinones III. Recent Advances*, Chapman & Hall, London, 1988; (c) J. Bérdy, A. Aszalos, N. Bostian, K. L. McNitt, *CRC Handbook of Antibiotic Compounds. Quinone and Similar Antibiotics*, vol. 3, CRC Press, Boca Raton, 1980; (d) R. H. Thomson, *Naturally Occurring Quinones*, 2nd edn, Academic Press, New York, 1971.
- (a) O. A. Kholdeeva, O. V. Zalomaeva, A. N. Smakov, M. S. Melgunov and A. B. Sorokin, *J. Catal.*, 2005, **236**, 62–68; (b) W. M. Owtin, *J. Chem. Soc., Perkin Trans. 1*, 1999, 2409–2420; (c) H. Ulrich, and R. Richter, in *Methoden der Organischen Chemie (Houben-Weyl)*, ed. E. Müller and O. Bayer, vol. 7/3a, Thieme, Stuttgart, 1977, pp. 13–89.
- (a) A. W. Jensen and C. Daniels, *J. Org. Chem.*, 2003, **68**, 207–210; (b) J. Cossy and D. Belotti, *Tetrahedron Lett.*, 2001, **42**, 4329–4331; (c) D. Murtinho, M. Pineiro, M. M. Pereira, A. M. d'A. Rocha Gonsalves, L. G. Arnaut, M. da Graça Miguel and H. D. Burrows, *J. Chem. Soc., Perkin Trans. 1*, 2000, 2441–2447; (d) A. S. Amarasekara, *Synth. Commun.*, 1999, **29**, 3063–3066; (e) H. M. Chawla, K. Kaul and M. Kaul, *Indian J. Chem. Sect. B*, 1993, **32**, 733–737; (f) S. Croux, M.-T. Maurette, M. Hocquaux, A. Ananides, A. M. Braun and E. Oliveros, *New J. Chem.*, 1990, **14**, 161–167; (g) H. Möhrle and H. Foltmann, *Arch. Pharm. (Weinheim)*, 1988, **321**, 167–170; (h) G. Wurm and U. Geres, *Arch. Pharm. (Weinheim)*, 1985, **318**, 931–937; (i) H.-J. Durchstein and G. Wurm, *Arch. Pharm. (Weinheim)*, 1984, **317**, 809–812; (j) J. Griffiths, K.-Y. Chu and C. Hawkins, *J. Chem. Soc., Chem. Commun.*, 1976, 676–677.
- K. Alfonsi, J. Colberg, P. J. Dunn, T. Fevig, S. Jennings, T. A. Johnson, H. P. Kleine, C. Knight, M. A. Nagy, D. A. Perry and M. Stefaniak, *Green Chem.*, 2008, **10**, 31–36.
- (a) L. F. C. Medina, V. Stefani and A. Brandelli, *Can. J. Microbiol.*, 2004, **50**, 951–956; (b) H. Yamaoe, S. Takamura and Y. Tanaka, *Yakugaku Zasshi - J. Pharm. Soc. Jpn.*, 1968, **88**, 1602–1609.

- 13 (a) D. P. Jindal, M. S. Coumar, G. Bruni and P. Massarelli, *Arzneim. Forsch.*, 2002, **52**, 654–663; (b) R. Neidlein and F. Moller, *Liebigs Ann. Chem.*, 1980, 971–979.
- 14 T. Razzaq and C. O. Kappe, *ChemSusChem*, 2008, **1**, 123–132.
- 15 As a safety precaution, the usage of a cold finger and an additional reflux condenser is highly recommended.
- 16 Y.-P. Zhao, R. O. Campbell and R. S. H. Liu, *Green Chem.*, 2008, **10**, 1038–1042.
- 17 For further examples, see: (a) N. Hoffmann, *Pure Appl. Chem.*, 2007, **79**, 1949–1958; (b) M. Veerman, M. J. E. Resendiz and M. A. Garcia-Garibay, *Org. Lett.*, 2006, **8**, 2615–2617; (c) A. V. Samoshin and V. V. Samoshin, *J. Undergrad. Chem. Res.*, 2006, **2**, 13–16;
- (d) A. G. Griesbeck, N. Maptue, S. Bondock and M. Oelgemöller, *Photochem. Photobiol. Sci.*, 2003, **2**, 450–451; (e) A. G. Griesbeck and A. Bartoschek, *Chem. Commun.*, 2002, 1594–1595; (f) A. G. Griesbeck, W. Kramer and M. Oelgemöller, *Green Chem.*, 1999, **1**, 205–207.
- 18 G. Ciamician, *Science*, 1912, **36**, 385–394.
- 19 Recently, micro-photochemistry, *i.e.* photochemistry in micro-structured reactors, has been proposed as ‘*the new photochemistry of the future*’, see: E. E. Coyle and M. Oelgemöller, *Photochem. Photobiol. Sci.*, 2008, **7**, 1313–1322; E. E. Coyle and M. Oelgemöller, *Chem. Technol.*, 2008, **7**((12)), T95, www.rsc.org/Publishing/ChemTech/Volume/2008/12/microphotochem_insight.asp.

Basic metal carbonate supported gold nanoparticles: enhanced performance in aerobic alcohol oxidation†

Jie Yang,^{a,b} Yejun Guan,^a Tiny Verhoeven,^a Rutger van Santen,^a Can Li^{*b} and Emiel J. M. Hensen^{*a}

Received 2nd December 2008, Accepted 8th January 2009

First published as an Advance Article on the web 20th January 2009

DOI: 10.1039/b821586c

Gold nanoparticles supported by basic hydrozincite or bismuth carbonate are excellent catalysts for liquid-phase aerobic alcohol oxidation: the performance of a series of metal (Zn, Bi, Ce, La, Zr) carbonate supported gold catalysts depends strongly on the basicity of the support material.

Selective oxidation of alcohols to more valuable aldehydes, ketones and carboxylic acids represents an important class of reactions in the fine chemicals industry. Current methods for alcohol oxidation are based on the use of stoichiometric amounts of toxic or corrosive reagents, mainly heavy metal salts in high oxidation states. Hence, there is a desire for their replacement by environmentally more benign approaches.¹ Particularly attractive is the use of air or molecular oxygen as a cheap and clean oxidizing agent for large scale oxidation processes.^{2–4} The use of solid catalysts is desirable because of the ease of metals recovery. Pd,⁴ Ru,⁵ Pt,⁶ and Au⁷ are active precious metals for liquid-phase aerobic oxidation of alcohols. Nanosized gold particles are very promising because they are not prone to leaching as a result of overoxidation of the metal. As supports, silica, carbon and metal oxides have been employed with ceria⁷ and titania⁸ giving outstanding performance because of facile activation of molecular oxygen. Liquid-phase alcohol oxidation requires addition of soluble bases (metal carbonates, acetates or borates),⁹ especially when inert supports such as silica, carbon or polymers¹⁰ are used to disperse gold. For instance, K₂CO₃ is widely used to promote the oxidation of benzyl alcohol, but adds an extra separation step. Here, we present novel gold catalysts supported by water-insoluble basic metal carbonates for the liquid-phase oxidation of alcohols with molecular oxygen. Gold nanoparticles dispersed over inexpensive basic carbonates such as hydrozincite or bismuth carbonate display excellent catalytic activity in liquid-phase aerobic alcohol oxidation.

Basic bismuth carbonate (BiO)₂CO₃, zirconium carbonate and zinc hydroxycarbonate Zn₅(CO₃)₂(OH)₆ were used as received. Lanthanum and cerium carbonates were prepared by

precipitation of La³⁺ and Ce³⁺ *via* decomposition of urea. Gold-containing catalysts were prepared by deposition–precipitation of aurochloric acid on these support materials.¹¹ The resulting catalysts are denoted by Au/M with M being the metal ion of the corresponding metal carbonate. The surface areas of the supports and the Au loadings of the catalysts are collected in Table 1.

Initially, we determined the catalytic performance of the metal carbonate supported gold nanoparticles in the liquid-phase oxidation of benzyl alcohol (BA) to establish the influence of the support. These experiments were carried out in a stirred glass batch reactor (25 mL) in the presence of a solvent (toluene) and O₂ at 373 K. After a reaction time of 1 h, the mixture was quenched and analyzed by GC-MS. Table 1 lists the results of these catalytic tests. Benzoic acid was not observed in the liquid phase. There was no conversion of benzyl alcohol for the parent metal carbonate supports. The maximum benzaldehyde yield was obtained for the hydrozincite supported gold catalyst (Au/Zn). The yield is considerably higher than that of Au/TiO₂ and Au/CeO₂ reference catalysts under similar conditions. The TOF is comparable to previous reports on the aerobic oxidation of alcohols over gold catalysts supported on metal oxides in the presence of a base.⁷ For the metal carbonate supported catalysts, the benzaldehyde yield decreases in the order Au/Zn ≈ Au/Bi > Au/La ≈ Au/Ce ≫ Au/Zr.

Previous results have revealed a strong influence of the support and the size of Au nanoparticles on the catalytic performance in alcohol oxidation.^{7,10} As the textural properties of the supports differ substantially, we first analyzed the gold particle size by transmission electron microscopy to establish differences in gold dispersion (Table 1). The particles in Au/Zn have a diameter of about 4–6 nm (Fig. 1). On bismuth carbonate, the metallic phase appears as 1–3 nm nanoparticles with a high density on the low surface area support. The gold nanoparticles on the CeCO₃OH support are less monodisperse: next to a few particles larger than 10 nm most particles are around 5 nm, giving an average gold particle size of 6 nm. On the LaCO₃OH support, we observed a relatively low density of gold particles with an average particle size of about 7 nm. No gold nanoparticles were observed in Au/Zr. As the gold loading in this catalyst is relatively high, gold could be present as a very well dispersed gold hydroxide that cannot be easily reduced. The reference Au/TiO₂ and Au/CeO₂ contained gold particles in the range 3–4 nm and 2–3 nm, respectively. The activity of these reference catalysts is lower than that of Au/Zn which contains larger gold particles. The differences in gold loading and metal dispersion in these metal carbonate supported gold catalysts are undoubtedly

^aSchuit Institute of Catalysis, Eindhoven University of Technology, P.O. Box 513, 5600 MB, Eindhoven, The Netherlands. E-mail: e.j.m.hensen@tue.nl; Fax: +31 40 245 5054; Tel: +31 40 247 5178

^bKey Laboratory of Catalysis, Dalian Institute of Chemical Physics, Chinese Academy of Sciences, Zhongshan Road 457, Dalian, China. E-mail: canli@dicp.ac.cn; Fax: +86 411 84694447; Tel: +86 411 84379070

† Electronic supplementary information (ESI) available: Transmission electron micrographs and XRD results. See DOI: 10.1039/b821586c

Table 1 Textural, chemical and catalytic properties of metal carbonates, titania and ceria supports and supported Au nanoparticle catalysts

Support	Formula	Surface area (m ² /g)	Basicity (pH)	Catalyst	Au loading (wt.%)	d_{Au} (nm)	Au oxidation state ^a			Y_{aldehyde} (%) ^b	TOF (h ⁻¹)
							Au ⁰	Au ⁺	Au ³⁺		
Zn ₅ CO ₃ (OH) ₆	34	8.4	Au/Zn	0.8	5	overlap ^c			54	135	
(BiO)CO ₃	4	8.7	Au/Bi	1.4	2	100%	0%	0%	50 (40 ^d /50 ^e)	70 (110 ^d /140 ^e)	
CeCO ₃ OH	6	6.4	Au/Ce	3.0	6	65%	12%	23%	16	10	
LaCO ₃ OH	10	6.9	Au/La	0.8	7	n.d. ^f			18	47	
ZrCO ₃ (OH) ₂	22	4.2	Au/Zr	1.7	—	0%	63%	37%	<0.5/12 ^g	<1/14 ^g	
CeO ₂	80	6.5	Au/CeO ₂	1.8	n.d.	100% ^h	0%	0%	0.5 ^h	<1 ^h	
TiO ₂ (P-25)	50	5.5	Au/TiO ₂	1.0	2–3	n.d.			27	31	
					3–4	n.d.			36	75	

^a From XP spectra Au 4f region of catalysts after one reaction cycle. ^b Yield benzaldehyde (100 mg catalyst, 1 mmol BA, 373 K, toluene, 20 ml/min O₂, $t = 1$ h). ^c Not possible because of strong overlap with Zn 3p. ^d 50 mg catalyst. ^e 50 mg catalyst and 50 mg (BiO)CO₃. ^f Not determined. ^g 40 mg NaOH was added. ^h Reduced in H₂ at 523 K.

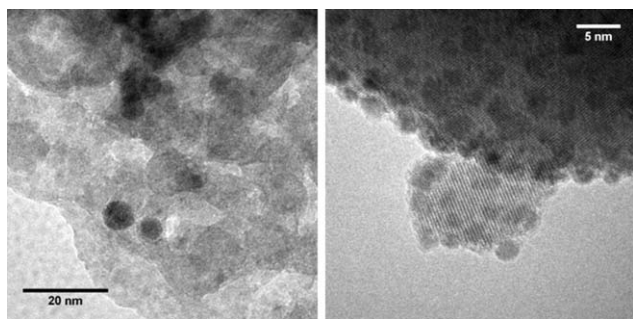


Fig. 1 Representative transmission electron micrographs of gold nanoparticles in Au/Zn (left) and Au/Bi (right).

related to the differences of the surface areas, hydroxyl densities and isoelectric points of the various supports, but do not appear to explain the large activity differences.

As bases facilitate alcohol oxidation by gold nanoparticle catalysts,¹² we surmised that differences in the surface basicity of the metal carbonate supports determine the activity ranking of the gold catalysts. Recently, Su *et al.*¹³ have found that the alcohol oxidation by gold nanoparticles is improved by a Ga-Al mixed oxide support that catalyzes the initial dehydrogenation of the alcohol. By measuring the pH of an equilibrated suspension of 0.5 g of support in 3 mL deionized water at room temperature (Table 1), we found that the various supports indeed exhibit considerable differences in basicity. The most active gold catalysts are obtained when metal carbonate supports with strong basic sites such as hydrozincite and bismuth carbonate are used. Gold catalysts supported on materials of intermediate basicity (Au/Ce and Au/La) display a benzaldehyde yield between that of the most active catalysts and Au/Zr. The latter catalyst has a very low activity. In accord with this, zirconium hydroxycarbonate has the lowest basicity. One notes that the TOF of Au/Zn (135 h⁻¹) is nearly twice that of Au/Bi (70 h⁻¹) despite similar basicity of the support. However, when the Au/Bi experiment was repeated with the same amount of gold as in the Au/Zn experiment, the TOF was 110 h⁻¹. The catalytic role of the basic sites of the support materials is further underpinned by an experiment with 50 mg of Au/Bi to which 50 mg of bismuth carbonate was added. In this case, the yield (TOF) increased from 40% (110 h⁻¹) to 50% (140 h⁻¹). The basic sites should be

involved in the deprotonation of the alcohol required as a first step towards dehydrogenation. Dehydrogenation has been found to be rate limiting in the gas-phase oxidation of ethanol.¹⁴ The involvement of supports such as ceria in this step has also been discussed.⁷

As noted above, an alternative explanation for the low activity of Au/Zr suggested by the absence of gold nanoparticles in electron micrographs is that the precursor Au phase is not fully reduced. Indeed, when immersed in benzyl alcohol the color of the white Au/Zr catalyst did not change. In contrast, the color of the catalysts that displayed good activity in alcohol oxidation changed to purple. XP spectra of the Au 4f core level of the catalysts after one reaction cycle (Fig. 2) show that the active catalysts contain metallic gold, whereas the gold phase in Au/Zr predominantly consists of Au⁺ and Au³⁺ ions (Table 1). When Au/Zr is calcined at 523 K in H₂, these gold ions become fully reduced as evidenced by the XP spectrum. After reduction, the catalytic activity remains negligible. Only when NaOH was added to the reaction mixture, a benzaldehyde yield of 12% was found. These findings support the claim that the basicity of the

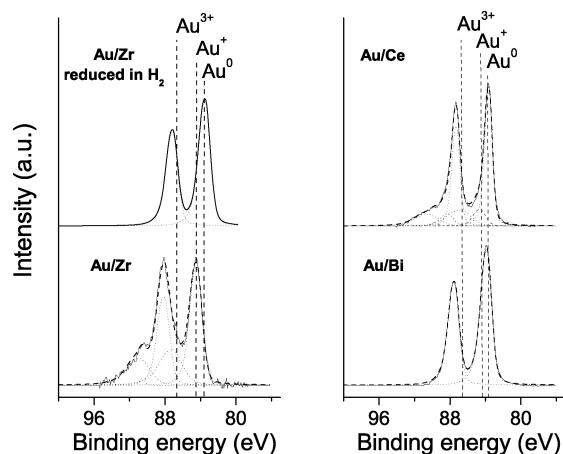


Fig. 2 XP spectra of the Au 4f region of supported catalysts after one reaction cycle in benzyl alcohol oxidation. The positions the Au³⁺, Au⁺ and Au⁰ 4f_{7/2} are indicated. The XP spectrum of Au/Zr after reduction at 523 K in H₂ is also shown (full lines: experimental data; dashed lines: fit).

zirconium carbonate support is too low to render an active gold oxidation catalyst.

We then focused on the Au/Zn catalyst and compared the possibilities of reusing this catalyst to reusing Au/TiO₂. After separation from the reaction mixture by centrifugation, the catalyst was washed in acetone and reused in the next run under the same conditions. Au/TiO₂ did not show any activity in the second run. The benzaldehyde yield for Au/Zn decreased to 13% in subsequent runs. The reason for this deactivation is not clear. Electron micrographs of Au/Zn after three subsequent runs did not show any changes in the gold phase (Fig. S2a). Elemental analysis did not evidence gold leaching during the catalytic tests nor during washing with acetone. In another experiment, after separation of Au/Zn from the reaction mixture after 0.5 h, the supernatant did not show any measurable further conversion under similar conditions. Also, washing in basic NaOH did not restore the initial catalyst activity. A possible deactivation mechanism is the deposition of carboxylic acids on the metallic surface.¹⁵ A reasonable explanation is that benzoic acid reacts with the basic sites of the support, thus leading to catalyst deactivation.¹⁶ Indeed, when we carried out benzyl alcohol oxidation in the presence of K₂CO₃, the activity of Au/Zn remained constant for three consecutive regenerations as it did for Au/TiO₂ (Fig. 3). Under these reaction conditions, the turnover frequencies of Au/Zn and Au/TiO₂ were higher at 190 h⁻¹ and 120 h⁻¹, respectively.

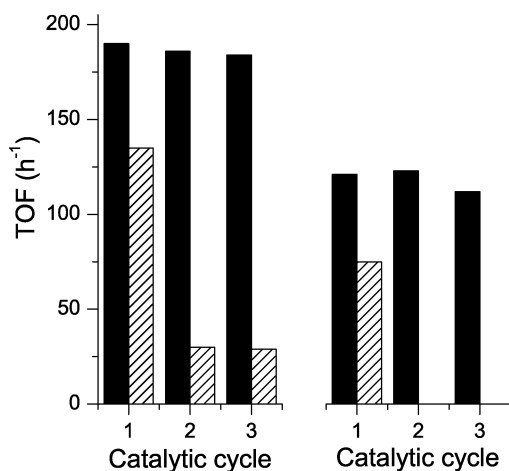
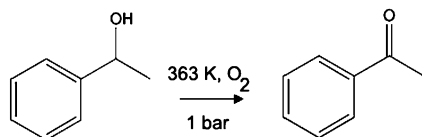


Fig. 3 Activities in benzyl alcohol oxidation (full (dashed) bars in presence (absence) of K₂CO₃) of Au/Zn (left) and Au/TiO₂ (right) for three consecutive cycles. After each cycle the catalyst was separated by centrifugation, washed in acetone and dried.

Finally, we found that our Au/Zn catalyst is very active for the solvent-free aerobic oxidation of (±)-1-phenylethanol to acetophenone (Scheme 1). In a typical experiment, we used 8 g (65.6 mmol) (±)-1-phenylethanol and 100 mg Au/ZnC. The mixture was refluxed at 363 K under flowing O₂ for 1 h. The



acetophenone conversion was 6.5% at a selectivity over 99%. The TOF of 1063 h⁻¹ is close to the value reported by Baiker and co-workers for Au/Cu₃Mg₁Al₂O_x.^{7b}

It should be noted that the TOF at 433 K under similar conditions as reported for polymer-microencapsulated Au^{10c} (TOF = 20 000 h⁻¹) and Au/Ga₃Al₃O₉¹³ (TOF = 25 000 h⁻¹) was nearly 25 000 h⁻¹ (164 mmol (±)1-phenylethanol, 14.5 mg Au/ZnC, *t* = 30 min, conversion 4.3%). However, in a control experiment without catalyst the conversion of 1-phenylethanol was found to be 2.3% under these conditions. As there was no conversion in a control experiment at 363 K, we conclude that the catalytic activity experiments at low temperature are more relevant.

In summary, we have demonstrated that basic metal carbonates are attractive supports for gold nanoparticles, resulting in excellent catalytic properties in liquid-phase alcohol oxidation under mild conditions. The high catalytic activity is related to the presence of accessible, strong basic sites. Tentatively, the initial O–H bond cleavage can occur on the support basic sites. This approach is promising to develop a truly heterogeneous catalyst for alcohol oxidation because soluble bases can be replaced in a straightforward manner by basic solid supports.

Experimental

Basic bismuth carbonate (BiO)₂CO₃·0.5H₂O and basic zirconium carbonate ZrCO₃(OH)₂ were purchased from Alfa–Aesar. Zinc carbonate hydroxide, Zn₃CO₃(OH)₄·xH₂O was purchased from Aldrich. Lanthanum and cerium carbonates were prepared by hydrolysis of La(NO₃)₃·6H₂O and Ce(NO₃)₃·6H₂O during urea decomposition. To this end, 10 g of the starting metal nitrate and 4.5 g urea were dissolved into 70 mL water. The solution was heated in an autoclave to 413 K for 4 h. The resulting precipitates were filtered and dried at 363 K overnight.

The gold catalysts were prepared by deposition–precipitation of aurochloric acid. The pH of a solution of 0.14 g HAuCl₄·3H₂O in 20 mL water was adjusted to pH = 12 by addition of 1 M NaOH. The solution was then added to a suspension of 2 g of the support in 20 mL distilled water. The resulting suspension was further stirred at room temperature for 18 h, filtered, washed with copious amounts of distilled water and finally dried at 363 K for 16 h. The resulting catalysts are denoted by Au/Zn, Au/Ce, Au/Bi, Au/Zr and Au/La. All chemicals were used as received unless stated otherwise.

The gold loading of the catalysts was determined by ICP-OES after an aliquot of the sample was dissolved in a mixture of HCl and HNO₃. Basicity measurements were carried out by suspending 0.5 g of support in 3 mL distilled water and stirring for 0.5 h. The pH of the upper clear liquid of the sedimented suspension was measured by an Inolab 730 pH meter. Transmission electron micrographs were acquired on a FEI Tecnai 20 electron microscope at an acceleration voltage of 200 kV with a LaB₆ filament. Typically, a small amount of sample was ground and suspended in ethanol or water, sonicated and dispersed over a Cu grid with a carbon film.

X-Ray photoelectron spectroscopic measurements were carried out on samples that underwent one catalytic cycle of benzyl alcohol oxidation followed by centrifugation, washing by acetone and drying in air. The catalysts were then introduced

into the X-ray photoelectron spectrometer (Kratos AXIS Ultra spectrometer equipped with a monochromatic Al K α X-ray source and a delay-line detector). Spectra were obtained using the aluminium anode (Al K α = 1486.6 eV) operating at 150 W. For survey and region scans, constant pass energies of 160 eV and 40 eV, respectively, were used. The background pressure was 2×10^{-9} mbar. Fitting was carried out with the CasaXPS program.

A reactor (25 ml round-bottle flask) was charged with 100 mg of catalyst, 1 mmol of benzyl alcohol and 9.9 mL of toluene. Molecular oxygen was bubbled through the reaction mixture (flow rate = 20 mL/min). The resulting mixture was then heated at 373 K for 1 h and cooled to room temperature. The reaction products were analyzed by a Shimadzu QP5050 GC-MS (CP-Sil 8CB, 50 m \times 0.32 mm, d_r = 0.15 μ m).

Acknowledgements

This work was financially supported by Program for Strategic Scientific Alliances between China and Netherlands funded by the Royal Netherlands Academy of Arts and Science and the Chinese Ministry of Science and Technology.

Notes and references

1 T. Mallat and A. Baiker, *Chem. Rev.*, 2004, **104**, 3037.

2 G. J. Ten Brink, I. W. C. E. Arends and R. A. Sheldon, *Science*, 2000, **287**, 636.

- 3 Z. Opre, D. Ferri, F. Krumeich, T. Mallat and A. Baiker, *J. Catal.*, 2006, **241**, 287.
- 4 K. Mori, T. Hara, T. Mizugaki, K. Ebitani and K. Kaneda, *J. Am. Chem. Soc.*, 2004, **126**, 10657.
- 5 K. Yamaguchi and N. Mizuno, *Chem.–Eur. J.*, 2003, **9**, 4353.
- 6 M. Besson and P. Gallezot, *Catal. Today*, 2000, **57**, 127.
- 7 (a) A. Abad, P. Concepción and H. García, *Angew. Chem., Int. Ed.*, 2005, **44**, 4066; (b) P. Haider and A. Baiker, *J. Catal.*, 2007, **248**, 175; (c) V. R. Choudhary, A. Dhar, P. Jana, R. Jha and B. S. Uphade, *Green Chem.*, 2005, **7**, 768; (d) V. R. Choudhary, R. Jha and P. Jana, *Green Chem.*, 2007, **9**, 267.
- 8 D. I. Enache, J. K. Edwards, P. Landon, B. Solsona-Espiriu, A. F. Carley, A. A. Herzing, M. Watanabe, C. J. Kiely, D. W. Knight and G. J. Hutchings, *Science*, 2006, **311**, 326.
- 9 N. F. Zheng and G. D. Stucky, *Chem. Commun.*, 2007, 3862.
- 10 (a) H. Tsunoyama, H. Sakurai, Y. Negishi and T. Tsukuda, *J. Am. Chem. Soc.*, 2005, **127**, 9374; (b) S. Kanaoka, N. Yagi, Y. Fukuyama, S. Aoshima, H. Tsunoyama, T. Tsukuda and H. Sakurai, *J. Am. Chem. Soc.*, 2007, **129**, 12060; (c) H. Miyamura, R. Matsubara, Y. Miyazaki and S. Kabayashi, *Angew. Chem., Int. Ed.*, 2007, **46**, 4151.
- 11 G. C. Bond, C. Louis and D. T. Thompson, *Catalysis by Gold*, IC Press, London, 2006, ch. 4.
- 12 A. Corma, V. Fornés and F. Rey, *J. Catal.*, 1994, **148**, 205.
- 13 F. Z. Su, Y. M. Liu, L. C. Wang, Y. Cao, H. Y. He and K. N. Fan, *Angew. Chem., Int. Ed.*, 2008, **47**, 334.
- 14 B. Jorgensen, S. E. Christiansen, M. L. D. Thomsen and C. H. Christensen, *J. Catal.*, 2007, **251**, 332.
- 15 A. Abad, A. Corma and H. Garca, *Chem.–Eur. J.*, 2008, **14**, 212.
- 16 C. Keresszegi, D. Ferri, T. Mallat and A. Baiker, *J. Phys. Chem. B*, 2005, **109**, 958.

A reusable $\text{FeCl}_3 \cdot 6\text{H}_2\text{O}$ /cationic 2,2'-bipyridyl catalytic system for the coupling of aryl iodides with thiols in water under aerobic conditions†

Wei-Yi Wu, Jui-Chan Wang and Fu-Yu Tsai*

Received 20th November 2008, Accepted 14th January 2009

First published as an Advance Article on the web 22nd January 2009

DOI: 10.1039/b820790a

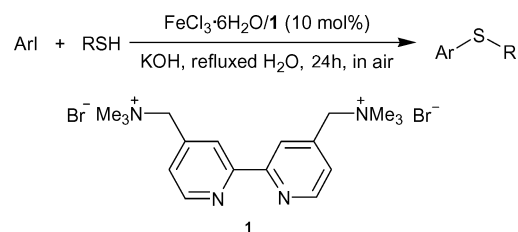
In this study, an $\text{FeCl}_3 \cdot 6\text{H}_2\text{O}$ /cationic 2,2'-bipyridyl system was employed as a catalyst in the coupling of aryl iodides with thiols to form an aryl–sulfur bond in refluxed water under aerobic conditions. The residual aqueous solution after extraction could be reused for several cycles without a significant decrease in activity.

Introduction

Transition-metal-catalyzed cross-coupling of aryl halides with thiols is a powerful method for the formation of carbon–sulfur bonds and is widely used in biological, pharmaceutical, and material science applications.¹ Since Migita and co-workers first reported the cross-coupling of aryl halides with thiols catalyzed by $\text{Pd}(\text{PPh}_3)_4$,² transition-metal-catalyzed formation of sulfur–carbon bonds has been widely employed by synthetic chemists. Several transition-metal catalysts, such as those based on palladium,³ nickel,⁴ copper,⁵ and cobalt,⁶ have been developed for use in this cross-coupling reaction. Recently, Bolm's group successfully developed a novel catalytic procedure for the S-arylation of aryl iodides with thiols, which uses anhydrous $\text{FeCl}_3/\text{DMEDA}$ as a catalyst and NaOtBu as a base in toluene under an Ar atmosphere.⁷ The benefits of this procedure are that iron salt is inexpensive and is less toxic to people and the environment than other transition metals. However, moisture-sensitive NaOtBu is employed as a base, so the use of a dried organic solvent under an inert atmosphere is required, leading to difficulties in recycling the catalyst.

On the other hand, the catalysis of organic reactions by water-soluble transition-metal complexes using water as a solvent has received much attention in recent years due to this green solvent being cheap, nontoxic, safe, and environmentally benign, as compared with organic solvents.⁸ Furthermore, the easy separation of the catalyst-containing aqueous solution from the organic products enables reuse of the catalyst. Despite the reporting of iron-catalyzed S-arylation by Bolm's group, this cross-coupling reaction catalyzed by iron in water under air has yet to be developed, and the design of a greener and reusable iron-containing catalytic system for S-arylation is considered of high practical value.

We have recently prepared a water-soluble cationic 2,2'-bipyridyl ligand **1** and used it to bring palladium and rhodium complexes into aqueous phases in order to develop green and reusable catalytic systems for carbon–carbon bond-forming reactions⁹ and phenylacetylene polymerizations in water.¹⁰ Herein, we report that the combination of **1** and $\text{FeCl}_3 \cdot 6\text{H}_2\text{O}$ was an efficient catalytic system for the cross-coupling of aryl iodides with thiols in neat water under air. This operationally-simple reaction enabled easy separation of the catalyst from the organic phase, and the residual aqueous solution could be reused for further reactions without any treatment (Scheme 1).



Scheme 1

Results and discussion

At the outset, 1-iodo-4-nitrobenzene and thiophenol were selected as representative reactants for optimization of the reaction conditions. The influence of bases, ligands, and the oxidation state of iron in the cross-coupling reaction was investigated, and the screening of reaction conditions is summarized in Table 1. The reaction gave the desired product, **4a**, in a 92% isolated yield when the reaction mixture, 1-iodo-4-nitrobenzene (3 mmol) and thiophenol (2 mmol), was stirred in refluxed water (5 mL) under aerobic conditions in the presence of $\text{FeCl}_3 \cdot 6\text{H}_2\text{O}/\mathbf{1}$ (10 mol%) and 4 mmol KOH for 24 h (Entry 1). Although it is known that iron catalysts can promote the homocoupling of thiols to produce disulfides,¹¹ in this reaction, the formation of such by-products was diminished by using thiol as the limiting reagent. A ligand-free system afforded the cross-coupling reaction less successfully, the product being afforded in a 55% isolated yield (Entry 2). When $\text{FeCl}_2 \cdot 4\text{H}_2\text{O}$ was used as the catalyst, 60 and 48% product yields were obtained in the presence and absence of ligand **1**, respectively, under the same conditions (Entries 3 and 4). We found that increasing the amount of ligand or KOH did not improve the yield for the formation of **4a** (Entries 5–7). Several common inorganic bases were employed in this reaction and their effects on the reaction studied: K_3PO_4 provided the arylated product in a 77% yield (Entry 8), whereas the other

Institute of Organic and Polymeric Materials, National Taipei University of Technology, Taipei, 106, Taiwan. E-mail: fuyutsai@ntut.edu.tw; Fax: +886 2 2731 7174

† Electronic supplementary information (ESI) available: Experimental procedures, spectroscopic characterization data of cross-coupling products, and copies of ^1H and ^{13}C NMR of compound **4d**. See DOI: 10.1039/b820790a

Table 1 Optimization studies for the Fe-catalyzed coupling of 1-iodo-4-nitrobenzene (**2a**) with thiophenol (**3a**) in water^a

Entry	Iron source	Base (mmol)	Yield (%) ^b
1	FeCl ₃ ·6H ₂ O	KOH (4)	92
2 ^c	FeCl ₃ ·6H ₂ O	KOH (4)	55
3	FeCl ₂ ·4H ₂ O	KOH (4)	60
4 ^c	FeCl ₂ ·4H ₂ O	KOH (4)	48
5 ^d	FeCl ₃ ·6H ₂ O	KOH (4)	81
6	FeCl ₃ ·6H ₂ O	KOH (6)	48
7	FeCl ₃ ·6H ₂ O	KOH (8)	40
8	FeCl ₃ ·6H ₂ O	K ₂ PO ₄ (4)	77
9	FeCl ₃ ·6H ₂ O	K ₂ CO ₃ (4)	41
10	FeCl ₃ ·6H ₂ O	KF (4)	22
11	FeCl ₃ ·6H ₂ O	CsF (4)	trace
12	FeCl ₃ ·6H ₂ O	Cs ₂ CO ₃ (4)	54
13	FeCl ₃ ·6H ₂ O	KOAc (4)	trace

^a Reaction conditions: **2a** (3 mmol), **3a** (2 mmol), [Fe] (10 mol%), **1** (10 mol%), base, H₂O (5 mL), refluxed for 24 h. ^b Isolated yields. ^c In the absence of **1**. ^d 20 mol% of **1** was used.

bases gave only trace amounts or moderate yields of the product (Entries 9–13).

The reusability of the aqueous catalytic system is very important from the practical and economic viewpoints. We chose the conditions of the presence and absence of ligand **1** for comparison (Table 1, Entry 1 and 2). For the reaction in the presence of **1**, after completion of the cross-coupling reaction of 1-iodo-4-nitrobenzene with thiophenol, the reaction mixture was extracted with hexane and the product was purified by column chromatography. The remaining aqueous solution was then charged with 1-iodo-4-nitrobenzene, thiophenol and base for the second-run reaction. As shown in Fig. 1, it was possible to use the catalyst-containing aqueous solution at least six times with only a slight decrease in activity. On the contrary, the activity of the iron catalyst was drastically decreased in each cycle and approached zero in the fifth cycle when the system lacked ligand **1**. Ligand **1** was therefore revealed to be important, not only through its stabilization of the iron salt in the aqueous phase, enabling the reuse of the catalytic system, but also because the ionic parts of the ligand may play a surfactant role and

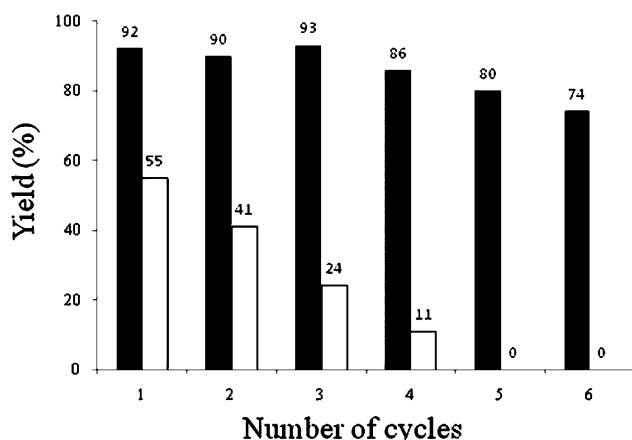


Fig. 1 Recyclability of FeCl₃·6H₂O/O1 (■) versus FeCl₃·6H₂O (□) for the coupling of 1-iodo-4-nitrobenzene with thiophenol. Reaction conditions: 1-iodo-4-nitrobenzene (3 mmol), thiophenol (2 mmol), KOH (4 mmol), and catalyst (10 mol%) under refluxed H₂O (5 mL) for 24 h for each cycle.

facilitate the reaction in neat water. It should be noted that the use of this water-soluble cationic 2,2'-bipyridyl/FeCl₃·6H₂O catalytic system enabled easy separation of the catalyst from the organic phase and the use of a simple reaction procedure under air.

In order to clarify whether the gradual loss of activity from the fourth cycle onwards in the presence of **1** was due to the successive extraction or deactivation of the catalyst, a successive addition experiment was performed. After completion of the first run (24 h), a fresh portion of 1-iodo-4-nitrobenzene, thiophenol, KOH, and water was added directly to the unseparated reaction mixture and the second cycle was executed under conditions identical to those of the first run; this procedure was repeated until the completion of the sixth cycle. We found that the overall isolated yield of **4a** was 558%, corresponding to an average of 93% yield for each cycle. This result excludes the possibility of deactivation of the catalyst during the reactions and indicates that the successive extraction in the previous recycling studies led to the decrease in the catalyst concentration in each cycle.

To explore the scope of this cross-coupling reaction catalyzed by our system, the reactions of a variety of aryl iodides and thiols were examined and the amount of disulfides formed was also analyzed (Table 2). 1-Iodo-4-nitrobenzene coupled with various aryl thiols efficiently to give the corresponding products **4b–d** in high yields (Entries 1–3), and the employment of 1-iodo-3-nitrobenzene resulted in the formation of **4e–h** in good yields. Although a slower cross-coupling rate led to the formation of a small amount of disulfide, it could be separated easily upon purification (Entries 4–7). Cross-coupling reactions with 1-chloro-4-iodobenzene proceeded exclusively at the C–I group, affording chloro-substituted thioethers (Entries 8–10). Entries 11–19 illustrate that iodobenzene and electron-rich iodotoluene were also effectively coupled with thiols, affording the corresponding thioethers in 64–96% yields. When 4-iodobenzonitrile and ethyl-4-iodobenzoate were used as the substrates, the hydrolyzed product **4r** was the sole cross-coupling product, obtained in high yields under such reaction conditions (Entries 20 and 21). Contrary to the first reported iron-catalyzed S-arylation system,⁷ aliphatic thiols such as benzyl mercaptan coupled with aryl iodides in our system to give **4s** and **4t** in 25 and 22% yields along with 11 and 12% of disulfides, respectively (Entries 22 and 23).

Experimental

General procedure for the iron-catalyzed carbon–sulfur bond formation reaction

A 20 mL reactor equipped with a condenser was charged with FeCl₃·6H₂O (54 mg, 0.2 mmol), ligand **1** (92 mg, 0.2 mmol) and H₂O (5 mL). After stirring at 50 °C for 0.5 h, aryl iodide **2** (3.0 mmol), thiol **3** (2.0 mmol) and KOH (4.0 mmol) were added to the solution, and the reaction mixture was then stirred under reflux conditions in air for 24 h. After cooling of the reaction mixture to room temperature, the aqueous solution was extracted with hexane; the organic layer was dried over MgSO₄ and the solvent was then removed under vacuum. Column chromatography on silica gel afforded the desired product.

Table 2 Results of $\text{FeCl}_3 \cdot 6\text{H}_2\text{O}$ /1-catalyzed coupling of aryl iodides (**2**) with thiols (**3**) in water^a

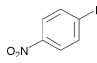
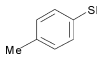
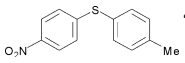
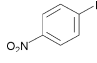
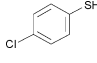
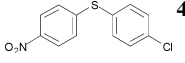
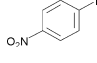
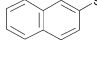
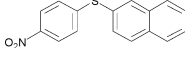
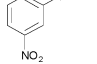
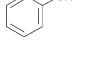
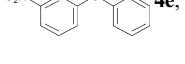
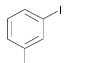
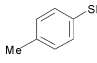
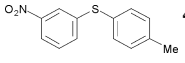
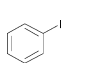
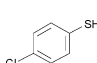
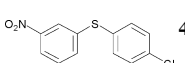
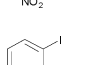
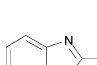
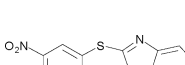
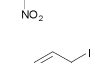
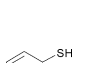
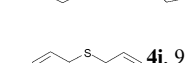
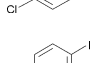
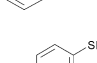
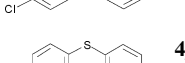
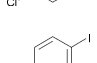
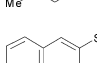
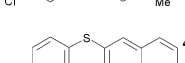
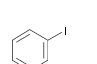
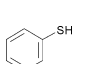
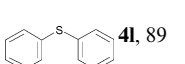
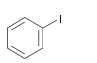
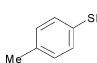
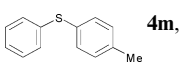
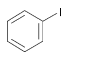
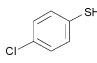
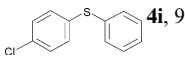
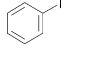
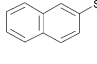
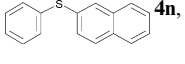
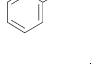
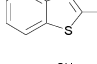
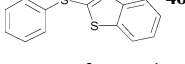
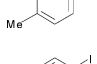
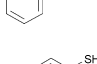
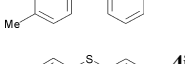
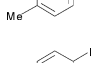
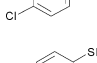
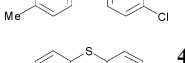
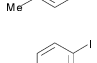
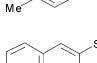
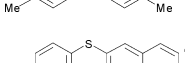
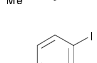
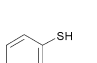
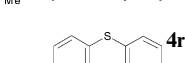
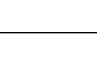
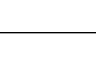
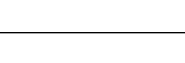
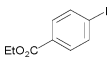
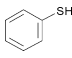
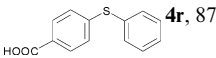
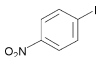
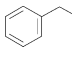
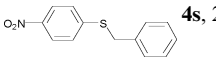
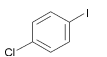
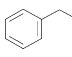
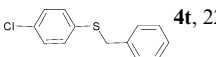
Entry	Aryl iodide (2)	Thiol (3)	Yield (%) ^b	
			ArSR (4)	RSSR (5)
1			 4b , 80	0
2			 4c , 99	0
3			 4d , 86	0
4			 4e , 68	10
5			 4f , 56	15
6			 4g , 77	8
7			 4h , 83	0
8			 4i , 99	0
9			 4j , 81	0
10			 4k , 87	0
11			 4l , 89	0
12			 4m , 96	0
13			 4i , 94	0
14			 4n , 70	13
15			 4o , 92	0
16			 4m , 82	0
17			 4j , 74	9
18			 4p , 87	0
19			 4q , 64	12
20			 4r , 92	0

Table 2 (Contd.)

Entry	Aryl iodide (2)	Thiol (3)	Yield (%) ^b	
			ArSR (4)	RSSR (5)
21			 4r , 87	0
22			 4s , 25	11
23			 4t , 22	12

^a Reaction conditions: **2** (3 mmol), **3** (2 mmol), FeCl₃·6H₂O (10 mol%), **1** (10 mol%), KOH (4 mmol), H₂O (5 mL), refluxed for 24 h. ^b Isolated yields.

Conclusions

In this paper, we have developed a green and reusable catalytic system for the coupling of aryl iodides with thiols using environmentally-friendly and cheap FeCl₃·6H₂O as a catalyst in the greenest solvent, water. This method avoids the use of air-sensitive reagents and the reaction can therefore be performed under air, rendering the experimental procedure very simple. In addition, the catalytic system can be reused at least six times with only a slight decrease in activity, indicating its potential for use in industrial applications. Further mechanistic studies on this reaction and the applicability of this green system in other organic syntheses are now under investigation in our group.

Acknowledgements

This research was financially supported by the National Science Council of Taiwan (NSC96-2113-M-027-003-MY2).

Notes and references

- D. J. Procter, *J. Chem. Soc., Perkin Trans. 1*, 2001, 335; G. Liu, J. R. Huth, E. T. Olejniczak, R. Mendoza, P. DeVries, S. Leitz, E. B. Reilly, G. F. Okasinski, S. W. Fesik and T. W. Von Geldern, *J. Med. Chem.*, 2001, **44**, 1202; J. Hassan, M. Seignion, C. Gozzi, E. Schulz and M. Lemaire, *Chem. Rev.*, 2002, **102**, 1359; S. V. Ley and A. W. Thomas, *Angew. Chem., Int. Ed.*, 2003, **42**, 5400; I. P. Beletskaya and A. V. Cheprakov, *Coord. Chem. Rev.*, 2004, **248**, 2337; G. De Martino, M. C. Edler, G. La Regina, A. Coluccia, M. C. Barbera, D. Barrow, R. I. Nicholson, G. Chiosis, A. Brancale, E. Hamel, M. Artico and R. Silvestri, *J. Med. Chem.*, 2006, **49**, 947; J.-P. Corbet and G. Mignani, *Chem. Rev.*, 2006, **106**, 2651; I.-P. Beletskaya and V. P. Ananikov, *Eur. J. Org. Chem.*, 2007, 3431; A. Gangjee, Y. Zeng, T. Talreja, J. J. McGuire, R. L. Kisliuk and S. F. Queener, *J. Med. Chem.*, 2007, **50**, 3046.
- T. Migita, T. Shimizu, Y. Asami, J. Shiobara, Y. Kato and M. Kosugi, *Bull. Chem. Soc. Jpn.*, 1980, **53**, 1385; M. Kosugi, T. Ogata, M. Terada, H. Sano and T. Migita, *Bull. Chem. Soc. Jpn.*, 1985, **58**, 3657.
- G. Y. Li, *Angew. Chem., Int. Ed.*, 2001, **40**, 1513; U. Schopfer and A. Schlappbach, *Tetrahedron*, 2001, **57**, 3069; M. Murata and S. L. Buchwald, *Tetrahedron*, 2004, **60**, 7397; T. Itoh and T. Mase, *Org. Lett.*, 2004, **6**, 4587; C. Mispelaere-Canivet, J.-F. Spindler,

S. Perrio and P. Beslin, *Tetrahedron*, 2005, **61**, 5253; M. A. Fernández-Rodríguez, Q. Shen and J. F. Hartwig, *J. Am. Chem. Soc.*, 2006, **128**, 2180.

- H. J. Cristau, B. Chabaud, A. Chêne and H. Christol, *Synthesis*, 1981, 892; K. Takagi, *Chem. Lett.*, 1987, 2221; V. Percec, J.-Y. Bae and D. H. Hill, *J. Org. Chem.*, 1995, **60**, 6895; C. Millois and P. Diaz, *Org. Lett.*, 2000, **2**, 1705.
- P. S. Herradura, K. A. Pendola and R. K. Guy, *Org. Lett.*, 2000, **2**, 2019; C. Palomo, M. Oiarbide, R. Lopez and E. Gomez-Bengoia, *Tetrahedron Lett.*, 2000, **41**, 1283; C. G. Bates, R. K. Gujadhur and D. Venkataraman, *Org. Lett.*, 2002, **4**, 2803; F. Y. Kwong and S. L. Buchwald, *Org. Lett.*, 2002, **4**, 3517; C. Savarin, J. Srogl and L. S. Liebeskind, *Org. Lett.*, 2002, **4**, 4309; Y.-J. Wu and H. He, *Synlett*, 2003, 1789; C. G. Bates, P. Saejueng, M. Q. Doherty and D. Venkataraman, *Org. Lett.*, 2004, **6**, 5005; W. Deng, Y. Zou, Y.-F. Wang, L. Liu and Q.-X. Guo, *Synlett*, 2004, 1254; Y.-J. Chen and H.-H. Chen, *Org. Lett.*, 2006, **8**, 5609; D. Zhu, L. Xu, F. Wu and B. Wan, *Tetrahedron Lett.*, 2006, **47**, 5781; L. Rout, T. K. Sen and T. Punniyamurthy, *Angew. Chem., Int. Ed.*, 2007, **46**, 5583; X. Lu and W. Bao, *J. Org. Chem.*, 2007, **72**, 3863; H. Zhang, W. Cao and D. Ma, *Synth. Commun.*, 2007, **37**, 25; M. Carril, R. SanMartin, E. Dominguez and I. Tellitu, *Chem.-Eur. J.*, 2007, **13**, 5100; L. Rout, P. Saha, S. Jammi and T. Punniyamurthy, *Eur. J. Org. Chem.*, 2008, 640.
- Y.-C. Wong, T. T. Jayanth and C.-H. Cheng, *Org. Lett.*, 2006, **8**, 5613.
- A. Correa, M. Carril and C. Bolm, *Angew. Chem., Int. Ed.*, 2008, **47**, 2880.
- For reviews see: C. J. Li, *Chem. Rev.*, 1993, **93**, 2023; G. Papadogiannakis and R. A. Sheldon, *New J. Chem.*, 1996, **20**, 175; B. Cornils, *J. Mol. Catal. A: Chem.*, 1999, **143**, 1; J. P. Genet and M. Savignac, *J. Organomet. Chem.*, 1999, **576**, 305; *Synthesis Methods in Organometallic and Inorganic Chemistry*, ed. W. A. Herrmann, Enke, Stuttgart, 2000; *Aqueous-Phase Organometallic Catalysis*, ed. B. Cornils and W. A. Herrmann, Wiley-VCH, Weinheim, Germany, 2004; C.-J. Li, and T.-H. Chan, *Organic Reactions in Aqueous Media*, John Wiley & Sons, New York, 1997; *Organic Synthesis in Water*, ed. P. A. Grieco, Blackie Academic and Professional, London, 1998; N. E. Leadbeater, *Chem. Commun.*, 2005, 2881; C. J. Li, *Chem. Rev.*, 2005, **105**, 3095; C. J. Li and L. Chen, *Chem. Soc. Rev.*, 2006, **35**, 68; I. T. Horvath and P. T. Anastas, *Chem. Rev.*, 2007, **107**, 2167; D. Dallinger and C. O. Kappe, *Chem. Rev.*, 2007, **107**, 2563.
- W.-Y. Wu, S.-N. Chen and F.-Y. Tsai, *Tetrahedron Lett.*, 2006, **47**, 9267; S.-N. Chen, W.-Y. Wu and F.-Y. Tsai, *Tetrahedron*, 2008, **64**, 8164.
- Y.-H. Wang and F.-Y. Tsai, *Chem. Lett.*, 2007, 1492.
- H. M. Meshram and R. Kache, *Synth. Commun.*, 1997, **27**, 2403; N. Iranpoor and B. Zeynizadeh, *Synthesis*, 1999, 49.

Study on Rh(I)-catalyzed cycloisomerization of dienes with alkenes in ionic liquids: effect of the structure of ILs on catalyst recyclability

Yoshihiro Oonishi, Akira Saito and Yoshihiro Sato*

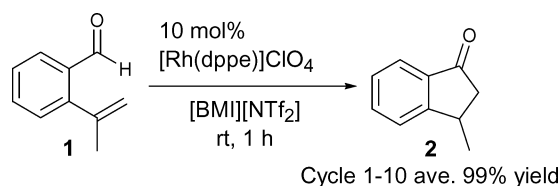
Received 22nd October 2008, Accepted 19th January 2009

First published as an Advance Article on the web 27th January 2009

DOI: 10.1039/b818725h

A Rh(I)-catalyzed cycloisomerization of dienes with alkenes using ionic liquids (ILs) as reaction media was investigated. In contrast to the hydroacylation promoted by the same cationic Rh(I) catalyst, the structure of ILs strongly affected the recyclability of the catalyst in this cycloisomerization, and a [BDMI (1-butyl-2,3-dimethyl imidazolium)]⁺-based IL was more effective than a [BMI (1-butyl-3-methyl imidazolium)]⁺-based one. It has also been proven that the addition of 2,2,2-trifluoroethanol (TFE) to the reaction mixture prevented the loss of reactivity of the catalyst, and the IL recovered after the reaction under the present conditions could be used repeatedly.

Recently, ionic liquids (ILs) have been widely used as environmentally benign solvents to replace common organic reaction media.¹ ILs are known to be miscible with polar organic solvents, such as alcohols, but non-miscible with water and less-polar organic solvents such as aliphatic or aromatic hydrocarbons. This property of ILs allows for easy separation of the catalyst and organic compounds by simple phase separation and recycling of the catalyst remaining in ILs. Many reactions catalyzed by transition metal complexes using ILs have been investigated, and efficient recyclability of the catalyst has been shown in some cases.¹ In this context, we have developed a cationic Rh(I)-catalyzed intramolecular hydroacylation in ILs in which recycling of the catalyst has been realized without loss of catalytic activity (Scheme 1).²



Scheme 1

We have also found a novel Rh(I)-catalyzed cycloisomerization between dienes and alkenes.^{3,4} This reaction was originally developed as a reaction proceeding in dichloroethane by the use of the same cationic Rh(I) catalyst as that used in the above-mentioned hydroacylation.³ Thus, we decided to examine this cycloisomerization in ILs as reaction media with the aim of developing environmentally benign processes.⁵

Table 1 Rh(I)-catalyzed cycloisomerization in various ILs

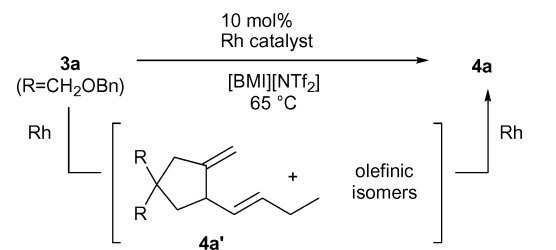
Run	Solvent	Time/h	Yield (%)
1	ClCH ₂ CH ₂ Cl	1.5	85
2	[BMI][BF ₄]	3	96
3	[BMI][PF ₆]	120	80
4	[BMI][NTf ₂]	2	98
5	[BDMI][BF ₄]	45	96
6	[BDMI][PF ₆]	72	— ^a
7	[BDMI][NTf ₂]	4	88

^a Complex mixture.

Initially, the cycloisomerization of **3a**³ using a cationic Rh(I) complex, [Rh(dppe)]ClO₄ (dppe = 1,2-bis(diphenylphosphanyl)ethane) generated *in situ* from [Rh(nbd)(dppe)]ClO₄ (nbd = norbornadiene) under an atmosphere of hydrogen,⁶ in various ILs⁷ was investigated. As a control experiment, the cyclization of **3a** was carried out in dichloroethane at 65 °C in the presence of 10 mol% [Rh(dppe)]ClO₄, and cyclic compound **4a**³ was obtained in 85% yield. In reactions using various ILs based on the butylmethylimidazolium cation [BMI]⁺ (runs 2–4), it was found that the cyclopentene derivative **4a** was obtained in high yield in each reaction, and the reaction in [BMI][NTf₂] showed the best result in the reactions using [BMI]⁺-based ILs. On the other hand, in the case of ILs based on the butyldimethylimidazolium cation [BDMI]⁺, the reaction time varied depending on the counter anion of the BDMI. Although the reaction in [BDMI][BF₄] was slow, the cyclized product **4a** was obtained in 96% yield after 45 hours (run 5). On the other hand, the reaction using [BDMI][PF₆] gave a complex mixture containing the desired compound **4a** (run 6), and the reaction in [BDMI][NTf₂] proceeded smoothly, giving **4a** in 88% yield (run 7) (Table 1).

These results indicated that the catalytic activity in this cycloisomerization using ILs as reaction media is strongly affected by the structure of the ILs and that [BMI][NTf₂] is the most effective IL in this cycloisomerization. It should be noted that [BMI][NTf₂] was also the most effective IL in the above-mentioned hydroacylation catalyzed by the same cationic Rh(I) complex.² Thus, we turned our attention to recycling of the IL containing the cationic Rh(I) complex (Table 2). After the reaction of **3a** had been completed, the product **4a**

Faculty of Pharmaceutical Sciences, Hokkaido University, Sapporo, 060-0812, Japan. E-mail: biyo@pharm.hokudai.ac.jp; Fax: +81 11 7064982; Tel: +81 11 7064982

Table 2 Recycling of IL containing Rh(I) catalyst using [BMI][NTf₂]


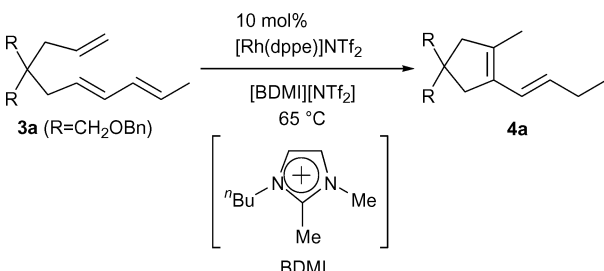
Catalyst	Cycle	Time/h	Yield (%)
[Rh(dppe)]ClO ₄	1	3	95
	2	3	92
	3	5	93
	4	48	44 ^a
[Rh(dppe)]NTf ₂	1	2	96
	2	2	95
	3	2	94
	4	2	91
	5	6	77 ^a

^a Mixture of cyclic compounds.

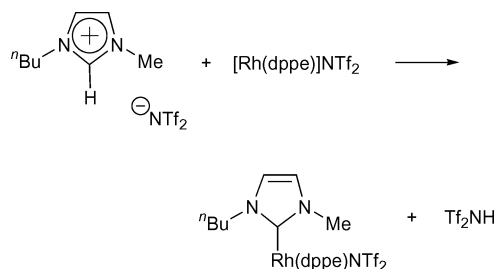
was extracted from the reaction media with Et₂O, and the remaining [BMI][NTf₂] phase containing the cationic Rh(I) complex was dried under reduced pressure and reused without further treatment. In the reaction using [Rh(dppe)]ClO₄ as a catalyst, the reaction could be repeated 3 times. However, in the 4th cycle, the cycloisomerization of **3a** was not completed and a complex mixture containing the cyclic compound **4a'** was obtained. These results indicated that recyclability of the catalyst in this cycloisomerization was less than that in the above-mentioned hydroacylation² despite the fact that these reactions were carried out in the same IL, [BMI][NTf₂], using the same cationic Rh(I) catalyst.

It was possible that the exchange of the counter anion of [Rh(dppe)]ClO₄ from ClO₄⁻ to NTf₂⁻ from [BMI][NTf₂] occurred to generate [Rh(dppe)]NTf₂, which would be less active than [Rh(dppe)]ClO₄. To examine this possibility, [Rh(dppe)]NTf₂ was prepared, and cyclization of **3a** using 10 mol% [Rh(dppe)]NTf₂ in [BMI][NTf₂] was carried out under the same conditions. It was found that the reaction proceeded smoothly, giving the cyclic compound **4a** in 96% yield. Furthermore, the catalyst seemed to be more active than [Rh(dppe)]ClO₄ and could be recycled 4 times without loss of activity. On the other hand, cycloisomerization of **3a** using [BDMI][NTf₂], having a methyl group on the C-2 position, was also investigated (Table 3). Interestingly, in the case of the reaction in [BDMI]⁺-based ILs, the IL containing the cationic Rh(I) catalyst could be recycled 8 times without significant loss of catalytic activity.

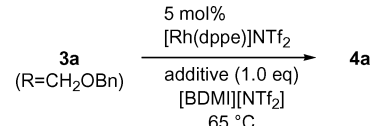
It was thought that the different recyclability in the reaction in the [BMI]⁺-based IL and in the [BDMI]⁺-based one is due to the formation of an Rh(I)-NHC complex under the reaction conditions. Thus, in the reaction in the [BMI]⁺-based IL, an NHC species would be generated from the imidazolium part. The NHC species would act as a ligand of the Rh center to produce an Rh(I)-NHC complex, which might be inactive in the cycloisomerization (Scheme 2).⁸

Table 3 Recycling of IL containing Rh(I) catalyst using [BDMI][NTf₂]


Cycle	Time/h	Yield (%)
1	4	99
2	4	98
3	4	97
4	4	96
5	4	95
6	4	96
7	4	94
8	5	82

**Scheme 2**

When the amount of [Rh(dppe)]NTf₂ catalyst was reduced to 5 mol% in the case of cycloisomerization of **3a** in [BDMI][NTf₂], the catalyst could be recycled 4 times without loss of the activity (Table 4). However, the 5th cycle reaction was not completed and

Table 4 Additive effect in recycling of IL containing Rh(I) catalyst


Additive	Cycle	Time/h	Yield (%)
None	1	4	97
	2	4	97
	3	5	96
	4	6	84
	5	24	47 ^a
TFE	1	3	99
	2	3	99
	3	3	97
	4	3	98
	5	3	99
	6	3	98
	7	6	98
	8	24	64 ^a

^a Mixture of cyclic compounds.

Table 5 Cycloisomerization of various substrates in [BDMI][NTf₂]

3 (R=CH₂OBn) $\xrightarrow[100\text{ }^\circ\text{C}]{\text{5 mol\% [Rh(dppe)]NTf}_2, \text{TFE (1.0 eq), [BDMI][NTf}_2]}$ 4

Substrate	Product	Cycle	Time/h	Yield (%)
 3b	 4b	1	1	94
		2	4	99
		3	4	99
		4	4	99
 3c	 4c	1	1	96
		2	4	98
		3	6	> 99
		4	10	> 99
 3d ^a	 4d	1	2	97
		2	4	98
		3	48	98

4e

^a The reaction was carried out using 10 mol% of Rh(I) catalyst at 65 °C.

a mixture of the cyclized products was obtained. On the other hand, it was found that the addition of 2,2,2-trifluoroethanol (TFE)⁹ to the reaction mixture prevented the loss of activity of the catalyst, and the recycling could be extended up to 7 times.

Having established the cycloisomerization in ILs, Rh(I)-catalyzed cycloisomerization of various substrates **3b–3d**³ [BDMI][NTf₂] was investigated (Table 5). In all cases using ILs, the cycloisomerization proceeded smoothly to give the desired compound **4b–4d**³ in higher yield than that in dichloroethane, and the catalyst could be reused at least 3 times. Noteworthy, the cyclization of **3d** selectively afforded the 6-membered ring **4d** in almost quantitative yield, while the 5-membered **4e** was produced along with **4d** in dichloroethane as a reaction medium.¹⁰

In summary, we have succeeded for the first time in developing Rh(I)-catalyzed cycloisomerization of dienes with alkenes using ILs as reaction media. In this reaction, in contrast to the hydroacylation promoted by the same catalyst, the structure of ILs strongly affected the recyclability of the catalyst, and a [BDMI]⁺-based IL was more effective than a [BMI]⁺-based one, in which a Rh-NHC complex would be formed from the imidazolium cation part. It has been proven that the addition of TFE to the reaction mixture prevented the loss of reactivity of the catalyst, and the IL recovered after the reaction under the present conditions could be used repeatedly. Further studies, including a study to confirm the formation of Rh-NHC species in the reaction in a [BMI]⁺-based IL, are now under way.

Experimental

Typical procedure for recycling of the IL containing [Rh(dppe)]NTf₂ in the presence of 2,2,2-trifluoroethanol (TFE) (Table 4)

A solution of [Rh(nbd)(dppe)]NTf₂ (14.0 mg, 0.016 mmol, 5 mol%) in [BDMI][NTf₂] (3.2 mL) was stirred under H₂ atmosphere at room temperature for 1 h. The reaction vessel was

flushed with argon gas, and to the reaction mixture was added a solution of **3a** (120.5 mg, 0.32 mmol) in Et₂O (1 mL). After removal of Et₂O under vacuum, 2,2,2-trifluoroethanol (TFE) (23.3 μL, 0.32 mmol) was added, and the reaction mixture was stirred at 65 °C for 3 h. The IL layer was extracted with Et₂O (5 mL × 3 times), and the combined Et₂O solution was concentrated. After removal of the solvent, the crude product was purified by filtration through a pad of silica gel eluting with Et₂O to give **4a** (118.7 mg, 99%) as a colorless oil. The IL layer that remained after extraction was dried under vacuum and reused for the next cycle.

Acknowledgements

This work was financially supported by Grant-in-Aids for Young Scientist (B) (No. 20790003) and for Scientific Research (B) (No. 19390001) from the Japan Society for the Promotion of Science (JSPS).

Notes and references

- (a) For reviews see: T. Welton, *Chem. Rev.*, 1999, **99**, 2071; (b) P. Wasserscheid and W. Keim, *Angew. Chem., Int. Ed.*, 2000, **39**, 3772; (c) R. Sheldon, *Chem. Commun.*, 2001, 2399; (d) J. S. Wilkes, *Green Chem.*, 2002, **4**, 73; (e) J. Dupont, R. F. de Souza and P. A. Z. Suarez, *Chem. Rev.*, 2002, **102**, 3667; (f) *Ionic Liquids in Synthesis*, ed. P. Wasserscheid and T. Welton, Wiley-VCH, Weinheim, 2003; (g) T. Welton, *Coord. Chem. Rev.*, 2004, **248**, 2459; (h) P. J. Dyson and T. J. Geldbach, *Metal Catalysed Reactions in Ionic Liquids*, Springer, Dordrecht, 2005.
- Y. Oonishi, J. Ogura and Y. Sato, *Tetrahedron Lett.*, 2007, **48**, 7505.
- Y. Sato, Y. Oonishi and M. Mori, *Organometallics*, 2003, **22**, 30.
- For a review of Rh(I)-catalyzed cycloisomerizations, see: *Modern Rhodium-Catalyzed Organic Reactions*, ed. P. A. Evans, Wiley-VCH, Weinheim, 2005.
- (a) For examples of palladium or ruthenium-catalyzed cycloisomerization of α,ω-dienes in ILs, see: A. Corma, H. García and A. Leyva, *J. Organomet. Chem.*, 2005, **690**, 3529; (b) X. Miao, J. Fender-Kubis, C. Fischmeister, J. Pernak and P. H. Dixneuf, *Tetrahedron*, 2008, **64**, 3687.
- D. P. Fairlie and B. Bosnich, *Organometallics*, 1988, **7**, 936.

- 7 (a) For preparation of ILs, see: J. G. Huddleston, A. E. Visser, W. M. Reichert, H. D. Willauer, G. A. Broker and R. D. Rogers, *Green Chem.*, 2001, **3**, 156; (b) J. Dupont, C. S. Consorti, P. A. Z. Suarez and R. F. de Souza, *Org. Synth.*, 2002, **79**, 236.
- 8 (a) For examples of the generation of metal-NHC complexes derived from ILs, see: L. Xu, W. Chen and J. Xiao, *Organometallics*, 2000, **19**, 1123; (b) C. J. Mathews, P. J. Smith, T. Welton, A. J. P. White and D. J. Williams, *Organometallics*, 2001, **20**, 3848 and references therein.
- 9 The Rh(I)-catalyzed cyclization was accelerated in TFE, see: R. S. Jolly, G. Luedtke, D. Sheehan and T. Livinghouse, *J. Am. Chem. Soc.*, 1990, **112**, 4965.
- 10 The cycloisomerization of **3d** in dichloroethane gave the 6-membered ring compound **4d** in 60% yield along with the 5-membered ring compound **4e** in 13%. See ref 3.

A stable biomimetic redox catalyst obtained by the enzyme catalyzed amidation of iron porphyrin†

Subhalakshmi Nagarajan,^{a,d} Ramaswamy Nagarajan,^c Ferdinando Bruno,^e Lynne A. Samuelson^e and Jayant Kumar^{b,d}

Received 8th August 2008, Accepted 13th November 2008

First published as an Advance Article on the web 18th December 2008

DOI: 10.1039/b813823k

Hematin, a hydroxyferritoporphyrin, is the more stable oxidized form of the free heme. The use of hematin as a catalyst for oxidative polymerization reactions has been restricted due to its limited aqueous solubility at low pH conditions. While there have been reports on the functionalization of hematin with poly (ethylene glycol), the esters formed are not very stable at low pH conditions. We report here the design and synthesis of hematin tethered with methoxypolyethylene glycol amine chains as a novel stable biomimetic catalyst. This one step amidation was performed under solventless conditions and catalyzed by a hydrolase (Novozyme-435). The amidation greatly improved the stability of hematin at low pH. Further, this catalyst was soluble in water and was able to catalyze the polymerization of aniline based monomers. The amide functionalized hematin serves as a robust cost-effective alternative to HRP, active even at lower pH conditions.

Introduction

In recent years, enzymatic polymerization has been investigated as a possible environmentally friendly route to the synthesis of polyphenols/polyanilines. Oxidoreductases such as Horseradish Peroxidase (HRP), Soybean Peroxidase (SBP) obtained from natural & renewable sources have been known to catalyze the polymerization of phenol^{1,2} and aniline³ based monomers under benign conditions in aqueous and mixed solvent systems. It has been reported that HRP catalyzes the oxidative coupling/polymerization of aniline and phenol based monomer derivatives to produce conjugated polymers with interesting properties. These biocatalytic reactions can be carried out in the presence of polyelectrolyte templates or in organized media such as micelles. The polyelectrolyte templates/micelles help in aligning the monomers through preferred electrostatic interactions or hydrogen bonding, and by providing a unique local environment that favors the formation of well-defined polymers. This template assisted enzymatic approach has overcome many of the limitations of traditional chemical methods of synthesis of polyaniline and polyphenol. While the advantages of

enzyme-catalyzed synthesis are numerous, there are also certain drawbacks associated with it.

The high cost of enzymes, low activity and poor stability of HRP at low pH is a major concern. In this context, metalloporphyrins have been studied both as models for cytochrome P-450 and as important catalysts for oxidative polymerization reactions.⁴

The heme prosthetic group is the active site in a number of metalloproteins and enzymes and has been reported to play a key role in electron transfer, oxygen transport and catalytic reactions.⁵ Interestingly, some metalloporphyrins have been shown to exhibit similar catalytic characteristics as that of peroxidases.⁶ Hence, there have been several reports on enhancing the activity of the porphyrins and trying to mimic naturally occurring peroxidases. The peroxidase-like activity of tetrakis(carboxyphenyl)porphyrin with different central metal ions has been evaluated.⁷ Metalloporphyrins of manganese, cobalt and iron were found to be the most efficient catalysts.⁸ Saito *et al.*⁹ reported an artificial metalloporphyrin and its ability to mimic peroxidases.

Among the iron containing metalloporphyrins, hemin has been shown to catalyze the oxidative polymerization of phenols.¹⁰ Nevertheless, the catalytic activity is still low.¹¹ Hemin has been modified by attaching pendant groups such as β -cyclodextrin.¹² The activity of the complex was still not appreciable.¹³ Wang *et al.*¹⁴ have reported the synthesis of a peroxidase mimic by modifying hemin. However the peroxidase mimic was not active below pH 9. Iron(III) tetra (p-sulfonatophenyl)porphyrin [(Fe(III)TPPS)] has been synthesized and found to oxidatively catalyze the polymerization of aniline.¹⁵ But, the synthetic route to prepare the Fe(III)TPPS is complex and involves multiple steps and purification. Hemoglobin, the major heme protein of red blood cells has by itself been shown to possess catalytic activity.¹⁶

^aDepartment of Chemistry, University of Massachusetts, Lowell, MA 01854, USA

^bDepartment of Physics, University of Massachusetts, Lowell, MA 01854, USA

^cDepartment of Plastics Engineering, University of Massachusetts, Lowell, MA 01854, USA. E-mail: Ramaswamy_Nagarajan@uml.edu; Fax: +1 978 458 9571; Tel: +1 978 934 3454

^dCenter for Advanced Materials, University of Massachusetts, Lowell, MA 01854, USA

^eU.S Army Natick Soldier Research, Development and Engineering Center, Natick, MA 01796, USA

† Electronic supplementary information (ESI) available: MALDI-TOF MS spectrum for the amidated hematin. See DOI: 10.1039/b813823k

Hematin, a hydroxy ferriprotoporphyrin, is also considered to be another promising biomimetic alternative to HRP. It is inexpensive and catalyzes the polymerization of a wide range of phenolic substrates.¹⁷ Hematin is an Fe(III) complex with a structure similar to the prosthetic iron protoporphyrin IX in HRP. One of the axial coordination sites of Fe(III) is occupied by a hydroxide ion instead of a histidine residue in HRP. Unlike peroxidases, hematin does not contain a protein environment and hence it is stable in organic solvents as well as high pH conditions. However hematin is water soluble only at high pH and ineffective for use as a catalyst at low pH aqueous conditions typically required for oxidative polymerization. To address this, we designed and synthesized a modified hematin [hematin tethered with poly (ethylene glycol) (PEG) groups].¹⁸ This PEG-hematin was soluble in water and was able to catalyze the polymerization of a wide variety of aniline and phenol monomers at a rate comparable to native HRP. However the pegylated hematin, being an ester, is also prone to hydrolysis at low pH conditions which are typically required for the oxidative polymerization of monomers like Ethylenedioxy Thiophene (EDOT). In order to overcome this limitation, we have modified hematin with Methoxypolyethylene glycol amine (MPEGNH₂). This amidation was performed in a single step using a lipase as a catalyst without the use of solvents. Novozyme-435 has been utilized as a catalyst for the amidation. The amide functionalized hematin was water-soluble, stable and catalytically active at a low pH. Initial results suggest that the amidated hematin could oxidatively catalyze the polymerization of aniline.

Results and discussion

As mentioned previously, although the PEG-hematin (ester) was able to catalyze the polymerization of a wide range of monomers, the pegylated ester by itself was not very stable at lower pH conditions. In highly acidic conditions, the ester bond between hematin and PEG chains is cleaved. As seen in Fig. 1, the pegylated hematin is not very stable at low pH. When a few drops of concentrated hydrochloric acid were added, the absorbance dropped drastically and the hematin precipitated out of the solution.

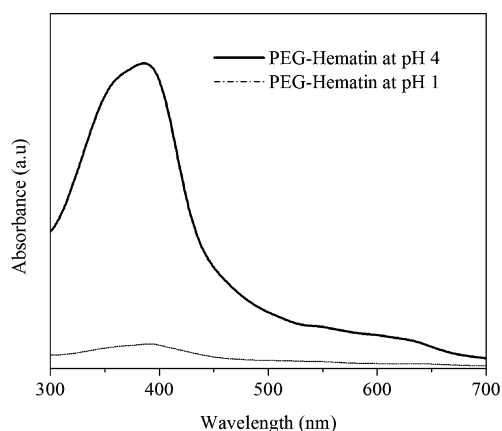


Fig. 1 Stability of the pegylated hematin at low pH conditions.

The primary goal of this research is to overcome this limitation by functionalizing hematin with polyethylene glycol containing a terminal amino group to form a more stable amide linkage. Lipases have been known to catalyze the amide formation reactions between acids and amines.¹⁹ We have used Novozyme-435 as a catalyst for the amidation of hematin as shown in Fig. 2. The reaction is performed in bulk at 85–87 °C and does not involve the use of solvents. Use of a mono functionalized PEG amine offers better control over the functionalization. The product formed can be separated from the starting materials by simple filtration and dialysis.

The resulting hematin functionalized with methoxypolyoxyethylene glycol amine was found to be water-soluble and is also soluble in organic solvents like DMF.

The molecular weight of the hematin tethered to poly(ethylene glycol amine) was also confirmed by Gel Permeation Chromatography (GPC) analysis. GPC confirms functionalization of the hematin with mPEG amine chains ($M_n \sim 10,711$ Da) indicating both the acid groups of the hematin have been functionalized.

GPC also indicates the small amounts of monofunctionalized hematin/unreacted PEG. However, for the intended use of this compound as a biomimetic catalyst, the presence of small

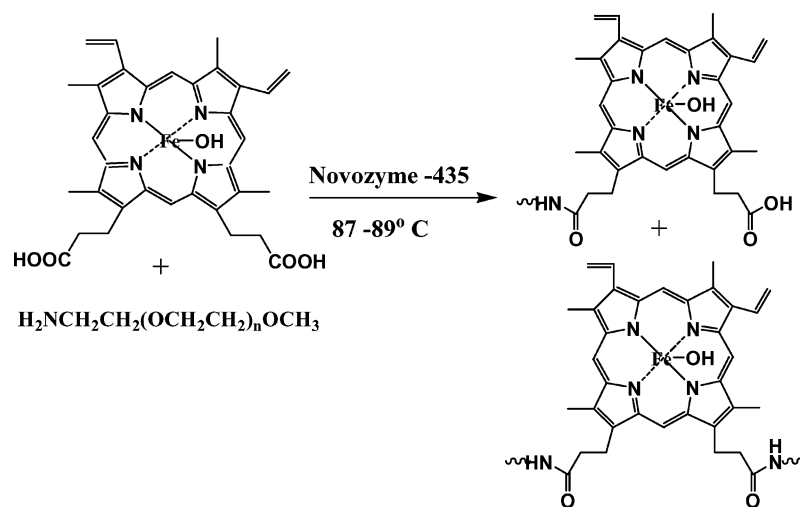


Fig. 2 Scheme for the amidation of hematin catalyzed by Novozyme-435.

amounts of unreacted PEG will not affect the efficacy of these compounds. MALDI-TOF results also confirm the presence of a bifunctionalized hematin (see ESI†).

The spectral changes of the infrared spectra in the carbonyl region of hematin and amidated hematin are indicative of the formation of an amide linkage. In particular, a strong band at 1712 cm^{-1} observed in the case of hematin shifts to 1684 cm^{-1} indicating the conversion of the carboxylic group into an amide. We attempted to further confirm the structure of the amidated hematin using NMR. The high paramagnetic resonance field of the Fe(III) present in the amidated hematin hampered unambiguous assignment of peaks in the NMR spectrum.

In order to assess the stability of the amidated hematin, the amide was dissolved in pH 4 phosphate buffer and the pH of the solution was lowered to pH 1. The UV-visible spectra were recorded two and five days after the solution was kept at pH 1. As seen in Fig. 3, the amide functionalized hematin is very stable even after 5 days (the Soret band of the hematin remains virtually unchanged) and the amide did not precipitate out of the solution.

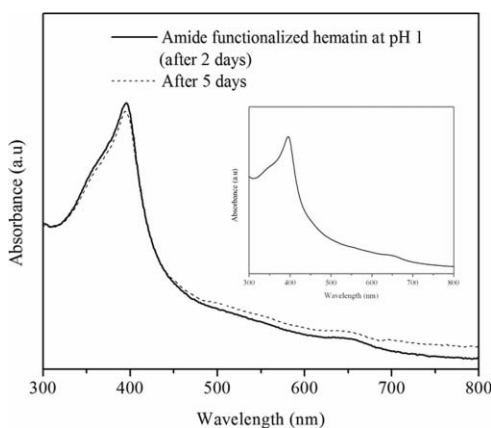


Fig. 3 UV-visible spectra for amidated hematin at pH 1 and pH 4 (inset).

The catalytic activity of peroxidases such as HRP is evaluated using the peroxidase assay originally developed by Willstaeter *et al.*^{20,21} The assay measures the rate of oxidation of pyrogallol to purpurogallin when catalysed by HRP. Specific activity of HRP is often expressed in terms of pyrogallol units. One pyrogallol unit will form 1.0 mg purpurogallin in 20 sec at pH 6.0 at $20\text{ }^{\circ}\text{C}$.

Since the catalytic center in HRP is an iron containing porphyrin, the peroxidase assay can also be extended to iron porphyrins like hematin. In addition, the pyrogallol assay has been used previously for studying the catalytic activity of different iron containing porphyrins.²²

Hematin was dissolved in water at pH 10 and then the pH was brought down gradually to a pH of 1 by addition of concentrated hydrochloric acid. Concentrations of hematin and the amidated hematin were chosen such that the optical densities were similar at the chosen concentration. In order to verify if the amidated hematin retained its catalytic activity at low pH, the enzymatic assay was performed at pH 1. The formation of purpurogallin was monitored at 420 nm for 8 minutes. As seen in Fig. 4, the amide functionalized hematin was active and could catalyze the transformation of pyrogallol to purpurogallin. In

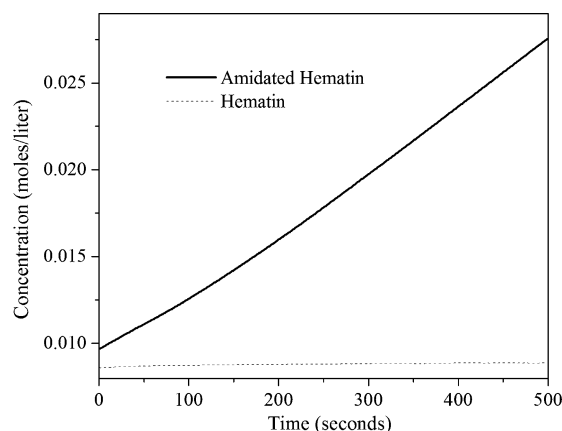


Fig. 4 Comparison of the time dependent formation of purpurogallin (moles/litre) catalyzed by hematin and amidated hematin at pH 1.

contrast, hematin by itself could not catalyze the formation of purpurogallin under identical conditions due to its poor solubility at this pH.

HRP has been modified with PEG and the pegylated HRP was found to be active in a number of organic solvents.²³ However the activity in aqueous solutions, determined using the peroxidase assay, was found to decrease with decrease in pH with optimal activity²⁴ seen at a pH around 10. Since the pegylated HRP is not active at low pH conditions, the activity of the amidated hematin was not compared with the pegylated HRP.

The amidated hematin was also effective in catalyzing the polymerization of aniline in the presence of sulfonated polystyrene (SPS). The UV-visible spectra of the polyaniline (PANI)/SPS complex formed at pH 4 after initiation of the polymerization is shown in Fig. 5. The UV-visible spectra showed the presence of polaron absorption bands at 400 nm and 800–1000 nm. This is consistent with earlier reports which have observed similar features for the PANI/SPS complex.²⁵

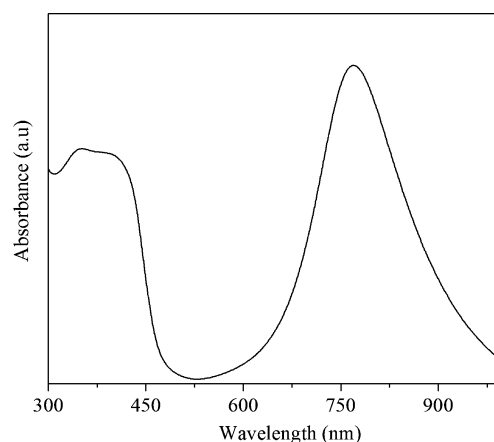


Fig. 5 UV Visible spectra for polymerization of aniline at pH 4 in the presence of SPS catalyzed by amide functionalized hematin.

The reversible redox behavior of the polyaniline was studied by dedoping and doping using base (NaOH) and acid (HCl), respectively, and the results are presented in fig. 6. The UV-visible spectra of the PANI/SPS obtained at pH 4 show some similarity to the spectra reported earlier for the SPS/PANI complex.³

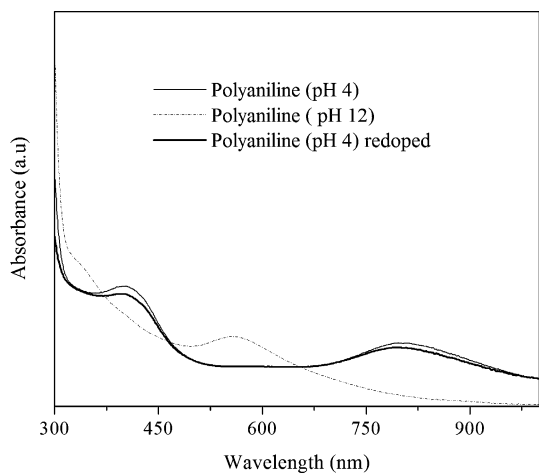


Fig. 6 UV-visible spectra of polyaniline/SPS complex during dedoping and redoping.

The polaron band at 407 nm and 800 nm confirms the presence of PANI in the doped state. When the pH of the solution is increased to 12, a strong absorption at 550–600 nm is seen due to the quinoid rings. The PANI can be redoped back to pH 4. Studies are underway to further characterize the polyaniline synthesized using amidated hematin.

The thermal stability of the catalyst was analyzed using thermal gravimetric analysis (TGA).

Fig. 7 shows the TGA for the MPEGNH₂ and the amide functionalized hematin. The free amine is known to start degrading at around 220 °C and is completely degraded by around 420 °C. In comparison, the amidated hematin is much more stable with over 20% remaining at 700 °C.

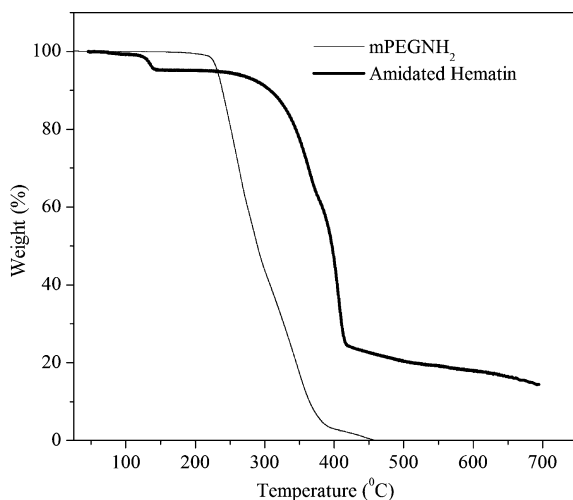


Fig. 7 TGA analysis of amidated hematin and mono-methoxy poly(ethylene glycol) amine [mPEGNH₂].

Conclusions

Hematin was modified through a one-step enzyme catalyzed reaction. The hematin functionalized amide exhibited better stability than PEG-hematin especially at low pH conditions. The modified hematin also serves as a catalyst for the polymerization of aniline. The enzymatically modified hematin can serve as a

versatile, more stable catalyst for the oxidative polymerization of a wider range of monomers like pyrrole and EDOT. This opens the possibility of using this catalyst at wider ranges of pH conditions, thus carrying out reactions that may not be possible using peroxidases. In addition, the improved stability of this amide functionalized hematin widens the scope for recycling thus making the catalyst more cost-effective.

Experimental section

Materials and methods

Hematin, aniline and sodium polystyrene sulfonate (SPS) (MW 70 kD) were purchased from Sigma Chemical Co. (St. Louis, MO) and used as received. Methoxypolyethylene glycol amine ($M_n \sim 5000$) was purchased from Aldrich, Allentown. Novozyme-435, an immobilized enzyme was a gift from Novozymes, Denmark. and was dried over P₂O₅ under vacuum prior to use. The hydrogen peroxide was diluted to 0.3% (in deionized water), and this solution was used for polymerization. All other chemicals were of reagent grade or better.

Synthesis of amidated hematin

Hematin (25mg, 0.03 mmol) and mono-methoxy poly(ethylene glycol) amine [mPEG-amine] (0.78 g, 0.15 mmol) were placed in a round-bottom flask and dried under vacuum at 87–89 °C. The enzyme (15% by weight with respect to reactants) was added to the reaction mixture and the reaction flask was placed in a constant temperature oil bath maintained at 87–89 °C under vacuum. The reaction was allowed to proceed for 48 hours. The reaction mixture was poured into water with a pH 3. The unreacted Hematin was filtered off along with the enzyme. The filtrate was dialyzed to remove unreacted [mPEG]. After the completion of dialysis, the product was obtained as a solid by freeze-drying. The gravimetric yield was between 75–78%.

Peroxidase assay

The peroxidase assay was performed based on the procedure provided by Sigma.²⁶ Concentrations of hematin and amidated hematin were chosen such that they have the same optical densities at the chosen concentration. 0.3% hydrogen peroxide was used for the assay. Absorbance was monitored at 420 nm for approximately 8 minutes.

Characterization

UV-visible near-IR spectra were obtained using a Perkin-Elmer Lambda 9 spectrophotometer. FT-IR measurements were carried out using a Perkin-Elmer 1720X series FT-IR spectrophotometer. Thermogravimetric analysis (TGA) was performed using a TA Instrument, Hi-Res 2950 thermogravimetric analyzer. The TGA of all samples was carried out under nitrogen. GPC analysis was carried out on a Agilent GPC with RI detector. GPC analysis was done on a water column calibrated with poly sodium polystyrene-sulfonate and containing 0.01% lithium bromide using a refractive index detector. 8 mg/ml of the amide functionalized with hematin was dissolved in water and a flow rate 1 ml/min was used.

MALDI experiments were done in the linear mode on a Waters MALDI-TOF MS instrument. Dithranol was used as a matrix. 10 mg/ml of the matrix was dissolved in THF: acetonitrile: water (1:1:1) ratio. A few drops of ammonium hydroxide was added to the compound before analysis. The sample and matrix solutions were mixed at 1/1 (v/v) ratio immediately before the analysis. Approximately 2 μ l of the above solution was spotted on a target plate.

References

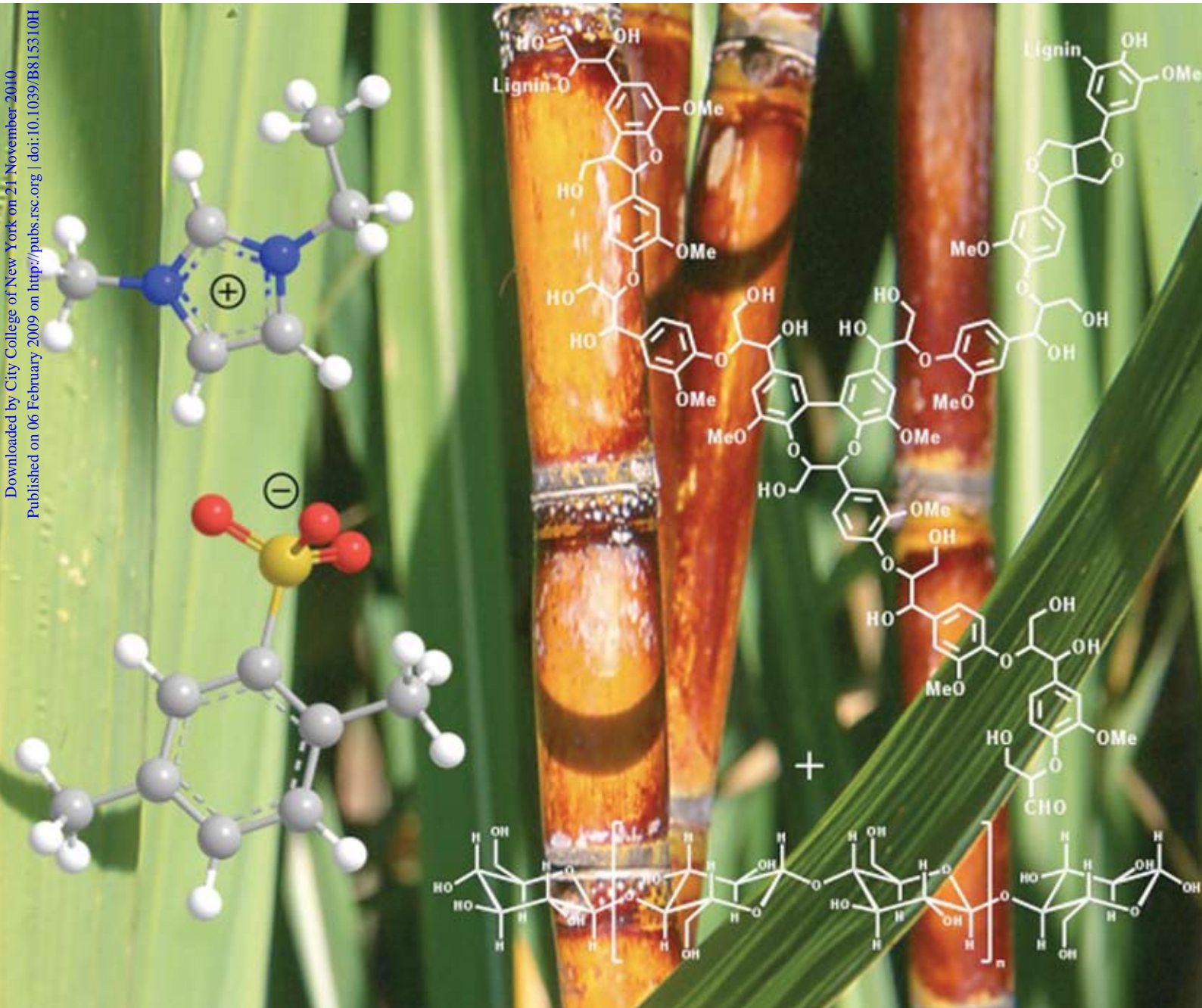
- 1 F. F. Bruno, R. Nagarajan, P. Stenhouse, K. Yang, J. Kumar, S. K. Tripathy and L. A. Samuelson, *J. Macromol. Sci. Part A—Pure Appl. Chem.*, 2001, **A38**(12), 1417–1426.
- 2 F. F. Bruno, S. Nagarajan, R. Nagarajan, J. Kumar and L. A. Samuelson, *J. Macromol. Sci. – Pure Appl. Chem.*, 2005, **42**(11), 1547–1554.
- 3 (a) W. Liu, J. Kumar, S. K. Tripathy, K. J. Senecal and L. A. Samuelson, *J. Am. Chem. Soc.*, 1999, **121**, 71–78; (b) F. F. Bruno, S. Fosey, S. Nagarajan, R. Nagarajan, J. Kumar and L. A. Samuelson, *Biomacromolecules*, 2006, **7**(2), 586–589.
- 4 T. G. Traylor, C. Kim, J. L. Richards, F. Xu and C. L. Perrin, *J. Am. Chem. Soc.*, 1995, **117**, 3468–3474.
- 5 (a) P. R. Ortiz de Montanallo, *Acc. Chem. Res.*, 1987, **20**, 289–294; (b) J. H. Dawson, *Science*, 1988, **240**, 433–439.
- 6 M. Sono, M. P. Roach, E. D. Coulter and J. H. Dawson, *Chem. Rev.*, 1996, **96**, 2841–2887.
- 7 Y. X. Ci, F. Wang and Fresenius, *J. Anal. Chem.*, 1991, **339**, 46–49.
- 8 Y. X. Ci and F. Wang, *Talanta*, 1990, **37**, 1133–1136.
- 9 Y. Saito, S. Nakashima, M. Mifune, J. Odo, Y. Tanaka, M. Chikuma and H. Tanaka, *Anal. Chim. Acta*, 1985, **172**, 285–287.
- 10 M. Akita, D. Tsutsumi, M. Kobayashi and H. Kise, *Biotechnology Letters*, 2001, **23**, 1827–1831.
- 11 K. Zhang, L. Mao and R. Cai, *Talanta*, 2000, **51**, 179–186.
- 12 L. Y. Mao and H. X. Shen, *Chem. J. Chin. Univ.*, 1998, **19**(Suppl.), 442.
- 13 K. Zhang, R. Cai, D. Chen and L. Mao, *Analytica Chimica Acta*, 2000, **413**, 109–113.
- 14 X. Wang, Y. Li and W. Chang, *Analytica Chimica Acta*, 1999, **400**, 135–142.
- 15 M. R. Nabid, R. Sedghi, P. R. Jamaat, N. A. Safari and A. Entezami, *J. Appl. Polym. Sci.*, 2006, **102**, 2929–34.
- 16 H. Xing, Z. Yu-Ying, T. Kai and Z. Guo-Lin, *Synth Met*, 2005, **150**, 1–7.
- 17 J. A. Akkara, J. Wang, D.-P. Yang and K. E. Gonsalves, *Macromolecules*, 2000, **33**, 2377–2382.
- 18 S. Nagarajan, R. Tyagi, R. Nagarajan, J. Kumar, A. C. Watterson, F. F. Bruno and L. A. Samuelson, *J. Macromol. Sci. Part A—Pure Appl. Chem.*, 2008, **45**(11), 952–957.
- 19 R. Irimescu and K. Kato, *Tetrahedron Letters*, 2004, **45**, 523–525.
- 20 R. Willstaetter and A. Stoll, *Liebigs Ann.*, 1918, **416**, 21.
- 21 R. Willstaetter and H. Weber, *Ann. Chem.*, 1926, **449**, 156.
- 22 Q. Wang, Z. Yang, X. Zhang, X. Xiao, C. K. Chang and B. Xu, *Angew. Chem., Int. Ed.*, 2007, **46**, 4285–4289.
- 23 P. A. Mabrouk, *J. Am. Chem. Soc.*, 1995, **117**, 2141–2146.
- 24 F.-Y. Jeng and S.-C. Lin, *Process Biochemistry*, 2006, **41**, 1566–1573.
- 25 S. Stafstrom, J. L. Breadas, A. J. Epstein, H.-S. Woo, D. B. Tanner, W.-S. Huang and A. G. MacDiarmid, *Phys. Rev. Lett.*, 1987, **59**, 1464–1467.
- 26 www.sigmaaldrich.com/img/assets/18160/Peroxidase.pdf.

Green Chemistry

Cutting-edge research for a greener sustainable future

www.rsc.org/greenchem

Volume 11 | Number 4 | April 2009 | Pages 437–592



ISSN 1463-9262

Tan *et al.*
Extraction of lignin from lignocellulose

Harmer *et al.*
Catalytic reactions using super acids in ionic liquids

Weinhold *et al.*
Improving the characterization of chitosan

Walsh *et al.*
Nanostructured membranes based on cellulose nanowhiskers

RSC Publishing

Extraction of lignin from lignocellulose at atmospheric pressure using alkylbenzenesulfonate ionic liquid†

Suzie S. Y. Tan,^{*a,c} Douglas R. MacFarlane,^a Jonathan Upfal,^b Leslie A. Edey,^c William O. S. Doherty,^c Antonio F. Patti,^{a,d} Jennifer M. Pringle^a and Janet L. Scott^a

Received 4th September 2008, Accepted 18th December 2008

First published as an Advance Article on the web 6th February 2009

DOI: 10.1039/b815310h

Lignocellulosic materials are a potentially valuable source of both aromatic compounds *via* the lignin component and sugars from the cellulose and hemicellulose components. However, efficient means of separating and depolymerising the components are required. An ionic liquid mixture containing the 1-ethyl-3-methylimidazolium cation and a mixture of alkylbenzenesulfonates with xylenesulfonate as the main anion was used to extract lignin from sugarcane plant waste at atmospheric pressure and elevated temperatures (170–190 °C). The lignin was recovered from the ionic liquid by precipitation, allowing the ionic liquid to be recycled. An extraction yield exceeding 93% was attained. The lignin produced had a molecular weight of 2220 g/mol after acetylation. The regenerated ionic liquid showed good retention of structure and properties. The other product of the extraction was a cellulose pulp, which can be used in further processing.

Introduction

Lignocellulosic materials have come under intense research scrutiny due to their potential as starting materials for biofuels and other commodity chemicals.^{1–3} Agricultural wastes such as bagasse, the residue from sugarcane processing, are a relatively cheap source of lignin, cellulose and hemicellulose. Lignin is a high molecular weight polymer based on phenylpropane units, and is potentially a renewable source of aromatic compounds if an economic means of extracting and depolymerising it could be developed. The presence of lignin within lignocellulose is also a major barrier to enzymatic hydrolysis of cellulose by cellulases, as well as inhibiting fermentation to form products such as ethanol. Hence its presence diminishes the value of lignocellulosic materials where the carbohydrate component provides the chemical feedstock for conversion to biofuels and commodity chemicals.

In order to fractionate biomass into useful chemicals, there are three general approaches. The first approach involves extracting lignin, usually at high temperature and pressure, leaving a cellulose-rich pulp. The second approach involves mass depolymerisation of the lignocellulose structure *via* even more severe conditions such as the temperatures and pressures used in

gasification, or the use of mineral acids at elevated temperatures to liberate sugars for fermentation. A third approach is the dissolution of cellulose, followed by re-precipitation, for example, using ionic liquids.

In this paper we describe a lignin extraction and partial depolymerisation method that uses a purpose designed ionic liquid. Extracting lignin from lignocellulose using this ionic liquid has several advantages, including reaction at atmospheric pressure, no emission of toxic or odourous gases, capability of recycling the ionic liquid, no requirement for prolonged drying of material and the ability to produce lignin with particular functional groups.

Traditional methods of extracting lignin from lignocellulose consist of a range of industrial processes for the production of papermaking pulp from wood chip and other fibres. These include the widely used kraft process, which accounts for 80% of chemical pulping,⁴ as well as the sulfite, soda, and organosolv processes. There are two main structural changes to lignin involved in chemical pulping, firstly, fragmentation of the lignin macromolecule into smaller parts, and secondly, the introduction of hydrophilic groups.⁵ The lignin fragments are then dissolved and removed. Pulping reactions are exclusively nucleophilic.⁵ The fragmentation reactions occur *via* cleavage of ether groups which are widely present within lignin. Cleavage of ethers produces highly reactive quinone methide or carbocation intermediates, which can then react with the nucleophilic species present, including pulping chemicals. The lignin fragments can also join with other lignin fragments in what are known as condensation reactions to form larger fragments. Lignin condensation reactions are undesirable for lignin removal as the carbon-carbon bonds formed are harder to break than the original ether bonds and the larger lignin fragments are harder to dissolve.

In almost all cases except organic acid pulping, the process requires high pressures and therefore capital intensive plant.

^aSchool of Chemistry and Centre for Green Chemistry, Monash University, Wellington Rd, Clayton, VIC 3800, Australia.
E-mail: suzie.tan@sci.monash.edu.au; Fax: +613 9905 4597;
Tel: +613 9905 4599

^bViridian Chemicals Pty Ltd, 1.2/193 Domain Rd, South Yarra, VIC 3141, Australia

^cSugar Research and Innovation, Queensland University of Technology, GPO Box 2434, Brisbane, QLD 4001, Australia

^dSchool of Applied Sciences and Engineering, Monash University, Churchill, VIC 3842, Australia

† Electronic supplementary information (ESI) available: ¹H NMR spectra of [C₂mim][ABS]. See DOI: 10.1039/b815310h

The high temperature (and therefore high pressure) processing is required in part because the glass transition temperature of lignin is around 150 °C. The main disadvantages associated with the kraft process are pollution and odour problems, high water use and large plant size,⁶ which creates a high cost for transporting lignocellulose. Newer methods of fractionating biomass using phosphoric acid,⁷ or acetic acid and formic acid⁸ under mild conditions have also been reported, but the corrosiveness of the acids is a major drawback and the processes have limitations in terms of energy usage, solvent recovery and ease of product isolation.

A lesser known pulping process, called *hydrotropic* pulping, which was patented by McKee in 1943^{9–11} involves the use of sodium xylenesulfonate (30–40%) in aqueous solution at temperatures between 150 °C and 180 °C, and pressures between 0.4 MPa and 1.4 MPa. As with the traditional pulping methods, the initial step in hydrotropic pulping involves fragmentation of the lignin, followed by solubilisation of the lignin fragments. After reaction at high pressure, the lignin dissolved in the hydrotrope solution is precipitated by dilution with water. Hydrotropic agents for lignin typically contain both polar and non-polar groups which enable them to solubilise the lignin *via* formation of strong ion-dipole bonds with water as well as interacting strongly with the lignin through, for example, π – π interactions.¹² It has also been suggested that they form micelles that envelop the lignin fragments.¹³

Due to their unusual properties and ability to act as solvents and catalysts in a wide variety of reactions, ionic liquids have been recently investigated in a range of biomass processing applications.¹⁴ Interest in using ionic liquids as biomass solvents has so far been centred on the dissolution and processing of pure cellulose using 1-butyl-3-methylimidazolium chloride ([C₄mim][Cl]),^{15,16} 1-allyl-3-methylimidazolium chloride,¹⁷ 1-ethyl-3-methylimidazolium acetate,¹⁸ 1-butyl-3-methylimidazolium acetate,¹⁸ 1-ethyl-3-methylimidazolium methylphosphate,¹⁹ and 1,3-dialkylimidazolium formates.²⁰ The dissolution of cellulose in [C₄mim][Cl] is attributed to disruption of hydrogen bonding and coordination of chloride ions to the hydroxyl groups of cellulose. It requires low moisture contents, typically below 1%, as water interferes by hydrogen bonding to the cellulose hydroxyl groups,¹⁶ or by coordinating to the chloride ions. Dissolution of wood using [C₄mim][Cl] has also been reported.^{21–23} Based on the same mechanism of cellulose dissolution, the dissolution of wood also requires the virtual absence of water, which necessitates extensive drying of the wood, drying of the ionic liquid and reaction under inert atmosphere, as well as small particle size and long dissolution times unless coupled with microwave heating.^{21–23}

Based on the effectiveness of sodium xylenesulfonate as a pulping agent, an ionic liquid which incorporates the xylenesulfonate anion, was designed in our laboratories for lignin extraction.²⁴ 1-Ethyl-3-methylimidazolium [C₂mim] is the cation, and the mixture of anions, which will be referred to as alkylbenzenesulfonate [ABS], is a commercially available mixture mainly made up of isomers of xylenesulfonate (74%) with smaller amounts of ethylbenzenesulfonate (13%), cumenesulfonate (9%) and toluenesulfonate (4%). The main component of [C₂mim][ABS] is shown in Fig. 1.

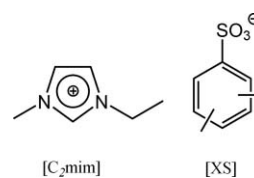


Fig. 1 Ionic liquid 1-ethyl-3-methylimidazolium xylenesulfonate ([C₂mim][XS]).

A more recent study on lignin solubility in ionic liquids has shown that up to 20 wt% kraft wood lignin can be dissolved in 1,3-dimethylimidazolium methylsulfate, 1-butyl-3-methylimidazolium methylsulfate and 1-hexyl-3-methylimidazolium trifluoromethanesulfonate.²⁵ Demonstrating the strong interest in using ionic liquids for lignocellulose processing is the large number of patents which have recently been published on the subject, mostly by BASF.^{26–31} In this paper we present a more extensive study of lignin extraction by the alkylbenzenesulfonate ionic liquid including characterisation of the lignin produced, the cellulose pulp and the recycling of the ionic liquid.

Results and discussion

Lignin was effectively extracted from sugarcane bagasse using the ionic liquid [C₂mim][ABS] at ambient pressure and elevated temperatures (Fig. 2). The initial step in delignification is hydrolytic fragmentation of the large lignin polymer, followed by solubilisation of lignin fragments. Hence the presence of water is important for the extraction of lignin. After steam pretreatment of bagasse, water was present at about 30% in the reaction mixture initially, but Karl-Fischer analysis showed a water content of approximately 2% in the reaction mixture after reaching 185 °C.



Fig. 2 (a) Bagasse (2–3 mm), (b) cellulose pulp, (c) recovered lignin.

As shown in Table 1, lignin extraction increases with increasing temperature from 170 °C to 190 °C. This is confirmed by the decreasing residual lignin content in the cellulose pulp shown in Fig. 3, where the maximum extraction corresponds to a total residual lignin content of 3.0% for reaction at 190 °C for 2 hours. Lignin extraction increases with increasing reaction time from 30 minutes to 120 minutes (Fig. 4) for reaction at 190 °C. In Table 1, the masses of recovered lignin are shown as a percentage of original lignin content in bagasse (21.5% on a dry basis). These percentages do not represent absolute yields due to the presence of other components which were difficult to separate. The maximum lignin extraction corresponds to a recovered lignin mass of 118 wt% of the original lignin content. This higher than theoretical mass may be partially due to the incorporation of the xylenesulfonate anion, as shown by

Table 1 Mass of recovered lignin

Run no	Condition	Mass of recovered lignin ^a (% ± 2)
1.	170 °C, 120 min	67
2.	180 °C, 120 min	78
3.	190 °C, 120 min	118
4.	190 °C, 90 min	97
5.	190 °C, 60 min	96
6.	190 °C, 30 min	67

^a As a percentage of original lignin content, corrected for ash content.

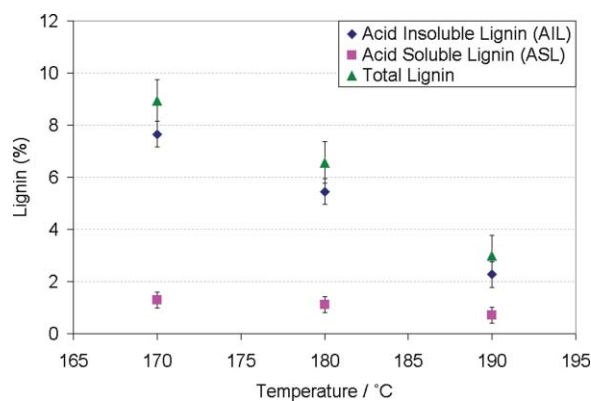


Fig. 3 Residual lignin in cellulose pulp vs. temperature (corrected for ash content).

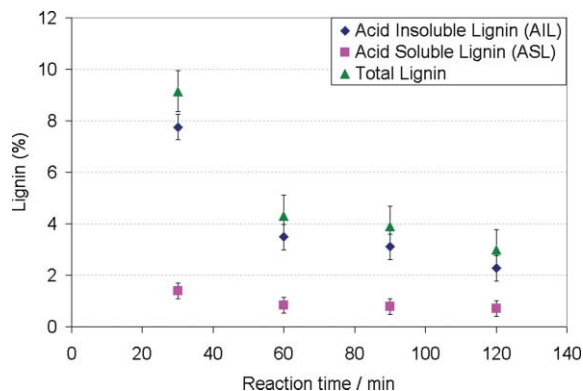


Fig. 4 Residual lignin in cellulose pulp vs. reaction time (corrected for ash content).

elemental analysis. Sulfur was absent in the original bagasse, but was found to be present in the recovered lignin at 1.5 wt% (Table 2). Assuming the sulfur is present as xylenesulfonate, this corresponds to 8.7% xylenesulfonate in the lignin. Subtracting the mass of xylenesulfonate gives a recovered mass of 108%. The high recovered lignin mass is also partly due to the reactions between lignin and hemicellulose breakdown products, as will be explained, *vide infra*. Small amounts of the [C₂mim] cation may also have been incorporated in the lignin.

It is quite plausible that the lignin carbonium ions formed during heating in the ionic liquid are able to react with the highly available xylenesulfonate anions, producing lignin with xylenesulfonate adducts. Indeed, the absence of “carbonium ion scavengers” has been reported to result in low lignin extraction in steam explosion experiments due to lignin condensation reactions.³² Thus the addition of a small amount of sodium

Table 2 Elemental analysis

	C (%)	H (%)	N (%)	S (%)
Bagasse	47.10	6.21	0.25	Nil
Cellulose pulp ^a	43.35	6.63	< 0.1	Nil
Lignin ^a	66.35	5.46	1.17	1.52
Organosolv lignin ^b	66.85	6.00	0.23	Nil

^a From reaction using [C₂mim][ABS] at 190 °C for 120 minutes.

^b Supplied by Sigma Aldrich.

xylenesulfonate into the reaction mixture, as in the procedure described here, may provide a source of carbonium ion scavengers required while still allowing complete regeneration of the ionic liquid.

The other possible additional contaminants of the recovered lignin are humins or “pseudo-lignin”. Humins are polymeric products commonly produced from degradation of glucose and fructose during heating under acidic conditions.^{33,34} The formation of “pseudo-lignin” from polysaccharide degradation products, which are known to react with lignin, has been reported in literature on delignification by autohydrolysis.^{32,35} Acid hydrolysis of the recovered lignin from reaction at 190 °C for 2 hours revealed less than 0.1% xylan and negligible levels of glucan and arabinan, indicating that carbohydrates were largely absent from the lignin; however the pseudo-lignin products would not be detected in this measurement as they are not carbohydrates.

The addition of a small amount of sodium xylenesulfonate to the ionic liquid mixture was also expected to aid cleavage of ether groups in lignin due to sodium ions coordinating to the ether oxygen, increasing the carbonium ion character of ether carbon atoms, thus facilitating nucleophilic attack on the latter by arylsulfonate groups of the ionic liquid. Generally, the catalytic effect of a counterion on a chemical process, known as metal ion catalysis or electrophilic catalysis, is traditionally attributed to Lewis acid complexation, although a more recent paper mentions the importance of the associated electrostatic effect.³⁶ While cleavage of alkyl aryl ethers can occur by either homolytic scission (dealkylation) or heterolytic scission (dealkoxylation), the study found that heterolytic scission was very much dependent on the electrophilic assistance of a counterion. The presence of alkali metal ions was found to increase the rate of cleavage of crown ether anisoles by up to three orders of magnitude with a toluenethiolate nucleophile.³⁷ Low levels of sodium ions were already present in the neat ionic liquid due to the use of a sodium salt as the starting material.

Sugarcane bagasse has a high silica content, which poses a problem for chemical recovery in traditional pulping systems.³⁸ The ash content of the bagasse used in these experiments was measured to be 1.58% (on dry basis). Silica is known to dissolve in the alkaline liquors of the kraft and soda processes.³⁸ Ash contents of the lignins were measured to be in the range of 0.6–2%, and were corrected for in the recovered lignin mass.

The mass of recovered cellulose pulps were between 45% and 55% of the original bagasse on a dry mass basis (Table 3), indicating relatively little degradation of cellulose. However, HPLC of acid-hydrolysed bagasse and pulp showed that the majority of the hemicellulose had been removed after reaction.

Table 3 Yield of cellulose pulp

Run no	Condition	Dry wt of cellulose pulp as percentage of original bagasse, dry wt (% \pm 2)
1.	170 °C, 120 min	55
2.	180 °C, 120 min	52
3.	190 °C, 120 min	45
4.	190 °C, 90 min	46
5.	190 °C, 60 min	48
6.	190 °C, 30 min	53

Xylan levels in the bagasse and cellulose pulp (190 °C, 2 hours) were 18.8% and 8.7%, respectively. Arabinan levels in the bagasse and cellulose pulp (190 °C, 2 hours) were 1.7% and 0%, respectively. The amount of hemicellulose removed during delignification correlates roughly with the amount of extra material in the recovered lignin, supporting the case that reactive breakdown products of hemicellulose have been incorporated within the recovered lignin.

Lignin characterisation

Solid state ^{13}C NMR was conducted on the bagasse, cellulose pulp and recovered lignin. Both spectra for bagasse and cellulose pulp (Fig. 5a and b) show the distinctive peaks for cellulose C1 at 107 ppm due to the anomeric carbon in the cellulose structure and overlapping signals from cellulose C2 to C6 at 60–100 ppm. The spectrum for lignin (Fig. 5c) shows sharp peaks for methoxy groups at 57.8 ppm, and methylene groups at 22.3 ppm. These lignin peaks can be observed in the spectrum for bagasse (Fig. 5a), but are distinctly absent from the spectrum of the cellulose pulp (Fig. 5b), confirming that delignification has taken place. Other peaks in lignin occurring at 110–160 ppm correspond to aromatic ring carbon.³⁹

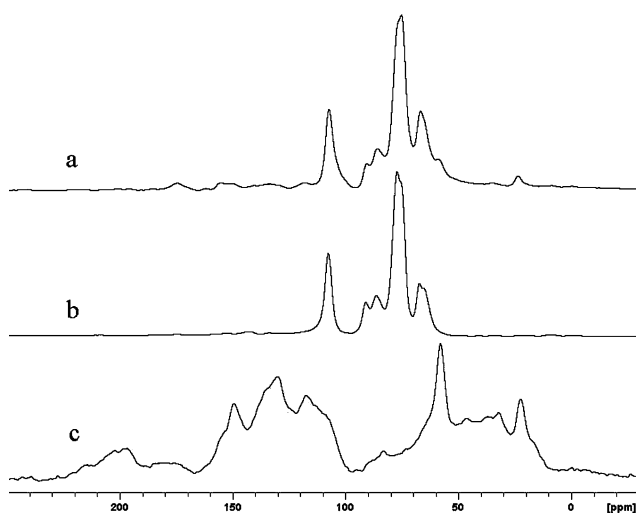


Fig. 5 Solid state ^{13}C NMR of (a) bagasse, (b) cellulose pulp (190 °C for 120 minutes), (c) recovered lignin (190 °C for 120 minutes).

Signals from the [ABS] anion are unable to be identified due to the overlapping signals from the aromatic groups in lignin. Signals from the [C₂mim] cation at 15.6, 35.9, 44.6 and 139.9 ppm are unable to be identified due to the relatively low levels of this cation resulting in the signals being obscured by other sources of carbon. The signals in the range 160–220 ppm are typically due

to carboxyl carbon (160–190 ppm) and carbonyl group carbons in quinones, ketones and aldehydes (190–220 ppm).⁴⁰ These are consistent with contamination from humic materials (humins), causing the high recovered mass of lignin. Humins have also been reported by others to give rise to ^{13}C NMR signals at 190–194 ppm.⁴¹ Carbonyl groups may be present in lignin to a small extent, but solid state NMR of milled wood lignins, a form of isolated lignin which most closely resembles native lignin within its plant source, do not show signals in the 170–220 ppm range,⁴² and neither do these signals appear in the spectrum of bagasse used in these experiments. No effort was made to exclude oxygen from the extraction procedure and oxidation of the isolated lignin (particularly phenolics) can account for the additional carbonyl groups observed at low field in the solid state ^{13}C NMR spectrum.

Infrared spectra of the recovered lignin and organosolv lignin from Sigma Aldrich (Fig. 6) are both dominated by a wide band at 3440–3200 cm^{-1} attributed to phenolic and aliphatic OH groups, followed by bands for C–H stretching in methyl and methylene groups (2936–2938 cm^{-1}), C–H stretching in methoxy groups (2842–2849 cm^{-1}), unconjugated C=O stretching (1701–1703 cm^{-1}), aromatic skeleton C–C stretching (1606–1610 cm^{-1}) and (1515–1516 cm^{-1}), asymmetric C–H deformation of methyl and methylene groups (1460–1461 cm^{-1}), aromatic skeleton C–C stretching (1425–1426 cm^{-1}), C–O stretching of syringyl groups (1328–1329 cm^{-1}), C–O stretching of guaiacyl groups (1270–1271 cm^{-1}), aromatic C–H deformation of guaiacyl groups (1216–1219 cm^{-1}), C–O(H) and C–O(C) stretching of first order aliphatic OH and ether groups (1031–1034 cm^{-1}), and aromatic C–H out of plane bending (830–834 cm^{-1}).^{43,44} Most interesting in the ionic liquid extracted lignin is the small band at 1168 cm^{-1} and larger band at 680 cm^{-1} , which are absent in organosolv lignin, and these may be attributed to symmetric SO_2 stretching and C–S stretching, respectively, supporting the hypothesis that [ABS]-derived groups are included in the extracted product.

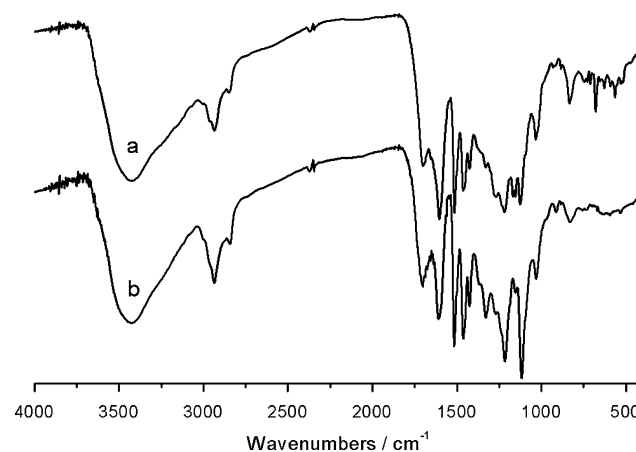


Fig. 6 Infra-red spectrum of (a) recovered lignin from reaction at 190 °C for 120 minutes, (b) Organosolv lignin from Sigma Aldrich.

Recovered lignin was acetylated and the molecular weight was determined using gel permeation chromatography with polystyrene standards and tetrahydrofuran as eluent. The weight average molecular weight was measured to be 3690 g/mol and number average molecular weight was 2220 g/mol with

polydispersity of 1.66. Acetylated autohydrolysis lignin from bagasse has been reported to have a weight average molecular weight of 19300 g/mol and a number average molecular weight of 1700 g/mol, with polydispersity of 11.4.⁴⁵ Thus the bagasse lignin extracted using ionic liquid has a much more uniform molecular weight than autohydrolysis bagasse lignin.

Thermogravimetric analysis conducted on extracted lignin (Fig. 7) showed that it begins to decompose at about 200 °C. This is quite similar to the thermal behaviour of acid insoluble lignin from alkaline extraction of bagasse, which begins decomposing at 186 °C.⁴⁶ The first derivative of the weight loss curve showed two minima at 290 °C and 370 °C.

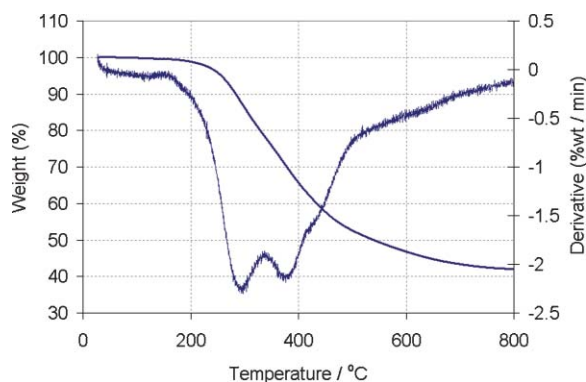


Fig. 7 Thermogravimetric analysis of lignin extracted using $[C_2mim][ABS]$.

Differential scanning calorimetry of dried lignin from $[C_2mim][ABS]$ extraction showed a glass transition temperature at about 144 °C (midpoint), which correlates well with literature values for soda bagasse lignin of between 140–145 °C.⁴⁷

Ionic liquid characterisation

Differential scanning calorimetry showed the ionic liquid $[C_2mim][ABS]$ to have no well-defined melting point, which is consistent with it being a mixture of different alkylbenzenesulfonate anions with residual levels of sodium and chloride. A glass transition was observed at -55 °C. At 70 °C, the viscosity of $[C_2mim][ABS]$ was 694 mPa s and its density was 1.209 g/cm³.

Recovery of ionic liquid

The ¹H NMR spectra of $[C_2mim][ABS]$ before and after reaction showed no change in structure. The recovered masses of ionic liquid were reasonably high, ranging from 96.1 to 99.4% (Table 4), indicating good potential for recycling.

Experimental

Purification of industrial grade sodium xylenesulfonate

An industrial grade of sodium xylenesulfonate was intentionally used in this work since, ultimately, the cost of the ionic liquid would be a major factor in its application. Sodium xylenesulfonate is typically produced as a mixture of isomers and all of the isomers can therefore be expected to be present in the ionic liquids made from these technical grade materials. Stepanate

Table 4 Recovery of ionic liquid

Run no	Recovery (% ± 0.5) ^a
1.	96.1
2.	97.9
3.	98.8
4.	96.4
5.	98.9
6.	99.4

^a Corrected for residual sodium and chloride content in recovered IL.

SXS-93 was obtained from Albright & Wilson, containing isomers of sodium xylenesulfonate, along with smaller amounts of sodium cumenesulfonate, sodium ethylbenzenesulfonate and sodium toluenesulfonate, and up to 4% sodium sulfate. This was dried under vacuum at 105 °C for 10 hours, and 100 g of the dried material was dissolved in 1.2 L of methanol. The insoluble sodium sulfate was removed by filtration and the filtrate was dried *in vacuo* to give solid $[Na][ABS]$, which was further dried at 105 °C overnight and ground in a mortar and pestle. From ¹H NMR, it was possible to estimate the amounts of each component: 74% sodium xylenesulfonate isomers, 9% sodium cumenesulfonate, 4% sodium toluenesulfonate, 13% sodium ethylbenzenesulfonate. ¹H NMR (D_2O , δ /ppm): 8.28 (s, ArH), 7.85–7.05 (m, ArH), 3.10–2.80 (m, $-CH_3-CH-CH_3$), 2.70–2.58 (q, $-CH_2-CH_3$), 2.58–2.48 (m, $-CH_3-Ar$), 2.34 (s, $-CH_3-Ar$), 2.31–2.20 (m, $-CH_3-Ar$), 1.20–1.11 (m, $-CH_2-CH_3$, $CH_3-CH-CH_3$). ES-MS: ES⁻ m/z 170.8 toluenesulfonate; 184.9 xylenesulfonate and ethylbenzenesulfonate; 198.9 cumenesulfonate.

Preparation of $[C_2mim][ABS]$

1-Ethyl-3-methylimidazolium chloride (99.2 g, 629 mmol) from Aldrich (98%) and purified Stepanate SXS-93 (182.6 g) from Albright & Wilson were dissolved in 560 mL of water and stirred overnight at room temperature. The water was removed under vacuum and 530 mL of acetone was added. Insoluble sodium chloride was removed by filtration. Acetone was removed under vacuum and the ionic liquid was dried under high vacuum at 70 °C for 12 hours. Dry acetone (280 mL) was used to dissolve the ionic liquid, with small amounts of sodium chloride forming a white precipitate. The mixture was refrigerated overnight. Sodium chloride was filtered off using glass fibre filter paper. Acetone was removed under vacuum and the ionic liquid was dried under high vacuum at 70 °C for 12 hours (205.5 g). ¹H NMR (D_2O , δ /ppm): 8.55–8.45 (s, $[C_2mim]$ ArH), 8.21–8.19 (s, $[ABS]$ ArH), 7.80–6.90 (m, $[ABS]$ ArH), 4.15–4.00 (q, $[C_2mim]$ $-CH_2-CH_3$), 3.73 (s, $[C_2mim]$ $-CH_3$), 3.00–2.75 (m, $[ABS]$ $-CH_3-CH-CH_3$), 2.65–2.55 (q, $[ABS]$ $-CH_2-CH_3$), 2.53–2.40 (m, $[ABS]$ CH_3-Ar), 2.28 (s, $[ABS]$ $-CH_3-Ar$), 2.24–2.12 (m, $[ABS]$ $-CH_3-Ar$), 1.45–1.25 (t, $[C_2mim]$ $-CH_2-CH_3$), 1.20–1.11 (m, $[ABS]$ $-CH_2-CH_3$, $CH_3-CH-CH_3$). ES-MS: ES⁺ m/z 110.9 $[emim]^+$. ES⁻ m/z 170.8 toluenesulfonate; 184.9 xylenesulfonate and ethylbenzenesulfonate; 198.9 cumenesulfonate. Sodium level 0.82% (atomic absorption spectroscopy). Chloride level 0.12% (ion-selective electrode). Thermal decomposition temperature 290 °C (approx.).

Delignification reactions

Three grams of bagasse (2–3 mm particles, 7% moisture) was weighed into a crucible and steamed in a beaker for 2 hours in order to pre-swell the fibres. Ionic liquid was re-dried at 70 °C for 2 hours under high vacuum and 27 g was placed into a 3-neck 100 mL round bottom flask with a small stirrer bar. Sodium xylenesulfonate [Na][ABS] (1.2 g) was dissolved in 3 mL of distilled water by heating on a hot plate. The sodium xylenesulfonate solution was added to the ionic liquid and stirred until completely mixed. The steamed bagasse was placed in the flask with the ionic liquid mixture. The reaction mixture was then heated to reaction temperature in a silicone oil bath with a digital controller on a hot plate. During the initial heating stage, excess water was allowed to boil off. When reaction temperature was reached, a reflux condenser was placed over the round bottom flask, with a thermometer and stopper in the second and third necks. The mixture was held at temperature for the set time.

After the reaction mixture was cooled to 80 °C, a total of 500 mL of 0.1 M sodium hydroxide was used to wash the ionic liquid and lignin away from the cellulose pulp. To remove traces of sodium hydroxide from the pulp, 300 mL of distilled water was washed through the pulp. Testing with pH paper showed the final drops of washing liquid to be pH neutral. The darkly-coloured caustic solution containing lignin and ionic liquid was acidified to pH 2 at room temperature by adding 1 M HCl dropwise, causing lignin to precipitate as a fine suspension. The suspension was then heated to 70 °C for 30 minutes and the lignin was isolated by filtering through a glass sinter. The filtered lignin was washed with 200 mL of distilled water at 70 °C. It was then air-dried and further dried in a convection oven at 60 °C for 18 hours. The recovered dry lignin mass was then measured.

After air-drying, the cellulose pulp samples were ball-milled, weighed and tested for moisture. Lignin extraction efficiency was quantified by measuring the mass of recovered lignin, as well as by measuring the acid insoluble lignin (AIL, or Klason lignin) and acid soluble lignin (ASL) in the cellulose pulp fraction as per TAPPI Test Method T222-om-02⁴⁸ and TAPPI useful method UM 250 um-83,⁴⁹ respectively.

Recovery of ionic liquid

The acidic aqueous filtrate containing ionic liquid, sodium chloride, hydrochloric acid and sodium xylenesulfonate (after removing lignin) was neutralised with 90 mL of 0.1 M NaOH. Water was removed under vacuum and the mixture was dried at 70 °C under high vacuum for 12 hours. Acetonitrile was added (100 mL) to dissolve the ionic liquid while leaving most of the sodium chloride and sodium xylenesulfonate as insoluble residue, which was removed by filtration. The acetonitrile was then removed under vacuum and the recovered ionic liquid was dried at 70 °C under high vacuum.

Characterisation

Infrared spectra of lignins were obtained using a Perkin-Elmer Spectrum RX1 FT-IR spectrophotometer, with KBr pellets made up of 1% sample. A total of 20 scans was taken for each sample, at resolution 4 cm⁻¹.

¹³C solid-state NMR was performed using a Bruker AM300 instrument equipped with a Bruker 4 mm solid-state probe operating at 75.5 MHz. The spectra were collected using a magic angle spinning speed of 5 KHz.

Differential scanning calorimetry was conducted on a TA Instruments DSC Q100 with 5–10 mg of sample in closed aluminium pans, at a ramp rate of 10 °C per minute. The ionic liquid sample was cooled to –100 °C, held for 2 minutes and heated to 200 °C. The lignin sample was heated from room temperature to 200 °C.

Elemental analysis was carried out by Campbell Microanalysis Laboratory, Department of Chemistry, University of Otago, Dunedin, New Zealand.

¹H Nuclear magnetic resonance spectra were obtained in D₂O and were recorded using a Bruker DPX300 at 300 MHz, referenced to water at 4.67 ppm.

Electro-spray ionisation mass spectra (ESI-MS) were recorded on a Micromass Platform II, with cone voltage 35 V and a capillary voltage of 3.5 kV.

Density measurements were conducted using an Anton Paar DMA 5000 density meter.

Viscosity measurements were conducted at an angle of 70 ° using an Anton Paar AmVn automated micro viscometer, and recorded as an average of four readings.

Thermogravimetric analysis was conducted on a Pyris 1 TGA by heating 5–15 mg of sample in a platinum pan at a rate of 10 °C per minute.

Conclusions

Extraction of lignin from bagasse using the ionic liquid mixture [C₂mim][ABS] was successfully achieved at atmospheric pressure, with over 93% yield. The fact that the process can be conducted at atmospheric pressure is significant in terms of plant and equipment requirements, and also illustrates a useful feature of ionic liquids in providing a reaction medium for hydrolysis reactions in which water is present but only at low activity. The lignin is of relatively uniform molecular weight, but contains some [ABS] adducts due to reaction of the [ABS] anion with carbonium ion lignin fragments. If necessary, the sulfonate ester groups may be hydrolysed under basic conditions. The recovered ionic liquid showed no structural change, as observed in the ¹H NMR spectra. Overall, the use of ionic liquids to extract lignin from lignocellulose has been successfully demonstrated, although a number of issues remain, such as simplification of ionic liquid recovery and tailoring an ionic liquid to create lignin with desirable adducts. Ionic liquids, for example, that exhibit desirable phase separation properties would be advantageous. In view of the environmental disadvantages of current processes, such as high water use, pollution, odour, high pressure operation, and the use of toxic, flammable and corrosive solvents, the use of an ionic liquid has significant advantages, especially with the possibility of designing new ionic liquids to overcome processing difficulties and to produce a specialised lignin product.

Acknowledgements

The Australian Sugar Research and Development Corporation and the Centre for Green Chemistry at Monash University are

acknowledged for their financial support. Thanks to Sally Duck of Monash University for ESI-MS data and Tanya Hutchins of Queensland University of Technology for carbohydrate determination by acid hydrolysis. JMP and DRM are extremely grateful to the Australian Research Council for QEII and Federation Fellowships respectively.

References

- 1 J. H. Clark, *J. Chem. Technol. Biotechnol.*, 2007, **82**, 603–609.
- 2 A. J. Ragauskas, C. K. Williams, B. H. Davison, G. Britovsek, J. Cairney, C. A. Eckert, W. J. Frederick, Jr., J. P. Hallett, D. J. Leak, C. L. Liotta, J. R. Mielenz, R. Murphy, R. Templer and T. Tschaplinski, *Science*, 2006, **311**, 484–489.
- 3 Y. H. P. Zhang, *J. Ind. Microbiol. Biotechnol.*, 2008, **35**, 367–375.
- 4 *Kirk-Othmer Encyclopedia of Chemical Technology [electronic resource]*, Web edn., John Wiley & Sons, New York, 1999–2008, Vol. 21.
- 5 J. Gierer, *Wood Sci. Tech.*, 1985, **19**, 289–312.
- 6 G. Wegener, *Ind. Crops Prod.*, 1992, **1**, 113–117.
- 7 Y. -H. P. Zhang, S. -Y. Ding, J. R. Mielenz, J. -B. Cui, R. T. Elander, M. Laser, M. E. Himmel, J. R. McMillan and L. R. Lynd, *Biotechnol. Bioeng.*, 2007, **97**, 214–223.
- 8 M. Delmas, *Chem. Eng. Technol.*, 2008, **31**, 792–797.
- 9 R. H. McKee, *US Pat.*, 2 308 564, 1943.
- 10 R. H. McKee, *Pulp & Paper Magazine of Canada*, 1954, **55**, 64–66.
- 11 R. H. McKee, *Paper Ind.*, 1960, **42**, 255–257, 266, 412–413, 420.
- 12 A. R. Procter, *Pulp and Paper Magazine of Canada*, 1971, **72**, 67–74.
- 13 D. E. Bland, *Research Review – Australia, Commonwealth Scientific and Industrial Research Organization, Division of Chemical Technology*, 1976, 27–41.
- 14 S. S. Y. Tan, and D. R. MacFarlane, *Top. Curr. Chem.*, 2009, in press.
- 15 R. P. Swatloski, R. D. Rogers, and J. D. Holbrey, *WO Pat.*, 2003/029329, 2003.
- 16 R. P. Swatloski, S. K. Spear, J. D. Holbrey and R. D. Rogers, *J. Am. Chem. Soc.*, 2002, **124**, 4974–4975.
- 17 H. Zhang, J. Wu, J. Zhang and J. He, *Macromolecules*, 2005, **38**, 8272–8277.
- 18 J. Zhang, Q. Ren, and J. He, *CN Pat.*, 1491974, 2004.
- 19 Y. Fukaya, K. Hayashi, M. Wada and H. Ohno, *Green Chem.*, 2008, **10**, 44–46.
- 20 Y. Fukaya, A. Sugimoto and H. Ohno, *Biomacromolecules*, 2006, **7**, 3295–3297.
- 21 D. A. Fort, R. C. Remsing, R. P. Swatloski, P. Moyna, G. Moyna and R. D. Rogers, *Green Chem.*, 2007, **9**, 63–69.
- 22 I. Kilpelainen, H. Xie, A. King, M. Granstrom, S. Heikkinen and D. S. Argyropoulos, *J. Agric. Food Chem.*, 2007, **55**, 9142–9148.
- 23 V. Myllymaeki, and R. Aksela, *WO Pat.*, 2005/017001, 2005.
- 24 J. Upfal, D. R. MacFarlane and S. A. Forsyth, *WO Pat.*, 2005/017252, 2005.
- 25 Y. Q. Pu, N. Jiang and A. J. Ragauskas, *J. Wood Chem. Technol.*, 2007, **27**, 23–33.
- 26 D. Argyropoulos, *US Pat.*, 2008/0185112, 2008.
- 27 T. Balensiefer, *WO Pat.*, 2008/090156, 2008.
- 28 T. Balensiefer, J. Brodersen, G. D'Andola, K. Massonne, S. Freyer, and V. Stegmann, *WO Pat.*, 2008/090155, 2008.
- 29 G. D'andola, L. Szarvas, K. Massonne and V. Stegmann, *WO Pat.*, 2008/043837, 2008.
- 30 L. A. Edey and W. O. S. Doherty, *WO Pat.*, 2008/095252, 2008.
- 31 V. Stegmann and M. Maase, *WO Pat.*, 2007/057235, 2007.
- 32 J. Li, G. Henriksson and G. Gellerstedt, *Bioresour. Technol.*, 2007, **98**, 3061–3068.
- 33 J. N. Chheda, Y. Roman-Leshkov and J. A. Dumesic, *Green Chem.*, 2007, **9**, 342–350.
- 34 K. -I. Seri, Y. Inoue and H. Ishida, *Bull. Chem. Soc. Jpn.*, 2001, **74**, 1145–1150.
- 35 M. G. S. Chua and M. Wayman, *Can. J. Chem.*, 1979, **57**, 1141–1149.
- 36 F. Casado, L. Pisano, M. Farriol, I. Gallardo, J. Marquet and G. Melloni, *J. Org. Chem.*, 2000, **65**, 322–331.
- 37 R. Cacciapaglia, L. Mandolini and F. S. Romolo, *J. Phys. Org. Chem.*, 1992, **5**, 457–460.
- 38 A. Leponiemi, *Appita Journal*, 2008, **61**, 234–243.
- 39 L. G. Akim, T. G. Fedulina and S. M. Shevchenko, *Holzforchung*, 1996, **50**, 237–244.
- 40 R. M. Silverstein, F. X. Webster and D. J. Kiemle, *Spectroscopic Identification of Organic Compounds*, 7th edn., John Wiley & Sons, New Jersey, 2005.
- 41 G. Almendros, J. Sanz and I. Sobrados, *Sci. Total Environ.*, 1989, **81–2**, 91–98.
- 42 M. Bardet, D. Gagnaire, R. Nardin, D. Robert and M. Vincendon, *Holzforchung*, 1986, **40**, 17–24.
- 43 A. Tejado, C. Pena, J. Labidi, J. M. Echeverria and I. Mondragon, *Bioresour. Technol.*, 2007, **98**, 1655–1663.
- 44 B. Xiao, X. F. Sun and R. C. Sun, *Polym. Degrad. Stab.*, 2001, **74**, 307–319.
- 45 W. G. Glasser, V. Dave and C. E. Frazier, *J. Wood Chem. Technol.*, 1993, **13**, 545–559.
- 46 J. X. Sun, X. F. Sun, R. C. Sun, P. Fowler and M. S. Baird, *J. Agric. Food Chem.*, 2003, **51**, 6719–6725.
- 47 D. P. Koullas, E. G. Koukios, E. Avgerinos, A. Abaecherli, R. Gosselink, C. Vasile, R. Lehnen, B. Saake and J. Suren, *Cellul. Chem. Technol.*, 2006, **40**, 719–725.
- 48 TAPPI, *TAPPI Test Methods*, TAPPI Press, 2004.
- 49 TAPPI, *Useful Test Methods*, TAPPI Press, 1991.

Purification of hexane with effective extraction using ionic liquid as solvent

Ana B. Pereiro and Ana Rodriguez*

Received 13th August 2008, Accepted 6th January 2009

First published as an Advance Article on the web 5th February 2009

DOI: 10.1039/b814032d

The separation of hexane and ethanol is valuable but difficult due to the formation of an azeotropic mixture. This work demonstrates the ability of the ionic liquid (IL) 1-butyl-3-methylimidazolium methyl sulfate [BMIM][MeSO₄] to act as an extraction solvent in petrochemical processes for the removal of hexane from its mixture with ethanol. Knowledge of the phase behavior of the system is key in order to optimize the separation process. For this reason, the experimental liquid–liquid equilibrium (LLE) for the ternary system hexane + ethanol + [BMIM][MeSO₄] is investigated at 298.15 K. The separation sequence of the extraction process is checked by using conventional software for simulation. Experimental data are obtained in a laboratory-scale packed column extraction system for the separation of this azeotropic mixture by using [BMIM][MeSO₄]. It is concluded that this IL has the highest extraction efficiency.

Introduction

An increasing concern about the environment has recently directed the attention of the scientific community to novel processes based on greener technologies. The separation of azeotropic mixtures has conventionally been one of the most challenging tasks in industrial processes due to the fact that the separation of these azeotropes in a simple distillation is basically impossible. It is essential to separate these mixtures into special components so that the separated parts may be reused in production cycles.

The azeotrope ethanol with hexane is present in a growing number of processes aiming at the production of oxygenated additives for gasolines. Most of these processes, which are under development or have already reached the industrial production stage,¹ are created in order to achieve the reduction of lead in gasoline. Albeit extractive distillation is the most widely used process for the removal of the components in the azeotropic system, this process needs energy to get a fluid phase system. Nevertheless, the liquid–liquid separation leads to an environmentally friendly extraction process of the azeotropic mixture ethanol with hexane as an alternative to azeotropic distillation,² a procedure which requires the use of considerable amounts of energy, volatile organic compounds, or high pressures.

Ionic liquids (ILs) are emerging as an appealing alternative in synthesis and extraction processes for the reduction of the amount of volatile organic solvents (VOSs) used in industry. ILs are receiving increasing attention due to notable properties such as negligible vapor pressure at room temperature, stable liquid phase over a wide temperature range, the possibility of designing the IL according to one's needs, high electrochemical stability, higher ionic conductivity in contrast with a regular solvent, non-flammability and non-odor.^{3–5}

The separation of azeotropic mixtures is an engineering problem often solved by using extracting agents or entrainers. ILs due to a nonvolatile property have more advantages as entrainer than conventional organic compounds. Experimentally, ILs have exhibited the ability to separate azeotropic mixtures including ethanol + water,^{6,7} THF + water,^{6–8} alcohols + alkanes mixtures,^{9–11} aromatic + aliphatic mixtures,^{12,13} ethyl acetate + alcohols,^{14,15} ethyl acetate + hexane,¹⁶ ketones + alkanes or alcohols mixtures,^{17,18} and ethyl *tert*-butyl ether (ETBE) + ethanol.¹⁹

In this work, 1-butyl-3-methylimidazolium methyl sulfate [BMIM][MeSO₄] (Fig. 1) has been preliminarily selected according to its low melting point (well below room temperature), its relatively low viscosity (thus facilitating fluid flow and mass transfer), its low cost, its low toxicity and the fact that the anion [MeSO₄][−] does not decompose in the presence of water²⁰ and at high temperatures²¹ to bring about the corresponding acid.

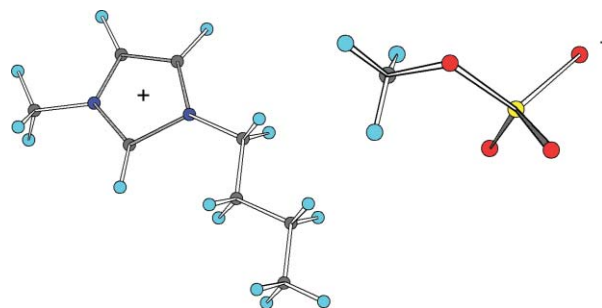


Fig. 1 Schematic 3D structure of [BMIM][MeSO₄].

For all the reasons explained above, [BMIM][MeSO₄] seems to be a good candidate to be tested as an extracting solvent or entrainer in purifying of hexane from its mixture with ethanol. In order to evaluate such a possibility, in this work we carry out an equilibrium thermodynamic study of the ternary system hexane + ethanol + [BMIM][MeSO₄]. Its liquid–liquid equilibrium (LLE) at 298.15 K and atmospheric pressure are

Department of Chemical Engineering, University of Vigo, P. O. Box 36310, Vigo, Spain. E-mail: aroque@uvigo.es; Fax: +34 986 81 23 80; Tel: +34 986 81 23 12

determined. The experimental data are successfully correlated, thus facilitating their implementation and use in computerized applications. The capacity of [BMIM][MeSO₄] as a solvent in liquid extraction processes is evaluated by using both the selectivity and the solute distribution ratio. This capacity is compared with the capacity of other ILs within the group of those based on the anion [PF₆]⁻. A simulation of the extraction process is performed by using the HYSYS software with the aim of optimizing the operation conditions for continuous extraction of ethanol from the azeotropic mixture. The optimized conditions are assessed in practice in a laboratory-scale packed column and the extraction efficiency of the extraction process in the packed column is calculated.

Results and discussion

Liquid–liquid equilibrium

The composition of both phases in equilibrium was determined at 298.15 K for mixtures with different global composition in the heterogeneous region of the system hexane + ethanol + [BMIM][MeSO₄]. The results are reported in Table 1, alongside the corresponding values of solute distribution ratio (β_2) and selectivity (S), which are defined by the following expressions:

$$\beta_2 = \frac{w_2^{\text{IL-phase}}}{w_2^{\text{HC-phase}}} \quad (1)$$

$$S = \left(\frac{w_1^{\text{HC-phase}}}{w_1^{\text{IL-phase}}} \right) \left(\frac{w_2^{\text{IL-phase}}}{w_2^{\text{HC-phase}}} \right) \quad (2)$$

In these equations, w is the mass fraction; subscripts 1 and 2 indicate the hexane and the ethanol, respectively; and HC-phase and IL-phase indicate the hydrocarbon (top phase) and IL (bottom phase) rich phase, respectively. The solute distribution ratio gives an idea of the solvent capacity of the IL, since it is related to the amount of solvent required for the process. Selectivity provides a measurement of the separation power of the IL, consequently conditioning the number of equilibrium stages needed in the unit. Since it deploys high values of these parameters, as desired, [BMIM][MeSO₄] can be considered good in this extraction process.

Table 1 Composition of the experimental tie-line ends, solute distribution ratio (β_2) and selectivity (S) for the ternary system hexane + ethanol + [BMIM][MeSO₄] at 298.15 K. The mass fraction of hexane and ethanol are w_1 and w_2 , respectively

Hydrocarbon-rich phase		Ionic liquid-rich phase		β_2	S
$w_1^{\text{HC-phase}}$	$w_2^{\text{HC-phase}}$	$w_1^{\text{IL-phase}}$	$w_2^{\text{IL-phase}}$		
0.994	0.005	0.013	0.030	5.51	432.0
0.994	0.006	0.016	0.045	7.64	482.1
0.993	0.007	0.020	0.070	10.27	523.0
0.992	0.008	0.024	0.123	15.98	651.7
0.991	0.009	0.033	0.156	18.28	553.9
0.988	0.012	0.040	0.213	17.62	437.3
0.987	0.012	0.048	0.282	23.31	483.2
0.979	0.019	0.076	0.334	17.89	231.0
0.962	0.035	0.101	0.381	11.01	105.0
0.951	0.044	0.128	0.409	9.30	68.9
0.934	0.060	0.160	0.441	7.31	42.6
0.905	0.088	0.199	0.466	5.27	24.0

The binodal curves of [BMIM][MeSO₄] with other ILs¹⁰ are shown in Fig. 2. This figure indicates a clear visualization of the change in the size and shape of the immiscibility region. It can be observed that the immiscibility region decreases when the length of the alkyl chain in the imidazolium ring increases.

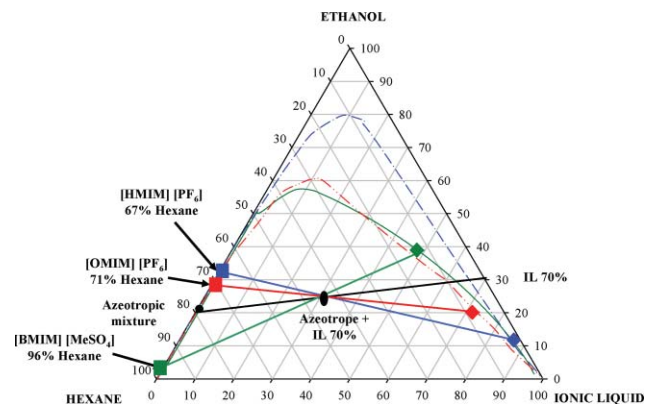


Fig. 2 Experimental binodal curves of the ternary systems hexane + ethanol + ionic liquid, where: (green solid line), [BMIM][MeSO₄]; (blue dash-dot line), [HMIM][PF₆]; (red dash-double dot line), [OMIM][PF₆] with the predictions of phase compositions when the azeotropic mixture ethanol + hexane and [BMIM][MeSO₄] containing 30% of ethanol (IL 70%) are mixed in solvent/feed ratio of 0.9, where: green ■, ◆, raffinate and extract of [BMIM][MeSO₄]; blue ■, ◆, raffinate and extract of [HMIM][PF₆]; red ■, ◆, raffinate and extract of [OMIM][PF₆].

Correlation of LLE

As design of a separation process requires knowledge of the phase equilibria; the NRTL equation²² is employed in order to correlate LLE data. Previous works confirm that the correlation equation is suitable to satisfactorily describe the phase equilibria involving electrolytes like ILs.^{23–26} The parameters were adjusted to minimize the difference between the experimental and the calculated mole fraction defined as:

$$O.F. = \sum_{i=1}^n \left[\left(x_{1i}^{\text{HC-phase}} - x_{1i}^{\text{HC-phase}}(\text{calc}) \right)^2 + \left(x_{2i}^{\text{HC-phase}} - x_{2i}^{\text{HC-phase}}(\text{calc}) \right)^2 \right] + \sum_{i=1}^n \left[\left(x_{1i}^{\text{IL-phase}} - x_{1i}^{\text{IL-phase}}(\text{calc}) \right)^2 + \left(x_{2i}^{\text{IL-phase}} - x_{2i}^{\text{IL-phase}}(\text{calc}) \right)^2 \right] \quad (3)$$

where $x_{1i}^{\text{HC-phase}}$, $x_{2i}^{\text{HC-phase}}$, $x_{1i}^{\text{IL-phase}}$, $x_{2i}^{\text{IL-phase}}$ are the experimental mole fraction; $x_{1i}^{\text{HC-phase}}(\text{calc})$, $x_{2i}^{\text{HC-phase}}(\text{calc})$, $x_{1i}^{\text{IL-phase}}(\text{calc})$ and $x_{2i}^{\text{IL-phase}}(\text{calc})$ are the calculated mole fraction.

The fitting parameters are listed in Table 2. The deviation was calculated by applying the following expression:

$$\sigma = \left(\frac{\sum_i \left(x_{ilm}^{\text{exp}} - x_{ilm}^{\text{calc}} \right)^2}{6k} \right)^{1/2} \quad (4)$$

where x is the mole fraction and the subscripts i , l and m provide the component, the phase and the tie-line, respectively. The k value refers to the number of experimental tie-lines.

The value of σ provides a measure of the accuracy of the correlation, which is 0.024 in this case. A comparison

Table 2 Binary interaction parameters from the correlation of the LLE data of the ternary system hexane + ethanol + [BMIM][MeSO₄] by the NRTL equation

Components i, j	Parameters ($\alpha = 0.19$)	
	$g_{ij} - g_{ji}$ (J mol ⁻¹)	$g_{ji} - g_{ii}$ (J mol ⁻¹)
1, 2	373.77	7776.8
1, 3	6845.4	12649
2, 3	35506	-2415.0

between the experimental data and those obtained from the NRTL equation demonstrates that the NRTL equation maps the liquid–liquid behavior.

Selection of column operation conditions

Operating conditions for the simulations and packed column experiments were selected in order to lessen cost while respecting the requirement of an elevated purity of the raffinate. Both cost and purity rise when the solvent/feed flow ratio in the column and the purity of the solvent stream increase. Moreover, the cost of solvent recovery grows when the purity is as high as desired. This study has been carried out for solvent purities of 70–100%. All the solvent streams considered can result in theoretical raffinate purities > 90 wt% within solvent/feed ratios ranging lower than 1.5. Overlooking formal optimization, we have selected a solvent/feed ratio of 0.9 and a 70% pure solvent stream, both of which afford a theoretical raffinate purity of 96.2 wt%, to be used in further research.

Fig. 2 shows a comparison of the predictions of phase compositions when the azeotrope ethanol + hexane (in azeotropic composition) and [BMIM][MeSO₄] with a pure solvent stream of 70% are mixed in these selected operation conditions. The plotted data for the systems with other ILs are taken from previous work.⁸ The corresponding separations are calculated from the tie-line data. A close look at this figure reveals that the [BMIM][MeSO₄] favors the separation of the azeotropic mixture ethanol + hexane. This conduct can also be found for other ternary systems in the literature.^{27,28}

Simulation results

The performance of the process shown schematically in Fig. 3, where a liquid–liquid extractor with one equilibrium stage models the packed column and a short-cut distillation process models solvent recovery, was optimized in the neighborhood of the chosen theoretical operating conditions *via* HYSYS v.3.2 (from Aspen Technology Inc., Cambridge, MA, USA) with the NRTL equation fitted to the experimental tie-line data. The solvent and feed compositions were kept constant, and flow rates were optimized in order to maximize raffinate purity. With the solvent and feed flow rates listed in Table 3, a raffinate with a purity of 97.8 wt% was achieved. Distillation of the extract stream afforded the recovery of 70:30 solvent (recycled to the first column). The ability of the [BMIM][MeSO₄] as an azeotrope breaker in liquid–liquid extraction processes for the separation of the mixture hexane + ethanol was proved.

Table 3 Properties of the main streams in the extraction of ethanol from its azeotropic mixture with hexane using [BMIM][MeSO₄] as solvent by means of HYSIS software

Stream name	Solvent	Feed	Raffinate	Extract	Alcohol
Temperature (K)	298.15	298.15	298.15	298.15	298.15
Pressure (kPa)	101.32	101.32	101.32	101.32	101.32
Molar flow (g mol/h)	7.52	12.55	7.107	12.96	5.44
Mass flow (kg/h)	0.8076	0.9156	0.6028	1.1204	0.3128
Liquid volume flow (ml/h)	770.7	1333.4	905.6	1198.5	427.8
Component mass fraction					
Hexane	0	0.7916	0.9777	0.1209	0.4289
Ethanol	0.3000	0.2084	0.0021	0.3757	0.5711
[BMIM][MeSO ₄]	0.7000	0	0.0021	0.5034	0

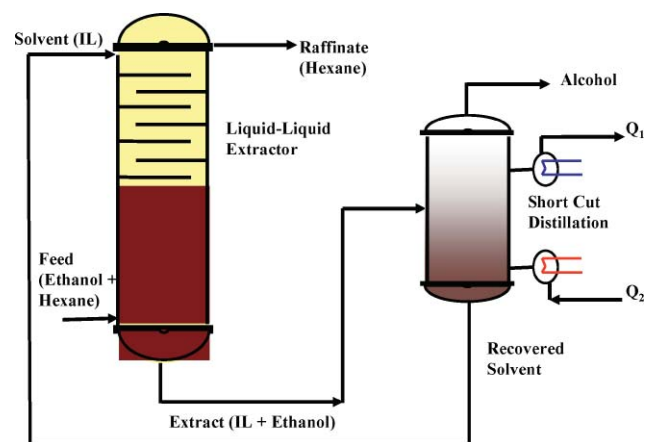


Fig. 3 Extraction process flow sheet in the separation of the azeotropic mixture ethanol + hexane using [BMIM][MeSO₄] as solvent.

Results of packed column experiment

Fig. 4 plots the evolution of the hexane content of raffinate, observed in a packed column countercurrent extraction experiment, carried out under operating conditions approximating those prescribed by the simulation results. In addition, Fig. 5 shows times, raffinate purity and the extract mass composition stabilized. The performance of the experimental column exceeded theoretical (96.2 wt.%) and simulation-based (97.8 wt.%)

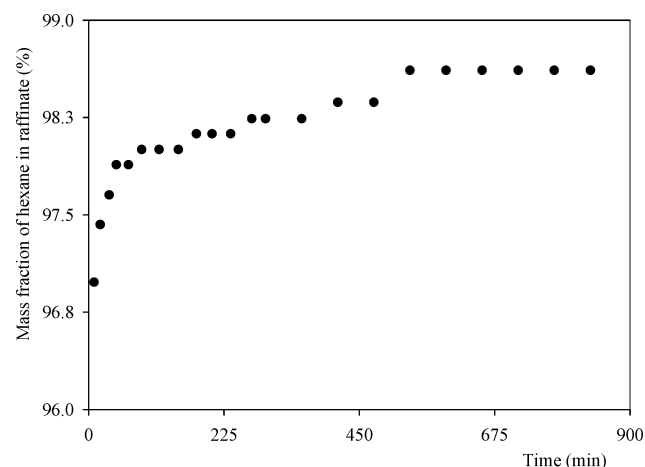


Fig. 4 Time dependence of the mass fractions of hexane in raffinate following start-up of the extraction column using [BMIM][MeSO₄] as solvent.

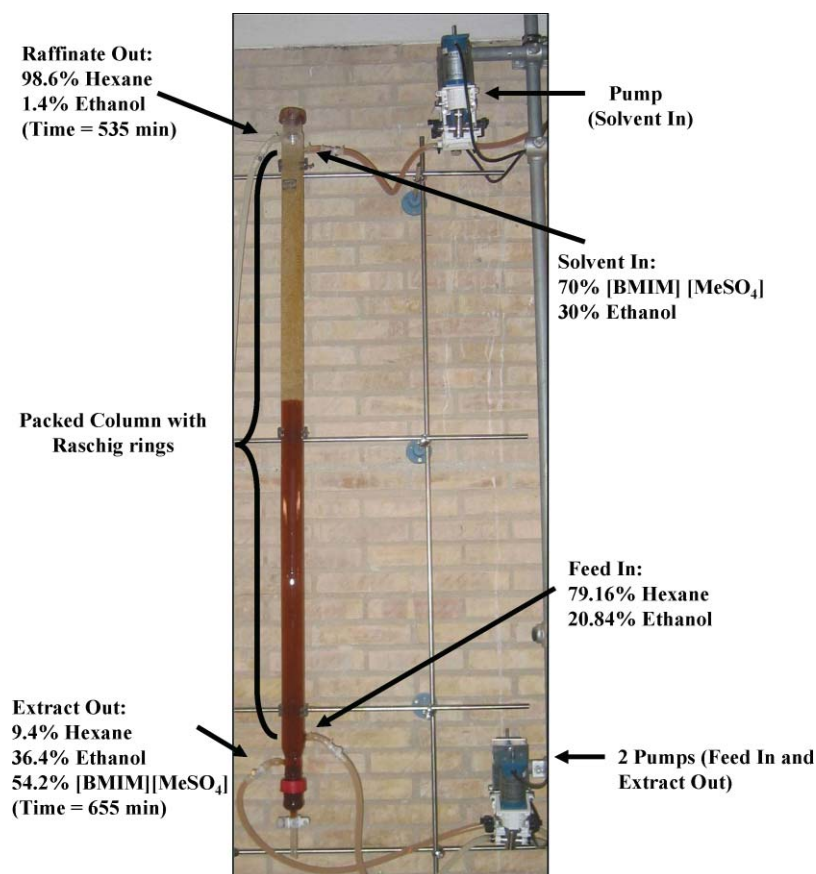


Fig. 5 The packed countercurrent extraction column with the experimental data in the steady state of extraction process.

expectations, undoubtedly because of superior mixing between feed and solvent. The extraction of hexane with a purity of 98.6 wt.% was feasible by using a packed extraction column and [BMIM][MeSO₄] as solvent.

The extraction efficiency, E , was calculated in order to study the extraction process in the packed column. This parameter points toward the ability of [BMIM][MeSO₄] to remove ethanol from the azeotropic mixture of ethanol and hexane in the extraction column. This parameter is defined as follows:

$$E = \frac{w_1^F - w_1^R}{w_1^F - w_1^{Eq}} \quad (5)$$

where w is the mass fraction, subscript 1 indicates the hexane and F, R and Eq provide the feed stream, the raffinate stream and one equilibrium stage, respectively. The extraction efficiency for [BMIM][MeSO₄] is 1.14 in the separation of the azeotrope ethanol with hexane.

Experimental methods

Materials

The synthesis of [BMIM][MeSO₄] was carried out as described in previous research.²⁹ It gave NMR and positive FAB mass spectra as a result, in keeping with the literature. This IL was always used directly following the reduction of its water content to a mass fraction < 0.02% (as determined in a Karl Fischer 756 coulometer) by vacuum (2×10^{-1} Pa) at 343.15 K. The

nominal purities of hexane (from Aldrich, ≥ 99.0 wt%) and ethanol (from Merck, ≥ 99.8 wt%) were verified by means of gas chromatography.

Regeneration of the IL

The [BMIM][MeSO₄] used during this experiment was recovered and purified from the extract stream by removing the rest of its components in a Büchi R 3000 rotary evaporator with a vacuum controller. This operation is straightforward due to the fact that vapor pressure is lower than the one of the rest of the components. The purity of this recovered compound was verified by comparing its density at 298.15 K and NMR with the density and NMR of the freshly synthesized product.

Experimental LLE procedure

Ternary LLE data were determined in a glass cell containing a magnetic stirrer and thermostatted by a water jacket connected to a bath controlled to ± 0.01 K. The temperature in the cell was measured with an ASL F200 digital thermometer with an uncertainty of ± 0.01 K. For the LLE measurements, 30 ml of ternary mixture of known composition was added to the cell, the temperature was brought to 298.15 ± 0.01 K, and the mixture was mixed vigorously for 1 h and left to settle for 4 h. Then, samples of both layers were taken with a syringe and their densities and refractive indices were determined. Lastly, their compositions were inferred by means of calibration curves which had been

previously constructed at 298.15 K. These curves were obtained after the determination of the binodal curve. Known masses of the three components were added slowly until one phase was obtained and then the binodal curve composition was detected visually. Forty miscible samples were prepared by mass near to the binodal curve and the density and refractive index were measured at 298.15 K to guarantee that the ternary physical properties were described properly. The calibration curves were obtained by fitting the composition on these samples by means of refractive indices and densities at 298.15 K. The uncertainty of the phase composition resulted in an estimation of ± 0.004 in mass fraction. All weight measurements were performed in a Mettler AX-205 Delta Range scale with an uncertainty of $\pm 10^{-4}$ mass fraction. Also, densities were measured with an Anton Paar DSA-48 digital vibrating tube densimeter with an uncertainty of $\pm 2 \times 10^{-4}$ g cm⁻³. Finally, refractive indices were calculated *via* a Dr. Kernchen ABBEMAT WR automatic refractometer with an uncertainty of $\pm 4 \times 10^{-5}$.

Packed column experiment

The practical performance of [BMIM][MeSO₄] as a hexane + ethanol azeotrope breaker was researched by using it for continuous countercurrent separation of the azeotropic mixture in a 54 × 1585 mm glass extraction column packed with 8 × 8 mm Raschig rings to a height of 1475 mm (Fig. 5). The experiment was carried out at room temperature under steady-state conditions with feed and solvent inflow rates of 1543 and 544 ml/h, respectively. First, the azeotropic mixture and solvent streams were pumped in, the extract stream was pumped out with FMI QV laboratory pumps and the raffinate stream came out of the column under gravity. Then, samples from the top and bottom of the column were taken periodically for the determination of their composition in relation to their density and refractive index. Lastly, [BMIM][MeSO₄] was recovered on-line from the extract stream and was recycled into the packed column.

Conclusions

The use of [BMIM][MeSO₄] as solvent for the separation of the azeotropic mixture ethanol with hexane by liquid–liquid extraction was analyzed. Experimental determination of LLE data for the ternary system hexane + ethanol + [BMIM][MeSO₄] at 298.15 K allowed the NRTL equation to be fitted and afforded the corresponding distribution ratios and selectivities for the extraction of ethanol from azeotropic hexane + ethanol mixtures. The phase diagram of [BMIM][MeSO₄] was compared with the phase diagram of [C_nMIM][PF₆] when both are used as solvent. [BMIM][MeSO₄] substantiates the best results in the separation of the azeotrope ethanol + hexane.

An extraction process was carried out with [BMIM][MeSO₄]. The LLE data were used for the identification of theoretically appropriate operating conditions for a room-temperature countercurrent continuous extraction process including a solvent recycling stage. The extraction process with this solvent was simulated by using conventional software. An experiment with a laboratory-scale packed column under steady-state conditions

close to the simulated optimum achieved a raffinate purity of over 98.6 wt%. It also confirmed the possibility of ready on-line recovery of [BMIM][MeSO₄]. The extraction efficiency of this extraction process was calculated and the results indicate that the [BMIM][MeSO₄] would be a suitable alternative as solvent in this separation process. If the raffinate purity of hexane obtained in the extraction process is taken into account, scaling up for industrial application seems viable.

Acknowledgements

We would like to thank the Ministerio de Educación y Ciencia (Spain) for the financial support through Project CTQ 2004–00454.

References

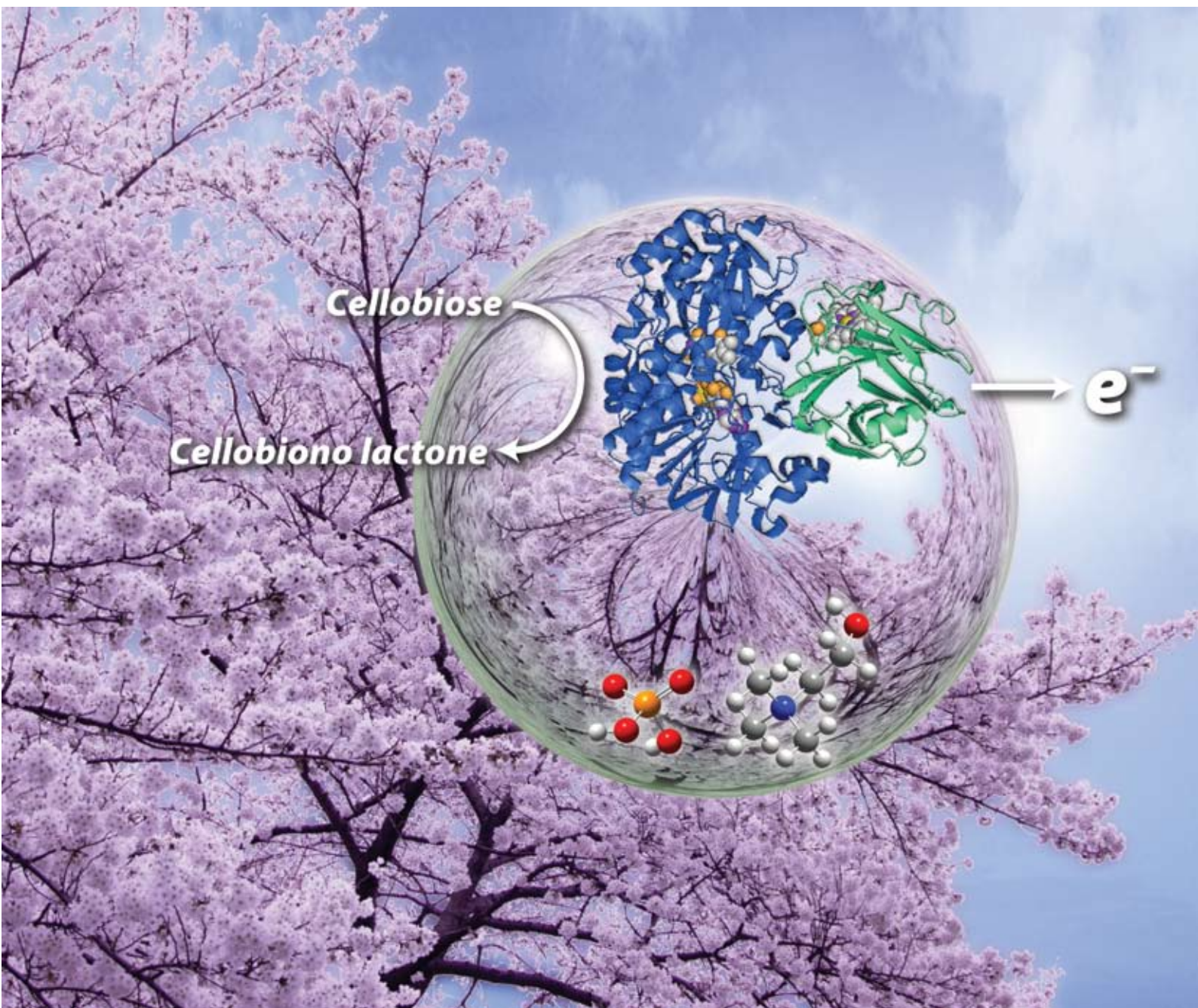
- 1 A. Pucci, *Pure Appl. Chem.*, 1989, **61**, 1363–1372.
- 2 S. J. Marwil, Separation of hydrocarbon and alcohol azeotropic mixtures by distillation with anhydrous ammonia. *US Pat.*, 4 437 941, 1984.
- 3 J. G. Huddleston, H. D. Willauer, R. P. Swatloski, A. E. Visser and R. D. Rogers, *Chem. Commun.*, 1998, 1765–1766.
- 4 A. G. Fadeev and M. M. Meagher, *Chem. Commun.*, 2001, 295–296.
- 5 J. G. Huddleston, A. E. Visser, W. M. Reichert, H. D. Willauer, G. A. Broker and R. D. Rogers, *Green Chem.*, 2001, **3**, 156–164.
- 6 C. Jork, M. Seiler, Y.-A. Beste and W. Arlt, *J. Chem. Eng. Data*, 2004, **49**, 852–857.
- 7 M. Seiler, C. Jork, A. Kavarnou, W. Arlt and R. Hirsch, *AIChE J.*, 2004, **50**, 2439–2454.
- 8 X. Hu, J. Yu and H. Liu, *Water Sci. Tech.*, 2006, **53**, 245–249.
- 9 A. B. Pereiro, E. Tojo, A. Rodriguez, J. Canosa and J. Tojo, *Green Chem.*, 2006, **8**, 307–310.
- 10 A. B. Pereiro and A. Rodriguez, *Fluid Phase Equilib.*, 2008, **270**, 23–29.
- 11 A. B. Pereiro and A. Rodriguez, *Sep. Purif. Technol.*, 2008, **62**, 733–738.
- 12 G. W. Meindersma, A. Podt and A. B. de Haan, *Fuel Proc. Technol.*, 2005, **87**, 59–70.
- 13 G. W. Meindersma and A. B. de Haan, *Chem. Eng. Res. Des.*, 2008, **86**, 745–752.
- 14 A. B. Pereiro and A. Rodriguez, *J. Chem. Thermodyn.*, 2007, **39**, 1608–1613.
- 15 L. Zhang, Y. F. Deng, C. B. Li and Ji. Chen, *Ind. Eng. Chem. Res.*, 2008, **47**, 1995–2001.
- 16 A. B. Pereiro and A. Rodriguez, *J. Chem. Eng. Data*, 2008, **53**, 1360–1366.
- 17 A. B. Pereiro and A. Rodriguez, *J. Chem. Eng. Data*, 2007, **52**, 2138–2142.
- 18 A. B. Pereiro and A. Rodriguez, *J. Chem. Thermodyn.*, 2008, **40**, 1282–1289.
- 19 A. Arce, H. Rodriguez and A. Soto, *Green Chem.*, 2007, **9**, 247–253.
- 20 R. P. Swatloski, J. D. Rogers and R. D. Rogers, *Green Chem.*, 2003, **5**, 361–363.
- 21 V. Najdanovic-Visak, J. M. S. S. Esperanca, L. P. N. Rebelo, M. Nunes da Ponte, H. J. R. Guedes, K. R. Seddon and J. Szydowski, *Phys. Chem. Chem. Phys.*, 2002, **4**, 1701–1703.
- 22 H. Renon and J. M. Prausnitz, *AIChE J.*, 1968, **14**, 135–144.
- 23 G. W. Meindersma, A. Podt and A. B. De Haan, *J. Chem. Eng. Data*, 2006, **51**, 1814–1819.
- 24 T. M. Letcher and P. Reddy, *J. Chem. Thermodyn.*, 2005, **37**, 415–421.
- 25 X. Hu, J. Yu and H. Liu, *J. Chem. Eng. Data*, 2006, **51**, 691–695.
- 26 A. Arce, M. J. Earle, H. Rodríguez and K. R. Seddon, *Green Chem.*, 2007, **9**, 70–74.
- 27 A. Arce, M. J. Earle, H. Rodríguez and K. R. Seddon, *J. Phys. Chem. B*, 2007, **111**, 4732–4736.
- 28 G. W. Meindersma, A. Podt, M. B. Klaren and A. B. De Haan, *Chem. Eng. Commun.*, 2006, **193**, 1384–1396.
- 29 A. B. Pereiro, P. Verdía, E. Tojo and A. Rodriguez, *J. Chem. Eng. Data*, 2007, **52**, 377–380.

Green Chemistry

Cutting-edge research for a greener sustainable future

www.rsc.org/greenchem

Volume 11 | Number 3 | March 2009 | Pages 297–436



ISSN 1463-9262

RSC Publishing

Ohno *et al.*
Biocatalytic oxidation of cellobiose

Guo *et al.*
Simultaneous esterification and transesterification of soybean oil

Tan *et al.*
Extraction of lignin from lignocellulose

Jessop *et al.*
Switching the hydrophilicity of a solute



1463-9262(2009)11:3;1-B

Biocatalytic oxidation of cellobiose in an hydrated ionic liquid

Kyoko Fujita,^a Nobuhumi Nakamura,^a Kiyohiko Igarashi,^b Masahiro Samejima^b and Hiroyuki Ohno^{*a}

Received 4th August 2008, Accepted 25th November 2008

First published as an Advance Article on the web 15th December 2008

DOI: 10.1039/b813529k

Extraction of electrons from cellobiose is realised by cellobiose dehydrogenase (CDH) in hydrated choline dihydrogen phosphate (dhp). Both inter- and intra-electron transfer of CDH were observed in the hydrated choline dhp suggesting a potential candidate of a non-aqueous solvent for enzymatic treatment of depolymerised biomass.

Introduction

Ionic liquids (ILs) typically possess almost no vapour pressure, have fascinating features such as high thermal, chemical and electrochemical stability. They are expected to be a maintenance free reaction media. ILs have gained increasing attention as green, multi-use reaction media, as well as solvents for electrochemistry and chemistry.^{1–3} ILs are also currently being investigated for a variety of bio-applications including use as media for biocatalytic reactions,^{4–7} biosensors,⁸ and protein stabilization.^{9–11}

A number of enzymes have been recognised to show catalytic activity in ILs.^{4,5} Lipases, in particular, maintain their activity in anhydrous ILs, as their selectivity and operational stability are often better than in traditional aqueous media.^{4,5} However in most cases, the enzymes are not in a homogeneously dissolved state, and are therefore acting like heterogeneous catalysts. Proteins are usually insoluble in organic solvents and ILs.^{4,12,13} Some hydrophilic ILs have been reported to accelerate dissociation of the proteins, but induced loss of secondary or higher ordered structures.^{9,14,15} To improve these problems, we have been studying hydrated ILs as solvents for proteins. Hydrated ILs maintain the basic properties of pure ILs, but a small amount of water was effective enough to improve the protein solubility considerably. We have already reported that cytochrome *c* (cyt *c*) is soluble, stable, and remains active in some hydrated ILs.¹⁰ Other proteins, including some enzymes, also showed excellent solubility and activity after dissolution in hydrated ILs (unpublished data). For example, hydrated choline dihydrogen phosphate (choline dhp) acts as an excellent preserver of proteins such as cyt *c*. Thus, cyt *c* maintained around 70% activity after 1.5 years storage at room temperature.¹⁰ Accordingly, these hydrated ILs may resolve troublesome conditions for proteins in technological uses.

Recently, it has become a pressing and important task to produce energy from biomass. For this, inedible biomass should be used instead of foods. Cellulose is the most abundant and

inedible biorenewable material in existence.¹⁶ However, natural cellulose is insoluble in water and most common organic molecular liquids because it consists of polydispersed linear glucose polymer chains, and furthermore, has a supramolecular complex structure stabilised by many hydrogen bonds.¹⁷ Degradation of cellulose in ILs should open a new strategy to construct sustainable energy conversion systems, such as biofuel cells. Three steps below should be clarified in ILs for the energy conversion of biomass. First step is cellulose treatment and dissolution. The second is depolymerization of cellulose. The third is generation of electrons from produced mono- or oligosaccharides. In an early stage, Rogers *et al.* reported that 1-butyl-3-methylimidazolium chloride, [bmim]Cl, has the potential to dissolve cellulose at high temperature.¹⁸ Furthermore, the dissolution at mild conditions with ILs has been reported.^{19,20} For the second step, solubilised cellulose was expected to be enzymatically converted into glucose in the IL. However, cellulase was irreversibly denatured in [bmim]Cl.²¹ Further investigations are necessary to design better ILs for enzymatic depolymerization. This work aims to realise the third step. Thus, we investigated the extraction of electrons from cellobiose by biocatalysis in the hydrated ILs. Hydrated choline dhp is used as an IL medium, since it has been found by Fujita *et al.* to be an excellent IL solvent for cyt *c*.¹⁰ Cellobiose dehydrogenase (EC 1.1.99.18; CDH) is investigated as one of the target enzymes for the extraction of electrons from biomass. CDH oxidises cellobiose, which is a repeating unit of cellulose (Fig. 1 enclosure).

CDH is an extracellular enzyme produced by a variety of fungi.^{22,23} CDH from white-rots has a proposed role in the early events of lignocellulose degradation and wood colonization.²⁴ CDH is an enzyme having two separate domains, one containing flavin (FAD) and the other containing a type-*b* heme. The molar ratio of FAD/heme is known to be 1:1.^{25,26} These separate domains work as an electron acceptor and donor, separately.^{22,27} From this structural characteristic, and given that separate sites in one molecule serve as the electron acceptor and donor, potential applications of CDH in biotechnology were exploited for bioelectrochemical and organic syntheses,²⁸ third generation biosensors,^{29,30} biofuel cells³¹ and biomass development.³² There have been many discussions regarding the electron transfer reaction of CDH.^{27,29} Although many candidates have been proposed as the electron acceptor of CDH, its natural electron acceptor is still uncertain.

^aDepartment of Biotechnology, Tokyo University of Agriculture and Technology, 2-24-16 Nakacho, Koganei, Tokyo, 184-8588, Japan. E-mail: ohnoh@cc.tuat.ac.jp; Fax: +81 42 388 7024; Tel: +81 42 388 7024

^bDepartment of Biomaterials Sciences, Graduate School of Agriculture and Life Sciences, The University of Tokyo, 1-1-1 Bunkyo-ku, Tokyo, 113-8657, Japan. E-mail: aqarius@mail.ecc.u-tokyo.ac.jp; Fax: +81 3 5841 5273; Tel: +81 3 5841 5258

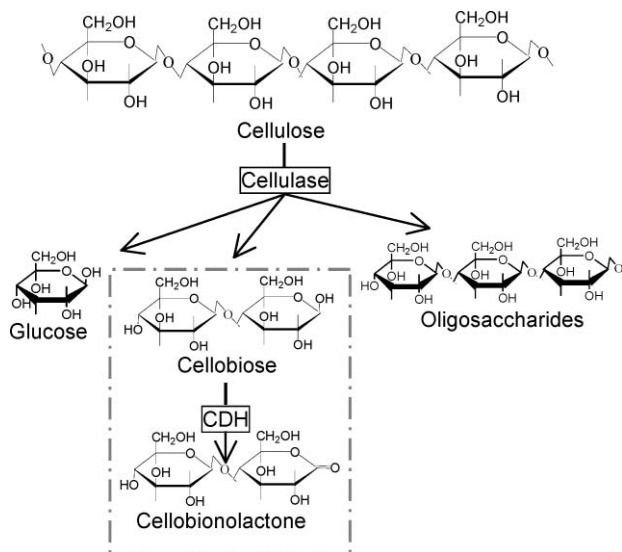


Fig. 1 CDH-catalysed oxidation of cellobiose that is one of depolymerised products of cellulose.

Experimental

D-Cellobiose was purchased from ICN Biomedicals (Irvine, CA, USA). Horse heart cytochrome *c* (cyt *c*) was purchased from Aldrich and used without further purification. Recombinant wild-type *P. chrysosporium* CDH was heterologously expressed in the methylotrophic yeast *Pichia pastoris* and purified as described previously.³³ 2,6-Dichloroindophenol sodium (DCIP) and other chemicals were purchased and used without further purification. Choline dihydrogen phosphate (choline dhp) was synthesised by a modified method.¹⁰ Choline bromide solution was treated on an ion exchange resin (Amberlite IRN77), then mixed with phosphoric acid solution. The solvent evaporated and the product was dried *in vacuo*. Choline dhp was identified using ¹H NMR, DSC, elemental analysis and electrospray mass spectrometry.

Absorption spectra and absorbance changes were recorded with Shimadzu UV-2450. Cellobiose (500 μM), cyt *c* (50 μM) and CDH (10 μM) were prepared with 20 mM sodium acetate (NaAc) buffer (pH 4.0). DCIP (50 μM) was prepared with 50 mM phosphate buffer (pH 7.0). Hydrated choline dhp (500 mg) was dissolved in 60 μL buffer first, then the prepared solution of cellobiose (70 μL), CDH (70 μL) and cyt *c* (70 μL) or DCIP (70 μL) were mixed with it. In both cases, a typical reaction mixture contained choline dhp, buffer, cellobiose, CDH and cyt *c* or DCIP in a final water content of 35 wt%. The viscosity was measured using a DV-|+ viscometer (Brookfield) with a CPE-40 spindle.

Results and discussion

When CDH solution is mixed with hydrated choline dhp, a clear liquid results. This would suggest successful dissolution of CDH in hydrated choline dhp. Generally, and as mentioned before, dissolution of proteins in most ILs is difficult. When a protein is insoluble in IL, a turbid solution results after mixing with a protein solution. To investigate the degradation process of CDH in choline dhp, first we prepared hydrated choline dhp

with 20 wt% water (about three water molecules per one ion pair), the same conditions as in our previous reports.¹⁰ However, the biocatalytic oxidation of CDH was not observed. Then, we changed the water content to find better conditions. The reaction was clearly observed when CDH was dissolved in hydrated choline dhp containing 35 wt% water. So, hydrated choline dhp with 35 wt% water (about six water molecules per one ion pair) was used as the reaction media in this study. The reason why no reaction was detected in choline dhp with 20 wt% water contents will be discussed later.

The electron transfer reactions of the FAD domain was first examined by DCIP. DCIP is used as a kind of indicator for the electron transfer reaction. DCIP receives two electrons directly from the FAD domain to form DCIPH₂ (Fig. 2). Generally, the electron transfer to DCIP from the FAD domain takes precedence over that occurring to the heme from the FAD domain, because the transfer of the former is faster than the latter. Fig. 3 shows the spectral change of DCIP before and after mixing with cellobiose solution in the hydrated IL. With cellobiose, the absorbance around 600 nm, based on DCIP, completely vanished after receiving electrons from CDH. It was confirmed that the FAD domain is active and able to execute the electron transfer in hydrated choline dhp.

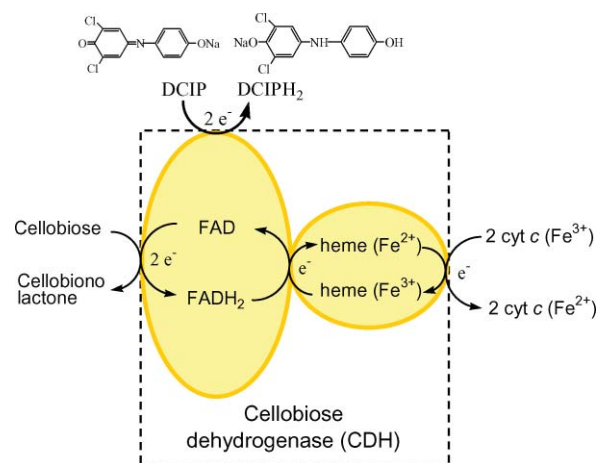


Fig. 2 Schematic representation of the pathway of electron transfer of cellobiose, CDH and cyt *c* or DCIP.

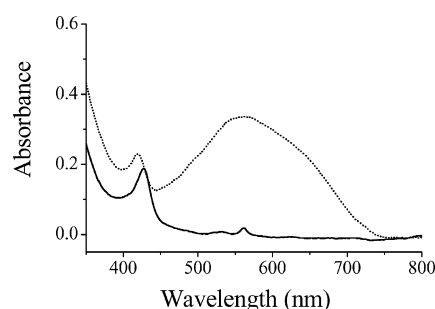


Fig. 3 Visible absorption spectra of DCIP in hydrated IL with CDH before (oxidised form; dotted line) and after (reduced form; solid line) mixing with cellobiose.

Next, cyt *c* was used as an indicator to confirm the intra-electron transfer reaction of CDH. Cyt *c* is one of several well

known electron acceptors of CDH *in vitro*. When cyt *c* works as an electron acceptor of CDH, the electron transfer path is proposed as shown in Fig. 2. In the oxidation reaction of cellobiose, two electrons are transferred at the FAD domain. These electrons must be sequentially delivered one by one from FAD to the heme *via* an internal electron transfer process. These electrons are then further transferred to the cyt *c* from the heme. When the inter- and intra-electron transfer reactions of CDH are in progress, it leads to cyt *c* reduction in the end. That is, the cyt *c* reduction means definite activity occurs for both domains of the CDH. When the absorption spectrum of cyt *c* was measured, no spectral change was observed without CDH or cellobiose. On the other hand, there was typical reduction of cyt *c* found after mixing cellobiose with CDH in hydrated IL, as shown in Fig. 4. This means that the electron was transferred from cellobiose to the two domains of CDH, and then to cyt *c* successfully in hydrated choline dhp. However, the reaction rate was slow compared with the aqueous system. There are two factors proposed to explain this slowing. One is the effect of viscosity; the viscosity of the reaction mixture (35 wt% water contents) was 25 cP at room temperature. That is quite a small value for ionic liquids, but it is still much larger than that of water (0.9 cP). Generally, the diffusion coefficient is inversely proportional to the viscosity, such that it must have a great effect on the two inter-electron transfers. In fact, even for the reaction of the FAD domain with DCIP as described above, the reaction was slow compared to that in an aqueous system. This means that the viscosity of the hydrated IL certainly affects the inter-electron transfer. In the case of hydrated choline dhp with 20 wt% water, the viscosity was 440 cp. In such high viscosity media, the diffusion must be very slow. That is, it must be a strong reason why we could not observe the biocatalytic oxidation in the hydrated choline dhp with 20 wt% water as mentioned above. Similar experiments are now in progress in the hydrated IL (with 20 wt% water) for a longer time span. In any case, if this system was applied for biofuel cells, immobilization of CDH on an electrode would be inevitable.³¹ Then, the viscosity of hydrated IL could almost be ignored.

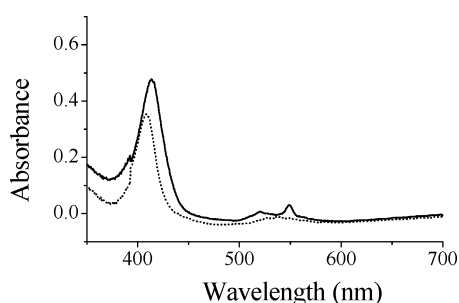


Fig. 4 Absorption spectra of cyt *c* in hydrated IL with cellobiose before (oxidised form; dotted line) and after (reduced form; solid line) mixing with CDH.

Meanwhile, the effect of pH in hydrated choline dhp is considered as another reason for this slow reaction. In an aqueous system, it is reported that although flavin reduction by cellobiose was observed in the range of pH 3.0–7.0, the velocity of the next electron transfer step to heme decreased with an increase in pH and it reached almost zero in solution

with pH of above 6.0.³³ Although pH value has little meaning in hydrated IL, the apparent pH value was measured to be 5.4 in the hydrated (35 wt%) choline dhp system with cyt *c*. Accordingly, it is suggested here that the electron transfer from the FAD domain to the heme become slow and consequently lowered the reduction rate of cyt *c* in the hydrated choline dhp. An investigation is in progress to further analyse the effect of pH in the hydrated choline dhp on the intra-electron transfer of CDH.

Conclusions

We investigated the biocatalysis of CDH in hydrated choline dhp. As such, CDH is successfully dissolved in hydrated choline dhp and maintains its activity. Generally, the electron transfer reaction of protein is considerably influenced by the salt concentration in the aqueous phase and often disappears with high salt concentration. In this study, on the other hand, the inter- and intra-electron transfer of CDH was observed in hydrated choline dhp without blocking. Although the reaction rate was thus far not as fast as that in an aqueous system, if the effect of diffusion was reduced in hydrated choline dhp, this is expected to be a great system for promoting development of biofuel cells after some improvements. For example, these could be operated under high temperature to reduce viscosity, because hydrated ILs are stable and show relatively small vapour pressure in spite of water-like properties. Also, CDH is able to realise the direct electron transfer reaction with an electrode.²⁹ These should be helpful to drive the system stably. Furthermore, an expansion of shelf-life is promising when an hydrated IL has been used. This research has shown that hydrated ILs can be used not just as novel solvents for biocatalysis, but also as working matrices with broad applications.

Acknowledgements

This study was supported by a Grant-in-Aid for Scientific Research to H.O. (no. 17205020) and K.I. (no. 19688016) from the Ministry of Education, Culture, Sports, Science and Technology, and by a Grant-in-Aid for Scientific Research to H.O. (no. 17073005) and K.I. (no. 20658040) from the Japan Society for the Promotion of Science. K.F. thanks the Japan Society for Promotion of Science (Research Fellowship for Young Scientists) for support.

Notes and references

- 1 T. Welton, *Chem. Rev.*, 1999, **99**, 2071.
- 2 K. R. Seddon, *J. Chem. Technol. Biotechnol.*, 1997, **68**, 351.
- 3 P. Wasserscheid, T. Welton, *Ionic liquids in synthesis*, Wiley-VCH, Weinheim, 2003.
- 4 U. Kragl, M. Eckstein and N. Kaftzik, *Curr. Opin. Biotechnol.*, 2002, **13**, 565.
- 5 F. van Rantwijk, L. R. Madeira and R. A. Sheldon, *Trends Biotechnol.*, 2003, **21**, 131.
- 6 S. Shipovskov, H. Q. N. Gunaratne, K. R. Seddon and G. Stephens, *Green Chem.*, 2008, **10**, 806.
- 7 H. Zhao, G. A. Baker, Z. Song, O. Olubajo, T. Crittle and D. Peters, *Green Chem.*, 2008, **10**, 696.
- 8 J. A. Laszlo and D. L. Compton, *J. Mol. Catal. B: Enzym.*, 2002, **18**, 109.

- 9 T. De Diego, P. Lozano, S. Gmouh, M. Vaultier and J. L. Iborra, *Biotechnol. Bioeng.*, 2004, **88**, 916; T. De Diego, P. Lozano, S. Gmouh, M. Vaultier and J. L. Iborra, *Biomacromolecules*, 2005, **6**, 1457.
- 10 K. Fujita, D. R. MacFarlane and M. Forsyth, *Chem. Commun.*, 2005, 4804; K. Fujita, D. R. MacFarlane, M. Forsyth, M. Yoshizawa-Fujita, K. Murata, N. Nakamura and H. Ohno, *Biomacromolecules*, 2007, **8**, 2080.
- 11 N. Byrne, L.-M. Wang, J.-P. Belieres and C. A. Angell, *Chem. Commun.*, 2007, 2714.
- 12 A. M. Klivanov, *Nature*, 2001, **409**, 241.
- 13 N. Kimizuka and T. Nakashima, *Langmuir*, 2001, **17**, 6759.
- 14 R. Madeira Lau, M. J. Sorgedraeger, G. Carrea, F. Van Rantwijk, F. Secundo and R. A. Sheldon, *Green Chem.*, 2004, **6**, 483.
- 15 M. Erbedinger, A. J. Mesiano and A. J. Russell, *Biotechnol. Prog.*, 2000, **16**, 1131.
- 16 Kirk-Othmer, *Encyclopedia of Chemical Technology*, 4th edn, Wiley, New York, 1993.
- 17 V. L. Finkenstadt and R. P. Millane, *Macromolecules*, 1998, **31**, 7776.
- 18 R. P. Swatloski, S. K. Spear, J. D. Holbrey and R. D. Rogers, *J. Am. Chem. Soc.*, 2002, **124**, 4974.
- 19 Y. Fukaya, A. Sugimoto and H. Ohno, *Biomacromolecules*, 2006, **12**, 3295; Y. Fukaya, K. Hayashi, M. Wada and H. Ohno, *Green Chem.*, 2008, **10**, 44.
- 20 A. P. Dadi, S. Varanasi and C. A. Schall, *Biotechnol. Bioeng.*, 2006, **5**, 904; G. Henriksson, G. Johansson and G. Pettersson, *J. Biotechnol.*, 2000, **78**, 93.
- 21 M. B. Turner, S. K. Spear, J. G. Huddleston, J. D. Holbrey and R. D. Rogers, *Green Chem.*, 2003, **5**, 443.
- 22 G. Henriksson, V. Sild, I. J. Szabo, G. Pettersson and G. Johansson, *Biochim. Biophys. Acta*, 1998, **1383**, 48; G. Henriksson, G. Johansson and G. Pettersson, *J. Biotechnol.*, 2000, **78**, 93.
- 23 M. D. Cameron and S. D. Aust, *Enzyme Microb. Technol.*, 2001, **28**, 129.
- 24 K.-E. Eriksson, N. Habu and M. Samejima, *Enzyme Microb. Technol.*, 1993, **15**, 1002.
- 25 M. Raices, R. Paifer, J. Cremata, R. Montesino, J. Stahlberg, C. Divne, I. J. Szabo, G. Henriksson, G. Johansson and G. Pettersson, *FEBS Lett.*, 1995, **369**, 233.
- 26 B. Li, S. R. Nagalla and V. Ranganathan, *Appl. Environ. Microbiol.*, 1996, **62**, 1329; B. Li, S. R. Nagalla and V. Ranganathan, *Appl. Environ. Microbiol.*, 1997, **63**, 769.
- 27 G. Henriksson, G. Pettersson, G. Johansson, A. Ruiz and E. Uzcategui, *Eur. J. Biochem.*, 1991, **196**, 101; M. G. Mason, P. Nicholls, C. Divne, B. M. Hallberg, G. Henriksson and M. T. Wilson, *Biochim. Biophys. Acta*, 2003, **47**, 1604.
- 28 E. Steckhan, *Top. Curr. Chem.*, 1994, **170**, 83.
- 29 L. Gorton, A. Lindgren, T. Larsson, F. D. Munteanu, T. Ruzgas and I. Gazaryan, *Anal. Chim. Acta*, 1999, **400**, 91; L. Stoica, R. Ludwig, D. Haltrich and L. Gorton, *Anal. Chem.*, 2006, **78**, 393.
- 30 E. Burestedt, C. Nistor, U. Schagerlöf and J. Emnéus, *Anal. Chem.*, 2000, **72**, 4171.
- 31 F. Tasca, L. Gorton, W. Harreither, D. Haltrich, R. Ludwid and G. Nöll, *J. Phys. Chem. C*, 2008, **112**, 9956.
- 32 M. Zamocky, R. Ludwig, C. Peterbauer, B. Hallberg, C. Divne, P. Nicholls and D. Haltrich, *Curr. Protein Pept. Sci.*, 2006, **3**, 255.
- 33 K. Igarashi, I. Momohara, T. Nishino and M. Samejima, *Biochem. J.*, 2002, **365**, 521; K. Igarashi, M. Yoshida, H. Matsumura, N. Nakamura, H. Ohno, M. Samejima and T. Nishino, *FEBS Lett.*, 2005, **272**, 2869.

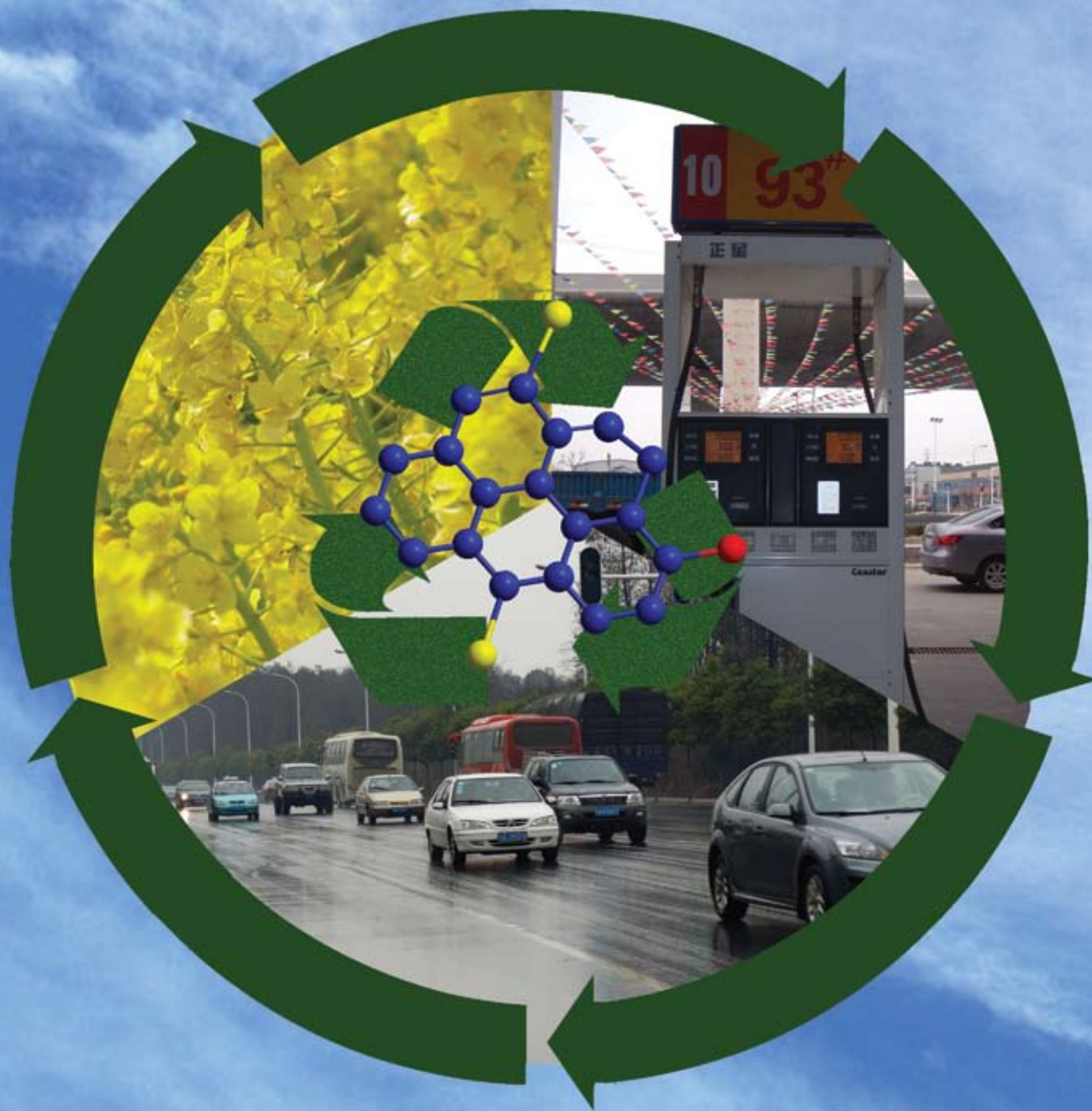
Green Chemistry

Cutting-edge research for a greener sustainable future

www.rsc.org/greenchem

Volume 11 | Number 3 | March 2009 | Pages 297–436

Downloaded by City College of New York on 21 November 2010
Published on 17 December 2008 on <http://pubs.rsc.org> | doi:10.1039/B812139G



ISSN 1463-9262

Zheng *et al.*
Biont shell catalyst for biodiesel
production

Oelgemöller *et al.*
Green photochemistry

Li *et al.*
Basic metal carbonate supported
gold nanoparticles

Nagarajan *et al.*
A stable biomimetic redox catalyst

RSC Publishing

Biont shell catalyst for biodiesel production

Jie Xie, Xinsheng Zheng,* Aiqin Dong, Zhidong Xiao and Jinhua Zhang

Received 8th August 2008, Accepted 25th November 2008

First published as an Advance Article on the web 17th December 2008

DOI: 10.1039/b812139g

A novel high performance solid biodiesel catalyst derived from biont shell has been prepared by a tri-step procedure: incomplete carbonization–KF impregnation–activation. The effects of carbonization temperature, concentration of KF solution and activation temperature on the activity of the catalyst were investigated. The activity of the biont shell catalyst was evaluated by transesterification of rapeseed oil with methanol and the mechanism of catalytic activity is discussed. The results indicate that the transesterification yield of rapeseed oil to biodiesel reaches 97.5% with 3 hours reaction and 3 wt% catalyst dosage (based on rapeseed oil mass). The activity of the catalyst for the transesterification came from the active sites formed by reaction of incompletely carbonized biont shell with KF in the procedure of synthesis catalyst. The matrix of the biont catalyst is weakly polar in nature, favoring transesterification of rapeseed oil to biodiesel and hindering the reverse glycerolysis reaction. Therefore, the biont catalyst displayed a higher catalytic activity compared with conventional solid base catalysts tested for biodiesel production.

1. Introduction

Depleting supplies of fossil fuel and increasing future energy demands will require development of alternative “clean” energy sources,^{1–5} such as biodiesel composed of monoalkyl esters of fatty acids. Biodiesel is produced from renewable biomass by the transesterification of triglycerides derived from vegetable oils or animal fats. It is biodegradable and non-toxic, has low emission profiles and so is environmentally beneficial.^{6–10} However, the process used for biodiesel production by homogeneous alkali or acid catalysts involves high consumption of energy and the separation of the catalysts from the homogeneous reaction mixtures is costly and chemically wasteful.^{11–15}

Increasing awareness of environmental factors has led to a profound evolution in the way we view the preparation of catalysts for biodiesel production. An efficient solid catalyst enables the process of biodiesel production to be fully ecologically friendly. Various solid-basic catalysts, including alkaline-earth oxides,^{16–18} zeolites,^{19,20} aluminium–magnesium mixed oxides,²¹ and hereogenized alkylguanidines,²² have exhibited some catalytic activity for transesterification of vegetable oils to biodiesel. However, some of the solid bases like CaO reported in the literature react easily with free fatty acids to form unwanted soap by-products and act as homogeneous catalysts in solution media.²³ Moreover, ETS-10(NA,K) and alkylguanidines/resin solid bases are found to leach out to the bulk solution even under mild conditions, losing much of their activity after only a few reaction cycles and contaminating the products.²⁴ In comparison

with homogeneous bases catalysts, the rate of transesterification reaction by major solid bases catalysts is lower and does not meet the requirements of practical production of biodiesel.²⁵ Therefore, it is still a big challenge to search for an ideal heterogeneous catalyst for biodiesel production, with the aim of integrating low-cost production, ecofriendly nature, and high catalytic activity characteristics into the promising biodiesel production.

To address these issues, we have developed a novel biont shell catalyst from incompletely carbonized natural products such as turtle shell, shrimp shell and crab shell to produce biodiesel from rapeseed oil. Our biont shell catalyst is recyclable and its activity markedly exceeds that of other solid base catalysts tested for biodiesel production. This high-performance catalyst does not produce saponification and emulsification in the process of catalytic reaction. Therefore, the production of biodiesel from rapeseed oil using this catalyst is a promising “green” process. The biont shell catalyst, which comes from renewable biomass and can be biodegraded easily, has the distinct characteristics of a “green” catalyst.

Biont shells are rich in chitin which is the second-largest renewable resources in the world and has been widely and deeply studied in the fields of food, chemistry, and environment.^{26–28} To the best of our knowledge, it is the first time a heterogeneous catalyst has been prepared for biodiesel production using the natural biont shell material. Incompletely sulfonated carbonized saccharide solid acid catalysts have been used successfully for esterification of oleic acid and stearic acid.²⁹ Although chitin is analogous to polysaccharides, this study is still a novel exploration in that the biont shell is firstly incompletely carbonized, the resulting material is then impregnated in KF solution, and subsequently undergoes a necessary activation step to prepare a high-performance solid base catalyst.

Institute of Chemical Biology, Department of Chemistry, Huazhong Agricultural University, Wuhan, 430070, P. R. China.
E-mail: xszheng@mail.hzau.edu.cn; Fax: +86-27-87282133;
Tel: +86-27-87281187

2. Results and discussion

2.1 Factors influencing the catalyst activity

As is well known, the biont shell used (the raw material is turtle shell in following discussion) is a natural, complicated material consisting mainly of chitin, protein and inorganic salt.^{30,31} Chitin, in the shape of fibers and in the state of interlacement, forms a layer which is parallel to the surface of the shell. The sheet protein grows along the chitin layer within the corresponding framework. The inorganic salt fills in the space between the chitin layers and the protein layers. The scheme we used to prepare biont shell catalyst is shown in Scheme 1. The natural material, turtle shell, was firstly incompletely carbonized, the resultant material was then impregnated in KF solution, and subsequently underwent a necessary activation step to prepare biont shell catalyst. A scanning electron microscope (SEM) was employed to characterize the microstructures of this catalyst. The activity of the catalyst was evaluated by transesterification of rapeseed oil with methanol. The effects of carbonization temperature, concentration of KF solution, and activation temperature on the catalyst activity were investigated.

To investigate the effect of carbonization temperature on catalytic activity, a series of the catalysts were prepared at different carbonization temperatures (all samples were treated by 25 wt% KF solution and 300 °C activation temperature) and were used for transesterification of rapeseed oil with methanol. As shown in Fig. 1a, the yield of transesterification of rapeseed oil is greatly improved with an increase of carbonization temperature in the range of 300 °C to 500 °C, then it displays a descending rate beyond 500 °C and is almost zero at 700 °C.

Clearly, the optimum carbonization temperature for the shell material should be 500 °C (as illustrated in Fig. 1a).

Fig. 2 shows the visible effect of the turtle shell with different carbonization temperatures during the carbonization treatment. It displays a black color under 400 °C carbonization temperature owing to the residues of organism, whereas it transformed to a gray color at 500 °C. The shell material turned white with blue components due to the complete vaporization of its organic components at 700 °C carbonization treatment, and changed into a very rigid solid.

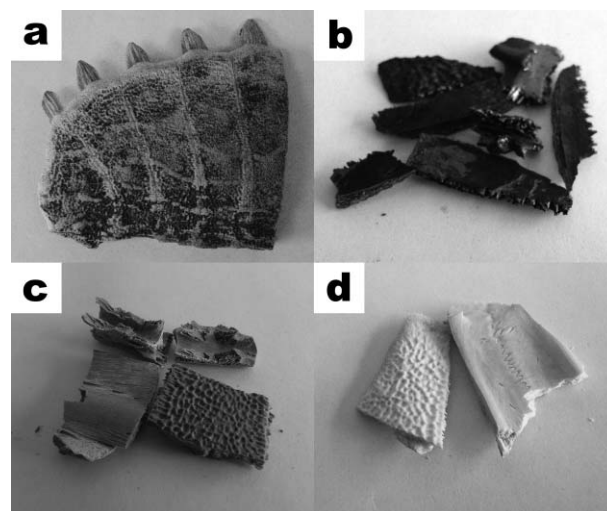
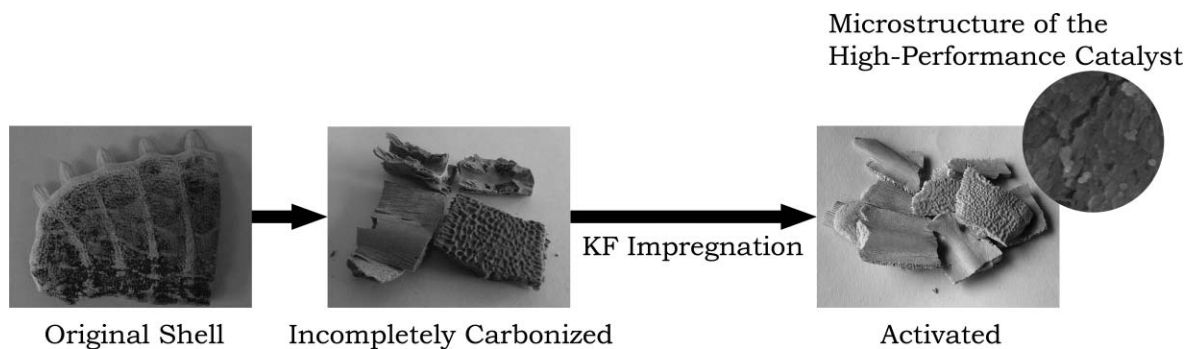


Fig. 2 The original appearance of turtle shell and visible alterations of appearance of the shell materials after carbonization at different temperatures: (a) the original turtle shell; (b), (c), (d) samples having undergone carbonization treatment at 400, 500, 600 °C, respectively.



Scheme 1 The tri-step synthesis procedure for obtaining the biont biodiesel catalyst.

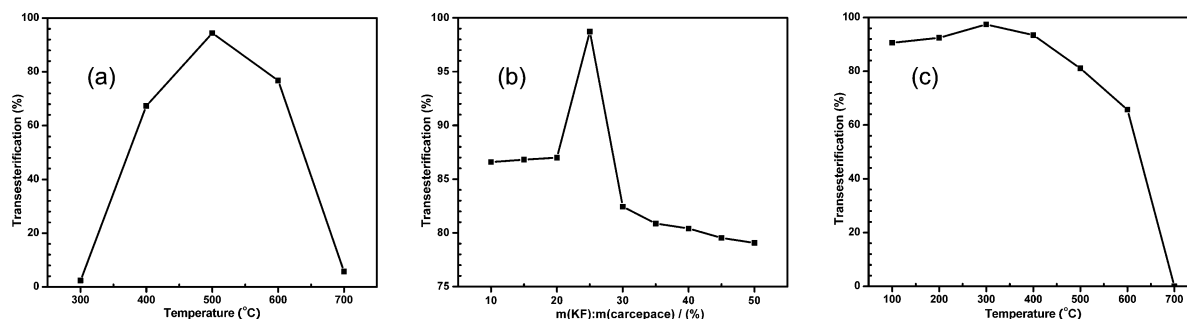


Fig. 1 The effect of (a) carbonization temperature; (b) concentration of KF solution; (c) activation temperature on activity of the catalyst. Mass ratio of catalyst to rapeseed oil: 3%; molar ratio of methanol to rapeseed oil: 9:1; reaction temperature: 70 °C; reaction time: 3 h.

Fig. 1b shows the results regarding the effect of concentration of KF solution on the activity of the catalysts. The yield of transesterification is improved from 87% to 98% when the concentration of KF solution increases from 10 wt% to 25 wt%. It can be assumed from this result that the increase of the concentration of KF solution contributes to an increase of the active sites in the shell materials. When the concentration of KF solution is beyond 25 wt%, however, the activity of the catalysts is reduced with the increasing of the concentration of KF solution, and the yield of transesterification was only 79% at 50 wt% KF solution, which means the active sites in the shell reach a saturation status when the concentration of KF is 25 wt%. Further increasing of the concentration of KF beyond 25 wt% only leads to the polymerization of the active sites. Thus, the optimum concentration of KF solution is 25 wt% in this regard.

The effect of the activation temperature on the activity of the catalyst was investigated in the temperature range of 200 °C to 500 °C, and all the samples were treated at 500 °C for incomplete carbonization and 25 wt% KF solution. Fig. 1c shows the yield of transesterification of rapeseed oil using biont catalysts prepared at different activation temperatures. Obviously, the rate of transesterification initially increased with the increase of the activation temperature, then reached the maximum value of 97% at 300 °C, and decreased when the activation temperature was over 300 °C. This is probably due to the fact that the number of active sites which were formed by a reaction of KF with incompletely carbonized turtle shell will increase with the elevation of activation temperature under 300 °C and will be decomposed above 300 °C.

The effects of the mole ratio of methanol to rapeseed oil on the transesterification of biodiesel are shown in Fig. 3.

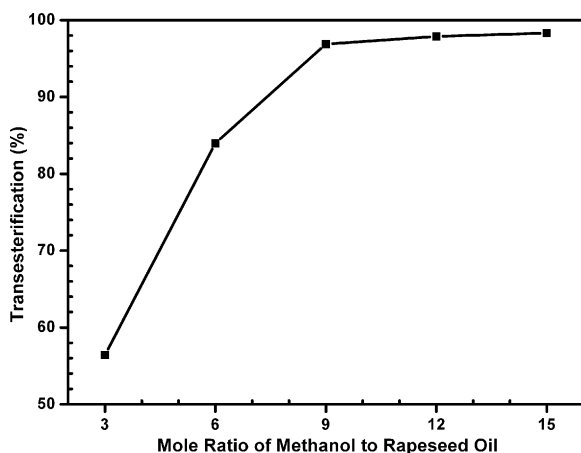


Fig. 3 The effect of mole ratio of methanol to rapeseed oil on transesterification reaction.

Theoretically, the transesterification of rapeseed oil to biodiesel requires three moles of methanol for each mole of oil. However, in practice, the mole ratio of methanol to oil should be higher than that of theoretical ratio in order to drive the reaction towards completion and produce more methyl esters as product. From Fig. 3, when the mole ratio of methanol to oil is below 9, the yield of transesterification of biodiesel increased with the ratio of methanol to oil; when the mole ratio of methanol to

oil was above 9, the transesterification yield remained almost unchanged with increases of the ratio of methanol to oil. Experimentally, the methanol can dilute rapeseed oil; the higher ratio of methanol to oil can enable full contact between reagents and catalyst, so as to accelerate the reaction. However, excessive methanol is not favorable for the purification of biodiesel in the following separation processes. Also, recovery of the unreacted methanol will consume large amounts of energy. According to our experiment results, the appropriate molar ratio of methanol to rapeseed oil should be 9:1.

2.2 Characterization of biont shell catalyst

The transesterification of rapeseed oil with methanol was carried out by using biont shell catalyst prepared at carbonation temperature 500 °C, 25 wt% KF aqueous solution treatment and activation temperature 300 °C. The reaction conditions were set at: reaction temperature 70 °C, mole ratio of methanol to rapeseed oil 9:1, and catalyst dosage 3% of rapeseed oil mass.

Fig. 4 shows typical transesterification rate profiles for rapeseed oil in the presence of the biont shell catalyst prepared at different activation temperatures. It can be seen that transesterification yield of rapeseed oil is over 90% at a reaction time of 2 h and reaches 97% at a reaction time of 3 h in the presence of biont shell catalyst prepared at activation temperature 300 °C. In recent studies using polymeric resin with QN^+OH^- terminated groups and QN^+OH^- functionalized silica as catalyst, respectively, around 90% triacetin conversion was achieved after reaction time of 4 h. However, by increasing the length of the fatty acid chain in triglycerides the catalytic activity of these catalysts will decrease further due to increasing steric hindrance.²⁴ For the transesterification of refined soybean oil with methanol (6:1) using 1% (by mass ratio of catalyst to oil) NaOH, methyl ester yield was 94.8% at reaction temperature 60 °C after reaction time of 1 h.¹¹ Although it was lower compared with the homogeneous NaOH catalyst, the catalytic activity exhibited by the biont shell catalyst in triglyceride transesterification was much higher than that of conventional solid base catalysts. Therefore, the biont shell catalyst can be used as a replacement for homogeneous NaOH catalyst in transesterification reaction owing to its environmental benefits.

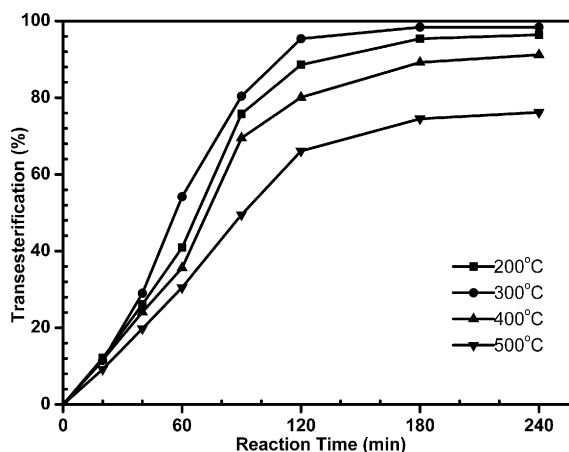


Fig. 4 The transesterification of rapeseed oil in the presence of the biont shell catalyst prepared at different activation temperature.

We also found that the biodiesel produced by transesterification of the rapeseed oil using biont shell catalyst is transparent, any subsequent purification step is not necessary. This indicates that there is no saponification in the process of transesterification of rapeseed oil with methanol by biont shell catalyst. Hence, the resultant mixture can be easily separated to remove the by-product, glycerol, and to recover the catalyst from the reaction mixture. Compared with conventional catalysts, the process of biodiesel production from rapeseed oil by using the biont shell catalyst omitted subsequent costly and chemically wasteful purification steps, indicating our catalyst is rather ecologically friendly.

2.2.1 Thermogravimetric analysis. The biont shell catalyst is insoluble in water, methanol, benzene, hexane, *N,N*-dimethylformamide and oleic acid, even at boiling temperature. The thermal stability of the catalyst was examined by thermogravimetric analysis (TGA). As shown in Fig. 5, biont shell catalyst has excellent thermal stability. The weight loss of the catalyst is almost zero at 70 °C (transesterification reaction temperature) and less than 5% even at 300 °C. The TGA curve of the catalyst is below that of incompletely carbonized turtle shell, which indicates that some new ingredients might be generated by KF and incompletely carbonized turtle shell. The rapid weight loss of all the samples above 700 °C can be attributed to the thermal decomposition of the turtle shell structure.

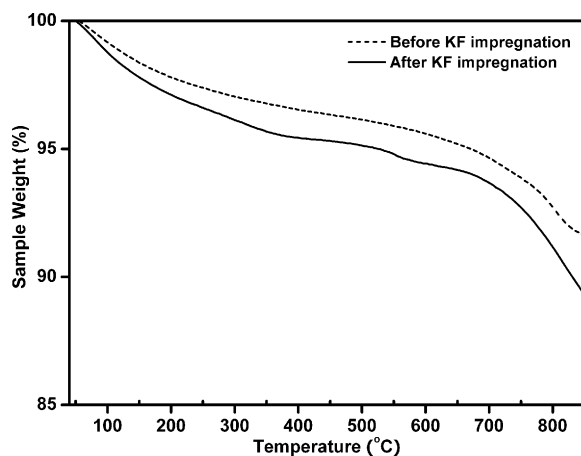


Fig. 5 TGA analysis of biont shell catalyst prepared from turtle shell before and after KF impregnation.

2.2.2 Catalyst deactivation and reusability. The reusability of the catalyst was investigated by carrying out subsequent reaction cycles. The catalyst, after 3 hours transesterification reaction, was separated from the reaction mixture and used again without any subsequent treatment in a second reaction cycle under the same reaction conditions as before. Results for all consecutive reaction cycles are given in Fig. 6. As can be seen, the biont shell catalyst was able to largely maintain its catalytic activity for all reaction cycles. However, it was found that the initial rate of transesterification of rapeseed oil with methanol decreased with each reaction cycle. This is probably due to some pores of the catalyst being blocked by the reactant and product, which influenced the diffusion of reactant to the activity center. So the catalyst has a lower initial rate of transesterification. With

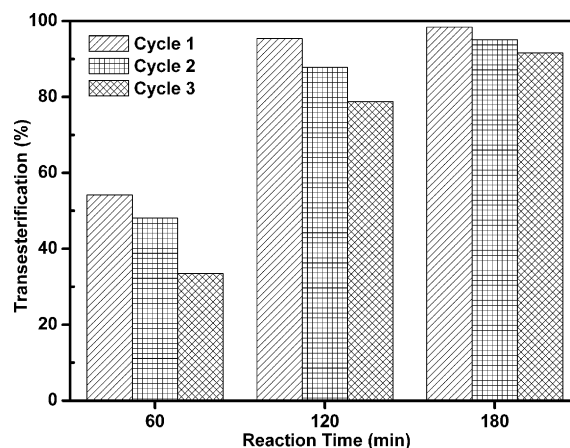


Fig. 6 The reusability performance of biont shell catalyst in biodiesel production.

the proceeding of reaction, the diffusion reached equilibrium and the yield of transesterification nearly reached the fresh catalyst level finally.

In order to investigate the reasons associated with the decrease of the activities, we took SEM characterization on the catalysts before and after use (Fig. 7). From the SEM images, many micro-nanometre crystals could be found at the surface of the catalysts. Through analyzing the SEM images of the catalyst before and after use, we found a layer of liquid membrane covered the micro-nanometre crystals of the used catalyst. This liquid membrane would decrease the activity of the catalysts. To remove this liquid membrane, the catalysts were treated in Soxhlet's Apparatus with petroleum ether as solvent for 3 hours, and the deposit build up on the catalyst surface was flushed away. The washed catalyst was used again with fresh reactants in the next reaction cycle under the same reaction conditions as before. After this treatment, the catalyst recovered its original high activity. The used catalysts were treated in Soxhlet's Apparatus with petroleum ether for 3 hours before the next cycle, then we found that the catalyst recovers its activity very well (the transesterification ratio remained at 70–80% even when used more than 10 times).

2.2.3 CO₂-TPD Experiments. In order to study the surfaces behavior of the catalyst, thermal programmed desorption (TPD) experiments were carried out. Chemisorption of small molecules can be used to estimate the basicity or acidity of catalyst. Because carbon dioxide is acidic, it is expected to adsorb strongly on the basic sites, CO₂ adsorption-desorption technique was used to detect the strength and concentration of basic sites present on the catalyst surface together with total basicity.

The CO₂-TPD profiles of catalysts before and after KF impregnation are shown in Fig. 8. The difference in the signal magnitude of catalyst is ascribed to the different basicity of material introduced. In this experiment, we will only take into account the position of desorption peaks but not their magnitude.

As shown in Fig. 8b, two CO₂ desorption peaks can be observed (the sample after KF impregnation and activation), one is a broad peak around 250 °C and the other is a sharp peak

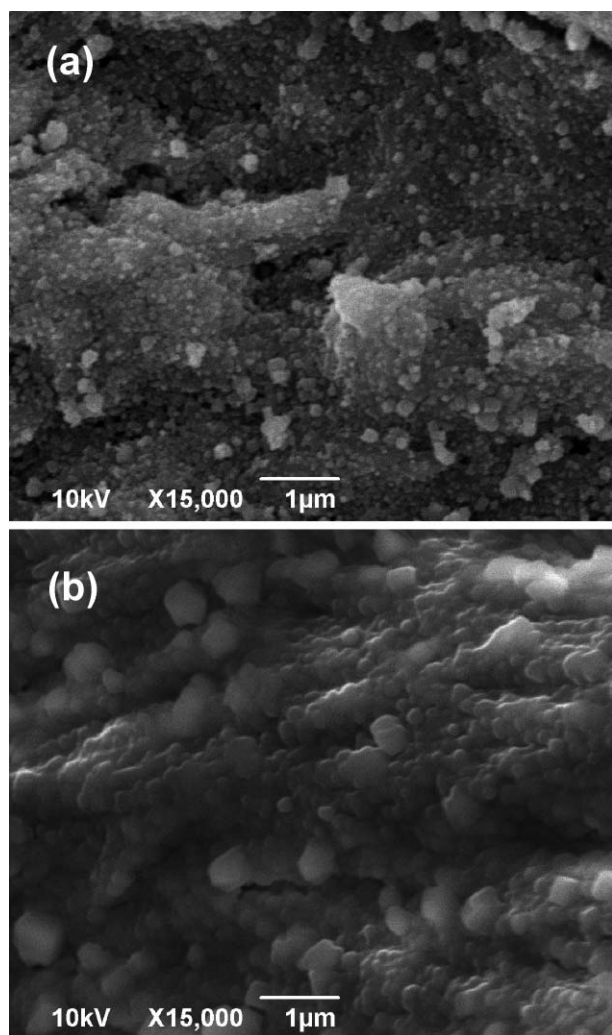


Fig. 7 SEM images showing the microstructural features of biont shell catalyst (a) before and (b) after transesterification reaction.

positioned at 550 °C. For the sample without KF impregnation, only one peak at around 250 °C can be observed.

The peaks in the different temperature region are associated with different types of sorption. The broad peak at low temperature can be attributed to the physisorption, and the peak at 550 °C resulted from desorption. We can only ascribe the difference in the peaks to the different preparation conditions of the samples. Some stronger basicity sites were formed in the sample after KF impregnation. The biont shell catalyst has a weak basicity, and one gram of the biont shell catalyst is able to neutralize 0.491 mmol hydrochloric acid by neutralization titration. The alkalinity of the catalyst is much lower than that of MgO, however, its catalytic activity markedly exceeds that of MgO.²⁴

2.2.4 Catalyst BET surface and pore size distribution. Surface area, total pore volume and pore size distribution are very important characters of solid catalyst because they are closely related to the activity of the catalyst. The Brunauer–Emmett–Teller (BET) surface area and total pore volume value of original biont shell and biont shell catalyst samples resulting from different conditions are shown in Table 1.

Table 1 BET surface area and total pore volume of biont shell catalyst (BSC) samples^a

	Surface area/m ² g ⁻¹	Total pore volume/cm ³ g ⁻¹
Original shell	15.43	0.0411
BSC-1	34.99	0.175
BSC-2	63.43	0.206
BSC-3	12.64	0.0311

^a BSC-1, BSC-2, BSC-3 samples were prepared with 25% KF impregnation and 300 °C activation treatment with different carbonization temperatures (300 °C, 500 °C and 700 °C, respectively).

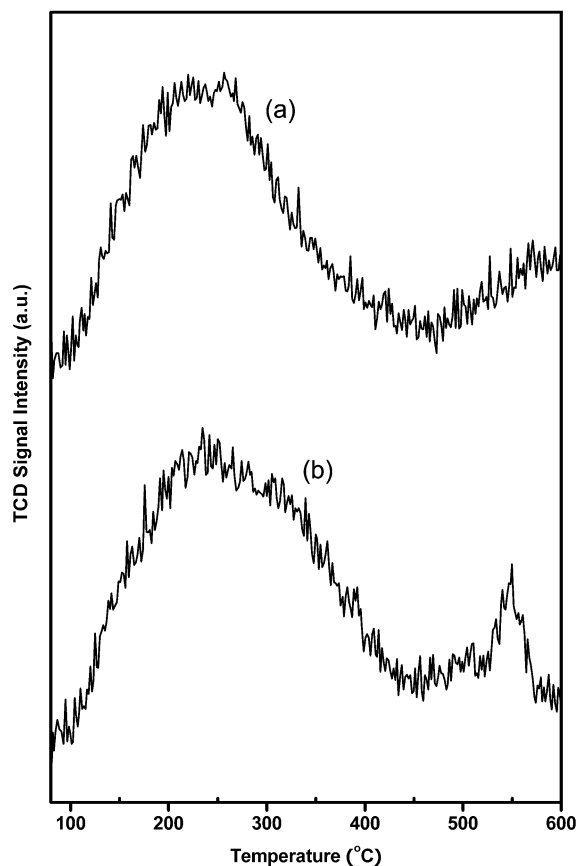


Fig. 8 CO₂-TPD spectra of biont shell catalyst samples: (a) without KF impregnation and (b) after activation.

From Table 1 we find that original biont shell has a small surface area and total pore volume value, but when the carbonization temperature was increased from 300 °C to 500 °C, the surface area increased from 34.99 m² g⁻¹ to 63.44 m² g⁻¹ with the total pore volume increased from 0.1750 cm³ g⁻¹ to 0.2060 cm³ g⁻¹, indicating that the biont shell structure changed when the carbonization temperature increased, and induced an increase of surface area and total pore volume value. The higher surface area will benefit the transesterification reaction of the catalyst. The surface area and total pore volume decreased obviously when the carbonization temperature increased to 700 °C.

We used SEM to analyze the change of microstructure of biont shell catalyst to elaborate the variation of catalyst surface area and total pore volume. As can be seen from Fig. 9a and b, the catalyst with a carbonization temperature below 500 °C has favorable surface area and total pore volume features because

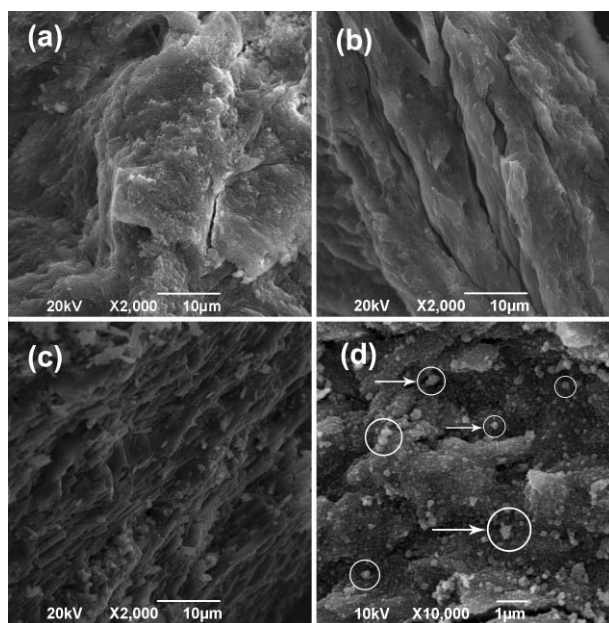


Fig. 9 SEM images showing the microstructural features of samples with different treatment: (a) sample after 300 °C carbonization treatment; (b) sample after 500 °C carbonization treatment; (c) sample treated with 500 °C carbonization and KF impregnation together with a 700 °C activation treatment; (d) high-resolution SEM image showing the details of the sample treated with 500 °C carbonization and KF impregnation together with a 300 °C activation treatment.

some small organic molecules were released from the shell to form a porous material under these conditions. The activity of the catalyst was enhanced with increasing specific surface area of turtle shell. Whereas, the structure of the shell was totally destroyed when the carbonization temperature was ramped up to 700 °C, and therefore the activity of the catalyst disappeared simultaneously (shown in Fig. 9c). This conclusion can be also supported by the TGA results (shown in Fig. 5).

The pore size distribution for original biont shell and different BSC samples can be clearly seen in Fig. 10. The original biont shell and BSC-3 sample show a very narrow pore distribution, centered at 30 to 100 nm pore diameter. The BSC-1 and BSC-2 samples show a broader pore distribution, and the pore diameter clustered around 80–300 nm, particularly for the BSC-2 sample. These macro-pores formed by the decomposition of organic substance associated with carbonization reaction. The macro-pores of this dimension provide appropriate space for the generating of active centers and suitable channels for the fast transfer of the product in the reaction.

These data indicated that the changes of carbonized biont shell structure will determine the surface area, total volume and pore diameter distribution and the activity of the catalyst.

2.2.5 XRD and IR analysis. Comparing the X-ray diffraction (XRD) results of the tri-step procedure catalyst and incomplete carbonized turtle shell, we found that in the curve of the tri-step procedure catalyst there was a wider but weaker diffraction peak at around $2\theta = 32^\circ$, and the peak height of two diffraction peaks at 28.42° and 35.14° increased obviously (indicated by the arrows in Fig. 11b). This result showed that after KF impregnation and activation, the randomness

of the molecular structure increased and the crystallinity of the molecular structure decreased. Meanwhile, more diffraction peaks were found in the XRD results of the tri-step procedure catalyst. This result showed that the crystal structure of the catalyst had a clear change after KF impregnation. The change of crystal structure means that new chemical bonds could possibly be formed.

Then, we did infrared spectrum (IR) analysis of these two catalyst materials. The result showed that tri-step procedure catalyst has two new absorption peaks at 833 and 703 cm^{-1} , and a stronger peak at 1652 cm^{-1} (indicated by the arrows in Fig. 12b). From these analyses we derived that new chemical bonds formed in the incomplete carbonized turtle shell after KF impregnation and activation, and the formation of new chemical bonds have direct relation with the impregnation of KF in incomplete carbonized turtle shell.

2.3 Reaction rate expressions and activation energies

The optimum reaction temperature, time and mole ratio of methanol to oil change with the different biont shell catalysts, so activation energy is always used to compare the activities of different catalysts. We analyzed the reaction rate and activation energies of biodiesel transesterification reaction using biont shell catalyst.

The reaction temperature was held constant (70 °C) to calculate the apparent reaction orders with respect to rapeseed oil and methanol, α and β , respectively. The power rate law model can be written as

$$-r_0 = k C_{\text{cat}} C_{\text{RO},0}^\alpha C_{\text{MeOH},0}^\beta$$

where, r_0 represents the initial reaction rate (transesterification rate $\leq 5\%$). k is the reaction rate constant and C_{cat} is the catalyst concentration. $C_{\text{RO},0}$ and $C_{\text{MeOH},0}$ are the initial rapeseed oil and methanol concentrations, respectively.

The reaction orders in this power rate model were obtained by varying one reactant concentration while keeping the other reactant concentration constant and in excess. $C_{\text{RO},0}$ and $C_{\text{MeOH},0}$ were 0.63–0.78 M and 5.7–8.7 M, respectively. The biont shell catalyst used in the transesterification is a heterogeneous catalyst, and the mass fraction of biont shell catalyst to rapeseed oil in all the reactions is fixed, so C_{cat} has no influence on the value of k .

By taking the logarithm of both sides of the reaction rate equation, we found that when we change the initial concentration of one reactant, the value of r_0 has a direct ratio correlation to the logarithm value of the initial concentration of this reactant, and the proportional coefficient is the reaction order of this reactant. The apparent reaction orders for rapeseed oil ($\alpha = 1.93$) and the methanol ($\beta = 0.97$) were calculated from the slopes of the fitted straight lines in Fig. 13a and b, with correlations for the fitted lines of 0.99 and 0.98, respectively.

The effect of reaction temperature was investigated in the 50–80 °C temperature range. The activation energies (E_a) were estimated from the Arrhenius plots shown in Fig. 14, with correlations for the fitted lines of 0.98. E_a for the conversion of rapeseed oil to biodiesel using biont shell catalyst was found to be 16.4 ± 2.4 kJ mol^{-1} . The activation energies of transesterification

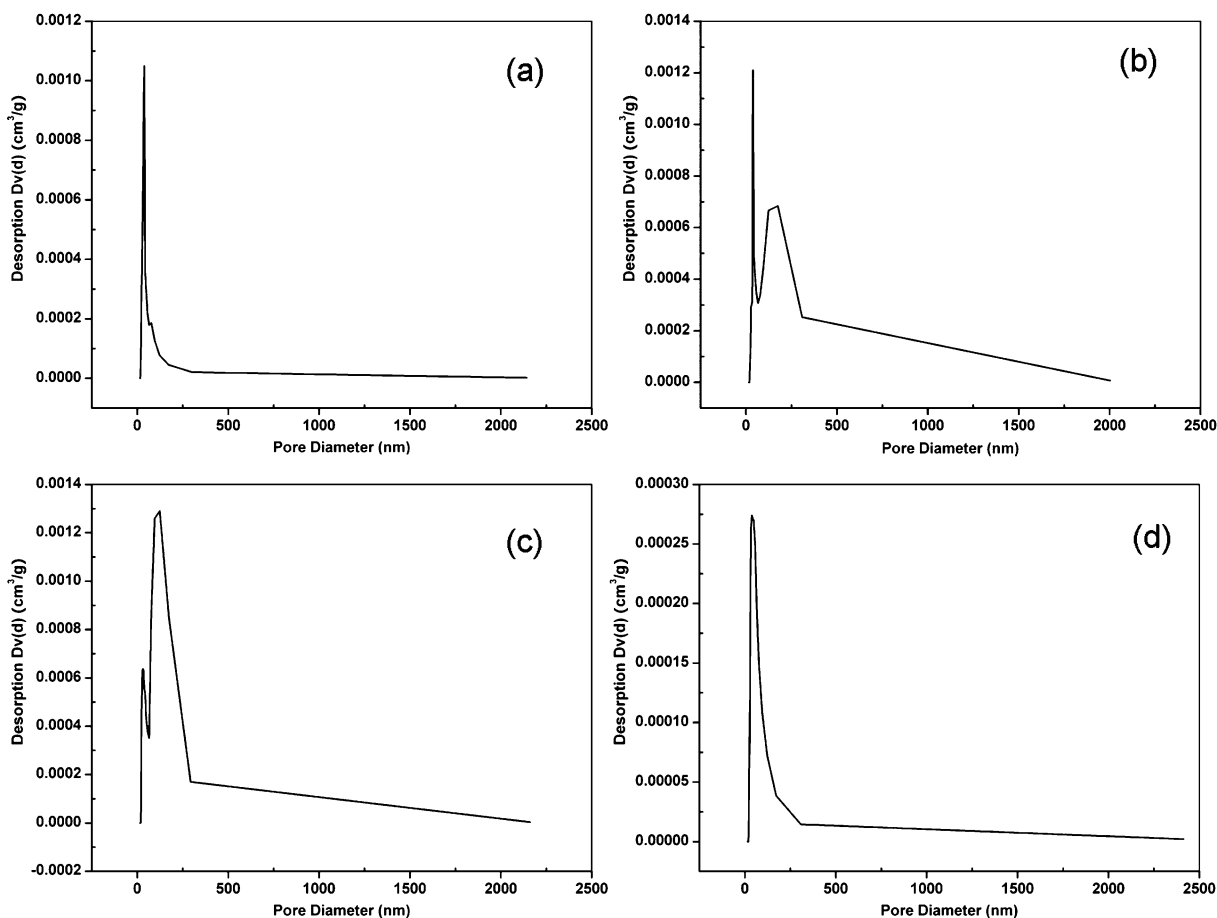


Fig. 10 Pore size distribution of biont shell catalyst samples: (a) original biont shell; (b) sample treated with 300 °C carbonization and KF impregnation together with a 300 °C activation treatment; (c) sample treated with 500 °C carbonization and KF impregnation together with a 300 °C activation treatment; (d) sample treated with 500 °C carbonization and KF impregnation together with a 700 °C activation treatment.

reaction using biont shell catalyst are all lower than Nafion[®] SAC-13 and H₂SO₄.³²

2.4 Proposed mechanism for transesterification using biont shell catalyst

The unique character and high catalytic activity of the biont shell catalyst for the transesterification of rapeseed oil with methanol prompted us to conjecture the mechanism of the catalytic activity. For comparison, KF, the original turtle shell and the incompletely carbonized turtle shell without the KF treatment were used independently as the catalyst for the transesterification of rapeseed oil with methanol and no biodiesel was obtained, indicating that the catalytic activity is originated from the chemical reaction of KF with the incompletely carbonized shell material in the synthesis procedure. Also, to determine the contribution of chitin in the turtle shell to the catalytic activity, a commercial chitosan (over 90% *N*-deacetylation of chitin) which underwent a tri-step treatment with the aforementioned optimum reacting conditions is used as catalyst for transesterification reaction. The resultant product showed relatively high catalytic activity (nearly 76% transesterification) for biodiesel production. The shell of shrimp or crab was used as raw material to synthesize catalyst for transesterification reaction through our devised tri-

step procedure. The activity of that shrimp or crab shell derived catalyst is also encouraging. Therefore, it is safe to say, the high catalytic activity of the catalyst probably comes from active sites formed by the reaction of KF with incompletely carbonized chitin.

The high-performance biont shell catalyst for biodiesel production can only be obtained *via* our carefully designed simple synthetic procedure, namely, the incomplete carbonization–KF loading–activation tri-step procedure. As we know, the turtle shell used is a natural material whose composition is very complicated.³¹ When the natural shell material was subjected to the incomplete carbonization treatment at 500 °C, the thermo decomposition and evaporation of small organic molecules will result in the formation of a micro–nano-structural porous framework with ultrahigh surface area (see SEM images in Fig. 9b). Meanwhile, the dehydration and elimination of ammonia in the chitin molecule will lead to the formation of a conjugated molecular structure. Then the following 25 wt% KF solution impregnation allows the fully loading of KF in the porous channels in the matrix, especially absorbed on the edge sites in the micro–nano-structural porous matrix due to their high surface energy status.³³ The key third activation step at 300 °C, on one hand, further stabilizes the KF adsorption,³⁴ together with forming the micro–nano scale crystallites on the surface

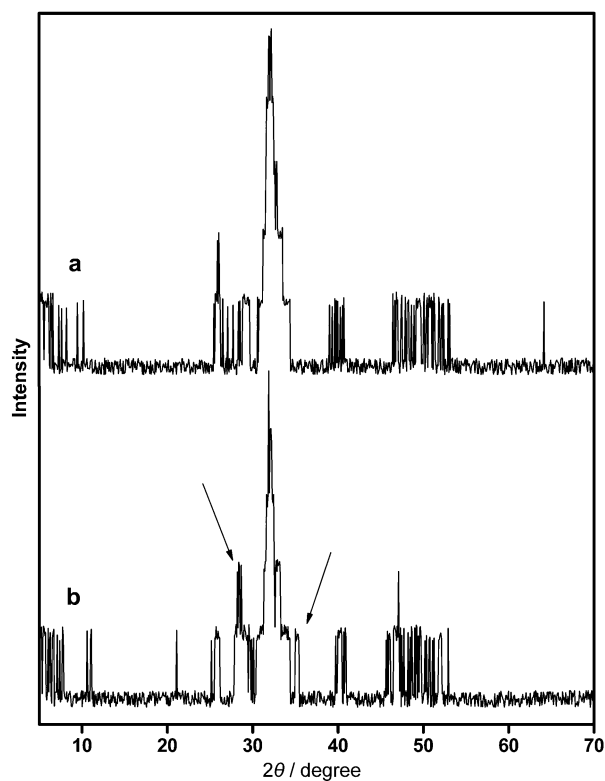


Fig. 11 XRD spectra of biont shell catalyst samples: (a) without KF impregnation and (b) after activation.

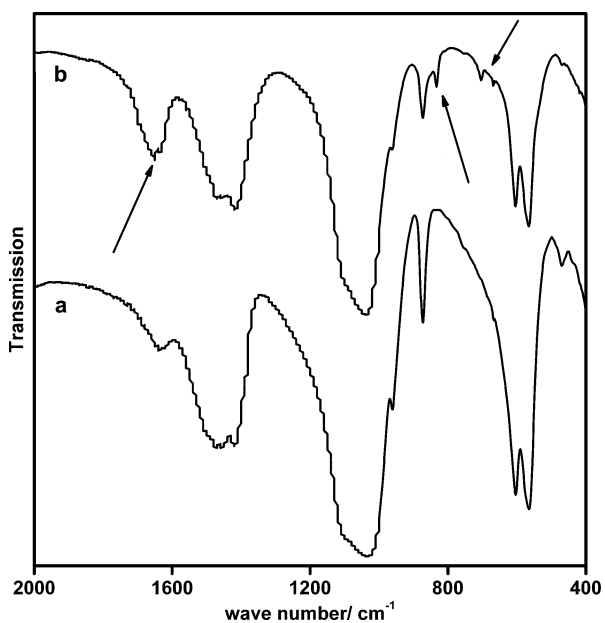


Fig. 12 IR spectra of biont shell catalyst samples: (a) without KF impregnation and (b) after activation.

of the incomplete carbonization shell matrix (shown in areas labelled with circles Fig. 9d). On the other hand, the additive reaction between the KF and the incomplete carbonized chitin resulted in the formation of RO^- , which intensifies the electron density of the oxygen atom in the molecular ring and generated the high active centers of the catalyst. Based on the results of

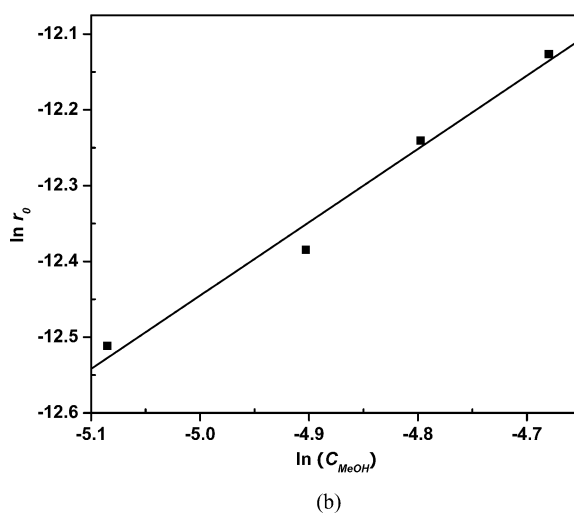
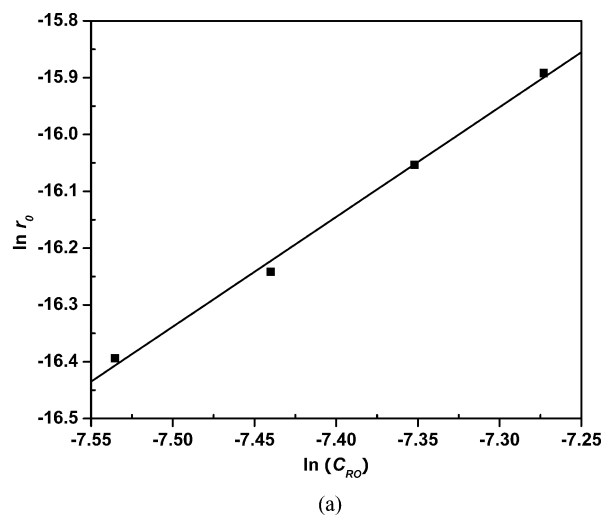


Fig. 13 Effect of reactant concentration on initial reaction rate (conversion $\leq 5\%$) at 70 °C: (a) rapeseed oil ($C_{\text{MeOH},0} = 5.7 \text{ M}$) and (b) methanol ($C_{\text{RO},0} = 0.63 \text{ M}$).

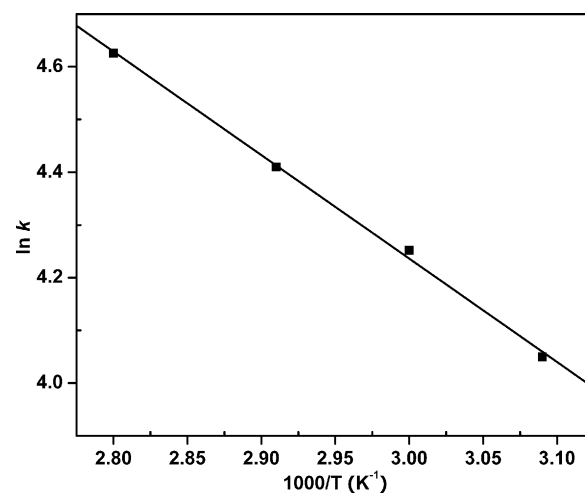
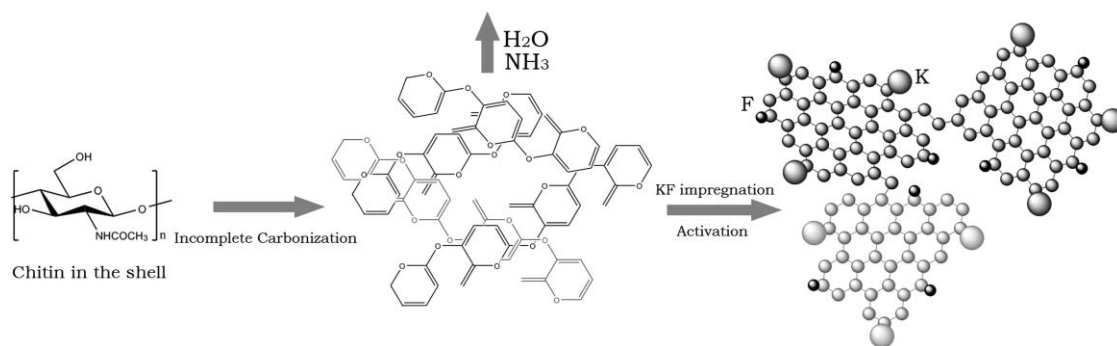


Fig. 14 Arrhenius plot for the transesterification of rapeseed oil to biodiesel using biont shell catalyst. Temperature range 50–80 °C and conversion $\leq 10\%$.



Scheme 2 Schematic illustration of the preparation of high-performance biodiesel catalyst derived from the Chinese turtle shell *via* our tri-step synthesis approach.

XRD, IR and other analysis, we can conjecture the possible preparation mechanism of our biont shell catalyst (as shown in schematic illustration in Scheme 2). When the carbonization temperature or activation temperature was ramped up beyond 700 °C, the complete destruction of conjugated molecular structure is accompanied by the disappearance of catalytic activity. Therefore, the high surface area features possessed by the porous framework combined with the ultrahigh active centers derived from the KF treated incomplete carbonized natural material can greatly enhance the accessibility of the rapeseed oil–methanol reactant to its catalytic sites,³⁵ leading to the high-performance catalytic ability.

3. Conclusions

The novel heterogeneous catalyst derived from the biont shell for biodiesel production from rapeseed oil exhibited an excellent catalytic activity and stability under mild reaction conditions. As a new catalyst, the biont shell catalyst, which comes from the natural material, turtle shell, is totally environment-friendly. As a solid catalyst, the biont shell catalyst has a large surface area, relatively broad particle size distribution, narrow pore size distribution, strong basicity, long catalyst lifetime and better stability in organic solvent. The biont shell was firstly incompletely carbonized at 500 °C, the resultant material was then impregnated in 25 wt% KF solution, and subsequently underwent a necessary activation step at 300 °C. After the tri-step treatment, we get the high-performance catalyst. In the transesterification of rapeseed oil to biodiesel using the biont shell catalyst, the yield of transesterification exceeded 97% within 3 hours. Meanwhile, the process of biodiesel production was clean because there is no soap generated in using the biont shell catalyst. The activity of the catalyst for the transesterification came from the active sites formed by the reaction of incompletely carbonized chitin with KF in the synthesis procedure of the catalyst. The matrix of the biont shell catalyst is weakly polar in nature, favoring transesterification of rapeseed oil to biodiesel and hindering the reverse glycerolysis reaction, therefore displaying a higher catalytic activity compared with conventional solid base catalysts tested for biodiesel production. Consequently, the use of biont shell from natural material and the promising synthesis strategy reported here should have significant benefits over existing technologies because this

synthesis is simple, inexpensive, environmentally benign, and adaptable for biodiesel production on a large scale.

4. Experimental

Materials

Commercial edible grade rapeseed oil, obtained from a market, was refined to reduce water content. The fatty acid composition consists of erucic acid 44.5%, stearic acid 1.3%, oleic acid 19.5%, linoleic acid 22.8%, linolenic acid 10%, and traces of other acids. Methanol, petroleum ether (boiling range: 60–90 °C) and di-*n*-butyl phthalate were analytical reagent (AR) and were purchased from Zhenxing Chemical Co. (Shanghai), Henxing Chemical Co. (Tianjin) and Kelong Chemical Co. (Chengdu), respectively.

Apparatus and procedure

Gas chromatography (GC) analysis was performed using HITACHI136 with a glass column (ov-17, 3 m × 0.5 mm) and nitrogen as carrier gas. The GC analytical conditions were as follows: isotherm at 190 °C (2 min), ramp rate at 10 °C min⁻¹ to 280 °C and held there for 20 min. The injector temperature was 300 °C and the detector temperature was 280 °C, the range of amplifier was 10² and attenuation 8. The flow rates of the H₂, N₂ and air were 40, 25 and 400 mL min⁻¹, respectively.

The thermal stability of the biont catalyst was examined using NETZSH TG 209C from room-temperature to 850 °C under an inert nitrogen atmosphere and a heating rate of 10 °C min⁻¹.

The microstructure features of samples during the fabrication steps were studied using a JEOL JSM-6390 SEM. The samples were mounted on stainless steel stubs using double-stick adhesive tape. Before analysis, the samples were coated with a thin layer of platinum in a Quorum K500X sputtering unit to prevent sample charging during SEM analysis.

The BET surface area, total pore volume, pore diameter and pore size distribution of biont shell catalyst were measured with a Quantachrome Autosorb-1-C chemisorption–physisorption analyzer. A weighed sample of the catalyst was prepared by outgassing for 6 h at 200 °C on the degas port. The BET surface area was calculated from the adsorption branches in the relative pressure range of 0.05–0.31 bar, and the total pore volume was evaluated at a relative pressure of about 1.00 bar. The pore diameter and the pore size distribution were calculated from the

desorption branches using the Barrett–Joyner–Halenda (BJH) method.

CO₂-TPD measurements spectra were recorded using an Altamira AMI-1. A 200 mg clay sample having a 0.1–0.2 mm particle size was introduced in the cylindrical glass microreactor (2 mm internal diameter) of the TPD device, which is then dried at 150 °C for 4 h under a nitrogen flow, at normal pressure. The clay sample was further cooled down to the injection temperature: 80 °C for CO₂-TPD. Carbon dioxide was injected through the clay fixed bed. Saturation is attained when no more absorption is observed, and the inlet and outlet amounts of the probe gas are balanced. Later, CO₂-TPD was achieved with a constant heating rate of 70 °C h⁻¹ and carrier gas throughputs 30 mL min⁻¹ in the temperature range of 80–700 °C. All experiments were achieved using N60 pure grade gases.

The XRD measurements were performed on a Rigaku D/MAX-3B powder X-ray diffractometer using the Cu radiation, over a 2θ range of 3–70° with a step size of 0.02 at a scanning speed of 5° min⁻¹.

The KBr pellet technique was applied for determining IR spectra of the samples. Spectra were recorded on a Nicolet AVATAR-330 spectrometer with 4 cm⁻¹ resolution.

Catalyst preparation and structural characterization

The turtle shell obtained from the market was incompletely carbonized in temperature range of 200 °C to 700 °C in a muffle furnace under ambient conditions after being cleaned, dried, and divided into small blocks. The incompletely carbonized turtle shell was completely dipped in the solution of KF with different mass ratios in the range of 5–50 wt% and then was activated in temperature range of 100 °C to 700 °C in muffle furnace. The resulting product was called turtle shell catalyst. The microstructure features of samples during the fabrication steps were investigated by SEM.

Reaction procedures

The transesterification reaction was carried out using different mass ratios of catalyst to oil and reaction times. A 100 mL round-bottom flask was charged with 30.0 g of rapeseed oil (34.5 mmol, calculated from the average molecular weight of the rapeseed oil), 12.6 mL methanol and varied amounts of catalyst. 15 ml di-n-butyl phthalate was added to the reaction mixture as an internal standard. The mixture was agitated and refluxed for the required reaction time by electric agitator, the temperature controlled by circulation of water. After the reaction finished, the mixture solution was pumped to the separatory funnel, and the mixture of the glycerol and methanol was separated. The superfluous methanol was removed from the biodiesel by decompressing distillation at 100 °C and the volume

of biodiesel was measured and recorded. The transesterification rate of rapeseed oil was measured by GC. Five microlitres of biodiesel was dissolved into 250 μl of methanol, and 2 μl of this mixture was injected into the GC.

References

- 1 J. A. Turner, *Science*, 1999, **285**, 687.
- 2 P. Moriarty and D. Honnery, *Int. J. Hydrogen Energy*, 2007, **32**, 1616.
- 3 F. Orecchini and E. Bocci, *Energy*, 2007, **32**, 1006.
- 4 W. Kaminski, J. Marszalek and A. Ciolkowska, *Biochem. Eng. J.*, 2008, **135**, 95.
- 5 V. Subramani, C. Song, M. Anpo and J. M. Andresen, *Catal. Today*, 2007, **129**, 263.
- 6 M. Toda, A. Takagaki, M. Okmura, J. N. Kondo, S. Hayashi, K. Domen and M. Hara, *Nature*, 2005, **438**, 178.
- 7 H. Stephan, *Nat. Biotechnol.*, 2006, **24**, 755.
- 8 J. Van Gerpen, *Fuel Process. Technol.*, 2005, **86**, 1097.
- 9 A. Lapinskienė, P. Martinkus and V. Rėbždaitė, *Environ. Pollut.*, 2006, **142**, 432.
- 10 J. A. DeMello, C. A. Carmichael, E. E. Peacock, R. K. Nelson, J. S. Arey and C. M. Reddy, *Mar. Pollut. Bull.*, 2007, **54**, 894.
- 11 F. Ma and M. A. Hanna, *Bioresour. Technol.*, 1999, **70**, 1.
- 12 H. Fukuda, A. Kondo and H. Noda, *J. Biosci. Bioeng.*, 2001, **92**, 405.
- 13 G. Vicente, M. Martinez and J. Aracil, *Bioresour. Technol.*, 2004, **92**, 297.
- 14 V. Mao, S. K. Konar and D. G. B. Boocock, *J. Am. Oil Chem. Soc.*, 2004, **81**, 803.
- 15 H. Nouredini and D. Zhu, *J. Am. Oil Chem. Soc.*, 1997, **74**, 1457.
- 16 Z. Yang and W. Xie, *Fuel Process. Technol.*, 2007, **88**, 631.
- 17 M. L. Granados, M. D. Z. Poves, D. M. Alonso, R. Mariscal, F. C. Galisteo, R. M. Tost, J. Santamaría and J. L. G. Fierro, *Appl. Catal., B*, 2007, **73**, 317.
- 18 X. Liu, H. He, Y. Wang and S. Zhu, *Catal. Commun.*, 2007, **8**, 1107.
- 19 G. J. Suppes, M. A. Dasari, E. J. Doskocil, P. J. Mankidy and M. J. Goff, *Appl. Catal., A*, 2004, **257**, 213.
- 20 J. Jitputti, B. Kitiyanan, P. Rangsunvigit, K. Bunyakiat, L. Attanatho and P. Jenvanitpanjakul, *Biochem. Eng. J.*, 2006, **116**, 61.
- 21 W. L. Xie, H. Peng and L. G. Chen, *J. Mol. Catal. A: Chem.*, 2006, **246**, 24.
- 22 U. Schuchardt, R. M. Vargas and G. Gelbard, *J. Mol. Catal. A: Chem.*, 1996, **109**, 37.
- 23 X. Liu, H. He, Y. Wang, S. Zhu and X. Piao, *Fuel*, 2008, **87**, 216.
- 24 Y. Liu, E. Lotero, J. G. Goodwin, Jr. and C. Lu, *J. Catal.*, 2007, **246**, 428.
- 25 X. Li, G. Lu, Y. Guo, Y. Guo, Y. Wang, Z. Zhang, X. Liu and Y. Wang, *Catal. Commun.*, 2007, **8**, 1969.
- 26 R. Jayakumar, N. Nwe, S. Tokura and H. Tamura, *Int. J. Biol. Macromol.*, 2007, **40**, 175.
- 27 M. N. V. Ravi Kumar, *React. Funct. Polym.*, 2000, **46**, 1.
- 28 R. A. A. Muzzarelli, *Carbohydr. Polym.*, 1983, **3**, 53.
- 29 M. Zong, Z. Duan, W. Lou, T. J. Smith and H. Wu, *Green Chem.*, 2007, **9**, 434.
- 30 F. Quignard, A. Choplin and A. Domard, *Langmuir*, 2000, **16**, 9106.
- 31 N. B. Clark, *Gen. Comp. Endocrinol.*, 1972, **3**, 430.
- 32 D. E. Lopez, J. G. Goodwin and D. A. Bruce, *J. Catal.*, 2007, **245**, 381.
- 33 Z. D. Xiao, L. D. Zhang, X. K. Tian and X. S. Fang, *Nanotechnology*, 2005, **16**, 2647.
- 34 D. E. Bergbreiter and J. J. Lalonde, *J. Org. Chem.*, 1987, **52**, 1601.
- 35 M. Hara, T. Yoshida, A. Takagaki, T. Takata, J. N. Kondo, S. Hayashi and K. Domen, *Angew. Chem., Int. Ed.*, 2004, **43**, 2955.

Bis{(trifluoromethyl)sulfonyl}amide ionic liquids as solvents for the extraction of aromatic hydrocarbons from their mixtures with alkanes: effect of the nature of the cation

Alberto Arce,^a Martyn J. Earle,^{*b} Héctor Rodríguez,^{a,b} Kenneth R. Seddon^b and Ana Soto^a

Received 14th August 2008, Accepted 19th November 2008

First published as an Advance Article on the web 19th December 2008

DOI: 10.1039/b814189d

The liquid–liquid equilibria of two ternary systems comprising hexane, benzene and a bis{(trifluoromethyl)sulfonyl}amide ionic liquid, [A][NTf₂] (where A = cation), have been determined at 40 °C. Specifically, the cations of the ionic liquids investigated are 1-ethylpyridinium, [C₂py]⁺, and (2-hydroxyethyl)trimethylammonium, [N_{1,1,1}(C₂OH)]⁺. The effectiveness of each ionic liquid as solvent for the separation of benzene from its mixtures with hexane was evaluated, and compared to that of 1-ethyl-3-methylimidazolium bis{(trifluoromethyl)sulfonyl}amide, [C₂mim][NTf₂], as well as of trihexyl(tetradecyl)phosphonium bis{(trifluoromethyl)sulfonyl}amide, [P_{6,6,6,14}][NTf₂]. It was observed that the ammonium ionic liquid leads to higher selectivities in a certain range of global compositions, but it presents lower distribution ratios. No significant difference was observed between the pyridinium and the imidazolium ionic liquids. It was concluded that these ionic liquids can be envisioned as potential alternatives for the replacement of conventional organic solvents currently used for the separation of aromatic and aliphatic hydrocarbons. The liquid–liquid equilibrium data were acceptably correlated by means of the ‘Non-Random Two-Liquid’ (NRTL) equation.

Introduction

Ionic liquids, currently defined as salts which melt below 100 °C,^{1–3} have been the object of a burgeoning research over the last decade.^{2,4,5} The possibility of tuning the chemical structures of the cation and the anion to yield an ionic liquid with customised properties^{6,7} has promoted a huge portfolio of applications of ionic liquids over a broad range of scientific and industrial fields.^{8–10} To date, important efforts have focused on investigating ionic liquids as neoteric solvents in reactors and separation processes. Due to their remarkable solvation ability and to their negligible or very low vapour pressure,¹¹ they constitute a potential alternative of great interest as replacements for the volatile organic compounds currently used in industry.^{12–14}

In the late 1990s, ionic liquids were firstly proposed as novel solvents in liquid–liquid extractions.¹⁵ Since then, numerous works around the opportunities of ionic liquids in this kind of processes have been published and reviewed,¹⁶ including different data categories such as partition coefficients, binary liquid–liquid equilibrium (LLE) data, activity coefficients, or ternary LLE data, the latter being of particular interest. Several challenging industrial separations, among which the separation of aromatic and aliphatic hydrocarbons holds a preferential position,¹⁷ have been investigated by determining the LLE of

ternary systems involving an ionic liquid as solvent. In a previous work,¹⁸ we found that an ionic liquid with the bis{(trifluoromethyl)sulfonyl}amide anion ([NTf₂][−]), namely 1-ethyl-3-methylimidazolium bis{(trifluoromethyl)sulfonyl}amide ([C₂mim][NTf₂]), exhibited an advantageous performance for the extraction of benzene from its mixtures with hexane, when compared to paradigmatic conventional solvents such as sulfolane¹⁷ (systematic name: 2,3,4,5-tetrahydrothiophene 1,1-dioxide). The ionic liquid [C₂mim][NTf₂] at the present time would be costly,¹⁹ but on the other hand the [NTf₂][−] anion would cause the ionic liquid to have good bulk properties such as comparatively low viscosity and melting point.^{20,21} An extended investigation to the series of 1-alkyl-3-methylimidazolium bis{(trifluoromethyl)sulfonyl}amide ionic liquids ([C_nmim][NTf₂], with *n* being the number of carbon atoms in the alkyl chain) was then carried out,²² thus providing an insight of how the length of the alkyl substituent chain in the cation influences the action of the ionic liquid in the extraction process; however it was concluded that, overall, the ionic liquid with the shortest chain would be preferable, mainly due to better selectivities.

One of the most striking features of ionic liquids is their tuneability.^{2,23,24} In fact, the number of possible combinations of cations and anions that will result in the formation of ionic liquids is huge.^{2,13,25} Thus, systematic studies on the influence of structural variations of ionic liquids for a specific objective become necessary in order to find the optimum ionic liquid to match such target. Ideally, simulation studies would do the job, but their development with systems including ionic liquids is still in the early stages, and their reliability to date is

^aDepartment of Chemical Engineering, University of Santiago de Compostela, E-15782, Santiago de Compostela, Spain

^bThe QUILL Centre, The Queen's University of Belfast, Belfast, UK BT9 5AG. E-mail: quill@qub.ac.uk

not enough;²⁶ therefore, at the present moment, experimental work is needed to bring accurate results towards the optimised structure of the ionic liquid needed. It can be said that there are three key structural variables within ionic liquids: the nature of the anion, the nature of the cation, and the length and number of the cationic substituents.²⁴ The [C₂mim][NTf₂] has already been justified as thermodynamically better, and/or with more favourable physical characteristics, than other imidazolium ionic liquids with different anions;¹⁸ also, as previously mentioned, a study of its homologous family, with variation of the length of the alkyl side chain, was developed.²² Therefore, it was decided to continue this analysis by introducing variation in the nature of the cation, thus investigating some [NTf₂]⁻ ionic liquids whose cation core was representative of classical families of the new generations of ionic liquids. In particular, 1-ethylpyridinium bis{(trifluoromethyl)sulfonyl}amide ([C₂py][NTf₂]) and (2-hydroxyethyl)trimethylammonium bis{(trifluoromethyl)sulfonyl}amide ([N₁₁₁(C₂OH)][NTf₂]) were selected, being members of the pyridinium and ammonium groups of ionic liquids. In choosing these representatives, factors like toxicity or availability, as well as a melting point sufficiently low, have been taken into consideration. A comparison will also be carried out with data available for a phosphonium ionic liquid, trihexyl(tetradecyl)phosphonium bis{(trifluoromethyl)sulfonyl}amide ([P₆₆₆₁₄][NTf₂]).²⁷ The latter, being essentially non-polar and having a much larger miscibility with hydrocarbons,²⁸ can be considered as helpful in disengaging the effects derived by the non-aromaticity and by the alcohol functionalisation introduced in the [N₁₁₁(C₂OH)]⁺ with regard to the [C₂mim]⁺ and [C₂py]⁺ cations. The chemical structures of the constituent ions of the ionic liquids involved in this work (including [C₂mim][NTf₂] and [P₆₆₆₁₄][NTf₂]) are shown in Fig. 1.

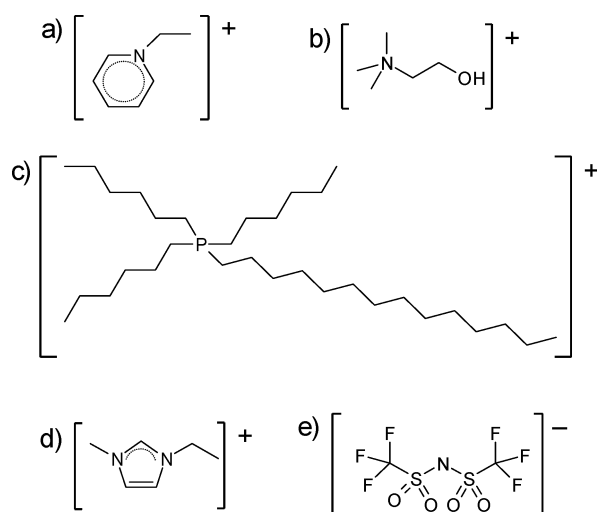


Fig. 1 Chemical structures of the constituent ions of the ionic liquids involved in this work. Cations: (a) 1-ethylpyridinium, [C₂py]⁺; (b) (2-hydroxyethyl)trimethylammonium, [N₁₁₁(C₂OH)]⁺; (c) trihexyl(tetradecyl)phosphonium, [P₆₆₆₁₄]⁺; (d) 1-ethyl-3-methylimidazolium, [C₂mim]⁺. Anion: (e) bis{(trifluoromethyl)sulfonyl}amide, [NTf₂]⁻.

A correlation of the LLE data reported herein has also been made, by means of the 'Non-Random Two-Liquid' (NRTL)

equation, in order to enhance their usefulness and facilitate their computational treatment.

Experimental

Materials

Benzene, with a nominal purity of 99%, was purchased from LabScan. Hexane, with a nominal purity of 97% and the other 3% being a mixture of isomers, was supplied by BDH. Both hydrocarbons were used as received, without further purification.

The ionic liquids were prepared by a metathetic reaction, following similar procedures to those described elsewhere,²⁹ by mixing the lithium salt of the desired anion, Li[NTf₂] (supplied by 3M with a nominal purity of 98%), in water with the hydrophilic bromide or chloride salts of the desired cation: [C₂py]Br or [N₁₁₁(C₂OH)]Cl. [C₂py]Br was synthesised by alkylation of pyridine (Acros, 99%) with bromoethane (Aldrich, 98%),³⁰ by dropwise addition of the latter over the former into a two-neck round-bottomed flask and heated under reflux, under a dried atmosphere, for several hours. The other precursor, [N₁₁₁(C₂OH)]Cl, was directly purchased from Aldrich with a purity of 98%.

By ion exchange in aqueous media, as mentioned above, the hydrophobic [NTf₂]⁻ ionic liquids were formed, creating a distinct phase while the lithium halide ions remained in the aqueous phase. Dichloromethane (Baker, 99.5%) was added, and the organic phase containing the desired ionic liquid was extracted in a separating funnel. Then, the extract was washed several times with fresh water, until no precipitation was observed by means of the silver nitrate test. The dichloromethane was removed in a rotary evaporator, and the purification of the ionic liquids was completed by heating them under reduced pressure (<1 mbar) at 70 °C for more than 24 h.

The final colourless products were characterised by nuclear magnetic resonance (NMR) spectroscopy. The ¹H NMR and ¹³C NMR spectra confirmed the desired structures. [C₂py][NTf₂] was obtained as a liquid at room temperature, which later solidified; whereas [N₁₁₁(C₂OH)][NTf₂] was also obtained as a liquid at room temperature with a remarkably viscous appearance, and remained in the liquid state throughout the development of the experiments. The melting points of these compounds were determined by differential scanning calorimetry (DSC), and were found to be 33 °C for [C₂py][NTf₂],³⁰ and 39 °C for [N₁₁₁(C₂OH)][NTf₂],³¹ thus indicating that the ionic liquids readily undergo supercooling.

Methods

Different mixtures of the hydrocarbons with one of the ionic liquids (with a total volume of about 10 cm³), lying in the immiscible region, were prepared and placed inside sealed glass cells especially designed for the determination of LLE data at a constant temperature. Taking into account the melting points of the ionic liquids used, the temperature selected to determine the LLE data was 40 °C. The global composition of the mixtures for both systems was such that the tie-lines generated would be distributed in an approximately even manner, covering the whole

immiscible region of the ternary diagram. Each mixture was vigorously stirred by magnetic agitation for at least 1 h, and then allowed to settle down for no less than 4 h. This period of time was checked to be sufficient for reaching the equilibrium. Then, a sample of each phase was taken with stainless steel needles attached to glass syringes, without disturbing the interphase or causing crosscontamination of the phases. The samples were transferred to NMR tubes and dissolved in a deuterated solvent, for compositional analysis.

A ^1H NMR spectroscopy technique was used for the determination of the composition of the samples. This technique is based on quantitative integration of the areas under certain peaks in the ^1H NMR spectra, so that the mole fraction of each compound in the sample can be calculated. This method has already been tested for similar systems, and its details can be found elsewhere.^{18,22} For benzene and hexane, the set of peaks selected for integration was identical to that in a previous work for the system (hexane + benzene + $[\text{C}_2\text{mim}][\text{NTf}_2]$):¹⁸ the sharp singlet peak at *ca.* 7.2–7.3 ppm for benzene, and the peak corresponding to the terminal methyl groups of the aliphatic chain for hexane. With regard to the ionic liquids, the following peaks were chosen for analysis: all five peaks corresponding to the aromatic pyridinium ring and the ethyl substituent of the pyridinium cation in $[\text{C}_2\text{py}][\text{NTf}_2]$, and the two methylene peaks of the (2-hydroxyethyl)trimethylammonium cation in $[\text{N}_{111}(\text{C}_2\text{OH})][\text{NTf}_2]$. The maximum error of the results obtained by using these sets of peaks in each of the systems studied was estimated to be no greater than 2% mole fraction for any composition in any of the investigated systems. The NMR spectra were recorded on a Bruker Avance DRX-500 spectrometer.

Results and discussion

LLE data

It is a common practice in the literature to determine the LLE of ternary systems at 25 °C, given that all compounds and their mixtures are liquid at such temperature. However, since $[\text{C}_2\text{py}][\text{NTf}_2]$ and $[\text{N}_{111}(\text{C}_2\text{OH})][\text{NTf}_2]$ melt slightly above that temperature, a value of 40 °C was chosen in this work. This is, in addition, a compromise value to avoid an excessive energy demand in keeping the working temperature in a hypothetical continuous extraction process. Moreover, LLE data for the system (hexane + benzene + $[\text{C}_2\text{mim}][\text{NTf}_2]$) are available at 40 °C in the literature,¹⁸ and consequently straightforward comparisons are possible.

Therefore, the LLE of the ternary systems (hexane + benzene + $[\text{C}_2\text{py}][\text{NTf}_2]$) and (hexane + benzene + $[\text{N}_{111}(\text{C}_2\text{OH})][\text{NTf}_2]$) were determined at 40 °C. The compositions of each pair of samples taken in a LLE experiment correspond to the ends of a LLE tie-line, and are reported for both systems in Tables 1 and 2. Interestingly, no presence of ionic liquid was detected in the upper phases of either system; thus, there would potentially be no need to install a unit for the recovery of solvent from the hydrocarbon-rich phase in a real process working in continuous operation, leading to the consequent reduction in installation and operation costs. Nonetheless, it must be noted that traces of ionic liquid may

Table 1 Composition of the experimental tie-line ends, and values of the solute distribution ratio (β) and selectivity (S) for the ternary system (hexane + benzene + $[\text{C}_2\text{py}][\text{NTf}_2]$) at 40 °C. The mole fractions of hexane, benzene and $[\text{C}_2\text{py}][\text{NTf}_2]$ are represented by x_1 , x_2 and x_3 , respectively

Upper phase			Lower phase			β	S
x_1	x_2	x_3	x_1	x_2	x_3		
1.000	0.000	0.000	0.048	0.000	0.952	—	—
0.937	0.063	0.000	0.039	0.078	0.883	1.24	29.7
0.857	0.143	0.000	0.037	0.171	0.792	1.20	27.7
0.762	0.238	0.000	0.035	0.271	0.694	1.14	24.8
0.646	0.354	0.000	0.037	0.371	0.592	1.05	18.3
0.493	0.507	0.000	0.036	0.483	0.481	0.95	13.0
0.331	0.669	0.000	0.032	0.614	0.354	0.92	9.5
0.164	0.836	0.000	0.024	0.688	0.288	0.82	5.6
0.085	0.915	0.000	0.015	0.716	0.269	0.78	4.4
0.000	1.000	0.000	0.000	0.773	0.227	0.77	—

Table 2 Composition of the experimental tie-line ends, and values of the solute distribution ratio (β) and selectivity (S) for the ternary system (hexane + benzene + $[\text{N}_{111}(\text{C}_2\text{OH})][\text{NTf}_2]$) at 40 °C. The mole fractions of hexane, benzene and $[\text{N}_{111}(\text{C}_2\text{OH})][\text{NTf}_2]$ are represented by x_1 , x_2 and x_3 , respectively

Upper phase			Lower phase			β	S
x_1	x_2	x_3	x_1	x_2	x_3		
1.000	0.000	0.000	0.015	0.000	0.985	—	—
0.946	0.054	0.000	0.014	0.037	0.949	0.69	46.3
0.880	0.120	0.000	0.014	0.080	0.906	0.67	41.9
0.754	0.246	0.000	0.015	0.135	0.850	0.55	27.6
0.608	0.392	0.000	0.013	0.206	0.781	0.53	24.6
0.421	0.579	0.000	0.018	0.290	0.691	0.50	11.7
0.298	0.702	0.000	0.016	0.341	0.642	0.49	9.0
0.207	0.792	0.000	0.015	0.395	0.590	0.50	6.9
0.109	0.891	0.000	0.008	0.422	0.570	0.47	6.5
0.000	1.000	0.000	0.000	0.491	0.509	0.49	—

enter the upper phases, in concentrations below the detection limit of the technique (estimated to be <0.0005 in mole fraction), as it was already observed and reported in a previous work.¹⁸ By inspection of the data, it can be inferred that hexane is quite insoluble in both ionic liquids, whereas benzene has a greater degree of miscibility with $[\text{C}_2\text{py}][\text{NTf}_2]$ than with $[\text{N}_{111}(\text{C}_2\text{OH})][\text{NTf}_2]$.

Fig. 2 shows the triangular diagrams with the graphical representation of the LLE of both ternary systems, together with that previously reported for the system (hexane + benzene + $[\text{C}_2\text{mim}][\text{NTf}_2]$) at the same temperature of 40 °C,¹⁸ as well as for the system (hexane + benzene + $[\text{P}_{66614}][\text{NTf}_2]$) which is available at 25 °C.²⁷ Although the temperature for the latter is not the same, it was previously shown that the temperature has little influence on this kind of systems.¹⁸ So, the direct visual comparison of the four triangular diagrams can be assumed as acceptable. In any case, it is clear that the immiscibility domain in the system (hexane + benzene + $[\text{P}_{66614}][\text{NTf}_2]$) is much smaller, the $[\text{P}_{66614}][\text{NTf}_2]$ not being suitable for its use as solvent on its own in a practical extraction process. This is undoubtedly due to the large alkyl chains of the cation, $[\text{P}_{66614}]^+$, causing a high or even total miscibility of the hydrocarbons in the ionic liquid.

In Fig. 2(b) and 2(c), the features previously indicated are graphically observed, with all compositional points of the upper phases lying on the edge corresponding to the binary subsystem

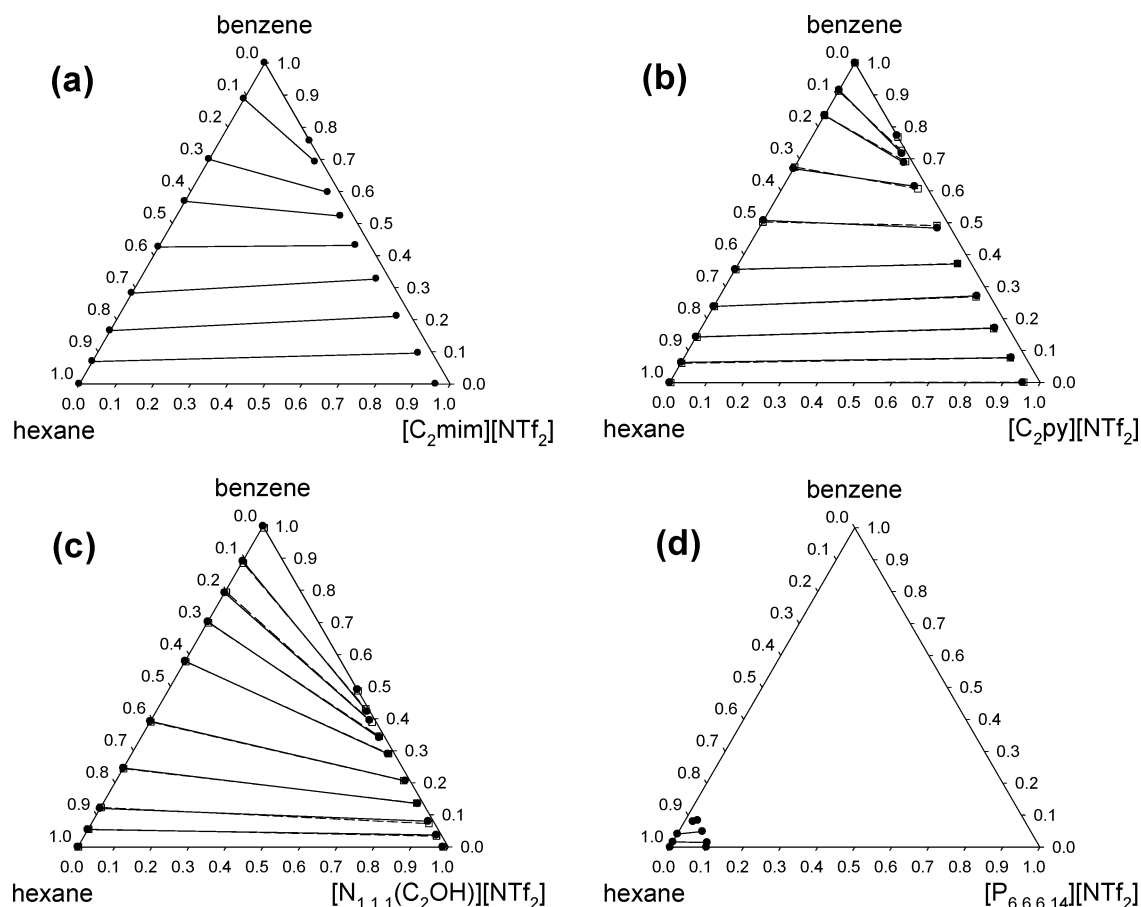


Fig. 2 Experimental (solid circles, solid lines) tie-lines for the LLE at 40 °C of the ternary systems (a) (hexane + benzene + [C₂mim][NTf₂]),¹⁸ (b) (hexane + benzene + [C₂py][NTf₂]), and (c) (hexane + benzene + [N_{1,11}(C₂OH)][NTf₂]); and for the LLE at 25 °C of the ternary system (hexane + benzene + [P_{6,6,6,14}][NTf₂]).²⁷ For the novel two systems reported in the present work, the correlated tie-lines (NRTL, with $\alpha = 0.30$ and $\alpha = 0.20$ respectively) are also drawn (open squares, dashed lines).

(hexane + benzene), and with tie-lines of different length on the other two edges of the triangle. Both these ternaries, as well as that with [C₂mim][NTf₂], correspond to Type 2 systems, according to the classification proposed by Sørensen *et al.*,³² since they present a completely miscible pair (hexane and benzene), two immiscible ones (the ionic liquid with either hydrocarbon) and only one continuum immiscibility domain. It can be seen that the aromatic hydrocarbon is much more soluble in these ionic liquids than the aliphatic hydrocarbon. In the case of the systems involving [C₂mim][NTf₂] and [C₂py][NTf₂], this is thought to be attributable to π - π interactions between the benzene and the aromatic core of the cation of the ionic liquid; whereas in the case of the system with [N_{1,11}(C₂OH)][NTf₂], its hydroxyl group is likely to better interact with the aromaticity of benzene rather than with the linear aliphatic molecule of hexane,³³ or it is due to a cation- π interaction.³⁴

Like in the system with [C₂mim][NTf₂], that with the more similar [C₂py][NTf₂] shows solutropy, *i.e.* the slope of the tie-lines changes from positive to negative as the concentration of benzene in the system increases; the solutrope, or horizontal tie-line, corresponds to a mole fraction of benzene in the range 0.4–0.5, which is a remarkably similar value to that of the solutrope for the system (hexane + benzene + [C₂mim][NTf₂]). On the other hand, for the system with [N_{1,11}(C₂OH)][NTf₂] all the

tie-lines have a negative slope, with the obvious exception of the horizontal tie-line for the binary pair (hexane + ionic liquid); and for the system (hexane + benzene + [P_{6,6,6,14}][NTf₂]) it is hard to draw any conclusion, since the slopes of the tie-lines are significantly sensitive to the experimental error, and the biphasic region is quite small.

Evaluation and comparison of the ionic liquids

The suitability of each ionic liquid to be used as solvent in the liquid extraction of benzene from its mixtures with hexane was analysed by means of classical evaluation parameters such as the solute distribution ratio (β) and the selectivity (S), defined by the following expressions:

$$\beta = \frac{x_2^{\text{II}}}{x_2^{\text{I}}} \quad (1)$$

$$S = \frac{x_2^{\text{II}}/x_1^{\text{I}}}{x_1^{\text{II}}/x_1^{\text{I}}} \quad (2)$$

where x stands for mole fraction, subscripts 1 and 2 represent the inert (hexane) and solute (benzene), and superscripts I and

II indicate the upper phase (raffinate) and lower phase (extract), respectively.

The calculated values of β and S for the systems (hexane + benzene + [C₂py][NTf₂]) and (hexane + benzene + [N₁₁₁(C₂OH)][NTf₂]) at 40 °C are displayed in Tables 1 and 2 along with the corresponding experimental LLE data. As expected from the aforementioned solutropic behaviour, the values of β for the system with [C₂py][NTf₂] are higher than the unity at low concentrations of benzene, and then decrease to values below the unity as the concentration of benzene in the system increases.

The solute distribution ratio and the selectivity as a function of the mole fraction of benzene in the organic (upper) phase, at 40 °C, are represented in Fig. 3 and 4 for the two novel systems in this work and also for the system (hexane + benzene + [C₂mim][NTf₂]) previously reported in the literature.¹⁸ Since the aromatic and aliphatic hydrocarbons, as well as the temperature, were the same for all three LLE data sets, a straightforward comparison of the ionic liquids (specifically of their cations, due to having a common anion) is possible. No LLE data were found in the literature for the system (hexane + benzene + sulfolane) at 40 °C, but they were available at 25 °C,³⁵ and the solute distribution ratio and selectivity calculated from them are also plotted. Assuming that the LLE behaviour of the system formed by the two hydrocarbons and sulfolane does not vary strongly with temperature, the graphs provide an acceptably valid visual comparison of the performance of the ionic liquids and sulfolane as solvents for the separation of hexane and benzene by liquid extraction.

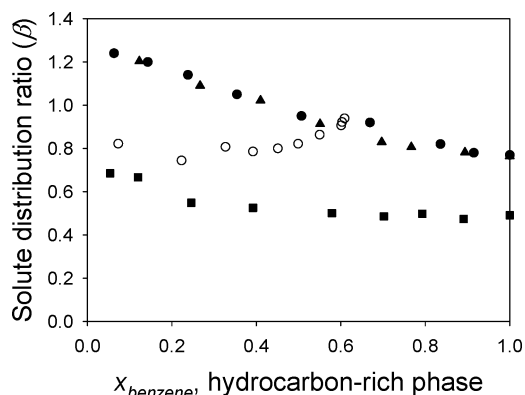


Fig. 3 Solute distribution ratio, as a function of the mole fraction of solute in the hydrocarbon-rich phase, for the ternary systems (hexane + benzene + [C₂mim][NTf₂])¹⁸ (▲), (hexane + benzene + [C₂py][NTf₂]) (●) and (hexane + benzene + [N₁₁₁(C₂OH)][NTf₂]) (■), at 40 °C. The data for the ternary system (hexane + benzene + sulfolane),³⁴ at 25 °C, are also plotted for comparison (○).

As observed in Fig. 3, the solute distribution ratio is practically identical for the systems with [C₂mim][NTf₂] or [C₂py][NTf₂] as solvents. When using [N₁₁₁(C₂OH)][NTf₂], however, the values of β are notably lower, at any composition in the system. This is consistent with the structures of the cations [C₂mim]⁺ and [C₂py]⁺ being much more similar to each other than to that of the cation [N₁₁₁(C₂OH)]⁺, and benzene being more soluble in [C₂mim][NTf₂] or [C₂py][NTf₂] than in [N₁₁₁(C₂OH)][NTf₂]. Although the length of the alkyl sub-

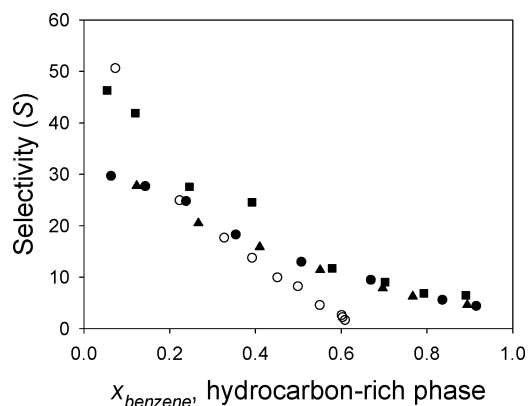


Fig. 4 Selectivity, as a function of the mole fraction of solute in the hydrocarbon-rich phase, for the ternary systems (hexane + benzene + [C₂mim][NTf₂])¹⁸ (▲), (hexane + benzene + [C₂py][NTf₂]) (●) and (hexane + benzene + [N₁₁₁(C₂OH)][NTf₂]) (■), at 40 °C. The data for the ternary system (hexane + benzene + sulfolane),³⁴ at 25 °C, are also plotted for comparison (○).

stituents in the cations of [P_{6,6,6,14}][NTf₂] and [N₁₁₁(C₂OH)][NTf₂] are notably different, the remarkably lower hydrocarbon solubility in the latter (visually observable by comparison of Fig. 2(c) and 2(d)) is likely to be influenced by the presence of the functional hydroxyl group in the [N₁₁₁(C₂OH)]⁺ cation. As a result of the above, a greater amount of [N₁₁₁(C₂OH)][NTf₂] would be needed to carry out a given degree of separation in a real extraction process.

A slight decrease with increasing the concentration of benzene is noticeable for the solute distribution ratio of all three systems (hexane + benzene + ionic liquid). This is explicable from the fact that, at global compositions with a high content of hydrocarbons, a significant amount of these is present in the ionic liquid rich phase. Thus, the molecules of hexane are more prone to partitioning towards such phase since it is considerably loaded with hydrocarbon molecules and the relative concentration of ionic liquid is lower.

Compared to sulfolane, the solute distribution ratios are notably higher when using [C₂mim][NTf₂] or [C₂py][NTf₂] over most of the comparable composition range, tending to be of the same magnitude as the plait point of the system (*i.e.* the global composition at which the compositions of the two phases in equilibrium converge)³⁶ with sulfolane is approached; but this region would not be of practical application, so the performance of the aforementioned ionic liquids would be better from this perspective. Conversely, the values for the system with [N₁₁₁(C₂OH)][NTf₂] lie below those for the system with sulfolane, then implying that a greater amount of this ammonium ionic liquid would be needed to treat a given hydrocarbon feed. The lower solubility of benzene in [N₁₁₁(C₂OH)][NTf₂], previously discussed, seems to be associated with this result.

For selectivities, as for solute distribution ratios, a decreasing trend is found with increasing the concentration of benzene in the systems (hexane + benzene + ionic liquid), as seen in Fig. 4. Again, a plausible explanation is based on the increasing presence of hydrocarbons in the ionic liquid rich phase as the global composition of the system becomes richer in hydrocarbons. Thus, at low concentrations of benzene and hexane in the system, the lower phase mainly consists of

ionic liquid and the partition of each hydrocarbon is strongly influenced by the direct specific interactions between them and the ionic liquid. However, as the ionic liquid phase becomes richer in hydrocarbons, the influence of the ionic liquid is somehow hindered, with the molecules of benzene and hexane acting as attenuators and promoting the gradual convergence of the distribution ratios of each hydrocarbon, thus resulting in a decrease of the selectivity. This theory would be also consistent with the tendency to converge that can be observed in the different series as the concentration of hydrocarbons in the systems becomes higher and higher.

As with the solute distribution ratios, no significant differences are detected when comparing the selectivities for the system with [C₂mim][NTf₂] and for the one with [C₂py][NTf₂], as a result of their structural similarity and consequent analogous interactions with the hydrocarbons. The behaviour of the system with [N₁₁₁(C₂OH)][NTf₂] is, in this case, relatively close to that of the other two systems; nonetheless, clearly higher values of *S* are observable at low concentrations of benzene, basically due to lower mole fractions of hexane in the ionic liquid rich phase. This region would be of particular interest from a practical application standpoint, since solvent extraction is currently understood as the most viable operation for the treatment of feedstreams with moderate to low content in aromatics.¹⁷

The comparison of the tested ionic liquids and sulfolane, with regard to selectivities, is similar to that already discussed in a previous work.¹⁸ In synthesis, the sulfolane leads to better selectivities at low concentrations of solute in the system, then dropping below the selectivities achieved with the ionic liquids. Since an extraction process exclusively operating in the region in which the sulfolane performs better is not economically viable with conventional solvents,¹⁷ it can be deduced that the ionic liquids will be overall as good or better than sulfolane, from a point of view based on selectivity.

Data correlation

Correlation of LLE data is desirable, as it permits a continuum treatment of the information rather than the discrete nature of the experimental tie-lines. Among the excess Gibbs energy models for the correlation of LLE data, the ‘Non-Random Two-Liquid’ (NRTL) model³⁷ has been commonly used over the last years for systems including ionic liquids. Although not originally developed for systems with electrolytes, the NRTL model has proven to acceptably correlate LLE data of ternary systems with ionic liquids, in particular those involving aromatic and aliphatic hydrocarbons plus ionic liquids.^{18,38–46}

In this work, the NRTL correlation of the ternary systems, with calculation of the binary interaction parameters (BIPs) of the model, was carried out by means of a computer program by Sørensen.⁴⁷ For each of the systems with practical applicability considered in the present work, the nonrandomness parameter of the model, α , was arbitrarily set to three different values, covering the usual range of values that it usually takes: 0.10, 0.20 and 0.30. The program was run for each of these values, and for all systems. An optimum value of $\alpha = 0.32$ had been already found for the ternary system (hexane + benzene + [C₂mim][NTf₂]) at 40 °C;¹⁸ but, for appropriate comparison,

it was preferred to correlate the data for this system again, following the protocol proposed herein.

The quality of the correlation was evaluated by calculating the mean error of the solute distribution ratio, $\Delta\beta$, and the residual function *F*, defined as:

$$\Delta\beta = 100 \times \left[\frac{1}{M} \sum_k \left(\frac{\beta_k - \hat{\beta}_k}{\beta_k} \right)^2 \right]^{0.5} \quad (3)$$

$$F = 100 \times \left[\sum_k \min_i \sum_j \frac{(x_{ijk} - \hat{x}_{ijk})^2}{6M} \right]^{0.5} \quad (4)$$

where subscripts and sum indices *i*, *j* and *k* refer to components, phases and tie-lines, respectively; *M* is the total number of experimental tie-lines; the circumflex symbol on top indicates a calculated value; ‘min’ refers to the minimum value obtained by the Nelder-Mead method; and *x* stands for mole fraction.

The residuals obtained are summarised in Table 3. The best results for the systems with [C₂mim][NTf₂] and [C₂py][NTf₂] are obtained for $\alpha = 0.30$. For the ammonium ionic liquid, however, the best values are achieved for $\alpha = 0.20$. It was preferred to keep these two distinct values instead of concluding a unique optimal value of α for the three systems analysed, in analogy to the relative similarity among the structures of the cations of the ionic liquids considered.

The BIPs of the NRTL model for the correlation of each system, using the values of α leading to the smallest residuals in each case, are shown in Table 4. No quantitative agreement exists between the BIPs corresponding to different systems, although in theory they should be the same for the pair (hexane + benzene). Nonetheless, a qualitative similarity among the sets of BIPs can be noticed.

The correlated tie-lines for the systems (hexane + benzene + [C₂py][NTf₂]) and (hexane + benzene + [N₁₁₁(C₂OH)][NTf₂]), generated from the reported BIPs, are plotted in Fig. 2, along with the corresponding experimental tie-lines. A simple visual inspection of both sets of tie-lines for each system confirms the closeness of the correlations performed. However, the NRTL model fails in a critical aspect, such as the absence of ionic liquid in the upper phase: the correlated compositions of the raffinate contain a small but not negligible amount of ionic liquid (barely perceptible in Fig. 2), whereas in the LLE experiments no ionic liquid was detected (see Tables 1 and 2). The same issue was

Table 3 Mean error of the solute distribution ratio ($\Delta\beta$) and residual function *F* for the NRTL correlation of the LLE data of the ternary systems (hexane + benzene + ([C₂mim][NTf₂] or [C₂py][NTf₂] or [N₁₁₁(C₂OH)][NTf₂])) at 40 °C, for different values of the nonrandomness parameter α

Ionic liquid	α	$\Delta\beta$	<i>F</i>
[C ₂ mim][NTf ₂]	0.10	6.5	0.7476
	0.20	6.3	0.5806
	0.30	3.8	0.3694
[C ₂ py][NTf ₂]	0.10	5.6	0.6589
	0.20	3.6	0.5774
	0.30	2.1	0.3816
[N ₁₁₁ (C ₂ OH)][NTf ₂]	0.10	5.1	0.4127
	0.20	6.2	0.3631
	0.30	11.6	0.4602

Table 4 Binary interaction parameters (Δg_{ij} , Δg_{ji}) of the NRTL model obtained from the correlation of the LLE data of the ternary systems (hexane (1) + benzene (2) + ([C₂mim][NTf₂] or [C₂py][NTf₂] or [N₁₁₁(C₂OH)][NTf₂]) (3)) at 40 °C, with the specified values of the nonrandomness parameter α

Ionic liquid	α	Components $i-j$	BIPs	
			$\Delta g_{ij}/$ J mol ⁻¹	$\Delta g_{ji}/$ J mol ⁻¹
[C ₂ mim][NTf ₂]	0.30	1–2	–2936.4	4910.4
		1–3	12250	6476.9
		2–3	15810	–3884.1
[C ₂ py][NTf ₂]	0.30	1–2	–3744.2	6986.4
		1–3	12099	6224.4
		2–3	27222	–2574.8
[N ₁₁₁ (C ₂ OH)][NTf ₂]	0.20	1–2	–1476.7	1981.6
		1–3	13379	6654.5
		2–3	16438	–3135.8

previously reported for the NRTL correlation of the system (hexane + benzene + [C₂mim][NTf₂]).¹⁸

Conclusions

The LLE of the ternary systems (hexane + benzene + [C₂py][NTf₂]) and (hexane + benzene + [N₁₁₁(C₂OH)][NTf₂]) were experimentally determined at 40 °C, and reasonably well correlated by means of the classical NRTL equation. Solute distribution ratios and selectivities were calculated to evaluate the ability of the ionic liquids to perform as solvents for the separation of aromatic and aliphatic hydrocarbons, particularised in the mixture of benzene and hexane.

Together with data of other systems (hexane + benzene + ionic liquid) previously reported,^{18,27} the current results enable an analysis of the effect of the nature of the cation of the bis{(trifluoromethyl)sulfonyl}amide ionic liquid on the targeted performance. It was already shown that [C₂mim][NTf₂] can be an effective alternative to the use of sulfolane in the separation of aromatics and aliphatics.¹⁸ No significant difference has been observed in terms of solute distribution ratio and selectivity with an analogous ionic liquid with an aromatic cation, [C₂py][NTf₂], in spite of the variation from a 5-member aromatic ring to a 6-member one. Hence, it turns out that the aromaticity factor plays a more relevant role than the ring size in determining the interactions in the system. On the other hand, non-aromatic cations such as tetraalkylammonium or tetraalkylphosphonium with linear alkyl substituents are unsuitable because of a too high oil solubility, in the case of long alkyl substituents, or of too high melting points, in the case of short alkyl substituents. The use of ammonium-functionalised cations may overcome these problems; thus, for example, the ionic liquid [N₁₁₁(C₂OH)][NTf₂], with a sufficiently low melting point, may lead to higher selectivities than those found with the bis{(trifluoromethyl)sulfonyl}amide ionic liquids containing an aromatic cation, albeit at the expense of a lower solute distribution ratio.

In order to conclude whether or not the performance of [N₁₁₁(C₂OH)][NTf₂] is better than that of [C₂mim][NTf₂] or [C₂py][NTf₂], other factors beyond the scope of this work need to be explored, such as physical property sets, toxicity and cost.

An overall economic balance of the engineered process would provide the definitive answer.

Acknowledgements

The authors are grateful to the Industrial Advisory Board of The QUILL Centre for their support. K.R.S. acknowledges the EPSRC (Portfolio Partnership Scheme, grant number EP/D029538/1) for support. A.A. and H.R. want to thank the Ministerio de Educación y Ciencia (Spain) for financial support through project CTQ2006–07687, and for the award of the FPI grant with reference BES-2004–5311.

References

- D. R. MacFarlane and K. R. Seddon, *Ionic Liquids—Progress in the Fundamental Issues*, *Aust. J. Chem.*, 2007, **60**, 3–5.
- A. Stark and K. R. Seddon, in *Kirk-Othmer Encyclopedia of Chemical Technology*, ed. A. Seidel, Vol. 26, John Wiley & Sons, Hoboken, 2007, pp. 836–920.
- R. D. Rogers and K. R. Seddon, *Ionic Liquids—Solvents of the Future?*, *Science*, 2003, **302**, 792–793.
- K. R. Seddon, *Ionic liquids—A taste of the future*, *Nature Materials*, 2003, **2**, 363–365.
- P. Wasserscheid, and T. Welton, (eds.), *Ionic Liquids in Synthesis*, 2nd ed., Wiley-VCH, Weinheim, 2008.
- M. Freemantle, *Designer solvents – Ionic liquids may boost clean technology development*, *Chem. Eng. News*, 1998, **76**[30th March], 32–37.
- G. Fitzwater, W. Geissler, R. Moulton, N. V. Plechkova, A. Robertson, K. R. Seddon, J. Swindall and K. Wan Joo, *Ionic Liquids: Sources of Innovation*, Report Q002, January 2005, QUILL, Belfast (2005). Available online at: <http://quill.qub.ac.uk/sources>.
- R. D. Rogers, and K. R. Seddon, (eds.), *Ionic Liquids IIIB: Fundamentals, Progress, Challenges, and Opportunities—Transformations and Processes*, *ACS Symposium Series*, vol. 902, American Chemical Society, Washington DC, 2005.
- M. Freemantle, *New frontiers for ionic liquids*, *Chem. Eng. News*, 2007, **85**[1st January], 23–26.
- N. V. Plechkova and K. R. Seddon, *Applications of ionic liquids in the chemical industry*, *Chem. Soc. Rev.*, 2008, **37**, 123–150.
- M. J. Earle, J. M. S. S. Esperança, M. A. Gilea, J. N. Canongia Lopes, L. P. N. Rebelo, J. W. Magee, K. R. Seddon and J. A. Widegren, *The distillation and volatility of ionic liquids*, *Nature*, 2006, **439**, 831–834.
- K. R. Seddon, *Ionic Liquids for Clean Technology*, *J. Chem. Tech. Biotechnol.*, 1997, **68**, 351–356.
- J. D. Holbrey and K. R. Seddon, *Ionic Liquids*, *Clean Prod. Proc.*, 1999, **1**, 223–236.
- R. D. Rogers, and K. R. Seddon, (eds.), *Ionic Liquids as Green Solvents—Progress and Prospects*, *ACS Symposium Series*, vol. 856, American Chemical Society, Washington DC, 2003.
- J. G. Huddleston, H. D. Willauer, R. P. Swatloski, A. E. Visser and R. D. Rogers, *Room temperature ionic liquids as novel media for ‘clean’ liquid–liquid extraction*, *Chem. Commun.*, 1998, 1765–1766.
- A. Heintz, *Recent developments in thermodynamics and thermophysics of non-aqueous mixtures containing ionic liquids. A review*, *J. Chem. Thermodyn.*, 2005, **37**, 525–535.
- K. Weissermel and H.-J. Arpe, *Industrial Organic Chemistry*, 3rd ed., VCH, Weinheim, 1997.
- A. Arce, M. J. Earle, H. Rodríguez and K. R. Seddon, *Separation of aromatic hydrocarbons from alkanes using the ionic liquid 1-ethyl-3-methylimidazolium bis{(trifluoromethyl)sulfonyl}amide*, *Green Chem.*, 2007, **9**, 70–74.
- As an example, the cost of this ionic liquid in the revised 2008 catalogue of the company Iolitec is: 1 kg for 920 euros, and 5 kg for 3680 euros (July 2008).
- J. D. Holbrey, and R. D. Rogers, in *Ionic Liquids in Synthesis* (eds. P. Wasserscheid, and T. Welton), 2nd ed., Wiley-VCH, Weinheim, 2008, vol. 1, pp. 57–72.

- 21 R. A. Mantz, and P. C. Trulove, in *Ionic Liquids in Synthesis* (eds. P. Wasserscheid, and T. Welton), 2nd ed., Wiley-VCH, Weinheim, 2008, vol. 1, pp. 72–88.
- 22 A. Arce, M. J. Earle, H. Rodríguez and K. R. Seddon, Separation of Benzene and Hexane by Solvent Extraction with 1-Alkyl-3-methylimidazolium Bis{(trifluoromethyl)sulfonyl}amide Ionic Liquids: Effect of the Alkyl-Substituent Length, *J. Phys. Chem. B*, 2007, **111**, 4732–4736.
- 23 M. J. Earle and K. R. Seddon, Ionic liquids. Green solvents for the future, *Pure Appl. Chem.*, 2000, **72**, 1391–1398.
- 24 J. F. Brennecke and E. J. Maginn, Ionic Liquids: Innovative Fluids for Chemical Processing, *AIChE J.*, 2001, **47**, 2384–2389.
- 25 K. R. Seddon, in *The International George Papatheodorou Symposium: Proceedings* (eds. S. Boghosian, V. Dracopoulos, C. G. Kontoyannis, and G. A. Voyiatzis), Institute of Chemical Engineering and High Temperature Chemical processes, Patras, 1999, pp. 131–135.
- 26 Z. Lei, B. Chen, C. Li and H. Liu, Predictive Molecular Thermodynamic Models for Liquid Solvents, Solid Salts, Polymers, and Ionic Liquids, *Chem. Rev.*, 2008, **108**, 1419–1455.
- 27 A. Arce, M. J. Earle, S. P. Katdare, H. Rodríguez and K. R. Seddon, Application of mutually immiscible ionic liquids to the separation of aromatic and aliphatic hydrocarbons by liquid extraction: a preliminary approach, *Phys. Chem. Chem. Phys.*, 2008, **10**, 2538–2542.
- 28 S. N. Falling, S. A. Godleski and L. W. McGarry, Process for the separation of oligomeric materials from a catalyst mixture, US Pat. App. 5,238,889 (1993).
- 29 P. Bonhôte, A.-P. Dias, M. Armand, N. Papageorgiou, K. Kalyanasundaram and M. Grätzel, Hydrophobic, Highly Conductive Ambient-Temperature Molten Salts, *Inorg. Chem.*, 1996, **35**, 1168–1178 (correction: *Inorg. Chem.*, 1998, **37**, 166).
- 30 A. Arce, M. J. Earle, S. P. Katdare, H. Rodríguez and K. R. Seddon, Phase equilibria of mixtures of mutually immiscible ionic liquids, *Fluid Phase Equilib.*, 2007, **261**, 427–433.
- 31 U. Fröhlich, Ph.D. Thesis, The Queen's University of Belfast, Belfast, UK, 2005.
- 32 J. M. Sørensen, T. Magnussen, P. Rasmussen and A. Fredenslund, Liquid–liquid equilibrium data: Their retrieval, correlation and prediction. Part I: Retrieval, *Fluid Phase Equilib.*, 1979, **2**, 297–309.
- 33 M. A. Muñoz, M. Galán, C. Carmona and M. Balón, Hydrogen-bonding interactions between 1-methylindole and alcohols, *Chem. Phys. Lett.*, 2005, **401**, 109–114.
- 34 J. C. Ma and D. A. Dougherty, The Cation- π Interaction, *Chem. Rev.*, 1997, **97**, 1303–1324.
- 35 J. Chen, L.-P. Duan, J.-G. Mi, W.-Y. Fei and Z.-C. Li, Liquid–liquid equilibria of multi-component systems including n-hexane, n-octane, benzene, toluene, xylene and sulfolane at 298.15 K and atmospheric pressure, *Fluid Phase Equilib.*, 2000, **173**, 109–119.
- 36 J. P. Novák, J. Matous and J. Pick, *Liquid–Liquid Equilibria*, Elsevier, Amsterdam, 1987.
- 37 H. Renon and J. M. Prausnitz, Local Compositions in Thermodynamic Excess Functions for Liquid Mixtures, *AIChE J.*, 1968, **14**, 135–144.
- 38 M. S. Selvan, M. D. McKinley, R. H. Dubois and J. L. Atwood, Liquid–Liquid Equilibria for Toluene + Heptane + 1-Ethyl-3-methylimidazolium Triiodide and Toluene + Heptane + 1-Butyl-3-methylimidazolium Triiodide, *J. Chem. Eng. Data*, 2000, **45**, 841–845.
- 39 T. M. Letcher and N. Deenadayalu, Ternary liquid–liquid equilibria for mixtures of 1-methyl-3-octyl-imidazolium chloride + benzene + an alkane at $T = 298.2$ K and 1 atm, *J. Chem. Thermodyn.*, 2003, **35**, 67–76.
- 40 T. M. Letcher and P. Reddy, Ternary (liquid + liquid) equilibria for mixtures of 1-hexyl-3-methylimidazolium (tetrafluoroborate or hexafluorophosphate) + benzene + an alkane at $T = 298.2$ K and $p = 0.1$ MPa, *J. Chem. Thermodyn.*, 2005, **37**, 415–421.
- 41 G. W. Meindersma, A. J. G. Podt and A. B. de Haan, Ternary liquid–liquid equilibria for mixtures of toluene + n-heptane + an ionic liquid, *Fluid Phase Equilib.*, 2006, **247**, 158–168.
- 42 G. W. Meindersma, A. Podt and A. B. de Haan, Ternary Liquid–Liquid Equilibria for Mixtures of an Aromatic + an Aliphatic Hydrocarbon + 4-Methyl-N-butylpyridinium Tetrafluoroborate, *J. Chem. Eng. Data*, 2006, **51**, 1814–1819.
- 43 U. Domańska, A. Pobudkowska and M. Królikowski, Separation of aromatic hydrocarbons from alkanes using ammonium ionic liquid C_2NTf_2 at $T = 298.15$ K, *Fluid Phase Equilib.*, 2007, **259**, 173–179.
- 44 U. Domańska, A. Pobudkowska and Z. Zolek-Tryznowska, Effect of an Ionic Liquid (IL) Cation on the Ternary System (IL + *p*-Xylene + Hexane) at $T = 298.15$ K, *J. Chem. Eng. Data*, 2007, **52**, 2345–2349.
- 45 R. Wang, J. Wang, H. Meng, C. Li and Z. Wang, Liquid–Liquid Equilibria for Benzene + Cyclohexane + 1-Methyl-3-methylimidazolium Dimethylphosphate or + 1-Ethyl-3-methylimidazolium Diethylphosphate, *J. Chem. Eng. Data*, 2008, **53**, 1159–1162.
- 46 R. M. Maduro and M. Aznar, Liquid–liquid equilibrium of ternary systems 1-butyl-3-methylimidazolium hexafluorophosphate + aromatic + aliphatic, *Fluid Phase Equilib.*, 2008, **265**, 129–138.
- 47 J. M. Sørensen, Ph.D. Thesis, Danmarks Tekniske Højskole, Lingby, Denmark, 1980.

Green glycosylation using ionic liquid to prepare alkyl glycosides for studying carbohydrate–protein interactions by SPR

F. Javier Muñoz,^a Sabine André,^b Hans-Joachim Gabius,^b José V. Sinisterra,^{a,c} María J. Hernáiz^{*a,c,d} and Robert J. Linhardt^{*e}

Received 14th August 2008, Accepted 25th November 2008

First published as an Advance Article on the web 24th December 2008

DOI: 10.1039/b814171a

Several simple glycosides of D-glucose (Glc) and N-acetyl-D-galactosamine (GalNAc) were prepared in a single step glycosylation reaction using unprotected and unactivated sugar donors. The resulting GalNAc glycoside, containing a bifunctional linker, was used to immobilize this glycoconjugate to a self assembled monolayer on a gold biosensor chip. Surface plasmon resonance (SPR) experiments demonstrated that this immobilized glycoconjugate bound to GalNAc specific lectin, *Viscum album* agglutinin.

Introduction

Glycoconjugates including proteoglycans, glycoproteins and glycolipids are involved in many different biological events, such as molecular recognition for cell–cell interaction.^{1–3} Owing to their ubiquitous presence at the cell membrane surface, carbohydrates are located in an environment containing many proteins, such as growth factors, cytokines, receptors, enzymes, and viruses and bacterial proteins. The numerous biological roles of carbohydrates are attributed to their interactions with these proteins, called lectins. Membrane surface carbohydrates, called glycoconjugates, modulate lectin activity at the cell–extracellular interface. Many studies have been directed towards understanding the recognition of these cell surface glycoconjugates by lectins from different sources.^{3,4} The most widely used techniques (*i.e.*, enzyme linked immunosorbent assays, microarrays, atomic force microscopy and surface plasmon resonance (SPR)) for the study of such molecular interactions require the immobilization of either the lectin or the glycoconjugate.⁵

A number of strategies have been developed to mimic the presentation of glycoconjugates on the membrane surface. In addition, many different methodologies have been investigated for the synthesis of glycoconjugates. Protecting groups for hydroxyl moieties in carbohydrates (acyl, ethers, *etc.*) and activation

methods for the anomeric position (halides, thioglycosides, trichloroacetimidates, *etc.*) are required in traditional synthetic chemistry to obtain new glycoconjugates.⁶ A major problem in the synthesis of glycoconjugates is the need for multiple protection, deprotection and activation steps. The crucial importance of glycoconjugates in the study of glycobiology cries out for alternative, simpler methods for their synthesis. Enzymatic synthesis of carbohydrates can be used to avoid many protection, deprotection and activation steps and the products are often obtained with high regio- and stereoselectivity.^{7–9} However, enzymes are often less efficient for the functionalization of glycoconjugates with linker chains required their immobilization to study their interaction with lectins.

Glycosylation using unprotected and unactivated donors is often preferable as it can reduce the number of steps, enhance reactivity, allow a different stereochemistry, and increase prospects for further process modifications.^{10,11} The chemical synthesis of unprotected carbohydrates possesses a number of challenges, including their poor solubility in most conventional solvents. It is important to investigate new solvent systems that dissolve carbohydrates and support glycosidation reactions of unprotected sugars.

Recently, room temperature ionic liquids (RTILs) have received attention as solvents for a wide range of chemical processes.¹² RTILs show exceptional solvent properties including thermal stability, low volatility and an ability to dissolve both polar and non-polar compounds. RTILs also have been widely researched as possible “green” replacements for organic solvents because they have very low vapour pressures and may be used to replace volatile organic solvents and may be easier to efficiently reuse than organic solvents.^{13,14} Carbohydrate chemistry is not an exception to this trend. In the past few years ionic liquids have been used in both protection and glycosylation reactions, resulting in new methodologies and enhanced yield.^{15–21}

We report a convenient method for the modification of unprotected and unactivated carbohydrates, of biological interest, with a bifunctional linker. The use of RTIL solvent allowed us to introduce a linker chain into carbohydrates in a single, simple step. The resulting glycoconjugates were immobilized

^aBiotransformations Group, Departamento de Química Orgánica y Farmacéutica, Facultad de Farmacia, Universidad Complutense de Madrid, Pz/ Ramón y Cajal s/n., 28040, Madrid, Spain.

E-mail: mjhernai@farm.ucm.es; Fax: +34 9139471822; Tel: +34 913947208

^bInstitut für Physiologische Chemie, Tierärztliche Fakultät, Ludwig-Maximilians-Universität, München, Veterinärstr. 13, 80539, München, Germany

^cServicio de Biotransformaciones Industriales, Parque Científico de Madrid C/ Santiago Grisolia, 28760, Tres Cantos, Spain

^dServicio de Interacciones Biomoleculares, Parque Científico de Madrid, Unidad de Proteómica, Pz/ Ramón y Cajal s/n, 28040, Madrid, Spain

^eDepartments of Chemistry and Chemical Biology, Biology, Chemical and Biological Engineering, Center for Biotechnology and Interdisciplinary Studies, Rensselaer Polytechnic Institute, 110 8th St., Troy, NY 12180-3590, USA. E-mail: linhar@rpi.edu; Fax: +1 518-276-3405; Tel: +1 518-276-3404

Table 1 Functionalization of carbohydrates with different linker chains^a

Donor	Acceptor	Compound	Yield
Glc	Allyl alcohol	1	35%
	Benzylamine	2	n.p.
	Benzylmercaptan	3	n.p.
	4-Aminobenzyl alcohol	4	n.r.
	2-(2'-Aminoethoxy)ethanol	5	n.p.
Lac	<i>t</i> Boc-2-(2'-Aminoethoxy)ethanol (6)	7	12%
	Allyl alcohol	8	n.p.
	GalNAc	Allyl alcohol	9
<i>t</i> Boc-2-(2'-Aminoethoxy)ethanol (6)		10	7%

^a n.p.: no product isolated. n.r.: no reaction observed.

on a carboxylated functionalized matrix and used in lectin interaction studies performed by SPR.

Results and discussion

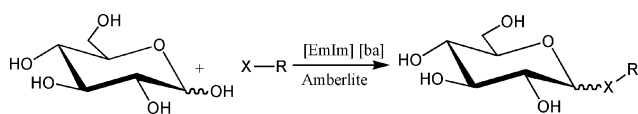
Synthesis of functionalized carbohydrates

In this study, we present the functionalization of non-activated carbohydrates in a single step to give a glycoconjugate having a free amino group. Thereby, it is possible to obtain various kinds of functionalized glycoconjugates without the need of protection, activation and deprotection steps required for the chemical synthesis chemistry of carbohydrates. For this purpose, we selected three substrates, D-glucose (Glc), N-acetyl-D-galactose (GalNAc) and lactose as model carbohydrates for study.

Glycosylation reactions were carried out in the presence of the RTIL, 1-ethyl-3-methylimidazolium benzoate [emIm][ba], and Amberlite IR-120 [H⁺] providing the acid milieu necessary to promote glycosylation. The application of [emIm][ba] RTIL was previously demonstrated in the protection and functionalization of carbohydrate.²¹

This RTIL was also previously used for the glycosylation of bulky acceptors, including monosaccharides and benzyl alcohol.¹⁵ These initial successes prompted us to examine if the same one-step glycosylation reaction could be similarly carried out using linear alkyl chain acceptors. For these purposes we initially tested the reactivity of an α,β -anomeric mixture of Glc monosaccharide donor with the allyl alcohol as acceptor (Table 1).

The reaction, carried out following the conditions described in the Experimental section, led to formation of the desired compound in 35% yield (Scheme 1, Table 2). Some stereoselectivity was observed in this glycosylation reaction, giving primarily the α -glycoside ($\alpha:\beta$, 77:23), as previously described for similar processes.^{15,22}



Scheme 1 General glycosylation reaction of Glc with various acceptors.

One of the most remarkable features of [emIm][ba] is its high viscosity at room temperature. The viscous nature of this

Table 2 Glycosylation of Glc with different linker chains^a

Compound	Product	<i>t</i>	Yield	$\alpha:\beta$
1		17 h	35%	77:23
2		6 h	n.p.	17:83
3		6 h	n.p.	59:41
4		7 d	n.r.	—
5		6 h	n.p.	50:50
7		24 h	12%	40:60

^a n.p.: no product isolated. n.r.: no reaction observed.

solvent posed a problem that was overcome by increasing the reaction temperature to 50 °C. Under the conditions, allyl alcohol afforded the complete conversion of Glc to the allyl glycoside **1**. However, the viscosity of this RTIL solvent posed additional problems in product purification. While a nearly quantitative yield was observed by TLC, the recovered yield of purified glucoside product was only 35%. Despite a yield of only 35%, the requirement of only one step makes this approach promising for glycosylation reactions, as protection, activation and deprotection steps would certainly decrease more greatly the yield of isolated product.

Allyl alcohol was selected as we expected it would be an excellent glycosidation acceptor due to its very small size when compared to the benzylamine, benzylmercaptan, 4-aminobenzyl alcohol or 2-(2'-aminoethoxy)ethanol acceptors (Table 2). This was demonstrated by the case when 4-aminobenzyl alcohol was used as acceptor: no reaction was observed, probably due to the poor solubility of the linker chain in the reaction medium. In addition, benzylamine, benzylmercaptan, and 2-(2'-aminoethoxy)ethanol acceptors afforded a mixture of products by TLC, possibly including the α,β -glycosides, the signals of which correspond to the anomeric protons identified by ¹H-NMR. Further isolation failed to afford the desired product due to the high viscosity of the RTIL at room temperature (Table 2). [emIm][ba] RTILs are relatively viscous RTILs with a viscosity of 425 cP at 25 °C, making both stirring and product recovery difficult.¹⁵

Next, a bifunctional linker chain was tested as a glycosylation acceptor in [emIm][ba], the *tert*-butoxycarbonyl (*t*Boc) amino protected 2-(2'-aminoethoxy)ethanol. The advantage of this linker is that once bound to the carbohydrate through the glycosylation of the hydroxyl group, selective removal of *t*Boc exposes an amino group that could be used for a covalent immobilization of the resulting glycoconjugate onto surfaces. Compound **7** was obtained as a mixture of α - and β -isomers

Table 3 Glycosylation of non-modified monosaccharides with allyl alcohol as linker chains in the presence of [emIm][ba]

Compound	Donor	Linker chain	Yield	Percentage of α -derivative
1	Glc	HOCH ₂ CH=CH ₂	35%	77%
9	GalNAc		35%	80%

(40:60) in 12% yield (Table 2). The α and β configurations were inferred from the chemical shifts and coupling constant of the anomeric proton signal.

The investigation of the glycosylation reaction in [emIm][ba] was next extended to other glycosyl donors, including GalNAc and lactose using allyl alcohol as acceptor (Table 1). Using lactose as a disaccharide donor afforded a mixture of products from which we were unable to detect the desired glycoconjugate by ¹H NMR.

Using GalNAc as donor and carrying out reactions under identical experimental conditions as described for Glc, afforded the desired glycoside product in 35% yield (Table 3). Interestingly, the conversion Glc and GalNAc afforded identical 35% isolated yields (Table 3); however, the Glc initial donor completely disappeared in 17 h, while the GalNAc reaction was terminated because no further evolution of product was observed after 28 h. On the other hand, the α -stereoselectivity observed using both Glc and GalNAc donors was surprising, as neighboring group participation of the 2-acetamido group typically affords the β -product using such donors. However, the α -selectivity was also described for the glycosylation of Man, Glc and GalNAc with benzyl alcohol by other authors.^{15,22}

The bifunctional linker, *t*Boc amino protected 2-(2'-aminoethoxy) ethanol was also examined as a glycosylation acceptor in [emIm][ba] using both Glc and GalNAc donors. The conversion was very low in both cases, 12% for Glc and 7% for GalNAc (Table 4). The high polarity of the solvent may explain the low reactivity towards this non-polar acceptor and also may have complicated the isolation of pure products. Again, compared to traditional glycosylation procedures, requiring several intermediate steps, the low overall yields associated with direct glycosylation in RTIL was considered acceptable. Interestingly, glycosylation by GalNAc exclusively afforded the α -glycoside (Table 4).

Deprotection of *t*-Boc with trifluoroacetic acid (TFA) quantitatively afforded the glycoconjugate **11**. This reaction, in the absence of water and at room temperature was complete within 3 min, and deprotected compound **11** decomposed to a complex mixture unless residual TFA was quickly removed and the sample was stored cold (< 4 °C). Thus, compound **11** was best immediately immobilized on the surface of the biosensor chip for carbohydrate-protein interaction studies.

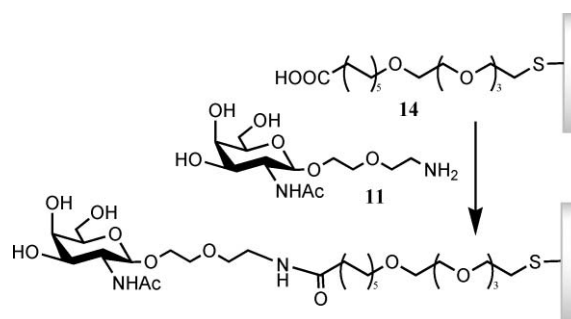
Table 4 Glycosylation of monosaccharides with 2-(2'-aminoethoxy)-ethanol protected with different protecting groups

Product	Donor	Linker chain	Yield	Percentage of α -derivative
7	Glc	HOCH ₂ CH ₂ OCH ₂ CH ₂ NH- <i>t</i> Boc	12%	43%
10	GalNAc		7%	99%

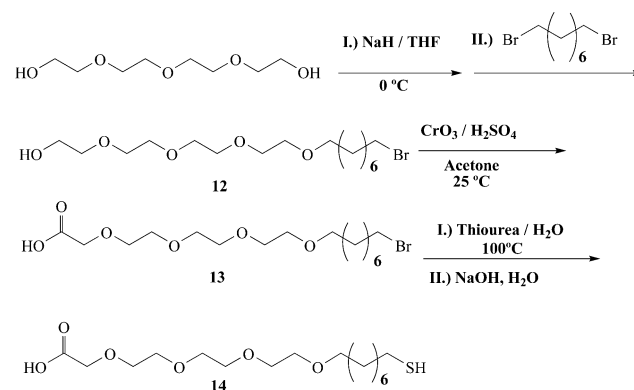
Functionalization of a biosensor chip

The basic SPR sensor chip contains a gold surface to which a ligand is immobilized. Commercially available biosensor chips, such as the CM5 chip, typically contain a functionalized matrix on the gold surface. Thus, when immobilizing low-molecular-weight ligands onto these types of surfaces, the greater the distance from the gold surface the lower the relative response (measured as "response units", RU), or sensitivity when a binding partner, in the solution phase, interacts with immobilized ligand. The problem of low sensitivity has been reported by others²³ when immobilizing small molecules on a commercial CM5 biosensor chips (Biacore).

Compound **11** was immobilized directly on a gold chip through a self-assembled monolayer (SAM) prepared using compound **14** (Fig. 1).

**Fig. 1** Preparation of the chip with mixed chains and immobilization of functionalized glycoconjugate **14**.

This thiol-reactive heterobifunctional linker **14** was synthesized as described in the Experimental section with good yield (Scheme 2). Tetra(ethylene glycol) reacted with 1,8-dibromooctane to afford compound **12** in 40% yield. Compound **12** was then oxidized with Jones reagent to afford **13** in good yield (70%). And finally, reaction with thiourea followed by base catalyzed hydrolysis afforded thiol group and carboxyl containing compound **14** in 60% yield. The resulting monolayer was very homogeneous judging from the similar RU values obtained for both flowcells. The linker chains forming the SAM contained a free carboxylic group for functionalization. The SAM was formed quickly and was quite stable due to the avidity of the thiol group for gold. Several washings with 50% aqueous MeOH were required to eliminate non-covalently bound linker.

**Scheme 2** Synthesis of compound **14**.

The GalNAc glycoconjugate **11** was immobilized to the SAM on the biosensor chip using standard EDC/NHS activation (Fig. 1). After several injections of glycoconjugate **11**, the response increased 600 RU and after the standard blocking of the remaining activated binding sites with ethanolamine, the increase of the response decreased to 374 RU. These results compare favorably to those obtained for the immobilization of the same concentration of glycoconjugate **11** on the carboxy dextran matrix of a CM5 chip, where no increase in RU was observed. Thus, the self-assembled monolayer considerably improves the sensitivity of SPR detection using small molecule ligands.

Interaction studies with lectin

The final step of this study was to determine the utility of SAM containing glycoconjugates to study a carbohydrate–protein interaction. VAA, a potent toxin and biohazard, was selected as a model lectin to examine the bioactivity of this surface. VAA recognizes and selectively binds to GalNAc residues. Different concentrations of VAA were injected over the GalNAc containing biochip and sensorgrams were obtained and analyzed (Fig. 2). The affinity parameters obtained were K_A : $6.72 \times 10^4 \text{ M}^{-1}$; K_D : $1.49 \times 10^{-5} \text{ M}$, clearly demonstrating binding in the micromolar range (Fig. 2). SPR, using the CM5 surface, showed no observable interaction.

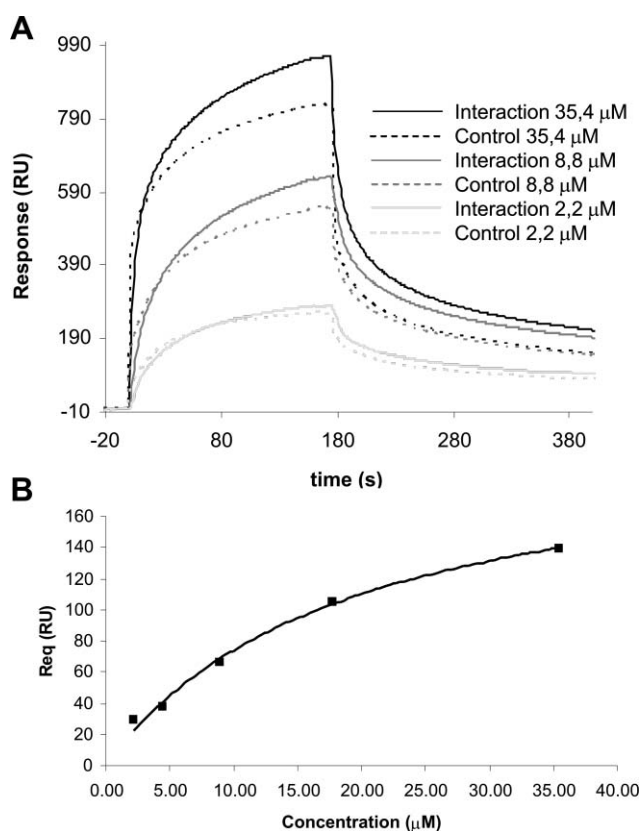


Fig. 2 A. Sensorgrams of the glycoconjugate–lectin interaction compared to the control sensorgrams. B. Steady-state affinity study of the interaction between B subunit from *Viscum album* lectin with glycoconjugate **11**, immobilized on an Au chip.

Experimental

The RTIL [emIm][ba] was synthesized according to the reported procedure¹⁵ and all chemicals were purchased from Fisher or Sigma–Aldrich. ¹H-NMR and ¹³C-NMR experiments were performed in a Varian 500 MHz (COSY or ¹H-¹³C heteronuclear experiments) were also carried out as required for making assignments). Chemical shifts (δ) are indicated in parts per million (ppm). LRMS was carried out with an Agilent 1100 series LC/MSD trap. TLC was performed on Kieselgel plates 60 F₂₅₄ (Merck). Product detection on TLC plates was carried out under a UV-lamp or with 5% H₂SO₄ in CH₃OH and heating. Column chromatography used silica gel 230–400 mesh (Natland International Corporation). Sensor chips and solutions used for the SPR assays were purchased from Biacore. SPR experiments were carried out with a BIAcore-3000 and the sensorgrams were analyzed with BIAEvaluation software version 4.1, 2003 (Biacore).

The *Viscum album* agglutinin (VAA) lectin was purified from mistletoe extracts of dried leaves by affinity chromatography on lactosylated Sepharose 4B obtained by divinyl sulfone activation and ligand coupling as crucial step and assays to ascertain purity and activity were run by one- and two-dimensional gel electrophoresis and gel filtration or haemagglutination and solid-phase/cell binding.^{24,25}

General method for glycosylation reactions in RTIL

Carbohydrate was dissolved in [emIm][ba] in the presence of Amberlite IR-120 (H⁺) and a excess of the linker (Scheme 1 and Table 1). The reaction mixture was stirred at 50 °C under argon atmosphere and monitored by TLC.

When reaction was complete, or no further conversion of substrates into products was observed, the Amberlite was removed by filtration and washed with CH₃OH. Solvent was removed and product purified by column chromatography (CH₂Cl₂–CH₃OH in the appropriate ratio depending on the polarity of compounds). If necessary, traces of RTIL could be removed from the product using a Dowex MR-3 mixed bed ion-exchange resin. All fractions containing carbohydrate were analyzed by ¹H-NMR.

Synthesis of 1-O-allyl-glucopyranoside (1)

Allyl alcohol (322 μL , 4.1 mmol) was added to a mixture of Amberlite IR-120 (H⁺) (300 mg) and Glc (50 mg, 0.28 mmol) [emIm][ba] (300 mg, 1.3 mmol) under the conditions described above. Compound **1** was purified by column chromatography eluting with CH₂Cl₂–CH₃OH gradient (9:1 to 3:1) affording 21 mg of product in 35% yield (Table 1).

¹H-NMR (500 MHz, D₂O): Allyl: 5.97 (m, 1H, H-2), 5.36 (dd, 1H, $J = 17.0$, $J = 1.8$ Hz, H-3a), 5.26 (dd, 1H, $J = 10.6$, $J = 0.7$ Hz, H-3b), 4.23 (dd, 1H, $J = 13.0$, $J = 5.7$ Hz, H-1a), 4.07 (dd, 1H, $J = 13.0$, $J = 6.2$ Hz, H-1b). Glc: 4.96 (d, 1H, $J = 3.8$ Hz, H-1 α), 3.85 (dt, 1H, $J = 12.1$, $J = 1.9$ Hz, H-6a), 3.75 (dd, 1H, $J = 11.6$, $J = 5.3$ Hz, H-6b), 3.69 (m, 1H, H-5), 3.68 (t, 1H, $J = 10.2$ Hz, H-3), 3.55 (dd, 1H, $J = 9.8$, $J = 3.9$ Hz, H-2), 3.40 (t, 1H, $J = 9.3$ Hz, H-4). ¹³C-NMR (125 MHz, D₂O): 133.69, 118.34, 97.47, 73.26, 71.99, 71.38, 69.81, 68.61, 60.66.

MS: [M + Na] calcd: 243.1, found: 242.7. [M + Cl] calcd: 255.6, found: 256.9.

Synthesis of *t*-Boc-2-(2'-aminoethoxy)ethanol (6)

2-(2'-Aminoethoxy)ethanol (10.5 μL, 0.95 mmol) was dissolved in 15 mL of anhydrous THF and cooled by stirring in an ice-water bath, NEt₃ (13 μL) was added and the reaction mixture was stirred under argon atmosphere at 0 °C. (*t*-Boc)₂O (311 mg, 1.42 mg) was slowly added to the reaction mixture at 0 °C, and then allowed to warm to room temperature with stirring. When reaction was complete, aqueous NaHCO₃ was added and this mixture was extracted with ethyl acetate (3 × 50 mL). The organic phase was dried with anhydrous MgSO₄, filtered and the solvent was removed by rotary evaporation. The final product was purified by column chromatography (hexanes–EtOAc gradient 1:1 to 1:9) affording compound **6** (158 mg, 81%).

¹H-NMR (500 MHz, CDCl₃): 5.15 (s, 1H, –NH–), 3.66 (t, 2H, *J* = 4.8 Hz, H-2'), 3.53 (t, 2H, *J* = 4.8 Hz, H-1'), 3.50 (t, 2H, *J* = 5.5 Hz, H-2), 3.23 (t, 2H, *J* = 5.5 Hz, H-1), 2.73 (s, –OH), 1.44 (s, 9H, –(CH₃)₃). ¹³C-NMR (125 MHz, CDCl₃): 156.10, 79.35, 72.16, 70.26, 61.62, 40.27. ESI-MS: [M + Na] calcd: 228.1, found: 228.0.

Synthesis of *t*-Boc-2-(2'-aminoethoxy)ethyl-glucopyranoside (7)

t-Boc-2-(2'-aminoethoxy)ethanol (58 mg, 0.28 mmol) was added to a mixture of Amberlite IR-120 (H⁺) (30 mg) and Glc (5 mg, 0.023 mmol) in [emIm][ba] (30 mg, 0.13 mmol) under identical purification and reaction conditions as described in the general procedure. Column chromatography was performed in CH₂Cl₂–CH₃OH (50:1 to 4:1) gradient, affording compound **7** (1 mg, 12% yield) (Table 1).

¹H-NMR (500 MHz, D₂O): 5.16 (d, 1H, *J* = 3.9, H-1α), 4.57 (d, 1H, *J* = 7.9, H-1β), 3.84–3.16 (14H, H-2 to H-6, and sugar), 1.44 (s, 9H, –(CH₃)₃). ¹³C-NMR (125 MHz, D₂O): 156.08, 107.78, 81.76, 79.38, 77.78, 75.83, 73.16, 70.15, 70.09, 65.30, 64.87, 40.54, 27.92. MS: [M + Na] calcd: 390.2, found: 389.1. [M + Cl] calcd: 402.7, found: 403.5.

Synthesis of 1-*O*-allyl-2-acetamido-2-deoxy-galactopyranoside (9)

Allyl alcohol (300 μL, 5.0 mmol) was added to a mixture of Amberlite IR-120 (H⁺) (60 mg) and GalNAc (10 mg, 0.05 mmol) in [emIm][ba] (60 mg, 0.26 mmol) under identical purification and reaction conditions as described in the general procedure. The solvent was removed with a high-vacuum pump to afford compound **9** (4 mg, 35%) (Table 1).

¹H-NMR (500 MHz, D₂O): Allyl: 5.90 (m, 1H, H-2), 5.28 (dd, 1H, *J* = 17.2, *J* = 1.5 Hz, H-3a), 5.23 (dd, 1H, *J* = 10.6, *J* = 1.1 Hz, H-3b), 4.13 (1H, H-1a), 3.98 (dd, 1H, *J* = 13.0, *J* = 6.1 Hz, H-1b). GalNAc: 4.89 (d, 1H, *J* = 3.8 Hz, H-1α), 4.10 (dd, 1H, *J* = 10.9, *J* = 3.8 Hz, H-2), 3.94–3.90 (m, 2H, H-6), 3.86 (dd, *J* = 10.9, *J* = 3.2 Hz, H-3), 3.72–3.64 (m, 2H, H-4, H-5), 1.90 (s, 3H, –CH₃). ¹³C-NMR (125 MHz, D₂O): 175.04, 134.10, 122.20, 118.34, 96.66, 71.41, 68.89, 68.11, 61.65, 50.33, 22.34. MS: [M + Na] calcd: 284.1, found: 283.7. [M + Cl] calcd: 296.6, found: 296.9.

Synthesis of *t*-Boc-2'-(2''-aminoethoxy)ethyl-2-acetamido-2-deoxy-galactopyranoside (10)

t-Boc-2-(2'-aminoethoxy)ethanol (232 mg, 1.13 mmol) was added to a mixture of Amberlite IR-120 (H⁺) (150 mg) and of GalNAc (25 mg, 0.11 mmol) in [emIm][ba] (150 mg, 0.65 mmol) under identical purification and reaction conditions as described in the general procedure. Purification by column chromatography CH₂Cl₂–CH₃OH (5:1) afforded compound **10** (3 mg, 7%) (Table 1).

¹H-NMR (500 MHz, D₂O): linker chain: 3.61–3.59 (4H, H-1' and H-2'), 3.53 (t, 2H, *J* = 5.5 Hz, H-1''), 3.20 (t, 2H, *J* = 5.2 Hz, H-2''), 1.27 (s, 9H, –(CH₃)₃). GalNAc: 4.96 (d, 1H, *J* = 2.1 Hz, H-1α), 4.11 (dd, 1H, *J* = 2.3, *J* = 4.4 Hz, H-2), 4.07 (dd, 1H, *J* = 4.5, *J* = 6.6 Hz, H-4), 3.96 (dd, 1H, *J* = 3.4, *J* = 6.6 Hz, H-3), 3.79 (m, 2H, H-5 and H-6a), 3.64 (dd, 1H, *J* = 3.7, *J* = 6.6 Hz, H-6b), 1.96 (s, 3H, –CH₃). ¹³C-NMR (125 MHz, D₂O): 174.99, 156.08, 101.78, 80.22, 79.01, 72.83, 71.16, 70.02, 69.91, 64.07, 63.85, 41.00, 27.82, 23.20. MS: [M + Na] calcd: 431.2 found: 430.8. [M + Cl] calcd: 443.5 found: 444.5.

Synthesis of 2'-(2''-aminoethoxy)ethyl-2-acetamido-2-deoxy-galactopyranoside (11)

Trifluoroacetic acid (100 μL) was added to 1 mg of compound **10** and reaction was stirred for 1 min. The mixture was dried under vacuum and compound **11** was analyzed by NMR without purification.

¹H-NMR (500 MHz, D₂O): 5.10 (d, 1H, *J* = 3.6, H-1α), 4.51 (d, 1H, *J* = 8.3, H-1β), 4.04–3.51 (H-2 to H-6, H-1' and H-2'), 3.51 (t, 2H, *J* = 5.5 Hz, H-1''), 3.09 (t, 2H, *J* = 5.5 Hz, H-2''), 1.92 (s, 3H, –CH₃). ¹³C-NMR (125 MHz, D₂O): 173.54, 100.35, 81.22, 74.55, 73.71, 71.39, 70.04, 65.11, 64.54, 60.01, 40.89, 23.21. ESI-MS: [M + Na] calcd: 331.2, found: 331.0.

Synthesis of 20-bromo-3,6,9,12-tetraoxatricosan-1-ol (12)

NaH (160 mg, 6.5 mmol) was added to a solution of tetraethyleneglycol (1 g, 5 mmol) in anhydrous THF and the reaction mixture was stirred under argon atmosphere at 0 °C. After 3 h the reaction mixture, under argon atmosphere at 0 °C, was added over a period of 4 h to a solution of 1,8-dibromooctane (1.4 g, 5 mmol). The NaBr formed was removed by filtration and the solvent was evaporated. Purification of final product was carried out by column chromatography (CH₂Cl₂–CH₃OH 20:1) affording **12** in 40% yield.

¹H-NMR (300 MHz, CDCl₃): 3.62 (m, 16H, H-1 to H-8), 3.43 (t, 2H, *J* = 6.56 Hz, H-9), 3.38 (t, 2H, *J* = 7.03 Hz, H-19), 1.83 (q, 2H, *J* = 7.2 Hz, H-18), 1.55 (q, 2H, *J* = 6.90 Hz, H-10), 1.38 (m, 2H, H-11), 1.25 (m, 12H, H-12 and H-17). ¹³C-NMR (125 MHz, CDCl₃): 72.63 (C-9), 71.52 (C-7), 70.61 (C-3, C-4, C-5, C-6), 70.28 (C-8), 70.05 (C-2), 61.50 (C-1), 34.00 (C-19), 32.89 (C-18), 29.56 (C-10, C-12, C-13, C-14, C-15), 28.72 (C-11), 28.18 (C-16), 26.13 (C-17). Analysis calculated for C₁₆H₃₃BrO₅: C: 49.87%; H: 8.63%; Found: C: 49.88%; H: 8.65%. ESI-MS: [M + Na] Calcd: 407.2. Found: 407.3.

Synthesis of 20-bromo-3,6,9,12-tetraoxatrieicosan-1-oic acid (**13**)

A mixture of **12** (650 mg, 1.7 mmol) in acetone (50 mL) was stirred at room temperature and Jones reagent (2.4 mmol in CrO₃) was added dropwise over 15 min. The reaction was stirred for an additional 30 min followed by the addition of few drops of 2-propanol. Saturated NaCl solution (20 mL) was added to the mixture and stirred for an additional 30 min followed by removal of the acetone. The aqueous mixture was extracted with CH₂Cl₂ (3 × 30 mL) and the solvent was removed by rotary evaporation. Purification of final product was carried out by column chromatography (CH₂Cl₂–CH₃OH 10:1) yielding **13** in 70%.

¹H-NMR (300 MHz, CDCl₃): 6.71 (s, 1H, COOH), 4.13 (s, 2H, H-2), 3.56 (m, 12H, H-3 a H-8), 3.39 (t, 2H, *J* = 6.90 Hz, H-9), 3.34 (t, 2H, *J* = 6.85 Hz, H-14), 1.81 (q, 2H, *J* = 7.16 Hz, H-15), 1.52 (m, 2H, H-10), 1.34 (m, 2H, H-11), 1.28 (m, 6H, H-12, H-13, H-14). ¹³C-NMR (125 MHz, CDCl₃): 173.03 (C-1), 72.07 (C-9), 71.97 (C-8), 70.84 (C-7), 70.74 (C-6), 70.65 (C-5), 70.45 (C-4), 70.34 (C-3), 69.11 (C-2), 34.44 (C-16), 33.10 (C-15), 29.70 (C-10), 29.55 (C-12), 29.00 (C-11), 28.41 (C-13), 26.24 (C-14). Analysis calculated for C₁₆H₃₁BrO₆: C: 48.12%; H: 7.82%. Found: C: 48.20%; H: 7.81%. ESI-MS: [M + Na] Calcd: 421.1. Found: 421.0.

Synthesis of 20-mercapto-3,6,9,12-tetraoxatrieicosan-1-oic acid (**14**)

A solution of **13** (230 mg, 0.5 mmol) and thiourea (120 mg, 1.5 mmol) in 30 mL of water was heated under reflux for 6 h. After the addition of NaOH (600 mg, 15 mmol), the heating was resumed for an additional period of 6 h. After the mixture was cooled at room temperature, the pH was adjusted to 1 with concentrated HCl. The resulting solution was extracted with CH₂Cl₂ (3 × 20 mL). The combined extracts were dried on MgSO₄ and evaporated to dryness, leaving an oil, which was purified by column chromatography (CH₂Cl₂–CH₃OH 5:2) with a 60% yield.

¹H-NMR (300 MHz, CDCl₃): 8.23 (s, 1H, COOH), 4.0 (s, 2H, H-2), 3.56 (m, 12H, H-3 and H-8), 3.38 (t, 2H, *J* = 6.93 Hz, H-9), 2.58 (t, 2H, *J* = 7.35 Hz, H-19), 1.58 (m, 4H, H-10, H-18), 1.20 (m, 14H, H-11, H-12, H-13, H-14, H-15, H-16, H-17). ¹³C-NMR (125 MHz, CDCl₃): 173.03 (C-1), 72.07 (C-9), 71.97 (C-8), 70.84 (C-7), 70.74 (C-6), 70.65 (C-5), 70.45 (C-4), 70.34 (C-3), 69.11 (C-2), 34.44 (C-16), 33.10 (C-15), 29.70 (C-10), 29.55 (C-12), 29.00 (C-11), 28.41 (C-13), 26.24 (C-14). Analysis calculated for C₁₆H₃₂O₆S: C: 54.52%; H: 9.15%; S: 9.10%. Found: C: 54.53%; H: 9.17%; S: 9.09%. ESI-MS: [M + Na] Calcd: 375.2. Found: 375.0.

Immobilization of glycoconjugates on the SPR chip

Immobilization of thiol chains on the gold surface. For the immobilization of the thiol linker functionalized with a carboxyl group, an Au chip (Biacore) was required. Flow was set at 2 μL min⁻¹ and temperature at 25 °C using HBS-P (0.01 M HEPES, 0.15 M NaCl, pH = 7.4) as running buffer. A solution of the linker **14** was injected into two different flow cells until 721 and 1228 RU (relative response unit) were obtained.

Immobilization of glycoconjugate **11** on the Au chip (Biacore).

For the immobilization of GalNAc glycoconjugate (**11**), the carboxylated groups of the self-assembled monolayer were activated by the injection of the amino coupling kit (Biacore): EDC/NHS, 35 μL, at a flow rate of 5 μL min⁻¹, at 25 °C, and HBS-P as running buffer. At the same conditions of flow and temperature, a solution of **11** (2 mM, 150 μL) in HBS-P was injected to get the maximum immobilization (605 RU), followed by the injection of ethanolamine (1 M, 35 μL) to block the possible remaining active sites and another injection of MeOH (5 μL). On the second flow cell, the activation and blocking standard procedures were carried out as described above, and it was left as a negative control of the interaction.

Immobilization of glycoconjugate **11 on the CM5 chip.** The immobilization of the functionalized GalNAc glycoconjugate (**11**) was carried out on commercially available CM5 chips (Biacore). The carboxylated dextran matrix was activated by the standard procedure (Biacore), as described above. A solution of glycoconjugate **11** (150 μL, 2 mM) in the running buffer (HBS-P) was injected at a flow rate of 5 μL min⁻¹ at 25 °C followed by the injection of ethanolamine (1 M, 35 μL) to block the remaining active sites. The same activation and blocking procedures were repeated in a different flow cell and used as negative control for the interaction studies.

Interaction with *Viscum album* lectin. The interaction experiments were carried at a constant flow of 5 μL min⁻¹ at 25 °C over GalNAc glycoconjugate **11** immobilized on the Au chip functionalized with the thiol chains as described above. For that purpose, 15 μL of different solutions of the VAA in the running buffer (HBS-P) were injected: 2.2, 5.4, 8.9, 17.9 and 35.7 μM. Sensorgrams obtained for the interaction of VAA with **11**, were analyzed and kinetic parameters of the interaction were determined with BIAEvaluation software (Biacore).

Conclusions

Different glycoconjugates were prepared in the presence of ionic liquids in order to carry out carbohydrate–protein interaction studies.

The direct functionalization of carbohydrates (Glc, GalNAc, lactose) with different linker chains (in the presence of ionic liquids) was carried out. Despite the poor yields obtained, the decrease in the number of steps made it a green alternative to the traditional carbohydrate chemistry.

An amino functionalized GalNAc was directly synthesized in the presence of ionic liquids and further immobilized on an alkanethiol-coated surface. The interaction of immobilized GalNAc derivative with a carbohydrate binding protein was studied, and kinetic parameters of this procedure were determined.

Acknowledgements

This work was supported by Spanish MEC (CTQ2006–09052/BQU) and EU grant (SOLVSAFE (Advanced safer solvents for innovative industrial eco-processing, FP-62003-NMP-SMF-3, proposal 011774–2), an EC Marie Curie Research Training Network grant (MRTN-CT-2005–019561), the

research initiative LMUexcellent and MEC-FPU predoctoral fellowship (AP2003–4820) and US National Institutes of Health (NIH grant AI065786).

References

- 1 C. R. Bertozzi and L. L. Kiessling, *Science*, 2001, **291**, 2357–2364.
- 2 A. Varki, *Glycobiology*, 1993, **3**, 97–130.
- 3 H.-J. Gabius, S. André, H. Kaltner and H.-C. Siebert, *Biochim. Biophys. Acta*, 2002, **1572**, 165–177.
- 4 C. Bies, C.-M. Lehr and J. F. Woodley, *Adv. Drug Delivery Rev.*, 2004, **56**, 425–435.
- 5 K. Larsen, M. B. Thygesen, F. Guillaumie, W. G. T. Willats and K. J. Jensen, *Carbohydr. Res.*, 2006, **341**, 1209–1234.
- 6 K. C. Nicolaou and H. J. Mitchell, *Angew. Chem., Int. Ed.*, 2001, **40**, 1576–1624.
- 7 D. H. G. Crout and G. Vic, *Curr. Opin. Chem. Biol.*, 1998, **2**, 98–111.
- 8 M. M. Palcic, *Curr. Opin. Biotechnol.*, 1999, **10**, 616–624.
- 9 M. Scigelova, S. Singh and D. H. G. Crout, *J. Mol. Catal. B: Enzym.*, 1999, **6**, 483–494.
- 10 S. Hanessian, *Preparative Carbohydrate Chemistry*, Marcel Dekker, New York, 1997.
- 11 S. Hanessian and B. L. Lou, *Chem. Rev.*, 2000, **100**, 4443–4463.
- 12 N. Jain, A. Kumar, S. Chauhan and S. M. S. Chauhan, *Tetrahedron*, 2005, **61**, 1015–1060.
- 13 J. M. DeSimone, *Science*, 2002, **297**, 799–803.
- 14 S. Park and R. J. Kazlauskas, *Curr. Opin. Biotechnol.*, 2003, **14**, 32–37.
- 15 T.-J. Park, M. Weïwer, X. Yuan, S. N. Baytas, E. M. Munoz, S. Murugesan and R. J. Linhardt, *Carbohydr. Res.*, 2007, **342**, 614–620.
- 16 J.-Y. Huang, M. Lei and Y.-G. Wang, *Tetrahedron Lett.*, 2006, **47**, 3047–3050.
- 17 A. Rencurosi, L. Lay, G. Russo, E. Caneva and L. Poletti, *Carbohydr. Res.*, 2006, **341**, 903–908.
- 18 K. Toshima, *Carbohydr. Res.*, 2006, **341**, 1282–1297.
- 19 S. Murugesan, N. Karst, T. Islam, J. M. Wiencek and R. J. Linhardt, *Synlett*, 2003, 1283–1286.
- 20 S. Murugesan and R. J. Linhardt, *Curr. Org. Synth.*, 2005, **2**, 437–451.
- 21 L. Poletti, A. Rencurosi, L. Lay and G. Russo, *Synlett*, 2003, 2297–2300.
- 22 M. Sharma, G. G. Potti, O. D. Simmons and W. Korytnyk, *Carbohydr. Res.*, 1987, **162**, 41–51.
- 23 C. Plath, T. Weimar, H. Peters and T. Peters, *ChemBioChem*, 2006, **7**, 1226–1230.
- 24 M. Jiménez, J. L. Sáiz, S. André, H.-J. Gabius and D. Solís, *Glycobiology*, 2005, **15**, 1386–1395.
- 25 S. André, H. Kaltner, T. Furuïke, S. I. Nishimura and H.-J. Gabius, *Bioconjug. Chem.*, 2004, **15**, 87–98.

Use of life cycle assessment to characterize the environmental impacts of polyol production options

Richard K. Helling^{*a} and David A. Russell^b

Received 10th September 2008, Accepted 16th December 2008

First published as an Advance Article on the web 21st January 2009

DOI: 10.1039/b815833a

Life cycle assessment (LCA) is a valuable tool that can be used to quantify potential environmental costs and benefits early in process research and development, allowing a company to focus development resources on products with both economic and environmental benefits.

Cradle-to-gate life cycle assessments show clear environmental benefits for flexible foam polyols made primarily from soy or castor oil compared to petrochemicals. Compared to petrochemical based polyols, the seed oil based polyols would use 33% to 64% of the fossil resources and could generate very low (−13% (*i.e.*, sequestration) to 46%) greenhouse gas emissions. The magnitude of impacts for polyols from castor oil is dominated by two key assumptions: castor farming inputs and emissions, and castor oil co-product value. The choice of farming model also has a significant impact on the gas emissions and water use for polyols from soy oil.

Introduction

The use of renewable feedstocks to make plastics is an idea with broad appeal. It offers the potential to create materials that perform many important, useful and common functions with minimal use of non-renewable resources and the environmental burdens that come from their use. But use of a renewable feedstock does not always bring such benefits, as the energy and resources required to produce the desired product can overwhelm the potential benefits. Life cycle assessment (LCA), the compilation and evaluation of the inputs, outputs, and potential environmental impacts of a product system throughout its life cycle, is a valuable tool to evaluate the potential environmental costs and benefits of new production options for chemicals and materials.

The goal of this study was to compare the sustainable chemistry attributes through a life cycle assessment under ISO standards of flexible foam polyols made through conventional petrochemical routes to a product with the same performance and mechanical characteristics but made largely from a renewable feedstock. The work was done prior to construction of the chemical production facilities for these options, as an aid for project evaluation and selection, and process and product development. The specific example is polyols for flexible foams made using Dow's RENUVA™ Renewable Resource Technology from either soy or castor oil.

A key part of LCA methodology is to define the “functional unit” of the study. It was 1 kg of unblown polymer solution, capable of being used to make a flexible polyurethane foam

identical to current petrochemical-derived materials. Three primary routes to this functional unit were compared:

- Petrochemical foam polyol solution, as described by the *PlasticsEurope* eco-profile.¹
- Foam polyol solution derived from soy oil.
- Foam polyol solution derived from Castor oil.

The solution is made by polymerizing either propylene oxide (PO) or a seed oil derivative with an initiator, made from glycerin and ethylene oxide (EO). EO is a petrochemical used in all three routes, so none of the final products is 100% bio-based, but the partially bio based products have identical mechanical properties to conventional foam.

Methodology

Life cycle assessment (LCA) is the compilation and evaluation of the inputs, outputs, and potential environmental impacts of a product system throughout its life cycle. A “cradle to grave” LCA starts with all materials extracted from nature (the earth, sea or atmosphere) and follows these through all their uses and manipulations by humans until they are returned in various forms back to nature. LCAs have been conducted for over 20 years, and the steps and procedures are well established. The four steps are goal and scope definition, inventory analysis, impact assessment, and interpretation. Life cycle inventories (LCI) include the summation of inputs and emissions, but not an impact assessment. There are ISO standards for LCA,² and many publications that describe the methodology and give examples.^{3,4} Any public disclosure of LCA results should be produced by following the ISO standards, including a sensitivity analysis for the impact of input errors on the results, and quantification of the impacts of assumptions, such as demonstrated in the work by Bernesson and co-workers.⁵

A partial LCA or LCI is the application of LCA methodology and tools to a portion of the life cycle. They are not a complete

^aThe Dow Chemical Company, Midland, Michigan, USA.
E-mail: rhelling@dow.com; Fax: +1 989-638-9674;
Tel: +1 989-638-5210

^bThe Dow Chemical Company, Horgen, Switzerland.
E-mail: DARUSSELL@dow.com; Fax: +41 1-728-2096;
Tel: +41 44-728-2855

LCA or LCI because they do not cover the whole life cycle, but are a building block for a complete LCA, and can be very useful for answering some questions. “Eco-profiles” are an example of a partial LCI that covers the “cradle to gate” inputs and emissions for a material, and can be used to create complete LCAs for downstream uses of these materials. These are typically created with great detail and extensive data. Examples include those assembled by Ian Boustead for *Plastics Europe*, which were collected by conducting surveys of multiple plants producing the same material. The surveys include all mass and energy inputs to a process, amounts and uses of water, and a complete description of air and water emissions. The data for polyol production for example was based on multiple plants in several European countries.⁶ The plants surveyed represent a European industry average.

This study used a “cradle to gate” partial LCA to compare different options for making an equivalent product. The use and disposal of the product will be the same for all the production options, so were neglected. Data for existing processes came from industry or field data, and numbers for new processes were estimated from engineering principles and analogy. The “Boustead Model v.5” software and database was used to organize the LCI information.

The level of detail done in typical published LCA is not possible during process development or other activities prior to having a commercial plant operating smoothly. There are also a variety of less quantitative or qualitative LCA approaches published. One approach is to take a high-level look, using data for economic sectors rather than individual operations.⁷ Another is to perform relative scoring of attributes of the different options.⁸ But if one has an estimate of the mass and energy inputs for a new process, one can put this information into an existing software tool for a rigorous LCA, use existing database information when it exists, and calculate the life cycle inventory (LCI) relatively quickly. This is the approach taken for this project in which we used the Boustead Model.⁹ All the calculated inventories include the total mass and energy inputs, pyramided back to material extraction from the earth. In most cases, transport of materials and intermediates was not included, except for those related to crops.

There are many possible measurements with which to compare processes, such as those from the Center for Waste Reduction Technology (CWRT) (affiliated with the American Institute of Chemical Engineers (AIChE)).¹⁰ This work used the following metrics to meet the project goals:

- Gross energy—this is the sum of all the energy used in any way and at any point in the production of the product and its raw materials, going back to material extracted from the ground. It is a well-established and often-utilized descriptor of life-cycle inventory calculations, because it can give a useful first indication of the magnitude of the total emissions or raw material use of a product. It can also be called the energy intensity of a product, expressed in the units of MJ/kg. It is a direct output of the Boustead Model (and other software systems). It is divided here into 4 categories:

- Fossil fuel energy—energy content of the various kinds of gas, oil and coal consumed as fuel to produce energy, plus the fossil energy used to produce and deliver any fuel or feedstock.

- Other fuel energy—energy produced from non-fossil sources, such as nuclear, hydro, solar, wind, and wood, plus any of these sources used to produce and deliver any fuel or feedstock.

- Fossil feedstock energy—the calorific heat (energy) of the various kinds of gas, oil and coal consumed as raw materials. This is based on the sum of the mass inputs to a process, not the heat value of the finished product.

- Biomass energy—the calorific heat (energy) of the biomass consumed as a raw material. This energy ultimately came from the sun. Farm inputs (fertilizer, tractor fuel, *etc.*) are included in the other categories.

- Raw material mass unit ratios or mass intensity—this is total mass of raw materials, organic and inorganic but excluding water, used for purposes other than energy, at any point in the production of the product and its raw materials, going back to material extracted from the ground (or ocean). It is expressed as kg per functional unit (typically kg of product). The Boustead model also includes the mass of hydrocarbons used as fuel, but since this is not a mass that is traditionally included in Dow as part of a mass balance, it was removed from the mass unit ratio. This required a simple calculation using the output from the Boustead Model.

- Water mass intensity—this is the total mass of supplied water throughout the upstream supply chain, but does not include rainwater taken up by crops. It is divided into two portions—process and irrigation water, which normally needs to be of potable quality, and cooling water, which may sometimes be seawater or other non-potable sources.

- Air emissions: 100-year CO₂ equivalents, SO_x calculated as SO₂, and NO_x calculated as NO₂—these are sums of all the calculated emissions for both energy use and chemical production, used at any point in the production of the product and its raw materials, going back to material extracted from the ground. These are dominated by production of the gases during energy production, which vary primarily by the source of electricity and heat, and also by emissions from farms. Combustion of biomass is modeled as zero net CO₂ emissions, since the natural cycle of plants is to take CO₂ from the atmosphere during growth and life, and to return it there, *via* decay, on death. These are direct outputs of the Boustead Model. CO₂ emissions are a global issue; SO_x and NO_x are regional issues.

Calculations of water pollutants or solid wastes are not presented here, although they are available from the Boustead Model. The importance of these terms depends in large part on the specific sites chosen for crop and chemical production, so that their importance cannot be determined early in process development, before sites are selected. Also, there are not good data available for these terms for either castor agriculture or its chemical conversion.

The primary source of data for soybean cultivation and processing were taken from NREL (National Renewable Energy Laboratory) bio-diesel study¹¹ (use of another data source is described later). Dow plant design information and vendor quotes were used for the process to make polyol (methanolysis, hydroformylation and polymerization). Boustead model data were used for fertilizers, methanol, steam, air and electricity. Dow internal eco-profiles were used for herbicides, insecticides,

EO (from ethylene), CO and H₂ (from steam reforming of natural gas). The LCA inputs for these two routes are shown in Figs. 1 and 2.

Castor cultivation information was taken from a COI (Castor Oil, Inc.) cost model for north Texas cultivation.¹² It was based in part from COI's experience with castor farming, and in part by analogy with soy farming. COI expects castor farm inputs per acre to be very similar to that for soy, with the addition of nitrogen-containing fertilizer (at 80 lbs nitrogen per acre). COI also anticipates using cold pressing to recover most of the oil, leaving some behind with the meats and hulls to make a higher-valued organic fertilizer. No solvent would be used in this process. This is the "base case" for castor. Energy and water inputs were estimated using engineering principles. The chemical

process to make polyols includes methanolysis, hydrogenation and polymerization. This route has not yet been demonstrated on any scale; the mass and energy inputs for this process were estimated by engineering principles. Boustead model data were used for urea, methanol, nickel, steam, air and electricity. Dow internal eco-profiles were used for ammonium phosphate, herbicides, EO (from ethylene) and H₂ (from steam reforming of natural gas). The LCA inputs for castor polyol are shown in Fig. 3.

In addition to the COI estimates of castor farming inputs, there is also a published analysis of energy and mass inputs for dry land castor farming in India.¹³ The land used in the US and India for growing castor or soybeans is assumed to be covered with native grasses in the other scenarios, so that the land is

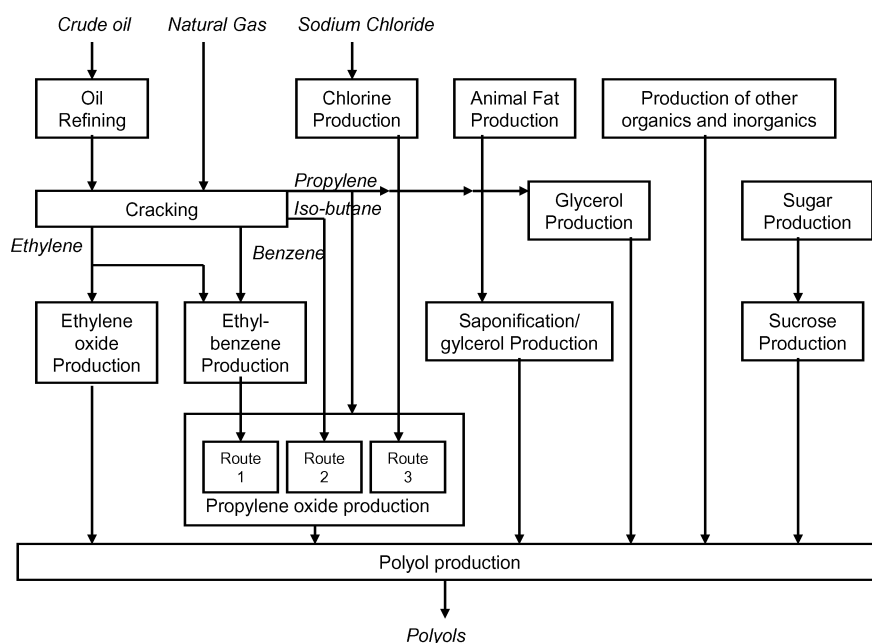


Fig. 1 Inputs to petrochemical polyol production.⁶

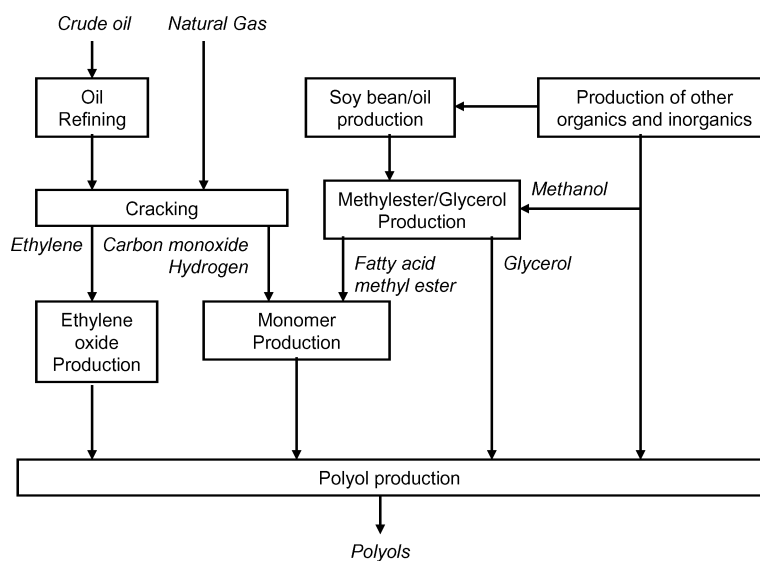


Fig. 2 Inputs to soy polyol production.

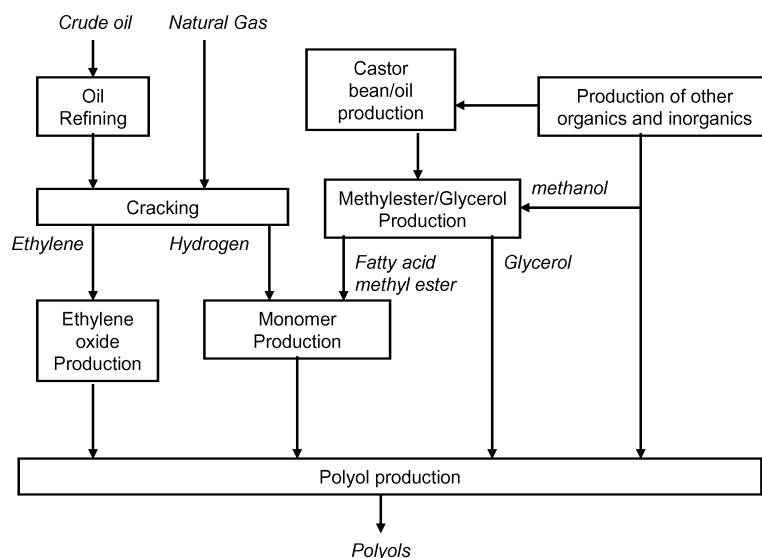


Fig. 3 Inputs for for castor polyol production.

in all cases participating in the natural carbon cycle, but has no inputs unless it is being farmed. The natural carbon flux is assumed to be the same for grasses and crops, so there is no change in biogenic carbon inventories (soil, plant matter) except for the carbon from the plants that ends up in the polyols. As a practical simplification, land and biodiversity were not included as specific resources in this work. Nevertheless, while the use of land for materials is an order of magnitude smaller than land used for fuels,¹⁴ there are current debates on “food vs. fuels” and on biodiversity loss through land use change that suggest these as useful additions to further work in this field.

The COI and Indian information on castor farming does not include emissions generated by farming activities, but do include quantified inputs, such as tractor fuel, pump power, and fertilizer. Emissions for all these activities are readily available, for both Texas and India, in the Boustead Model.

Nitrous oxide (N_2O) is a powerful greenhouse gas—298 times that of CO_2 on a mass basis with a 100-year time horizon. It can also be a significant emission from agriculture, from the natural decomposition of plant nitrogen in roots and crop residues and from decomposition of nitrogen-containing fertilizers. The Intergovernmental Panel on Climate Change (IPCC) has defined models for estimating N_2O emissions from farm and field activities that are widely used.¹⁵ Their models were used to calculate the N_2O emissions from castor farming, based on both the COI and Indian data for fertilizer inputs, and by assuming a ratio of crop to residue of 4.5,¹⁶ and a nitrogen content of the residue of 1.6% (on an 85% dry matter basis), an estimate based on data from a broad range of crops.

The inputs and emissions for crop production must be assigned or allocated to the useful products from that crop as part of the LCA process. There are many ways and much debate in the literature on how to do this allocation, such as by mass proportion or economic value proportion. This study uses a mass allocation, since this can be directly calculated from a simple mass balance, and is also reasonable for co-products of similar value. The “base case” for castor production assigns no value or inputs to roots, stems, leaves, or stalks (these will all

return to CO_2 by natural decay or burning), and allocates the inputs equally to the fertilizer product (hulls, meats and some oil) and oil, with no other, non-valued, byproduct. An input of X units of something *per kg of beans* will thus produce fertilizer with an allocated input of X units per kg of fertilizer and also oil with an allocated input of X units per kg of oil. Both fertilizer and castor oil are assumed to be useful, similar to the situation for soybeans, where meal and oil are the co-products. The use of cold-press castor meal and hulls as a higher-value organic fertilizer is the subject of current work by Castor Oil, Inc, and the USDA. It may also be possible to use the meal and hulls in other applications, such as adhesives. The impact of other allocations (seeds produce useful oil and meal and not useful hulls; seeds produce useful oil, but not useful meal and hulls) is discussed later.

As mentioned earlier, the functional unit was 1 kg of unblown polymer solution, capable of being used to make a flexible polyurethane foam functionally identical to current petrochemical-derived materials. Production of this functional unit from castor or soy also makes meal or fertilizer and glycerin as co-products, and these share the inputs and burdens as explained above (“allocation”).

Results and discussion

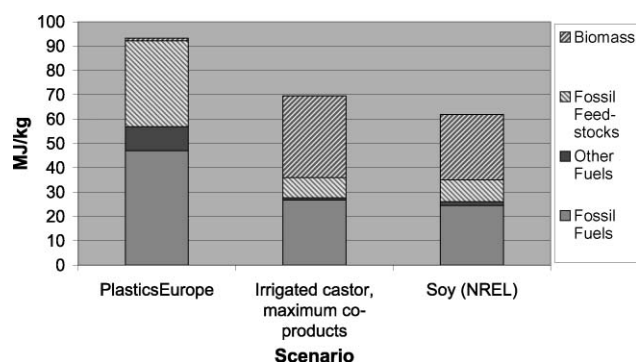
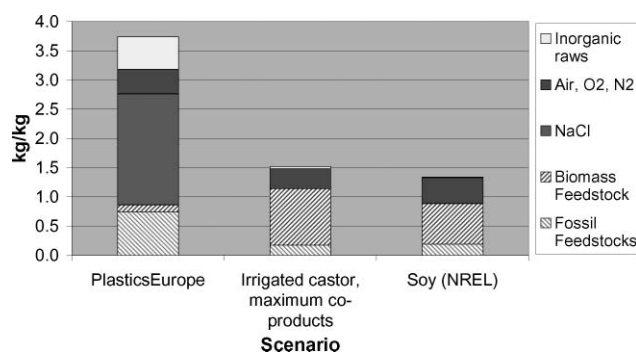
The results from several scenarios for polyol production are described in the following sections. A list of the scenarios is shown in Table 1.

The three basic routes

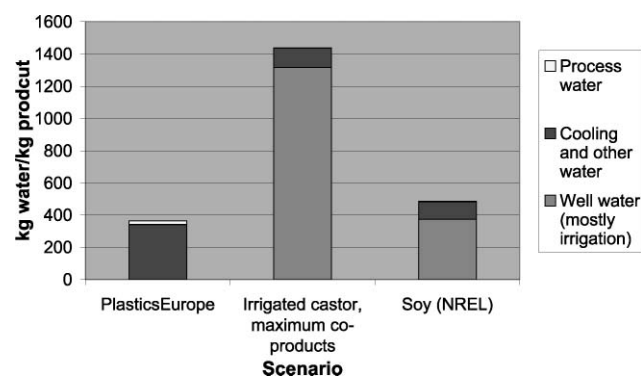
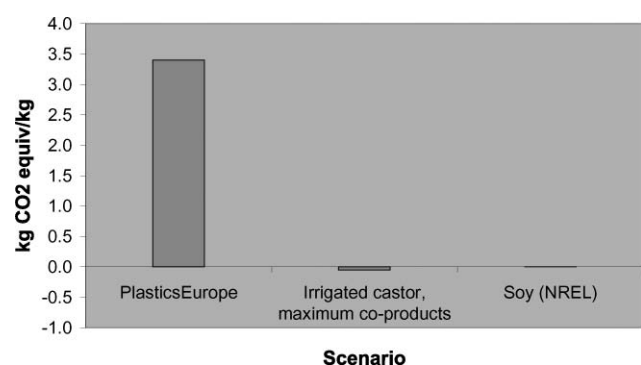
Figs. 4 to 8 present the calculated life cycle inventories (energy, mass and water) and impacts (greenhouse gas and acid gas emissions) for the three compared routes to make a functionally identical polymer solution for flexible foam polyurethanes as described in Table 1: *PlasticsEurope*, soy (NREL) and irrigated castor with fertilizer coproduct.

Table 1 Polyol LCA scenarios evaluated

Scenario name	Rationale	Key attributes
PlasticsEurope Soy (NREL) Irrigated castor, maximum co-products	Reference case for petrochemical polyols Base case for soy-based polyols Base case for castor-based polyols (lowest burden on castor oil)	Uses NREL model for US soy farming Castor oil has a valuable fertilizer co-product (includes hulls); farming based on limited information for north Texas
Soy (NIST) Irrigated castor, no co-products	Quantify impact of using alternative farming model Quantify impact of alternative co-product assumption	Uses NIST model for US soy farming Castor co-products have no value; oil carries maximum burden. Farming model based on limited information for north Texas
Irrigated castor, partial co-products	Quantify impact of alternative co-product assumption	Castor meal co-product has value, but hulls do not; oil carries an intermediate burden
Dryland India castor, no co-products	Quantify impact of castor farming and supply region (vs. the irrigated castor w/o co-product scenario)	Farming based on published data for current practices in a major castor supply region.
US average castor, no co-products	Quantify impact of castor farming and supply region (vs. the irrigated castor w/o co-product scenario)	Farming based on expectations for inputs required in areas of US with less required irrigation, <i>i.e.</i> NREL soy inputs per acre

**Fig. 4** Gross energy intensity for three polyol options.**Fig. 5** Raw material unit ratios for three polyol options.

The partial life cycle calculations demonstrate some of the significant potential benefits for bio-based polyols. Both seed oil polyols have lower gross energy (including biomass) than the European average. More importantly, polyols made from soy used only 41% of the fossil resources compared to the European average, and polyols from castor used only 43%. Use of either seed oil would decrease the use of fossil resources. For this cradle-to-gate study (which excludes the use and disposal of the polyol) there were essentially zero net greenhouse gas emissions for polyol made from either oil. The seed oil polyols also have a reduced regional air impact, with 32% and 37% of the SO_x and NO_x emitted from the soy route compared to the European average, and 28% and 32% for castor.

**Fig. 6** Water intensity for three polyol options.**Fig. 7** Greenhouse gas emissions for three polyol options.

Seed-oil polyols decouple polyol production from chlorine-based chemistry, as shown in Fig. 5 by the lack of NaCl as a raw material unit ratio compared to the European average. Although chlorine can be safely used in industrial processes, its use requires a relatively large capital infrastructure, and may create unwanted chlorinated organic by-products that can be expensive to destroy. If one faces capacity limits in chlorine supply or chlorinated organic destruction, then non-chlorine chemistries can be more economical.

Water use for seed oil polyols is 134% (soy) to 396% (castor) of the European average. Most of the increase is due to water

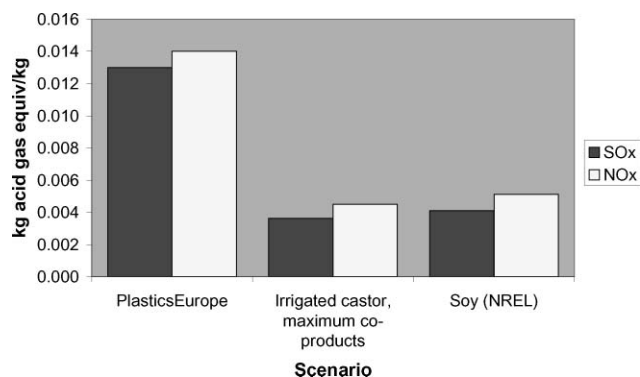


Fig. 8 Acid gas emissions for three polyol options.

used in irrigation. It is possibly not of the same source type and quality as the water used in the chemical production plant.

Quantitative impact of soy farming assumptions

An additional source of information on soy cultivation was available but not selected as the base case for this study of soy polyol LCA,¹⁷ and is the Soy (NIST) scenario defined in Table 1. The data were also used by Omni Tech International in a life cycle comparison of soy polyols.¹⁸ The NIST description of soybean cultivation has a lower primary energy input per kg of soybeans than NREL's analysis (2.16 vs. 3.14 MJ/kg), but much higher field emissions of N₂O (3.9 g/kg vs. 0). NREL felt that the N₂O emissions data for soybeans were too widely variable to know the "true" value, and were likely not distinguishable from fallow land. NIST was based on the IPCC methods to estimate N₂O emissions from soy fields. The NIST data also differed from the NREL approach in how to assign the CO₂ uptake from air. NREL does this based on the carbon content of the oil used, and does not take credit for CO₂ used in roots, stalks, stems, and meal. NREL assumed that biomass used in food, crop residue and fuel are merely different pathways for the same net-zero CO₂ flux between plants and air. It also carries an implicit assumption that land not used for soy agriculture would be used to grow biomass of some sort, with a similar carbon flux. The NIST data assigned CO₂ uptake during plant growth, and also during use of the oil in the polyol. This overstates the biomass CO₂ in the polyol compared to the NREL approach.

We used the NREL model as the base case for soy farming because it is well-documented, with complete documentation of their assumptions and methods, so is a more "transparent" set of data to use. But the choice of soy farming model has a significant impact on the soy polyol LCA, especially the greenhouse gasses, as shown in Fig. 9. The NREL model used much more irrigation water, but produced much less N₂O so had less greenhouse gas emissions. The other metrics for the polyols based on the two farming models are very similar.

The NIST data does not clearly define the method use to calculate the "cradle to gate" LCI data or methods for delivered fuels and power, nor the manufacturing process used to convert the soy oil into polyol and calculates a gross energy of 12 MJ/kg for a soy polyol, of which 11.4 was for non-renewable energy inputs and 0.5 MJ/kg for fossil feedstocks. This is much lower than the soy case calculated here, which had (excluding biomass energy) 34.74MJ/kg gross energy, of which 24.4 MJ/kg were

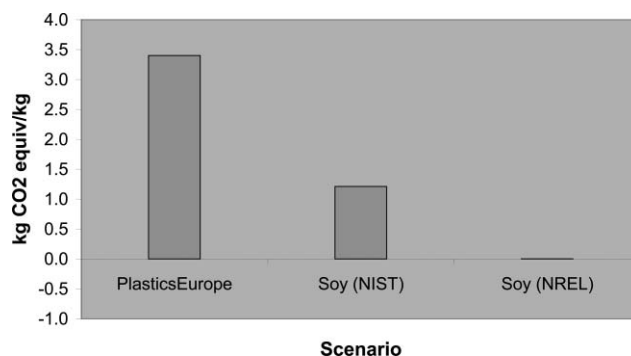


Fig. 9 Impact of soy farming model on greenhouse gas emissions of polyols.

for fuel use, production and transport and 8.9 MJ/kg was for fossil feedstocks. The first key difference is that the soy polyol in this study included ethylene oxide (EO) as part of the polymer and the NIST polyol does not. EO contributes 8.6 MJ/kg of feedstock energy and 5.4 MJ/kg of other fossil and non-fossil energy to the Dow polyol. The next key difference is that the current study's polyol includes hydroformylation as a chemical process step, and the synthesis gas used for this adds another 6.6 MJ/kg. The NIST polyol does not appear to include this step or these materials. Subtracting these raw materials from the current polyol, and increasing the unit ratio of soy oil to polymer in the Dow material from 0.678 to 1.0, produces a same-basis estimate of soy polyol gross energy of 15.4 MJ/kg. This is 28% higher than the NIST calculation, which is due to their lower estimate of soy farm inputs. The polymer NIST modeled (100% soy based) is intended for carpet backing. The current LCA is a comparison of directly equivalent materials for flexible foams, so cannot be compared with the Omni Tech work.

Quantitative impact of castor co-product assumptions

An essential feature of LCAs conducted according to ISO standards is consideration of the impact of key assumptions on the results. The impact of soy farming model was discussed above, and since soy produces two clearly valuable products (oil and protein-rich meal), there is clear need to include them both, as has been done. The results described above were also based on several key assumptions about castor co-products and their value and also castor farm inputs.

The "base case" assumed all non-oil parts of the seed are useful as an organic fertilizer and thus share equally the per kg burdens from farming and seed processing. This assumption was made as it would increase the revenue stream to the farmer and would make castor a more likely commodity crop in the future. But it is not the case today. Currently, only the oil has significant value—the meal and hulls do not (allergens in the meal and toxic ricin in the hulls hamper the use of these materials, especially as feed, although these can be detoxified by steam). The impact of this assumption is explored in the following graphs, Figs. 10 and 11. These are similar to the ones above, and for reference include the three bars shown in the previous graphs: the *PlasticsEurope* data on the far left, soy (NREL) polyol on the far right, and the base-case castor scenario (irrigated farms in north Texas, where the fertilizer co-product includes hulls), in the column adjacent to the soy data. The two added bars are polyols made

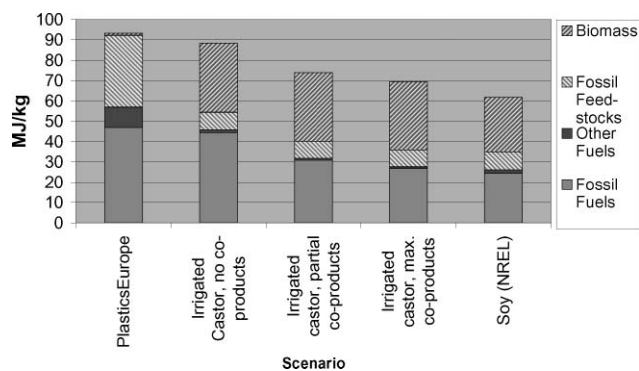


Fig. 10 Impact of co-products on gross energy.

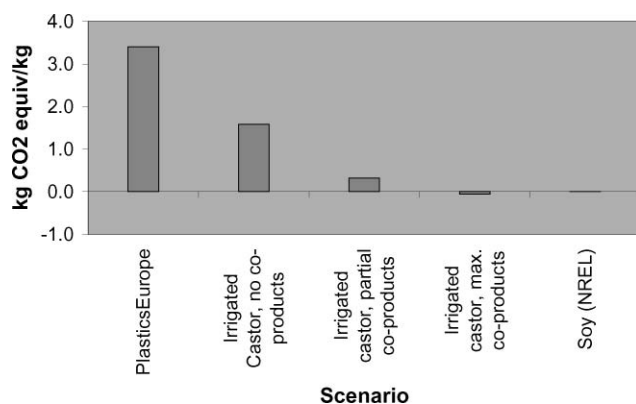


Fig. 11 Impact of co-products on greenhouse gasses.

from castor from irrigated north Texas farms, but where the useful (steamed) meal co-product does *not* contain the hulls (the center column), and the scenario using irrigated north Texas castor with *no* byproduct value (the column adjacent to the *PlasticsEurope* column). This last scenario is the closest to the situation today. The two added scenarios increase the proportion of the farm and processing inputs from 1.0 in the base case to 1.33 in the case without hulls and 2.22 in the case without meal. They also use the current hexane extraction process to recover the castor oil and steam in the meal co-product case to detoxify it. The inputs and emissions were estimated using engineering principles from a published flowsheet.¹⁹

For all the metrics, the case with partial co-products (meal but without hulls) yielded results between the base case of maximum co-products (fertilizer including hulls) and the case with no useful by-product, so the following discussion will describe the results going from the one extreme (all products useful—oil and fertilizer) to the other (no useful by-products). The gross energy of the castor polyol increased from 75% to 95% of the *PlasticsEurope* European average, with the fossil resource use increasing from 43% to 64%. Water use increased from 396% to 840%. Greenhouse gas emissions increased from -2% to 47% of the average. Acid gases increased from 28% to 44% for SO_x and from 32% to 52% for NO_x . These are all significant impacts. In all cases, the inputs to the farm per acre planted and many of the factory inputs per mass of seeds are unchanged (there are differences for co-product processing), so the total burden to the environment is nearly the same. The major change is in the sharing of those burdens ranging from complete (base case)

to none (no meal—the oil carries it all). The work also shows the inherent benefit to producing useful products rather than waste streams—one gets more benefit for a given quantity of environmental burden.

Quantitative impact of castor farming assumptions

The other key assumption was the model for castor farming. Castor is not yet a mature commercial crop in the US, unlike soybeans or corn. Comprehensive field data do not exist for castor farming. A new reference case for this analysis used farming inputs from Castor Oil, Inc., but with *no* useful co-products. This is a different reference case for the castor polyol than the one used previously, which did include useful co-products, and was chosen to more clearly show the impact of the farming assumptions. The impact of the farming assumption is explored in the following graphs, Figs. 12 and 13. These are similar to the ones above, and for reference include the three columns from previous graphs: the *PlasticsEurope* data on the far left, soy (NREL) polyol on the far right, and the new reference case castor scenario (irrigated farms in north Texas, where the meal and hulls are *NOT* useful products), in the column adjacent to the *PlasticsEurope* data. The two added bars are: polyols made from castor from dryland Indian (Andhra Pradesh) farms, including transport to US Gulf Coast (the center column); and US farming, assuming the same farm inputs per acre as per NREL's soy data (the center-right column) but with the yield of seed per acre being that of castor rather than soy (castor seed has about twice the mass yield per acre as soy beans) This scenario is meant as a "best guess" for possible

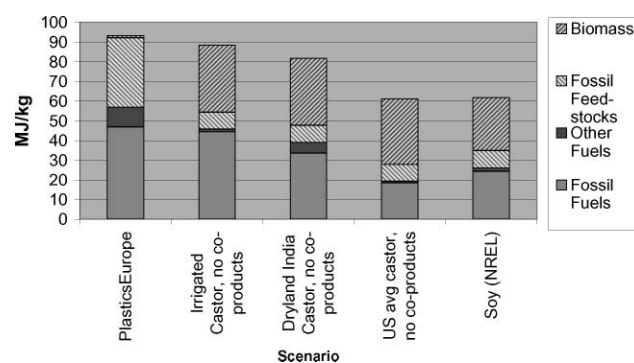


Fig. 12 Impact of castor farming model on gross energy intensity.

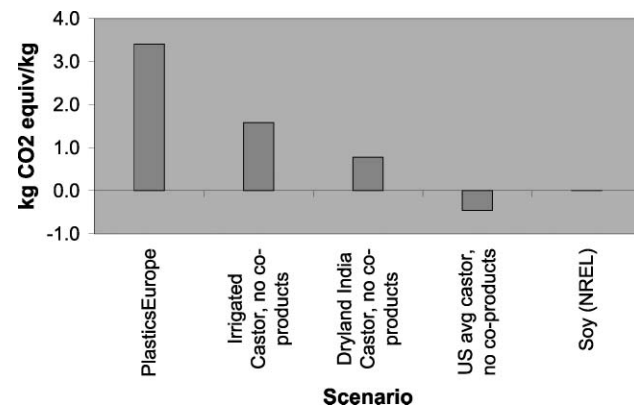


Fig. 13 Impact of castor farming model on greenhouse gas intensity.

Table 2 Sensitivity of key metrics to $\pm 20\%$ variations in largest inputs

Input variable	Gross energy	Fossil use	GHG reduction	Inorganic waste	Water use
Electricity use in oil plant	1.1%	1.5%	1.4%	0.0%	0.0%
Ethylene oxide production	4.5%	8.8%	3.8%	10.3%	1.1%
Yield (grow, harvest soy)	0.7%	1.3%	0.9%	1.3%	15.4%
Natural gas use in oil plant	0.6%	1.1%	0.8%	0.0%	0.0%
Carbon monoxide prod'n	1.9%	3.2%	1.3%	7.4%	0.0%

Table 3 Impact of farm model assumption on key sensitivity metrics

Input variable	Gross energy	Fossil use	GHG reduction	Inorganic waste	Water use
Farming model (NIST)	-4.3%	-3.6%	45.2%	39.7%	-70.2%

castor farming in other, less irrigated (more natural rainfall), sections of the country.

These graphs clearly show that the choice of farm model is of tremendous importance. The magnitude of the possible benefits for polyols from castor depends on the success and system of farming. Fossil resource use ranges from 33% to 64% of the *PlasticsEurope* European average data, greenhouse gas emissions range from -13% to 47%, acid gas emissions range from 33% to 52%, and water use ranges from 35% to 840% higher. The assumption about farm inputs changes many impacts by more than two-fold. The impact of the farm model impact is less, but still significant, if co-products are assumed to be useful.

The farming system in India is much different than that of the US, primarily as it is dryland farming. Two tractor passes were done on the fields (first plough, then harrow plus sow), but harvesting and other work was done by hand or animals (the human and animal input was modeled as a biomass energy input (this assumes they are 100% efficient vegetarians), but only for the work performed, and not other living). The yield was about half that expected in the US. Even though the Indian data had lower mass and energy inputs per acre than the US, the lower yield led to very comparable product gross energy and higher mass inputs on a per-mass-polyol basis.

The major difference between the north Texas and US (*i.e.*, soy) models for castor farming is the energy required for irrigation. The total energy input to US soy farming is ~ 3 MJ/kg-bean, but for north Texas castor it is about 13.3 MJ/kg-seed, of which 9.4 MJ/kg is the pumping energy for irrigation. This is a very large burden, which makes farming in other regions—if it can be done with the same inputs as soy beans—much more beneficial. Other possible impacts, such as CO₂ sequestration or biodiversity, for converting non-farm land into farmland were not included in this analysis. It was assumed that unused land was supporting native grasses and thus participates in the natural carbon cycle.

Sensitivity analysis for major energy inputs to soy polyol

A key aspect of an LCA done to ISO standards is a sensitivity analysis for the impact of variations in the input parameters on the calculated results. The parameters selected for this analysis were determined by using the Boustead Model to calculate the contribution of the different inputs to the gross energy of polyol

made from soy oil (NREL farming model). The top five inputs, and their contribution as a percentage of the total gross energy, were:

- Electricity use in oil plant—24%
- EO production—23%
- Grow and harvest soy beans—15%
- Natural gas use in oil plant—12%
- Carbon monoxide production—9%

These five inputs accounted for 85% of the gross energy of the soy polyol. Each of these inputs was individually varied by $\pm 20\%$, the results recalculated, and tabulated as a percentage change from the base case for five key metrics: gross energy, fossil resource use, reduction in greenhouse gas emissions, total inorganic raw materials used, total water used. The impact on the metrics and calculations other than those listed was typically $< 5\%$ (Table 2).

The usually small impact of the $\pm 20\%$ input changes shows the robustness of the results to errors in details of process knowledge. The sensitivity results can also be put into perspective by doing a similar calculation for the impact of the soy farm model assumption (Table 3).

These results confirm the much larger impact of the co-product and farm input assumptions on the LCA results than variations in input parameters.

Sensitivity analysis for major energy inputs to castor polyol

A similar analysis was done for the polyols from castor oil. The parameters selected for this analysis were determined by using the Boustead Model to calculate the contribution of the different inputs to the gross energy of polyol made from irrigated north Texas castor, with fertilizer as the useful co-product. The top five inputs, and their contribution as a percentage of the total gross energy, were:

- Natural gas (Texas (ERCOT) source and production data) used for irrigation pumps—41.0%
- Ethylene oxide production—18.8%
- Fertilizers (both ammonium phosphate and urea)—13.9%
- Electricity (Texas (ERCOT) grid average) used in seed and oil processing—14.1%
- Steam used for energy in the polyol plant—6.1%

These five inputs accounted for 94% of the gross energy of the castor polyol. Each of these inputs was individually varied by $\pm 20\%$, the results recalculated, and tabulated as a percentage

Table 4 Sensitivity of key metrics to $\pm 20\%$ variations in largest inputs

Input variable	Gross energy	Fossil use	GHG reduction	Inorganic waste	Water use
Crop yield	3.8%	6.7%	9.9%	9.0%	17.1%
Irrigation energy (nat'l gas)	2.7%	4.8%	5.3%	0.0%	0.0%
EO mass in polymer	3.3%	6.1%	4.2%	10.9%	0.3%
Fertilizer use	1.0%	1.4%	1.5%	9.0%	0.0%
Elect. in seed oil prod'n	0.8%	1.3%	1.7%	0.0%	0.0%
Steam use polymer plant	1.7%	2.8%	3.3%	0.0%	0.0%

Table 5 Impact of assumptions on key sensitivity metrics

Input variable	Gross energy	Fossil use	GHG reduction	Inorganic waste	Water use
No useful co-products	27.1%	51.3%	47.3%	121%	112%
"Best" farm (soy inputs, castor output)	-4.3%	-3.6%	45.2%	39.7%	-70.2%

change from the base case for five key metrics: gross energy, fossil resource use, reduction in greenhouse gas emissions, total inorganic raw materials used, total water used. The crop yield was also varied by 20% around a base of 845 kg oil per acre (4638 kg seeds/hectare). These calculations are summarized in the table below. The impact on the metrics and calculations other than those listed was typically $<5\%$ (Table 4).

The usually small impact of the $\pm 20\%$ input changes shows the robustness of the results to errors in details of process knowledge. The sensitivity results can also be put into perspective by doing a similar calculation for the impact of the assumptions described earlier using a series of graphs. The table below shows the absolute value of the changes. The first line compares polyols from Texas irrigated castor with no useful products to that from the castor co-produced in Texas with fertilizer. The second line compares the best farm model (soy inputs) to the worst (irrigated Texas), both with no co-products (Table 5).

These results again confirm the much larger impact of the co-product and farm input assumptions on the LCA results than variations in input parameters.

Data gaps

Discussion of data gaps is an essential element of LCA. The most significant gaps here are related to castor farming, since castor is a small crop compared to soy, and there have not been extensive LCA studies of castor farming. Neither of the two descriptions of castor farming—north Texas or India—contained information on air or water emissions, other than those generated by farm equipment. N_2O gas emissions were estimated using a widely-used method, but was not based on data specifically for castor. Contaminants in the farm run-off have been important in other studies of agricultural systems. Data on emissions may also need to be compared to those for the likely land use if it is not used for farming. The primary source of castor farm inputs (from Castor Oil, Inc.) is also an estimate rather than historical data from fields. Since fertilizer and irrigation input are important to the LCA, more specific data would provide an improved assessment of castor-based polyols. Finally, the usefulness of castor meals and hulls needs to be understood better. The use of these as a higher-value organic

fertilizer is the subject of current work by Castor Oil, Inc, and the USDA. It may also be possible to use the meal and hulls in other applications, such as adhesives. If castor production expands and more is used in chemical products, then data from this expansion would be important in any future assessments of castor-based products.

For both the soy and castor polyols, the data for bio-based polyol manufacturing inputs were based on less-than-kilogram-scale lab work for castor and pilot plant work for soy. LCA are typically based on surveys of multiple production plants. Data from a larger scale could be different and yield different results than the research-scale inputs used in this study.

Conclusions

Life cycle assessment (LCA) is a valuable tool that can be used to quantify potential environmental costs and benefits early in process research and development, allowing a company to focus development resources on products with both economic and environmental benefits. Cradle-to-gate life cycle assessments show clear environmental benefits for flexible foam polyols made primarily from soy or castor oil compared to petrochemicals. Compared to petrochemical based polyols, the seed oil based polyols would use 33% to 64% of the fossil resources and could generate very low (-13% (*i.e.*, sequestration) to 46%) greenhouse gas emissions. The magnitude of impacts for polyols from castor oil is dominated by two key assumptions: castor farming inputs and emissions, and castor oil co-product value. The choice of farming model also has a significant impact on the gas emissions and water use for polyols from soy oil.

Acknowledgements

We are thankful for the support of the United States Department of Energy for partial funding of this work (DOE contract DE-FC36-01ID14213 "Development of Improved Chemicals and Plastics from Oilseeds"). We appreciate the thorough and helpful critical review of this work provided by Prof. David Shonnard of Michigan Technological University. We also thank Rick Graves

of Castor Oil Inc. (Plainview, Texas) for information about potential castor farming in the US.

References

- 1 Ian Boustead, Eco-profiles of the European Plastics Industry: Polyols, March, 2005 (available from <http://lca.plasticseurope.org/index.htm>).
- 2 International Organization for Standardization, ISO 14040: 1997(E), Environmental management—Life Cycle Assessment—Principles and Framework, Geneva, 1997.
- 3 Mary Ann Curran, *Environmental Life Cycle Assessment*, ISBN 0-07-015063-X, McGraw-Hill, 1996.
- 4 <http://www.epa.gov/ord/NRMRL/lcaccess/resources.html>.
- 5 Sven Bernesson, Dan Nilsson, Per-Anders Hansson, A limited LCA comparing large and small scale production of rape methyl ester (RME) under Swedish conditions, *Biomass and Bioenergy*, vol 26, pp. 545–559, 2004.
- 6 Ian Boustead, Polyols, as reported at www.apme.org, “information produced in collaboration with ISOPA—The European Isocyanate Producers Association”, August 13, 2003.
- 7 A. Horvath, C. Hendrickson, S. Joshi and L. Lave, Economic Input Output Models for Environmental Life-Cycle Assessment, *Environmental Science and Technology*, A-pages, **32**(7), 184A–191A, 1998.
- 8 T. E. Graedel, *Streamlined Life-Cycle Assessment*, Prentice Hall, New Jersey, 1998.
- 9 W. T. Dove, Life cycle assessment: an argument for a detailed approach, *Proceedings of the LCM 2005 Innovation by Life Cycle Management International Conference*, Barcelona, Spain 5th–7th September 2005, pub. LCM, volume 2, pp. 481–484.
- 10 Jeanette Schwarz, Beth Beloff and Earl Beaver, Use Sustainability Metrics to Guide Decision-Making, *Chemical Engineering Progress*, pp. 58–62, July 2002.
- 11 Life Cycle Inventory of Biodiesel and Petroleum Diesel for Use in an Urban Bus: A joint study sponsored by: US Department of Agriculture and US Department of Energy, NREL/SR-580–24089 UC Category 1503, National Renewable Energy Laboratory, Final report, May, 1998.
- 12 Rick Graves, castor input cost spreadsheet.xls, Castor Oil, Inc., Plainview, Texas, received via e-mail, 14 January 2004.
- 13 J. P. Mittal, K. C. Dhawan and C. R. Thyagraj, Energy scenario of castor crop under dryland agriculture of Andhra Pradesh, *Energy Convers*, vol. 32, no. 5, pp. 425–430, 1991.
- 14 W. F. Banholzer, K. J. Watson and M. E. Jones, How Might Biofuels Impact the Chemical Industry?, *Chemical Engineering Progress*, vol. 104, no. 3, p. s7, 2008.
- 15 IPCC, IPCC Good Practice Guidance and Uncertainty Management in National Greenhouse Gas Inventories, Chapter 4, Agriculture (2001) as found at <http://www.ipcc-nggip.iges.or.jp/public/gp/english/>.
- 16 Rick Graves, Castor Oil Incorporated, Plainview, Texas, telephone conversation, 6 December 2004.
- 17 Obtained from Barbara Lippiatt, NIST (U.S. National Institute of Standards & Technology), 14 April 2004.
- 18 J. Pollack, Soy vs. Petro Polyols, A Life Cycle Comparison, *GPEC 2004 Paper Abstract 37*, Omni Tech International, Inc., Midland, MI, 2004.
- 19 E. A. Weiss, Oilseed processing, in *Castor, Sesame and Safflower*, pp. 761–793, 1971; available at http://www.wsu.edu/~gmhyde/433_web_pages/433Oil-web-pages/castor/castor-oil2.html via the Jayant Oil Mills web page.

Kinetic model for the hydrolysis of lignocellulosic biomass in the ionic liquid, 1-ethyl-3-methyl-imidazolium chloride†

Laurent Vanoye,^a Markus Faselow,^a John D. Holbrey,^a Martin P. Atkins^b and Kenneth R. Seddon^a

Received 13th October 2008, Accepted 19th December 2008

First published as an Advance Article on the web 21st January 2009

DOI: 10.1039/b817882h

The kinetics of the acid-catalysed hydrolysis of cellobiose in the ionic liquid 1-ethyl-3-methylimidazolium chloride, [C₂mim]Cl, was studied as a model for general lignocellulosic biomass hydrolysis in ionic liquid systems. The results show that the rate of the two competing reactions, polysaccharide hydrolysis and sugar decomposition, vary with acid strength, and that for acids with an aqueous pK_a below approximately zero, the hydrolysis reaction is significantly faster than the degradation of glucose, thus allowing hydrolysis to be performed with a high selectivity in glucose. In tests with soluble cellulose, hemicellulose (xylan), and lignocellulosic biomass (*Miscanthus* grass), comparable hydrolysis rates were observed with bond scission occurring randomly along the biopolymer chains, in contrast to end-group hydrolysis observed with aqueous acids.

Lignocellulosic biomass is an important chemical resource;^{1,2} a great deal of research has been directed at discovering ways to effectively utilise biomass both as source of value-added chemicals,¹ and as source of liquid biofuels.²

The three major components of lignocellulosic biomass are cellulose, hemicellulose and lignin. Cellulose and hemicellulose, are polymers of simple carbohydrates. Cellulose, formed from linear chains β(1→4) linked D-glucose units, is the primary structural component of plant cell walls and is a water-insoluble polymer, characterised by its chemical stability. Hemicelluloses, in contrast, contain a variety of sugar monomers (mainly xylose) and can incorporate both branched and linear chains. Hemicelluloses tend to have little structural strength and are readily hydrolysable by acids in aqueous solution. Lignins are highly crosslinked polymeric aromatic materials that compose the secondary structure of woody biomass.³ Lignins are formed from predominantly aromatic alcohols, *i.e.* from reduced forms of carbohydrates, and when removed from biomass, as for example during the Kraft process for pulp and paper manufacture, are often burned as a direct fuel source.

In combination, cellulose and hemicelluloses are the principle carbohydrate components of biomass and the most abundant renewable carbon resources (The worldwide raw biomass energy potential has been estimated to be between 3.4 and 10.2 Gtoe);⁴ however, challenges remain in successfully abstracting simple, and defined, chemical building blocks from the natural complexity of the biomass.

First generation bioethanol production from fermentable sugars is a well developed process with in excess of 4 × 10¹⁰ l produced worldwide in 2004.⁵ Nevertheless, competition with food production and a concomitant increase in crops prices are serious limiting factors for their use and so the development of second generation bioethanol from lignocellulosic biomass (which can be produced from crops on marginal land) is the objective of considerable current research.⁴

The first studies to understand biomass hydrolysis in water and the digestion of biomass were initiated by Saeman in 1945,⁶ and reported by many others since then.⁷ The hydrolysis of cellulose can be described as a *pseudo*-first-order homogeneous sequential reaction followed by degradation of glucose, as shown in Fig. 1. However, as this is a solid-liquid reaction, no model can reliably predict the behaviour of each source of cellulose and its physical changes during the course of the experiment. Moreover, only few of the numerous products of acid degradation of glucose have been adequately characterised (mainly 5-(hydroxymethyl)furfural (5-hmf), 4-oxopentanoic acid and methanoic acid). Most of them are reported as humin (humic substances).

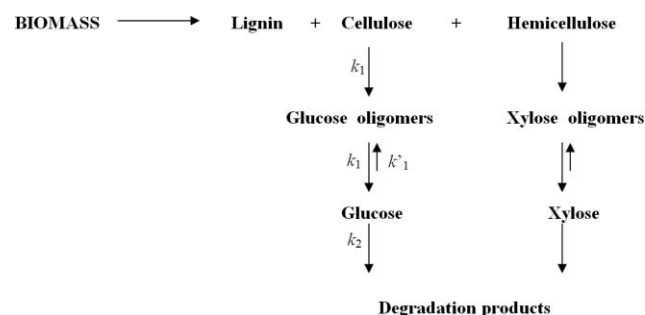


Fig. 1 Proposed mechanism for biomass digestion.⁶

^aQUILL Research Centre, School of Chemistry and Chemical Engineering, The Queen's University of Belfast, David Keir Building, Stranmillis Road, Belfast, UK BT9 5AG. E-mail: quill@qub.ac.uk

^bBP, 457 Zhongshan Road, Dalian Institute of Chemical Physics (DICP), Dalian, 116023, P.R. China

† Electronic supplementary information (ESI) available: Data calculations and HPLC chromatograms. See DOI: 10.1039/b817882h

Recent work has shown that some ionic liquids, such as 1-butyl-3-methylimidazolium chloride [C₄mim]Cl, are exceptional solvents for cellulose.^{8,9} Swatloski *et al.*⁸ demonstrated that refined and pure natural celluloses could all be readily dissolved to high concentrations in these ionic liquids and, more recently, it has been reported that even untreated biomass sources such as wood can be, at least partially dissolved or swollen in ionic liquids.^{10–13} This approach has been used successfully to prepare swollen amorphous regenerated celluloses that can be converted to glucose through enzymatic hydrolysis more readily than the native forms.¹⁴ Moreover, it has been shown that ionic liquids are suitable solvents for the acidic hydrolysis of lignocellulosic biomass,¹⁵ and these results have since been confirmed.¹⁶

Here we describe the results of our investigation of the kinetics of the acid catalysed hydrolysis¹⁷ of cellobiose as a model for cellulose hydrolysis in the ionic liquid, 1-ethyl-3-methylimidazolium chloride,¹⁸ paying particular attention to the competition between hydrolysis¹⁹ and subsequent decomposition of glucose, as a model to help understand the hydrolysis of cellulose and lignocellulosic biomass in ionic liquids.

Experimental

Materials

Anhydrous 1-ethyl-3-methylimidazolium chloride, [C₂mim]Cl, was supplied by Accelrys, China (recrystallised from ethyl ethanoate, anhydrous, 99% purity). Cellobiose, maleic acid, ethanedioic acid, sulfamic acid, 1,1,1-trifluoroethanoic acid, methanesulfonic acid and sulfuric acid were *ex* Aldrich (99% purity). Cellulose fibres (Ref Aldrich C6663, batch 055K0166), hemicellulose (xylan from birch wood, 90% xylose, Ref Sigma X0502, batch 096K1248) were *ex* Aldrich and used as received. *Miscanthus* grass was provided by the National Renewable Energy Laboratory (Golden, CO), and was dry milled to a 0.5 mm powder before use. Nylon filters (45 μm) were from VWR.

Work-up procedure

Experiments were carried out using a magnetically stirred (700 rpm) glass micro-batch reactor (15 cm³). 1-Ethyl-3-methylimidazolium chloride (5 g) was placed in the reactor and heated to temperature, melting at 89 °C. The saccharide source (0.5 g) was then added and stirred; glucose and cellobiose dissolved rapidly, whereas with cellulose and xylan, the mixtures were stirred at 700 rpm for 20–60 min to solubilise the polysaccharide. As the solubility of the cellulose dropped in the presence of acid, the yields obtained with non-presolubilised substrates are lower. Acid catalyst was then added (with water, if needed) at the reaction temperature and the start time, *t*^o, for kinetic measurements was taken as the time of catalyst addition.

Analysis

Analyses were performed using an Agilent 1200 series HPLC unit equipped with a refractive index detector (RI-HPLC) and a Biorad HPX-87H column, eluting with deionised water (flow 0.6 cm³ min⁻¹). The presence of glucose was confirmed by ¹H-NMR and ¹³C-NMR spectroscopy using a 500 MHz Bruker apparatus.

Progress of the reaction was monitored by periodically taking small (10 μl) aliquots from the reactor which were quenched with water (1 cm³), filtered through 45 μm nylon filters and then analysed by RI-HPLC. The ionic liquid was used as an external standard.

Initially, glucose production was also monitored using a colorimetric assay with dinitrosalicylic acid (dns, see Fig. 2) to test for reducing sugars. However, as previously recognised by Rivers *et al.*,²⁰ this assay significantly overestimates the yields of reducing sugars when used for acid hydrolysis of cellulose, largely due to interference from glucose degradation products. The RI-HPLC method proved to be much more reliable.

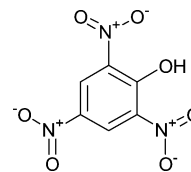


Fig. 2 Structure of dinitrosalicylic acid.

Cellulose digestion was followed by monitoring the change in solution viscosity of parallel reactions performed directly in the viscosimeter using a Brookfield CAP 2000 cone and plate viscometer with Capcalc V1.02 control and data acquisition software using a shear rate of 1666 rpm.

Mass balances for cellulose and biomass experiments were not evaluated, the production of carbohydrate being the sole objective.

Kinetic modelling

Cellobiose hydrolysis was approximated by a simple “two successive first order reactions” model given in Equation 1; glucose dimerisation was neglected and water was present in a large excess. It is worth noting that since cellobiose contains two glucose units per β(1→4) link, the rate of glucose formation is twice the rate of hydrolysis, Equation 2.

$$d[\text{glucose}]/dt = r_{1(\text{cellobiose hydrolysis})} - r_{2(\text{glucose degradation})} \quad (1)$$

where $r_1 = 2 \times 2k_1[\text{cellobiose}]$; $r_2 = k_2[\text{glucose}]$

So as a function of time:

$$[\text{glucose}]/2[\text{cellobiose}]^0 = (2k_1/(k_2 - k_1)) \times (e^{-2k_2t} - e^{-k_1t}) \quad (2)$$

Both reactions were studied and initial rates of cellobiose hydrolysis r_1^0 and glucose degradation r_2^0 were directly measured and both expressed in μmol_{glucose} s⁻¹ cm⁻³. As expected by the model, the maximum yield in glucose achieved during the course of each experiment increases as twice the ratio of the rate constants k_1/k_2 , which is equal to the ratio of the initial rates, r_1^0/r_2^0 . So, its optimisation will be the objective of the following experiments.

For cellulose hydrolysis, there is only one glucose unit per β(1→4) link so the optimum will depend directly on the ratio of the rate constant k_1/k_2 . As cellulose was soluble in [C₂mim]Cl, the hydrolysis was still a homogeneous reaction with each link equally accessible to the acid catalyst. So the model used for cellulose hydrolysis was based on a first-order random chain

scission followed by a first-order glucose degradation. Glucose concentration as a function of time is shown in Equation 3.

$$[\text{glucose}]/[\text{glucose/cellulose}]^0 = \frac{(2k_2 - k_1)}{(k_1 - k_2)} \times e^{-k_1 t} + \frac{(k_2 - k_1)}{(k_2 - 2k_1)} \times e^{-2k_1 t} + \frac{(k_1 \times k_1)}{(k_2 - k_1) \times (k_2 - 2k_1)} \times e^{-k_2 t} \quad (3)$$

Results and discussion

Solubility

The solubility of glucose and cellobiose in $[\text{C}_2\text{mim}]\text{Cl}$ were determined to be around 250 g kg^{-1} in dry liquid $[\text{C}_2\text{mim}]\text{Cl}$ at 90°C . Cellulose is highly soluble, too, as previously reported⁷ and solutions containing 200 g kg^{-1} of cellulose in $[\text{C}_2\text{mim}]\text{Cl}$ can be readily obtained. However, it should be noticed that such solutions are very viscous and solutions of $<10 \text{ wt}\%$ are far easier to handle on a bench scale. Contrary to some reports that claim that unrefined biomass sources can be readily dissolved in ionic liquids,¹⁰ we found that *Miscanthus* switch grass was not completely solubilised by $[\text{C}_2\text{mim}]\text{Cl}$ after 24 h at 100°C , however swelling of the grass fibres was observed as shown in Fig. 3.

Cellobiose hydrolysis and glucose degradation

The two reactions at the core of the present investigation of cellobiose as a model for longer-chain polysaccharide oligomers, are hydrolysis of cellobiose into two equivalents of glucose (Scheme 1), and the subsequent competing decomposition of glucose, forming 5-hydroxymethylfurfural, levulinic and formic acids, and uncharacterised products (humin), following the overall scheme presented previously (Fig. 1).

If cellulose is used as the starting material, the chains are, of course, much longer than the two glucose units shown above, however, the crucial reaction is still the addition of water across the $\beta(1 \rightarrow 4)$ ether linkage between two glucose moieties. The

rate of the hydrolysis reaction, k_1 is assumed to be constant, regardless of the chain length of the substrate. The rate of glucose degradation, k_2 , has also been determined.

No attempts have been made to determine the rate constant for the hydrolysis of hemicellulose, the rate constant for degradation of xylose, or to elucidate the pathway of the subsequent degradation of the resultant sugars (glucose from cellulose and xylose from hemicellulose) in the ionic liquid. Isomerisation of glucose into mannose or fructose was not considered, as only trace quantities of these sugars were detected. Indeed, under the reaction conditions in the acidic ionic liquid media, fructose was dehydrated immediately into 5-hmf as reported elsewhere.²¹

Water content

The physicochemical properties of ionic liquids have been shown to be very sensitive to water content;²² reactions in ionic liquids can be strongly influenced by the moisture content and this reaction is no exception. In the present case, water plays a dual role as a necessary reactant for cellobiose hydrolysis and as a base which limits the strength of the acid used as catalyst. Moreover, for cellulose hydrolysis reactions, water can act as an anti-solvent causing precipitation of cellulose from solution,⁷ so it is imperative that the water content is carefully controlled.

Initial reaction rates, determined as a function of the water content, are presented in Fig. 4. The influence of water on the hydrolysis of cellobiose (r_1^0) and the degradation of glucose (r_2^0) were very different. The glucose degradation rate decreased regularly with the amount of water, as the basicity of water neutralises partially the acidity of the media. The overall reaction rate is reduced by a factor of four when the water content increased from 1 to 4 mmol cm^{-3} . In contrast, the rate of cellobiose hydrolysis first increased with water content, due to the role as reactant of the water, then decreased.

Balancing these two competing factors, an optimum composition for this reaction is one where the water content of the initial system is between 2.5 to 5 mmol cm^{-3} (5–10% by weight), the upper limit bounded by cellulose solubility in ionic liquid/water mixtures.

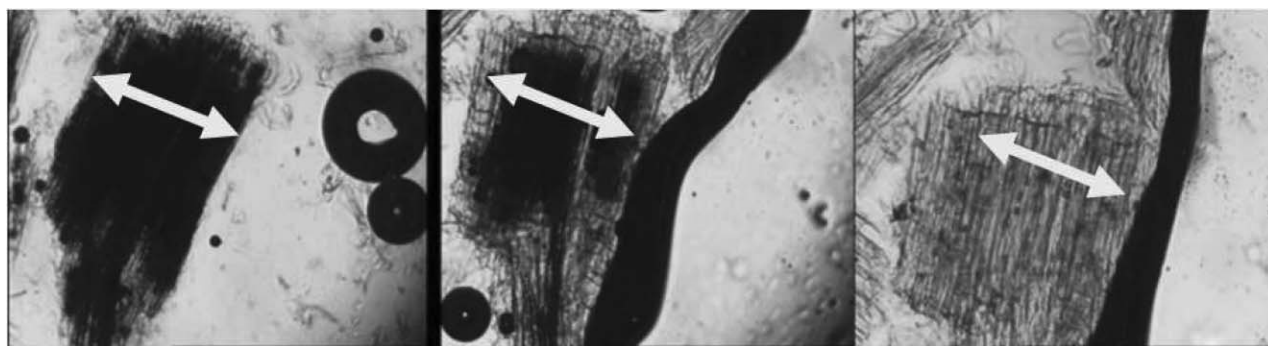
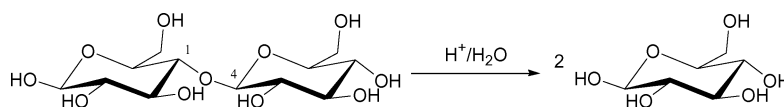


Fig. 3 Swelling of *Miscanthus* grass particles (0.5 mm mesh) in the ionic liquid, $[\text{C}_2\text{mim}]\text{Cl}$, heated at 100°C as a function of time; (a): t^0 , (b): $t = 2 \text{ h}$, (c): $t = 20 \text{ h}$; white arrow is 0.34 mm.



Scheme 1 Hydrolysis of cellobiose under acidic conditions to form glucose.

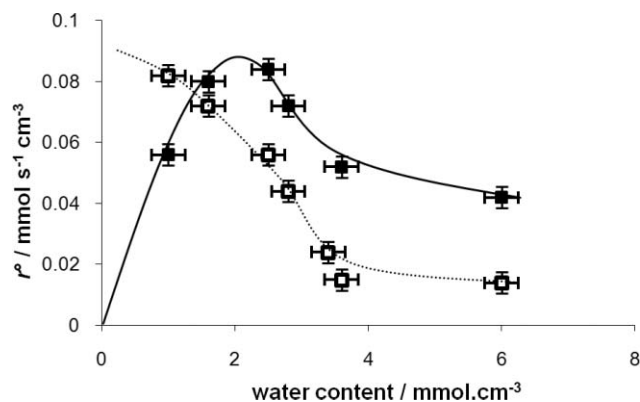


Fig. 4 Effect of water content for cellobiose hydrolysis (■) and glucose degradation (□). Reaction conditions: 90 °C, 5 cm³ of ionic liquid, 0.22 mmol cm⁻³ of methane sulfonic acid and 0.5 mmol cm⁻³ of glucose equivalent.

Acid strength

A range of acids were screened as catalysts for both reactions. The initial rates are plotted against the respective pK_a of the acids^{23–26} in Fig. 5. It should be noted that the pK_a values used are those of the acids in water, despite the fact that the reactions here take place in an ionic liquid rather than aqueous environment. MacFarlane and co-workers have shown that the relative order of the acidities for non ionic acids will be the same in water, and in the ionic liquid ($pK_a(\text{IL})$ and $pK_a(\text{H}_2\text{O})$) related by a constant.²⁷ Thus, although the magnitudes of the acidities may differ, the relative ordering of acid strengths should remain constant.

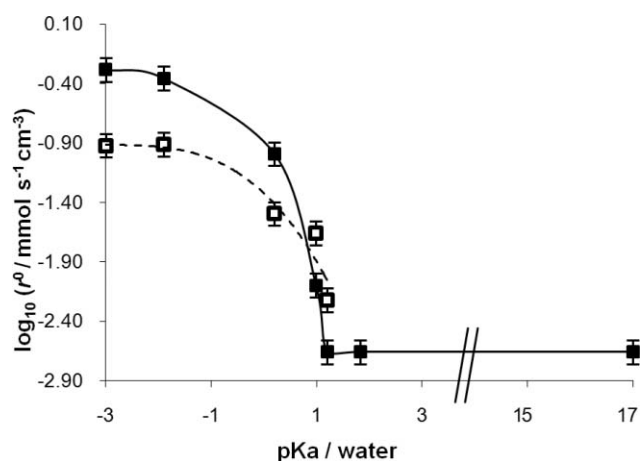


Fig. 5 Influence of the pK_a of the acid catalyst on the initial rates of cellobiose hydrolysis to glucose (■) and glucose degradation (□) reactions. Reactions performed using the following acids: None, maleic acid ($pK_a = 1.92$),²³ ethanedioic acid ($pK_a = 1.2$),²³ sulfamic acid ($pK_a = 0.99$),²⁴ 1,1,1-trifluoroethanoic acid ($pK_a = 0.2$),²⁵ methanesulfonic acid ($pK_a = -1.9$),²³ sulfuric acid ($pK_a = -3$).²⁶ Reaction conditions: 90 °C, 5 cm³ of ionic liquid, 0.5 mmol cm⁻³ of glucose equivalents, 3.5 mmol cm⁻³ water and 0.22 mmol cm⁻³ of the respective acid.

As shown in Fig. 5, cellobiose hydrolysis occurs only when the acid present is a strong acid whereas glucose degradation occurs even in the presence of weaker acids.

In order to increase selectivity, acids with negative pK_a in water are required. For a $pK_a > 1$ in water, cellobiose hydrolysis

is slower compared to glucose degradation, yielding less than 5% glucose in solution at any time, even at high conversion. For a $pK_a < -2$ in water, water present is preferentially protonated and therefore, the actual catalytic species was the hydronium ion (levelling effect by water).

From this it follows, and is observed, that for an acid of $pK_a < -2$ the actual acid strength does not influence the reaction rate, with comparable rates using H₂SO₄ ($pK_a \sim -3$) and MeSO₃H ($pK_a \sim -2$) as catalysts.

Carbohydrate concentration

The initial reaction rates for the two reactions, using methanesulfonic acid as catalyst, are plotted as a function of carbohydrate concentration in Fig. 6. For an initial concentration of less than 0.5 mmol cm⁻³, both cellobiose hydrolysis and glucose degradation are *pseudo*-first-order reactions, thus the initial rates were directly proportional to the amount of carbohydrate introduced and the kinetic model previously described (Equation 1 and 2) was valid. Nevertheless, for higher concentrations, the glucose degradation rate increased more than expected. A third competing reaction, dimerisation of glucose into cellobiose (dehydration) occurs; the hydrolysis reaction was in equilibrium resulting in lower conversion and selectivity. This dehydration product is not observed starting from glucose at higher water contents, *i.e.* when the acid is predominantly aqueous.

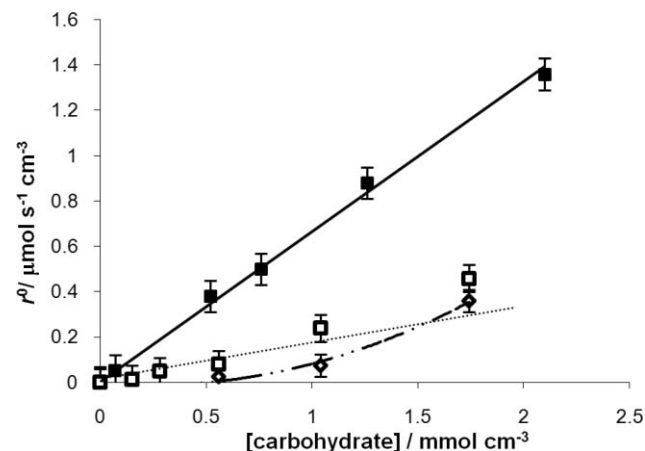


Fig. 6 Effect of carbohydrate concentration on the initial rate of cellobiose hydrolysis (■, $r^0 = 0.66 \times [\text{Cellobiose}]$, $R^2 = 0.99$), glucose degradation (□, $r^0 = 0.15 \times [\text{glucose}]$ for lower concentration, $R^2 = 0.97$) and glucose dimerisation (◇). Reaction conditions: 90 °C, 5 cm³ of ionic liquid, 0.22 mmol cm⁻³ of methane-sulfonic acid and 3.5 mmol cm⁻³ water.

Both glucose dimerisation and the viscosity of the cellulose solution are limiting factors to the maximum carbohydrate contents suitable for this reaction, such that effectively a maximum content of 5 mmol cm⁻³ of glucose equivalents can be used.

Acid concentration

The initial rates of acid catalysed cellobiose hydrolysis and glucose degradation dissolved in [C₂mim]Cl in the presence of methanesulfonic acid, at 90 °C, are shown in Fig. 7 as a function of acid concentration for both cellobiose hydrolysis and glucose degradation. Initial rates are directly proportional to the amount

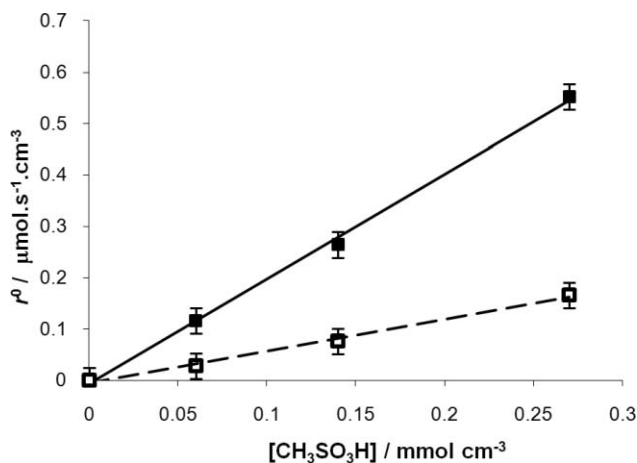


Fig. 7 Variation in the initial rate of cellobiose hydrolysis to glucose (■, $r^0 = 2.0 \times [\text{CH}_3\text{SO}_3\text{H}]$, $R^2 = 0.99$) and glucose degradation (□, $r^0 = 0.6 \times [\text{CH}_3\text{SO}_3\text{H}]$, $R^2 = 0.99$) with concentration of methanesulfonic acid catalyst under identical reaction conditions ($T = 90$ °C, 5 cm^3 of ionic liquid, 0.5 mmol cm^{-3} of glucose (and $0.25 \text{ mmol cm}^{-3}$ of cellobiose) and 3.5 mmol cm^{-3} water).

of acid introduced, as shown by the linear dependence on the acid concentration. It can also be clearly seen that the rate of hydrolysis is higher than the rate of glucose degradation. No significant differences in the overall yield of the reactions were found as a function of acid concentration. Similarly, no gross effects on the product selectivity were observed.

Temperature effect

Activation parameters for both reactions were determined from the Arrhenius plots of rate vs. reciprocal temperature and are shown in Fig. 8, with the activation energies obtained from the slope. Both activation energies, $111 \pm 12 \text{ kJ mol}^{-1}$ for cellobiose hydrolysis and $102 \pm 9 \text{ kJ mol}^{-1}$ for glucose degradation in

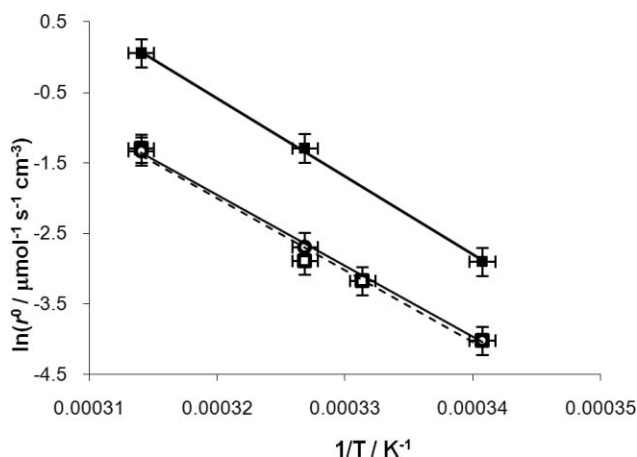


Fig. 8 Effect of temperature on the initial rate of cellulose hydrolysis to glucose (■, $y = -11092x + 34.91$, $R^2 = 0.99$) and glucose degradation (□, $y = -10187x + 30.59$, $R^2 = 0.98$), and for values calculated from the model and the maximum yield obtained for cellobiose hydrolysis (○, $y = -10055x + 30.22$, $R^2 = 0.99$). Reaction conditions: 5 cm^3 of ionic liquid, 0.1 mmol cm^{-3} of methane sulfonic acid, 3.5 mmol cm^{-3} of water and 0.5 mmol cm^{-3} of glucose equivalent.

[C_2mim] Cl , were comparable to the respective literature data in water⁶ (respectively $110 \text{ kJ} \pm 29 \text{ mol}^{-1}$ for cellobiose hydrolysis and between $72.6 \pm 22 \text{ kJ mol}^{-1}$ and $118 \pm 37 \text{ kJ mol}^{-1}$ for glucose degradation). Moreover recent study of cellulose hydrolysis in presence of solid acid catalyst in water reported a similar activation energy (110 kJ mol^{-1}).²⁸

Since the activation energies for both reactions were indistinguishably within experimental error, an increase of temperature has only a very small influence on the yield of the reaction, provided the reaction was carried out between 80 and 150 °C, the working temperature range of [C_2mim] Cl .

Optimised results

The optimum reaction conditions for cellobiose hydrolysis (strong acid, water content between 5–10% (w/w), carbohydrate content less than 10% (w/w), temperature between 80 – 150 °C) have been determined. These conditions were then applied to the hydrolysis of cellobiose, cellulose and *Miscanthus* grass. The ratio of the reaction rate constants were $2k_1/k_2 = 4.8$ for cellobiose hydrolysis and $k_1/k_2 = 2.4$ for cellulose hydrolysis so the anticipated yields in glucose were respectively 65% and 50% from the two systems.

Hydrolysis of cellobiose

The extent of hydrolysis of cellobiose under the best conditions is shown in Fig. 9. The maximum yield of glucose obtained during the course of the experiment was 68% in solution, comparable to that predicted from the model. Nevertheless it would be useful to stop the reaction and extract the products at $\sim 50\%$ conversion in order to optimise and control the selectivity of the reaction to glucose. However, because the degradation rate is still quite high, it may be necessary to perform the reactions under conditions of continuous product extraction in order to optimise yields. Extraction and partitioning of sugars from ionic liquids is an interesting topic not yet covered in literature.

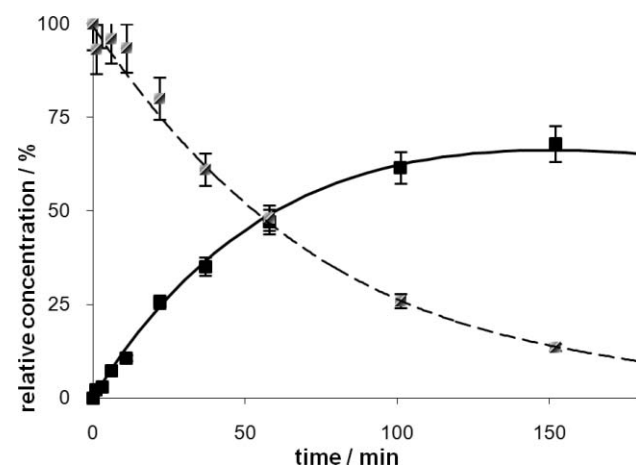


Fig. 9 Reduction in cellobiose concentration (□) and formation of glucose (■) as a function of time during hydrolysis under optimised reaction conditions ($T = 90$ °C, 5 cm^3 of ionic liquid, $0.03 \text{ mmol cm}^{-3}$ of methane sulfonic acid, 3.5 mmol cm^{-3} of water and 0.5 mmol cm^{-3} of glucose equivalent). The fitted lines show predicted conversions from the kinetic model (Equation 2).

Hydrolysis of cellulose and hemicellulose

In order to justify application of the reaction model to the hydrolysis of real, rather than model, systems, cellulose and hemicellulose were studied under the same reaction conditions and the results fitted with the model previously presented.

The reactions were followed by HPLC to determine reaction product distribution, and by following the change in solution viscosity to monitor the rate of depolymerisation of polysaccharide chains. Results are shown in Fig. 10. As anticipated, a final yield of 50% glucose was obtained from the hydrolysis of cellulose. Comparison of the data with the model developed for cellobiose using the same constants shows a good fit. This demonstrates that the cellobiose hydrolysis model can be successfully applied to hydrolysis of more complex, polysaccharides in ionic liquids.

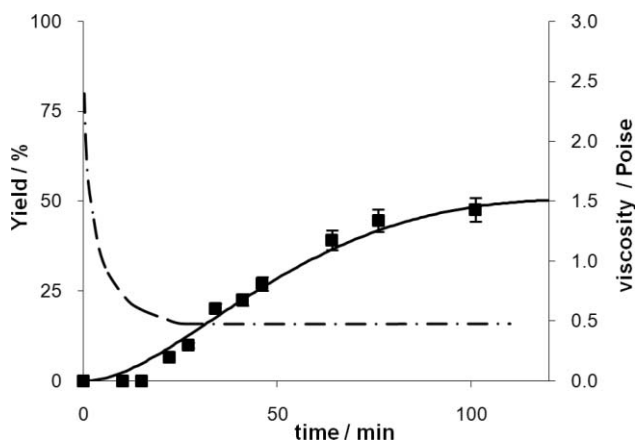


Fig. 10 Yield in glucose (■) from the acid catalysed hydrolysis of cellulose, and change in viscosity of the cellulose/ionic liquid solution over the reaction timescale (---). Reaction conditions: 90 °C, 5 cm³ of ionic liquid, 0.23 mmol cm⁻³ of methane sulfonic acid, 6 mmol cm⁻³ of water and 0.23 mmol cm⁻³ of glucose equivalent. The fitted lines show predicted conversions from the kinetic model.

The experimental results fit the model well and it can be seen that the system viscosity drops drastically after fifteen minutes of reaction, before any glucose can be detected. This implies that during this period, hydrolysis does not form glucose, and thus, that the hydrolysis of cellulose in [C₂mim]Cl occurs at random points along the cellulose chains, in contrast to the mechanism of cellulose hydrolysis in aqueous systems or in enzymatic saccharification, where cellulose chains are hydrolysed preferentially in non crystalline areas and from their ends. These results are consistent with those recently published on cellulose depolymerisation using solid acid catalyst in ionic liquids by Rinaldi *et al.*²⁹ In both studies there is a latency before glucose is detected in solution, corresponding of the hydrolysis of long chain cellulose to oligomers.

Fig. 11 shows the results from the comparable reaction with a hemicellulose (xylan from Birchwood) as the substrate. The yield of xylose, the direct hydrolysis product, was lower (35%) than the corresponding glucose yield from cellulose hydrolysis. This is mainly due to the rapid competing xylose dehydration reaction to furfural (furfural contents up to 20% were detected by RI-HPLC). However, the rate of reaction for the hydrolysis of xylan is similar to that obtained for the hydrolysis of cellulose. It should also be noted that furfural is not stable under the

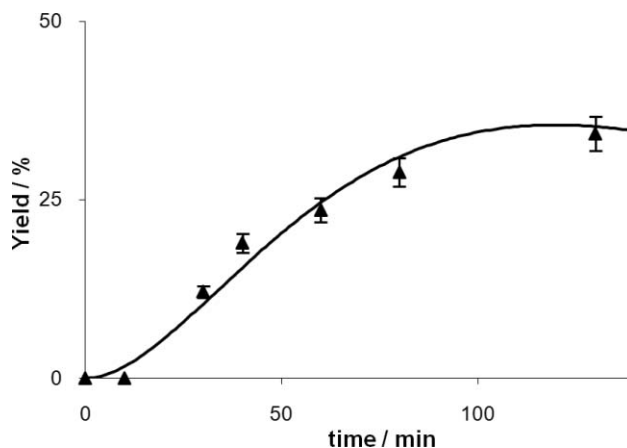


Fig. 11 Yield in xylose (▲) from the acid catalysed hydrolysis of hemicellulose over the reaction timescale. Reaction conditions: 100 °C, 5 cm³ of ionic liquid, 0.09 mmol cm⁻³ of methane sulfonic acid, 4.7 mmol cm⁻³ of water and 0.5 mmol cm⁻³ of xylose equivalent. Fitted lines show predicted conversions from the kinetic model.

acidic reaction conditions and also readily undergoes further degradation.

Lignocellulosic biomass hydrolysis

As a conclusion to the work described above, hydrolysis of samples of miscanthus grass, an example of unprocessed lignocellulosic biomass, was attempted. A straight translation of the reaction conditions found favourable for purified cellulose did not yield efficient hydrolysis and conversion of the cellulosic components to glucose (Fig. 12), in contrast to the results from the reactions of the isolated components, cellulose and hemicellulose.

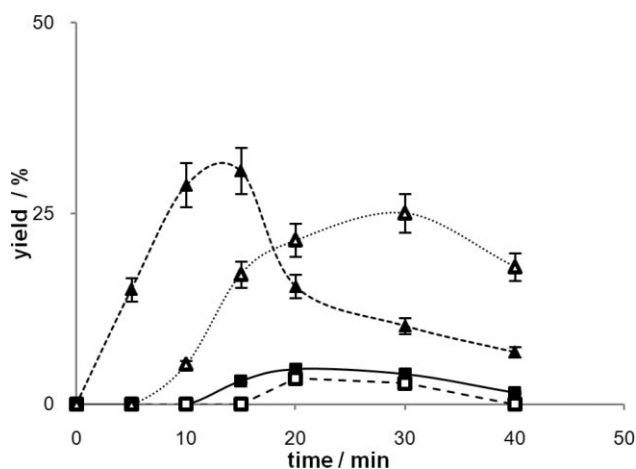


Fig. 12 Yields in glucose (■), xylose (▲), 5-hmf (□) and furfural (△) detected in solution during the acid catalysed hydrolysis of Miscanthus grass in the ionic liquid [C₂mim]Cl as a function of time. Reaction conditions: 100 °C, 5 cm³ of ionic liquid, 0.11 mmol cm⁻³ of methanesulfonic acid, 3 mmol cm⁻³ of water and 0.1 g cm⁻³ of starting biomass (miscanthus, 44% cellulose (0.25 mmol cm⁻³), 24% hemicellulose (0.16 mmol cm⁻³).

Xylose was obtained as a hydrolysis product of the miscanthus with yields similar to those obtained from hemicellulose, showing that the hemicellulosic components could be successfully

hydrolysed and extracted from the biomass by ionic liquids. However, the formation of glucose was very low, with a maximum production of 5% at the peak of conversion. It was noted previously that the biomass did not dissolve in ionic liquids and thus the reaction was conducted under heterogeneous conditions, rather than in a homogeneous solution as for the isolated cellulose and hemicellulose hydrolyses. It seems likely that this is the most significant limiting factor in the efficient hydrolysis of unrefined biomass. Nevertheless, by using a two-stage process (ionic liquid extraction of lignin as reported elsewhere,¹¹ followed by solubilisation of the cellulose/hemicellulosic components in [C₂mim]Cl and hydrolysis as described here) up to 30% yields in glucose could be obtained as shown in Fig. 13, with concurrent xylose yields maintained.

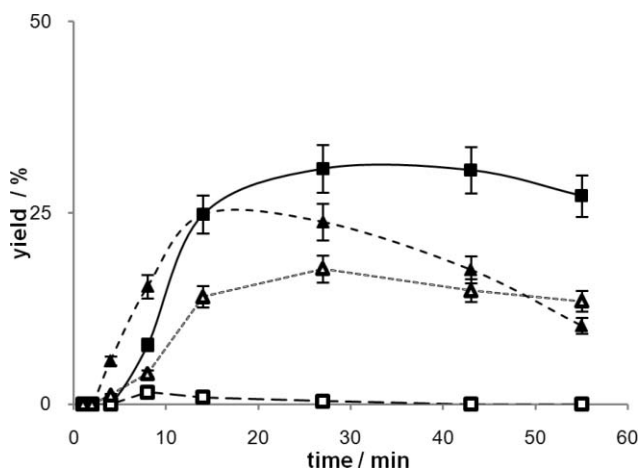


Fig. 13 Change in relative concentrations of glucose (■), xylose (▲), 5-hmf (□) and furfural (△) detected in solution during the acid catalysed hydrolysis of delignified *Miscanthus* grass in the ionic liquid [C₂mim]Cl as a function of time. Reaction conditions: 90 °C, 5 cm³ of ionic liquid, 0.63 mmol cm⁻³ of methanesulfonic acid, 5 mmol cm⁻³ of water and 0.1 g/cm³ of starting biomass (*miscanthus*, 44% cellulose (0.25 mmol cm⁻³), 24% hemicellulose (0.16 mmol cm⁻³) lignin removed by action of triisobutyl methyl phosphonium tosylate at 150 °C for 1 h).

Conclusions

It has been shown that acid catalysed hydrolysis of cellobiose may easily be performed in ionic liquids, and may serve as a model for designing an efficient process for the hydrolysis of cellulose and biomass. The reaction requires very mild conditions in comparison to the same reaction with aqueous acids and when the acid strength is lower than about $pK_a = 0.5$, hydrolysis yielding monosaccharides is favoured with respect to the competing decomposition of glucose. The hydrolysis results from long chain oligosaccharides are consistent with the model cellobiose system, demonstrating that the competition between acid hydrolysis of polysaccharides and subsequent decomposition of monosaccharide in ionic liquid can be controlled by choice of acid catalyst and can be optimised to monosaccharide formation. An advantage of using an ionic liquid based system is the high degree of cellulose solubility and the opportunity to use stronger acids than in water. Even though degradation of glucose cannot be avoided, a continuous extraction system would help to obtain higher yields at high conversion.

Acknowledgements

We would like to thank BP for funding and Dr Brian Dancer and Juliet Hynes (Department of Biosciences, Cardiff University) for performing dns colorimetric assays.

Notes and references

- 1 A. J. Ragauskas, C. K. Williams, B. H. Davison, G. Britovsek, J. Cairney, C. A. Eckert, W. J. Frederick, J. P. Hallett, D. J. Leak, C. L. Liotta, J. R. Mielenz, R. Murphy, R. Templer and T. Tschaplinski, *Science*, 2006, **311**, 484–489.
- 2 R. Luque, L. Herrero Davila, J. M. Campelo, J. H. Clark, J. M. Hidalgo, D. Luna, J. M. Marinas and A. A. Romero, *Energy Environ. Sci.*, 2008, **1**, 57.
- 3 A. Effendi, H. Gerhauser and A. V. Bridgwater, *Renewable Sustainable Energy Rev.*, 2008, **12**, 2092–2116.
- 4 G. W. Huber, S. Iborra and A. Corma, *Chem. Rev.*, 2006, **106**, 4044–4098.
- 5 A. K. Chandel, C. Es, R. Rudravaram, M. Lakshmi, Narasu, L. Venkateswar, Rao and P. Ravindra, *Biotechnol. Mol. Biol. Rev.*, 2007, **2**, 14–32.
- 6 J. F. Saeman, *Ind. Eng. Chem.*, 1945, **37**, 43–52.
- 7 N. S. Mosier, C. M. Ladisch and M. R. Ladisch, *Biotechnol. Bioeng.*, 2002, **79**, 610–618.
- 8 R. P. Swatloski, S. K. Spear, J. D. Holbrey and R. D. Rogers, *J. Am. Chem. Soc.*, 2002, **124**, 4974–4975.
- 9 V. Stegmann, K. Massone, M. Maase, E. Uerdingen, M. Lutz, F. Hermanutz and F. Gaeher, "Solution system based on molten ionic liquid e.g. imidazolium salt for dissolving carbohydrate e.g. starch, cellulose or derivative and regeneration e.g. for fiber production also contains water and /or other protic solvent", European patent DE102005062608 (2007).
- 10 V. Myllymaki and R. Aksela, "Dissolution method for lignocellulosic materials", World patent application WO 2005/017001 (2005).
- 11 I. Kilpeläinen, H. Xie, A. King, M. Granstrom, S. Heikinen and D. S. Argyropoulos, *J. Agric. Food Chem.*, 2007, **55**, 9142.
- 12 J. Upfal, D. R. MacFarlane, and S. A. Forsyth, "Solvents for use in the treatment of lignin-containing materials", World Patent Application, WO/2005/017252 (2005).
- 13 D. A. Fort, R. C. Remsing, R. P. Swatloski, P. Moyna, G. Moyna and R. D. Rogers, *Green Chem.*, 2007, **9**, 63–69.
- 14 L. Liyang and C. Hongzhang, *Chinese Science Bulletin*, 2006, **51**, 2432–2436.
- 15 M. Fanselow, J. Holbrey, and K. R. Seddon, "Conversion method", World Patent Application WO/2007/138256 (2007).
- 16 C. Li, Q. Wang and Z. K. Zhao, *Green Chem.*, 2008, **10**, 177–182.
- 17 J. A. Bootsma and B. H. Shanks, *Appl. Catal., A*, 2007, **327**, 44–51.
- 18 J. S. Wilkes, J. A. Levisky, R. A. Wilson and C. L. Hussey, *Inorg. Chem.*, 1982, **21**, 1263–1264.
- 19 S. E. Jacobsen and C. E. Wynan, *Appl. Biochem. Biotechnol.*, 2000, **84–86**, 81–96.
- 20 D. B. Rivers, S. J. Gracheck, L. C. Woodford and G. H. Emert, *Biotechnol. Bioeng.*, 1984, **26**, 800–802.
- 21 C. Moreau, A. Finiels and L. Vanoye, *J. Mol. Catal. A: Chem.*, 2006, **253**, 165–169.
- 22 K. R. Seddon, A. Stark and M.-J. Torres, *Pure Appl. Chem.*, 2000, **72**, 2275–2287.
- 23 E. P. Serjeant and B. Dempsey, (eds.), *Ionization Constants of Organic Acids in Solution*, IUPAC Chemical Data Series No. 23, Pergamon Press, Oxford, UK, 1979.
- 24 J. L. Kurz and J. M. Farrar, *J. Am. Chem. Soc.*, 1969, **91**, 6057–6062.
- 25 S. Kutsuna and H. Hori, *Atmos. Environ.*, 2008, **42**, 1399–1412.
- 26 I. M. Kolthoff, *Treatise on Analytical Chemistry*, New York, Interscience Encyclopedia, Inc., 1959.
- 27 D. R. MacFarlane, J. M. Pringle, K. M. Johansson, S. A. Forsyth and M. Forsyth, *Chem. Commun.*, 2006, 1905–1917.
- 28 Suganuma K. Nakajima, M. Kitano, D. Yamaguchi, H. Kato, S. Hayashi and M. Hara, *J. Am. Chem. Soc.*, 2008, **38**, 12787–12793.
- 29 R. Rinaldi, R. Palkovits and F. Schüth, *Angew. Chem., Int. Ed.*, 2008, **47**, 8047–8050.

Effects of water-miscible ionic liquids on cell growth and nitro reduction using *Clostridium sporogenes*

Olutosin Dipeolu,^a Edward Green^b and Gillian Stephens^{*a}

Received 22nd July 2008, Accepted 12th December 2008

First published as an Advance Article on the web 23rd January 2009

DOI: 10.1039/b812600c

Water miscible ionic liquids had various effects on the physiology of *Clostridium sporogenes* when tested as additives in culture media or reaction media for reduction of nitrobenzene. 2-Hydroxy ethyl trimethyl-ammonium dimethyl phosphate ([EtOHMe₃][Me₂PO₄]) and *N,N*-dimethylethanolammonium acetate (DMEAA) increased the growth rate of *C. sporogenes* by as much as 28%, suggesting that they were either metabolised or increased the availability of nutrients. By contrast, 1-butyl-3-methylimidazolium tetrafluoroborate ([BMim][BF₄]) and AMMOENG™ 100 inhibited growth. Although 1-ethyl-3-methyl imidazolium ethylsulfate ([EMim][EtSO₄]; 2% w/v) inhibited growth by 58%, it was sufficiently non-toxic to allow efficient reduction of nitrobenzene using harvested cells, providing aniline yields up to 79%. The high product yield with reactions in [EMim][EtSO₄] represented a significant improvement over conventional solvents, since the yield was only 8% in aqueous ethanol (4% v/v) and 45% in a biphasic heptane/aqueous system (phase ratio 0.33). The ionic liquid appeared to suppress unproductive substrate consumption by an unknown mechanism

Introduction

Ionic liquids are salts in which the crystal packing is so defective that they are liquid at room temperature.^{1,2} Since they are composed of ions, their behaviour is different from conventional organic solvents, and this has led to intense interest in this unique class of compounds. Most importantly, the polarity and solvent miscibility are adjustable over the whole range required for chemical processing, through modification of the composite cation and anion structure. This provides unprecedented opportunities to tune the solvent to match the needs of the process with exquisite precision. In addition to this, most ionic liquids have near-zero vapour pressure and excellent thermal stability, and biodegradable and non-toxic ionic liquids can be designed.^{3–11} This means that ionic liquids offer the prospect of cleaner, greener chemical manufacturing. These 'futuristic' solvents are now finding uses in a wide range of chemical and biocatalytic processes.^{1,2,12,13}

Ionic liquids are particularly attractive for biocatalysis because there is such a restricted range of conventional solvents that is suitable for use in biotransformations.¹⁴ There are already numerous examples of improved enzyme biocatalysis in ionic liquids, resulting from the ability to tune the solvent structure for optimal solvation of substrate and product whilst also retaining enzyme activity. Additional benefits include improved enantioselectivities, higher yields, improved enzyme

stability and stimulated activity in comparison to organic solvents.^{2,9}

In contrast, there have been rather few reports on the use of ionic liquids for whole cell biotransformations,^{15–23} even though ionic liquids may offer considerable advantages over conventional solvents. In particular, conventional solvents tend to be toxic to whole microbial cells, and there is a real need for better solvents.^{14,24–26} Indeed, there have been some notable successes in using ionic liquids for whole cell biotransformations^{16,17,21,22} and some preliminary rules for solvent selection are beginning to emerge.^{27,28} However, most of the studies have focused on water-immiscible ionic liquids. Whilst two-liquid phase reaction systems are extremely useful for biotransformations involving non-polar toxic substrates, there are numerous examples of biotransformations where substrate delivery depends simply on solubilisation of relatively non-toxic substrates, and there is no need to resort to the complexity of multi-phase processing.^{24,25} In such cases, water-miscible, conventional solvents^{29–31} or detergents³² are frequently used for substrate delivery. However, these materials can be extremely toxic to cells unless used at low concentrations,^{25,26,33} and this restricts the substrate concentrations that can be achieved in the process. Therefore, water miscible ionic liquids may provide an alternative to deliver poorly water soluble substrates in whole cell biotransformations.¹⁵

In this study, we tested the effect of water-miscible ionic liquids on *Clostridium sporogenes*, a proteolytic spore-forming anaerobe. This organism is an extremely versatile biocatalyst for transformation of nitrogen-containing precursors to chiral and achiral amines,^{34–37} which together comprise the single most useful group of precursors for manufacturing pharmaceuticals.^{38,39} Nitro reduction is a particularly attractive target, due to the

^aManchester Interdisciplinary Biocentre, University of Manchester, 131 Princess Street, Manchester, UK M1 7DN. E-mail: gill.stephens@manchester.ac.uk; Fax: +44 161 3068918; Tel: +44 161 3064377

^bGreen Biologics Limited, 45A Milton Park, Abingdon, Oxfordshire, UK OX 14 4RU

ease with which the substrates can be prepared. *C. sporogenes* is known to reduce *p*-nitrobenzoate and 2-nitroethanol.^{34,35} Although these substrates are water soluble, the most useful substrates are much less soluble and this would restrict productivity in the biotransformations. Therefore, we studied the use of water-miscible ionic liquids to deliver water-insoluble substrates. We used nitrobenzene as a simple example of a poorly water soluble substrate to provide a suitable model for initial feasibility studies.

We wish to report that 1-ethyl-3-methyl imidazolium ethylsulfate **5** ([EMim][EtSO₃]; Fig. 1) provided improved reduction of nitrobenzene to aniline using *Clostridium sporogenes* compared with the conventional solvents, heptane and ethanol. In addition, we report that selection of water-miscible ionic liquids for biotransformations requires care, due to unpredictable effects on cell physiology and the potential for reactions with microbial culture media.

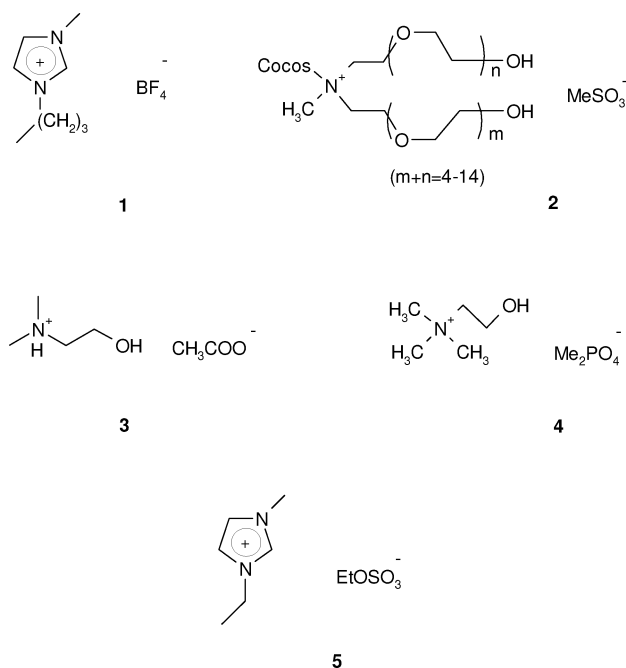


Fig. 1 Ionic liquids tested for biocompatibility with *Clostridium sporogenes*.

Results and discussion

Reaction optimisation

Reduction of nitrobenzene has not been determined using *Clostridium sporogenes*, and therefore, we started by confirming that nitrobenzene was reduced to aniline as expected. Nitrobenzene is rather insoluble in water (1.9 g/L at 20 °C; 0.015 mM), whereas the reduced product, aniline, is water soluble (36 g/L at 20 °C; 2.57 mM).⁴⁰ Therefore, we used a two phase heptane/water reaction system for initial tests, in which the Log D heptane/water for nitrobenzene was 1.7.

C. sporogenes was grown on phenylalanine, and then harvested and washed anaerobically. The cell suspensions were then tested anaerobically for reduction of nitrobenzene (3.5 mM in heptane). The reduction was successful when H₂ was used as the electron donor, providing aniline in 45% yield. We found

Table 1 Effect of electron donors on the reduction of nitrobenzene by *Clostridium sporogenes*

Electron donor	Aniline (mM)	Yield (%)
H ₂	1.44 ± 0.25	41
Fructose	1.36 ± 0.16	39
Starch	1.23 ± 0.02	35
Glucose	0.95 ± 0.14	32

Harvested cells (92 g_{dry wt} L⁻¹) were incubated with nitrobenzene with the electron donors shown. The data are the mean of duplicate reactions and the standard deviations are shown. The experiment was repeated on 3 occasions and representative data are shown.

that H₂ was the best electron donor, since yields with fructose, starch and glucose were 13, 16 and 29% lower, respectively, than with H₂ (Table 1). Therefore, H₂ was chosen as the electron donor for further experimental studies. Nevertheless, it should be noted that glucose and starch can be produced from plant biomass, and are relatively cheap and safe to use. Therefore, the carbohydrates may be better candidates than H₂ for future industrial use, since product yields were only slightly lower.

Nitrobenzene was consumed completely with each of the electron donors, even though the product yield was less than 45% (Table 1). This could be attributed to formation of side products, since the aqueous phase of the reaction mixtures contained either phenol or an unidentified product. The product ratios varied when the experiment was repeated with different cell preparations, although the aniline yields were similar. However, the side products were not characterised further because we obtained higher yields in later experiments (see below). We also checked for product consumption by incubating *C. sporogenes* with aniline (2 mM) for 24 h under H₂. Less than 2 (± 0.5)% of the aniline was consumed, suggesting that the low yields were not due to product consumption.

Effect of ionic liquids on growth of *C. sporogenes*

The next step was to investigate the biocompatibility of ionic liquids to determine their suitability for use as a replacement for heptane in the biotransformation. Since water-miscible ionic liquids have rarely been used in whole cell biotransformations,¹⁵ we decided to test diverse structures. We tested for biocompatibility by measuring the growth rate of *C. sporogenes* on phenylalanine under anaerobic conditions in the presence and absence of various concentrations of ionic liquids (Table 2). Growth of *C. sporogenes* was also monitored in the presence of ethanol, as an example of a conventional, water miscible organic solvent.

Ethanol was only slightly inhibitory, even at 2% (v/v). By contrast, 1-butyl-3-methylimidazolium tetrafluoroborate **1** ([BMim][BF₄]) allowed growth at low concentrations, but inhibited growth completely when added to 0.5% (w/v), indicating that *C. sporogenes* is more sensitive to this ionic liquid than *E. coli*.⁴¹ However, the sensitivity may not be due to the ionic liquid *per se*, since [BMim][BF₄] hydrolyses in water, forming HF.⁴² Indeed, we found that the pH fell from 7.0 to 5.9 in uninoculated medium containing 2% [BMim][BF₄] after 24 h, whereas the pH did not change significantly in the absence of

Table 2 Growth of *Clostridium sporogenes* in the presence of ionic liquids and ethanol

Ionic liquids		Growth rate ^a (%) at different concentrations of ionic liquids (% w/v)				
		0.10	0.25	0.50	1.0	2.0
[BMim][BF ₄]	1	91 ± 2	59 ± 3	0 ± 0	0 ± 0	19 ± 0
AMMOENG TM 100	2	9 ± 0	0 ± 0	0 ± 0	0 ± 0	0 ± 0
DMEAA	3	117 ± 3	85 ± 2	98 ± 6	83 ± 5	59 ± 3
[EtOHNMe ₃][Me ₂ PO ₄]	4	98 ± 6	128 ± 15	102 ± 6	123 ± 12	91 ± 2
[EMim][EtSO ₄]	5	79 ± 2	81 ± 2	89 ± 11	77 ± 2	42 ± 5
Ethanol (% v/v)		92 ± 6	98 ± 10	96 ± 6	87 ± 7	76 ± 5
No solvent (control)		100 ± 9				

^a *C. sporogenes* was grown anaerobically in the presence of ionic liquids or ethanol at the concentrations shown. The control contained water in place of solvent. The growth rates (shown as a percentage relative to the control experiments) are the average of 4 cultures and the standard deviations are shown.

ionic liquid. This suggests that the observed toxicity may be associated with HF formation.

Next, we tested AMMOENGTM 100 **2** as an example of an ethylene glycol functionalized ammonium salt. There was almost no growth even at 0.1% (w/v) ionic liquid, but AMMOENGTM 100 caused immediate precipitation of the culture medium. This suggested that the apparent growth inhibition was due to a decreased availability of essential nutrients. We assume that the ionic liquid was reacting with ionic substances in the culture medium and forming an insoluble precipitate. The precipitate dissolved again after incubation for 24 h, but there was still no growth. We have encountered precipitation with other ionic liquids using different media (data not shown), so it seems that this is a fairly general problem. However, it is dependent on the type of culture medium and the type of ionic liquid.

Two of the ionic liquids stimulated growth, causing an increased growth rate and a shorter lag phase. Thus, *N,N*-dimethyl-ethanolammonium acetate **3** (DMEAA) increased the growth rate by 17% when provided at 0.1% (v/v), but caused slight inhibition at higher concentrations. 2-Hydroxy ethyl trimethylammonium dimethyl phosphate **4** ([EtOHNMe₃][Me₂PO₄]) also increased the growth rate (up to 28%), and growth stimulation continued at concentrations up to 1% before slight inhibition was observed. We were surprised to see such a large increase in growth rate, since the cells were growing in a complex culture medium, containing amino acids, peptone and yeast extract which has already been optimised to support rapid growth of *C. sporogenes*.^{34,35,43} It is possible that the cells were able to use the ionic liquids as an additional nutrient source, but it is difficult to explain why these xenobiotics would support more rapid growth than naturally-occurring amino acids and protein hydrolysates, which are the natural substrates for this proteolytic organism.⁴⁴ Therefore, it is also possible that the ionic liquids increased the availability of other nutrients in the medium. However, phenylalanine has a solubility of 20 g/L in water,⁴⁰ but the solubility only increased slightly, to approximately 23–24 g/L in 4% DMEAA or [EtOHNMe₃][Me₂PO₄]. Therefore, it seems more likely that the growth stimulation may have been due to solubilisation of other nutrients or utilisation of the ionic liquids as nutrients. To distinguish between these possibilities, it would be necessary to test for growth in minimal medium with the ionic

liquids as the sole carbon and energy source. However, such studies would be fraught with difficulty because *C. sporogenes* has an absolute requirement for supplementary amino acids in the culture medium⁴⁵ and it would not be possible to distinguish between growth on the amino acids and the ionic liquids. Whatever the explanation, the uncertainty about the effects of DMEAA and [EtOHNMe₃][Me₂PO₄] on *C. sporogenes* makes these ionic liquids unsuitable for use in biotransformations.

1-Ethyl-3-methyl imidazolium ethylsulfate **5** ([EMim][EtSO₄]) caused growth inhibition (23%) at all concentrations up to 1% (w/v), with further inhibition (58%) as the concentration was increased to 2%. This inhibition was relatively modest compared with [BMim][BF₄] and AMMOENGTM 100. Therefore, it was possible that this ionic liquid might be useful for biotransformations, because we have shown that biotransformations can be less sensitive to inhibition by ionic liquids than growth.²² Therefore, we selected [EMim][EtSO₄] for use in nitrobenzene reduction.

Nitrobenzene reduction in ionic liquid solutions

We found that nitro reduction was more efficient in the ionic liquid solutions than in conventional solvents. Thus, washed, harvested *C. sporogenes* cells were able to reduce nitrobenzene in 4% [EMim][EtSO₄], forming aniline in 45% yield (Fig. 2). By contrast, the average yield was only 8% in 4% ethanol. Therefore, the water-miscible ionic liquid provided better biocatalyst performance than the conventional solvent. When ethanol or [EMim][EtSO₄] were used, the substrate was still consumed completely, as with heptane, but side products were not formed. This suggests that the formation of the side product was associated specifically with use of heptane as solvent.

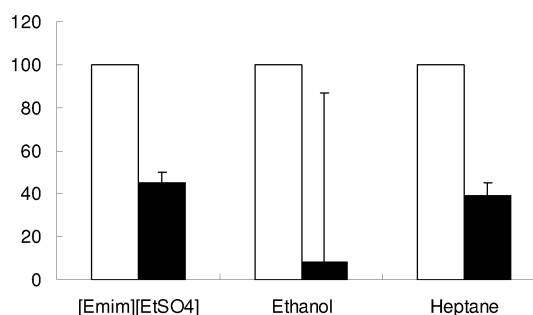


Fig. 2 Reduction of nitrobenzene with *Clostridium sporogenes* in different solvent systems. Nitrobenzene was reduced using harvested cells (24 g_{dry wt} L⁻¹) with H₂ as the electron donor using the solvent systems shown and the substrate consumed (■) and product formed (□) expressed as percentages. Data are a mean of duplicate reactions and error values are the standard deviations.

When nitro reduction was tested in heptane, the aniline yield was only 39%, compared with 45% in Table 1. However, the cell concentration (24 g_{dry wt} L⁻¹) was much lower in this experiment compared with the experiment reported in Table 1 (92 g_{dry wt} L⁻¹). This suggested that the product yield might be related to cell concentration. Therefore, we tested nitrobenzene reduction in 4% [EMim][EtSO₄] using an increased cell concentration (92 g_{dry wt} L⁻¹). In this case, the aniline concentration increased to 2.76 ± 0.18 mM, and the yield was 79%. Therefore, unproductive substrate conversion had decreased, and more of the substrate

was converted to the desired product. Most importantly, the yield was 43% higher than in heptane under equivalent reaction conditions.

Interpreting the results is complex. All three solvent systems provided effective solubilisation of the substrate, nitrobenzene. Therefore, it seems that the superior performance of the ionic liquid may be due to suppression of unproductive substrate conversion. As noted above, this ionic liquid inhibited growth by up to 58%, so it is fairly toxic. This suggests that it may inhibit metabolic processes that are associated with unproductive substrate conversion. However, further speculation about the mechanism would be premature at this stage, and further studies will be needed to investigate the biological basis of this phenomenon.

Experimental

Chemicals

Ionic liquids were obtained as follows: [BMim][BF₄] from Fluka; [EMim][EtSO₄], AMMOENG™ 100, and [EtOHNMe₃][Me₂PO₄] from Solvent Innovation; DMEA from Bioniqs Limited. All other chemicals were obtained from Sigma-Aldrich at the highest purity unless otherwise stated.

Measurement of growth rates

Clostridium sporogenes was maintained and cultured in an anaerobic cabinet as described previously.³⁷ Ionic liquids were deoxygenated by purging with N₂.⁴⁶ The ionic liquids and ethanol were mixed with deoxygenated, sterile distilled water in the anaerobic cabinet and then added to the culture medium. AMMOENG™ 100 was hygroscopic and solidified immediately on contact with air, and was dissolved by mixing with water at 50 °C and cooling anaerobically. The cultures were inoculated (4% v/v) from pre-cultures that had been grown overnight to an OD₆₆₀ of 3. There was no growth in uninoculated controls, showing that the solvents were self sterile. The cultures were mixed anaerobically on a IKA Vibrax® shaker at 120 rpm at 30 °C. Samples were taken aseptically, the OD₆₆₀ (N_t) was measured and the growth rates (μ) were calculated from data collected during the exponential growth phase using the following equation: $\ln N_t/N_o = \mu t$.

Biotransformations

Cells were grown and harvested anaerobically as described previously.³⁷ The cells were resuspended in 50 mM potassium phosphate buffer pH 7.0 to approximately 10% of the original culture volume and used as the biocatalyst. Nitrobenzene was dissolved in the solvent, deoxygenated, and then transferred to the anaerobic cabinet. Solutions in heptane were added to a phase ratio of 0.33, with nitrobenzene at 3.5 mM across both phases. For the water miscible systems, nitrobenzene was dissolved in ethanol or [EMim][EtSO₄], deoxygenated, transferred to the anaerobic cabinet, mixed with an equal volume of anaerobic water and then added to the reaction mixture to 3.5 mM nitrobenzene and 4% solvent. For reactions with H₂ as electron donor, the H₂ was passed over the headspace of the reaction vessel for 5 min before sealing the reaction vessels

and inverting them to minimise gas loss. For reactions with fructose, glucose or starch, the electron donor was added as an anaerobic aqueous solution (1 mL; final concentration 0.45% w/v) and the headspace of the reaction vessel was flushed with N₂. In all cases, the total volume of reaction mixtures was 12 mL and the cell concentrations (stated in the text) were adjusted to the same concentration across the whole reaction mixture by diluting with buffer as necessary. The reaction mixtures were incubated in Supelco® bottles with polypropylene screw tops and PTFE septum seals.

Analytical methods

The cells were removed from all samples by centrifugation at 4000 rpm for 20 min in an Eppendorf 5210R bench centrifuge (UK). The heptane phases from biphasic reactions were separated before centrifuging the aqueous phase, and the heptane phase and aqueous supernatant were analysed directly without further extraction. The supernatants containing water miscible solvents were extracted once with 3 mL ethyl acetate for samples containing [EMim][EtSO₄] or dichloromethane for samples containing ethanol. Samples were analysed using a Thermo Finnigan ISD gas chromatograph coupled to an ion trap mass spectrometer detector. Samples (1 μL, split ratio 33:1) were analysed on a ZB-5MS capillary column (0.25 mm × 30 m, 0.25 μm nominal film thickness; Phenomenex, USA) with He as the carrier gas (1 mL/min). The column was held at 80 °C for 2 min, and the temperature was increased by 15 °C min⁻¹ to 190 °C, and then maintained for 1 min. Mass spectra were acquired using positive ion electron impact ionization at 70 eV with the source temperature at 200 °C. Mass spectra were scanned from 50–350 mass units at a rate of 3 scans/s. Aniline and nitrobenzene concentrations were determined using calibration curves made with authentic standards.

Conclusion

Water-miscible ionic liquids have a variety of different effects on the physiology of *Clostridium sporogenes*. Thus, DMEA and [EtOHNMe₃][Me₂PO₄] caused large increases in the growth rate of *C. sporogenes*, by an unknown mechanism. We also found that AMMOENG™ 100 can react with culture media. Whilst this causes growth inhibition, it is not because the ionic liquid is toxic but because the reaction reduces the availability of essential nutrients. Therefore, great care has to be exercised when selecting ionic liquids for use with whole microbial cells. It is becoming evident that simple tests for cell viability are insufficient,^{15,17,21} and tests for growth, with suitable controls, are needed to rule out effects on cell physiology or reactions with growth media. In addition, the lessons learned in this study suggest that care may also be needed to ensure that the ionic liquid does not react with components of reaction media for biotransformations, although there were no such problems with the media used in this study.

The unexpected effects on cell physiology also extended to nitro reduction using *C. sporogenes*. [EMim][EtSO₄] was as an effective additive to increase the solubility of nitrobenzene in aqueous reaction mixtures. However, the benefits extended beyond improved substrate delivery. Remarkably, the ionic liquid increased the yield of the amine product, compared with

reactions run in aqueous ethanol or a biphasic heptane/water system. The yield increase appeared to be due to suppression of unproductive substrate consumption by an unknown mechanism, so that more of the substrate was converted to product. [EMim][EtSO₄] inhibited growth rather strongly, and it is possible that the target for growth inhibition was associated with the side reactions on the biotransformation substrate, so that both growth and side reactions were inhibited. This unexpected outcome has considerable practical benefit.

Our finding that a growth inhibitory ionic liquid can provide benefits for nitro reduction shows that it is not necessary to use completely non-toxic ionic liquids for biotransformations. Indeed, this is consistent with our earlier finding that moderately toxic ionic liquids are also suitable for oxygenase-catalysed whole cell biotransformations.²² Therefore, we recommend that both non-inhibitory and partially inhibitory ionic liquids should be screened for use in biotransformations.

Overall, we conclude that water-miscible ionic liquids may have considerable potential as additives in culture media and reaction media to obtain improved growth and biotransformation using *C. sporogenes*. Further work is now needed to determine the generality of such phenomena amongst microbial biocatalysts.

Acknowledgements

OD is grateful to Green Biologics Limited (Oxford, UK) and the University of Manchester, UK for funding her Ph.D. studentship.

Notes and references

- N. Plechkova and K. Seddon, *Chem. Soc. Rev.*, 2008, **37**, 123–150.
- F. van Rantwijk and R. A. Sheldon, *Chem. Rev.*, 2007, **107**, 2757–2785.
- M. Garcia, N. Gathergood and P. Scammells, *Green Chem.*, 2005, **7**, 9–14.
- N. Gathergood, M. Garcia and P. Scammells, *Green Chem.*, 2004, **6**, 166–175.
- N. Gathergood, P. Scammells and M. Garcia, *Green Chem.*, 2006, **8**, 156–160.
- J. Ranke, S. Stolte, R. Stoermann, J. Arning and B. Jastorff, *Chem. Rev.*, 2007, **107**, 2183–2206.
- M. Deetlefs and K. Seddon, *Chim. Oggi*, 2006, **24**, 16–23.
- P. Scammells, J. Scott and R. Singer, *Aust. J. Chem.*, 2005, **58**, 155–169.
- U. Kragl, M. Eckstein and N. Kaftzik, *Curr. Opin. Biotechnol.*, 2002, **13**, 565–571.
- K. Docherty and C. J. Kulpa, *Green Chem.*, 2005, **7**, 185–189.
- J. Ranke, K. Moelter, F. Stock, U. Bottin-Weber, J. Poczobutt, J. Hoffmann, B. Ondruschka, J. Filser and B. Jastorff, *Ecotox. Environ. Saf.*, 2004, **58**, 396–404.
- R. Sheldon, *Chem. Commun.*, 2001, 2399.
- T. Welton, *Chem. Rev.*, 1999, **99**, 2071–2084.
- A. J. J. Straathof, *Biotechnol. Prog.*, 2003, **19**, 755–762.
- W. Hussain, D. Pollard and G. Lye, *Biocatal. Biotransform.*, 2007, **25**, 443–452.
- S. Bräutigam, S. Bringer-Meyer and D. Weuster-Botz, *Tetrahedron: Asymmetr.*, 2007, **18**, 1883–1887.
- H. Pfruender, R. Jones and D. Weuster-Botz, *J. Biotechnol.*, 2006, **124**, 182–190.
- S. Cull, J. Holbrey, V. Vargas-Mora, K. Seddon and G. Lye, *Biotechnol. Bioeng.*, 2000, **69**, 227–233.
- J. Howarth, P. James and J. Dai, *Tetrahedron Lett.*, 2001, **42**, 7517–7519.
- W. Lou, M. Zong and T. Smith, *Green Chem.*, 2006, **8**, 147–155.
- H. Pfruender, M. Amidjojo, U. Kragl and D. Weuster-Botz, *Angew. Chem., Int. Ed.*, 2004, **43**, 4529–4531.
- R. Cornmell, C. Winder, S. Schuler, R. Goodacre and G. Stephens, *Green Chem.*, 2008, **10**, 685–691.
- A. Lenourry, J. M. Gardiner and G. Stephens, *Biotechnol. Lett.*, 2005, **27**, 161–165.
- R. Leon, P. Fernandes, H. Pinheiro and J. Cabral, *Enzyme Microb. Technol.*, 1998, **23**, 483–500.
- G. Salter and D. Kell, *Crit. Rev. Biotechnol.*, 1995, **15**, 139–177.
- C. Laane, S. Boern, K. Vos and C. Veeger, *Biotechnol. Bioeng.*, 1987, **30**, 81–87.
- D. Weuster-Botz, *Chem. Rev.*, 2007, **7**, 334–340.
- S. Park and R. Kazlauskas, *Curr. Opin. Biotechnol.*, 2003, **14**, 432–437.
- H. Mang, J. Gross, M. Lara, C. Goessler, H. E. Schoemaker, G. M. Guebitz and W. Kroutil, *Tetrahedron*, 2007, **63**, 3350–3354.
- A. Adams, J. Demyttenaere and N. De Kimpe, *Food Chem.*, 2003, **80**, 525–534.
- R. J. Steffan and K. R. Mcclay, in *US Pat.*, 10/088991, United States of America, 2007.
- D. Pamperin, H. Hopf, C. Syldatk and M. Pietzsch, *Tetrahedron: Asymmetr.*, 1997, **8**, 319–325.
- F. R. Bettley, *Br. J. Dermatol.*, 1968, **80**, 635–642.
- L. Angermaier and H. Simon, *Hoppe-Seyler's Z. Physiol. Chem.*, 1983, **364**, 961–975.
- L. Angermaier and H. Simon, *Hoppe-Seyler's Z. Physiol. Chem.*, 1983, **364**, 1653–1663.
- T. P. Chirpich, V. Zappia, R. N. Costlow and H. A. Barker, *J. Biol. Chem.*, 1970, **245**, 1778–1789.
- O. Dipeolu, J. Gardiner and G. Stephens, *Biotechnol. Lett.*, 2005, **27**, 1803–1807.
- A. Czarnik, *Acc. Chem. Res.*, 1996, **29**, 112–113.
- R. N. Patel, *Coord. Chem. Rev.*, 2007.
- D. Lide, *CRC handbook of chemistry and physics: a ready-reference book of chemical and physical data*, Boca Raton, FL.; London, CRC, 2000.
- F. Ganske and U. Bornscheuer, *Biotechnol. Lett.*, 2006, **28**, 465–469.
- K. R. Seddon, A. Stark and M. Torres, *Pure Appl. Chem.*, 2000, **72**, 2275–2287.
- H. Giesel and H. Simon, *FEBS Lett.*, 1983, **123**, 107–110.
- D. H. Bergey, R. E. Buchanan and N. E. Gibbons, *Bergey's manual of determinative bacteriology- 8th edition*, Williams & Wilkins, Baltimore, 1974.
- H. A. Barker, *Annu. Rev. Biochem.*, 1981, **50**, 23–40.
- M. Martinez, N. Kelessidou, Z. Law, J. Gardiner and G. Stephens, *Anaerobe*, 2008, **14**, 55–60.

A high throughput screen to test the biocompatibility of water-miscible ionic liquids

Martin Rebros,^a H.Q. Nimal Gunaratne,^b Jamie Ferguson,^b Kenneth R. Seddon^b and Gillian Stephens^{*a}

Received 12th September 2008, Accepted 12th December 2008

First published as an Advance Article on the web 23rd January 2009

DOI: 10.1039/b815951c

The Agar Diffusion test has been used for many years for testing antibiotic susceptibility in clinical laboratories. We wish to report that this simple, rapid test can also be applied to screen ionic liquids for toxicity to microorganisms. We screened 14 water miscible ionic liquids for toxicity for *Clostridium butyricum* using the test, and compared the results with EC₅₀ values calculated from measurements of growth rates in the presence of the ionic liquids. The Agar Diffusion test could be used reliably to identify ionic liquids which were toxic to *C. butyricum*, with EC₅₀ values below 0.034 M, and relatively non-toxic structures, with EC₅₀ values above 0.063 M. Therefore, the Agar Diffusion test can be used with confidence to distinguish between toxic and biocompatible ionic liquids.

Introduction

Ionic liquids have enormous potential for use as safer and more versatile alternatives to conventional organic solvents in chemical and biocatalytic processes.^{1–3} There are literally millions of possible ionic liquid structures, and this provides unprecedented opportunities to design the solvent to match the needs of the process with exquisite precision.⁴ Despite these attractions, there is a growing realisation that ionic liquids can be just as toxic^{4,6,7} as any other class of chemicals.^{5,8} Therefore, it is crucial to ensure that new ionic liquids are tested for toxicity before contemplating their use in industrial processes.

Unfortunately, it is still difficult and time-consuming to measure the toxicity of ionic liquids. The industry standard tests for toxicity include EC₅₀ and IC₅₀ measurements, using a range of unicellular and multicellular organisms.^{6,8–23} The studies are then followed up with more detailed analysis, including histological effects, mutagenicity and metabolic fate.^{24–27} The methods for EC₅₀ and IC₅₀ measurements are prescribed by the regulatory agencies (e.g. ref. 28) and give accurate, reliable results, although they are rather slow and require significant operator expertise. Therefore, the tests are most suitable for assessing the toxicity of materials that have already been selected as strong candidates for process development. They are much less suitable for initial testing of completely new, uncharacterised structures. In these cases, it would be better to have simpler, cheaper, first pass screens to measure toxicity, so that unpromising structures can be rejected at the earliest possible stage.

A number of alternative screens are available, although each has disadvantages. In general, microorganisms are used as

indicator organisms because they can be grown quickly in inexpensive media using simple, widely available equipment. The simplest methods are minimum inhibitory concentration (MIC) or minimal biocidal concentration (MBC) tests.^{29–33} Further detail can be obtained by measuring growth rates,^{29,34,35} and biocidal effects can be measured using dyes³⁶ or viable counts.^{37–39} Membrane integrity measurements are quicker and require very small quantities of test material,^{36,40} but may give rather high values due to changes in cellular morphology in the presence of ionic liquids.⁴¹ Luminometry-based screens are also available, but these depend on the availability of specialised instrumentation and are restricted to specific luminescent species of bacteria.^{10,15,22,23} All of these tests require several steps to grow the organisms and to prepare samples for analysis, and considerable operator skill is needed to obtain reliable results.

In this paper, we describe the use of the Agar Diffusion method for testing the toxicity of ionic liquids towards microorganisms. The Agar Diffusion method is an extremely well established test for the sensitivity of microorganisms to antibiotics (e.g. ref. 42–46) and other toxic compounds,⁴⁷ and is used very widely in clinical laboratories. The popularity of the method is due to its simplicity. It involves soaking the test substance into filter paper discs and then placing them on lawns of microbial cells spread on the surface of agar plates. The microbial lawns can be prepared quickly and easily from a single pre-culture, without the need for dilution. The plates are incubated to allow the cells to grow, and a gradient of the test substance is established by diffusion through the agar or transport over the surface. If the test substance is inhibitory, a clear zone with no growth appears around the disc, and the diameter is related to toxicity. The results are best analysed qualitatively simply by visual inspection,⁴² but limited quantitative information can be obtained by measuring the size of the inhibition zone. This can be done using nothing more complex than a ruler, although automation is also possible.⁴⁴ Thus, the materials are cheap, the equipment is simple and only the most basic microbiological training is needed.

^aManchester Interdisciplinary Biocentre, University of Manchester, 131 Princess Street, Manchester, UK M1 7DN. E-mail: gillian.stephens@manchester.ac.uk; Fax: +44 161 3068918; Tel: +44 161 3064377

^bQueen's University Ionic Liquid Laboratories (QUILL), The Queen's University of Belfast, David Keir Building, Stranmillis Road, Belfast, BT9 5AG, UK. E-mail: k.seddon@qub.ac.uk; Fax: +44 28 90665297; Tel: +44 28 90975420

Here, we show that the Agar Diffusion method can be used as a first stage screen for rapid detection of ionic liquid toxicity using as little as 5 μl of ionic liquid. We used the obligately anaerobic bacterium, *Clostridium butyricum*, for this initial study. We are interested in *C. butyricum* because it can ferment glycerol to 1,3-propanediol,^{48–50} and we wished to develop design rules for non-toxic ionic liquids to extract 1,3-propanediol from the fermentation broths. We ran Agar Diffusion tests with 14 ionic liquids. We validated the screen by measuring growth rates and calculating EC_{50} values for comparison with the Agar Diffusion tests. The screen is now ready for deployment for preliminary, low cost, high throughput screening of new ionic liquids for toxicity.

Experimental

Organism and culture conditions

Clostridium butyricum was re-isolated from the freeze-dried culture of DSM10703 provided by Deutsche Sammlung von Mikroorganismen und Zellkulturen GmbH, since the culture produced two colony morphologies on RCM agar. The larger, spreading colonies were selected for use, since they produced 1,3-propanediol more quickly than the small, compact colonies (data not shown). Cultures were grown at 30 °C in an anaerobic cabinet (DW Scientific) except where stated, and stock cultures were maintained on Reinforced Clostridial Medium (RCM) agar (Sigma). Experimental cultures were grown in Y5 medium (modified from ref. 49) and contained (per l): glycerol (20 g), KH_2PO_4 (5 g), K_2HPO_4 (5 g), $\text{CoCl}_2 \cdot 6\text{H}_2\text{O}$ (0.01 g), acetic acid (2 g), and yeast extract (3 g). The pH was adjusted to 7 with 8 M NH_4OH and sterilized anaerobically⁵¹ $\text{MgSO}_4 \cdot 7\text{H}_2\text{O}$ (0.2 g) was autoclaved separately, and $\text{FeSO}_4 \cdot 7\text{H}_2\text{O}$ (0.01 g) was filter sterilized anaerobically, and the medium components were mixed in the anaerobic cabinet.

Agar Diffusion tests

Agar Diffusion tests were prepared by inoculating RCM liquid medium (Fisher) with a single colony and growing the culture for 12–20 h at 150 rpm (using an IKA VXR Vibrax shaker). Undiluted culture (200 μl) was spread on RCM agar to prepare a lawn, and 1–4 filter discs were placed with even spacing on the agar plate after soaking them in different ionic liquids. The filter discs (diameter 7 mm; Whatman 3MM) were cut with an office hole punch and autoclaved in screw capped bottles. The discs were then transferred aseptically to sterile Eppendorf tubes using forceps which had been autoclaved in Falcon tubes and kept in the tube between transfers. The Eppendorf tubes and filter discs were weighed, and the ionic liquids were added aseptically using an automatic pipette set to 5 μl . The tubes, filter and ionic liquids were reweighed, and then the discs were placed on the agar. The tubes and residual ionic liquids were reweighed again, and the weight of ionic liquid soaked into the disc was calculated. The lawns of *C. butyricum* were cultivated overnight, with the Petri dish upside down (as usual), because the filters adhered to the agar. After incubation, the inhibition zones were measured. The ionic liquids were proved to be self sterile, since there was no growth when filter discs were incubated on uninoculated RCM

agar. In addition, all cultures were checked for contaminating colonies after growth.

Measurement of growth rates and calculation of EC_{50} values

Growth rates of triplicate cultures of *C. butyricum* were measured in the presence and absence of ionic liquids in 96 well plates. Ionic liquids were added to sterile Eppendorf tubes on a tared balance using an automatic pipette set to 200 μl and the weight of ionic liquid was recorded. The Eppendorf tubes were transferred to the anaerobic cabinet, and sterile, anaerobic Y5 medium was added to produce a solution containing approximately 50% (v/v) of the ionic liquid. The solution was then serially diluted in Y5 medium and aliquots of the dilutions (40 μl) were added to 96 well plates. *C. butyricum* was inoculated into Y5 medium (2% v/v), and aliquots (200 μl) were added to the wells. The cultures were then sealed with Breathe Easy film (R.B. Radley and Co.) and transferred into a plate reader (Nephelostar; BMG Labtech Ltd.). Anaerobic conditions were maintained by placing the plate reader in an Atmos bag (Sigma Aldrich) and flushing with N_2 for 2 h prior to use. The 96 well plates were quickly transferred into the bag, the bag was resealed and then flushed with N_2 throughout the experiment (half a cylinder per experiment). The cultures were incubated in the plate reader at 30 °C with orbital shaking (shaking width, 4 mm). The plate reader operates automatically, and was set to interrupt the shaking every 1200 s so that light scattering could be measured (2 s/well with the period delay set at 0.5 s) and then resume shaking. The gain was set at 40, with the laser beam focus set at 2.5 mm. The incubation and measurement regime were optimized by comparing growth rates in the plate reader and in conventional cultures, in which growth was measured by conventional OD measurements. Maximum specific growth rates were calculated in the exponential growth phase, using the equation, $\ln N_t/N_0 = \mu t$, where N_t is light scattering units (arbitrary values measured in the nephelometer) at time t (h), and μ is the growth rate (h^{-1}). The growth rates in the presence of the ionic liquids were calculated as a percentage of the growth rate in control cultures without ionic liquid and the mean values are reported. EC_{50} values were calculated from the plots of percentage growth inhibition (y) against ionic liquid concentration (x) by linear regression of the linear parts of the plots, and solving the equation $y = mx + c$ to find the value of x (EC_{50}) when y is equal to 50%, where m is the gradient and c the intercept on the ordinate.

Synthesis of ionic liquids

All but four of the ionic liquids used in this study (Table 1) were known, well characterised materials whose syntheses have been described elsewhere; the four novel ionic liquids were $[\text{N}_{2,4}(\text{C}_2\text{OH})_2][\text{C}_2\text{OSO}_3]$, $[\text{N}_{1,1,2,4}][\text{C}_2\text{OSO}_3]$, $[\text{N}_{2,4}(\text{C}_2\text{OH})_2][\text{N}(\text{CN})_2]$ and $[\text{N}_{1,1,4}(\text{C}_2\text{OH})][\text{N}(\text{CN})_2]$, and the details of their preparation will be published elsewhere, together with the analytical data. 1-Alkyl-3-methylimidazolium halides were synthesised by treating 1-methylimidazole with the appropriate haloalkane.^{52,53} Dicyanamide ionic liquids were synthesized by treating equimolar quantities of silver dicyanamide with the appropriate 1-alkyl-3-methylimidazolium or tetraalkylammonium halides in aqueous solution and then

Table 1 Ionic liquids used in this study

Name	Abbreviation	Structure
1-Butyl-methylimidazolium bromide	[C ₄ mim]Br	
1-Hexyl-methylimidazolium bromide	[C ₆ mim]Br	
1-Octyl-methylimidazolium bromide	[C ₈ mim]Br	
1-Butyl-methylimidazolium iodide	[C ₄ mim]I	
1-Hexyl-methylimidazolium iodide	[C ₆ mim]I	
1-Ethyl-methylimidazolium ethylsulfate	[C ₂ mim][C ₂ OSO ₃]	
1-Butyl-methylimidazolium methylsulfate	[C ₄ mim][C ₁ OSO ₃]	
<i>N</i> -Butyl- <i>N</i> -ethyl- <i>N,N</i> -di(2-hydroxyethyl)-ammonium ethylsulfate	[N _{2,4} (C ₂ OH) ₂][C ₂ OSO ₃]	
<i>N</i> -Butyl- <i>N</i> -ethyl- <i>N,N</i> -dimethylammonium ethylsulfate	[N _{1,1,2,4}][C ₂ OSO ₃]	
1-Ethyl-3-methylimidazolium 3,6,9-trioxodecylsulfate	[C ₂ mim][C ₁ OC ₂ OC ₂ OSO ₃]	
<i>N</i> -Butyl- <i>N</i> -ethyl- <i>N,N</i> -di(2-hydroxyethyl)-ammonium Dicyanamide	[N _{2,4} (C ₂ OH) ₂][N(CN) ₂]	
1-Butyl-3-methylimidazolium dicyanamide	[C ₄ mim][N(CN) ₂]	
<i>N</i> -Butyl- <i>N</i> -(2-hydroxyethyl)- <i>N,N</i> -dimethylammonium dicyanamide	[N _{1,1,4} (C ₂ OH)][N(CN) ₂]	
1-Butyl-1-methylpyrrolidinium dicyanamide	[bmpyrr][N(CN) ₂]	

removing the precipitated silver halide by filtration.^{54,55} The removal of water from the filtrate under reduced pressure yielded the appropriate dicyanamide ionic liquid. All ionic liquids were characterised by standard analytical tools such as NMR, MS, *etc.* $[\text{N}_{2,4}(\text{C}_2\text{OH})_2][\text{C}_2\text{OSO}_3]$ was synthesized by adding diethylsulfate (0.2 mol) dropwise to *N*-butyldiethanolamine (0.2 mol) and stirring at room temperature overnight. No solvent was used. The resulting viscous ionic liquid was shown to have undergone a complete and clean reaction by ^1H NMR spectroscopy. $[\text{N}_{1,12,4}][\text{C}_2\text{OSO}_3]$ was synthesized by adding diethylsulfate (0.2 mol) dropwise to *N,N*-dimethylbutylamine (0.2 mol), with initial cooling in ice, followed by warming to room temperature and overnight stirring. The resulting viscous ionic liquid was shown to have undergone a complete and clean reaction by ^1H NMR spectroscopy.

Both $[\text{N}_{2,4}(\text{C}_2\text{OH})_2][\text{N}(\text{CN})_2]$ and $[\text{N}_{1,14}(\text{C}_2\text{OH})][\text{N}(\text{CN})_2]$ were prepared by mixing equimolar aqueous solutions of corresponding [cation]Br and silver dicyanamide.^{54,55} The resulting slurry was stirred in the dark for 18 h, and then silver (I) bromide was collected by filtration to give a clear aqueous filtrate. Water was removed under reduced pressure and the resulting ionic liquids were dried at 60–70 °C under very high vacuum (0.1 mm). The halide content in the dicyanamide ionic liquids was determined to be in the range 1.1–1.46% (w/w).

Results and discussion

Agar Diffusion tests

We synthesized a series of water-miscible ionic liquids (Table 1) and tested them for toxicity using the Agar Diffusion method. Water-miscible ionic liquids were chosen to ensure that they would dissolve in the agar and diffuse through it, thus simplifying the interpretation of the data in this pilot study. A wide range of structural classes was used, since the purpose of this study was to develop a new high throughput screen for toxicity and it was necessary to establish that the method would be generally applicable.

Agar diffusion tests were set up by placing filter paper discs soaked in ionic liquids onto lawns of *Clostridium butyricum* cells on agar plates. Ionic liquids can be extremely viscous, and so cannot be pipetted accurately. Therefore, we set an automatic pipette to 5 μl , and pipetted the ionic liquids onto sterile filter discs in vials, which had both been pre-weighed together. The volume was small enough to ensure that all of the added ionic liquid soaked into the filters. We then weighed the filter discs and vials again to calculate the weight of added ionic liquid, and placed the filters aseptically onto the lawn of cells. The cultures were then incubated overnight. If the ionic liquid was non-inhibitory, the cells grew and produced a confluent lawn over the entire surface of the agar. If the ionic liquid was toxic, there was a zone of inhibition near to the filter disc and a zone of confluent growth at the outer margins of the agar plate (Fig. 1). The size of the inhibition zones varied with the structure of the ionic liquid (Table 2). The 1-alkyl-3-methylimidazolium halides produced relatively large inhibition zones, indicating that they were toxic. The size of the inhibition zone was larger for the iodides than the respective bromides, and the size increased with alkyl chain length for both the bromides and the

Table 2 Toxicity of ionic liquids determined by the Agar Diffusion method

Ionic liquid	Weight of ionic liquid on filter paper disc (mg)	Size of inhibition zone (mm)
$[\text{C}_4\text{mim}]\text{Br}$	7.9	0.5
$[\text{C}_6\text{mim}]\text{Br}$	6.6	2.25
$[\text{C}_8\text{mim}]\text{Br}$	6.2	9
$[\text{C}_4\text{mim}]\text{I}$	8.4	1.5
$[\text{C}_6\text{mim}]\text{I}$	5.4	6
$[\text{C}_4\text{mim}][\text{C}_1\text{OSO}_3]$	8.8	2.25
$[\text{C}_4\text{mim}][\text{N}(\text{CN})_2]$	8.5	1.5
$[\text{C}_2\text{mim}][\text{C}_2\text{OSO}_3]$	7.6	0
$[\text{C}_2\text{mim}][\text{C}_1\text{OC}_2\text{OC}_2\text{OC}_2\text{OSO}_3]$	13.6	0
$[\text{N}_{2,4}(\text{C}_2\text{OH})_2][\text{C}_2\text{OSO}_3]$	6.1	0
$[\text{N}_{1,12,4}][\text{C}_2\text{OSO}_3]$	6	0
$[\text{N}_{2,4}(\text{C}_2\text{OH})_2][\text{N}(\text{CN})_2]$	5.4	0
$[\text{N}_{1,14}(\text{C}_2\text{OH})][\text{N}(\text{CN})_2]$	7.4	0
$[\text{bmpyrr}][\text{N}(\text{CN})_2]$	5.3	0.5

C. butyricum lawns were prepared on agar plates. Ionic liquids (nominal volume, 5 μl) were added to filter paper discs and the actual weights of the ionic liquid were recorded. The filter discs were then placed on the 5 lawns and the cultures were incubated for 16–20 h. The size of the inhibition zones (indicated as B in Fig. 1) were then recorded.

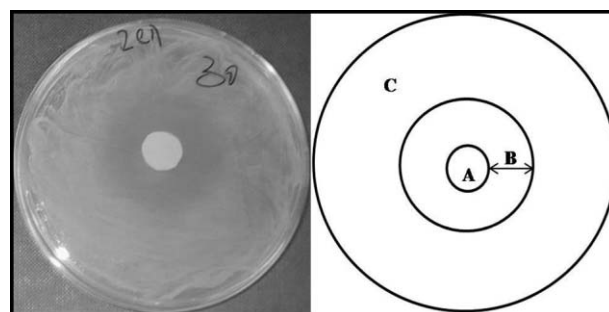


Fig. 1 Example of an Agar Diffusion test. A lawn of *C. butyricum* was spread on an agar plate (9 cm diameter). The ionic liquid was soaked onto a filter paper disc (A), which was placed on the lawn of cells (C). The plate was incubated overnight (16–20 h), the diameter of the inhibition zone was measured and the plate was photographed. The zone of inhibition is indicated (B).

iodides. $[\text{C}_4\text{mim}][\text{N}(\text{CN})_2]$ and $[\text{C}_4\text{mim}][\text{C}_1\text{OSO}_3]$ also produced inhibition zones. By contrast, $[\text{C}_2\text{mim}][\text{C}_2\text{OSO}_3]$ and $[\text{C}_2\text{mim}][\text{C}_1\text{OC}_2\text{OC}_2\text{OC}_2\text{OSO}_3]$ did not produce inhibition zones, suggesting that the decreased alkyl chain length of the cation and increased chain length of the anion combined to make the ionic liquids non-toxic. Similarly, $[\text{N}_{2,4}(\text{C}_2\text{OH})_2][\text{C}_2\text{OSO}_3]$ and $[\text{N}_{1,12,4}][\text{C}_2\text{OSO}_3]$ seemed to be non-toxic. $[\text{N}_{2,4}(\text{C}_2\text{OH})_2][\text{N}(\text{CN})_2]$ and $[\text{N}_{1,14}(\text{C}_2\text{OH})][\text{N}(\text{CN})_2]$ also appeared to be non-toxic, but $[\text{bmpyrr}][\text{N}(\text{CN})_2]$ was toxic. Thus, ionic liquids seemed to be less toxic when they were made with non-cyclic tetraalkylammonium cations rather than alkylmethylimidazolium cations, confirming and extending findings made with other organisms.¹³

Effect of ionic liquids on the growth rate of *C. butyricum*

The Agar Diffusion test has been thoroughly validated for antibiotic testing, and the diameter of the zone of inhibition is known to be related to the potency of the antibiotic.⁵⁶ Therefore, we tested the hypothesis that the size of the inhibition zones

produced by ionic liquids may also be related to toxicity. For microbial cells, the most reliable quantitative measure of the toxicity of a substance is to determine the growth rates of the cells over a range of concentrations of the toxic substance.⁵⁷ The data can then be used to calculate an EC_{50} value. Therefore, we grew *C. butyricum* at various concentrations of each ionic liquid in 96 well plates and measured growth rates by high throughput nephelometry.

Initially, we tested alkylmethylimidazolium halides, to benchmark our data against previously published work.³⁰ In general, the ionic liquids had little effect on growth at the lowest concentrations tested, and a threshold concentration had to be reached before inhibition started to become significant, as noted for other organisms^{9,11,15,21} (Fig. 2; we did not test $[C_4mim]Br$ at concentrations below 1.6 g l^{-1} [7.3 mM], and this may explain the absence of a toxicity threshold in this case). After that, the growth rate appeared to decrease linearly with increasing concentration, although the growth rate decreased so quickly with concentration for $[C_8mim]Br$ and $[C_6mim]I$ that it was not possible to collect enough data points to confirm linearity in these two cases. There was considerable variation in the rate at which the growth rate decreased beyond the toxicity threshold, and in the ionic liquid concentrations that caused complete growth inhibition. Thus, $[C_8mim]Br$ caused complete inhibition when the concentration was only 0.73 g l^{-1} (2.7 mM), compared with 6.9 g l^{-1} (28 mM) for $[C_6mim]Br$ and 12.9 g l^{-1} (59 mM) for $[C_4mim]Br$. Therefore, the ionic liquids became less toxic as the alkyl chain length decreased, confirming the Agar Diffusion tests, and previous findings by others.^{11,13–19,21,30,33}

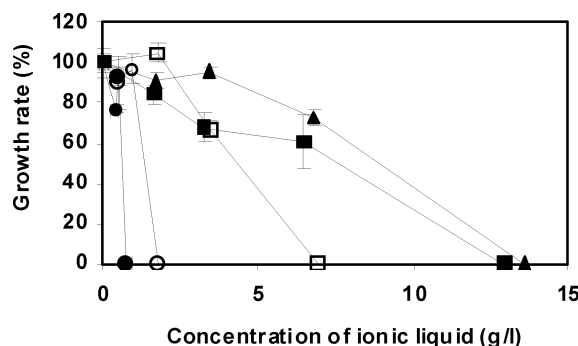


Fig. 2 Growth of *C. butyricum* in the presence of ionic liquids with halide anions. *C. butyricum* was grown in the presence of various concentrations of $[C_8mim]Br$ (●), $[C_4mim]Br$ (■), $[C_4mim]I$ (▲), $[C_6mim]I$ (○), or $[C_6mim]Br$ (□). The growth rates were determined and are expressed as a percentage of the growth rate of a control culture grown without ionic liquids. The data are the mean of 3 replicates and the error bars show the standard deviation.

The iodides seemed to be more toxic than the bromides, since $[C_6mim]I$ was completely inhibitory at 1.77 g l^{-1} (6 mM). However, $[C_4mim]I$ did not become completely inhibitory until the concentration reached 13.6 g l^{-1} (51 mM), which is similar to $[C_4mim]Br$. $[C_4mim][C_1OSO_3]$ seemed to inhibit growth as strongly as the corresponding halides, since complete inhibition was observed at 12.5 g l^{-1} (50 mM ; Fig. 3). Therefore, these anions seemed to have less effect on toxicity than the cation, as observed with other organisms.^{12,13,15,19} However, $[C_4mim][N(CN)_2]$ was more toxic (complete inhibition at 5.56 g l^{-1} ; 27 mM ; Fig. 4),

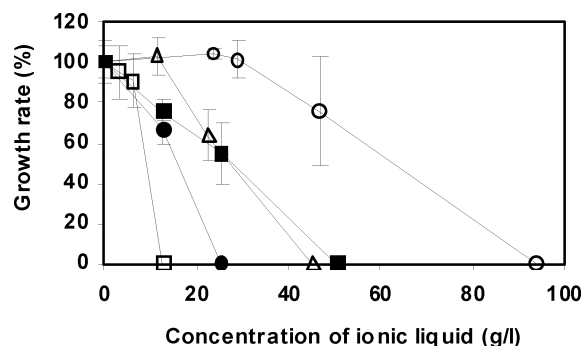


Fig. 3 Growth of *C. butyricum* in the presence of ionic liquids with sulfate anions. *C. butyricum* was grown in the presence of various concentrations of $[C_2mim][C_1OC_2OC_2OC_2OSO_3]$ (■), $[C_4mim][C_1OSO_3]$ (□), $[N_{2,4}(C_2OH)_2][C_2OSO_3]$ (○), $[C_2mim][C_2OSO_3]$ (●), or $[N_{1,1,2,4}][C_2OSO_3]$ (△). The growth rates were determined and are expressed as a percentage of the growth rate of a control culture grown without ionic liquids. The data are the mean of 3 replicates and the error bars show the standard deviation.

confirming that the anion can still have significant effects on toxicity, depending on its structure.^{17,19} The halides and the C_4mim^+ -containing ionic liquids all produced inhibition zones in the Agar Diffusion tests.

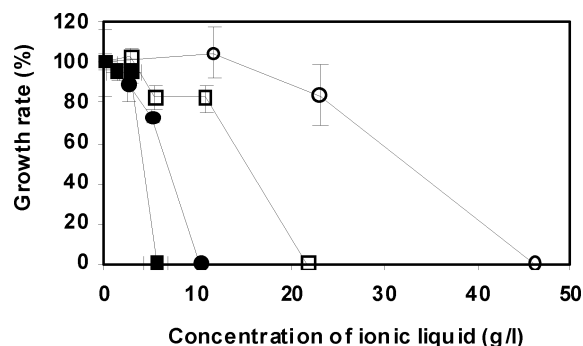


Fig. 4 Growth of *C. butyricum* in the presence of ionic liquids with dicyanamide anions. *C. butyricum* was grown in the presence of various concentrations of $[C_4mim][N(CN)_2]$ (■), $[bmpyr][N(CN)_2]$ (●), $[N_{1,1,4}C_2OH][N(CN)_2]$ (□), or $[N_{2,4}(C_2OH)_2][N(CN)_2]$ (○). The growth rates were determined and are expressed as a percentage of the growth rate of a control culture grown without ionic liquids. The data are the mean of 3 replicates and the error bars show the standard deviation.

The ethylsulfates were relatively non-toxic (Fig. 3). Thus, $[C_2mim][C_2OSO_3]$, $[N_{1,1,2,4}][C_2OSO_3]$ and $[C_2mim][C_1OC_2OC_2OC_2OSO_3]$ did not cause complete inhibition until 25.5 (108 mM), 45.4 (178 mM) and 50.5 g l^{-1} (142 mM), respectively. $[N_{2,4}(C_2OH)_2][C_2OSO_3]$ was the least toxic ionic liquid used in this study, since it did not cause complete growth inhibition until the concentration was increased to 93.9 g l^{-1} (298 mM). It had no effect on the growth rate up to 28.9 g l^{-1} (92 mM), and the cells could still grow in ionic liquid concentrations as high as 46.9 g l^{-1} (149 mM). None of the ethylsulfates caused an inhibition zone in the Agar Diffusion tests.

$[N_{2,4}(C_2OH)_2][N(CN)_2]$ was also the least toxic of the dicyanamides, since the cells could still grow at 23.1 g l^{-1} (90 mM), and complete growth inhibition was not observed

until the concentration reached 46.2 g l^{-1} (180 mM ; Fig. 4). For other dicyanamides, the concentrations causing 100% growth inhibition decreased in the order $[\text{N}_{1,1,4}(\text{C}_2\text{OH})][\text{N}(\text{CN})_2]$ (21.7 g l^{-1} ; 102 mM) > $[\text{bmpyrr}][\text{N}(\text{CN})_2]$ (10.32 g l^{-1} ; 50 mM) > $[\text{C}_4\text{mim}][\text{N}(\text{CN})_2]$ (5.56 g l^{-1} ; 27 mM). Of these, $[\text{bmpyrr}][\text{N}(\text{CN})_2]$ and $[\text{C}_4\text{mim}][\text{N}(\text{CN})_2]$ produced inhibition zones in the Agar Diffusion test, whereas $[\text{N}_{1,1,4}(\text{C}_2\text{OH})][\text{N}(\text{CN})_2]$ did not.

Considering the growth rate data and the results of the Agar Diffusion test for all of the ionic liquids, it appears that toxicity needs to reach a certain threshold value before it can be detected by the Agar Diffusion test. Thus, an inhibition zone was only detected when the ionic liquids caused complete growth inhibition at concentrations at 59 mM or lower. However, the next highest concentration of ionic liquid causing complete growth inhibition was 90 mM ($[\text{N}_{2,4}(\text{C}_2\text{OH})_2][\text{N}(\text{CN})_2]$). Therefore, the threshold inhibitory concentration correlated with production of an inhibition zone actually lies between 59 – 102 mM , and a wider study including more ionic liquids will be needed to define the threshold concentration more precisely.

Validation of the Agar Diffusion test as a screen for ionic liquid toxicity

The final stage of this study was to validate the Agar Diffusion test as a toxicity screen, and to define the scope and limitations of the screen. The growth rate data provide an absolute measure of ionic liquid toxicity, and were, therefore, used to calibrate the Agar Diffusion test. Molar EC_{50} values were calculated using the data shown in Fig. 2–4 and were plotted as the abscissa, with the diameters of the inhibition zones in the Agar Diffusion tests as the ordinate (Fig. 5).

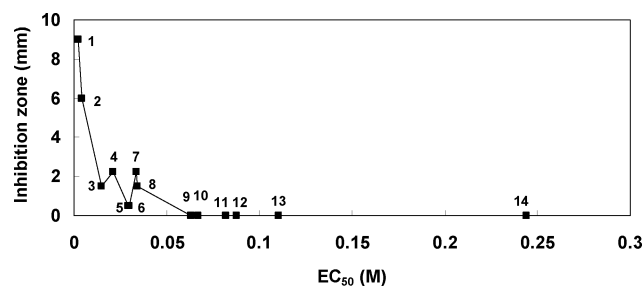


Fig. 5 Correlation between data from the Agar Diffusion tests and growth rate measurements. The diameters of the inhibition zones measured in the Agar Diffusion tests are plotted against the EC_{50} values for each ionic liquid. (1) $[\text{C}_8\text{mim}]\text{Br}$; (2) $[\text{C}_6\text{mim}]\text{I}$; (3) $[\text{C}_4\text{mim}][\text{N}(\text{CN})_2]$; (4) $[\text{C}_6\text{mim}]\text{Br}$; (5) $[\text{bmpyrr}][\text{N}(\text{CN})_2]$; (6) $[\text{C}_4\text{mim}]\text{Br}$; (7) $[\text{C}_4\text{mim}][\text{C}_1\text{OSO}_3]$; (8) $[\text{C}_4\text{mim}]\text{I}$; (9) $[\text{N}_{1,1,4}(\text{C}_2\text{OH})][\text{N}(\text{CN})_2]$; (10) $[\text{C}_2\text{mim}][\text{C}_2\text{OSO}_3]$; (11) $[\text{C}_2\text{mim}][\text{C}_1\text{OC}_2\text{OC}_2\text{OC}_2\text{OSO}_3]$; (12) $[\text{N}_{2,4}(\text{C}_2\text{OH})_2][\text{N}(\text{CN})_2]$; (13) $[\text{N}_{1,1,2,4}][\text{C}_2\text{OSO}_3]$; (14) $[\text{N}_{2,4}(\text{C}_2\text{OH})_2][\text{C}_2\text{OSO}_3]$. It should be noted that the EC_{50} values for $[\text{C}_8\text{mim}]\text{Br}$ and $[\text{C}_6\text{mim}]\text{I}$ were calculated from only 2 data points (Fig. 2), since the ionic liquids were too toxic to obtain enough data points to calculate EC_{50} accurately.

An inhibition zone was produced when the EC_{50} was 0.034 M or less. Therefore, the Agar Diffusion test seems to be a reliable method to identify toxic ionic liquids that inhibit growth of *C. butyricum* at low concentrations. Conversely, there was no inhibition zone when the EC_{50} was in the range 0.063 – 0.24 M (none of the ionic liquids tested had higher EC_{50} values). These

EC_{50} values were relatively high, so these ionic liquids were relatively non-toxic. Therefore, the absence of an inhibition zone in the Agar Diffusion test provides a reliable indication that the ionic liquids are sufficiently biocompatible to merit further investigation for use as green solvents. Conversely, the ionic liquids which do produce an inhibition zone are toxic enough to be rejected from further study.

Nevertheless, there are still some limitations. $[\text{C}_4\text{mim}]\text{I}$ had the highest EC_{50} value (0.034 M) of all the toxic ionic liquids that produced an inhibition zone, whereas $[\text{N}_{1,1,4}(\text{C}_2\text{OH})][\text{N}(\text{CN})_2]$ had the lowest EC_{50} value (0.063 M) of the ionic liquids that did not produce an inhibition zone. Therefore, the maximum EC_{50} value which correlates with production of an inhibition zone must lie between these two concentrations. Since none of the ionic liquids turned out to have EC_{50} values between these boundary values, a larger number of ionic liquids will need to be synthesized and tested to find ionic liquids with EC_{50} values between the two boundary values. This could be quite a lengthy process, because there are too few data points at present to predict which structures would have the desired range of EC_{50} values. Therefore, we recommend that the screen should be deployed in any case, so that the necessary data points will become available through use.

The original intention of this study was to develop a qualitative high throughput screen to distinguish between toxic and biocompatible ionic liquids. Whilst this has been achieved, it is worth examining the scope to use the Agar Diffusion test as a quantitative assay for toxicity. Fig. 5 seems to show an exponentially decaying correlation between size of the inhibition zone and the lowest EC_{50} values, for the most toxic ionic liquids. However, the correlation is rather poor for ionic liquids with intermediate toxicities, with EC_{50} values between 0.015 and 0.035 M , since there is considerable scatter in the data. This is hardly surprising, since it was very difficult to dispense defined volumes of ionic liquids onto the filter discs, due to their viscosity, and there was considerable variation in the weight of ionic liquids used in the tests. It is also possible that the diffusion of some ionic liquids may have been hindered by their viscosity, reaction with medium components or non-covalent interactions between the ionic liquids and the agar matrix. Given these potential sources of error, it is impressive that the plot (Fig. 5) shows even a reasonable correlation between the size of the inhibition zone and the EC_{50} values. Therefore, we conclude that the screen is not suitable for quantitative testing of ionic liquid toxicity. However, it may have some limited value to rank the toxicity of ionic liquids that produce an inhibition zone, provided that the data are used judiciously and confirmed in more detailed follow-up studies. It should be emphasised that, of course, it is not possible to rank the ionic liquids that do not produce an inhibition zone. Overall, we recommend that the Agar Diffusion test is best used as a first stage screen to distinguish between toxic ionic liquids and those which are sufficiently biocompatible to merit further investigation for use as green solvents.

Conclusions

The Agar Diffusion test has been validated as a method to identify toxic ionic liquids with EC_{50} values below 0.034 M .

This is immensely valuable, because such ionic liquids would be too toxic for exploitation in truly green processes, and so can be rejected from further evaluation with confidence. The screen has also been used to identify relatively non-toxic ionic liquids with EC₅₀ values above 0.063 M. Further work needs to be done to define the lower limit of EC₅₀ value correlated with the absence of an inhibition zone in the Agar Diffusion test. Nevertheless, the screen can still be used to short list structures that are sufficiently biocompatible for detailed toxicity testing, and further deployment of the screen will resolve the uncertainties very quickly. Indeed, deployment of the screen is recommended, because it is quick, cheap and easy to do, and does not require specialist equipment or significant microbiological expertise. Most importantly, it uses microlitre quantities of ionic liquids. Therefore, the Agar Diffusion test can be interfaced with high throughput synthetic methods as a first stage screen to select or reject new ionic liquids on the basis of their toxicity. This will allow selection of the most promising candidate structures at a much earlier stage of the characterisation process. This will greatly accelerate the development of next generation, non-toxic ionic liquids for use as truly “Green” solvents in chemical and biocatalytic processes.

Acknowledgements

We are grateful to the UK Engineering and Physical Science Research Council for financial support *via* grant number EP/E010687/1.

References

- M. Deetlefs and K. R. Seddon, *Chim. Oggi*, 2006, **24**, 16–23.
- N. V. Plechkova and K. R. Seddon, *Chem. Soc. Rev.*, 2008, **37**, 123–150.
- F. Van Rantwijk and R. A. Sheldon, *Chem. Rev.*, 2007, **107**, 2757–2785.
- K. R. Seddon, in *The International George Papatheodorou Symposium: Proceedings*, eds S. Boghosian, V. Dracopoulos, C. G. Kontoyannis, and G. A. Voyiatzis, Institute of Chemical Engineering and High Temperature Chemical Processes, Patras, 1999, pp. 131–135.
- H. Nishimura and S. Miyamoto, *Acta Anat.*, 1969, **74**, 121–124.
- A. S. Wells and V. T. Coombe, *Org. Process Res. Dev.*, 2006, **10**, 794–798.
- D. Zhao, Y. Liao and Z. Zhang, *Clean*, 2007, **35**, 42–48.
- J. Ranke, S. Stolte, R. Stoermann, J. Arning and B. Jastorff, *Chem. Rev.*, 2007, **107**, 2183–2206.
- C.-W. Cho, T. Phuong Thuy Pham, Y.-C. Jeon and Y.-S. Yun, *Green Chem.*, 2008, **10**, 67–72.
- K. M. Docherty and C. F. Kulpa, Jr., *Green Chem.*, 2005, **7**, 185–189.
- K. J. Kulacki and G. A. Lamberti, *Green Chem.*, 2008, **10**, 104–110.
- M. Matzke, S. Stolte, K. Thiele, T. Juffernholz, J. Arning, J. Ranke, U. Welz-Biermann and B. Jastorff, *Green Chem.*, 2007, **9**, 1198–1207.
- D. J. Couling, R. J. Bernot, K. M. Docherty, J. K. Dixon and E. J. Maginn, *Green Chem.*, 2006, **8**, 82–90.
- J. Ranke, A. Mueller, U. Bottin-Weber, F. Stock, S. Stolte, J. Arning, R. Stoermann and B. Jastorff, *Ecotoxicol. Environ. Saf.*, 2007, **67**, 430–438.
- J. Ranke, K. Molter, F. Stock, U. Bottin-Weber, J. Poczobutt, J. Hoffmann, B. Ondruschka, J. Filser and B. Jastorff, *Ecotoxicol. Environ. Saf.*, 2004, **58**, 396–404.
- A. Garcia-Lorenzo, E. Tojo, J. Tojo, M. Teijeira, F. J. Rodriguez-Berrocal, M. P. Gonzalez and V. S. Martinez-Zorzano, *Green Chem.*, 2008, **10**, 508–516.
- S. Stolte, J. Arning, U. Bottin-Weber, M. Matzke, F. Stock, K. Thiele, M. Uerdingen, U. Welz-Biermann, B. Jastorff and J. Ranke, *Green Chem.*, 2006, **8**, 621–629.
- S. Stolte, M. Matzke, J. Arning, A. Boeschen, W.-R. Pitner, U. Welz-Biermann, B. Jastorff and J. Ranke, *Green Chem.*, 2007, **9**, 1170–1179.
- S. Stolte, J. Arning, U. Bottin-Weber, A. Mueller, W.-R. Pitner, U. Welz-Biermann, B. Jastorff and J. Ranke, *Green Chem.*, 2007, **9**, 760–767.
- J. Salminen, N. Papaiconomou, R. A. Kumar, J.-M. Lee, J. Kerr, J. Newman and J. M. Prausnitz, *Fluid Phase Equilib.*, 2007, **261**, 421–426.
- C.-W. Cho, T. P. T. Pham, Y.-C. Jeon, K. Vijayaraghavan, W.-S. Choe and Y.-S. Yun, *Chemosphere*, 2007, **69**, 1003–1007.
- P. Luis, I. Ortiz, R. Aldaco and A. Irabien, *Ecotoxicol. Environ. Saf.*, 2007, **67**, 423–429.
- M. T. Garcia, N. Gathergood and P. J. Scammells, *Green Chem.*, 2005, **7**, 9–14.
- I. G. Sipes, G. A. Knudsen and R. K. Kuester, *Drug Metab. Dispos.*, 2008, **36**, 284–293.
- R. P. Swatloski, J. D. Holbrey, S. B. Memon, G. A. Caldwell, K. A. Caldwell and R. D. Rogers, *Chem. Commun.*, 2004, 668–669.
- C. Pretti, C. Chiappe, D. Pieraccini, M. Gregori, F. Abramo, G. Monni and L. Intorre, *Green Chem.*, 2006, **8**, 238–240.
- K. M. Docherty, S. Z. Hebbeler and C. F. Kulpa, Jr., *Green Chem.*, 2006, **8**, 560–567.
- OECD Guidelines for the Testing of Chemicals Section 2: Effects on Biotic Systems Test Nos. 201–227*, OECD.
- F. Ganske and U. Bornscheuer, *Biotechnol. Lett.*, 2006, **28**, 465–469.
- J. Pernak, K. Sobaszekiewicz and I. Mirska, *Green Chem.*, 2003, **5**, 52–56.
- J. M. Andrews, *J. Antimicrob. Chemother.*, 2001, **48**, 5–16.
- A. Cieniecka-Roslonkiewicz, J. Pernak, J. Kubis-Feder, A. Ramani, A. J. Robertson and K. R. Seddon, *Green Chem.*, 2005, **7**, 855–862.
- J. Pernak, I. Goc and I. Mirska, *Green Chem.*, 2004, **6**, 323–329.
- R. J. Cornmell, C. L. Winder, S. Schuler, R. Goodacre and G. Stephens, *Green Chem.*, 2008, **10**, 685–691.
- A. Latala, P. Stepnowski, M. Nedzi and W. Mroziak, *Aquat. Toxicol.*, 2005, **73**, 91–98.
- H. Pfruender, R. Jones and D. Weuster-Botz, *J. Biotechnol.*, 2006, **124**, 182–190.
- W. Hussain, D. J. Pollard and G. J. Lye, *Biocatal. Biotransform.*, 2007, **25**, 443–452.
- M. Matsumoto, K. Mochiduki, K. Fukunishi and K. Kondo, *Sep. Purif. Technol.*, 2004, **40**, 97–101.
- M. Matsumoto, K. Mochiduki and K. Kondo, *J. Biosci. Bioeng.*, 2004, **98**, 344–347.
- S. Bräutigam, S. Bringer-Meyer and D. Weuster-Botz, *Tetrahedron: Asymmetry*, 2007, **18**, 1883–1887.
- H. Pfruender, M. Midjojo, U. Kragl and D. Weuster-Botz, *Angew. Chem., Int. Ed.*, 2004, **43**, 4529–4531.
- Difco Manual*, Difco Laboratories, Detroit, 1953, pp. 331–337.
- J. J. Gavin, *Appl. Microbiol.*, 1957, **5**, 25–33.
- W. W. Davis and T. R. Stout, *Appl. Microbiol.*, 1971, **22**, 659–665.
- G. Vedel, M. Peyret, J. P. Gayral and P. Millot, *Res. Microbiol.*, 1996, **147**, 297–309.
- J. M. Andrews, *J. Antimicrob. Chemother.*, 2001, **48**, 43–57.
- H. Richardson, A. H. Emslie-Smith and B. W. Senior, *Appl. Microbiol.*, 1968, **16**, 1468–1474.
- S. Saint-Amans, P. Perlot, G. Goma and P. Soucaille, *Biotechnol. Lett.*, 1994, **16**, 831–836.
- M. Gonzalez-Pajuelo, I. Meynial-Salles, F. Mendes, J. C. Andrade, I. Vasconcelos and P. Soucaille, *Metab. Eng.*, 2005, **7**, 329–336.
- J. R. O'Brien, C. Raynaud, C. Croux, L. Girbal, P. Soucaille and W. N. Lanzilotta, *Biochemistry*, 2004, **43**, 4635–4645.
- H. Li, P. Williams, J. Micklefield, J. M. Gardiner and G. Stephens, *Tetrahedron*, 2004, **60**, 753–758.
- W. Kubo, T. Kitamura, K. Hanabusa, Y. Wada and S. Yanagida, *Chem. Commun.*, 2002, 374–375.
- P. Nockemann, K. Binnemans and K. Driesen, *Chem. Phys. Lett.*, 2005, **415**, 131–136.
- D. R. MacFarlane, S. A. Forsyth, J. Golding and G. B. Deacon, *Green Chem.*, 2002, **4**, 444–448.
- D. R. MacFarlane, J. Golding, S. Forsyth, M. Forsyth and G. B. Deacon, *Chem. Commun.*, 2001, 1430–1431.
- M. K. R. Chowdhury, R. Goswami and P. Chakrabarti, *Anal. Biochem.*, 1980, **108**, 126–128.
- S. J. Pirt, *Principles of microbe and cell cultivation*, Blackwell, Oxford, 1975, pp. 170–185.

The continuous self aldol condensation of propionaldehyde in supercritical carbon dioxide: a highly selective catalytic route to 2-methylpentenal†

James G. Stevens, Richard A. Bourne and Martyn Poliakoff*

Received 5th November 2008, Accepted 18th December 2008

First published as an Advance Article on the web 23rd January 2009

DOI: 10.1039/b819687g

The aldol reactions of propionaldehyde and butyraldehyde have been explored in supercritical CO₂, scCO₂, using an automated continuous flow reactor. The reaction was found to proceed over a variety of heterogeneous acidic and basic catalysts and with increased selectivity compared to using neat reactants.

Introduction

The aldol reaction is one of the most widely used reactions for C–C bond formation,^{1,2} yet it has several drawbacks from an environmental standpoint. Some of these issues have been highlighted by Mestres³ and Kelly *et al.*⁴ Industrially, the aldol synthesis has to overcome poor selectivity³ and the use of stoichiometric quantities of aqueous base with neutralisation and separation of the aldol product after completion of the reaction. This neutralisation generates large volumes of aqueous inorganic waste which require disposal.⁴

The continuous synthesis of 2-ethylhexanal (**5**), a commercially important aldol product, from crotonaldehyde (**1**) has been elegantly demonstrated by Baiker and co-workers,^{5,6} who performed the reaction continuously in scCO₂ over a palladium doped acidic resin (Amberlyst® 15) Scheme 1. Their process combined the aldol condensation and the hydrogenation of the unsaturated aldol product into a single process, hence driving the reaction equilibrium. They achieved >99% hydrogenation of **1** to **2** but the further conversion to **5** (*via* the hydrogenation

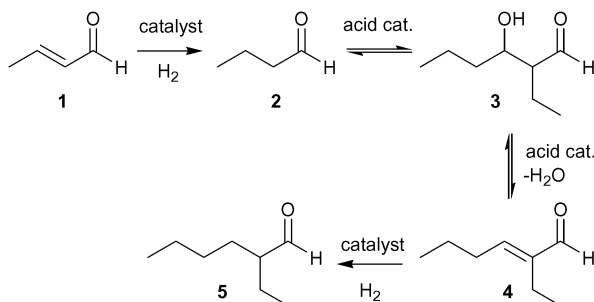
of the aldol intermediate, **4**) only reached a maximum of 70%. However, they were unable to produce **5** directly from **2** with high selectivity.

The work described in this paper aims to build on the work carried out by Baiker and co-workers by studying the aldol reaction further in scCO₂, and by exploring whether the use of hydrogen can be avoided and, hence, whether unsaturated aldols can be produced with high selectivity. Hydrogen acts as a driving force in Scheme 1 because **5** does not participate in the acid catalysed equilibrium steps, thus forcing the reaction towards the saturated aldehyde product.

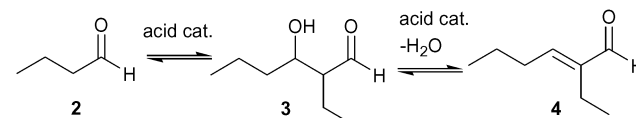
All our reactions were carried out on an automated continuous reactor⁷ which is described briefly in the Experimental section at the end of the paper. The reactor has on-line GC analysis. This allows the operator to program a series of reaction conditions, for example ramping of the temperature, while analytical data are collected automatically under computer control.

Proof of concept

The self aldol reaction of butyraldehyde (**2**) was explored over Amberlyst® 15 in continuous flow *without* the addition of hydrogen (Scheme 2) utilising scCO₂ as the reaction medium. This is the first stage of the reaction that Baiker and co-workers reported to give only 70% of the saturated aldehyde **5**. Fig. 1 shows the conversion of **2** and selectivity to **4** as a function of reactor temperature at 8 MPa pressure with fixed flow rates of both CO₂ and **2**. It can be seen that the conversion increases over the whole temperature range studied. A marked increase in the selectivity is also observed from 50 to 70 °C, but above this temperature the selectivity for **4** remains constant and high, >90%.



Scheme 1 The hydrogenation^{5,6} of crotonaldehyde (**1**) to yield butyraldehyde (**2**), with subsequent self aldol condensation to form 2-ethylhexenal (**4**) and hydrogenation of the unsaturated aldol product to form 2-ethylhexanal (**5**).



Scheme 2 Self aldol condensation of **2** showing both the aldol intermediate (**3**), and the unsaturated dehydration product (**4**).

School of Chemistry, The University of Nottingham, Nottingham, UK NG7 2RD. E-mail: Martyn.Poliakoff@nottingham.ac.uk; Fax: +44 (0)115 951 3508; Tel: +44 (0)115 951 3520

† Electronic supplementary information (ESI) available: Phase behaviour of propionaldehyde and 2-methylpentenal in supercritical carbon dioxide. See DOI: 10.1039/b819687g

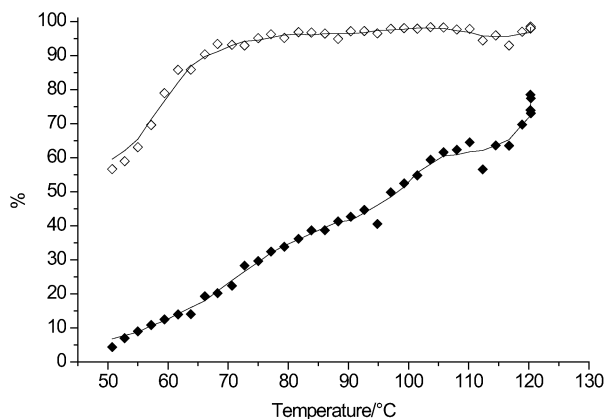
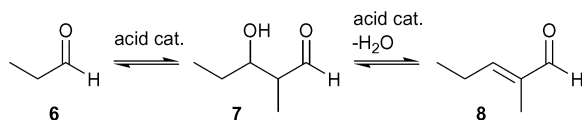


Fig. 1 The formation of the unsaturated butyraldehyde aldol product **4** in scCO_2 showing the temperature dependence of the conversion (◆) and selectivity (◇) of the self aldol condensation of **2** at flow rates of 0.1 mL min^{-1} of **2** and 1.0 mL min^{-1} of CO_2 at 8 MPa using a 10 mL reactor filled with Amberlyst® 15.

This result indicates that it is indeed possible to conduct the aldol reaction effectively in scCO_2 using a heterogeneous acid catalyst to produce the unsaturated aldol product in high yields.

Reaction of propionaldehyde

Following this successful proof of concept experiment with butyraldehyde, we have studied the self aldol condensation of propionaldehyde (**6**) to yield 2-methylpentenal (**8**) (Scheme 3).



Scheme 3 The self aldol condensation of propionaldehyde (**6**) showing both the aldol intermediate, 3-hydroxy-2-methylpentanal (**7**), and the unsaturated dehydration product 2-methylpentenal (**8**).

Aims and strategy

Compound **8** is a commercially important compound that is used widely in the fragrance, flavour,⁸ and cosmetic industries⁹ as well as being an important intermediate in the synthesis of pharmaceuticals^{10,11} and plasticisers.¹² Compound **8** is manufactured industrially by the aldol condensation of **6** in the presence of stoichiometric amounts of an aqueous base such as NaOH or KOH. Under optimum conditions, 99% conversion of **6** is achieved with 86% selectivity to **8**. Additionally, it has been demonstrated that the inclusion of an inert solvent can reduce the formation of any unwanted by-products.¹²

Mehnert *et al.* have studied the base catalysed aldol condensation of **6** in ionic liquids. They reported 100% conversion at 80 °C in 3 h with 83% selectivity for **8** using NaOH in [BMIM][PF₆].^{13,14} The solvent-free condensation of **6** has also been explored using a batch process at 100 °C using solid base catalysts by Sharma *et al.*¹⁵ Their optimum results were achieved using an activated Mg/Al hydrotalcite catalyst, giving 97% conversion of the **6** with 99% selectivity to **8**. The aldol condensation of **6** has also been carried out by Scheidt¹⁶ in the gas phase over lithium phosphate at 270 °C. This gave 95% selectivity to **8** at 32% conversion of **6**.

Table 1 Maximum yield of **8** achieved during temperature ramp over various catalysts from the self condensation of **6** at flow rates of 0.1 mL min^{-1} **6**, 1.0 mL min^{-1} CO_2 at 10 MPa (*base catalysts in italics*)

Catalyst	% Yield 8 ^a	% Sel. 8	Temp / °C
γ -Alumina	78	89	210
Amberlyst® 15	76	88	135
<i>Amberlyst® A26</i>	<i>10</i>	<i>83</i>	<i>180</i> ^b
Deloxan® ASP	49	77	125
<i>Magnesium oxide</i>	<i>39</i>	<i>95</i>	<i>240</i>
Nafion® SAC13	48	84	125
Purolite® CT175	63	81	155
<i>Supported NaOH</i>	<i>70</i>	<i>83</i>	<i>285</i>

^a Determined by GC. ^b Catalyst undergoing rapid degradation.

Matsui *et al.*^{17,18} have explored the effect of a pressure of CO_2 , in a batch reaction, on the selectivity of the aldol condensation of **6** whilst using a MgO catalyst. At 12 MPa, under supercritical conditions, 94% selectivity towards **8** was achieved, whereas at the subcritical pressure of 5 MPa, 85% selectivity towards the aldol product was observed.

Our aim was to use the continuous flow scCO_2 apparatus⁷ to screen rapidly a variety of both acidic and basic heterogeneous catalysts, see Table 1, for their suitability for the selective self condensation of propionaldehyde across a range of temperatures. Once a suitable catalyst has been found it would then be tested under a wide variety of conditions to optimise the performance of the reaction further. The high solubility of gaseous hydrogen and organic compounds in scCO_2 ¹⁹ can be used in combination with the aldol reaction to allow hydrogenation of the unsaturated product *in situ* if desired.^{5,6}

Catalyst screening

For each catalyst system the reaction was performed using identical reaction conditions at a pressure of 10 MPa. Further details of the catalysts used in this study are outlined later in Table 4 (Experimental section). Fig. 2 shows the conversion and selectivity towards **8** for each catalyst across the temperature range tested. The maximum yields are summarised in Table 1. However, from the point of view of environmental sustainability, selectivity towards the desired product, Table 2, is more important than conversion, because of the ease of separation of unreacted **6** from the product **8** by simple distillation due to the large difference in boiling point of the two compounds; this enables unreacted **6** to be easily repassed through the reaction system.

At temperatures <70 °C, with Brønsted acid catalysts such as Amberlyst® 15 or Purolite® CT-175 (Fig. 2b and 2e), the by-products consisted of the aldol intermediate, **7**, and a variety of other compounds including C₉ aldehydes. These arise from further aldol reactions, and Michael additions to the α,β -unsaturated product **8**. A typical product distribution can be seen in the gas chromatogram, shown in Fig. 3.

A similar profile of conversion and selectivity was obtained with the basic catalyst, NaOH/silica, although higher temperatures were required to achieve this reactivity (Fig. 2h). Magnesium oxide (Fig. 2f) also gave excellent selectivity albeit with a poor conversion. The experiments suggested that the MgO underwent rapid deactivation with a decrease in the

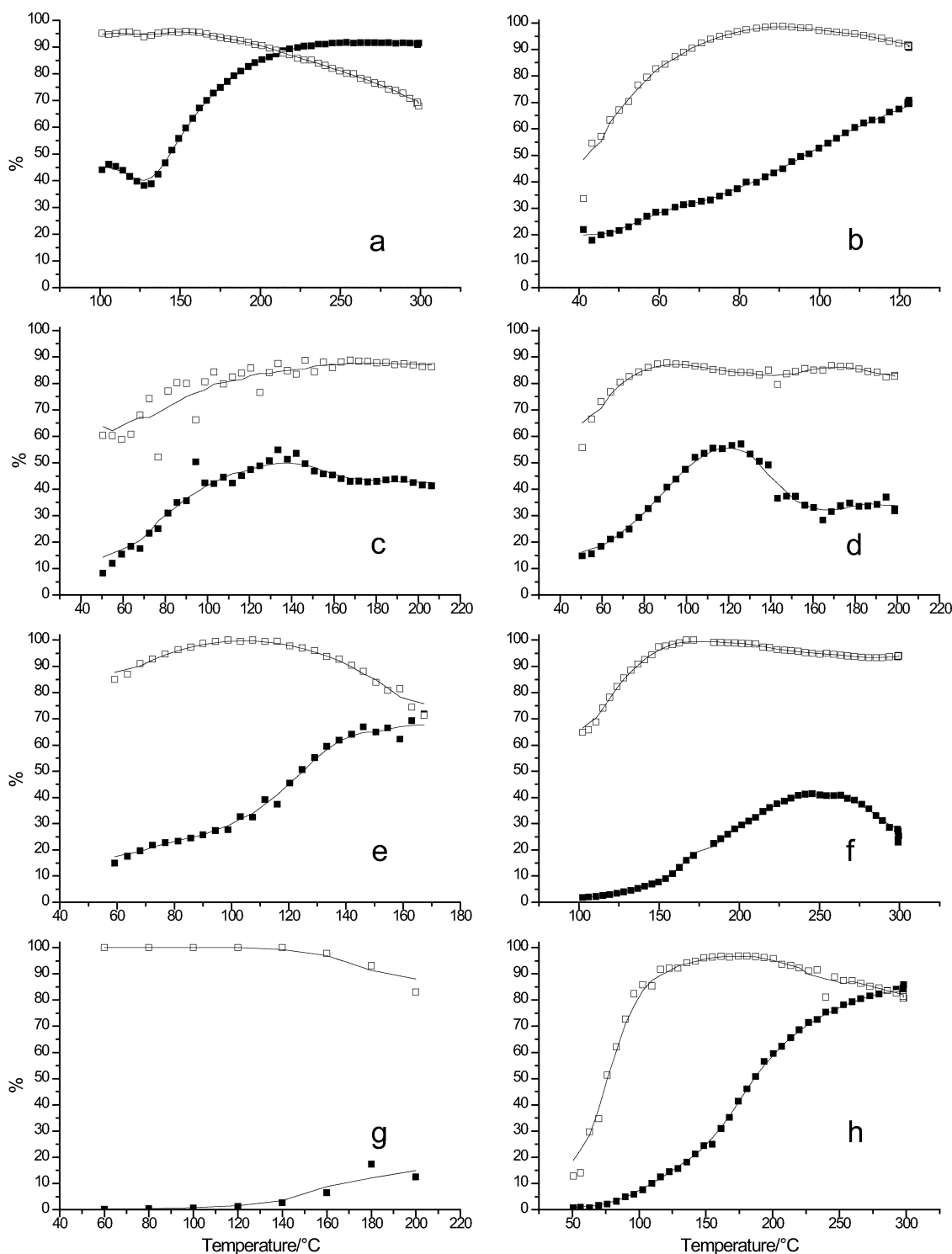


Fig. 2 Summary of catalyst performance over a range of temperatures, showing rare examples of base catalysis in scCO_2 . The plots show the temperature dependence of the conversion (■) and selectivity (□) of the self aldol condensation of **6** to **8** in the presence of a variety of catalysts, each packed into a 10 mL reactor tube. The reactions were carried out at flow rates of 0.1 mL min^{-1} of **6** and 1.0 mL min^{-1} of CO_2 at 10 MPa. The catalysts are: **Amphoteric**: a, γ -alumina; **Bronsted acids**: b, Amberlyst® 15; c, Deloxan® ASP IV/6-2; d, Nafion® SAC-13; e, Purolite® CT-175; **Bases**: f, magnesium oxide; g, Amberlyst® A26; h, supported NaOH. A moving average line has been drawn between data points to aid visualisation.

conversion as the temperature was increased over time. This rapid deactivation may be due to the removal of catalytically active hydroxide groups from the surface of MgO. The freshly exposed MgO can then form inactive carbonates upon reaction

with CO_2 .²⁰ Amberlyst® A26 had poor activity (Fig. 2g) with only minor conversion over the temperature range studied. This is probably due to the formation of carbamate species by the reaction of CO_2 with the amine groups of the catalyst.

Table 2 Maximum selectivity achieved during temperature ramp over various catalysts for the self condensation of **6** at flow rates of 0.1 mL min⁻¹ **6**, 1.0 mL min⁻¹ CO₂ at 10 MPa (*base catalysts in italics*)

Catalyst	% Conv. 6 ^a	% Sel. 8	Temp/°C
γ-Alumina	46	96	158
Amberlyst® 15	43	99	95
<i>Amberlyst® A26</i>	7	97	160 ^b
Deloxan® ASP	50	89	146
<i>Magnesium oxide</i>	22	>99	184
Nafion® SAC13	47	87	100
Purolite® CT175	37	>99	116
<i>Supported NaOH</i>	41	97	174

^a Determined by GC. ^b Catalyst undergoing rapid degradation.

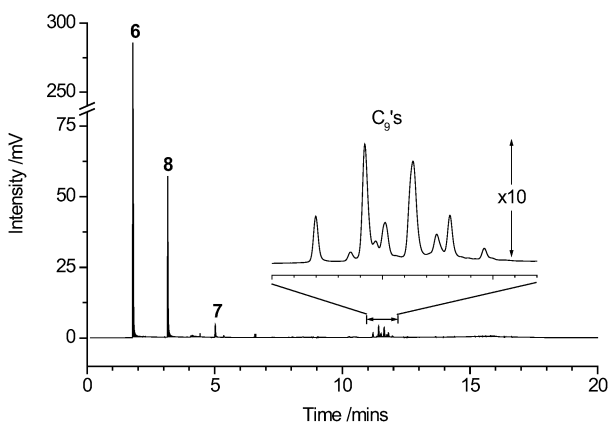


Fig. 3 GC chromatogram (see Experimental for details) taken from Fig. 2b. This shows the range of products from the self condensation of **6** over Amberlyst® 15 at 50 °C. The main peaks are due to **6**, **7** and **8**; the inset figure shows the region from 11.0–12.2 mins with expanded scales. (Other minor peaks remain unidentified.)

Lower selectivity was achieved with Nafion® SAC13 than with Amberlyst® 15 possibly because the higher acidity of Nafion® accelerated the rate of side reactions. Proportionately more **7** was formed at <60 °C with up to 10% selectivity. Even at 140 °C there was up to 5% selectivity towards **7** with Nafion® SAC13.

Overall, γ-alumina, Amberlyst® 15, and Purolite® CT-175 appeared to have the greatest potential for further optimisation whilst maintaining a high selectivity for **8**.

Optimisation of the reaction with Amberlyst® 15

Following the catalyst screening, Amberlyst® 15 was chosen for optimisation due to its low operating temperature, high selectivity and high yield compared to Purolite® and γ-alumina (Table 1). Optimisation of the reaction in scCO₂ was carried out by varying several reactor parameters. Firstly, the reaction was carried out under the same conditions both with and without CO₂. Three reactions were performed to study the effect of CO₂ on the system: 0.1 mL min⁻¹ **6** without CO₂; 0.5 mL min⁻¹ **6** without CO₂; 0.1 mL min⁻¹ **6** with 1.0 mL min⁻¹ CO₂, these results are shown in Fig. 4, Fig. 5 and Fig. 6. The scCO₂ reaction system produced much lower amounts of **7**, the aldol intermediate, to **8**.

Similarly, Fig. 5 shows that the presence of scCO₂ increases the selectivity toward the desired product **8**. However, the conversion at low temperatures was significantly higher *without* CO₂ (Fig. 6).

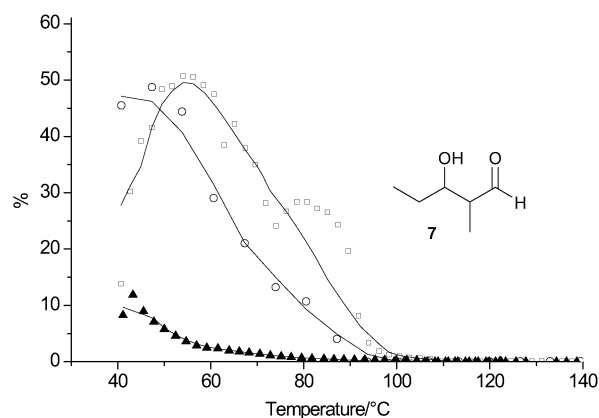


Fig. 4 Demonstration of how the addition of CO₂ reduces the amount of the intermediate **7** in the product stream at lower temperatures. The plot shows the temperature dependence of the selectivity for **7** during the self aldol condensation of **6** over Amberlyst® 15 at 10 MPa, flow rates of: □, 0.1 mL min⁻¹ of **6**, no CO₂; ○, 0.5 mL min⁻¹ of **6**, no CO₂; ▲, 0.1 mL min⁻¹ of **6** and 1.0 mL min⁻¹ of CO₂.

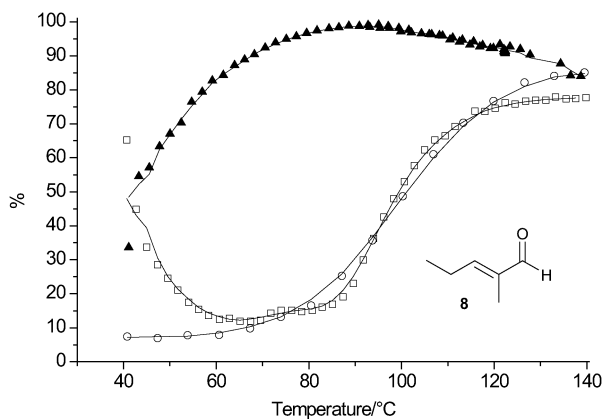


Fig. 5 Plot demonstrating the increase in selectivity for **8** in the presence of CO₂ during the self aldol condensation of **6** over Amberlyst® 15. Carried out at 10 MPa, flow rates of: □, 0.1 mL min⁻¹ of **6**, no CO₂; ○, 0.5 mL min⁻¹ of **6**, no CO₂; ▲, 0.1 mL min⁻¹ of **6** and 1.0 mL min⁻¹ of CO₂.

As the temperature was increased, the conversion in scCO₂ increased markedly and scCO₂ has little effect on conversion at ≥130 °C.

It is postulated that the reaction is driven to completion by the insolubility of the polar aldol intermediate **7** in scCO₂. Intermediate **7** will most likely exist in a liquid-like phase with a higher affinity for the catalyst surface. It can then react forming **8** which is then removed from the catalyst due to its higher solubility in scCO₂. See ESI† for details of phase behaviour of **6** and **8** in scCO₂ – unfortunately it was not possible to isolate the intermediate **7** in sufficient purity to analyse its phase behaviour with CO₂.

Because the selectivity is higher for the reaction in scCO₂, the overall yield of **8** is higher with CO₂, than without, between 60 and 140 °C (see Fig. 6).

Entries 1–4 in Table 3 show the effect of altering the residence time by varying the flow rates of CO₂ and **6** whilst maintaining a constant 6 mol% organic ratio at an isothermal reactor temperature of 90 °C. As the residence time was decreased, a

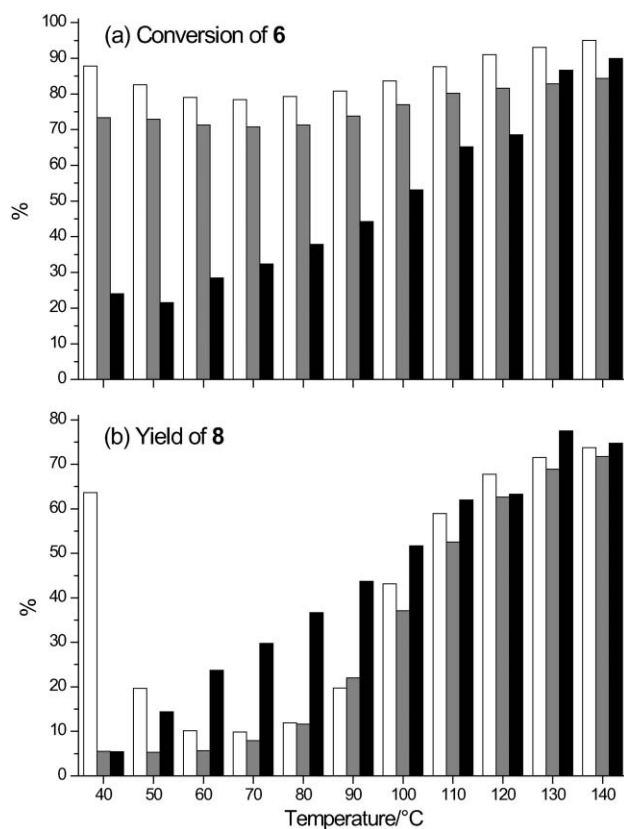


Fig. 6 At lower temperatures the conversion of **6** is higher without CO₂, but the yield of **8** is higher with CO₂ due to the significant increase in selectivity. Temperature dependence of: (a), the conversion of **6** during its self aldol condensation over Amberlyst® 15 and (b), the yield of **8** from the self condensation of **6** over Amberlyst® 15 is illustrated. Carried out at 10 MPa, flow rates of: □, 0.1 mL min⁻¹ of **6**, no CO₂; ▒, 0.5 mL min⁻¹ of **6**, no CO₂; ■, 0.1 mL min⁻¹ of **6** and 1.0 mL min⁻¹ of CO₂.

marginal decrease in conversion was observed (51% → 44%, as total flow rate was increased from 0.825 mL min⁻¹ → 3.85 mL min⁻¹). To test further the effect of residence time a second reactor was added downstream of the first. Fig. 7 shows that an additional catalyst bed gives an extra 20% in conversion from 60 to 105 °C, accompanied by an increase in selectivity to >99%.

Entries 5–8 in Table 3 show that the molar ratio of CO₂ : **6** has only a minimal effect on the conversion and selectivity of

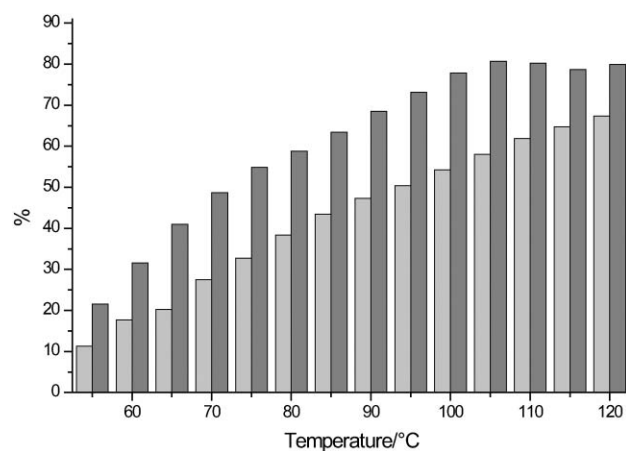


Fig. 7 Effect of temperature on the yield of **8** with: □ a single reactor; ▒ two reactors in series (doubling the reactor volume). Carried out at flow rates of 0.1 mL min⁻¹ of **6** and 1.0 mL min⁻¹ of CO₂ at 8 MPa in the presence of Amberlyst® 15. The addition of a second reactor had no observable effect on the selectivity.

the reaction. Therefore, the benefits of using CO₂ on selectivity can be retained even when using high concentrations of **6**.

The effect of pressure was also explored (Table 3, *N* = 9–12). No definitive change in selectivity was observed as the pressure was varied from 6 to 20 MPa.

The activity of the catalyst was monitored over time under constant conditions of 90 °C and 8 MPa with no pre-equilibration of the system. These conditions were chosen to maximise the conversion with >99% selectivity. There was a rapid reduction in conversion from 86% to 50% over the first 8 h with a small percentage of side products being observed. The conversion then stabilised at 43% and was maintained at this level up to 65 h with no observable side products (by GC) (Fig. 8). A loss of activity was also observed by Baiker and co-workers⁵ when performing the aldol reaction in scCO₂. The stabilisation of conversion following an initial rapid drop suggests that a partial desulfonation of Amberlyst® 15 has occurred, rather than a coking process. We have previously observed a similar desulfonation with the Friedel–Crafts alkylation of anisole.²¹

The *in situ* hydrogenation of the unsaturated product **8** is also of interest, see Scheme 4. The hydrogenation was carried out by replacing the Amberlyst® 15 with a 50 wt% mixture of

Table 3 Study on the effect of reaction parameters on the conversion and selectivity of **6** to **8**

<i>N</i>	<i>T</i> /°C	<i>P</i> /MPa	CO ₂ flow/mL min ⁻¹	6 flow/mL min ⁻¹	Mol% of 6	Conv. (%)	Sel. (%)
1 ^a	90	10	0.75	0.075	6	51	95
2 ^a	90	10	1.00	0.100	6	48	92
3 ^a	90	10	2.25	0.225	6	46	96
4 ^a	90	10	3.50	0.350	6	44	95
5 ^b	120	10	0.97	1.027	40	56	90
6 ^b	120	10	1.04	0.645	28	57	88
7 ^b	120	10	1.10	0.335	16	50	88
8 ^b	120	10	1.15	0.077	4	59	87
9 ^c	120	6	1.00	0.100	6	66	64
10 ^c	120	10	1.00	0.100	6	71	65
11 ^c	120	15	1.00	0.100	6	62	68
12 ^c	120	20	1.00	0.100	6	68	76

The parameters were varied as follows: ^a residence time; ^b concentration of substrate **6**; ^c system pressure.

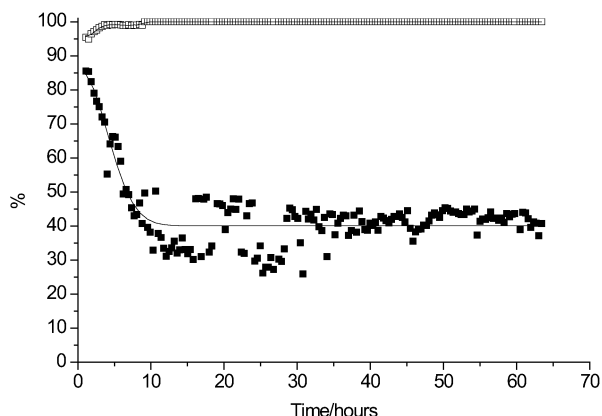
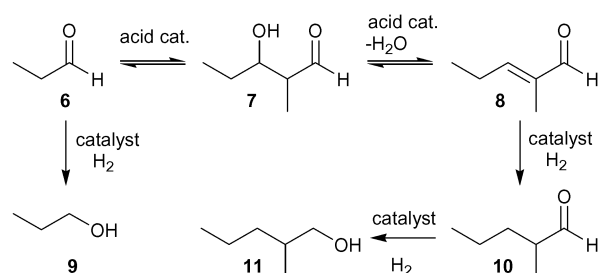


Fig. 8 Effect of catalyst activity over an extended time period on the conversion (■) and selectivity (□) of the self aldol condensation of **6** to **8** in the presence of Amberlyst® 15. The catalyst was loaded into two reactors in series and the reaction was carried out isothermally at 90 °C, 8 MPa with flow rates of 0.1 mL min⁻¹ of **6** and 1.0 mL min⁻¹ of CO₂.



Scheme 4 Self aldol condensation of propionaldehyde (**6**) with possible hydrogenation products: propan-1-ol (**9**), 2-methylvaleraldehyde (**10**) and 2-methyl-1-pentanol (**11**).

Amberlyst® 15 and 2% Pd on silica/alumina (Johnson Matthey Type 31) and dosing hydrogen into the system at 0.55 molar equivalents (based on **6**). Fig. 9 shows the conversion of **6** and selectivity to **10** as a function of temperature. No hydrogenation of the carbonyl group to **11** was observed even when complete

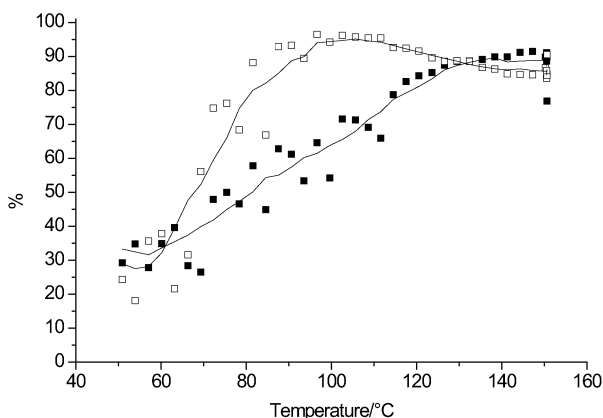


Fig. 9 Plot of the temperature dependence of the conversion (■) and selectivity (□) of the self aldol condensation and *in situ* hydrogenation of **6** to **10** in the presence of Amberlyst® 15 mixed with 2% Pd on silica/alumina (JM Type 31). The reactions were carried out at flow rates of 0.1 mL min⁻¹ of **6** and 1.0 mL min⁻¹ of CO₂ at 8 MPa with 0.55 equivalents of hydrogen. No hydrogenation of the carbonyl group to **9** or **11** was observed.

hydrogenation of **8** was achieved. The conversion was slightly elevated higher than that achieved with Amberlyst® 15 alone (Fig. 7) suggesting that the hydrogenation of **8** to **10** may drive the dehydration of **7** to some extent.

Conclusions

The self condensation of butyraldehyde and propionaldehyde in scCO₂ has been successfully conducted, yielding the α,β -unsaturated aldol products with high selectivity. A series of catalysts has been evaluated, using an automated continuous flow reactor. Surprisingly, two basic catalysts were effective in scCO₂, but overall the experiments showed that Amberlyst® 15 was the most effective of the catalysts screened. The reaction parameters with Amberlyst® 15 parameters were then studied in more detail. The formation of the unsaturated aldol product, **8**, was more selective in scCO₂ than in neat propionaldehyde, over the whole temperature range studied, an effect attributed to the postulated insolubility of the polar aldol intermediate, **7**, in scCO₂. The additional selectivity which is observed in the scCO₂ system delivers higher yields of **8**, whilst any unreacted starting material could be easily recycled. Finally, it was possible to perform an *in situ* hydrogenation of **8** by using a mixed catalyst bed consisting of a 50 wt% mixture of Amberlyst® 15 and 2% Pd on silica/alumina (Johnson Matthey Type 31) producing 2-methylvaleraldehyde in high yield. Thus, overall, our experiments demonstrate that aldol condensations in scCO₂ have even wider potential than reported by previous workers in this field.

Experimental

Safety hazard

CAUTION! *The experiments described in this paper involve the use of relatively high pressures and require equipment with the appropriate pressure rating.*

Catalysts and reagents

Commercially available catalysts were employed: γ -alumina (SI Group), Amberlyst® 15 (Lancaster Synthesis), Amberlyst® A26 (Alfa Aesar), Deloxan® ASP (Degussa Hüls), magnesium oxide (Acros), Nafion® SAC 13 (Sigma Aldrich), Purolite® CT-175 (Purolite International Ltd). NaOH was used as NaOH on a silica support, see Table 4. Commercially available propionaldehyde (Acros, 97%) and butyraldehyde (Acros, 97%) were used without further purification.

Automated continuous flow apparatus and reaction procedure

Fig. 10 shows a schematic view of the experimental apparatus. A programmable CO₂ pump, CP (Jasco PU-1580-CO₂) and HPLC pump, OP (Jasco PU-980) were connected to a 1/4 inch tee-piece, packed with glass beads, PH. The tee-piece acts as both mixer and pre-heater, heated by cartridge heaters within an aluminium heating block. Hydrogen was dosed into the system *via* a 6-port Rheodyne, HD, and was premixed with the CO₂ in a static mixer, M. The reactor, R, consisted of a 10 mL 316 SS tube (100 mm \times 12 mm OD), packed with catalyst and heated by cartridge heaters

Table 4 Catalysts employed in this study

Catalyst	Support	Active group	Catalyst loading
γ -Alumina	N/A	N/A ^a	N/A
Amberlyst® 15	Macroreticular polystyrene cross-linked with divinylbenzene	-SO ₃ H	4.7 eq/kg
Amberlyst® A26	Macroreticular polystyrene cross-linked with divinylbenzene	-N(Me) ₃ OH	0.80 eq/L
Deloxan® ASP IV/6-2	Polysiloxane	-SO ₃ H	Unknown
Magnesium oxide	N/A	N/A ^a	N/A
Nafion® SAC13	Copolymer resin (of tetrafluoroethane and perfluoro-2-(fluorosulfonylethoxy)propyl vinyl ether)	-CF ₂ CF ₂ SO ₃ H	0.13 eq/kg
Purolite® CT-175	Macroporous polystyrene cross-linked with divinylbenzene	-SO ₃ H	4.9 eq/kg
Supported NaOH	Silica	NaOH	3.5 eq/kg

^a The metal oxides, Al₂O₃²² and MgO²⁰ possess a variety of different active sites and modes of catalysis.

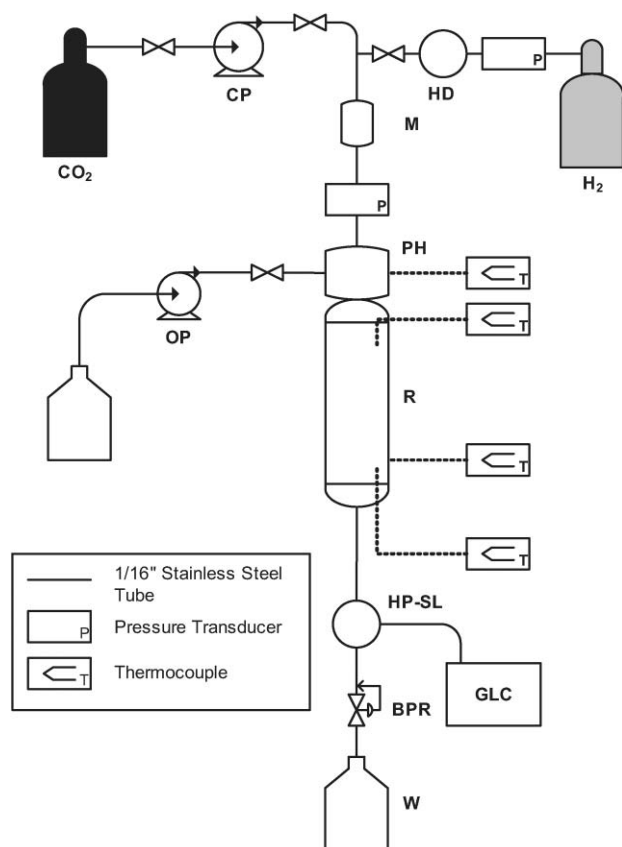


Fig. 10 Schematic of the automated supercritical fluid continuous flow apparatus. The components are labelled as follows: **CP**, chilled CO₂ pump; **HD**, H₂ dosing unit; **M**, mixer; **OP**, organic pump; **PH**, pre-heater and mixer; **R**, reactor; **HP-SL**, high pressure sample loop; **BPR**, back pressure regulator; **GLC**, gas liquid chromatograph; **W**, organic waste.

in an aluminium heating block, controlled *via* a programmable heating controller (Eurotherm 2416). The mixture of products and gases passed through a HPLC 4-port sample loop, HP-SL, which injects the sample into the carrier gas flow of a GLC (Shimadzu GC-17A), where product separation and analysis was carried out.

The system pressure was maintained by a programmable Back Pressure Regulator, BPR (Jasco BP-1580-81). Products were collected in the waste bottle, W. The temperature and

pressure was logged at several points throughout the system on a computer, *via* a PicoLog® data recorder.

In a typical experiment, the reactor was filled with catalyst and sealed into the apparatus. After the equipment had stabilised at the required pressure and flow rate of CO₂, the reactor was heated to the reaction temperature and the substrate was pumped into the system. Experimental parameters were programmed into the pumps, back pressure regulator and GC. Unless otherwise stated, the standard reaction conditions were: flow of CO₂ 1.0 mL min⁻¹ at -10 °C and 5.8 MPa, flow of the substrate 0.1 mL min⁻¹, 10 MPa operating pressure. The GC was fitted with an RTX-5 column (30 m, ID 0.32 mm, film thickness, 0.25 μm), held at 40 °C for 1 minute, ramped at 17 °C/min to 280 °C and then held for 2 min. Quantification was performed by integration of the peak areas; response factors and conversions were calculated by the internal normalisation method. The products were identified by comparing the GC retention time with known standards and by GC-MS.

Acknowledgements

We thank the EPSRC and Thomas Swan & Co. Ltd. for support. We also thank Dr P. N. Gooden, Miss K. A. Scovell, Dr P. Licence and Dr S. K. Ross for scientific discussion and Mr M. Dellar, Mr M. Guyler, Mr R. Wilson and Mr P. Fields for their technical support at the University of Nottingham.

References

- 1 J. Clayden, N. Greeves, S. Warren and P. Wothers, *Organic Chemistry*, Oxford University Press, Oxford, UK, 2001.
- 2 M. M. Green and H. A. Wittcoff, *Organic Chemistry Principles and Industrial Practice*, Wiley-VCH, Weinheim, 2003.
- 3 R. Mestres, *Green Chem.*, 2004, **6**, 583–603.
- 4 G. J. Kelly, F. King and M. Kett, *Green Chem.*, 2002, **4**, 392–399.
- 5 T. Seki, J. D. Grunwaldt, N. van Vegten and A. Baiker, *Adv. Synth. Catal.*, 2008, **350**, 691–705.
- 6 T. Seki, J. D. Grunwaldt and A. Baiker, *Chem. Commun.*, 2007, 3562–3564.
- 7 B. Walsh, J. R. Hyde, P. Licence and M. Poliakoff, *Green Chem.*, 2005, **7**, 456–463.
- 8 T. Aida, T. Nagasawa and Y. Yamazaki, *WO Pat.*, 065851, 2008.
- 9 S. Tanaka, K. Fukuda and T. Asada, *WO Pat.*, 029033, 2004.
- 10 S. Aratake, T. Itoh, T. Okano, T. Usui, M. Shoji and Y. Hayashi, *Chem. Commun.*, 2007, 2524–2526.
- 11 R. H. Fan, D. M. Pu, F. Q. Wen, Y. Ye and X. L. Wang, *J. Org. Chem.*, 2008, **73**, 3623–3625.

- 12 A. D. Godwin, R. H. Schlosberg, F. Hershkowitz, M. G. Maturro, G. Kiss, K. C. Nadler, P. L. Buess, R. C. Miller, P. W. Allen, H. W. Deckman, R. Caers, E. J. Mozeleski and R. P. Reynolds, *US Pat.*, 6,307,093, 2001.
- 13 C. P. Mehnert, N. C. Dispenziere and R. H. Schlosberg, *US Pat.*, 6,552,232, 2003.
- 14 C. P. Mehnert, N. C. Dispenziere and R. A. Cook, *Chem. Commun.*, 2002, 1610–1611.
- 15 S. K. Sharma, P. A. Parikh and R. V. Jasra, *J. Mol. Catal. A: Chem.*, 2007, **278**, 135–144.
- 16 F. M. Scheidt, *J. Catal.*, 1964, **3**, 372–378.
- 17 K. Matsui, H. Kawanami, Y. Ikushima and H. Hayashi, *Chem. Commun.*, 2003, 2502–2503.
- 18 K. Matsui, H. Kawanami and H. Hayashi, in *Carbon Dioxide Utilization for Global Sustainability*, Elsevier Science Bv, Amsterdam, 2004, pp. 363–368.
- 19 M. G. Hitzler, F. R. Smail, S. K. Ross and M. Poliakoff, *Org. Process Res. Dev.*, 1998, **2**, 137–146.
- 20 H. Hattori, *Chem. Rev.*, 1995, **95**, 537–558.
- 21 R. Amandi, P. Licence, S. K. Ross, O. Aaltonen and M. Poliakoff, *Org. Process Res. Dev.*, 2005, **9**, 451–456.
- 22 G. W. Kabalka and R. M. Pagni, *Tetrahedron*, 1997, **53**, 7999–8065.

Extended dissolution studies of cellulose in imidazolium based ionic liquids†

Jürgen Vitz,^{a,b} Tina Erdmenger,^{a,b} Claudia Haensch^{a,b} and Ulrich S. Schubert^{*a,b,c}

Received 14th October 2008, Accepted 5th January 2009

First published as an Advance Article on the web 23rd January 2009

DOI: 10.1039/b818061j

Ionic liquids (ILs) have become advantageous solvents for the dissolution and homogeneous processing of cellulose in recent years. However, despite significant efforts, only a few ILs are known for their capability to efficiently dissolve cellulose. In order to overcome this limitation, we screened a wide range of potentially suitable ILs. From our studies, some remarkable results were obtained, for example, an odd–even effect was found for different alkyl side-chain lengths of the imidazolium chlorides which could not be observed for the bromides. Furthermore, 1-ethyl-3-methylimidazolium diethyl phosphate was found to be best suitable for the dissolution of cellulose; dissolution under microwave irradiation resulted in almost no color change. No degradation of cellulose could be observed. In addition, 1-ethyl-3-methylimidazolium diethyl phosphate has a low melting point which makes the viscosity of the cellulose solution lower and, thus, easier to handle.

Introduction

Cellulose (C₆H₁₀O₅)_n is a linear β-1,4-glycosidically linked polyglucane and the most abundant form of terrestrial biomass. It can be extracted from wood or cotton. Cellulose is also a biodegradable polymer (1000 < DP < 15 000) and the starting material for a variety of products, including cellophane, rayon, cellulose acetate, carboxymethyl cellulose, and many more. These products are used for a large number of industrial applications, for example fibers, tissues, or paper. Furthermore, polysaccharides are used in medical areas for tissue engineering, drug delivery systems or specialized hydrogels.^{1–4} One of the major drawbacks of cellulose concerning its industrial application is the insolubility in common solvents due to its fibril structure and the pronounced presence of intra- and intermolecular hydrogen bonds (Fig. 1).^{5,6}

Nevertheless, cellulose can be transferred to the above mentioned products by solubilization and processing followed by subsequent precipitation or solvent evaporation. Another possibility is the heterogeneous derivatization of cellulose.⁷ The most commonly applied industrial process to obtain regenerated, processible cellulose is the xanthogenate route during which cellulose is swollen with aqueous NaOH and subsequently treated with CS₂ leading to a highly viscous sodium

xanthogenate solution. This solution is later treated with acidic solution to reform the cellulose, CS₂ and NaOH. The main drawbacks of this process are the degradation of the cellulose backbone and the formation of toxic H₂S as a byproduct.^{8–10} Other derivatizing solvents like trifluoroacetic acid, formic acid, or *N,N*-dimethylformamide/N₂O₄ could also be applied for the functionalization of cellulose with or without isolation of the intermediates.

Generally, the easiest way to regenerate cellulose would be its direct dissolution in a solvent and subsequent precipitation (or the evaporation of the solvent) without the formation of a cellulose derivative. Newer examples for non-derivatizing solvents with aqueous inorganic complexes include cuprammonium hydroxide (Cuoxam, Cuam), cupriethylene diamine (Cuen) and CdO/ethylenediamine (Cadoxen), or non-aqueous solvents together with inorganic salts or gases, e.g. DMA/LiCl, DMSO/SO₂, or DMSO/TBAF.^{5,11–13} However, until now, such processes could not be industrially applied. Efforts to overcome the dissolution problem of cellulose by utilizing ionic liquids (ILs) were made in the last few years.^{14–16} In 1934, Graenacher already recognized the ability of molten salts to dissolve cellulose very easily.¹⁷ The value of his research was not fully noticed at that time, most probably due to the high melting points of these salts. Almost seven decades later, in 2002, Rogers and co-workers picked up his ideas and showed that ILs with lower melting points can also be used as non-derivatizing solvents for cellulose.^{14,18} They assumed that anions, which are strong hydrogen bond acceptors, are most effective. The greatest solubility was achieved with 1-butyl-3-methylimidazolium chloride which could dissolve up to 25 wt% of cellulose under microwave irradiation.¹⁸ In particular, 1-butyl-3-methylimidazolium chloride ([C₄MIM]Cl) and 1-allyl-3-methylimidazolium chloride ([AllylMIM]Cl)¹⁹ are now commonly used; etherification²⁰ and esterification,²¹ acetylation,^{16,22} carboxy-methylation²¹ and tritylation²³ are some examples of possible reactions in these solvents. However, besides their promising properties, the already described ILs also show

^aLaboratory of Macromolecular Chemistry and Nanoscience, Eindhoven University of Technology, P. O. Box 513, NL-5600, MB, Eindhoven, The Netherlands. E-mail: u.s.schubert@tue.nl; Web: www.schubert-group.com; Fax: +31 40 247 4186; Tel: +31 40 247 5303

^bDutch Polymer Institute (DPI), P.O. Box 902, NL-5600, AX, Eindhoven, The Netherlands; Fax: +31 40 247 2462; Tel: +31 40 247 56 29

^cLaboratory of Organic and Macromolecular Chemistry, Friedrich-Schiller-University Jena, Humboldtstr. 10, D-07743, Jena, Germany. E-mail: ulrich.schubert@uni-jena.de; Fax: +49 3641 9482 02; Tel: +49 3641 9482 00

† Electronic supplementary information (ESI) available: Analytical data. See DOI: 10.1039/b818061j

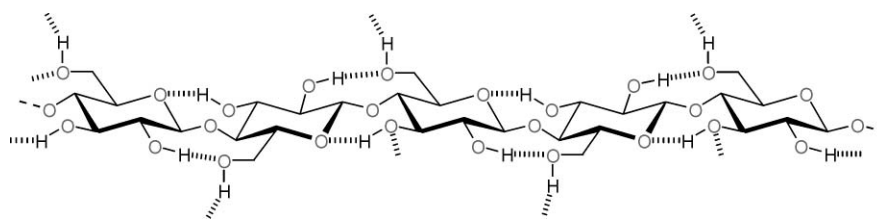


Fig. 1 Schematic representation of the structure of cellulose (with hydrogen bonds).

disadvantages like high melting points, high hygroscopicity and sometimes even degradation of cellulose.²¹ Therefore, we decided to investigate a broader range of ILs for the dissolution of cellulose. In our studies, we used commercially available ILs as well as tailor-made compounds. We investigated the influence of different side-chains and different side-chain lengths in combination with various anions on the dissolution properties. Moreover, the possible degradation of the cellulose during the dissolution process was studied and tried to be minimized by applying thermal heating or microwave irradiation. With this technology, based on homogeneous reactions, a better control of the degree of functionalization of modified cellulose should be possible. The intention is to provide an easier, more environmentally friendly and industrially applicable method of processing cellulose. In addition, novel modified cellulose products might be accessible in particular to the field of advanced and smart bio-based materials, which have not been synthetically available until now.

Results and discussion

Synthesis of ionic liquids

Although there are already some ILs described in the literature, which are able to dissolve cellulose in high amounts, they all show some disadvantages. For example, the IL 1-butyl-3-methylimidazolium chloride, used in our group for the homogeneous tritylation of cellulose,²³ can dissolve up to 25wt% of cellulose (as reported by Rogers *et al.*).¹⁸ However, a melting point above 70 °C, the high viscosity of the [C₄MIM]Cl solution and the high hygroscopicity—in general valid for all imidazolium based ILs with a chloride counter anion—makes their handling difficult. In order to extend the potential application of ILs for cellulose processing, we screened other effective ILs circumventing the mentioned drawbacks. In a recently published paper, the influence of the dissolution properties of the side-chain lengths for the imidazolium based ILs with chlorides as counter ions was described.²³ Thereby, we observed a distinct odd–even effect for short side-chain lengths. As a consequence of these results, the synthesis of 1-alkyl-3-methylimidazolium based ILs also with the bromide anion, was envisioned to support the previously described effect. The mentioned ILs could be obtained in the Emrys Liberator microwave (Biotage) after short reaction times in high yields and high purities.^{24,25} Furthermore, ILs with substituted side-chains were synthesized, e.g. containing double bonds, halides, the CN or the hydroxyl group (Table 1).

The bromide or chloride anions could be exchanged to yield different 1-butyl-3-methylimidazolium and 1-ethyl-3-

Table 1 Melting points and decomposition temperatures of synthesized as well as commercially available ILs

Ionic liquid	Conversion (%)	Purity ^b (%)	T _{decomp} ^c / °C	T _m ^d / °C
[DiMIM]I	>99 ^a	>99	—	—
[DiMIM]Me ₂ PO ₄	>99 ^a	~80	268	— ^e
[C ₂ MIM]F	>99 ^a	98	—	—
[C ₂ MIM]Cl	—	—	256	— ^e
[C ₂ MIM]OAc	>99 ^a	95	—	— ^e
[C ₂ MIM]Et ₂ PO ₄	>99 ^a	90	264	— ^e
[C ₄ MIM]F	>99 ^a	98	234	— ^e
[C ₄ MIM]I	>99 ^a	92	271	— ^e
[C ₄ MIM]OH	—	—	160 ^f	— ^e
[C ₄ MIM]OAc	95	95	221	— ^e
[C ₄ MIM]NO ₃	>99 ^a	99	224	— ^e
[C ₄ MIM]NTf ₂	99	95	369	— ^e
[C ₄ MIM]Bu ₂ PO ₄	96	95	238	— ^e
[AllylMIM]Br	>99 ^a	99	263	— ^e
[NCC ₃ MIM]Br	>99 ^a	~80	289	— ^e
Br[MIM-C ₆ -MIM]Br	~94	~94	278	128
Cl[MIM-C ₄ -MIM]Cl	~96	~95	239	151

^aNo starting material detectable (determined by ¹H NMR). ^bPurity determined by ¹H NMR spectroscopy. ^cTemperature of thermal decomposition. ^dMelting point. ^eMelting point could not be determined by DSC. ^fDecomposition of product.

methylimidazolium based ILs. Whereas, for some exchange reactions water was found to be the best solvent,²⁶ other exchange reactions must be carried out in dichloromethane or acetonitrile.^{27–29} The completeness was checked by adding a silver nitrate solution to a solution of the IL in water.²⁶ An Amberlite IRA-400 exchange resin³⁰ could be used for the preparation of 1-ethyl-3-methylimidazolium acetate ([C₂MIM]OAc) and 1-butyl-3-methylimidazolium acetate ([C₄MIM]OAc).

Due to the fact that the exchange potential increases with increasing atomic number, the exchange resin could not be used for synthesizing ILs with a fluoride anion. Therefore, silver fluoride (AgF) was used to synthesize 1-ethyl-3-methylimidazolium fluoride ([C₂MIM]F) and 1-butyl-3-methylimidazolium fluoride ([C₄MIM]F). During the exchange, the poorly soluble silver chloride precipitates from the solution. The completeness of the reaction was checked after purification using a silver nitrate solution.²⁶

Unfortunately, in the case of 1-butyl-3-methylimidazolium fluoride, some excess of the silver fluoride used remained in the product and could not be separated.

Dissolution studies

The newly synthesized ILs as well as commercially available ILs were subsequently used for the dissolution studies of cellulose. In this context, also a correlation of the water content and the

Table 2 Water content of different ILs and starting materials/reagents used^a

Entry	IL	Water content (ppm) ^a	Remark ^b
1	[C ₂ MIM]Et ₂ PO ₄	5865	i ^c
2	[C ₂ MIM]Et ₂ PO ₄	11 475	ii ^c
3	[C ₂ MIM]Et ₂ PO ₄	6153	iii ^c
4	[C ₂ MIM]OAc	6762	iv ^d
5	[C ₂ MIM]OAc	8895	iii ^d
6	[C ₄ MIM]Cl	2200	v
7	[C ₂ MIM](CN) ₂ N	1234	iv ^e
8	[C ₂ MIM](CN) ₂ N	426	iii ^e
9	[C ₄ MIM]triflate	633	iv ^f
10	[C ₄ MIM]BF ₄	141	iv ^f
11	[C ₄ MIM]PF ₆	101	iv ^f
12	[C ₄ MIM]PF ₆	63	iii ^f
13	1-Methylimidazole	996	iv ^d
14	Triethyl phosphate	178	iv ^d
15	Pyridine (dry)	88	iv ^g

^a Karl-Fischer titration. ^b (i) After preparation; (ii) wet sample, vacuum oven dried; (iii) freeze dried; (iv) as received from supplier; (v) results of Huddleston *et al.*³¹ ^c Synthesized. ^d Aldrich. ^e Solvent Innovation. ^f ToLiTec. ^g Acros Organics.

solubility was found. When using non-dried ILs, the solubility of cellulose was reduced and it was necessary to dry all ILs carefully before use. Therefore, the water content before and after drying was checked by Karl-Fischer titration (Table 2). As a result, it was found that in particular the vacuum oven (at 40 °C) was not sufficient to dry the ILs; only a freeze dryer was able to remove the water. Interestingly, with the used freeze dryer it was not possible to completely dry [C₂MIM]Et₂PO₄ and [C₂MIM]OAc. Once water was absorbed, it was no longer possible to reach the initial values directly obtained for the synthesized [C₂MIM]Et₂PO₄ (entries 1–3) or the commercially available ones [C₂MIM]OAc (entries 4–5). On the other hand, less hygroscopic ILs, *e.g.* [C₂MIM](CN)₂N (entries 7–8) or [C₂MIM]PF₆ (entries 11–12), could be dried significantly. For comparison, [C₄MIM]triflate and [C₂MIM]BF₄ were also measured. As a result, the water content decreases with the anions in the order of OAc⁻ ≈ Et₂PO₄⁻ > (CN)₂N⁻ > triflate > BF₄⁻ > PF₆⁻. The chemicals used for synthesizing [C₂MIM]Et₂PO₄

(entries 13–14) show a lower water content than the obtained IL (entry 1).

For the dissolution studies we used small 2 mL vials. After the IL was filled in, the cellulose was added and the vial was placed into a metal holder and heated to about 100 °C. Thereby, the dissolution of cellulose was checked visually and the time needed for a complete dissolution was between 15 min and 1 h. The results of the dissolution studies are shown in Table 3 together with literature values. As already mentioned above, an odd–even effect was found for the imidazolium based ILs having chloride as the counter ion (Table 3, row 2).²³ As a result, cellulose was more soluble in 1-alkyl-3-methylimidazolium based ILs with even-numbered alkyl chains compared to odd-numbered alkyl chains. Since this result was remarkable, we also used the synthesized bromides to dissolve cellulose. Thereby, the earlier recognized effect for the chlorides was not observed for the bromides (row 3). A response to different side-chain lengths is not clearly visible in that case, maybe due to the overall lower solubility of cellulose in these ILs containing bromide as the counter anion. During these screening tests, a different behavior of the cellulose in the dissolution experiments was also observed. Whereas the solutions of cellulose in compatible ILs like 1-butyl-3-methylimidazolium chloride and 1-hexyl-3-methylimidazolium chloride ([C₆MIM]Cl) became clear and stayed congealed at room temperature (whereby, in particular, the pure chlorides are solids at room temperature; see Fig. 2A), other solutions tend to crystallize back at room temperature, *e.g.* 1-ethyl-3-methylimidazolium chloride (Fig. 2B). If no dissolution can be observed, the cellulose is either only ‘suspended’ in the IL as shown in Fig. 2 (picture C for 1-ethyl-3-methylimidazolium ethyl sulfate), or is rapidly degraded, visible by a deep coloration of the solution seen in picture D. This effect was often observed, in particular when using higher amounts of cellulose.

Whereas all the chlorides—on average—show very good dissolving properties, almost all other ILs show less or no dissolution of cellulose. Only the ILs with acetate and phosphate counter anions revealed good dissolving properties for cellulose. For instance, 8 wt% of cellulose could be dissolved in 1-ethyl-3-methylimidazolium acetate and 12 wt% in 1-butyl-3-methylimidazolium acetate, whereby the solutions became

Table 3 Overview of the results from the dissolution studies for imidazolium based ILs

IL/anion	DiMIM	C ₂ MIM	C ₃ MIM	C ₄ MIM	C ₅ MIM	C ₆ MIM	C ₇ MIM	C ₈ MIM	C ₉ MIM	C ₁₀ MIM	AllylMIM
F ⁻		2%									
Cl ⁻		10–14%	no sol.	20% ^a	1%	6%	5%	4%	2%	no sol.	15% ^c
Br ⁻		1–2%	1–2%	2–3%	1–2%	1–2%	1%	1%	1%	no sol.	no sol.
I ⁻	no sol.			1–2%							
SCN ⁻				5–7% ^b							
BF ₄ ⁻				no sol. ^b							
PF ₆ ⁻				no sol. ^b							
NO ₃ ⁻				no sol.							
NTf ₂ ⁻				no sol.							
F ₃ CSO ₃ ⁻				no sol.							
EtSO ₄ ⁻		no sol.									
(CN) ₂ N ⁻		no sol.									
TsO ⁻		1%									
AcO ⁻		8%		12%							
R ₂ PO ₄ ⁻	10% ^d	12–14% ^e		no sol. ^f							

^a 25% under microwave irradiation according to Rogers *et al.*¹⁸ ^b Results of Rogers *et al.*¹⁸ ^c Results of Wu *et al.*^{16,19} ^d R = Me. ^e R = Et. ^f R = Bu.

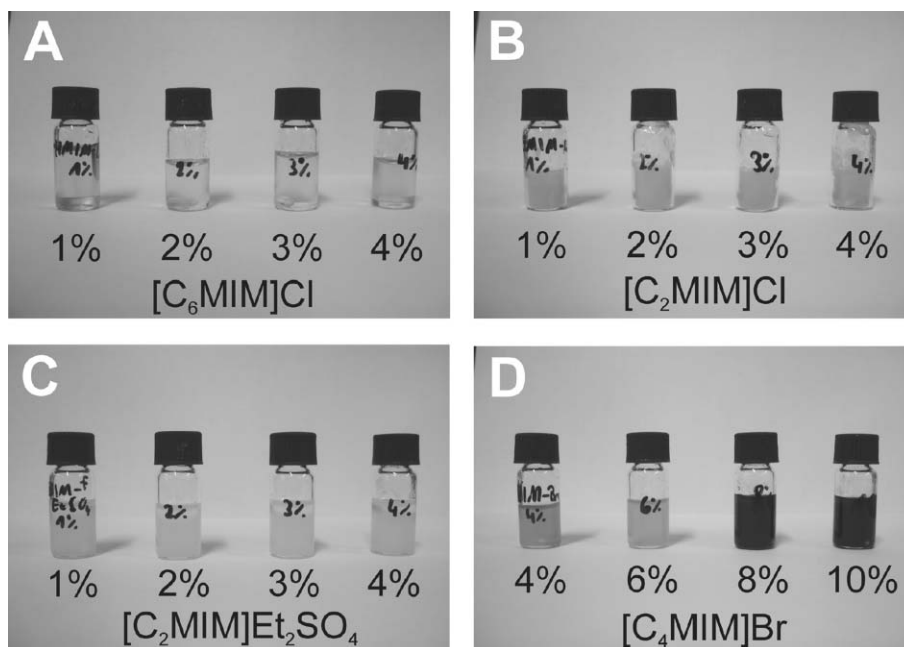


Fig. 2 Cellulose dissolved in $[C_6MIM]Cl$ (A), $[C_2MIM]Cl$ (B), $[C_2MIM]Et_2SO_4$ (C) and $[C_4MIM]Br$ (D), respectively.

colored, indicating degradation of cellulose. Surprisingly, 1-ethyl-3-methylimidazolium diethyl phosphate ($[C_2MIM]Et_2PO_4$) has the ability to dissolve up to 14 wt% of cellulose and 1,3-dimethylimidazolium dimethyl phosphate ($[DiMIM]Me_2PO_4$) up to 10 wt%, whereas 1-butyl-3-methylimidazolium dibutyl phosphate ($[C_4MIM]Bu_2PO_4$) could not dissolve cellulose. The results are summarized in Table 3.

Subsequently, a selection of ILs was studied for the dissolution of cellulose under microwave irradiation in the Biotage Emrys Liberator and Initiator microwave synthesizers. First tests were less successful and showed mostly brownish solutions after heating. This suggests a strong degradation of the cellulose under these conditions.

However, with the Initiator or Swave microwave it is possible to set the maximum power introduced into the solvent. By using different power/temperature settings, we found a relationship between the colorization of the cellulose solution and the maximum power introduced. Typical heating and power profiles for the dissolution of cellulose under microwave irradiation show similar temperature and power profiles for different concentrations of cellulose in $[C_2MIM]Cl$. Although a reduced maximum power was chosen, a thermal overshoot could not be avoided when using concentrations above 4 wt%. In addition, the maximum power of 60 W was reduced automatically after the final temperature was reached. Since the dissolution was performed in the absence of additional solvent and the IL used showed no significant vapor pressure, the pressure is negligible. For example by dissolving 6 wt% of cellulose in $[C_2MIM]Cl$, the power could be varied between 60 and 140 W without any color change at 100 °C. By using a higher concentration of cellulose (up to 10 wt%), a color change was clearly visible at 140 and 160 °C (constant temperature/power). In addition between both test series, a deeper color was visible for the higher temperature.

Not only the power/temperature/concentration settings are important, but the IL used also has an influence. In particular,

$[C_4MIM]Cl$ showed a trend for higher degradation of cellulose. These visual results were supported by DP measurements from dissolved and precipitated cellulose according to the described method by Barthel and Heinze.²² In our experiments, we used the three ILs $[C_4MIM]Cl$, $[C_2MIM]Cl$ and $[C_2MIM]Et_2PO_4$ to dissolve cellulose. As a general procedure the solution contained 8 wt% of cellulose and the mixture was heated up to 100 °C and left at this temperature for 2 h. The automated ChemSpeed A100 AutoPlant robot with its internal anchor stirrers was used to ensure an efficient heating, stirring and cooling. Subsequently, the DP values of both the starting cellulose and the regenerated samples were determined by capillary viscometry in Cuen (Table 4).

These values indicate that the highest degradation of cellulose appears in $[C_4MIM]Cl$ and a slightly lower degradation in $[C_2MIM]Cl$. The lowest degradation after 2 h of heating at 100 °C was found in $[C_2MIM]Et_2PO_4$. The high yield of cellulose with 96% after the regeneration shows a significant benefit for the use of this IL. Furthermore, the low melting point of about 25 °C supports the handling of this IL. It must be noted that the melting point can only be observed visually since it could not be determined by DSC (Table 1) because this IL—like many others—behaves like a supercooled melt.³²

Table 4 DP of cellulose samples after dissolution and re-precipitation from $[C_4MIM]Cl$, $[C_2MIM]Cl$, and $[C_2MIM]Et_2PO_4$, respectively

IL	Temperature/°C	Time/min	Yield (%)	DP
Avicel PH-101	—	—	—	398 ^a
$[C_4MIM]Cl$	100	120	79	311 ^b
$[C_2MIM]Cl$	100	120	86	358 ^b
$[C_2MIM]Et_2PO_4$	100	120	96	378 ^b

^a Before processing. ^b After regeneration.

The dissolution of cellulose in $[C_4MIM]Cl$ has also been carried out under microwave heating. Four samples were heated for between 30 and 120 min at 100 °C. The degradation under microwave irradiation seems to be higher than under classical heating conditions. However, no real correlation between the DP values and the heating time was observed. Therefore, we assumed that a 'stirring problem' caused the higher degradation of cellulose in this case. In the Initiator microwave only magnetic stirring bars can be used.

Remarkable abilities for the absorption of water were observed for $[C_2MIM]Cl$, $[C_4MIM]Cl$, $[C_2MIM]Et_2PO_4$, $[C_2MIM]OAc$ and $[C_2MIM](CN)_2N$ with the dynamic vapor sorption (DVS) technique. Applying this measurement technique, a sample is subjected to varying conditions of humidity and temperature, the response of the sample is measured gravimetrically. Our attempt was to understand the effect of water content especially on the dissolving properties of the ILs. For an initial measurement, the standard heated vacuum oven was used to dry the IL. Then, $[C_2MIM]Cl$ was dried for 3 days in a freeze dryer. In general, the weight of the sample decreases slightly at the drying step. The resulting weight (if the weight change is smaller than 0.05% for a period of 60 min) is used to set the weight change to zero at this point. In Fig. 3 it is visible for $[C_2MIM]Cl$ that at the 'drying-step' this freeze dried IL is very hygroscopic and able to absorb 6 wt% of water at 60 °C in a 0% humidity atmosphere (dried N_2 flow). In contrast, the weight decreased in the case of the vacuum oven dried IL. As a consequence, we assume that the normal vacuum oven is not sufficient to dry in particular highly hygroscopic ILs. After the saturation, the temperature was adjusted to 25 °C and the relative humidity was subsequently increased stepwise to 20%, 50% and 80% relative humidity (RH), respectively (Fig. 3).

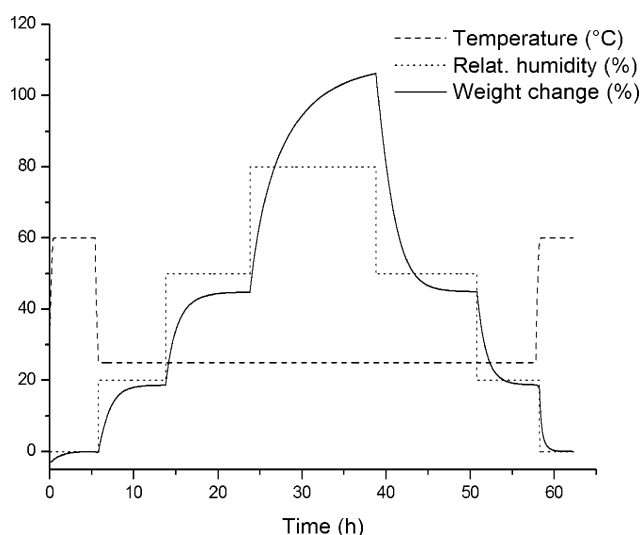


Fig. 3 Water uptake measurement of $[C_2MIM]Cl$ at 25 °C.

In the same manner, the humidity was decreased and an additional drying step was included to compare the initial and final sample weights. From these data, a sorption isotherm was contracted revealing that the absorption and desorption of water is completely reversible (Fig. 4). The sorption isotherm

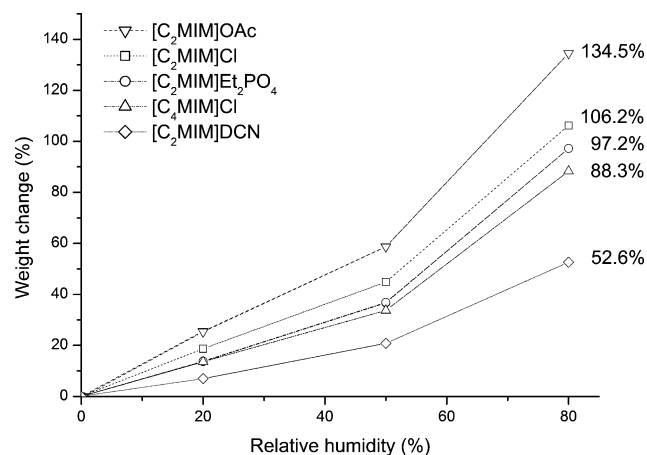


Fig. 4 Water uptake measurements of different ILs showing the weight change (%) as a function of the relative humidity (%) (sorption isotherm).

indicates that for ILs with the same counter ion the water uptake decreases with longer side-chains ($[C_2MIM]Cl$ (106%) > $[C_4MIM]Cl$ (88%)). For the same $[C_2MIM]$ cation the ability to attract water decreases with the anions in the order of $OAc^- > Cl^- > Et_2PO_4^- > (CN)_2N^-$. The water uptake for $[C_2MIM]Et_2PO_4$ (97%) lies in between $[C_2MIM]Cl$ (106%) and $[C_4MIM]Cl$ (88%) and the ability of dissolving cellulose for $[C_2MIM]Et_2PO_4$ is slightly higher than for $[C_2MIM]Cl$. When comparing the results for the cellulose dissolution (Table 3) with the water uptake (Fig. 4), it seems that a lower water uptake in the direction $OAc^- > Cl^- > Et_2PO_4^-$ improves the dissolution of cellulose. But at a certain point, the dissolution property of cellulose drops. In the case of $[C_2MIM](CN)_2N$, cellulose cannot be dissolved at all. On the other hand, it is known from measurements in our group³³ that $[C_3MIM]Cl$ and $[C_5MIM]Cl$ show similar water absorbance compared to $[C_2MIM]Cl$ but they dissolve only very low amounts of cellulose (< 1%, see Table 3, 'odd-even' effect). In comparison with the Karl-Fischer titration (Table 2), the ability to take up water is in line with the water content of the measured ILs. Due to the lack of additional data, it is not yet possible to deduce a detailed correlation between the water uptake and the cellulose dissolving ability of the ILs. Additional measurements are necessary to elucidate the relationship more intensively.

Furthermore, the viscosity behavior of $[C_2MIM]Et_2PO_4$ was investigated. The viscosity was measured on an automated microviscometer by Anton Paar (AMVn) based on the approved and acknowledged rolling/falling ball principle according to DIN 53015 and ISO 12058. Fig. 5 shows the plots of the dynamic viscosity against the temperature for different measuring angles. Assuming that the viscosity is independent from the measuring angle, it can be deduced that the IL used behaves like a Newtonian liquid. This result is similar to the already described behavior of imidazolium dialkylphosphates.³² The viscosity is reduced to approximately half of its starting value only by heating it up by 10 °C (Fig. 5). Since water can influence the viscosity of ILs dramatically, it is essential that the ILs are severely dried before its use. In addition, only a closed viscometer should be used because ILs can absorb a high amount of water as visible from the water uptake measurements.

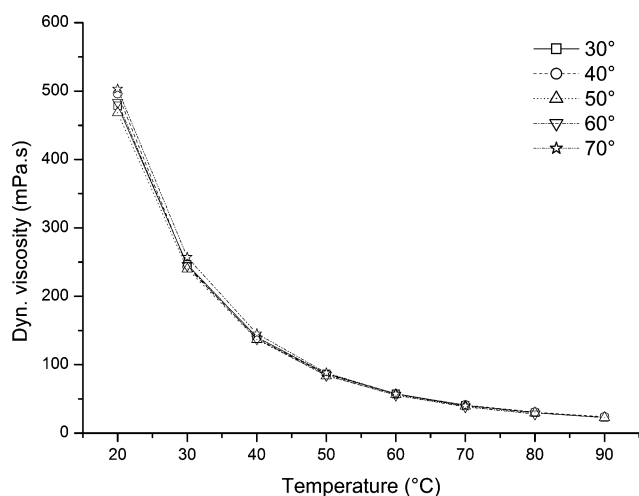
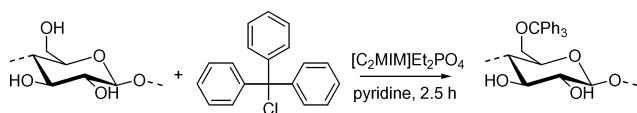


Fig. 5 Viscosity measurements of $[\text{C}_2\text{MIM}]\text{Et}_2\text{PO}_4$ at 30°, 40°, 50°, 60°, and 70°, respectively.

Processing of cellulose

As a result of the dissolution studies, we found the most compatible IL for dissolving cellulose to be $[\text{C}_2\text{MIM}]\text{Et}_2\text{PO}_4$. To show its usability as a reaction medium in a homogeneous functionalization, the tritylation of cellulose was chosen and performed by using pyridine as a base according to a previously described method (Scheme 1).²³



Scheme 1 Schematic representation of the tritylation of cellulose in $[\text{C}_2\text{MIM}]\text{Et}_2\text{PO}_4$.

From elemental analysis a degree of substitution (DS) of 1.17 was obtained for the product after a 2.5 h reaction time using a six fold excess of trityl chloride. This result was checked by ¹H NMR measurements of the pure trityl cellulose but also for their acetylated and propionylated samples showing DS values of 1.09, 1.10 and 1.12, respectively. The completeness of the esterifications was proven by IR measurements. These results are in alignment with results published earlier in our group for $[\text{C}_4\text{MIM}]\text{Cl}$ (DS values of 1.09 (elemental analysis, EA) and 0.97 (¹H NMR for propionylated product) after 3 h of reaction time).²³ Elemental analysis also revealed that small amounts of IL (0.4%) were still present after purification.

Conclusions

Since ILs became advantageous solvents for the dissolution of cellulose, they were used for a number of different reactions to process cellulose. To extend the range of suitable ILs, we screened known but also new tailor-made ILs. Savagely dried ILs are indispensable for the dissolution of cellulose. The earlier found odd–even effect for the 1-alkyl-3-methylimidazolium chlorides was not observed for the bromides. Whereas all the even chlorides with shorter side-chains showed good dissolving properties, mostly all other ILs revealed less or no dissolution

of cellulose. Only the ILs with chloride, acetate and phosphate counter anions revealed good dissolving properties for cellulose. When using microwave irradiation for the dissolution of cellulose, a correlation of power, temperature, and concentration was found. By using low amounts of cellulose, the influence of the power introduced into the solution as well as the temperature is relatively low. A color change indicating a degradation of the polymer backbone was clearly visible in the direction to higher concentrations of cellulose. In conclusion, we found that $[\text{C}_2\text{MIM}]\text{Et}_2\text{PO}_4$ is better suitable for the dissolution of cellulose because almost no color change, and therefore a very low degradation of cellulose, was observed. These visual results were supported by DP measurements from dissolved and precipitated cellulose showing a DP value of 378 after 2 h of heating when starting with a DS of 398 for Avicel PH-101. In addition, the $[\text{C}_2\text{MIM}]\text{Et}_2\text{PO}_4$ melts at low temperatures just above room temperature (melting point could not be determined by DSC) which makes the handling easier. Furthermore, this IL shows advantages in processing cellulose; less degradation could be observed and no ‘acetylation’ as known for $[\text{C}_2\text{MIM}]\text{OAc}$ takes place.³⁴ With this IL, the experimental investigations will be continued for the processing of cellulose and the preparation of new, advanced as well as biocompatible and/or biodegradable cellulose derivatives.

Experimental

Materials

Avicel PH-101 cellulose (Fluka) and pyridine (Acros) were purchased commercially. The ILs 1-ethyl-3-ethylimidazolium chloride, 1-hexyl-3-methylimidazolium chloride, 1-octyl-3-methylimidazolium chloride, 1-decyl-3-methylimidazolium chloride, trihexyl(tetradecyl) phosphonium chloride and 1-ethyl-3-methylimidazolium ethyl-sulfate were donated by Merck. The ILs 1-butyl-3-methylimidazolium chloride, 1-ethyl-3-methylimidazolium tosylate, 1-butyl-3-methylimidazolium tetrafluoroborate, 1-butyl-3-methylimidazolium hexafluorophosphate, 1-ethyl-3-methylimidazolium dicyanamide and 1-butyl-3-methylimidazolium trifluoromethanesulfonate were donated by Solvent Innovation. All other ILs were synthesized according to the literature,^{24,32,35,36} using microwave reactors (Emrys Liberator and Initiator, Biotage, Sweden, and Swave, ChemSpeed, Switzerland) and anion exchange reactions.²⁶ The Avicel cellulose was dried for 12 h at 100 °C under reduced pressure (10 mbar) before use.

Dissolving of cellulose in ionic liquid

The IL was filled into a small vial (1.5 mL, approx. 1 mL of IL, weighted on a micro balance) and preheated before the cellulose was added (8 wt%). This mixture was stirred with a magnetic stirrer at 100 °C for a maximum of 1 h. The solubility of cellulose in the IL was checked visually. Some dissolution tests were performed under microwave irradiation in microwave vials (0.5–2 mL and 2–5 mL vials) in the above mentioned microwave reactors from Biotage (Uppsala, Sweden).

The examination for the degradation of cellulose was performed in an automated ChemSpeed AutoPlant 100 robot (August, Switzerland) equipped with internal anchor stirrers to

ensure efficient heating, stirring and cooling. Again, the cellulose was filled into the preheated IL and heated for 2.5 h. Then dimethylsulfoxide was added (approx. 15 mL) and the dissolved cellulose was precipitated in methanol (500 mL).

DVS measurements³⁷

The water uptake measurements of the ILs were performed on a TA Instruments Q-5000 SA thermo gravimetric analyzer containing a micro balance in which the sample and reference pans were enclosed in a humidity and temperature controlled chamber. The temperature was controlled by Peltier elements. A dried N₂ gas flow and a water saturated stream with 100% relative humidity (RH) were mixed (regulated by mass flow controllers) to obtain the desired RH for the measurements. The standard measurement consisted of a number of subsequent steps. First, the sample was dried at 60 °C at 0% RH for a specific time until the weight change was stabilized to be less than 0.05% for a time period of 60 min. In the second step, the temperature was decreased to 25 °C and the humidity was increased stepwise (with steps of 20% RH and 30% RH) to a maximum of 80% RH. The weight change of the sample was stabilized after each step until it was smaller than 0.05% for a time period of 60 min. The reverse isotherm was measured, too. For further information see ref. 37.

Characterization

¹H NMR and ¹³C NMR spectra were recorded on a Varian Mercury spectrometer (400 MHz) or on a Varian Gemini spectrometer (300 MHz). Chemical shifts are given in ppm downfield from TMS.

IR spectra were recorded on a Perkin Elmer 1600 FT-IR ATR spectrometer. Also, a Bruker TENSOR 37TM equipped with a HTS-XT (High Throughput Screening eXTension) compartment and a HYPERIONTM 3000 microscope was used.

Elemental analyses were carried out on a EuroVector EuroEA3000 elemental analyzer for CHNS-O. Melting points were determined on a DSC 204 F1 by Netzsch under a nitrogen atmosphere from -50 to 200 °C with a heating rate of 10 K min⁻¹ (a first heating cycle was not considered for calculations).

Thermogravimetric analyses were performed on a TG 209 F1 Iris by Netzsch under a nitrogen atmosphere in the range from 25 to 600 °C with a heating rate of 20 K min⁻¹.

The intrinsic viscosities of the cellulose samples were determined by capillary viscosimetry according to DIN 54270 applying copper(II)-ethylenediamine (Cuen) as the solvent.²² From the intrinsic viscosities, the DP can be calculated. A LAUDA PVS 1/4 with four measuring stands and automatic cleaning was used as a viscosimeter. It has an automatic flow time measurement and online cleaning. A maximum temperature stability (variation < 0.01 °C) over a large temperature range (-20 °C up to 200 °C) is possible. The system was fitted with a micro-Ubbelohde capillary with a filling volume of 2–3 mL and a total length of 290 mm (accuracy of ±0.5%, calibrated for absolute and automatic measurements). The measurements were performed at 20 °C.

Dynamic and kinetic viscosities were measured on an AMVn microviscometer by Anton Paar which is based on the approved and acknowledged rolling/falling ball principle according to

DIN 53015 and ISO 12058. The system allows a variable inclination angle of the measurement capillary and, therefore, both the variation of shear stress and shear rate and the easy repetition of measurements on a wide viscosity range (0.3–2500 mPa s). A Peltier thermostat makes it possible to measure over a large temperature range (+5 to 135 °C).

The water content of the ILs was measured on a METTLER TOLEDO Karl-Fischer titrator DL39 equipped with a cell without a diaphragm. This compact coulometric titrator allows measurements for water contents in the range 1 ppm to 5%. As reagent CombiCoulomat (apura[®]) from MERCK was used.

Representative synthesis of trityl cellulose

To 1-butyl-3-methylimidazolium chloride (21.58 g, 81.66 mmol) cellulose (1.88 g, 11.57 mmol) was added. The mixture was heated for 30 min to ensure a complete dissolution before pyridine (9.40 mL, 115.7 mmol) was poured in. After a short mixing, a six-fold excess of trityl chloride (19.35 g, 69.42 mmol) was added and the mixture was heated to 100 °C and kept at this temperature for 2.5 h. The reaction mixture was precipitated in 200 mL methanol. The trityl cellulose was filtered-off and washed several times with methanol. The trityl cellulose was redissolved in 200 mL THF and reprecipitated in 700 mL methanol. After filtration and washing several times with methanol, the product was dried at 45 °C in a vacuum oven (Yield: 5.24 g).

EA, Found: C, 76.15; H, 6.10; DS_{Trityl} = 1.17. Calc. for [C₂₅H₂₄O₃]_n: C, 74.24; H, 5.98; O, 19.78; DS = 1.

FT-IR: $\nu_{\max}/\text{cm}^{-1}$ 3578 (–OH), 3466 (–OH), 3086 (=C–H), 3059 (–C–H), 3028, 2928 (–C–H), 2882 (CH), 1491, 1449 (C–C_{arom}), 1329, 1219, 1159 (C–O–C), 1065 (C–O), 1034, 901, 750, 704 (=C–H), 633. ¹H NMR: δ_{H} (400 MHz, CD₂Cl₂) 0.64–4.20 (H_{Cellulose}), 6.38–7.84 (H_{Trityl}).

Determination of DS by ¹H NMR spectroscopy

The propionylation of trityl cellulose was performed according to the literature (263 mg, DS_{Trityl} = 1.12).³⁸

FT-IR: $\nu_{\max}/\text{cm}^{-1}$ 3059 (=C–H), 3034, 2978 (–C–H), 2942, 2882 (CH), 1757, 1724 (CO_{Ester}), 1651, 1599, 1493, 1449 (C–C_{arom}), 1323, 1275, 1155 (C–O–C), 1078 (C–O), 1040, 764, 748, 706 (CH), 633. ¹H NMR: δ_{H} (400 MHz, CD₂Cl₂) 0.20–1.42 (CH₃), 1.92–2.74 (CH₂), 2.76–5.10 (H_{Cellulose}), 6.35–8.69 (H_{Trityl}).

For the acetylation, a modified procedure of the propionylation was used: A mixture of pyridine (6 mL, 74.2 mmol), acetic acid anhydride (6 mL, 63.5 mmol) and 4-(dimethylamino)pyridine (50 mg) was added to the trityl cellulose (225 mg, 0.56 mmol). The reaction mixture was heated for 24 h at 80 °C. After cooling to room temperature the product was precipitated in an ethanol/hexane mixture (1 : 2), filtered-off, washed with ethanol and dried in a vacuum oven at 45 °C (307 mg, DS_{Trityl} = 1.10).

FT-IR: $\nu_{\max}/\text{cm}^{-1}$ 3059 (=C–H), 3032, 2938, 2882 (CH), 1761 (CO_{Ester}), 1665, 1491, 1449 (C–C_{arom}), 1370, 1221 (C–O–C), 1109 (C–O), 1063, 764, 748, 706 (CH), 635. ¹H NMR: δ_{H} (400 MHz, CD₂Cl₂) 0.38–1.37 (CH₃), 2.52–5.10 (H_{Cellulose}), 6.18–8.33 (H_{Trityl}).

Acknowledgements

The authors would like to thank the Dutch Polymer Institute (DPI) and the Fonds der Chemischen Industrie for financial support and Solvent Innovation and Merck KGaA for supplying their ILs as a kind gift. In addition, we would like to thank Rebecca Eckardt and Christoph Ulbricht for performing the elemental analysis.

Notes and references

- 1 F. T. Moutos, L. E. Freed and F. Guilak, *Nat. Mater.*, 2007, **6**, 162–167.
- 2 D. J. Mooney and E. A. Silva, *Nat. Mater.*, 2007, **6**, 327–328.
- 3 R. Langer, *Science*, 1990, **249**, 1527–1533.
- 4 T. Coviello, P. Matricardi, C. Marianecchi and F. Alhaique, *J. Controlled Release*, 2007, **119**, 5–24.
- 5 T. Heinze and T. Liebert, *Prog. Polym. Sci.*, 2001, **26**, 1689–1762.
- 6 K. J. Edgar, C. M. Buchmann, J. S. Debenham, P. A. Rundquist, B. D. Seiler, M. C. Shelton and D. Tindall, *Prog. Polym. Sci.*, 2001, **26**, 1605–1688.
- 7 J. Haftrén, W. Zou and A. Córdova, *Macromol. Rapid Commun.*, 2006, **27**, 1362–1366.
- 8 C. F. Coss and D. C. Spruance, *US Pat.*, 763 266, 21.06.04.
- 9 P. Green, *J. Chem. Soc., Trans.*, 1906, **89**, 811–813.
- 10 H. Lyncke, *GB Pat.*, 190 808 023, 03.09.08.
- 11 A. L. Horvath, *J. Phys. Chem. Ref. Data*, 2006, **35**, 77–92.
- 12 T. Heinze, R. Dicke, A. Koschella, E.-A. Klohr, W. Koch and A. H. Kull, *Macromol. Chem. Phys.*, 2000, **201**, 627–631.
- 13 S. Köhler and T. Heinze, *Macromol. Biosci.*, 2007, **7**, 307–314.
- 14 R. P. Swatloski, R. D. Rogers and J. D. Holbrey, (The University of Alabama, PG Research Foundation Inc.), *WO Pat.*, 03 029 329, 10.04.03.
- 15 M. B. Turner, S. K. Spear, J. D. Holbrey and R. D. Rogers, *Biomacromolecules*, 2004, **5**, 1379–1384.
- 16 J. Wu, J. Zhang, H. Zhang, J. He, Q. Ren and M. Guo, *Biomacromolecules*, 2004, **5**, 266–268.
- 17 C. Graenacher, (Chem. Ind., Basel), *US Pat.*, 1 943 176, 09.01.34.
- 18 R. P. Swatloski, S. K. Spear, J. D. Holbrey and R. D. Rogers, *J. Am. Chem. Soc.*, 2002, **124**, 4974–4975.
- 19 H. Zhang, J. Wu, J. Zhang and J. He, *Macromolecules*, 2005, **38**, 8272–8277.
- 20 V. Myllymaeki and R. Aksela, (Kemira Oyj, Helsinki), *WO Pat.*, 2005 054 298, 16.06.05.
- 21 T. Heinze, K. Schwikal and S. Barthel, *Macromol. Biosci.*, 2005, **5**, 520–525.
- 22 S. Barthel and T. Heinze, *Green Chem.*, 2006, **8**, 301–306.
- 23 T. Erdmenger, C. Haensch, R. Hoogenboom and U. S. Schubert, *Macromol. Biosci.*, 2007, **7**, 440–445.
- 24 M. Deetlefs and K. R. Seddon, *Green Chem.*, 2003, **5**, 181–186.
- 25 R. S. Varma and V. V. Namboodiri, *Chem. Commun.*, 2001, 643–644.
- 26 X. Creary and E. D. Willis, *Org. Synth.*, 2005, **82**, 166.
- 27 N. Jain, A. Kumar, S. Chauhan and S. M. S. Chauhan, *Tetrahedron*, 2005, **61**, 1015.
- 28 N. Jain, A. Kumar and S. M. S. Chauhan, *Tetrahedron Lett.*, 2005, **46**, 2599–2602.
- 29 Y. Génisson, N. Lauth-de Viguierie, C. André, M. Baltas and L. Gorrichon, *Tetrahedron: Asymmetry*, 2005, **16**, 1017–1023.
- 30 W. C. Bass, (Ecodyne Corp.), *US Pat.*, 4 252 905, 24.02.81.
- 31 J. G. Huddleston, A. E. Visser, W. M. Reichert, H. D. Willauer, G. A. Broker and R. D. Rogers, *Green Chem.*, 2001, **3**, 156–164.
- 32 E. Kuhlmann, S. Himmler, H. Giebelhaus and P. Wasserscheid, *Green Chem.*, 2007, **9**, 233–242.
- 33 T. Erdmenger, J. Vitz, F. Wiesbrock and U. S. Schubert, *J. Mater. Chem.*, 2008, **18**, 5267–5273.
- 34 S. Köhler, T. Liebert, M. Schöbitz, J. Schaller, F. Meister, W. Günther and T. Heinze, *Macromol. Rapid Commun.*, 2007, **28**, 2311–2317.
- 35 V. V. Namboodiri and R. S. Varma, *Org. Lett.*, 2002, **4**, 3161–3163.
- 36 B. M. Khadilkar and G. L. Rebeiro, *Org. Process Res. Dev.*, 2002, **6**, 826–828.
- 37 H. M. L. Thijs, C. R. Becer, C. Guerrero-Sanchez, D. Fournier, R. Hoogenboom and U. S. Schubert, *J. Mater. Chem.*, 2007, **17**, 4864–4871.
- 38 D. Gräbner, T. Liebert and T. Heinze, *Cellulose*, 2002, **9**, 193–201.

Ligand-less palladium-catalyzed direct 5-arylation of thiophenes at low catalyst loadings

Julien Roger,^a Franc Požgan^b and Henri Doucet^{*a}

Received 10th November 2008, Accepted 5th January 2009

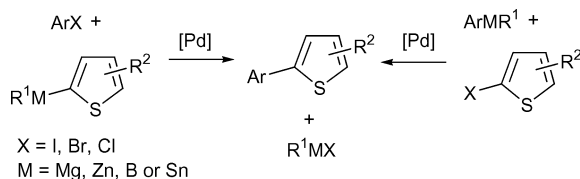
First published as an Advance Article on the web 6th February 2009

DOI: 10.1039/b819912d

Ligand-less Pd(OAc)₂ provides a very efficient catalyst for the direct 5-arylation of thiophene derivatives. With this catalyst, a low palladium concentration (0.1–0.001 mol%) should be employed in order to obtain high yields of coupling products. At higher concentrations a fast formation of inactive “Pd black” generally occurs. Substrates/catalysts ratios up to 100000 can be employed with the most reactive aryl bromides. A very wide variety of functional groups is tolerated on both coupling partners. The major waste of this reaction is HBr associated with KOAc. Therefore this procedure is more economically and environmentally attractive than the traditional cross-coupling procedures employing organometallic derivatives.

Introduction

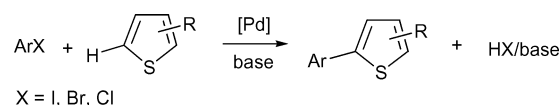
In recent years, much attention has been given to the synthesis of arylthiophenes, due to the biological or physical properties demonstrated by this class of compounds.¹ 2-Arylthiophene derivatives can be prepared by classical palladium-catalyzed cross-coupling procedures such as Suzuki,² Stille³ or Negishi⁴ type reactions. These reactions are performed using an organometallic derivative of the thiophene with an aryl halide or using an organometallic derivative of an aryl with a halothiophene (MR¹ = ZnX, SnR₃, B(OR)₂) (Scheme 1). The major drawback of these reactions is that they require the preparation of organometallic derivatives and also provide either an organometallic or a salt (MX) as a by-product.



Scheme 1

In 1990, Ohta and co-workers reported the direct arylation of thiophenes with aryl halides *via* a C–H bond activation of thiophene in medium to good yields using 5 mol% Pd(PPh₃)₄ as catalyst.⁵ Since these results, this methodology has been demonstrated to be very powerful for the synthesis of 2-arylthiophenes.^{6,7} This reaction is attractive for the environment since the major by-product is HX (X = I, Br or Cl) associated to a base instead of a metallic salt using more

classical coupling procedures. Moreover, no preparation of an organometallic derivative is required reducing the number of steps to prepare these compounds (Scheme 2).



Scheme 2

The major disadvantage of this reaction is the relatively high catalyst loadings which are actually employed for such couplings. So far, most of these reactions have been performed using 1–10 mol% palladium catalyst.^{5,8,9} Moreover, in most cases, palladium was associated with 1–20 mol% of monophosphines⁸ or diphosphines as ligands.⁹ Only a few examples of ligand-free palladium procedures have been reported.^{10–12} An intramolecular Pd(OAc)₂ in the absence of ligand or stabilizing agent gave the target products in 60–100% yields.¹⁰ However, in most cases, for ligand-free palladium procedures, a stoichiometric amount of an ammonium salt or of a crown ether was added to the reaction mixture as palladium-stabilizing agent, increasing the amount of wastes.^{11,12} Additionally, to the best of our knowledge, such ligand-less palladium couplings using low catalyst concentration have not been reported.

Recently, de Vries and co-workers have reported that Heck and Suzuki reactions can be performed under very low catalyst loadings (0.1–0.01 mol%) using a ligand-free catalyst Pd(OAc)₂.^{13,14} They have demonstrated that, when Pd(OAc)₂ is employed as catalyst precursor at elevated temperature, soluble palladium(0) colloids or nanoparticles are formed. With this ligand-less catalytic system, the Heck or Suzuki reactions takes place *via* the interaction of the arylating agent with the palladium atoms in the outer rim of the nanoparticles. This leads to formation of monomeric or dimeric anionic palladium complexes that undergo the usual catalytic steps. However, this promising procedure has not yet been extended to C–H activation reactions.

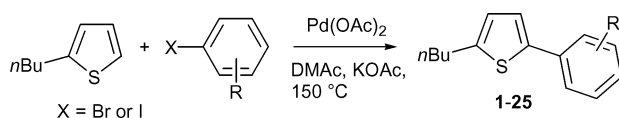
^aUMR 6226 CNRS-Université de Rennes, “Catalyse et Organometalliques”, Campus de Beaulieu, 35042, Rennes, France. E-mail: henri.doucet@univ-rennes1.fr; Tel: +33 (0)2 23 23 63 84

^bFaculty of Chemistry and Chemical Technology, University of Ljubljana Aškerčeva 5, SI-1000, Ljubljana, Slovenia. E-mail: franc.pozgan@fkt.uni-lj.si

For the past few years we have been studying the efficiency of palladium catalysts for activation followed by arylation or vinylation of C–H bonds of heteroaromatics such as furans,^{15a,b} thiazoles,^{15c} benzoxazoles.^{15d,e} We have already reported preliminary results for the direct 5-arylation of thiophenes using ligandless Pd(OAc)₂ as catalyst.¹⁶ Here, we wish to report on the use of the “de Vries procedure” for palladium-catalyzed 5-arylation of a large set of thiophene derivatives using a wide variety of aryl bromides under very low catalyst loadings.

Results and discussion

First, we examined the reactivity of a variety of *para*-substituted aryl bromides and also iodobenzene with 2-*n*-butylthiophene (Scheme 3, Table 1). The coupling of the electron-deficient aryl bromides, 4-bromoacetophenone, 4-bromobenzophenone, 4-bromobenzaldehyde, 4-(trifluoromethyl)bromobenzene or 4-bromobenzonitrile with 2-*n*-butylthiophene proceeded in high yields using only 0.1–0.001 mol% catalyst (Table 1, entries 3–10). With these substrates the target compounds **2–6** were selectively obtained in very high turnover numbers (TONs) of 1900–85000. Poorly activated 4-fluorobromobenzene was found to be slightly less reactive, and 0.1 mol% catalyst had to be employed in order to obtain a high conversion of the starting material and a good yield of **7** (81%) (Table 1, entry 11). As expected, a lower reactivity of the deactivated aryl bromide, 4-bromoanisole, was observed. Using 0.1 mol% catalyst, a yield of 62% of **9** was obtained (Table 1, entry 14). With this substrate, an increase of the catalyst loading to 1 mol% led to



Scheme 3

Table 1 Reaction of 2-*n*-butylthiophene with *para*-substituted aryl bromides or iodobenzene (Scheme 3)

Entry	Aryl halide	Substrate/ catalyst ratio	Yield Prod. (%)
1	Iodobenzene	1000	1 63 (49)
2	Iodobenzene	10000	1 52 (46)
3	4-Bromoacetophenone	10000	2 100 (85)
4	4-Bromobenzophenone	10000	3 100 (86)
5	4-Bromobenzaldehyde	1000	4 100 (89)
6	4-Bromobenzaldehyde	10000	4 19
7	4-(Trifluoromethyl)- bromobenzene	10000	5 100 (90)
8	4-(Trifluoromethyl)- bromobenzene	100000	5 85
9	4-Bromobenzonitrile	1000	6 100 (88)
10	4-Bromobenzonitrile	10000	6 30
11	4-Bromofluorobenzene	1000	7 98 (81)
12	4-Bromotoluene	1000	8 73 (67)
13	4-Bromoanisole	100	9 60 (50)
14	4-Bromoanisole	1000	9 76 (62)
15	4-Bromo- <i>N,N</i> -dimethylaniline	100	10 0
16	4-Bromo- <i>N,N</i> -dimethylaniline	1000	10 0

Conditions: Pd(OAc)₂, aryl halide (1 mmol), 2-*n*-butylthiophene (2 mmol), KOAc (2 mmol), DMAc, 20 h, 150 °C, GC and NMR yields, yields in parentheses are isolated.

Table 2 Reaction of 2-*n*-butylthiophene with *meta*- or *ortho*-substituted aryl bromides (Scheme 3)

Entry	Aryl bromide	Substrate/ cat. ratio	Yield Prod. (%)
1	3-Bromobenzaldehyde	1000	11 100 (88)
2	3-Bromoacetophenone	1000	12 100 (91)
3	3-Bromoacetophenone	10000	12 65
4	3-(Trifluoromethyl)-bromobenzene	1000	13 100 (93)
5	3,5-Bis(trifluoromethyl)- bromobenzene	10000	14 100 (90)
6	2-Bromobenzaldehyde	1000	15 91 (84)
7	2-Bromoacetophenone	1000	16 0
8	2-(Trifluoromethyl)-bromobenzene	1000	17 100 (92)
9	2-Bromobenzonitrile	10000	18 81 (67)
10	1-Bromonaphthalene	1000	19 100 (87)
11	2-Bromotoluene	100	20 52 (42)
12	2,6-Difluorobromobenzene	1000	21 94 (86)

Conditions: Pd(OAc)₂, aryl bromide (1 mmol), 2-*n*-butylthiophene (2 mmol), KOAc (2 mmol), DMAc, 20 h, 150 °C, GC and NMR yields, yields in parentheses are isolated.

a lower yield of product **9** (50%) (Table 1, entry 13). This result was confirmed using the strongly deactivated aryl bromide: 4-bromo-*N,N*-dimethylaniline. In the presence of 0.1 mol% or 1 mol% of catalyst no conversions were detected (Table 1, entries 15 and 16). For this ligand-free procedure, under higher palladium concentrations, so-called “palladium black” forms more rapidly. The concentration of active palladium species is not increased, and the conversions of aryl bromides are not improved. Therefore, this ligand-free procedure is limited to relatively reactive substrates.

Surprisingly, this ligand-free procedure was also found to give disappointing results using iodobenzene. With this very reactive aryl halide, moderate conversions of 52 and 63% and yields of 46 and 49% of **1** were obtained using 0.01 or 0.1 mol% catalyst (Table 1, entries 1 and 2). In the course of this reaction, the formation of side-products was also observed. The major one was biphenyl arising from the homocoupling of iodobenzene.

Then, we studied the reactivity of *meta*- and *ortho*-substituted aryl bromides with 2-*n*-butylthiophene (Table 2, Scheme 3). As expected, *meta*-substituted aryl bromides gave quite similar results than the *para*-substituted ones. For example, 3-bromoacetophenone gave **12** with a TON of 6500, whereas a TON of 10000 had been obtained using 4-bromoacetophenone (compare Table 2, entry 3 with Table 1, entry 3). In general, *ortho*-substituents on aryl halides have a more important effect on the rates and yields of palladium-catalysed reactions, due to their different steric hindrance and coordination properties. *Ortho*-substituted 2-bromobenzonitrile reacted with 2-*n*-butylthiophene leading to the expected product **18** in a high TON of 8100 (Table 2, entry 9). 2-Bromobenzaldehyde, 2-(trifluoromethyl)bromobenzene or 1-bromonaphthalene also led to the desired 5-arylated thiophenes **15–17** in good yields and TONs of 910–1000 (Table 2, entries 6, 8 and 10). On the other hand, 2-bromoacetophenone gave no coupling product (Table 2, entry 7). This is probably due to some coordination of the acetyl function to palladium. A low reactivity was observed using 2-bromotoluene. With this non-activated congested substrate, the product **20** was obtained in 42% yield using 1 mol% catalyst (Table 2, entry 11). This lower reactivity probably comes from

Table 3 Reaction of 2-*n*-butylthiophene with heteroaryl bromides (Scheme 3)

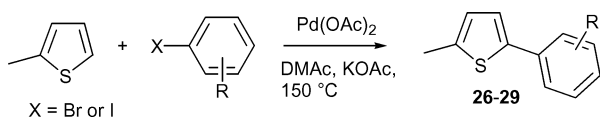
Entry	Heteroaryl bromide	Substrate/ cat. ratio	Prod.	Yield (%)
1	3-Bromopyridine	1000	22	100 (91)
2	3-Bromopyridine	10000	22	53
3	3-Bromoquinoline	1000	23	100 (90)
4	3-Bromoquinoline	10000	23	23
5	5-Bromopyrimidine	1000	24	100 (88)
6	2-Bromo-5-methylthiophene	100	25	0
7	2-Bromo-5-methylthiophene	1000	25	0

Conditions: Pd(OAc)₂, heteroaryl bromide (1 mmol), 2-*n*-butylthiophene (2 mmol), KOAc (2 mmol), DMAc, 20 h, 150 °C, GC and NMR yields, yields in parentheses are isolated.

a slow oxidative addition to palladium. On the other hand, the di-*ortho*-substituted 2,6-difluorobromobenzene gave the target compound **21** in good yield using only 0.1 mol% catalyst (Table 2, entry 12).

Palladium chemistry involving heterocycles has its unique characteristics stemming from the heterocycles' inherently different structural and electronic properties in comparison to the corresponding carbocyclic aryl compounds.¹ Pyridines, quinolines or pyrimidines are π -electron deficient heterocycles, while thiophenes or furans are π -electron excessive. If the oxidative addition of the aryl bromides to the palladium complex is the rate-limiting step of the reaction with this catalyst, the reactions should be slower with thiophenes or furans than with pyridines. We observed that the coupling of 3-bromopyridine, 3-bromoquinoline or 5-bromopyrimidine proceeded nicely using only 0.1–0.01 mol% catalyst and gave **22–24** in 88–91% yields (Table 3, entries 1–5). On the other hand, 2-bromo-5-methylthiophene gave no coupling product **25** using 0.1 or 1 mol% catalyst (Table 3, entries 6 and 7). This result seems to confirm that the oxidative addition of the aryl bromide to palladium is the rate-limiting step of the catalytic cycle with this catalyst. With such challenging substrates, palladium associated to phosphine ligands should be preferred as catalysts.^{7c}

Then, we examined the reactivity of 2-methylthiophene (Scheme 4, Table 4). Due to its very similar electronic and steric properties with 2-*n*-butylthiophene, we expected to obtain similar reaction rates with this substrate. Indeed, we observed almost identical TONs. 4-Bromobenzaldehyde and 4-bromobenzonitrile gave **26** and **27** in 2800 and 2300 TONs, respectively (Table 4, entries 1–4). 4-Fluorobromobenzene was slightly less reactive (Table 4, entry 5). Again, only a partial conversion of 4-bromoanisole was observed to give **29** in 41% isolated yield (Table 4, entry 6).

**Scheme 4**

The functionalised thiophene, thiophene-2-carbonitrile can also be employed with this ligand-less palladium procedure (Scheme 5, Table 5). When this substrate was reacted with 4-bromoacetophenone it gave very selectively the expected

Table 4 Reaction of 2-methylthiophene with aryl bromides (Scheme 4)

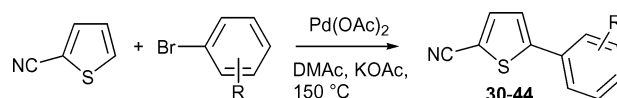
Entry	Aryl bromide	Substrate/ catalyst ratio	Prod.	Yield (%)
1	4-Bromobenzaldehyde	1000	26	100 (89)
2	4-Bromobenzaldehyde	10000	26	28
3	4-Bromobenzonitrile	1000	27	100 (92)
4	4-Bromobenzonitrile	10000	27	23
5	4-Bromofluorobenzene	1000	28	95 (87)
6	4-Bromoanisole	1000	29	48 (41)

Conditions: Pd(OAc)₂, aryl bromide (1 mmol), 2-methylthiophene (2 mmol), KOAc (2 mmol), DMAc, 20 h, 150 °C, GC and NMR yields, yields in parentheses are isolated.

Table 5 Reaction of thiophene-2-carbonitrile with aryl bromides (Scheme 5)

Entry	Aryl bromide	Substrate/ catalyst ratio	Prod.	Yield (%)
1	4-Bromoacetophenone	10000	30	100 (80)
2	4-Bromobenzaldehyde	1000	31	100 (85)
3	4-Bromobenzaldehyde	10000	31	79
4	Methyl 4-bromobenzoate	1000	32	100 (87)
5	Methyl 4-bromobenzoate	10000	32	57
6	4-(Trifluoromethyl)-bromobenzene	10000	33	97 (90)
7	4-Bromobenzonitrile	1000	34	100 (89)
8	4-Bromobenzonitrile	10000	34	68
9	4-Bromofluorobenzene	10000	35	97 (84)
10	4- <i>tert</i> -Butylbromobenzene	1000	36	72 (62)
11	4- <i>tert</i> -Butylbromobenzene	10000	36	44
12	4-Bromoanisole	1000	37	87 (77)
13	4-Bromo- <i>N,N</i> -dimethylaniline	1000	38	0
14	3-Bromobenzonitrile	10000	39	100 (89)
15	2-Bromobenzaldehyde	1000	40	98 (87)
16	2-(Trifluoromethyl)-bromobenzene	10000	41	100 (90)
17	2-Bromobenzonitrile	10000	42	100 (91)
18	2-Bromoanisole	1000	43	0
19	3-Bromopyridine	10000	44	98 (86)
20	3-Bromopyridine	100000	44	46

Conditions: Pd(OAc)₂, aryl bromide (1 mmol), thiophene-2-carbonitrile (2 mmol), KOAc (2 mmol), DMAc, 20 h, 150 °C, GC and NMR yields, yields in parentheses are isolated.

**Scheme 5**

product **30** in a very high TON of 10000 and 80% isolated yield (Table 5, entry 1). Quite similar TONs of 5700–9700 were obtained using the other electron-deficient *para*-substituted aryl bromides, 4-bromobenzaldehyde, methyl 4-bromobenzoate, 4-(trifluoromethyl)bromobenzene or 4-bromobenzonitrile (Table 5, entries 2–8). Good yields and TONs were also obtained using 4-*tert*-butylbromobenzene or 4-bromoanisole. With these two deactivated substrates, TONs of 4400 and 870 were obtained, respectively (Table 5, entries 10–12). Again, the strongly deactivated aryl bromide 4-*N,N*-dimethylaniline was found to be unreactive using this procedure (Table 5, entry 13). Electron-deficient *meta*- and *ortho*-substituted aryl bromides reacted with thiophene-2-carbonitrile gave **39–42** in 98–10000 TONs (Table 5, entries 14–17). On the other hand,

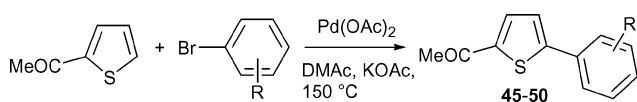
Table 6 Reaction of 2-acetylthiophene with aryl bromides (Scheme 6)

Entry	Aryl bromide	Substrate/ catalyst ratio	Prod.	Yield (%)
1	4-Bromoacetophenone	1000	45	91 (78)
2	Methyl 4-bromobenzoate	1000	46	89 (76)
3	Methyl 4-bromobenzoate	10000	46	36
4	4-(Trifluoromethyl)- bromobenzene	1000	47	94 (80)
5	4-(Trifluoromethyl)- bromobenzene	10000	47	81
6	4-Bromobenzonitrile	1000	48	90 (78)
7	4-Bromobenzonitrile	10000	48	15
8	4-Bromofluorobenzene	1000	49	92 (79)
9	4-Bromoanisole	1000	50	78 (63)

Conditions: Pd(OAc)₂, aryl bromide (1 mmol), 2-acetylthiophene (2 mmol), KOAc (2 mmol), DMAc, 20 h, 150 °C, GC and NMR yields, yields in parentheses are isolated.

the deactivated and congested aryl bromide: 2-bromoanisole was recovered unreacted (Table 5, entry 18).

The coupling reactions using 2-acetylthiophene were found to be less selective than those in the presence of 2-alkylthiophenes or thiophene-2-carbonitrile. With this substrate, the formation of some side-products was observed with most aryl bromides, mostly due to some arylation of the acetyl function. Therefore, the isolated yields of desired products **45–50** were slightly lower (Scheme 6, Table 6). However, also with this substrate, the reactions can be performed using only 0.1–0.01 mol% catalyst when using electron-poor aryl bromides (Table 6, entries 1–7). For the coupling of 4-fluorobromobenzene or 4-bromoanisole, we used 0.1 mol% catalyst (Table 6, entries 8 and 9).

**Scheme 6**

Then, we employed 2-acetylthiophene ethylene acetal as coupling partner (Scheme 7, Table 7). This reactant is commercially available on large scale at an affordable cost. With this substrate, we expected to reduce the formation of side-products. Moreover, the direct access to protected 5-aryl-2-acetylthiophenes might be very convenient in total synthesis. We observed that, in all cases, the desired 5-arylated thiophenes were obtained very cleanly. Almost no side-products were formed in the presence of this reactant. Using *para*-substituted electron-deficient aryl bromides, the compounds **51–54** were obtained in 2800–9800 TONs (Table 7, entries 1–7). 4-*tert*-Butylbromobenzene or 4-bromoanisole gave **55** and **56** in lower TONs of 620 and 810, respectively (Table 7, entries 8 and 9). The *ortho*-substituted 2-bromobenzaldehyde, 2-bromobenzonitrile or 1-bromonaphthalene also gave the expected 5-arylation products **57–59** using only 0.1–0.01 mol% catalyst (Table 7, entries 10–14). In the presence of the same catalyst loadings, heteroaromatic substrates, 3-bromopyridine or 4-bromoisoquinoline gave **60** and **61** in very high yields (Table 7, entries 15–17). 2-Formylthiophene reacted with a variety of aryl bromides gave the desired products **62–68** in 31–78% isolated yields using 0.1 mol% catalyst (Scheme 8, Table 8). The formation of a small

Table 7 Reaction of 2-acetylthiophene ethylene acetal with aryl bromides (Scheme 7)

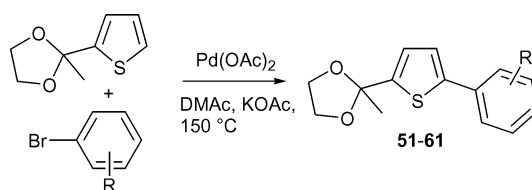
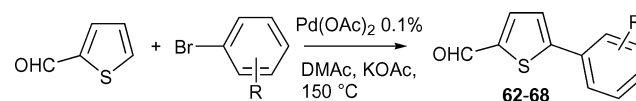
Entry	Aryl bromide	Substrate/ catalyst ratio	Prod.	Yield (%)
1	4-Bromobenzaldehyde	1000	51	100 (89)
2	4-Bromobenzaldehyde	10000	51	53
3	4-(Trifluoromethyl)- bromobenzene	10000	52	98 (87)
4	4-Bromobenzonitrile	1000	53	100 (89)
5	4-Bromobenzonitrile	10000	53	39
6	4-Bromofluorobenzene	1000	54	100 (88)
7	4-Bromofluorobenzene	10000	54	28
8	4- <i>tert</i> -Butylbromobenzene	1000	55	62 (56)
9	4-Bromoanisole	1000	56	81 (72)
10	2-Bromobenzaldehyde	1000	57	100 (88)
11	2-Bromobenzaldehyde	10000	57	16
12	2-Bromobenzonitrile	1000	58	100 (90)
13	1-Bromonaphthalene	10000	59	100 (87)
14	1-Bromonaphthalene	1000	59	74
15	3-Bromopyridine	1000	60	100 (91)
16	3-Bromopyridine	10000	60	50
17	4-Bromoisoquinoline	1000	61	100 (88)

Conditions: Pd(OAc)₂, aryl bromide (1 mmol), 2-acetylthiophene ethylene acetal (2 mmol), KOAc (2 mmol), DMAc, 20 h, 150 °C, GC and NMR yields, yields in parentheses are isolated.

Table 8 Reaction of 2-formylthiophene with aryl bromides (Scheme 8)

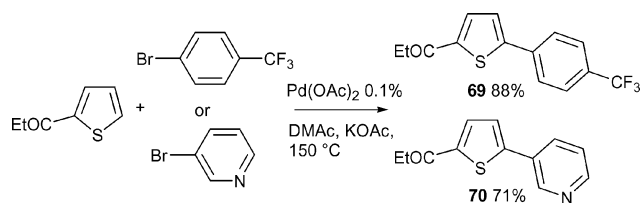
Entry	Aryl bromide	Prod.	Yield (%)
1	4-Bromobenzaldehyde	62	78 (67)
2	4-(Trifluoromethyl)-bromobenzene	63	85 (77)
3	4-Bromobenzonitrile	64	96 (78)
4	4-Bromofluorobenzene	65	95 (76)
5	4- <i>tert</i> -Butylbromobenzene	66	40 (31)
6	4-Bromoanisole	67	78 (68)
7	3-Bromopyridine	68	72 (65)

Conditions: Pd(OAc)₂ (0.001 mmol), aryl bromide (1 mmol), 2-formylthiophene (2 mmol), KOAc (2 mmol), DMAc, 20 h, 150 °C, GC and NMR yields, yields in parentheses are isolated.

**Scheme 7****Scheme 8**

amount of unidentified side-products was observed in all cases thus lowering the yields. Again, electron-deficient aryl bromides generally gave higher yields than the electron-rich ones.

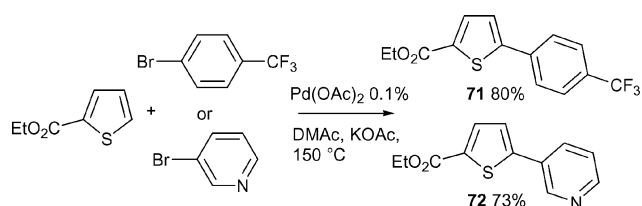
As expected, 2-propionylthiophene gave quite similar results than 2-acetylthiophene (Scheme 9). The formation of lower amounts of side-products than with 2-acetylthiophene was observed. The reaction of 2-propionylthiophene with 4-(trifluoromethyl)bromobenzene or 3-bromopyridine gave



Scheme 9

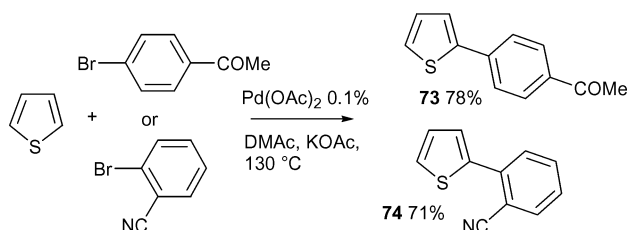
69 and **70** in 88 and 71% yields, respectively, employing 0.1 mol% catalyst.

Next, a thiophene substituted by an ester function in 2 position was employed (Scheme 10). Ethyl 2-thiophenecarboxylate coupled with 4-(trifluoromethyl)bromobenzene or 3-bromopyridine gave **71** and **72** in good yields using again only 0.1 mol% catalyst.



Scheme 10

Finally, thiophene was employed as reactant (Scheme 11). Using 4-bromoacetophenone or sterically hindered 2-bromobenzonitrile in the presence of as little as 0.1 mol% Pd(OAc)₂, the compounds **73** and **74** were obtained in 78 and 71% yields, respectively.



Scheme 11

Conclusions

We have demonstrated that, using this ligand-free procedure, the direct 5-arylation *via* C–H bond activation of thiophene derivatives proceeded in moderate to very high yields. In the presence of as little as 0.1–0.001 mol% of Pd(OAc)₂ as catalyst precursor, a wide range of aryl bromides were selectively arylated. With this ligand-free procedure, an increase of the catalyst loading to 1 mol% generally led more rapidly to aggregation of palladium to form so-called “palladium black” and gave lower yields of coupling products. This procedure gave the best results using electron-deficient aryl bromides, and several functions such as acetyl, benzoyl, nitro, nitrile, fluoro or trifluoromethyl are tolerated. Deactivated or congested aryl bromides also gave satisfactory results in some cases. Several functions on the thiophene derivative are also tolerated. This ligand-less low catalyst loading procedure is economically and environmentally

attractive. There is no need to eliminate phosphine derivatives at the end of the reaction. Under such low catalyst concentration, palladium stabilizing agents such as ammonium salts, are useless, thus reducing the amount of wastes. With this C–H activation procedure, no preparation of an organometallic derivative is required, reducing the number of steps and therefore the mass of waste product to prepare these compounds, compared to Negishi, Stille or Suzuki type coupling reactions. Moreover, as it should be possible to recover most of DMAc, the major waste is the relatively non-toxic AcOH/KBr instead of metallic salts with more classical coupling procedures. For these reasons, the methodology developed here is very promising for the sustainable synthesis of 5-arylthiophenes.

Experimental section

General procedure

As a typical experiment, the reaction of the aryl halide (1 mmol), thiophene derivative (2 mmol) and KOAc (0.196 g, 2 mmol) at 150 °C during 20 h in dry DMAc (3 mL) in the presence of Pd(OAc)₂ under argon affords the corresponding coupling product after extraction with dichloromethane, evaporation and filtration on silica gel: pentane/ether: 1/4 or ether for compounds **10**, **22**, **23**, **24**, **38**, **44**, **60**, **61** and **68**.

2-*n*-Butyl-5-phenylthiophene^{7a} (**1**). Iodobenzene (0.204 g, 1 mmol) and 2-*n*-butylthiophene (0.280 g, 2 mmol) affords **1** in 46% (0.100 g) yield.

4-(5-*n*-Butylthiophen-2-yl)acetophenone^{7a} (**2**). 4-Bromoacetophenone (0.199 g, 1 mmol) and 2-*n*-butylthiophene (0.280 g, 2 mmol) affords **2** in 85% (0.220 g) yield.

4-(5-*n*-Butylthiophen-2-yl)benzophenone^{7a} (**3**). 4-Bromobenzophenone (0.261 g, 1 mmol) and 2-*n*-butylthiophene (0.280 g, 2 mmol) affords **3** in 86% (0.275 g) yield.

4-(5-*n*-Butylthiophen-2-yl)benzaldehyde^{7a} (**4**). 4-Bromobenzaldehyde (0.185 g, 1 mmol) and 2-*n*-butylthiophene (0.280 g, 2 mmol) affords **4** in 89% (0.217 g) yield.

2-*n*-Butyl-5-[4-(trifluoromethyl)phenyl]thiophene^{7a} (**5**). 4-(Trifluoromethyl)bromobenzene (0.225 g, 1 mmol) and 2-*n*-butylthiophene (0.280 g, 2 mmol) affords **5** in 90% (0.256 g) yield.

4-(5-*n*-Butylthiophen-2-yl)benzonitrile^{7a} (**6**). 4-Bromobenzonitrile (0.182 g, 1 mmol) and 2-*n*-butylthiophene (0.280 g, 2 mmol) and KOAc (0.196 g, 2 mmol) affords **6** in 88% (0.212 g) yield.

2-*n*-Butyl-5-(4-fluorophenyl)thiophene (**7**). 4-Bromofluorobenzene (0.175 g, 1 mmol) and 2-*n*-butylthiophene (0.280 g, 2 mmol) and KOAc (0.196 g, 2 mmol) affords **7** in 81% (0.190 g) yield.

2-*n*-Butyl-5-*p*-tolylthiophene (**8**). 4-Bromotoluene (0.171 g, 1 mmol) and 2-*n*-butylthiophene (0.280 g, 2 mmol) affords **8** in 67% (0.154 g) yield.

2-*n*-Butyl-5-(4-methoxyphenyl)thiophene^{7a} (**9**). 4-Bromoanisole (0.187 g, 1 mmol) and 2-*n*-butylthiophene (0.280 g, 2 mmol) affords **9** in 62% (0.153 g) yield.

3-(5-*n*-Butylthiophen-2-yl)benzaldehyde (11). 3-Bromo-benzaldehyde (0.185 g, 1 mmol) and 2-*n*-butylthiophene (0.280 g, 2 mmol) affords **11** in 88% (0.215 g) yield.

3-(5-*n*-Butylthiophen-2-yl)acetophenone (12). 3-Bromo-acetophenone (0.199 g, 1 mmol) and 2-*n*-butylthiophene (0.280 g, 2 mmol) affords **12** in 91% (0.235 g) yield.

2-*n*-Butyl-5-[3-(trifluoromethyl)phenyl]thiophene (13). 3-(Trifluoromethyl)bromobenzene (0.225 g, 1 mmol) and 2-*n*-butylthiophene (0.280 g, 2 mmol) affords **13** in 93% (0.264 g) yield.

2-[3,5-Bis(trifluoromethyl)phenyl]-5-*n*-butylthiophene (14). 3,5-Bis(trifluoromethyl)bromobenzene (0.293 g, 1 mmol) and 2-*n*-butylthiophene (0.280 g, 2 mmol) affords **14** in 90% (0.317 g) yield.

2-(5-*n*-Butylthiophen-2-yl)benzaldehyde (15). 2-Bromo-benzaldehyde (0.185 g, 1 mmol) and 2-*n*-butylthiophene (0.280 g, 2 mmol) affords **15** in 84% (0.205 g) yield.

2-*n*-Butyl-5-[2-(trifluoromethyl)phenyl]thiophene^{7a} (17). 2-(Trifluoromethyl)bromobenzene (0.225 g, 1 mmol) and 2-*n*-butylthiophene (0.280 g, 2 mmol) affords **17** in 92% (0.262 g) yield.

2-(5-Butylthiophene-2-yl)benzonitrile (18). 2-Bromobenzonitrile (0.182 g, 1 mmol) and 2-*n*-butylthiophene (0.280 g, 2 mmol) affords **18** in 67% (0.162 g) yield.

2-*n*-Butyl-5-(naphthalen-1-yl)thiophene^{7a} (19). 1-Bromonaphthalene (0.207 g, 1 mmol) and 2-*n*-butylthiophene (0.280 g, 2 mmol) affords **19** in 87% (0.232 g) yield.

2-Butyl-5-*o*-tolylthiophene^{7a} (20). 2-Bromotoluene (0.171 g, 1 mmol) and 2-*n*-butylthiophene (0.280 g, 2 mmol) affords **20** in 42% (0.097 g) yield.

2-*n*-Butyl-5-(2,6-difluorophenyl)thiophene (21). 2,6-Difluorobromobenzene (0.193 g, 1 mmol) and 2-*n*-butylthiophene (0.280 g, 2 mmol) affords **21** in 86% (0.217 g) yield.

3-(5-*n*-Butylthiophen-2-yl)pyridine^{7a} (22). 3-Bromopyridine (0.158 g, 1 mmol) and 2-*n*-butylthiophene (0.280 g, 2 mmol) affords **22** in 91% (0.198 g) yield.

3-(5-*n*-Butylthiophen-2-yl)quinoline^{7a} (23). 3-Bromoquinoline (0.208 g, 1 mmol) and 2-*n*-butylthiophene (0.280 g, 2 mmol) affords **23** in 90% (0.240 g) yield.

5-(5-*n*-Butylthiophen-2-yl)pyrimidine (24). 5-Bromopyrimidine (0.159 g, 1 mmol) and 2-*n*-butylthiophene (0.280 g, 2 mmol) affords **24** in 88% (0.192 g) yield.

4-(5-Methylthiophen-2-yl)benzaldehyde (26). 4-Bromobenzaldehyde (0.185 g, 1 mmol) and 2-methylthiophene (0.196 g, 2 mmol) affords **26** in 89% (0.180 g) yield.

4-(5-Methylthiophen-2-yl)benzonitrile (27). 4-Bromobenzonitrile (0.182 g, 1 mmol) and 2-methylthiophene (0.196 g, 2 mmol) affords **27** in 92% (0.183 g) yield.

2-(4-Fluorophenyl)-5-methylthiophene (28). 4-Bromofluorobenzene (0.175 g, 1 mmol) and 2-methylthiophene (0.196 g, 2 mmol) affords **28** in 87% (0.168 g) yield.

2-(4-Methoxyphenyl)-5-methylthiophene^{17a} (29). 4-Bromoanisole (0.187 g, 1 mmol) and 2-methylthiophene (0.196 g, 2 mmol) affords **29** in 41% (0.084 g) yield.

5-(4-Acetylphenyl)thiophene-2-carbonitrile (30). 4-Bromoacetophenone (0.199 g, 1 mmol) and thiophene 2-carbonitrile (0.218 g, 2 mmol) affords **30** in 80% (0.182 g) yield.

5-(4-Formylphenyl)thiophene-2-carbonitrile (31). 4-Bromobenzaldehyde (0.185 g, 1 mmol) and thiophene 2-carbonitrile (0.218 g, 2 mmol) affords **31** in 85% (0.181 g) yield.

Methyl 4-(5-cyanothiophen-2-yl)benzoate (32). Methyl 4-bromobenzoate (0.215 g, 1 mmol) and thiophene 2-carbonitrile (0.218 g, 2 mmol) affords **32** in 87% (0.212 g) yield.

5-[4-(Trifluoromethyl)phenyl]thiophene-2-carbonitrile^{7a} (33). 4-(Trifluoromethyl)bromobenzene (0.225 g, 1 mmol) and thiophene 2-carbonitrile (0.218 g, 2 mmol) affords **33** in 90% (0.228 g) yield.

5-(4-Cyanophenyl)thiophene-2-carbonitrile^{17b} (34). 4-Bromobenzonitrile (0.182 g, 1 mmol) and thiophene 2-carbonitrile (0.218 g, 2 mmol) affords **34** in 89% (0.187 g) yield.

5-(4-Fluorophenyl)thiophene-2-carbonitrile^{7a} (35). 4-Bromofluorobenzene (0.175 g, 1 mmol) and thiophene 2-carbonitrile (0.218 g, 2 mmol) affords **35** in 84% (0.171 g) yield.

5-(4-*tert*-Butylphenyl)thiophene-2-carbonitrile^{7a} (36). 4-*tert*-Butylbromobenzene (0.213 g, 1 mmol) and thiophene 2-carbonitrile (0.218 g, 2 mmol) affords **36** in 62% (0.150 g) yield.

5-(4-Methoxyphenyl)thiophene-2-carbonitrile^{7a} (37). 4-Bromoanisole (0.187 g, 1 mmol) and thiophene 2-carbonitrile (0.218 g, 2 mmol) affords **37** in 77% (0.166 g) yield.

5-(3-Cyanophenyl)thiophene-2-carbonitrile (39). 3-Bromobenzonitrile (0.182 g, 1 mmol) and thiophene 2-carbonitrile (0.218 g, 2 mmol) affords **39** in 89% (0.187 g) yield.

5-(2-Formylphenyl)thiophene-2-carbonitrile (40). 2-Bromobenzaldehyde (0.185 g, 1 mmol) and thiophene 2-carbonitrile (0.218 g, 2 mmol) affords **40** in 87% (0.186 g) yield.

5-(2-Trifluoromethylphenyl)thiophene-2-carbonitrile^{7a} (41). 2-(Trifluoromethyl)bromobenzene (0.225 g, 1 mmol) and thiophene 2-carbonitrile (0.218 g, 2 mmol) affords **41** in 90% (0.228 g) yield.

5-(2-Cyanophenyl)thiophene-2-carbonitrile (42). 2-Bromobenzonitrile (0.182 g, 1 mmol) and thiophene 2-carbonitrile (0.218 g, 2 mmol) affords **42** in 91% (0.191 g) yield.

5-(Pyridin-3-yl)thiophene-2-carbonitrile (44). 3-Bromopyridine (0.158 g, 1 mmol) and thiophene 2-carbonitrile (0.218 g, 2 mmol) affords **44** in 86% (0.160 g) yield.

1-[4-(5-Acetylthiophen-2-yl)phenyl]ethanone^{17c} (45). 4-Bromoacetophenone (0.199 g, 1 mmol) and 2-acetylthiophene (0.252 g, 2 mmol) affords **45** in 78% (0.191 g) yield.

Methyl 4-(5-acetylthiophen-2-yl)benzoate^{17d} (46). Methyl 4-bromobenzoate (0.215 g, 1 mmol) and 2-acetylthiophene (0.252 g, 2 mmol) affords **46** in 76% (0.198 g) yield.

1-[5-[4-(Trifluoromethyl)phenyl]thiophen-2-yl]ethanone^{7a} (47). 4-(Trifluoromethyl)bromobenzene (0.225 g, 1 mmol) and 2-acetylthiophene (0.252 g, 2 mmol) affords **47** in 80% (0.216 g) yield.

4-(5-Acetylthiophen-2-yl)benzonitrile^{7a} (48). 4-Bromobenzonitrile (0.182 g, 1 mmol) and 2-acetylthiophene (0.252 g, 2 mmol) affords **48** in 78% (0.177 g) yield.

1-[5-(4-Fluorophenyl)thiophen-2-yl]ethanone^{7a} (49). 4-Bromofluorobenzene (0.175 g, 1 mmol) and 2-acetylthiophene (0.252 g, 2 mmol) affords **49** in 79% (0.174 g) yield.

1-[5-(4-Methoxyphenyl)thiophen-2-yl]ethanone^{17c} (50). 4-Bromoanisole (0.187 g, 1 mmol) and 2-acetylthiophene (0.252 g, 2 mmol) affords **50** in 63% (0.146 g) yield.

4-[5-(2-Methyl-1,3-dioxolan-2-yl)thiophen-2-yl]benzaldehyde (51). 4-Bromobenzaldehyde (0.185 g, 1 mmol) and 2-acetylthiophene ethylene acetal (0.340 g, 2 mmol) affords **51** in 89% (0.244 g) yield.

2-Methyl-2-[5-[4-(trifluoromethyl)phenyl]thiophen-2-yl]-1,3-dioxolane (52). 4-(Trifluoromethyl)bromobenzene (0.225 g, 1 mmol) and 2-acetylthiophene ethylene acetal (0.340 g, 2 mmol) affords **52** in 87% (0.273 g) yield.

4-[5-(2-Methyl-1,3-dioxolan-2-yl)thiophen-2-yl]benzonitrile (53). 4-Bromobenzonitrile (0.182 g, 1 mmol) and 2-acetylthiophene ethylene acetal (0.340 g, 2 mmol) affords **53** in 89% (0.242 g) yield.

2-[5-(4-Fluorophenyl)thiophen-2-yl]-2-methyl-1,3-dioxolane (54). 4-Bromofluorobenzene (0.175 g, 1 mmol) and 2-acetylthiophene ethylene acetal (0.340 g, 2 mmol) affords **54** in 88% (0.233 g) yield.

2-[5-(4-tert-Butylphenyl)thiophen-2-yl]-2-methyl-1,3-dioxolane (55). 4-tert-Butylbromobenzene (0.213 g, 1 mmol) and 2-acetylthiophene ethylene acetal (0.340 g, 2 mmol) affords **55** in 56% (0.169 g) yield.

2-[5-(4-Methoxyphenyl)thiophen-2-yl]-2-methyl-1,3-dioxolane (56). 4-Bromoanisole (0.187 g, 1 mmol) and 2-acetylthiophene ethylene acetal (0.340 g, 2 mmol) affords **56** in 72% (0.199 g) yield.

2-[5-(2-Methyl-1,3-dioxolan-2-yl)thiophen-2-yl]benzaldehyde (57). 2-Bromobenzaldehyde (0.185 g, 1 mmol) and 2-acetylthiophene ethylene acetal (0.340 g, 2 mmol) affords **57** in 88% (0.241 g) yield.

2-[5-(2-Methyl-1,3-dioxolan-2-yl)thiophen-2-yl]benzonitrile (58). 2-Bromobenzonitrile (0.182 g, 1 mmol) and 2-acetylthiophene ethylene acetal (0.340 g, 2 mmol) affords **58** in 90% (0.244 g) yield.

2-Methyl-2-(5-naphthalen-1-yl)thiophen-2-yl]-1,3-dioxolane (59). 1-Bromonaphthalene (0.207 g, 1 mmol) and 2-acetylthiophene ethylene acetal (0.340 g, 2 mmol) affords **59** in 87% (0.258 g) yield.

3-[5-(2-Methyl-1,3-dioxolan-2-yl)thiophen-2-yl]pyridine (60). 3-Bromopyridine (0.158 g, 1 mmol) and 2-acetylthiophene ethylene acetal (0.340 g, 2 mmol) affords **60** in 91% (0.225 g) yield.

4-[5-(2-Methyl-1,3-dioxolan-2-yl)thiophen-2-yl]isoquinoline (61). 4-Bromoisoquinoline (0.208 g, 1 mmol) and 2-acetylthiophene ethylene acetal (0.340 g, 2 mmol) affords **61** in 88% (0.262 g) yield.

5-(4-Formylphenyl)thiophene-2-carbaldehyde^{17f} (62). 4-Bromobenzaldehyde (0.185 g, 1 mmol) and 2-formylthiophene (0.224 g, 2 mmol) affords **62** in 67% (0.145 g) yield.

5-[4-(Trifluoromethyl)phenyl]thiophene-2-carbaldehyde^{17g} (63). 4-(Trifluoromethyl)bromobenzene (0.225 g, 1 mmol) and 2-formylthiophene (0.224 g, 2 mmol) affords **63** in 77% (0.197 g) yield.

4-(5-Formylthiophen-2-yl)benzonitrile^{17h} (64). 4-Bromobenzonitrile (0.182 g, 1 mmol) and 2-formylthiophene (0.224 g, 2 mmol) affords **64** in 78% (0.166 g) yield.

5-(4-Fluorophenyl)thiophene-2-carbaldehyde¹⁷ⁱ (65). 4-Bromofluorobenzene (0.175 g, 1 mmol) and 2-formylthiophene (0.224 g, 2 mmol) affords **65** in 76% (0.157 g) yield.

5-(4-tert-Butylphenyl)thiophene-2-carbaldehyde (66). 4-tert-Butylbromobenzene (0.213 g, 1 mmol) and 2-formylthiophene (0.224 g, 2 mmol) affords **66** in 31% (0.076 g) yield.

5-(4-Methoxyphenyl)thiophene-2-carbaldehyde¹⁰ (67). 4-Bromoanisole (0.187 g, 1 mmol) and 2-formylthiophene (0.224 g, 2 mmol) affords **67** in 68% (0.149 g) yield.

5-(Pyridin-3-yl)thiophene-2-carbaldehyde^{17j} (68). 3-Bromopyridine (0.158 g, 1 mmol) and 2-formylthiophene (0.224 g, 2 mmol) affords **68** in 65% (0.123 g) yield.

1-[5-[4-(Trifluoromethyl)phenyl]thiophen-2-yl]propan-1-one (69). 4-(Trifluoromethyl)bromobenzene (0.225 g, 1 mmol) and 2-propionylthiophene (0.280 g, 2 mmol) affords **69** in 88% (0.250 g) yield.

1-[5-(Pyridin-3-yl)thiophen-2-yl]propan-1-one (70). 3-Bromopyridine (0.158 g, 1 mmol) and 2-propionylthiophene (0.280 g, 2 mmol) affords **70** in 71% (0.154 g) yield.

Ethyl 5-[4-trifluoromethyl]phenyl]thiophene-2-carboxylate (71). 4-(Trifluoromethyl)bromobenzene (0.225 g, 1 mmol) and ethyl 2-thiophenecarboxylate (0.312 g, 2 mmol) affords **71** in 80% (0.240 g) yield.

Ethyl 5-(pyridin-3-yl)thiophene-2-carboxylate (72). 3-Bromopyridine (0.158 g, 1 mmol) and ethyl 2-thiophenecarboxylate (0.312 g, 2 mmol) affords **72** in 73% (0.170 g) yield.

1-(4-Thiophen-2-ylphenyl)-ethanone (73)^{17k}. 4-Bromoacetophenone (0.199 g, 1 mmol) and thiophene (0.420 g, 5 mmol) affords **73** in 78% (0.158 g) yield.

2-Thiophen-2-yl-benzonitrile (74)^{17l}. 2-Bromobenzonitrile (0.182 g, 1 mmol) and thiophene (0.420 g, 5 mmol) affords **74** in 71% (0.132 g) yield.

Acknowledgements

This research was supported by a Marie Curie Intra-European Fellowships within the 6th European Community Framework Programme. J. R. is grateful to "Ministère de la Recherche" for a grant. We thank P. H. Dixneuf for useful discussions.

Notes and references

- 1 J. J. Li and G. W. Gribble, *Palladium in Heterocyclic Chemistry*, Pergamon, Amsterdam, 2000.
- 2 (a) I. Kondolff, H. Doucet and M. Santelli, *Synlett*, 2005, 2057; (b) N. Kuhnert, C. Patel and F. Jami, *Tetrahedron Lett.*, 2005, **46**, 7575; (c) S. P. G. Costa, R. M. F. Batista, P. Cardoso, M. Belsley and M. M. M. Raposo, *Eur. J. Org. Chem.*, 2006, 3938; (d) A. N. Cammidge, V. H. M. Goddard, H. Gopee, N. L. Harrison, D. L. Hughes, C. J. Schubert, B. M. Sutton, G. L. Watts and A. J. Whitehead, *Org. Lett.*, 2006, **8**, 4071; (e) J.-H. Li, Q.-M. Zhu and Y.-X. Xie, *Tetrahedron*, 2006, **62**, 10888; (f) V. Promarak, A. Pankvuang and S. Ruchirawat, *Tetrahedron Lett.*, 2007, **48**, 1151; (g) C.-L. Deng, S.-M. Guo, Y.-X. Xie and J.-H. Li, *Eur. J. Org. Chem.*, 2007, 1457; (h) L. M. Klingensmith, M. M. Bio and G. A. Moniz, *Tetrahedron Lett.*, 2007, **48**, 8242; (i) D. P. Hagberg, T. Marinado, K. M. Karlsson, K. Nonomura, P. Qin, G. Boschloo, T. Brinck, A. Hagfeldt and L. Sun, *J. Org. Chem.*, 2007, **72**, 9550; (j) E. Paunescu, N. Matuszak and P. Melynyk, *Tetrahedron*, 2007, **63**, 12791; (k) I. Kondolff, H. Doucet and M. Santelli, *J. Het. Chem.*, 2008, **45**, 109.
- 3 (a) C. Fave, Y. Leroux, G. Trippe, H. Randriamahazaka, V. Noel and J.-C. Lacroix, *J. Am. Chem. Soc.*, 2007, **129**, 1890; (b) D. Kim, J. K. Lee, S. O. Kang and J. Ko, *Tetrahedron*, 2007, **63**, 1913; (c) N. Negishi, Y. Ie, M. Taniguchi, T. Kawai, H. Tada, T. Kaneda and Y. Aso, *Org. Lett.*, 2007, **9**, 829; (d) J. Ohshita, S. Kangai, H. Yoshida, A. Kunai, S. Kajiwara, Y. Ooyama and Y. Harima, *J. Organomet. Chem.*, 2007, **692**, 801; (e) J. Ohshita, S. Kangai, Y. Tada, H. Yoshida, K. Sakamaki, A. Kunai and Y. Kunugi, *J. Organomet. Chem.*, 2007, **692**, 1020; (f) A. Pietrangelo, M. J. MacLachlan, M. O. Wolf and B. O. Patrick, *Org. Lett.*, 2007, **9**, 3571; (g) P.-L. T. Boudreaux, S. Wakim, N. Blouin, M. Simard, C. Tessier, Y. Tao and M. Leclerc, *J. Am. Chem. Soc.*, 2007, **129**, 9125; (h) C. Zhao, Y. Zhang and M.-K. Ng, *J. Org. Chem.*, 2007, **72**, 6364; (i) M. Endou, Y. Ie, T. Kaneda and Y. Aso, *J. Org. Chem.*, 2007, **72**, 2659; (j) X. Zhang, Y. Qu, L. Bu, H. Tian, J. Zhang, L. Wang, Y. Geng and F. Wang, *Chem. Eur. J.*, 2007, **13**, 6238; (k) S. Lois, J.-C. Flores, J.-P. Lere-Porte, F. Serein-Spirau, J. J. E. Moreau, K. Miqueu, J.-M. Sotiropoulos, P. Baylere, M. Tillard and C. Belin, *Eur. J. Org. Chem.*, 2007, 4019.
- 4 (a) B. Betzemeier and P. Knochel, *Angew. Chem. Int. Ed. Eng.*, 1997, **36**, 2623; (b) J. Sirieix, M. Ossberger, B. Betzemeier and P. Knochel, *Synlett*, 2000, 1613; (c) M. Iyoda, K. Nakao, T. Kondo, Y. Kuwatani, M. Yoshida, H. Matsuyama, K. Fukami and S. Nagase, *Tetrahedron Lett.*, 2001, **42**, 6869; (d) W.-L. Jia, D.-R. Bai, T. McCormick, Q.-D. Liu, M. Motala, R.-Y. Wang, C. Seward, Y. Tao and S. Wang, *Chem. Eur. J.*, 2004, **10**, 994; (e) F. F. Kneisel, M. Dochnahl and P. Knochel, *Angew. Chem. Int. Ed.*, 2004, **43**, 1017; (f) K. Krascenicsova, P. Walla, P. Kasak, G. Uray, C. O. Kappe and M. Putala, *Chem. Commun.*, 2004, 2606.
- 5 A. Ohta, Y. Akita, T. Ohkuwa, M. Chiba, R. Fukunaga, A. Miyafuji, T. Nakata, N. Tani and Y. Aoyagi, *Heterocycles*, 1990, **31**, 1951.
- 6 (a) V. Ritleng, C. Sirlin and M. Pfeffer, *Chem. Rev.*, 2002, **102**, 1731; (b) D. Alberico, M. E. Scott and M. Lautens, *Chem. Rev.*, 2007, **107**, 174; (c) T. Satoh and M. Miura, *Chem. Lett.*, 2007, **36**, 200; (d) H. Doucet and J. C. Hierso, *Curr. Opin. Drug Discov. Devel.*, 2007, **10**, 672; (e) L.-C. Campeau, D. R. Stuart and K. Fagnou, *Aldrichimica Acta*, 2007, **40**, 35.
- 7 (a) A. Battace, M. Lemhadri, T. Zair, H. Doucet and M. Santelli, *Adv. Synth. Catal.*, 2007, **349**, 2507; (b) J. Roger and H. Doucet, *Org. Biomol. Chem.*, 2008, **6**, 169; (c) F. Derridj, A. L. Gottumukkala, S. Djebbar and H. Doucet, *Eur. J. Inorg. Chem.*, 2008, 2550.
- 8 For direct 2- or 5-arylations of thiophenes using palladium associated to monophosphine ligands: (a) S. Pivsa-Art, T. Satoh, Y. Kawamura, M. Miura and M. Nomura, *Bull. Chem. Soc. Jpn.*, 1998, **71**, 467; (b) R. R. Hark, D. B. Hauze, O. Petrovskaia and M. M. Joulie, *Can. J. Chem.*, 2001, **79**, 1632; (c) T. Okazawa, T. Satoh, M. Miura and M. Nomura, *J. Am. Chem. Soc.*, 2002, **124**, 5286; (d) B. Glover, K. A. Harvey, B. Liu, M. J. Sharp and M. F. Tymoschenko, *Org. Lett.*, 2003, **5**, 301; (e) C. W. G. Fishwick, R. Grigg, V. Sridharan and J. Virica, *Tetrahedron*, 2003, **59**, 4451; (f) A. Yokooji, T. Satoh, M. Miura and M. Nomura, *Tetrahedron*, 2004, **60**, 6757; (g) E. M. Beccalli, G. Brogini, M. Martinelli, G. Paladino and C. Zoni, *Eur. J. Org. Chem.*, 2005, 2091; (h) K. Kobayashi, A. Sugie, M. Takahashi, K. Masui and A. Mori, *Org. Lett.*, 2005, **7**, 5083; (i) L. Joucla, A. Putey and B. Joseph, *Tetrahedron Lett.*, 2005, **46**, 8177; (j) M. Nakano, T. Satoh and M. Miura, *J. Org. Chem.*, 2006, **71**, 8309; (k) J. Fournier, D. Chabert, G. Chatelain, S. Pellet-Rostaing, D. Bouchu and M. Lemaire, *Tetrahedron Lett.*, 2006, **47**, 1015; (l) A. Martins, D. Alberico and M. Lautens, *Org. Lett.*, 2006, **8**, 4827; (m) K. Kobayashi, M. S. Mohamed, Ahmed and A. Mori, *Tetrahedron*, 2006, **62**, 9548; (n) A. K. Mohanakrishnan, P. Amaladass and J. A. Clement, *Tetrahedron Lett.*, 2007, **48**, 539; (o) H. A. Chiong and O. Daugulis, *Org. Lett.*, 2007, **9**, 1449; (p) E. David, S. Pellet-Rostaing and M. Lemaire, *Tetrahedron*, 2007, **63**, 8999; (q) P. Amaladass, J. A. Clement and A. K. Mohanakrishnan, *Tetrahedron*, 2007, **63**, 10363; (r) H. Ohno, M. Iuchi, N. Fujii and T. Tanaka, *Org. Lett.*, 2007, **9**, 4813; (s) S. H. Wunderlich and P. Knochel, *Angew. Chem. Int. Ed.*, 2007, **46**, 7685; (t) G. L. Turner, J. A. Morris and M. F. Greaney, *Angew. Chem. Int. Ed.*, 2007, **46**, 7996; (u) E. David, J. Lejeune, S. Pellet-Rostaing, J. Schulz, M. Lemaire, J. Chauvin and A. Deronzier, *Tetrahedron Lett.*, 2008, **49**, 1860.
- 9 For direct 2- or 5-arylations of thiophenes using palladium associated to diphosphine ligands: (a) K. Masui, A. Mori, K. Okano, K. Takamura, M. Kinoshita and T. Ikeda, *Org. Lett.*, 2004, **6**, 2011; (b) K. Masui, H. Ikegami and A. Mori, *J. Am. Chem. Soc.*, 2004, **126**, 5074.
- 10 I. C. F. R. Ferreira, M.-J. R. P. Queiroz and G. Kirsch, *Tetrahedron*, 2003, **59**, 3737.
- 11 For direct 2- or 5-arylations of thiophenes using Pd(OAc)₂ and an ammonium salt: (a) L. Lavenot, C. Gozzi, K. Ilg, I. Orlova, V. Penalva and M. Lemaire, *J. Organomet. Chem.*, 1998, **567**, 49; (b) M. Smet, J. Van, Dijk and W. Dehaen, *Synlett*, 1999, 495; (c) J. Fournier, D. Chabert, C. Gozzi and M. Lemaire, *Tetrahedron Lett.*, 2002, **43**, 1829; (d) J. Fournier, D. Chabert, L. Joucla, E. David and M. Lemaire, *Tetrahedron*, 2004, **60**, 3221; (e) A. Borghese, G. Geldhof and L. Antoine, *Tetrahedron Lett.*, 2006, **47**, 9249; (f) S. H. Mashraqui, M. Ashraf and S. G. Ghadigaonkar, *Synlett*, 2006, 2423; (g) K. Mitsudo, P. Thansandote, T. Wilhelm, B. Mariampillai and M. Lautens, *Org. Lett.*, 2006, **8**, 3939.
- 12 (a) E. David, J. Perrin, S. Pellet-Rostaing, J. Fournier, dit Chabert and M. Lemaire, *J. Org. Chem.*, 2005, **70**, 3569; (b) E. David, C. Rangheard, S. Pellet-Rostaing and M. Lemaire, *Synlett*, 2006, 2016.
- 13 (a) A. H. M. de Vries, J. M. C. A. Mulders, J. H. M. Mommers, H. J. W. Henderickx and J. G. de Vries, *Org. Lett.*, 2003, **5**, 3285; (b) M. T. Reetz and J. G. de Vries, *Chem. Commun.*, 2004, 1559; (c) J. G. de Vries, *Dalton Trans.*, 2006, 421.
- 14 A. Alimardanov, L. Schmieder-van, de Vondervoort, A. H. M. de Vries and J. G. de Vries, *Adv. Synth. Catal.*, 2004, **346**, 1812.
- 15 (a) A. Battace, M. Lemhadri, T. Zair, H. Doucet and M. Santelli, *Organometallics*, 2007, **26**, 472; (b) A. L. Gottumukkala and H. Doucet, *Adv. Synth. Catal.*, 2008, **350**, 2183; (c) A. L. Gottumukkala and H. Doucet, *Eur. J. Inorg. Chem.*, 2007, 3629; (d) F. Derridj, S. Djebbar, O. Benali-Baitich and H. Doucet, *J. Organomet. Chem.*, 2008, **693**, 135; (e) A. L. Gottumukkala, F. Derridj, S. Djebbar and H. Doucet, *Tetrahedron Lett.*, 2008, **49**, 2926.
- 16 F. Požgan, J. Roger and H. Doucet, *ChemSusChem*, 2008, **1**, 404.
- 17 (a) D. R. Shridhar, M. Jogibhukta, P. S. Rao and V. K. Handa, *Synthesis*, 1982, 1061; (b) V. Tralic-Kulenovic, G. Karminski-Zamola, L. Racane and L. Fiser-Jakic, *Heterocyclic Commun.*, 1998, **4**, 423; (c) E. L. Anderson, J. E. Casey, Jr., M. Emas, E. E. Force, E. M. Jensen, R. S. Matz and D. E. Rivard, *J. Med. Chem.*, 1963, **6**, 787; (d) F. F. Kneisel, M. Dochnahl and P. Knochel, *Angew. Chem. Int. Ed.*, 2004, **43**, 1017; (e) J. C. Meslin, Y. T. N'Guessan and H. Quiniou, *Tetrahedron*, 1975, **31**, 2679; (f) S. P. G. Costa, R. M. F. Batista, P. Cardoso, M. Belsley and M. M. M. Raposo, *Eur. J. Org. Chem.*, 2006, 3938; (g) S. Ando, J.-i. Nishida, H. Tada, Y. Inoue, S. Tokito and Y. Yamashita, *J. Am. Chem. Soc.*, 2005, **127**, 5336; (h) S. Mallena, M. P. H. Lee, C. Bailly, S. Neidle, A. Kumar, D. W. Boykin and W. D. Wilson, *J. Am. Chem. Soc.*, 2004, **126**, 13659; (i) J. C. Bussolari and D. C. Reborn, *Org. Lett.*, 1999, **1**, 965; (j) T. E. Barder and S. L. Buchwald, *Org. Lett.*, 2004, **6**, 2649; (k) S. Sase, M. Jaric, A. Metzger, V. Malakhov and P. Knochel, *J. Org. Chem.*, 2008, **73**, 7380; (l) B. Sain and J. S. Jagir, *J. Org. Chem.*, 2008, **55**, 2545.

'I wish the others were as easy to use.'



'ReSource is the best online submission system of any publisher.'

'It leads the way for online submission and refereeing.'

ReSource



A selection of comments received from just a few of the thousands of satisfied RSC authors and referees who have used ReSource to submit and referee manuscripts. The online portal provides a host of services, to help you through every step of the publication process.

authors benefit from a user-friendly electronic submission process, manuscript tracking facilities, online proof collection, free pdf reprints, and can review all aspects of their publishing history

referees can download articles, submit reports, monitor the outcome of reviewed manuscripts, and check and update their personal profile

NEW!! We have added a number of enhancements to ReSource, to improve your publishing experience even further.

New features include:

- the facility for authors to save manuscript submissions at key stages in the process (handy for those juggling a hectic research schedule)
- checklists and support notes (with useful hints, tips and reminders)
- and a fresh new look (so that you can more easily see what you have done and need to do next)

A class-leading submission and refereeing service, top quality high impact journals, all from a not-for-profit society publisher ... is it any wonder that more and more researchers are supporting RSC Publishing? Go online today and find out more.

RSCPublishing

www.rsc.org/resource

Registered Charity Number 207890



Top Quality Bioscience Journals

Molecular BioSystems - a journal with a focus on the interface between chemistry and the -omic sciences and systems biology. www.molecularbiosystems.org

Organic & Biomolecular Chemistry - an international journal covering the breadth of synthetic, physical and biomolecular chemistry. www.rsc.org/obc

Natural Product Reports (NPR) - a critical review journal which stimulates progress in all areas of natural products research. www.rsc.org/npr

Photochemical & Photobiological Sciences - publishing high quality research on all aspects of photochemistry and photobiology, encouraging synergism between the two areas. www.rsc.org/pps

Chemical Biology - a news supplement which draws together the latest developments in chemical biology from all RSC publications. www.rsc.org/chembiology

NEW for 2009

Integrative Biology - a journal focusing on quantitative multi-scale biology using enabling technologies and tools to exploit the convergence of biology with physics, chemistry, engineering, imaging and informatics. www.rsc.org/ibiology

Metallomics - a journal covering the research fields related to metals in biological, environmental and clinical systems. www.rsc.org/metallomics

Take a look today!

RSC Publishing

www.rsc.org/journals

Registered Charity Number 207890



Renewable Energy themed issue

This themed issue of *Chem Soc Rev* on Renewable Energy collects the work of scientists that seek to transform the dream of a solar-powered society into reality. Topics include bioenergy conversion and biocatalysis, solar capture and conversion materials and catalysts used to store energy in hierarchical materials or in the form of the chemical bonds of fuels.

Reviews include:

Small molecule mimics of hydrogenases: hydrides and redox

Frédéric Gloaguen and Thomas B. Rauchfuss

Biology and technology for photochemical fuel production

Michael Hambourger, Gary F. Moore, David M. Kramer, Devens Gust, Ana L. Moore and Thomas A. Moore

Photosynthetic energy conversion: natural and artificial

James Barber

Single Nanowire photovoltaics

Bozhi Tian, Thomas J. Kempa and Charles M. Lieber

Multifunctional 3D nanoarchitectures for energy storage and conversion

Debra R. Rolison, Jeffrey W. Long, Justin C. Lytle, Anne E. Fischer, Christopher P. Rhodes, Todd M. McEvoy, Megan E. Bourg and Alia M. Lubers

Photodriven heterogeneous charge transfer with transition-metal compounds anchored to TiO₂ semiconductor surfaces

Shane Ardo and Gerald J. Meyer

Guest editor



Daniel G. Nocera
 Massachusetts Institute of
 Technology, Cambridge,
 MA, USA



Dirk M. Guldi
 Interdisciplinary Center for
 Molecular Materials (ICMM)
 Germany

"The aim of this thematic issue is to be a timely showcase for the latest cutting edge international research in this most important of multidisciplinary fields, and to show how the latest research can lead a path to ground-breaking new alternative renewable energy technologies."

010992

RSC Publishing

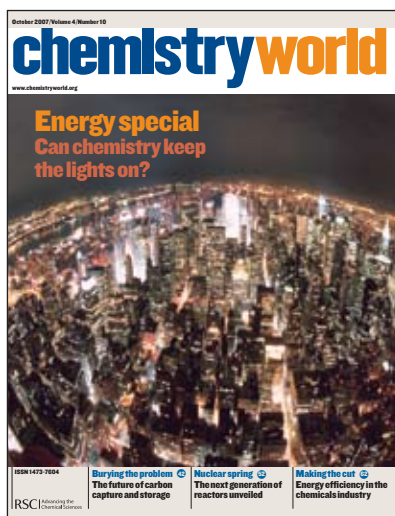
www.rsc.org/chemsocrev/energy

Registered Charity Number 207890

Take the global perspective



Chemistry World, the award-winning monthly magazine from the Royal Society of Chemistry, has something for everyone with daily online news, articles on all aspects of the chemical sciences, job vacancies and award-winning columnists.



Named Best monthly and business professional magazine of the year at the 2006 PPA Magazine Awards, *Chemistry World* reflects the ubiquitous importance of the chemical sciences in the world today, providing a more complete picture and informed opinion on the issues that matter.

Daily web updates and e-mail alerts give the magazine a strong online presence that enhances and expands on the monthly print issue. Plus, with the *Chemistry World* Podcast and Blog, there's a chance to go interactive.

Go online today!

RSC | Advancing the
Chemical Sciences

www.chemistryworld.org

Registered Charity Number 207890

10080743